CRANFIELD UNIVERSITY

GREGORY ROSS JAMES

DEVELOPMENT OF MODELS TO ASSESS PENETRATING INJURY FROM BALLISTIC PROJECTILES

DEFENCE ACADEMY

PhD THESIS
Academic Year: 2013 - 2020

Supervisors: Ian Horsfall 2013 - 2018
Clare Knock 2018 - 2020

CRANFIELD UNIVERSITY

DEFENCE ACADEMY

PhD THESIS

Academic Year 2013 - 2020

GREGORY ROSS JAMES

DEVELOPMENT OF MODELS TO ASSESS PENETRATING INJURY FROM BALLISTIC PROJECTILES

Supervisors: Ian Horsfall 2013 - 2018
Clare Knock 2018 - 2020

DSTL/PUB118063

ABSTRACT

Injuries from penetrating ballistic projectiles, such as fragments and bullets, are the major cause of military (and civilian) casualties in conflict, as well as casualties in terrorist incidents.

This research project had the primary aim of developing models that facilitate the assessment of injury from penetrating ballistic projectiles, in both a physical and virtual environment.

Existing models and literature in this area has been limited to a narrow range of scenarios (such as specific projectile types) or with limited validation of the models.

Collation of ballistic data for muscle tissue and simulants from the literature, in addition to an extensive original dataset and novel data analysis techniques allowed a definitive assessment of the validity of skin and muscle tissue simulants for wound ballistics research, relevant to fragments and bullets.

A range of physical and virtual models were developed and are applicable to assessing the risk of penetrating projectiles in ballistic and blast scenarios.

Considered particularly novel was the development of a new fragment witness pack to assess the hazard from low density and low energy fragments by predicting the risk of eye penetration, skin perforation and to estimate the impact velocity of the projectile.

The range of physical and virtual models developed have been used to provide insights to (and describe implications of) the target factors that influence the outcomes of physical testing when using real tissue or tissue simulants.

The exploitation of these models has led to improvements in tactics, techniques, and procedures and equipment for UK Armed Forces and police, ultimately reducing injuries and saving lives.

Keywords:

Fragment, tissue, gelatin, retardation, model

ACKNOWLEDGEMENTS

Firstly, I want to say a huge thank you to my wife, who has been through the PhD process herself and understands many of the challenges I have faced. She has been supportive, encouraging and understanding. I could not have done it without her.

I would like to thank my supervisors; Professor Ian Horsfall and Dr Clare Knock for their support and guidance.

Special thanks to Alan Hepper for his insightful and knowledgeable review of the plans and technical content of this work through the duration of my studies.

For their support, advice, guidance and discussion of many ideas on various aspects of this work: Alan Hepper, James Keirl, Mark Laird, Rebecca Livesey Ruth McGuire, Scott Reeve, Andrew Sedman, Warren Tam and Jane Weir.

I am grateful to all who assisted in the preparation and conduct of the numerous ballistic trials:

Daniel Armstrong, James Badger, Lisa Baker, Rajesh Dhokia, Rebecca Dyer, Alun Fortes, Lucy Gant (nee Allanson-Bailey), Craig Girdlestone, Pete Harwood, Alan Hepper, Phil Homer, Sarah Jones, James Keirl, Warren Kitchen, Mark Laird, Iain Larcombe, Stuart Maitland, Brett Martin, Charles Masey, Kris Piper, Amy Pullen, Scott Reeve, Jon Russell, Brian Sainsbury, Andrew Sedman, Ian Softley, Julie Softley, Laura Stebbings, Warren Tam, Emma Teasdale, Kathryn Waterworth, Jane Weir, Pete West, Alex Wright and the Dstl Engineering Capability.

Trials support from the individuals listed above contributed to one or more of the following: target preparation and/or disposal, data capture equipment supply, set-up and/or operation, weapon system operation and range safety roles.

Robert Fryer for his support and advice relating to the Weapon Target Interaction model.

Dstl Intellectual Property Group for generating the patent applications made in relation to the work in this thesis.

Dr Richard Critchley as secondary supervisor and Dr Peter Zioupos as review chair. Both provided insightful comments and considerations which helped guide aspects of this work.

Alan Peare and Professor Debra Carr for their assistance with the tensile testing setup. Additionally Deb for her willingness to help and advice, even after the closure of the Impact and Armour Group at Cranfield University.

International partners who advised, verified, exploited and/or fed back on the models developed in this thesis. In particular Patrick Gillich and Randy Mrozek (Army Research Laboratory, US) and Simon Ouellet (Defence Research and Development Canada). Randy Mrozek for supply of Stabili-Gel for ballistic testing and the raw data from his previously published results.

Lt. Col. Johno Breeze for his collaboration on some of the experiments detailed in this thesis (and publications) that were conducted prior to the start of the registration period for this PhD.

David Kieser for sharing his raw data on 10%, 11.5% and 20% gelatin calibration.

Tom Stevenson for supply of the high speed video for some shots against Cranfield 10% gelatin, used as part of the retardation comparison in different simulants.

TABLE OF CONTENTS

LIST OF FIGURES

LIST OF TABLES

LIST OF EQUATIONS

LIST OF ABBREVIATIONS

AD	Areal Density
AIS	Abbreviated Injury Scale
APM	Anti-Personnel Mine
ARL	Army Research Laboratory
BABT	Behind Armour Blunt Trauma
BAD	Behind Armour Debris
BB	Ball Bearing
BMI	Body Mass Index
BSE	Bovine Spongiform Encephalopathy
CDM	Collateral Damage Model
CI	Confidence Interval
CN	Chisel Nosed
CPA	Critical Perforation Analysis
CSA	Chief Scientific Advisor
DES	Duma Eye Score
DIC	Digital Image Correlation
DoP	Depth of Penetration
Dstl	Defence Science and Technology Laboratory
E_{50}	Energy at which 50% of projectiles perforate
EM	Engineering Model
EPS	Expanded Polystyrene
E_{th}	Threshold energy
FEA	Finite Element Analysis
FREM	Fast Running Engineering Model
FSP	Fragment Simulating Projectile
HD	High Density
HME	Home Made Explosive
HSV	High Speed Video
HTPH	Honed Tube Pressure Housing
IED	Improvised Explosive Device
LD	Low Density
LLW	Less Lethal Weapon
MD	Medium Density
MDFPIM	Multiple Discrete Fragment Physical Injury Model

MOD	Ministry of Defence
MPH	Mann Pressure Housing
MTC	Maximum Temporary Cavity
NATO	North Atlantic Treaty Organisation
NIJ	National Institute of Justice
ORCA	Operational Requirements-based Casualty Assessment (model)
PC	Permeant Cavity
PMHS	Post Mortem Human Subject
PP	Pelvic Protection
PPE	Personal Protective Equipment
rFVIIa	recombinant Factor VIIa
RH	Relative Humidity
S&K	Sperrazza and Kokinakis
SDVB	polyStyrene-DiVinyl Benzene
SE	Standard Error
SEBS	poly(Styrene-b-Ethylene-co-Butylene-b-Styrene)
SFPIM	Single Fragment Physical Injury Model
STANAG	Standardisation Agreement
UTS	Ultimate Tensile Strength
V&V	Verification & Validation
V_{50}	Velocity at which 50% of projectiles perforate
V_{th}	Threshold velocity
WSU	Wayne State University
WTI	Weapon Target Interaction (model)
ZMR	Zone of Mixed Results

LIST OF SYMBOLS

Symbol	Description
a	Parameter for the simple empirical skin perforation equation
A	Cross sectional area of the projectile (cm^2)
Ā	Entrance region attenuation factor for cavity formation
a’	Parameter for the expanded empirical skin perforation equation
A_{av}	Average presented area of the projectile (cm^2)
A_c	Local cross sectional area of the MTC (cm^2)
A_s	Total surface area of the projectile (cm^2)
b	Parameter for the simple empirical skin perforation equation
b’	Parameter for expanded empirical skin perforation equation
C	Curve fitting constant for the probability of skin perforation (simple and expanded forms) equation
C_D	Velocity independent drag coefficient
D	Curve fitting constant for the probability of skin perforation (simple and expanded forms) equation
d	Projectile diameter (mm)
d_6	Reference value for projectile diameter (6 mm)
d_{av}	Average diameter of the projectile (mm)
DoP	Permanent Depth of Penetration (mm)
DoP’	The modified DoP to account for the skin
DoP_{maxT}	The maximum temporary depth of penetration (mm)
E	Kinetic energy (J)
e	Base of the natural logarithm (≈2.718)
E_{50}	Energy at which the estimated probability of the outcome (penetration or perforation) is 50% (J)
G	Curve fitting constant for the probability of eye penetration
$\bar{g}$	Temporary cavity formation parameter
$\bar{g}_\infty$	Asymptotic value of g at large *v/U*
H	Curve fitting constant for the probability of eye penetration
L	Layer number of the MDFPIM polythene sheeting
m	Projectile mass (g)
n	The total number of fragment impacts

Symbol	Description
P_{hk}	The probability (given a hit) that single, random hits with steel fragments will incapacitate
P_{hki}	The probability of incapacitation (given a hit) from the i^{th} fragment
P_k	The total probability that *n* hits will incapacitate
r_{MTC}	Radius of the MTC at a given depth in gelatin (mm)
$r_{MTCtissue}$	Radius of the MTC at a given depth in tissue (mm)
r_{PC}	Radius of the PC in tissue (mm)
S	Sectional density of the projectile (g cm^{-2})
T_a	Parameters for different tissue types within the equivalent tissue thickness scaling equation
T_b	
T_c	
T_d	
U	Rupture modulus (for gelatin or tissue)
U_6	Reference value related to rupture modulus for a 6 mm diameter projectile (m s^{-1})
v	Velocity (m s^{-1})
V_{50}	The velocity at which the estimated probability of the outcome (penetration or perforation) is 50% (m s^{-1})
V_R	Residual velocity (m s^{-1})
V_s	Strike or impact velocity (m s^{-1})
V_{th}	Threshold velocity (m s^{-1}). The lowest experimental velocity at which a penetration or perforation occurs.
α	Parameters for expanded empirical skin perforation equation dependent on penetration/perforation and prediction method
β	
γ_a	Parameters for expanded empirical skin perforation equation for target type
γ_b	
δ_a	Parameters for expanded empirical skin perforation equation for target area
δ_b	
ε_a	Parameters for expanded empirical skin perforation equation for backing type
ε_b	
κ_a	Parameters for expanded empirical skin perforation equation for storage condition
κ_b	

Symbol	Description
λ	Parameter in the generic, non-linear least squares regression form of conservation of energy equation, assuming a constant projectile mass.
η_a	Parameters for expanded empirical skin perforation equation for normalised nose length of the projectile
η_b	
μ	Parameter in the generic, non-linear least squares regression form of conservation of energy equation, assuming a constant projectile mass.
π	Pi (3.1415...)
ρ_T	Target density (g cm^{-3})
ρ_p	Projectile density (g cm^{-3})
σ_{rMTC}	Standard deviation the radius of the MTC
σ_{rPC}	Standard deviation the radius of the PC
Φ	Standard normal cumulative distribution (with a mean of zero and a standard deviation of one)

1 Introduction

1.1 Background

1.1.1 General

Injuries from penetrating ballistic projectiles (such as fragments and bullets) are the major cause of military (and civilian) casualties in conflict [1-13], as well as in terrorist incidents [14-16].

Injuries from penetrating projectiles may be caused by a variety of different threats. In a military setting this includes small arms (bullets) and explosive weapons such as grenades, mortars, artillery shells, mines and Improvised Explosive Devices (IEDs).

For explosive weapons, the fragments from the weapon itself, such as those from the steel casing of grenades, mortars and artillery shells are termed primary fragments. The fragments energised from the surrounding environment such as from soil, buildings, etc. are termed secondary fragments [17].

Primary and secondary fragments are of interest as both cause injuries, although primary fragments have generally been the main focus of fragment injuries and modelling in the literature. This is likely because primary fragments are designed into the weapon performance and therefore will be repeatable from one example of the weapon to the next. Secondary fragments, by their nature, will be more unpredictable in their properties (sizes, materials, geometries, etc.) and are therefore more challenging to characterise.

Many of the casualty statistics reported in the literature do not supply sufficient detail to provide the exact proportion of casualties with penetrating injuries caused by fragments. However, the potential scale of the problem can be estimated, noting that not all casualties caused by explosive incidents will have penetrating fragment wounds (for example if they were in an armoured vehicle at the time of the incident).

The reported incidence of military casualties[1] from fragment injuries ranges from 33% to 92% [1-13] across World War I, World War II, Korea, Vietnam, Northern Ireland, Falklands, Somalia, Iraq and Afghanistan. In the more recent conflicts the proportion of casualties from fragment injuries was generally reported as >60% [1-13], although these were not further divided into primary and secondary fragments.

For terrorist bombings, the incidence of casualties from fragments or classed as soft tissue injury ranges from 48% to 87% [14-16].

In a civilian setting, air rifles have been well documented in causing penetrating injuries [18; 19], the hazard of these systems may need to be assessed (e.g. References [18-21]).

Understanding how different projectiles perforate the skin and penetrate tissue is critical for a number of applications. This includes understanding the injury potential of different threats, models to inform safety cases, development of predictive models of penetration and for casualty prediction models.

There are a variety of models that are needed to assess the risk or potential injury from penetrating projectiles. The UK Ministry of Defence (MOD) defines a model as "*A representation of something. A model may be physical (e.g. a wooden mock-up) or virtual (computer-based). The 'something' may be physical (e.g. a vehicle) or abstract (e.g. a relationship between variables in a graph).*" [22]

In this thesis, the terminology 'simulant' is used interchangeably with 'model', particularly when describing physical models for skin and muscle tissue.

The field of study of the projectile – tissue interaction is often termed 'Wound Ballistics' and can be considered as two related branches: clinical considerations (i.e. surgical management or treatment) and 'engineering' based (i.e. more fundamental understanding of the physics). This explains why much of the literature is from (military) surgeons as well as scientists and engineers from a

[1] Does not include Non-Battle Injuries (NBI) which can equate to approximately half of field hospital admissions [1].

range of backgrounds. In this thesis, the main focus is on the 'engineering' approach, although many of the conclusions are relevant to clinical aspects and are discussed.

Despite copious wound ballistics studies on many different projectile and tissue types, including tissue simulants, there are very few sources that aim to provide a more holistic validation of the penetration process, particularly in both the physical and virtual environment.

1.1.2 Eye injuries

Penetration of the eye or perforation of skin by ballistic projectiles is important as it marks the onset of penetrating injury. Any projectiles that do not have the ability to penetrate the eye or perforate skin can be ignored in terms of their penetrating injury potential; however, any blunt injury potential may still need to be considered. Low mass projectiles, less than 20 grams, are broadly considered outside the range expected to cause (serious) blunt injuries [23][2], without causing a penetrating injury.

Eye penetration is also of particular interest because it can have severe impact on morbidity (quality of life), rather than mortality (threat to life) that is normally considered from penetrating fragments.

1.1.3 Ballistic models

A generally accepted and adopted approach to physically model ballistic impacts for the whole body is to use either use an animal cadaver or tissue simulant such as gelatin (which is homogeneous and repeatable). Using animal cadavers cause a number or practical and ethical issues, although may enable direct prediction of injury effects. The use of gelatin as a muscle tissue simulant provides a model which is more repeatable and reduces some of the practical and ethical problems to allow comparative assessment, but by itself cannot provide a predictive outcome. Predicting the target response (i.e. the resulting damage in real tissue)

[2] Assuming an impact to an unprotected person. For impacts to a protected person, Behind Armour Blunt Trauma (BABT) is still a potential risk, even with low mass projectiles.

from a simulant is challenging and generally is limited to comparative studies (i.e. the ‘wound profile method’ illustrated in Reference [24]). It is rarely considered how the effects of penetration through multiple different tissue types influence the resulting outcome, instead assuming a tissue simulant (i.e. gelatin for a muscle tissue simulant) models the whole body, or just considering each tissue in isolation. A major stumbling block is considered to be the objective and predictive assessment of the target response.

1.1.4 Bullets

Whilst bullets are frequently used in wound ballistics studies as they are of specific interest, their behaviour in tissue or tissue simulants is difficult to control experimentally and to measure the relevant variables. Coupled to this is large inherent variation in biological tissues, meaning conclusions (or validation) cannot normally be extrapolated to other projectile types or tissues. The key variables specific to bullets that limit the generalisation of these studies are: tumbling in the target[3], deformation and/or fragmentation of the bullet. These behaviours are projectile and tissue specific (meaning results cannot easily be extrapolated to other tissue types).

1.2 Aims and objectives

1.2.1 Aims

The field of wound ballistics is extremely broad. In order to focus the work within this thesis, the work was limited to understanding and modelling the projectile response in different tissues (i.e. penetration and retardation of the projectile) and the target response of eye, skin and muscle tissue (i.e. damage). The response of other tissue types was not considered as part of the thesis (although potential routes for generating these outcomes are discussed).

The aims of this work were to:

[3] The depth at which this occurs is variable even from the same weapon, at the same range and with the same batch of ammunition [25; 26].

- Develop (a suite of complementary) models that facilitate the assessment of injury from penetrating ballistic projectiles, in both a physical and virtual environment.
- Use these models to further the understanding of the penetration process, access the validity and limitations of the models developed.

1.2.2 Objectives

The objectives of this work were to:

- Review the existing data for skin perforation, eye penetration and penetration into muscle tissue and tissue simulants, (Section 3).
- Use the above to focus the subsequent research to address some of the shortcomings identified, by performing a series of practical experiments (Section 5).
- Develop empirical equations for skin perforation and eye penetration that can be used in computer simulations (Section 6).
- Develop a physical model for single projectile impacts to muscle tissue (Section 7) and muscle tissue with skin (Section 8) that can be used in laboratory physical trials.
- Evaluate and develop equations, known as Fast Running Engineering Models (FREMs), for predictions of penetration and cavitation in muscle tissue and tissue simulants (Section 9).
- Develop a physical model to assess injury from multiple simultaneous projectile impacts that can be used in physical threat assessments (Section 10).

Throughout the thesis, additional objectives were placed on each of the models developed:

- Be applicable to a broad a range of input parameters to enable their use over a wide variety of scenarios.

- Verify and then validate the models over a broad range of input parameters and determine the model accuracy and reliability compared to experimental data (to allow potential model users to make a sound judgement on model ‘fitness for purpose’).

1.3 Declaration

I, Gregory James, state that the work presented within this PhD thesis is my own.

Development based on existing models is clearly referenced and acknowledged where relevant. Some data from unpublished experiments are included within this thesis that were conducted by the author, prior to the registration of this PhD. These have been indicated in the relevant section.

All of the original experiments described were planned and conducted by the author for the purposes of this PhD. Support from a large number of individuals (listed in the Acknowledgements) was required for the numerous ballistic tests conducted. All original ballistic experiments took place at the Defence Science and Technology Laboratory (Dstl) Porton Down, Building 390 South Ballistic Laboratories.

Ethical approval for this research was granted through the Cranfield University Research Ethics System with reference CURES/9292/2019. No live animals were used within the experiments conducted as part of this thesis. The animal cadavers or tissues used for the original work were either obtained following other (non-ballistic) experiments, where it would otherwise have been disposed of, or the animals were humanely killed by qualified personnel using schedule 1 methods according to the Animals (Scientific Procedures) Act 1986.

2 Model definitions and types

2.1 Introduction

The ‘targets’ used for ballistic research, be that live or dead animals, Post Mortem Human Subjects (PMHS) or tissue simulants are all models of a live person. Some of the key issues that need consideration when using models are not always properly or fully considered in the wound ballistics literature [27]. This section covers an explanation of model types and use, leading into the models developed within this thesis.

2.2 Predictive and comparative models

Models may be comparative; such that a measured output from the model can be used to rank different scenarios, but may not be able to be related directly back to the real world. For example a comparative model could be used to discriminate between threats A and B. Comparative models are often used when there are limited data to validate the model, or simple comparison is all that is required[4].

Models may be predictive; such that the output is expected to relate directly to the real world, for example a velocity or penetration depth in a given material.

2.3 Model types

2.3.1 Virtual (computer-based) models

There are a wide range of different virtual/mathematical models of varying levels of complexity and accuracy.

The simplest (least accurate, least complex) type of virtual model is a ‘rule of thumb’, for example the ‘80 Joule rule’ which generalises that a projectile with greater than 80 J of kinetic energy on impact is required “*to immobilize a human from the battlefield*” [28; 29].

[4] A comparative model may be able to say threat A is less injurious than threat B, but may not be able to determine the significance of that difference in terms of injury, e.g. that both may be lethal.

Models based purely on data (i.e. the relationship between variables in a graph) are termed empirical. Empirical models are only as good as the data on which they are based and may be appropriate when interpolated. Extrapolation may cause erroneous or illogical model outputs.

Analytical (e.g. physics based or engineering based) models may be better for extrapolation, but rely on the fact that they must suitably describe the system they model. Analytical models are not necessarily more complex than empirical models; just have different benefits and drawbacks. In this thesis, analytical models will be in a form of an equation, or set of equations that can be implemented in Microsoft® Excel® 2010 or similar. These types of analytical models are sometimes referred to as Engineering Models (EM) or Fast Running Engineering Models (FREM).

A shot line model is a type of virtual model where a 3D representation of a target can be implemented (e.g. a person or vehicle) and then a threat projected at it within the model, in order to get a damage or injury outcome. Shots are normally repeated at the target over a grid to get an averaged output. A shot line model may have lots of underpinning empirical and analytical models that allow the predictions to be made. Examples of shot line models are the US developed ComputerMan [30], the Operational Requirements-based Casualty Assessment (ORCA) [31] and the UK Human Vulnerability Tool within the Weapon Target Interaction (WTI) architecture [32].

Finite Element Analysis (FEA) is a complex physics/engineering based mathematical model. This can be in a complex 3D geometry, for example an entire vehicle, but generally takes a long time to run due to the complexity. FEA is not used in this thesis, but has been included in the model descriptions to help illustrate where the other model types sit in comparison. The outputs from this thesis may be used to validate FEA models in the future.

An overview of how these different types of mathematical models relate to each other in terms of complexity and run time is given in Figure 1[5]. It is important to note that just because a model is more complex does not mean it is more accurate. In these relationships run time can be thought of as analogous to resource required to run the model (independent of computational power).

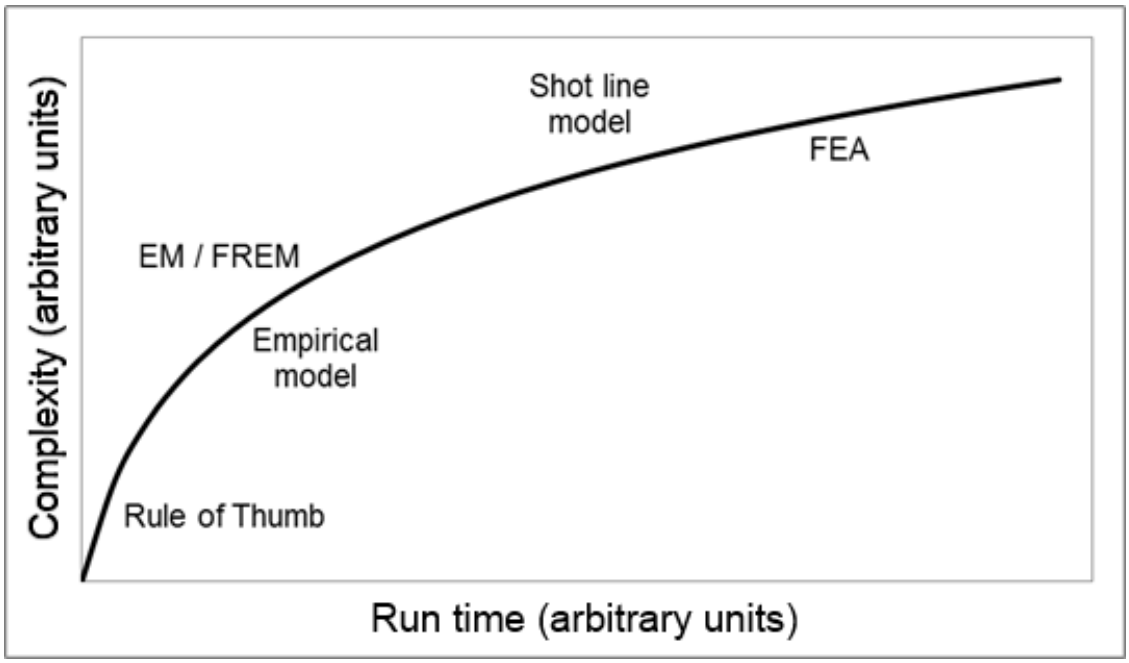

Figure 1: Generalised representation of the relationship between complexity and run time for different mathematical models

2.3.2 Physical models

Physical models may have varying levels of complexity and accuracy, as with virtual models.

A physical model is designed to simplify the system, or part of the system of interest; be that in terms of reduced complexity, time required, affordability, ease of analysis/interpretation, ethics, storage, supply, etc.. Additionally, due to the highly variable nature of biological tissues and the desired model applications,

[5] Subject Matter Expert (SME) opinion could also be thought of as a virtual model, but is not shown here.

physical models are normally intended to be more repeatable than the system they represent.

In this thesis, physical models are sub-categorised as biological or synthetic, not by their complexity. For example PMHS and animals (live or dead) are physical biological models of live humans.

2.4 Fit for purpose

Models must be fit for purpose. This (seemingly common sense statement) often does not appear to be properly considered. The 'best' model for a particular application depends on the requirements. The most accurate model is not always the best model. For example if an output is required in a short timeframe, then the 'best' model may be one that is toward the left of Figure 1, sacrificing accuracy in the answer as a trade-off for reduced run time. Even if a model has been used to answer a similar question 10 or 100 times previously, does not automatically mean it is fit for purpose to do so again.

In order to determine what model to use for any situation, a robust requirement or user need statement is needed. The intended model should then be checked against this requirement to determine if it meets these criteria. This process should be conducted every time a model is used.

References [33-35] discuss the need for, and how to ensure that models used are fit for purpose. A key part of ensuring a model is fit for purpose is Verification and Validation (V&V).

2.5 Verification and Validation (V&V)

Verification is ensuring that the model works as expected. For example verification could involve inputting test data to the model where the results that should be output are already known, to ensure that the model outputs match. For a physical model this is often referred to as calibration.

Validation is ensuring the accuracy of the model outputs (within a given range or scenario).

The need for verification and validation is given in many sources. Reference [22] provides an overview of the need for V&V relating it to a risk based application of the model output:

> "*When to do V&V? V&V should be conducted when the risk of making an incorrect decision … outweighs the risk of conducting the V&V activity.*" [22]

The verification and validation requirements for the same model may differ depending on how the output is used (relating back to fitness for purpose). Model verification and validation is an ongoing process [35; 36].

Reference [37] discussed V&V procedures for models used in vulnerability and lethality analysis software in the Army Research Laboratory (ARL) and promotes the use of observed versus predicted value plots or model residual fits in order to show how well a model fits the data. As each model is generated throughout this thesis, consideration is given to its verification and validation. Observed versus predicted value plots are used in a number of instances to show model accuracy and reliability in this manner.

2.6 Model relationships

In this thesis, multiple models were developed, some of which are linked together or predicated on other models or datasets. In order to meet the aims and objectives (Section 1.2), both virtual and physical models were required.

The approach taken for the prediction of penetration and retardation in tissue was to use a simple, homogeneous physical model that with the supporting FREMs could be used to interpret the projectile response in a range of different tissues. This is in contrast to other approaches described in the literature where a physical model specific to a given tissue type or scenario was created [38-41]. The objective baseline response of the selected physical model (i.e. without scaling by the FREMs) was desired to match that of (live) muscle tissue.

The exception to this was for the eye penetration and skin perforation physical model(s) where the requirement was to have direct predictions of the penetration/perforation outcome directly from the physical model for simplicity.

The focus in this thesis is on ‘simple’ virtual models (i.e. FREMs) and physical models. The use of FREMs was considered to allow more scope for exploitation of the outputs, compared to more complex virtual models, such as FEA. For example, this enables the FREMS developed to be integrated into shot-line or casualty prediction models and still achieve the run time required from these models.

Figure 2 shows how these models and datasets used and/or developed relate to each other in terms of the model development. Not all of the data/models displayed in Figure 2 were generated as part of this thesis; some have been drawn from external sources. For example this includes data that fed into each of the datasets; ComputerMan scaled retardation [42] (Section 9.9) and the basis of the FREM for tissue penetration and retardation (Section 9). The information that has come from external sources is detailed in the relevant section for that model or dataset.

Injury algorithms (such as that in Reference [43]) and shot line models are shown in Figure 2 (in yellow) as potential exploitation of the outputs from preceding models in order to generate an injury outcome. However, these models are not within the scope of this thesis other than as examples of potential exploitation routes.

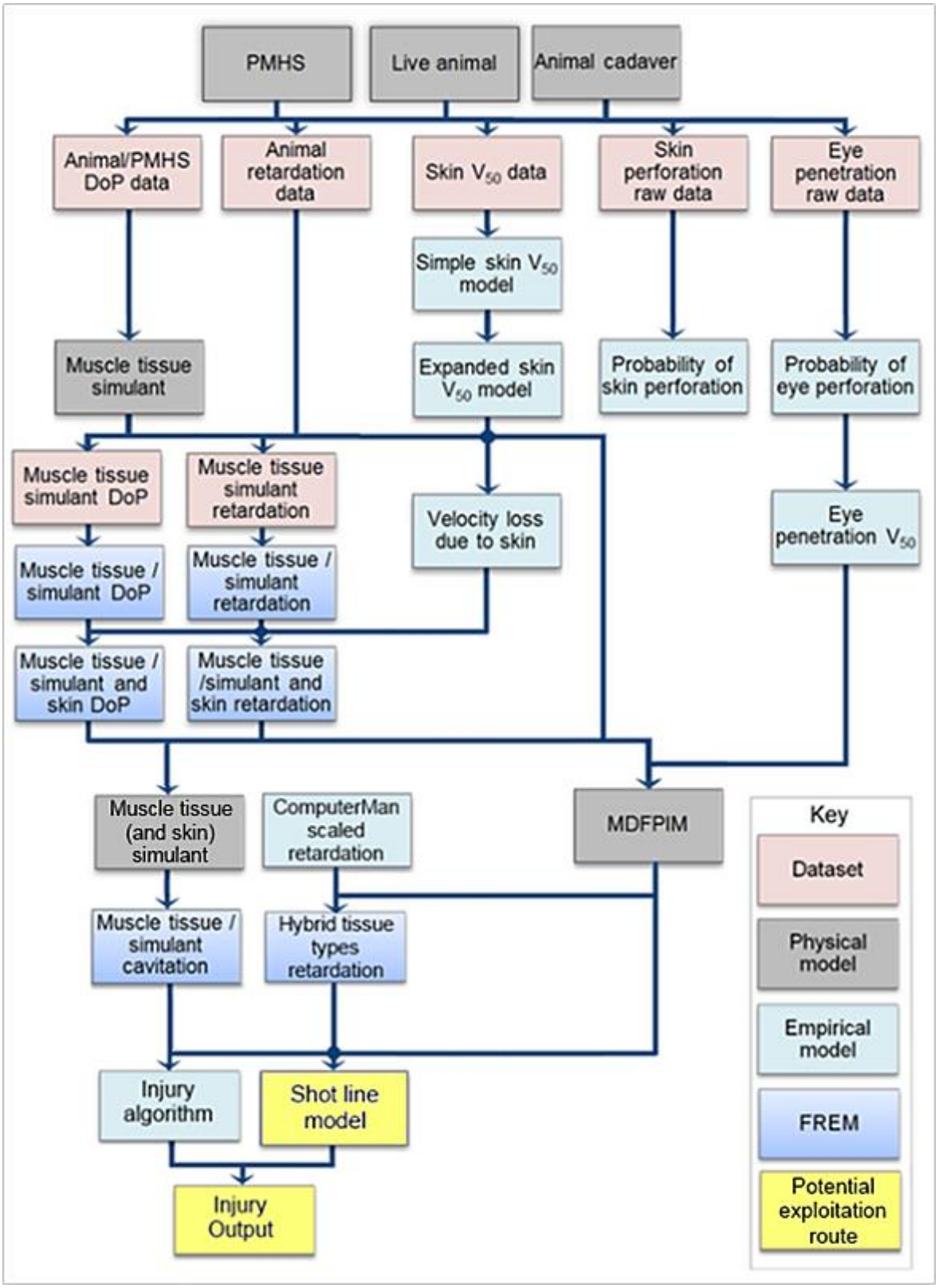

Figure 2: Overview of model linkages. Arrows indicate direction of data flow / model development (MDFPIM = Multiple Discrete Fragment Physical Injury Model).

3 Literature review

3.1 Scope of literature review

To understand the scale of penetrating ballistic injuries, for which the models developed in this thesis can be applied to assess, the incidence of military and civilian casualties were evaluated.

In order to model (mathematically or physically) the response of human tissue to penetration from projectiles, the first step that has been taken was to evaluate the penetration response from experimental studies on ex-vivo humans, referred to as PMHS and animals in the form of a review of the literature. This review of the literature allowed performance metrics to be generated for the risks of skin perforation and eye penetration as well as velocity – penetration into tissue, which has been used as the basis for the models developed.

This literature review was conducted for:

- Skin penetration and perforation
    - Raw penetration and perforation data and/or V_{50} response from experiments (discussed separately for PMHS and animal targets).
    - Mathematical predictions
    - (Physical skin simulants are reviewed in Section 8)
- Muscle tissue and tissue simulants
    - Physical muscle tissue simulants
    - Penetration data for muscle tissue and simulants from experiments
- Ballistic penetration of the eye
    - Types and incidence of penetrating eye injury
    - Raw penetration and perforation data from experiments
    - V_{50} response data from experiments
    - Mathematical predictions

3.2 Penetration and perforation of skin data

3.2.1 Objective

The aim of the review of the skin penetration and perforation data was to establish the ballistic performance of skin against a range of different projectiles and determine the dominant properties (of the projectile and the target) influencing the skin perforation process.

The data was gathered for as wide a range of projectiles and impact conditions as possible to ensure that any empirical equation or physical model developed could be validated against the response over this wide range, reducing the need for extrapolating outside of the bounds on which it is based.

The review focused on finding raw data (i.e. for a given projectile, an impact velocity and if it penetrated or perforated skin) in addition to studies where the threshold velocity or 50% penetration or perforation risk was reported. To be included in the dataset, sufficient detail was required to identify the target[6], the projectile properties and the projectile had to be non-deforming. One of the projectile properties used to describe the skin perforation risk was the cross sectional area or sectional density of the projectile. Time-variable sectional density projectiles, e.g. some less lethal weapon impact rounds that expand on impact, are beyond the scope of this thesis.

3.2.2 Skin and muscle structure

Skin is made up of several layers (see Figure 3), with different properties. The outermost layer is the epidermis which ranges from 0.05 mm to 1.5 mm in thickness [47]. Below this is the dermis, containing blood vessels and nerve endings as well as the main elements that contribute to the skins mechanical properties (elastin and collagen). The dermis is between 0.3 mm and 3 mm thick [47]. The dermis contains collagen and elastin fibres, which dominate the flexibility and strength of the skin [48]. Further beneath the dermis is

[6] Some target types were discounted from the review, such as data for cows [18; 44], horses [45] and chickens [18; 46] due to their dissimilarities in skin to humans.

subcutaneous tissue (referred to as hypodermis), not part of the skin itself, but connects the skin to the underlying tissues. Figure 3 shows these layers of the skin.

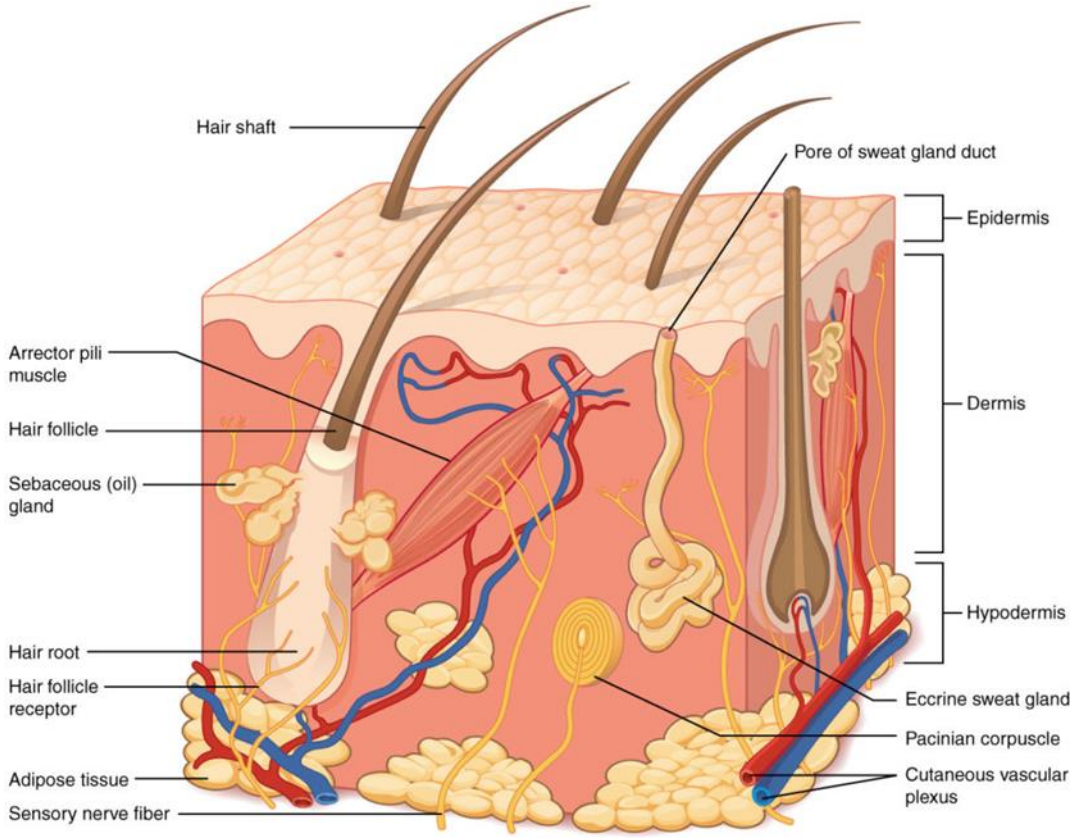

Figure 3: Skin structure in cross section. Original image from Reference [49], used under license *CC BY: Attribution*.

At low strains the elastin fibres dominate the skins mechanical performance and are responsible for its elastic performance [48].

At higher strains (greater than approximately 0.3) the collagen fibres dictate the mechanical performance of skin [48]. The collagen is under greater tension parallel to the so called Langer's lines compared to the fibres perpendicular the Langer's lines. Because of this, the skin exhibits anisotropy; it has different mechanical properties in different directions. It is also considered that skin is anisotropic in it's through thickness direction [48].

Whilst the orientation of skin in respect to Langer's lines is critical for mechanical testing, it is less relevant for ballistic testing where the skin will be stretched in all

directions. For skin simulants, the material construction needs to be understood in order to consider any potential anisotropy for mechanical testing.

Skin (epidermis and dermis) thickness and mechanical properties can vary greatly between individuals, particularly people of different genders, ages, ethnicity, Body Mass Index (BMI), as well as different places on the same person. A large number of sources are available that have measured skin thickness accounting for these factors using different methods. For this thesis, Reference [50] has been used and provides data to show that there was no significant difference found in average skin thickness for four body regions (thigh, waist, deltoid and suprascapula) between 4 different age ranges (18-30, 31-40, 41-50, 51-70 years old), although mechanical properties would be expected to differ.

The average male skin thickness has been shown to be 2.16 mm (averaged across 4 sites; thigh, waist, deltoid and suprascapula) [50].

3.2.3 Definitions

All the data in the literature has been based on different measures of skin 'performance' in terms of the type of skin damage and how the corresponding velocity result was calculated or averaged.

In order to study the ballistic response of skin, certain terms need to be defined (Section 3.2.3.1). The existing data in the literature has been re-interpreted in line with these definitions where possible.

The terms and methods used to calculate skin perforation velocities used in this thesis are described in Section 3.2.3.2.

3.2.3.1 Skin penetration and perforation terms

- Skin is defined as the epidermis and dermis.
- Penetration: the projectile has passed through a partial thickness of the skin, without completely perforating it. The projectile may bounce off or remain embedded in the skin. Any partial thickness laceration or similar damage to the skin is classed as a penetration.

- Non-penetration: the projectile has not broken or punctured the skin.
- Perforation: the projectile has passed completely through the entire thickness of the skin. During physical testing this is simple to determine for isolated skin as there will be a hole that allows light through if a perforation has occurred. For intact skin, perforation can be determined if there is a hole in the dermis and epidermis that allows a thin rod to pass through into the subcutaneous tissue or muscle. Perforation can occur even if the projectile bounces off, or remains embedded in the skin. In this latter case, the projectile would have to be removed in order to determine if perforation had occurred.
- Non-perforation: the projectile has not passed (or created a hole) through the entire skin thickness.
- Zone of Mixed Results (ZMR): the velocity region that contains mixed penetration or perforation data. It is the zone that is bounded the slowest perforating shot and the fastest non-perforating shot. A ZMR does not always occur during testing.
- Sectional density (*S*): the projectile mass (*m*, in grams) over the cross sectional area (sometimes called presented area) of the projectile (*A*, in cm^2). $S = m/A$, with units of g cm^{-2}.
- Energy density (*E/A*): the projectile energy (*E*, in joules) over the cross sectional area of the projectile (*A*, in cm^2). *E/A* in units of J cm^{-2}.

3.2.3.2 Penetration and perforation velocities

There are a number of different methods for calculating and defining the velocity at which a material (in this case skin) “fails” due to ballistic penetration or perforation. Most can be applied to either penetrations or perforations. Each value calculated is only applicable to the specified target and projectile combination. In addition, repeating the testing under exactly same conditions may not give the same result. A description of the different terms and methods are below:

- Threshold velocity (V_{th}): This is the lowest experimental velocity at which a penetration or perforation was observed[7].

- V_{50}: A mathematical calculation of the velocity at which the estimated probability of the outcome (penetration or perforation[7]) is 50%. There are several different ways of calculating this value that will each yield different results. Some methods are also able to calculate other probability values (e.g. the velocity at which the estimated probability of the outcome is 1%). Similarly the V_{50} can be converted into the energy (E_{50}) or energy density (E_{50}/A) at which the estimated probability of the outcome is 50%.

    - Average method: the arithmetic mean of an even number of shots, half of which perforate the material and the other half do not.

    - Calculation based on shots from the Zone of Mixed Results: for instances where there is a (wide) ZMR, the V_{50} can be calculated by only considering the shots within the ZMR [51].

    - Probit method: A mix of perforations and non-perforations are used to fit a probit curve to the data. A probit model can then be used to calculate the corresponding velocity for a given probability value. For the data analysed within this thesis, the statistical package R [52] (with a bias reduced generalized linear model, brglm [53]) was used to calculate V_{50} velocities with 95% confidence intervals.

    - Extrapolation or interpolation of V_{50}[8] from Depth of Penetration (DoP) or residual velocity data[9]: The penetration depths (or residual velocity for isolated skin) of all 'fair'[10] shots are plotted against the impact velocity. This method can be applied even where there are no non-perforating shots. The V_{50} perforation value is the extrapolated or

[7] Unless stated in the text, this should be taken to refer to perforation.
[8] The calculated velocity is not the V_{th} or V_0 as sometimes referred to: any experimental data with a ZMR will, by definition, have perforations at velocities lower than the calculated V_{50}.
[9] Can only be used for V_{50} perforation calculations
[10] Those that hit bone etc. must be removed. Non-perforations are given a DoP of zero and are included in the analysis.

interpolated value corresponding to a zero penetration depth. This can be calculated by fitting a regression model to the data and therefore requires a range of velocities. It is a standard model developed for finding the "*velocity limit*" when projectiles perforate armour and the residual velocity is known [54]. Replacing the residual velocity parameter with the DoP (which is a function of the residual velocity after perforating the skin) allows this standardised method to be applied to calculate the V_{50}. There are several different sub-methods of curve fitting the data to calculate the V_{50}.

A discussion of the benefits and drawbacks of the different skin perforation calculations are given in APPENDIX A, along with further detail on each.

3.2.4 Structure of the review of experimental studies on skin perforation

There have been many separate investigations of the projectile properties required to penetrate and/or perforate skin, with multiple attempts to produce predictive equations based on disparate data sets.

The majority of studies use skin intact on PMHS or animal cadavers and fire the projectiles at skin on the thigh or abdomen. This has been done with a variety of different projectiles including handgun bullets, air rifle pellets, spheres, cylinders, cones, cubes, flechettes and Less Lethal Weapon (LLW) impact rounds.

Other body regions are less frequently used, or data from multiple regions combined to provide sufficient data to analyse for a V_{50}.

Some studies remove the skin from the target and test it by itself or backed by a different material (for example on gelatin). Removal of skin is likely done for practical purposes or to give a more repeatable backing; however, the backing (or lack of) can affect the measured skin response. Additionally, skin has an intrinsic level of tension when on the body. Once removed, the skin relaxes. How the skin is removed and then tensioned for testing is critical to ensure it replicates the in-situ performance (and is not damaged in the process).

The review of the literature for skin perforation data was split into different target types; PMHS or animal, and further sub divided by the backing method (intact, isolated and backed or completely isolated).

Previous studies, especially those reviewing other experimental data sets, have frequently confused the definition of penetration, perforation, threshold and the different methods of calculating the 50% probability of penetration or perforation. This has resulted in different, non-comparable data being combined, potentially giving flawed outputs.

The V_{50} values attained from the literature review are not given individually in the text, as many have been recalculated in line with the definitions and methods in Section 3.2.3 where raw data was obtained. Instead, the data collated from each study is summarised in Section 3.5.

This review focuses on the experimental setups and results rather than the original interpretation of each individual dataset, as this is done more effectively with a larger dataset once all the data is collated. Key insights are given in respect to individual studies where appropriate.

All the data was obtained from the original sources where possible. However, in a few cases (where indicated) secondary sources had to be used. This was generally due to the classification of the original source, but where the data had been openly reported by others.

3.3 Review of experimental studies using PMHS

3.3.1 Intact PMHS skin

The first reported experimental study was performed by Journée [45] in 1907[11]. The work contains descriptions of a number of different tests performed using lead spheres and various bullets with intact PMHS. Only a limited amount of the testing was directed at determining the skin penetration or perforation thresholds.

[11] The review of this work was based on a professionally translated copy of the original article from French [55]. A copy of the original French text [45] was used to verify the numerical data and equations.

Two experiments on PMHS targets yielded skin perforation threshold velocities, but both based on very limited data.

DiMaio et al. tested PMHS legs, either fresh or refrigerated for a few days, with three different projectiles, two air rifle pellets and a 0.38" bullet [56]. It was stated that "*refrigeration, at least for a short time, does not significantly change any ballistic characteristics of skin*" [56][12].

The raw data, including DoP into the muscle for two of the projectiles were presented and the results given as penetration and perforation V_{th}, in line with the definitions used in Section 3.2.3.2. Due to the fact that all the raw data was presented, including the DoP for perforations, re-calculation of the V_{50} for penetration and perforation by the average, ZMR[13] and probit method was possible, in addition to the perforation V_{50} from extrapolation of DoP data for two of the projectiles.

It was assumed in the recalculation of the data, that any shots resulting in a non-penetration, by definition, resulted in a non-perforation, although in the original work it is given as "*determination cannot be made*" [56]. There were a large number of shots completed for each projectile (average of 31), ensuring the subsequent V_{50} calculations are reliable.

By far the most comprehensive experimental study (and one of the most useful in terms of the range of data obtained and conclusions that could be drawn) was that performed by Missliwetz [59][14], published in 1987. Over 2,500 shots were performed using eight different projectiles. Three of the projectiles were 4.5 mm (0.177") air rifle pellets of different shapes and the remainder spheres (4 mm or 4.5 mm diameter) made of lead, steel, brass, glass or plastic. This gave a set of projectiles with a wide range of densities.

[12] This statement is supported by testing on dead pig skin in References [57; 58], discussed in Section 3.4.2.
[13] Perforation $V_{50\,ZMR}$ couldn't be calculated for the 0.38" projectile.
[14] Article published in German and translated via machine.

Impacts were conducted on the thigh and back region of adult PMHS, on the thigh of child PMHS (up to 3 years old) and on adult PMHS thigh skin isolated and backed by cork. This yielded 28 separate evaluations and in the reference statistical comparisons were made between some of the different variables. The outcomes of the main comparisons are summarised below:

- "*A statistically significant difference in perforation velocity between males and females could not be found;*
- *The influence of age between the child and adult group on the perforation velocity was statistically significant, for each of the projectiles tested (where the child group required a lower velocity to perforate);*
- *No correlation between age in years and the perforation velocity was observed within the adult group (aged between 18 and 90 years);*
- *The inter-individual threshold velocities differed considerably, with the highest individual values usually more than twice as large as the lowest;*
- *A statistically significant difference in perforation velocity between the intact skin in adults on the thigh and back was found, for each of the projectiles tested (where the back skin required a higher velocity to perforate);*
- *No statistically significant differences in the perforation velocity between the intact thigh skin and isolated-backed thigh skin could be detected (although the individual values showed a clear trend to deviate from each other);*
- *A statistically significant linear correlation was found between the perforation velocity and sectional density, but not energy density when considering all the projectiles"* [59].

Definitions for the different skin 'failure' modes were provided in order to interpret the results. However, the definitions given are different to those in used in this thesis (Section 3.2.3.1). The penetration and perforation thresholds and V_{50}'s are likely to be shifted to slightly higher velocities than if they were calculated in line

with the definitions in Section 3.2.2. The extent of this shift cannot be determined without re-evaluating every shot for the damaged caused to the skin, which is not possible without the original data.

The description of the V_{50} calculation in Reference [59] referred to Mascianica [51], although it appears that the average and not the ZMR method was used. It was stated that at best 10 shots were conducted, half of which perforated and the other half did not. The standard deviations on the V_{50} values calculated were also presented. For skin perforation testing, 10 shots for a V_{50} calculation is a small, but reasonable number to give some confidence in the outcome along with the reported standard deviation values.

Certain details, such as the distinction between V_{th} and V_{50}, as well as the data for the intact back skin and isolated thigh skin appear to have been completely ignored by other subsequent literature reviews, possibly due to the fact that it was published in German.

Rathman reported a study to compare the energy density required to penetrate and perforate the skin of refrigerated PMHS in the thigh, calf and buttock regions (data grouped from all regions) for projectiles of different shapes [60]. This study used five different projectiles; a pointed and flat air rifle pellet each in 0.177” and 0.22” calibres and a 0.177” sphere.

The results showed that projectile shape was a factor in the resulting skin perforation response: the sphere required the lowest energy density to penetrate and perforate the skin, followed by the pointed pellets, then the flat pellets.

Extraction of the key velocities from the graphed data in reference [60] was performed to determine the threshold velocities (lowest value of the ZMR) as well as the V_{50} which was estimated as the midpoint of the ZMR.

Bir et al. [61] conducted a study on PMHS using a 12 gauge fin-stabilize rubber rocket kinetic energy munition, a LLW round. The study utilised eight subjects, four male and four female over 10 different body regions.

The authors refer to penetration of the skin, but no definition is given and it is assumed that they meant perforation as defined in Section 3.2.2. They evaluated the data in terms of energy density with the 50% risk of skin perforation determined from a logistic regression fit to at least 10 shots for each region. It is one of the few studies to have used a logit or probit model in order to estimate a 50% probability of penetration or perforation. This study used the largest diameter projectile from the literature included in dataset (17.7 mm).

The study demonstrated that the 50% risk of skin penetration/perforation varied considerably between different body regions, with double the energy density required for the posterior rib compared to the anterior rib locations. This large difference between seemingly similar locations was attributed to the amount of muscle, the rib contours and skin thicknesses between the two sites[15].

The publication by Bir et al. [61] was based on the ballistic data produced in a PhD thesis by Stewart [62]. This thesis presented the raw data in terms of the velocity and penetration/perforation response for the majority of the impacts used in Reference [61] (139 of the 166). Form this, recalculation of the V_{th} and V_{50}'s calculated by the average, ZMR and probit methods could be made here for both penetration and perforation. Due to the fact that these determinations were not based on the entire data set used by Bir et al. [61], some differences in the resulting values were seen (and could be expected).

Previously unpublished testing from Wayne State University tested refrigerated[16] PMHS skin on the neck [63]. 0.49 g cylinder and 1.1 g chisel nosed cylinder Fragment Simulating Projectiles (FSPs) were used with the average age of the PMHS of 58. The yaw and pitch of the projectile pre-impact were measured via high speed camera and were found not to be a significant predictors of penetration for either projectile (even though they varied considerably). The raw

[15] The skin overlying the posterior ribs was stated as being significantly thicker, although the quoted values of skin thickness (0.0161 cm and 0.0255 cm [61]) seem an order of magnitude out compared to Reference [50] (average of 0.216 cm).
[16] Never frozen or embalmed, tested within a maximum of 14 days after death with storage at 4±2°C.

perforation and DoP data was made available from this testing (24 shots with each projectile) on which the skin V_{50}'s could be calculated.

Mattoo et al. published a study using a 4.5 g lead sphere into samples of cadaver thigh muscle and skin, removed from the limb[17] [64]. It appears that Mattoo made an error in the description of the lead shot used in the experiment. This error was highlighted by Jussila [65], correcting the diameter of the "*buck shot 000* ≡ *British LG*" from 8.5 mm as stated by Mattoo to 9.14 mm. The description of the type of shot matches the given mass and the corrected diameter is in line with the 0.38" revolver case used to propel the shot. A number of references [59; 61; 66-70] have subsequently quoted the incorrect diameter and their calculations based on sectional density or energy density will be incorrect.

In Reference [64] the penetration depth for each shot into the thigh muscle and corresponding velocity were plotted and the perforation V_{50} from extrapolation of DoP data given. In addition, the raw data was tabulated, from which the penetration and perforation V_{th} and V_{50}'s could be re-calculated here. The value given in the text by Mattoo of ≈ 200 ft s^{-1} (61.0 m s^{-1}) is the perforation V_{50} from extrapolation of DoP data from a linear fit. However, due to the apparent error in the diameter of the projectile used, the quoted energy density value is incorrect.

3.3.2 Intact and isolated - backed PMHS skin

Tausch et al. [71] completed a large series of tests against isolated PMHS skin backed by a material called Mipoplast® (a thin, ~0.5 mm plastic film) in addition to a smaller number of tests on intact PMHS thigh skin. This was done with 8 different projectiles; 3 spheres and a mixture of different shaped bullets (9 mm and 0.45" calibre) for the isolated-backed skin. The samples mainly consisted of deeply frozen, then thawed skin, with some fresh samples. It was stated that "*preliminary tests did not reveal a conclusively different behaviour*" [71], but no data was shown[12].

[17] As the muscle and skin were kept together and not separated, despite not being part of an intact limb, the results are treated as an 'intact' condition for later analysis.

The number of shots conducted in different velocity bands were reported for each series of shots. Additionally, the velocity and penetration depth is reported for each series. However, this shows there were significantly more shots conducted than are reported with corresponding velocity and DoP data in Reference [71]. It also appears that when the details for specific shots were not reported, these were not included in the subsequent skin penetration/perforation determinations. No reason for this was given in the paper. The penetration depth for each shot into the skin and Mipoplast® was plotted with the corresponding velocity. In the reference, the perforation V_{50} from extrapolation of DoP data was calculated based on the average value from a linear, second order polynomial and logarithmic fit. The "*critical velocity, V_{cr}*", as it was referred to, differed by up to 80% between these different best fits, highlighting the requirement for a reliable and standard method to use to fit the penetration data[18]. The validity of the empirical fits used to determine the 'critical velocities' in Reference [71] were also questioned by Reference [72].

As mentioned, some of the raw velocity and DoP data was reported. This, along with the figures depicting the ricochet and penetration region for each projectile (their Figures 4a and 4b) allowed subsequent determinations of the perforation V_{th}, estimation of the perforation V_{50}[19] and in one case the perforation V_{50} from the ZMR and probit methods. The perforation V_{50} from extrapolation of DoP data were also recalculated.

It was noted that the perforation velocities for the conical bullets fell in line with the expected values based on the data from the spherical projectiles, based on the relationship between the sectional density and perforation velocity as well as the mass and perforation velocity [71].

[18] This is done within Section 9.4.
[19] Based on the mid-point of the ZMR

3.3.3 Isolated PMHS skin

The testing performed by Grundfest et al. [73][20] and reported by References [66; 74; 75] appears to have performed a limited number of impacts with 4 different projectiles on isolated human skin. Without access to the original article, the data from the review by DiMaio [66] was used. The data appears to be very limited and testing on isolated skin is not ideal compared to an intact target.

Sperrazza and Kokinakis conducted firings with steel cubes, spheres and cylinders at isolated goat and human skin, reported in 1968 [76]. Although the raw data is not given to verify their conclusions, they stated that there were no significant differences between the goat and human skin and so the results were combined. The data presented was in terms of the perforation V_{50} by extrapolation from the residual velocity method [54].

The actual V_{50} values were taken from their graphed results (their Figure 3) and not those from their Table 2 which describes points along their empirical fit equation. It was stated that "*as many as 30 data points were used for each average value*" [76]. It was also stated that "*based upon some limited experiments, skin in situ…. possesses a lower ballistic limit, on the average, than isolated skin*" [76].

3.4 Review of experimental studies using animals

3.4.1 Choice of animal

The choice of animal for skin penetration and perforation assessments has varied considerably across the literature. Different animals have different benefits and drawbacks [77]. A review by Schantz [78] discussed these for general applications in wound ballistics. The choice of animal is a trade-off between factors such as the likeness of the skin to human skin (including hair) and size of muscle tissue available for the assessments.

[20] The original work by Grundfest [73] is not openly available, and when quoted (if not originating from, or under direct contract from US DoD) is likely to be from a secondary source.

Horses [55] and cattle [18; 44] have previously been used, but any data has been discounted for use in this work as the skin is too thick [78]. Sheep and goats in particular have been frequently used as the skin in the thigh region is generally accepted to offer similar ballistic resistance to that of PMHS [76; 79].

Pigs (swine) are one of the most common animals used for ballistic research and are generally accepted as the 'best' animal for general wound ballistic studies due to the large muscle mass on the thighs that can be impacted [78]. However, for skin penetration and perforation studies pigs are not ideal as the skin is thicker and tougher than human skin [69].

There is not considered to be a suitable validation in the available literature for the use of a given animal species (be that pig, goat, etc.) to be used in place of PMHS targets. Reference [76] did not report or show any of the data for the separate PMHS and goat targets, so their conclusions cannot be verified. The comparison in Reference [65] used data from the literature (rather than experimental testing under matched conditions) and did not control the variables sufficiently in order to reach valid outcomes[21].

3.4.2 Intact animal skin

The Kokinakis et al. work [43][22] gave the results of testing with the same steel projectiles to those in Reference [76], in addition to a selection of steel flechettes, all against intact goat tissue.

Due to the focus on developing an incapacitation criterion, for which the skin perforation aspect was a very small part, there is limited information on how the skin perforation data was collected. It is likely (although not confirmed) that the velocities calculated were the perforation V_{50} by extrapolation from the residual velocity method [54], but with the skin and muscle tissue together. This is due to

[21] The comparison in Reference [65] used a mixture of intact and isolated skin data, mixed skin penetration and perforation calculations and a mix of projectile geometries to show no difference between animal and PMHS skin, where the type of animal (pig or goat) was not considered.

[22] Due to the original classification, it was not made publicaly available until ~ 1995. Reviews of the literature prior to this are unlikely to have included this data.

the fact that firings appear to have been conducted only at set velocities all of which would perforate skin.

Lewis et al. [80] conducted a study on goat skin backed by 20% gelatin. The original source could not be obtained and so experimental details were taken from Reference [81] and results from Reference [68]. This data included a steel sphere, steel and tungsten cubes and wooden cylinders. It was stated in Reference [81] that the projectiles chosen were to help understand "*environmental debris such as rocket motor fragments and other secondary projectiles that pose a hazard to personnel*". It is also not known the number of shots or calculation method used to determine each V_{50} value.

A study by Haag in 1995 [82] (re-reported in Reference [83]) conducted 2 or 3 shots each at the abdomen and thorax of a pig cadaver with four different types of 0.38" bullet. Although the data is not extensive enough to enable calculation of V_{50}'s in the normal manner, other sources have combined all the data for the different bullets and impact locations together [68; 84]. Although this enables sufficient data to facilitate a calculation, the potential effect of bullet shape and impact location is ignored. There was some distinction between bullet shapes, even with the limited data: the flat faced bullet needed a higher velocity in order to perforate the skin compared to a round nose bullet [82; 83].

McKenzie et al. performed a series of impacts with three 0.177" air rifle pellets at a freshly killed pig [85]. Impacts were conducted against the abdomen and thorax regions with a view to determining the type of underlying injuries resulting from perforation of the body wall into the internal organs. In addition to this main aim, skin (and body wall) perforation velocities were given for two of the different shaped pellets, a pointed and blunt nosed design, separately for the thorax and abdomen.

The raw data is not given, and it is unknown how many shots were conducted with each pellet, although it was stated that approximately 50% of the pellets perforated the body wall. The skin perforation velocities were quoted with a small uncertainty, but it is not known where this uncertainty originated. The perforation V_{th}'s given were identical for the abdomen and thorax region, but is unknown if

these were determined separately or the data combined. The results did show that the pointed pellet perforated the skin (and body wall) at a lower velocity than the blunt tip pellet [85].

Dahlstrom et al. conducted a study to investigate the injury potential of a LLW 12 gauge bean bag round [86]. Part of their study involved impacting isolated pig skin backed by 10% gelatin with the LLW round. Before this was conducted, they calibrated the pig skin backed by gelatin using two 0.177" air rifle projectiles so that the V_{50} could be correlated to previously reported PMHS skin data for similar projectiles in Reference [84]. This calibration of the pig skin is the only known instance in an experimental study where the animal skin performance has been compared to PMHS data prior to testing with the 'objective' projectile.

The raw data (velocity and resulting skin damage) for the 0.177" sphere (22 shots) and round nosed pellet (11 shots) were reported, as well as the values for the V_{50}. This allowed subsequent determination of the penetration and perforation V_{th} and V_{50}'s calculated by the average, ZMR and probit methods.

Haag conducted a study where fresh isolated pig skin from the abdominal area was backed by 10% gelatin at 4°C and impacted with a 0.177" Ball Bearing (BB) [87]. Impacts were conducted on the isolated-backed skin and the testing was repeated with the skin and gelatin having been refrigerated for 6 days at 4°C.

As the raw data was given, subsequent determination of the penetration and perforation V_{th} and V_{50}'s calculated by the average, ZMR, probit and from extrapolation of DoP data methods was possible here. Comparison of the probit V_{50} data shows no significant difference between the fresh and refrigerated samples, but this may be due to the skew of the data to higher velocities for recording DoP in addition to skin perforation. As reported in the article, there was comparable penetration depths for velocities about 30% over the V_{50} into the bare gelatin and when the skin was present on the front of the gelatin (their Figure 1A and 1B) [87].

A study by Breeze et al. [88] (also included in [58]) reported the penetration of steel FSPs (0.16 g, 1.10 g and 2.84 g cylinders) into four different regions of pig

cadavers (abdomen, thorax, thigh and neck). This was primarily to investigate the utility of 20% gelatin at 10°C as a tissue simulant by comparison of the DoP. The pig penetration data was plotted and the skin "*perforation V_{th}*" was calculated by extrapolation of linear best fit lines. The value given for the skin perforation is not the threshold, V_{th} as stated in the paper, but the perforation V_{50} from extrapolation of DoP by linear fit.

The conclusions of the study, comparing the DoP in pig tissue to 20% gelatin are unreliable due to the fact that all the comparisons were based on statistical differences in the linear fits, which was a flawed model choice. The inappropriate choice of model appears to be at least partially acknowledged by the fact that a polynomial fit was applied when all fragments were considered together and stated that it gave a good correlation [88].

The raw data from this study was re-analysed here to determine the perforation V_{50} from extrapolation of DoP data for each of the body region and fragment combination where sufficient data was present. The value given for the 1.1 g FSP into the leg was discounted here for V_{50} analysis as it was based on only 3 data points which was considered insufficient for a reliable extrapolation. Calculation of the perforation V_{50} from extrapolation of DoP data was achieved for a total of 8 of the 11 fragments and body region combinations.

Breeze et al. published a study examining the perforation of goat skin [79] (also included in [58]). This used three different projectiles; 0.16 g and 0.49 g steel cylinders and a 1.1 g chisel nosed cylinder. The raw data for each fragment (velocity, penetration/perforation and DoP for every shot) were re-analysed here to determine the V_{th} and V_{50}'s calculated by the average, ZMR, probit and extrapolated DoP methods for both penetration (where possible) and perforation.

References [57; 58] considered the potential effect of refrigeration and freezing on the resulting skin and muscle tissue response. Although skin perforation V_{50}s were not determined in References [57; 58] (due to focus on retardation in muscle tissue) the raw data was presented and has been re-analysed here. Whilst this pilot study had limited data on which to base to conclusions, no difference was observed between the different storage conditions on the retardation response of

the tissue. Whilst the potential effect of tissue storage on its subsequent response is a key aspect for consideration, both in terms of skin perforation and penetration into muscle tissue, References [57; 58] has insufficient data, coupled with the inherent variability of real tissue to make firm conclusions on the effect of storage conditions.

Reference [89] investigated the impact of 6 mm steel spheres into pig faces (and eyes) in order to evaluate the risk and appropriate impact protection for the face for occupational environments. A number of impacts were conducted to establish the penetration thresholds for the pig skin and eye[23].

3.5 Summary of collated skin perforation data

An overview of all studies identified in the previous sections that contain useful skin penetration or perforation data are given below in Table 1, with a brief overview of the data. If the primary reference could not be obtained, the secondary source of the data is stated.

Study	**Target description**	**Projectile description**	**Number of assessments[24]**	**Raw data (shots)**
Bir et al. [61] (also in Stewart [62])	Intact PMHS: various locations	LLW impactor	10	Y (142)
Bowyer et al. [90]	Pig skin isolated and backed by gelatin	0.20 g cylinder FSP	1	Y (35)
Breeze et al. [88]	Intact pig; thorax, abdomen, neck and thigh	0.16 g, 1.1 g and 2.84 g FSPs	8	Y (68)

[23] The skin perforation V_{50}s have not been calculated within this thesis for the raw data from Reference [89] as this reference was found after completion of the skin perforation model development (Sections 6.1 and 8).
[24] Number of separate V_{th} or V_{50} determinations (i.e. different projectile or body region), made either in the original work or based on subsequent re-analysis of the data here.

Study	Target description	Projectile description	Number of assessments	Raw data (shots)
Breeze et al. [79]	Intact goat: thigh	0.16 g, 0.49 g and 1.1 g FSPs	3	Y (46)
Breeze et al. [91] and Breeze [58]	Intact pig; Thigh refrigerated and frozen	5 mm sphere 0.49 g and 1.1 g FSPs	5	Y (77)
Dahlstrom et al. [86]	Pig skin isolated and backed by gelatin	0.177” bb and air rifle pellet	2	Y (36)
Dain [89]	Pig head	6 mm steel sphere	1	Y[23]
DiMaio et al. [56]	Intact PMHS: legs	0.38” Bullet and air rifle pellets	3	Y (94)
Grundfest et al. [73] values taken from [66; 74; 75]	Isolated abdominal skin	Steel sphere and bullet	4	Y (4)
Haag et al. [83] (republished data from Haag [82])	Intact pig: abdomen and thorax	0.38” bullets	5	Y (17)
Haag [87]	Pig skin isolated and backed by gelatin	0.177” BB	2	Y (27)
Journée [45; 55]	Intact PMHS	lead sphere	2	Y (6)
Kokinakis et al. [43]	Intact goat	Sphere, cubes and flechettes	7	N
Lewis et al. [80] values taken from Hudgins [68]	Intact goat	Spheres, cylinders and cubes	8	N

Study	Target description	Projectile description	Number of assessments	Raw data (shots)
MacPherson [84]	Pig skin isolated and backed by gelatin	Various	5	N
Mattoo et al. [64]	Intact PMHS	Lead sphere	1	Y (30)
McKenzie [85]	Intact Pig – thorax and abdomen	0.177” air rifle pellets	4	N
Missliwetz [59]	Intact and isolated, adult and child PMHS	Various spheres and air rifle pellets	28	N
Rathman [60]	Intact PMHS	0.177” and 0.22” air rifle pellets	5	N
Salziger et al. [92] reported in [83]	Pig	9 mm bullet	1	N
Sperrazza et al. [76]	Isolated PMHS and goat	Cubes and spheres	5	N
Tausch [71]	Intact and isolated-backed PMHS	Spheres and bullets	11	Y (114)
Andrecovich [63]	Intact PMHS	0.49 g and 1.1 g FSPs	2	Y (48)
Total			123	998

Table 1: Source and overview of skin penetration and perforation data identified.

Additional data comprising of only skin perforations at higher velocities has also been collated [93-96], despite not being able to generate V_{50} directly (n=244).

Additional data for other projectiles has been identified, but not included. Data for 12 gauge bean bag rounds on fresh pigs [97] was excluded due to the deformable nature of the projectiles. Data for glass shards penetrating animal skin have also been excluded [98; 99], due to a different penetration mechanism from the sharp, knife like geometry of the projectiles.

3.6 Assessment of previous literature reviews

Previous reviews of the skin penetration/perforation literature were also considered [58-61; 64-71; 75; 83; 84; 100-103]. Most of the experimental studies also included a (limited) review of the data in order to introduce their own data and findings.

Each of the previous literature reviews had various flaws (some of which are considered extremely significant), such as: omitted large sections of the previously available data (some deliberately due to their specific focus), were published before much of the current data was available, discrepancies in interpreting V_{th} and V_{50} data from previous work and/or mix up of penetration and perforation data.

These previous reviews are not discussed, other than to identify existing empirical equations for skin perforation (Section 3.7) and to support the summary of key findings from the literature review (Section 3.8).

3.7 Existing empirical equations for skin perforation

A number of studies have used portions of the existing published skin perforation data to create empirical equations to predict the skin penetration or perforation response based on the projectile properties. The majority of equations have related the velocity required to penetrate or perforate the skin to the sectional density of the projectile.

There are a number of equations available from the literature; some of these equations were directly reported and others were abstracted from other relationships given. Some authors produced multiple equations to describe alternative relationships or prediction types.

A valid projectile for these equations is a projectile that does not plastically (or significantly elastically) deform or fragment, with a constant mass and definable cross sectional area.

These equations with some details on their applicability are given below in Table 2, ordered chronologically. For ease of comparison and where possible,

equations have been converted into a similar form and modified to bring them in line with mass in grams, velocity in m s^{-1} and Sectional density in g cm^{-2}. The prediction type is given in line with the definitions from Section 3.2.3.1.

Source	Prediction type	Target(s)	Projectiles	Equation
Journée (PMHS) [45; 55]	Perforation V_{th}	Intact PMHS	Lead spheres and bullets	$v_{th} = 204S^{-0.5}$
Based on Feinstein [104; 105]	Probability of penetration	Intact PMHS	Spherical bullets[25]	$P = \phi(1.272ln(mv^4) - 23.63)$
Based on Feinstein [104; 105]	Penetration V_{50}	Intact PMHS	Spherical bullets [25]	$v_{50} = 98.7m^{-0.25}$
Based on Feinstein [104; 105]	Probability of perforation	Intact PMHS	Spherical bullets [25]	$P = \phi(1.3066ln(mv^4) - 25.02)$
Based on Feinstein [104; 105]	Perforation V_{50}	Intact PMHS	Spherical bullets [25]	$v_{50} = 120m^{-0.25}$
Sellier [69; 75; 100]	Penetration V_{th}	PMHS and animal, intact, isolated and isolated-backed	Spheres, bullets and cubes	$v_{th} = 141.2S^{-0.5}$
Sperraza and Kokinakis [76]	Perforation V_{50}	Isolated PMHS and goat skin	Steel cubes and spheres	$v_{50} = 124.71S^{-1} + 22.03$
Tausch et al. [71]	V_{50} from DoP data[26]	PMHS, intact and isolated-backed	Bullets and spheres	$v_{th} = 162.1e^{-0.38\sqrt{m}}$
Tausch et al. [71]	V_{50} from DoP data [26]	PMHS, intact and isolated-backed	Bullets and spheres	$v_{th} = 277.7e^{-0.482\sqrt{S}}$
Lewis [80; 81]	Probability of perforation	Goat, isolated and backed by gelatin	Metal sphere, cubes and wooden cylinders	$P = \frac{1}{1 + e^{(28.42 - 2.94ln[Sv^2])}}$

[25] Taken to mean spheres and hemispherical / rounded nose bullets. ϕ is the cumulative normal distribution function

[26] Stated as penetration V_{th} in the reference

Source	Prediction type	Target(s)	Projectiles	Equation
Based on Lewis [80; 81] [27]	Perforation V_{50}	Goat, isolated and backed by gelatin	Metal sphere, cubes and wooden cylinders	$v_{50} = 125.6S^{-0.5}$
Mattoo [67]	Perforation V_{th} [28]	Intact PMHS	Spheres, bullets and pellets	$v_{th} = 182.75S^{-0.5}$
MacPherson [84]	Penetration V_{th}	PMHS and isolated-backed pig	Spheres, bullets and pellets	$v_{th} = 128.7S^{-0.3}$
Hudgins (bare skin) [68]	Perforation V_{50}	PMHS and animal, intact, isolated and isolated-backed	Various metallic projectiles	$v_{50} = 153.9S^{-0.38708}$
Breeze [58][29]	Perforation V_{th}	PMHS and animal, intact and isolated	Metallic projectiles	$v_{th} = -29.143ln(S) + 129.44$
Ouellet [106]	Perforation V_{50}	Intact PMHS and animal	Various projectiles	$v_{50} = -49.25\ln(S) + 172.08$

Table 2: Empirical skin penetration and peroration equations from the literature

The majority of references that have developed an empirical equation shown in Table 2 for the V_{th} or V_{50} have based it on the form given in Equation 1 (where V_{50} may be substituted for V_{th}):

$$v_{50} = aS^b$$

Equation 1: Simple empirical skin perforation equation

Where:

[27] Simplified version of the original for V_{50} prediction
[28] Penetration or perforation not explicitly stated. Assumed perforation.
[29] Seven additional equations are given in Reference [65] for some different target factors, although not all are reported correctly. Reference [58] is taken to supersede Reference [65] and therefore these additional equations are not included in Table 2.

S is the sectional density of the projectile = mass, *m*, over the cross sectional area, *A*, of the projectile (g cm^{-2}) [30].The cross sectional area is taken as:

- The maximum value for hemispherical nosed projectiles (i.e. spheres and some pistol bullets).
- For projectiles that have increasing A along the projectile length, the value for the maximum cross sectional area in the first 5 mm length.
- For cubes, A is taken as the area of one face (even if randomly orientated)[31]

a and *b* are constants determined by each individual author, based on the datasets they used to generate the equation.

When b=−0.5, the equation gives a constant energy density (E_{50}/A or E_{th}/A), as given by Equation 2:

$$v_{50} = a\left(\frac{2000E_{50}}{SA}\right)^{0.5}$$

Equation 2: Simple empirical skin perforation equation for constant energy density

Where;

a is a constant as for Equation 1.

E_{50}/A (or E_{th}/A) is the energy density in J cm^{-2}.

Due to the issues discussed in Section 3.8 many of these equations, even if based on large data sets, have faults due to combinations of mixed data (whether that is mixed target types, backing methods, V_{50} calculation methods, etc.).

[30] It is recognised that Sectional density in g cm^{-2} is not a standard SI unit, but the values are required in this format due to how the model has been constructed and to remain consistent with previous work in this field.
[31] This gave the best match to the PMHS and animal skin perforation data, see Section 6.1.

Of all the equations summarised in Table 2, the one from Hudgins [68] has the most utility and best base data from which it was calculated. The main drawback of the Hudgins equation [68] (as well as others given in Table 2) is that many of the target factors that have been identified as (potentially) significant in Section 3.8 cannot be separated out and therefore the predictions will not be accurate.

A new empirical equation is therefore required and is addressed in Section 6.1.

3.8 Summary of key findings from literature review of skin perforation data

Skin can be highly variable in its response to penetration or perforation, even with all conditions controlled as far as possible. References [61; 62] showed high variability within a specific location: the average range of the zone of mixed results (velocity of slowest perforation to the fastest non-perforation) across the 10 body regions used was 45.8 m s^{-1} (which equates to around 30% of the skin V_{50} velocity). The data from References [61; 62] also showed a 56 m s^{-1} difference in perforation V_{50} between two sets of experiments on different locations on the back. Other references comment on this variability: *"The inter-individual threshold velocities differed considerably, with the highest individual values usually more than twice as large as the lowest"* [59].

Based on the literature review the following factors are deemed to be potentially significant for determinations of skin perforation:

- Distinction between penetration and perforation
- V_{50} prediction method (i.e. V_{th}, V_{50} by average method, V_{50} by probit method, etc.).
- Projectile properties;
    - Mass
    - Velocity
    - Cross sectional area or presented area
    - Shape/ geometry[32]

[32] Although not all may give (significant) differences

    - Sectional density[33] correlated with perforation V_{50}
- Target properties;
    - Species (i.e. human, goat, pig, etc.)[32]
    - Age distinction in terms of child / adult[34]
    - Target area[32]
    - Backing method (intact, isolated backed or isolated)[32]

The following factors are deemed to be less significant for skin perforation:

- Projectile properties;
    - Energy density[33] correlated with perforation V_{50}
- Target properties;
    - Sex[34]
    - Age for adults[34]
    - Storage condition (live, fresh, refrigerated, frozen-thawed) [35]

The following limitations have been drawn from the literature review of skin perforation data and associated literature.

- There is limited data for low density and non-metallic fragments. Only 17/123 (14%) of dataset of which the majority of these are a large LLW impactor [61; 62]. For 'typical' fragments only 7/113 (6%) are non-metallic from References [59; 80].
- There is very little quantitative comparison of the effect of target storage conditions on the resulting V_{50}. The single reference that published their data relating to storage conditions [57] conducted limited shots, leading to no apparent differences.
- A considerable number of references confused the definitions of penetration and perforation, either miss reporting data or combining data of mixed types.

[33] As a method of combining some of the significant projectile properties
[34] At least for PMHS
[35] Within the bounds of the experimental setups reviewed.

- Very few references considered the effect of comparing different V_{th} or V_{50} calculation methods.
- There is a requirement for a standard or consistent method to use to fit DoP-velocity data in order to calculate a V_{50}.
- There is no (explicit) consideration of the effect of post-mortem changes on resulting skin response.

The best predictors of skin perforation in terms of projectile properties, as determined from the literature review were the impact velocity and projectile sectional density. These metrics will be used in the remainder of this thesis to understand skin perforation.

Whilst multiple attempts to produce predictive equations to address the velocity required to penetrate or perforate the skin have been made (Section 3.7), none have accounted for the different factors deemed to be (potentially) significant above.

3.9 Muscle tissue and simulants

3.9.1 Animal tissues

There is debate about the best tissue simulant for human muscle to use in a physical model for assessing or comparing the injury potential of different projectiles (fragments and bullets). Animal muscle such as horse, pig, goat, sheep, dog and cat (live, cadaveric, whole and isolated tissues) have all been previously used to look at the mechanisms of ballistic injury.

Animals are also not always ethical or practical to use, especially for assessments of a large number of projectiles, and experiments are affected by the inherent variability in biological tissues and between different individuals. This is where tissue simulants are required.

Different simulants can be used to simulate different tissues [107-109]. Initially in this thesis, the focus is on muscle tissue (and Section 8 investigates skin simulants).

In order to understand the requirements for a muscle tissue simulant, first the mechanisms by which real muscle tissue is damaged by ballistic projectiles needs to be considered.

3.9.2 Damage mechanisms in (muscle) tissue

When a projectile (bullet or fragment) penetrates into tissue, there are several mechanisms by which the tissue is damaged. These mechanisms are described in terms of their effects in muscle tissue, as this is the most common type of tissue used for wound ballistics studies and the focus of this thesis.

One difficulty in describing tissue damage is how (and when) to categorise the 'damage'. Viable tissue can be assessed (e.g. by "*colour, consistency, contractibility and bleeding"* [90; 110]), but judgement can be very subjective from a surgical perspective [111; 112]. Tissue will also undergo progressive necrosis, and then (partial) healing following an injury [90; 113; 114]. Therefore the extent of 'damaged' tissue will differ between time=0 to hours or days after wounding.

The main 'damage' mechanisms have been previously described, such as in References [69; 115-117]. The mechanisms can be summarised as:

1. Crushing. The area in direct contact with the projectile is crushed as the projectile penetrates through the tissue. This is approximately a projectile diameter.

2. Stretching past the elastic limit of the tissue. This is caused by the expansion of a temporary cavity within the (muscle) tissue. A typical temporary cavity in a muscle tissue simulant[36] is shown in Figure 4.

[36] The temporary cavity is opaque in muscle tissue and can be observed by flash or high speed x-ray, compared to high speed video in a transparent tissue simulant. Its formation in opaque tissues are easily inferred without x-ray due to surface bulging.

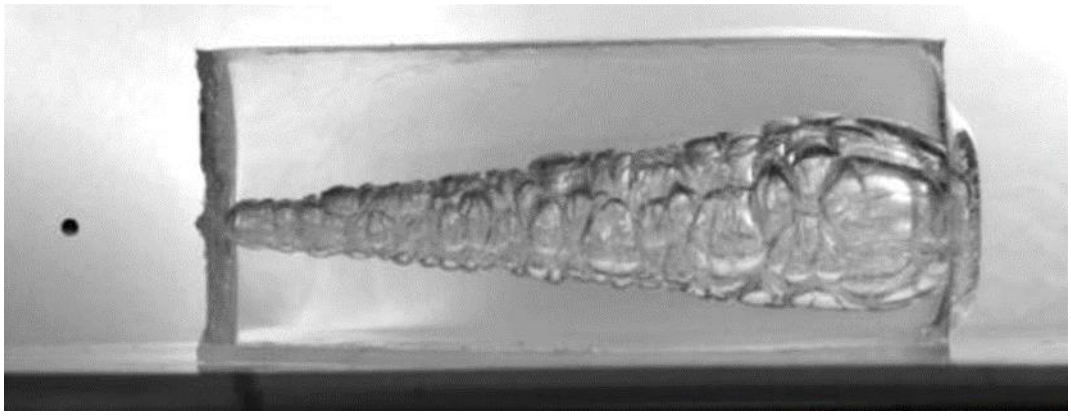

Figure 4: Frame from high speed video showing the temporary cavity formed in 20% gelatin at 10°C (a muscle tissue simulant) after penetration by a 6 mm steel sphere.

The magnitude of the temporary cavity is related to the energy deposited by the projectile (more energy deposited gives larger cavities) and can be many times the projectile diameter. Energy lost by bullets is maximised when they deform, fragment or tumble to a side on orientation due to increasing presented area and drag coefficient. The cavity forms dynamically; it reaches a maximum size, called the Maximum Temporary Cavity (MTC) and will then collapse back down, oscillating and finally leaving a Permanent Cavity (PC). The temporary cavity will be at sub-atmospheric pressure and is responsible for drawing in air and environmental debris (deep) into the wound as the pressure equalises, potentially leading to infection.

References [69; 116] also describe the ability of the temporary cavity to cause damage in air filled organs/tissues (within the zone of temporary cavitation) due to expansion of the trapped air to counteract the forces of the sub-atmospheric temporary cavity.

3. Distant or remote effects due to the temporary cavity. Other tissue types (such as bones or blood vessels) not directly damaged by the direct impact of the projectile can be damaged by the expansion of the temporary cavity [69; 115; 118]. Non-contact (from the projectile) bone fracture may be caused due to flexure past its elastic limit [69; 119].

4. At very high impact velocities, pressure waves can cause distant damage in other tissues [120] (such as damage to the colon when the impact was to the thigh with impact velocities >3000 m s^{-1} [120]). Due to requiring 'hypervelocity' impacts, remote damage from pressure waves is not considered further in this thesis.

The temporary cavity reaches a maximum size in the order of a millisecond after impact by the projectile and will then start to collapse. Whilst the temporary cavity does not contain damaged tissue (it's a sub atmospheric cavity) it can be used to indicate the maximum extent of potentially damaged tissue[37]. The size of the resulting permanent cavity is proportional to the size of the maximum temporary cavity (see Section 9.7).

Reference [115] describes how different researchers place different importance on the temporary or permanent cavity as metrics to relate to the actual tissue damaged. In reality neither the temporary or permanent cavity actually represents the extent of tissue damage:

- The permanent cavity is, as its name suggests, empty space. The tissue that originally occupied this volume will have been displaced and the resulting cavity may be sub-calibre or a few times the projectile diameter.
- The temporary cavity shows the maximum extent to which the tissue has stretched. The local tissue properties will determine the extent to which the tissue strained within the temporary cavity will be damaged. Some tissues are more susceptible to this stretching/strain damage such as the liver, whilst others are less, such as intestines [26]. Only in very brittle tissues will the extent of the temporary cavity approximate the zone of damaged tissue.

In most cases and tissue types, the zone of damaged tissue will occupy a volume between the extent of the permanent and temporary cavities. Figure 5 shows a cross sectional view of the different zones within a tissue after a projectile has

[37] No damage should occur to tissue outside the maximum temporary cavity radius by mechanisms 1-3.

penetrated through. Remote effects from the temporary cavity are likely to be within the MTC radius, but more distant to the projectile than the zone of damaged tissue caused by stretching past its elastic limit. Tissue damage by the pressure wave may be more distant than the MTC radius, if this occurs (for hypervelocity impacts).

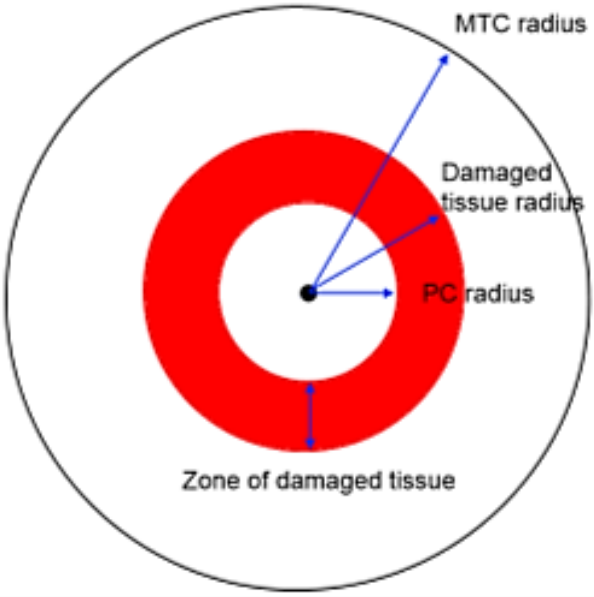

Figure 5: Cross sectional view of the MTC, PC and zone of damaged tissue predictions (not to scale).

Figure 5 shows a circular cross sectional view of the different zones. However, in real tissue this may be a different geometry due to inhomogeneous tissue properties.

Depending on the requirement, a muscle tissue simulant may be used to replicate aspects of these damage mechanisms observed in real muscle tissue. Often a muscle tissue simulant is used to assess the projectile response; i.e. the permanent depth of penetration and/or retardation. In order to compare the magnitude or location of 'tissue damage', a target response such as the temporary cavity measured using high speed video is frequently used.

3.9.3 Introduction to muscle tissue simulants

Tissue simulants are required for a number of reasons:

- Using animals or PMHS may not be ethical.
- There is large variability in real tissue, even within the same animal / PMHS as well as between individuals of the same species. Tissue simulants are homogeneous and can be made to meet a verification test to ensure repeatability and reproducibility.
- There are a variety of practical limitations to using real tissue:
    - Ethical issues if animals are killed specially for wound ballistics research. This can be partially mitigated by using tissue from the human food chain, or from other experiments.
    - Extracting the required information is challenging. Tissue is opaque; it requires (flash) x-ray equipment. Tissue simulants are either transparent allowing the use of High Speed Video (HSV), or are plastically deformed, preserving the required information.
    - Real tissue degrades post-mortem, so storage becomes an issue, as well as the storage method (refrigerated or frozen) may affect the tissue properties. Tissue simulants can be made on demand and some can be stored for long periods prior to use.
    - Sourcing real tissue can be challenging. It needs to be from certain species to be most representative, needs to contain a sufficient target size, but sourcing from the food chain limits the control over how soon the tissue can be tested after death. Tissue simulant raw materials can be stored prior to mixing, or produced and stored until required for testing. The target size of tissue simulants can be varied according to the user need.
    - Availability, especially of representative PMHS (the average ages of PMHS were 58 and 72 from References [59; 61]).
    - Real tissue is highly variable in its response and limited sample sizes mean it may not represent the entire population from which it

was obtained, or that prohibitively large numbers of tests may be required.

- PMHS or animal tissues may contain disease which could be passed onto the people conducting the testing. For example live or dead cows, sheep and goats can cause transmissible spongiform encephalopathy infection (of which Bovine Spongiform Encephalopathy (BSE) is an example)[38] [121].
- Manual handling risks if whole intact animals are used.

Whilst an ideal muscle tissue simulant would exactly match the penetration and cavitation response of (live human) muscle tissue, this is not a vital requirement. More important is that the tissue simulant behaves in a similar manner to real tissue in terms of projectile penetration and retardation response, so that effects such as tissue cavitation, projectile tumbling, fragmentation or deformation can be more easily measured and occur to a similar extent, at similar depths and results can be extrapolated to real tissue under the required impact conditions. Other key requirements are that the simulant behaves in a repeatable and reproducible manner.

The requirements for a tissue simulant vary depending on the desired use or output. In this thesis, the ability to measure and provide the same permanent DoP, retardation, temporary cavity dimensions and tumbling for bullets as expected in muscle tissue are required. This drives the requirement for a tissue simulant to a transparent material.

Numerous reviews of tissue simulants have been conducted in the past, examples include References [94; 108; 111; 122-125] and will not be discussed in detail. Not all of these previous reviews were directly aimed at identifying a suitable muscle tissue simulant. However, the limitations of previous reviews in

[38] The BSE infectious agent may be present in certain tissues: skull, brains, eyes, spinal cord and intestines [121].

relation to selection of an appropriate muscle tissue simulant selection can be summarised as one or more of:

- Comparison of simulants to each other without any relation back to real tissue (e.g. [122; 125; 126]).
- Comparisons of tissue and tissue simulants using bullets. Bullets cause variable results due to a number of factors which are difficult to control or account for, based on their propensity to tumble, deform or fragment in tissue or a simulant, but to different degrees or at different depths from shot to shot (e.g. [111]).
- Comparisons of tissue and tissue simulants conducted over very limited data ranges. For example with a single projectile type and/or at a single velocity (e.g. [94]).
- The comparison of 1 (or limited number) of simulants to (limited) animal data (e.g. [79; 88; 123]). The simulant being compared can be judged as to how well it matches real tissue, but does not allow selection of the most appropriate simulant.
- Comparison of the DoP response of tissue and tissue simulants used to provide retardation or cavitation predictions[39] (e.g. researchers that use Reference [94] as 'validation' for bullet assessments).

As described by Fackler, a suitable tissue simulant "*must cause the same projectile deformation and the projectile must stop at the same depth as in living animal tissue. This requirement is often ignored by wound ballistic investigators*" [27]. For a simulant to cause the same projectile deformation as in live tissue (consistently across all impact conditions), it must provide the same retardation on the projectile as real tissue. The retardation (or deceleration) is directly proportional to the force acting on the projectile.

[39] The DoP and retardation in a material (e.g. a muscle tissue simulant) are independent of each other, i.e. a material can be made to match the DoP response to muscle tissue but not retardation, or vice versa. It would be possible for a simulant to have very large elastic recoil from its maximum temporary penetration depth (compared to muscle tissue), but match the required DoP behaviour. In this case the retardation behaviour would not match the desired response.

Against the requirements set out in this thesis for a muscle tissue simulant, there has been no suitable validation in the literature of any of the potential simulants identified (which are described below).

The most widely-used tissue simulant for both penetrating bullets and fragments is ballistic gelatin. Gelatin is produced from the collagen in skin and bone. This is typically from cattle bones, cattle hide or pig skin. Type A gelatin (acidic) is produced by conditioning the collagen in a dilute acid to extract water. Acid processed and lime processed gelatin differ in their properties [127]. Gelatin is often used as a tissue simulant because it is a transparent and homogeneous material. Being transparent allows the interaction of the projectile within the target to be viewed during penetration via HSV and is a desirable quality of (elastically deformable) tissue simulants.

There is much discussion on the benefits and drawbacks of different gelatin concentrations in the literature. Most of the debate on how closely a given gelatin mix matches real tissue is not necessarily a critical factor as only the ability to be able to extrapolate back to real muscle tissue is needed [128]. However, the better the match to real tissue, the more confidence can be placed on the observed behaviour of the projectile in the simulant and therefore its likely behaviour in real tissue.

The main discussion on different gelatin concentrations are between the use of 10% (referred to as Fackler method[40] [129]) or 20% (normally the North Atlantic Treaty Organisation (NATO) method [130]) gelatin concentration by mass:

- The use of 10% gelatin at 4°C was predominantly advocated by Martin Fackler at the Letterman Army Institute of Research, Wound Ballistics Laboratory during the 1980's and 90's [24-27; 93; 94; 129; 131-136].
- The use of 20% gelatin at 10°C can be attributed to the Ballistic Research Laboratory (BRL) in the United States[41]. Haag [137] stated that he had correspondence with the BRL in 1981 quoting:

[40] Also commonly called the FBI method.
[41] The validation details not openly available or published, so it is assumed.

"Edgewood Arsenal researchers had established that 20% w/w ordnance gelatin at 10°C provided a medium which "best approximated projectile retardation in tissue"… the 20% w/w at 10°C was adopted by Edgewood for all subsequent terminal ballistic studies".

One of the issues that have compounded the discussion on suitable muscle tissue simulants is that large amounts of the underlying validation data have not been openly available, for both 10% and 20% gelatin mixes.

Reference [138] reproduced a figure from Dubin [139] which shows the measured cavity in pig muscle tissue compared to that predicted in 20% gelatin and states that the work by Dubin "*has shown a remarkable similarity of cavities in gelatin with those in freshly excised pig muscle"* [138]. Despite the original report from Dubin [139] not being openly available to confirm or to use the data to validate the work within this thesis, it originated from BRL and as such is highly likely that this relates to the use of 20% gelatin at 10°C as detailed above.

Gelatin usage temperature as well as the method used to mix it can affect its ballistic response (for example the long chain fibres of the gelatin can be broken down by excessive heating during mixing) [129; 137; 140-142].

Gelatin is considered a good simulant to use for the dynamic and permanent depth of penetration (temporary cavitation[42]), but not the permanent cavity (except for using it to show the projectile path or as a way to estimate the size of the temporary cavity from the permanent cracks [143]).

Glycerine soap (1.06 g cm^{-3}, commercial grade cold stirred, based on animal and vegetable fat) has been widely used as a muscle tissue simulant (particularly in in Sweden), normally with high velocity bullets [75; 118; 144-150].

The soap is plastically deformed on impact, so the resulting permanent cavity in soap is compared to the maximum temporary cavity that would be seen in real tissue[42]. This cavity can be easily viewed by sectioning the block after shooting,

[42] Considered as a useful metric for the comparative or relative 'damage' in muscle tissue. It has not been suitably validated as a direct predictor for the temporary cavity in real muscle tissue.

without the need for expensive high speed video equipment and analysis. For bullets, the soap is often quoted as producing similar cavities as the temporary cavity formed in animal tissue and similar projectile behaviour (tumbling and fragmenting) [75; 118].

However, although soap has a longer shelf life to mixed gelatin, it is still sensitive to usage temperature [94; 144; 145].

Paraffin candle wax (white paraffin oil and kraton) has also been shown to give similar penetration depths as 10% gelatin and pig tissue with air rifle pellets [19; 151]. However, it has not been widely utilised as a ballistic tissue simulant.

A number of synthetic (non-biological) replacements or alternatives to both 10% and 20% gelatin have been developed:

- Physically Associating Gel commercially known as Perma-Gel, and has been developed to replicate 10% gelatin, whilst being highly transparent and re-useable [152; 153].
- Clear Ballistics have developed synthetic alternatives to both 10% and 20% gelatin; Clear Ballistics Gel® [154].
- Army Research Laboratory (ARL) have developed a poly(styrene-b-ethylene-co-butylene-b-styrene) triblock copolymer (SEBS) powder and mineral oil referred to as “Stabili-gel” to be a synthetic alternative to 10% and 20% gelatin [155].

These synthetic gelatin alternatives are aimed to provide all the benefits of gelatin without the drawbacks of the limited shelf life and temperature sensitivity. Additional benefits these synthetic simulants bring are that they be used in scenarios such as outdoor tests / trials where gelatin or soap would be impractical [156].

The main limitation of the synthetic gelatin simulants is that due to their relatively recent availability compared to standard gelatin, there is limited validation data on their performance [125].

An overview of the main muscle tissue simulants is given in Table 3 showing their general properties, main uses and some typical drawbacks. Deliberately omitted from Table 3 is their match to penetration of actual muscle tissue which is addressed in Section 7.2.

Simulant	Dominant response	Transparency	Ease of storage and use	Primary uses	Drawbacks
Gelatin (20% at 10°C)	Elastic	Good	Poor – temperature controlled storage, very limited shelf life. Not normally reused.	Temporary cavitation, projectile retardation and DoP testing. NATO testing. Wealth of legacy data.	Usage temperature and limited shelf life (impractical for blast trials).
Gelatin (10% at 4°C)	Elastic	Good		Temporary cavitation, projectile retardation and DoP testing. Typically used by (non-UK) law enforcement. Wealth of legacy data.	
Synthetic gelatin alternatives	Elastic	Very good	High. Limited temperature dependencies and long shelf life. Reusable	Temporary cavitation, projectile retardation and DoP testing. Outdoor/blast trials. Ease of use.	Limited data (especially for bullets).
Soap	Plastic	Normally poor (transparency not normally required)	Good. Some temperature dependencies and moderate shelf life. May be reusable	Permanent cavitation and DoP testing. No need for HSV. Typically Scandinavian countries (for small arms rounds).	Only permanent penetration and cavities. Temperature sensitive.
Wax	Plastic	Can be good	High. Limited temperature dependencies and long shelf life. May be reusable	Permanent cavitation and DoP testing. HSV may not be needed. Retardation if sufficiently transparent (with HSV).	Only permanent penetration and cavities. Very limited data.

Table 3: Summary of main muscle tissue simulants with general properties

A critical factor for any simulant is being able to verify it prior to use.

3.9.4 Muscle tissue ballistic data

The muscle tissue simulants being investigated for a physical model are based on the assumption that human muscle can be represented by a homogeneous material. This is a simplistic approach, but a good starting point for the development of the model. On this basis, only fragment penetrations into (approximately) homogeneous animal tissue are used for the comparison at this stage, where the final penetration depth of the fragment was measured. Shots where the fragment is known to have hit a bone, or exited the tissue have been discounted (a separate analysis is performed based on shots that fully perforated the target).

All the sources of data outlined in Section 3.5 which tested the skin intact and reported the resulting DoP were added to a database. A summary of this PMHS and animal penetration data (both total shots and those with non-zero penetration depths) are given in Table 4 for comparison to tissue simulants.

Reference	Target type	Total Shots	Shots with non-zero DoP data
[56]	PMHS	67	15
[62]	PMHS	123	44
[63]	PMHS	48	36
[64]	PMHS	30	26
[71]	PMHS	16	16
[79]	Goat	41	22
[58]	Pig	59	55
[88]	Pig	27 (for muscle tissue)	27
[94]	Pig	1[43]	1[43]
[90]	Pig	12	12
Total shots included		424	254

Table 4: Summary of PMHS and animal muscle tissue DoP data from the literature

[43] 10 repeats at the same velocity. The average value and limits were reported.

In addition to this ballistic data, the relationship between velocity and DoP used for muscle tissue in ComputerMan was extracted from Reference [42] (see Section 7.2.3).

Data for shots that fully perforated muscle tissue and where an exit velocity was recorded were also collated and is given in Table 5 (limited to non-deforming, non-tumbling projectiles).

Reference	**Target type**	**Number of data points**	**Impact energy range (J)**
[95]	Live anesthetised pig thigh	48	96-1056
[96] (APPENDIX E)	Live anesthetised pig thigh	17 (+2 outliers)	970-1175 (182, 1870)
[113]	Live anesthetised pig thigh	3 [44]	~440
[123]	Live anesthetised pig thigh	1 [45]	298
[157]	Live anesthetised dog thigh	3 [46]	112-741
[58]	Dead pig thigh	18	3-12
[109]	Dead pig thigh, no skin	3 [46]	~5.7
Total		93 (+2)	3-1175

Table 5: Summary of animal muscle tissue energy loss data.

The data from reference [96] has not been previously published, but was made available for this analysis with overview of the testing provided in APPENDIX E, E.2.

[44] Grouped data, average of 10 shot per group.
[45] Based on the fitted model retardation equation generated from 14 shots.
[46] 3 sets of grouped data, average of 18 shots per group.

3.9.5 Muscle tissue simulant ballistic data

To help identify what muscle tissue simulants may be suitable, any ballistic data available for the simulants were collated from the literature. In addition to results directly reported, raw data from References [155] and [158] was made available [159; 160]. Only data for simple[47] projectile types were considered.

A summary of the data collated is given Table 6.

Reference	Simulant(s)	Projectile(s)	Velocity range (m s^{-1})	Shots with DoP data
Mabbott [38]	Perma-Gel 10% gelatin at 4°C 20% gelatin at 10°C	5.5 mm steel sphere	114 - 1075	103 [48] 108 70
Bourget [42]	10% gelatin at 4°C 20% gelatin at 10°C	5.5 mm steel sphere	185 - 631	33 32
Breeze [91]	20% gelatin at 10°C	5.0 mm steel sphere	79 - 1156	48
Breeze [58]	20% gelatin at 10°C	0.49 g CN FSP, 1.1 g CN FSP, 5 mm sphere	40 – 190	47
Breeze [88]	20% gelatin at 10°C	0.16 g cylinder, 1.1 g CN FSP and 2.84 g CN FSP	100-994	51
Dziemian [161]	20% gelatin at 10°C	Various steel spheres (4.8 – 11.1 mm)	71 - 973	94
Swaina [162]	5% gelatin at 4°C 7.5% gelatin at 4°C 10% gelatin at 4°C 15% gelatin at 4°C	Various steel spheres (7 – 11 mm)	17 - 73	28 36 26 29
Maiden [140]	Various 10% gelatin at 4°C mixes and 20% gelatin at 10°C mixes	4.5 mm steel sphere	175-185[49]	14 [50]

[47] Non-tumbling, non-deforming, non-fragmenting.
[48] Of which 43 were with the Perma-Gel re-melted.
[49] The actual velocity of each shot was not measured. Shots are assumed to be within this velocity range.
[50] 3-4 repeats for each mix type. Only the average value for each mix is included.

Reference	Simulant(s)	Projectile(s)	Velocity range (m s^{-1})	Shots with DoP data
Mahoney [163]	10% gelatin at 4°C	5.5 mm steel sphere	651 - 730	36
Fackler [94]	10% gelatin at 4°C 20% gelatin at 4°C 20% gelatin at 20°C Soap at 4°C Soap at 20°C	4.3 mm steel sphere	181±4	1[51] 1[51] 1[51] 1[51] 1[51]
Uzar [151]	10% gelatin at 4°C 11%, 13% and 15% Kraton - Paraffin candle wax	4.5 mm steel sphere	154	1 [52] 3 [52]
Ogunc [19]	10% gelatin at 4°C 15% Kraton - Paraffin candle wax	4.5 mm and 5.5 mm air rifle pellets	123 - 188	3 [53] 3 [53]
Mrozek [155; 159]	Stabili-gel. 15-40% SEBS in mineral oil	5.56 mm steel sphere	104 - 500	60
Scepanovic [164]	Soap (glycerine, commercial grade)	6 mm steel sphere	237 - 1718	44
Guey, Kieser [158; 160]	10% gelatin at 4°C 11.25% gelatin at 4°C 20% gelatin at 10°C	4.5 mm steel sphere	73 - 216	151 253 238
Haag [137]	10% gelatin at 4°C 10% gelatin at 10°C 20% gelatin at 4°C 20% gelatin at 10°C 20% gelatin at 20°C	4.5 mm and 7.8 mm steel sphere, 8.3 mm lead sphere	82 - 204 120 - 190 119 - 204 80 - 410 82 - 228	20 10 7 27 8
Eisler [165]	10% gelatin 15% gelatin 20% gelatin (all assumed at 10°C)	Steel spheres and cylinders	170 - 183 140 - 424 56 – 533	2 6 29
Stevenson [166]	10% gelatin at 4°C	5.5 mm steel sphere	668 - 774	34
Freitas [167; 168]	Perma-Gel	Steel cylinders	152 - 1280	52 [54]

[51] 5-30 repeats at the same velocity. The average value and limits were reported.
[52] 10 repeats at the same velocity. Only the average value for each set is included.
[53] 25 repeats at the same velocity. Only the average value for each set is included.
[54] Data were limited to impact velocities below 1400 m s^{-1}.

Reference	Simulant(s)	Projectile(s)	Velocity range (m s^{-1})	Shots with DoP data
Grand Total				1718

Table 6: Summary of muscle tissue simulant DoP data from literature

3 additional shots were excluded from the data obtained from Reference [137] for 8.3 mm lead spheres, as they were reported to deform at higher velocities (over approximately 335 m s^{-1}).

Data from Reference [39] was not included as the projectile dimensions were not reported, only the mass and cylindrical geometry.

These data in Table 6 will be used in Section 7 (along with original testing) to select a suitable muscle tissue simulant.

3.10 Review of penetrating eye injuries

3.10.1 Types and incidence of penetrating eye injury

The eye is such a sensitive and easily damaged organ that even relatively minor injuries can result in incapacitation, long-term, or permanent suffering for an individual.

Military casualties suffering from penetrating eye injuries as a result of fragmenting weapons are well documented in the literature [169-172]. The proportion of casualties documented to have sustained this type of injury vary from about 2% in the First and Second World Wars, to rates of 10-16% in modern conflicts [169-171]. This is despite the eye being only a very small portion of the body surface area (approximately 0.5%). In addition, a large proportion of these injuries may be bilateral. Around 30% of penetrating eye injuries were bilateral for UK Military casualties in Iraq and Afghanistan between 2004 and 2008 [169]. Bilateral injuries will massively increase their impact on morbidity, as well as combat effectiveness and mission success.

Eye injuries by penetrating and blunt mechanisms are also common in the general public from airsoft weapons [70; 173], paintballs [174-179], sporting equipment [180-182] and Conducted Electrical Weapons[55] [183].

There are many different types of eye injury, ranging from corneal abrasions which could occur from any foreign body rubbing the surface of the eye, to retinal damage and globe rupture that could result in complete loss of vision in that eye. Figure 6 shows an example of different ocular injuries with energy for paintball impacts to porcine eyes, ordered by the relative level of impact energy required to generate them.

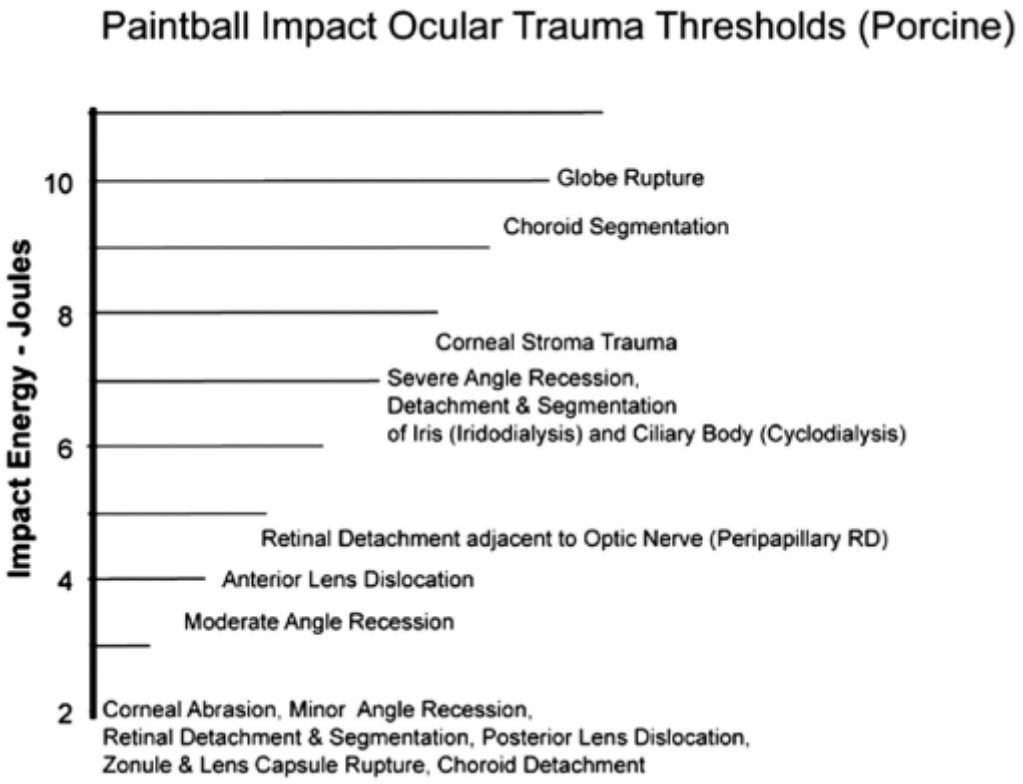

Figure 6: Ocular trauma levels for porcine eyes from paintballs, given in increasing order of impact energy required to inflict. Reproduced from Reference [174]

For the purposes of this work, penetrating injury to the eye (cornea) will be used, which is clinically termed (open) globe rupture or open globe laceration. Globe

[55] An example of which is TASER.

rupture and open globe laceration are defined as any full-thickness injury to the sclera, cornea or both (i.e. corneal or scleral perforation)[56]. This type of injury represents a severe clinical consequence [186], with a 46% chance of complete loss of vision in civilian trauma, even with specialist ophthalmological treatment within 24 hours of arrival at the treatment centre, most of which was within 24 hours of sustaining the injury [186].

Globe rupture (and laceration) from ballistic impact has been widely studied in the literature and it is relatively easy to determine when they have occurred based on gross pathology of a traumatised eye. Globe rupture or laceration will be referred to generically here as “eye penetration”.

Corneal abrasion is also used during this work, which Figure 6 shows is one of the lowest (energy) level injuries that can occur. According to the Duma Eye Score (DES) from the Abbreviated Injury Scale (AIS) handbook [187], a corneal abrasion type of injury would have a DES of severity 2, “*Minor injury to eye*”. A cornea laceration (penetration) would have a DES of severity of at least 3, “*More serious eye injury that may require surgery and present guarded long-term prognosis*” [187].

3.10.2 Eye penetration data

Penetration data of the eyes for ballistic projectiles have been collated from previous studies [70; 174; 188-193]. Either the slowest velocity that resulted in the projectile penetrating the eye (V_{th}), or the V_{50} were reported. Different projectiles were used which included a range of materials (plastic, steel and lead), different sizes (4.4 mm to 17 mm diameter) and geometries (spheres and cylinders).

The V_{th}/V_{50} tests were conducted mainly on pig eyes, with limited data points for rabbits, PMHS and dog eyes. In some cases, the eyes remained in the head

[56] Classified as open globe laceration if caused by a sharp object and globe rupture if by a blunt projectile [184; 185]. However, in the ballistic testing literature it is often simply termed globe rupture irrespective of causal agent.

during testing, in others they were removed and inserted into gelatin, Styrofoam or a plastic orbit.

This resulted in a dataset containing 18 unique results, of which V_{th} data was available for 16 and V_{50} data available (or could be calculated) for 11.

Data in Reference [188] allowed a V_{50} to be calculated that had a zone of mixed results (velocity range of the slowest penetration to the highest non-penetration) of 20 m s^{-1} on a V_{50} of 78.1 m s^{-1}, showing the potential variability in eyes, even from the same species.

Another problem is that very few of these studies looked at human eyes and a suitable animal model has not been validated by ballistic testing. Figure 7 shows all the combined V_{th} and V_{50} data, by target type.

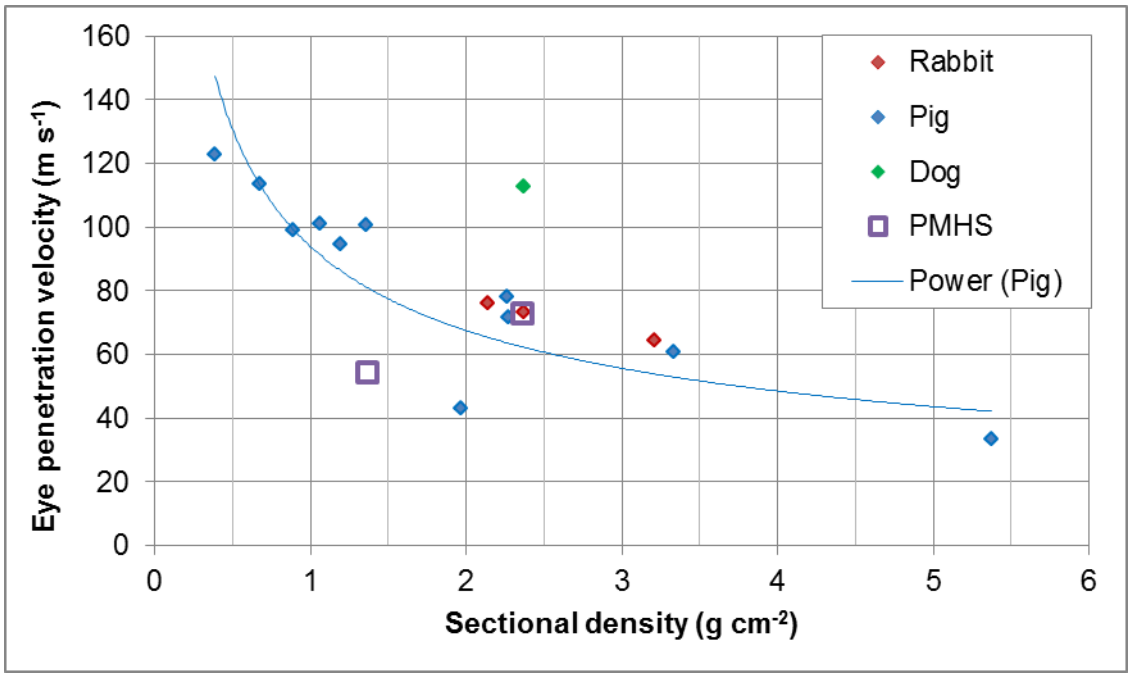

Figure 7: Eye penetration velocities for small projectiles showing data from different animal species and PMHS [70; 174; 188-193].

Given the limited data and scatter shown in Figure 7, it cannot be determined how the values for PMHS compare to the other targets over the range of interest of projectile sectional densities.

Given these limitations, an alternative approach to generate performance data for PMHS eyes was needed. Raw data from the V_{th} and V_{50} tests, as well as from other studies that in isolation could not calculate a suitable V_{th} or V_{50} were collated. This resulted in 403 data points obtained from 11 References [89; 171; 174; 181; 188; 192-197][57]. This included data for cat, human and pig eyes. Additional data from References [198; 199] were not included as they used heavy projectiles (282 g and 303 g respectively) and may have resulted in a blunt rather than penetrating rupture mechanism.

The V_{th}, V_{50} and raw data that has been collated is summarised in Table 7.

Reference	**Target**	**Projectile(s)**	**Number of V_{50} assessments**	**Raw data (# shots)**
[171]	Human, pig	Spheres, cylinders, various materials	3	Y (131)
[174]	Pig	Sphere	1	Y (34)
[181]	Human	Spheres	1	Y (21)
[188]	Pig	Steel sphere	1	Y (19)
[192]	Pig	Sphere	1	Y (4)
[193]	Pig	Sphere and cylinder	1	Y (36)
[194]	Pig	Steel cylinder	0	Y (19)
[197]	Pig	Foam	0	Y (13)
[195]	Cat	Sphere	0	Y (17)
[196]	Pig	Sphere	0	Y (105)
[70]	Pig	Spheres (plastic, aluminium and lead)	5	N
[89]	Pig	Steel sphere	1	Y (4)

[57] Raw data was included from studies that conducted firings at pre-determined impact velocities using the reported average velocities for each group [195; 196], and also partial data sets where the minimum and maximum velocities causing penetration and non-penetration were reported [192].

Reference	Target	Projectile(s)	Number of V_{50} assessments	Raw data (# shots)
[189; 190]	Rabbit	Spheres	2	N
[191]	Rabbit, dog	Steel sphere	2	N
Total raw shots				403

Table 7: Summary of collated eye penetration data.

3.10.3 Eye penetration predictions

References [171; 197] have produced predictive curves based on a probit or logit regression. Reference [197] produced a prediction based on combined animal and PMHS data, whereas Reference [171] produced curves separately for humans and pigs.

These predictive equations were based on energy density, rather than velocity and sectional density as commonly done for skin perforation.

The data collated in Table 7 was used to generate a predictive probit model and compared to these previous predictive models from References [171; 197] in Section 6.2.

4 Normalisation of depth of penetration

In order to simultaneously compare the depth of penetration results from a range of different projectiles in tissue or a tissue simulant throughout this thesis, the penetration depths have been normalised. This normalisation was performed to get all the data to fall onto (approximately) a single curve when plotted against impact velocity. Commonly DoP is normalised by dividing it by the projectile diameter [88; 162; 200; 201].

Reference [161] normalised DoP using $(m/A)^{1.21}$ for steel spheres which had the same effect of collapsing data onto a single curve (and can be applied to projectiles of other densities). The power of 1.21 used was based on empirical fit to their available gelatin data.

In this thesis, the DoP was divided by the projectile diameter and additionally divided by the projectile density to get a 'normalised DoP over density' function to enable comparisons between projectiles of different diameters and densities.

$$\text{Normalised DoP over density} = \frac{DoP}{d_{av}\rho}$$

Equation 3: Normalised depth of penetration over density empirical model

Where:

d_{av} is the average diameter of the projectile (simply the diameter for spheres and cylinders) in mm.

ρ is the projectile density (g cm^{-3}).

For randomly orientated cubes (in 3D), the average diameter is given by Equation 4:

$$d_{av} = 3d\sqrt{\frac{2}{7}}$$

Equation 4: Average diameter (projection length) of a randomly orientated cube in 3D [202]

Where *d* is the side length of the cube (mm)

Figure 8 to Figure 10 show penetration data into Dstl 20% gelatin at 10°C for 3, 6 and 9 mm spheres of different densities collapsing the data from DoP to normalised DoP to normalised DoP over density. All data was original from Section 7 and forms part of the dataset detailed within Table 23.

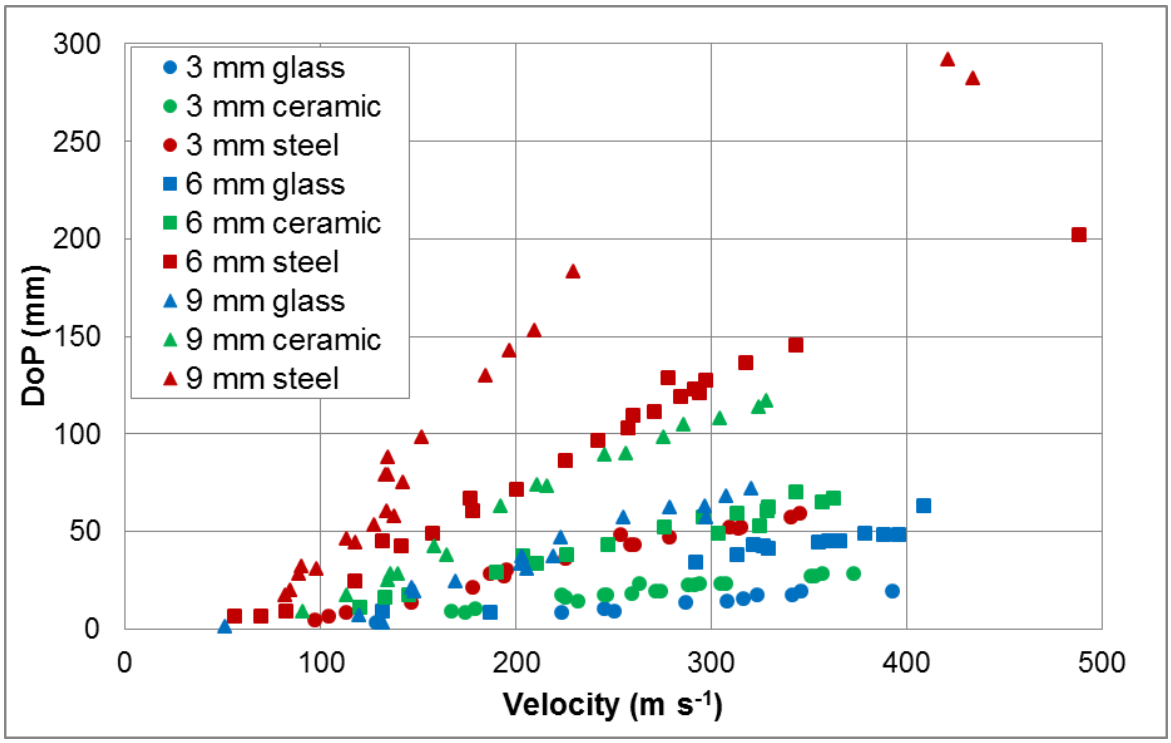

Figure 8: Impact velocity against DoP for 3, 6 and 9 mm spheres of different densities in Dstl 20% gelatin at 10°C.

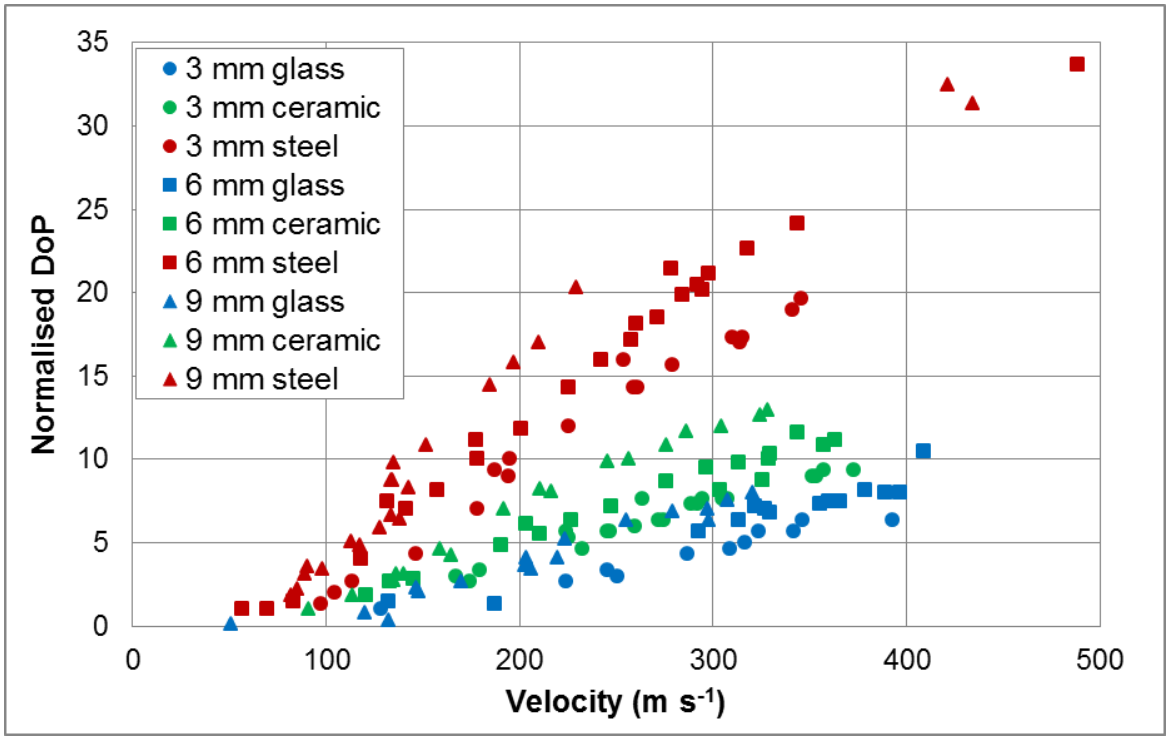

Figure 9: Impact velocity against normalised DoP for 3, 6 and 9 mm spheres of different densities in Dstl 20% gelatin at 10°C.

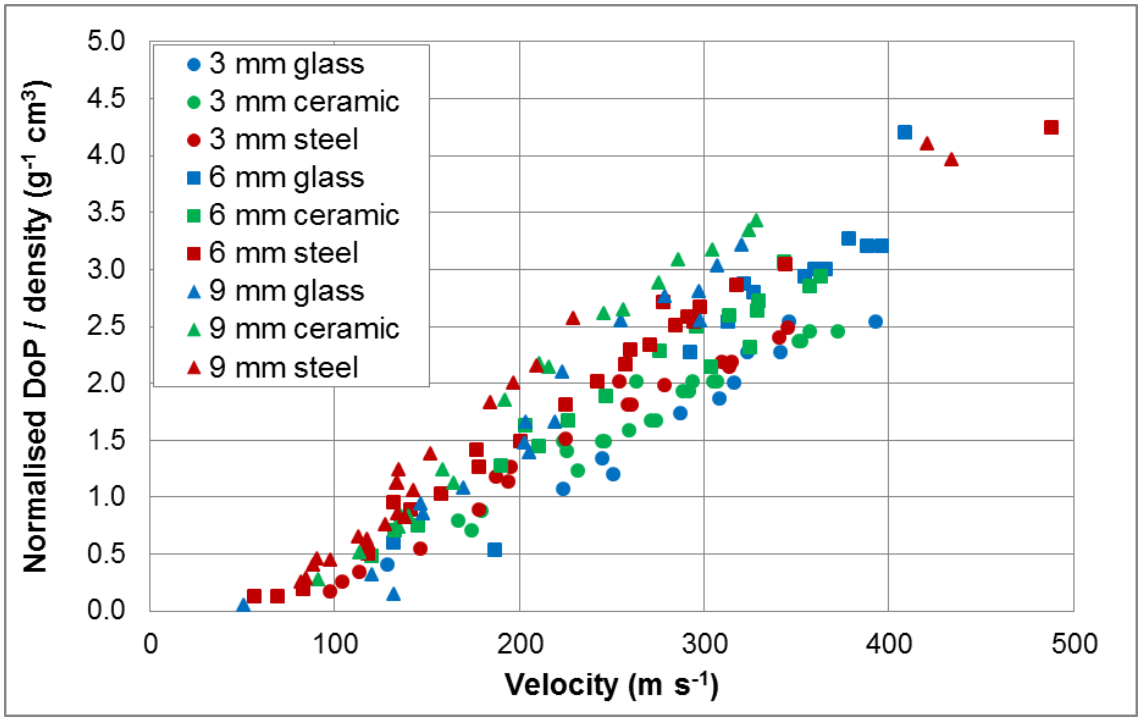

Figure 10: Impact velocity against normalised DoP over density for 3, 6 and 9 mm spheres of different densities in Dstl 20% gelatin at 10°C.

Figure 10 shows there is still some scatter in the normalised DoP over density against velocity data.

Reference [200] suggests that this is (at least partially) due to strain rate behaviour in the target, which itself is dependent on the projectile diameter (based on a virtual model to describe penetration into 20% gelatin at 10°C).

The scatter may also be partially due to the data coming from trials conducted at different times, with potential variability between the gelatin batches. It shows that the normalised DoP over density is potentially a useful method for collapsing the penetration data, although it is not ideal. One major limitation is that it does not account for projectile geometry.

Subsequent improvement of this normalisation process has shown that the data reduction can be optimised. For this specific dataset, $d^{1.4}$ provides an optimal fit instead of d in Equation 3. However; this optimisation was conducted after completion of the analysis within this thesis and the original normalisation (as given by Equation 3) was used throughout. The differences between the two processes are unlikely to alter the conclusions reached; it may just make the data appear less variable.

The outcome of the normalisation process on the 3 mm, 6 mm and 9 mm spheres is given in Figure 11 to show the improvement of this optimisation, in comparison to that in Figure 10.

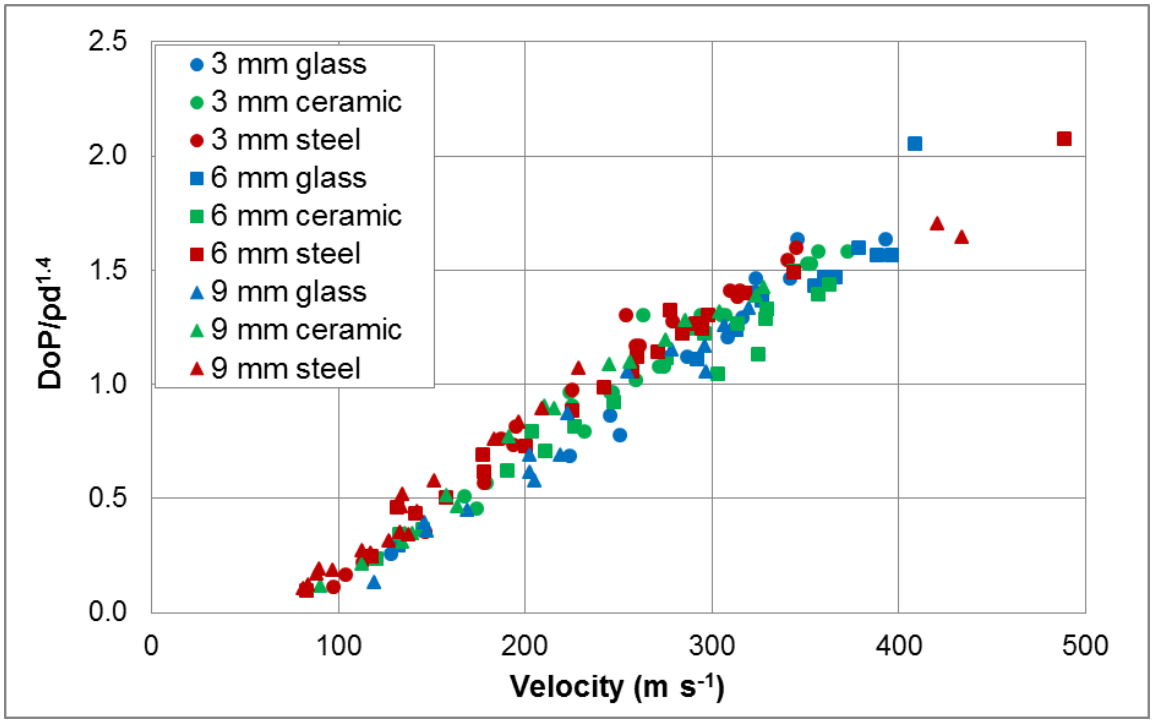

Figure 11: Impact velocity against 'optimised' normalisation of the DoP for 3, 6 and 9 mm spheres of different densities in Dstl 20% gelatin at 10°C.

As suggested in Reference [200], the strain rate behaviour of the target is dependent on the projectile diameter. This means that for targets tested with other diameter projectiles, or targets with different rate sensitivity to 20% gelatin at 10°C, may require revision of the power to which *d* is raised in Equation 3 to result in an optimised fit[58].

Additionally, the normalisation with Equation 3 does not exhibit the same diameter dependence on rate sensitivity for the Multiple Discrete Fragment Physical Injury Model data, which is discussed in Section 10 (see Figure 132).

Due to the desire to use the normalised DoP over density process to compare multiple different targets, tested with different sets of projectiles, it is not practical to optimise the power of *d*. Equation 3 as given (d^1) is considered suitable.

[58] For example, $d^{1.1}$ is the optimised value for Equation 3 for the Perma-Gel data given in Table 23 (spheres only).

5 Skin perforation and DoP comparisons

5.1 Introduction

To address some of the findings from the literature review of skin perforation data in Section 3.8, data from unpublished studies[59] were analysed and a series of experiments were performed to address:

- The lack of skin perforation (and DoP into muscle tissue) data for low density projectiles[59]
- The effect of skin on penetration depth
- The effect of storage condition on skin perforation V_{50} and DoP
- A direct comparison of skin V_{50} across different target types (utilising existing data from the literature [63; 79; 88] and some data from experiments listed above).

5.2 Skin perforation by low density projectiles

5.2.1 Aim

The majority of literature is focused on projectiles from conventional military threats like steel fragments or civilian injuries from air rifle pellets. There is a lack of information on low density projectiles, such as the soil particles or stones that might be generated from an Anti-Personnel Mine (APM) or buried Improvised Explosive Device (IED) common on recent operations in Afghanistan [203; 204].

In order to build on the existing data, ballistic impacts were conducted into the thighs of one freshly killed goat and one sheep with ceramic and glass spheres (to represent stone and glass secondary fragments). As the experiment was not published[59], the testing details are described here, as well as the original analysis conducted on the data.

[59] Experiments performed by the author with Maj. Johno Breeze and Matthew Mouland, prior to the registration period for this PhD.

5.2.2 Method

Six different low density projectiles were chosen to evaluate the goat and sheep skin response. The projectiles were spheres constructed from soda lime glass (2.50 ± 0.05 g cm^{-3}) or ceramic (Al_2O_3, 3.80 ± 0.02 g cm^{-3}) to Reference [203]. Projectile details for each target are given in Table 8.

Target	Material	Diameter (mm)	Mass (g)	Sectional density (g cm^{-2})
Sheep	Glass	6.0	0.28	1.00
Sheep	Ceramic	6.0	0.43	1.52
Goat	Glass	3.0	0.04	0.50
Goat	Ceramic	6.0	0.43	1.52
Goat	Glass	9.0	0.95	1.50
Goat	Ceramic	9.0	1.45	2.28
Goat	Ceramic	20.0	15.92	5.01

Table 8: Non-metallic projectiles used for assessment of sheep and goat skin perforation.

The projectiles were chosen to give repeatable test projectiles, for their low densities compared to the majority of projectiles in the skin pentration/perofration data (Table 1) and determine if the sectional density is a key determining factor for the velocity required to perforate the skin for low-density projectiles.

The ballistic testing was initiated approximately 30 minutes after death. Prior to firing, the hairs covering the thighs were clipped to remove them. The impacts were conducted against the skin overlaying the muscle mass on the front and rear thighs.

The Honed Tube Pressure Housing (HTPH) weapon system was used with either 37 mm rechargeable compressed Airmunition cartridges, or 7.62x17 mmSR (0.32” ACP) blank pyrotechnic charges and smooth bore barrels for each fragment type. Details of the weapon system used are given in APPENDIX B as they are commmon to a number of different tests.

Impact velocities were recorded using MSI solid state velocity equipment [205] with a 1 m separation between the velocity heads. Impacts were viewed using a Photron SA3 high speed camera [206] at 10,000 frames per second.

Assessment of skin penetration and perforation was performed by visual inspection and probing with a rod after each shot.

DoP was measured by inserting a stiff rod down the resulting wound (in the perforating shots) until it contacted the back of the projectile. The DoPs for shots impacting bone were discounted.

The penetration and perforation V_{th}'s and V_{50}'s calculated by the average, ZMR, probit and extrapolated DoP methods were determined (where possible) as described in Section 3.2.3.

5.2.3 Results

In total, 94 shots were conducted, giving an average of 13 (and minimum of 10) shots for the seven projectile-target combinations. The projectile sectional density along with the skin perforation V_{50} determined by the probit method were chosen as metrics to evaluate the results, in line with Section 3.7 and Equation 1. The resulting skin perforation V_{50}s determined by the probit method with 95% confidence intervals are shown in Figure 12.

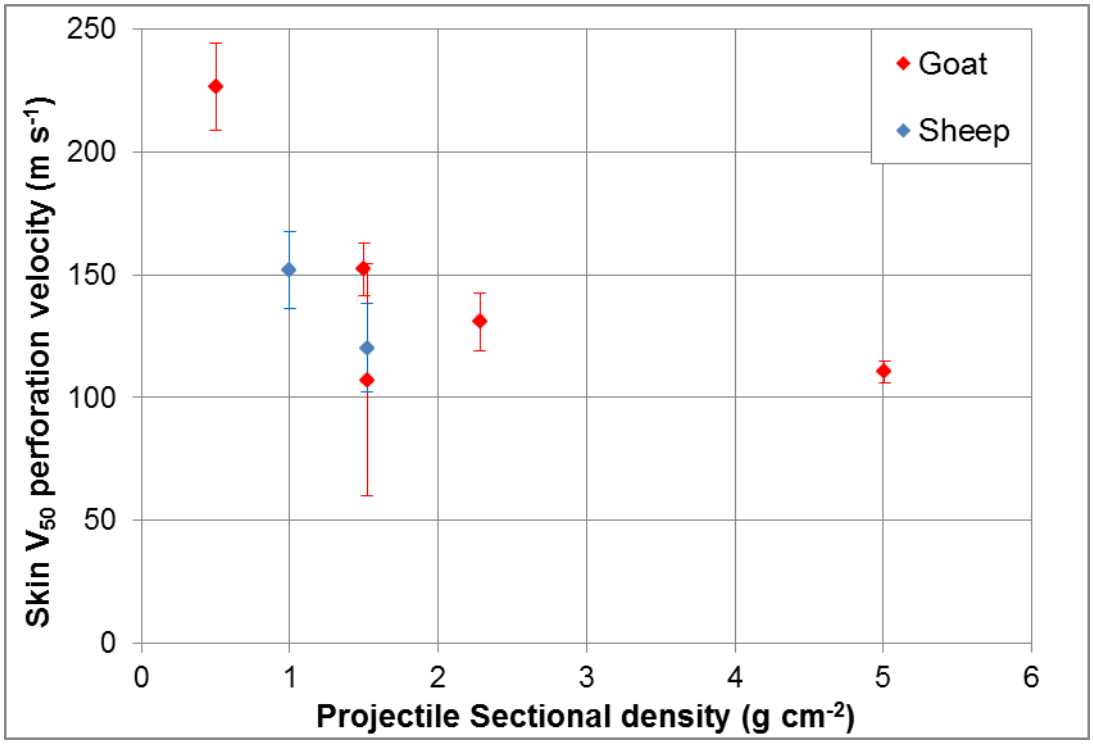

Figure 12: Low density projectile skin perforation V_{50}s for fresh goat and sheep thighs. Error bars show the 95% Confidence Interval (CI).

5.2.4 Discussion

The V_{50} results for the 6 mm ceramic sphere showed no significant difference at the 95% confidence level between the sheep and goat skin perforation V_{50} (p=0.276). This, along with the other V_{50} data for the sheep and goat in Figure 12 suggests a similar skin performance between the two animals.

This testing was limited to an individual target of each type. The review of the literature (Section 3) showed large potential variations between individuals, which the current testing is not able to account. Whilst unlikely, it may be that either or both of the targets were atypical in their skin properties (and therefore skin perforation response). Additional testing across multiple individuals of the same species would address this.

This data for the low density projectiles in sheep and goat skin was plotted against equivalent data for goat skin for a variety of other projectiles to determine if using sectional density as a predictor of skin perforation was valid for these fragment types. This comparison is shown in Figure 13.

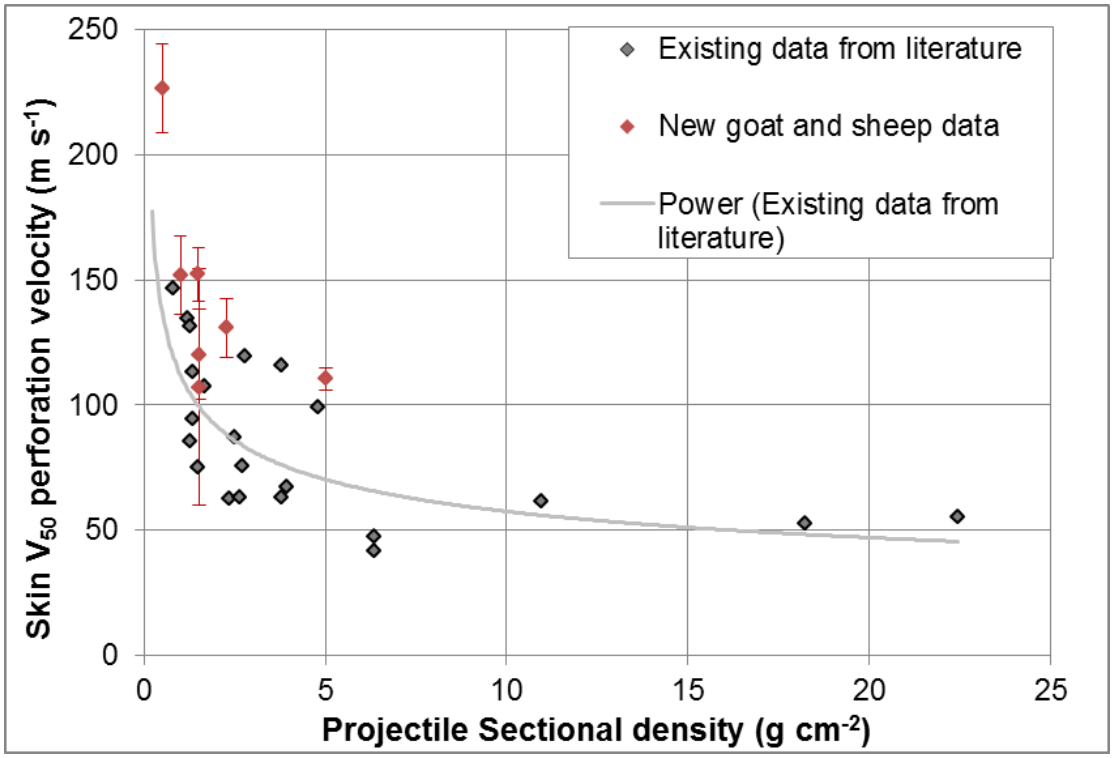

Figure 13: Skin perforation V_{50}s for fresh goat and sheep thighs compared to the existing data for goats (and mixed PMHS/goat targets) from the literature [43; 76; 79; 80].

Figure 13 shows the V_{50} (probit) data for the low density, non-metallic fragments aligned reasonably well with the previous data in the literature [43; 76; 79; 80] (perforation V_{50} by the average or extrapolation from DoP methods). It can be seen that it follows the same general trends for the relationship between V_{50} and sectional density, although the new data is offset to slightly higher V_{50} velocities.

An explanation for this velocity offset between the two datasets may be due to other target factors that were not accounted for in this comparison, such as target storage condition or backing type. In most cases the storage condition of the comparison data from the literature was not known [43; 76; 80]. The data from Reference [80] removed the skin and backed it by 20% gelatin at 10°C.

This new data helps populate the lower projectile density spectrum of the skin perforation dataset.

During this testing, the DoP data was recorded for those shots that perforated the skin. As the testing was optimised for skin perforation determination there were limited data points for each target and projectile. This DoP data is not particularly useful in isolation to produce a comparison between targets and/or projectiles, but can be combined with similar data and will be used later (Section 7) to aid comparison of penetration into different tissue and tissue simulants.

5.3 Presence of skin on penetration depth

5.3.1 Aim

The aim of this work was to examine the effect of the presence of skin on the subsequent penetration into the underlying muscle. Pig thighs, with and without the skin were impacted. The velocity required for perforation of the skin (for the legs with skin intact) or corresponding penetration of muscle tissue (for the legs with skin removed) was compared. Additionally the resulting depth of penetration was compared in each target for shots that penetrated into the muscle tissue.

5.3.2 Method

The rear legs were removed from recently killed large white pigs, following the conclusion of other (non-ballistic) trials. These were frozen (for approximately 2 months) and then thawed prior to the testing. Half of the legs had their skin surgically removed.

Three different projectiles, all 9 mm diameter but different densities were impacted against each of the bare and intact pig thighs at a range of velocities. Additional shots were planned with a 4.4 mm steel sphere to replicate the gelatin calibration procedure. Table 9 summarises the properties of the projectiles used. All impacts were conducted against the main muscle mass on the thighs.

Diameter (mm)	Material	Mass (g)
4.4	Steel	0.35
9.0	Glass	0.95
9.0	Ceramic	1.45
9.0	Steel	3.00

Table 9: Projectiles used for the comparison of the presence of skin on penetration depth.

Impact velocities were measured using Oehler Model 57 infrared ballistic screens [207] with 0.8 m separation, connected to a Nicolet Sigma 10 oscilloscope and impacts were viewed using a Photron SA3 high speed camera [206] at 10,000 frames per second.

DoP was measured by inserting a stiff rod down the resulting wound (in the penetrating shots) until it contacted the back of the projectile. The DoPs for shots impacting bone were discounted. If the projectile fully perforated the target and exited the other side, the thickness traversed was measured, but was not considered a valid DoP measurement.

Perforation of the skin was assessed for the legs with skin intact after each shot and corresponding penetration of muscle tissue was assessed for the legs with skin removed. The penetration or perforation V_{50}'s calculated by the average, probit and extrapolated DoP methods were determined (where possible).

5.3.3 Results and discussion

54 shots were completed against the targets. Of these, six shots fully perforated the target, three hit bone and three could not be positively located after the shot. One shot did not trigger the velocity equipment or HSV and no velocity was recorded. 50 shots were considered valid for skin perforation determinations[60] and 26 for non-zero DoP measurements.

[60] Shots that hit bone or fully perforated the target were still considered valid for skin perforation assessments.

The deepest DoP measured with the projectile remaining within the target was 140 mm. The first shot with the 4.4 mm steel sphere against the pig leg with skin removed fully perforated the target (62 mm thickness) at an impact velocity of 185 m s^{-1}. Due to this full perforation of the target, further shots with the 4.4 mm steel sphere were not conducted.

Exit velocities of fully perforating shots could not be measured from the HSV due to the setup being optimised to aid assessment of skin perforation.

Table 10 details the number of valid shots conducted against each target with each projectile.

	Number of valid shots for 'perforation' assessment			**Number of valid non-zero DoP shots**		
	9 mm glass	9 mm ceramic	9 mm steel	9 mm glass	9 mm ceramic	9 mm steel
Skin intact	13	7	7	4	4	2
Skin removed	7	7	9	5	6	5

Table 10: Number of valid shots conducted for each target and projectile combination.

Due to the limited data collected, the probit V_{50} could not be calculated for some of the conditions. However, the extrapolation from the DoP could be calculated in each case to enable comparisons. Probit V_{50}s are shown in Table 11 to validate the V_{50} by extrapolation from the DoP where it was possible to calculate both values, for the skin intact and removed.

	Skin removed		**Skin intact**	
Projectile	**Penetration V_{50} (probit) (m s^{-1})**	**Penetration V_{50} (extrapolation from DoP) (m s^{-1})**	**Perforation V_{50} (probit) (m s^{-1})**	**Perforation V_{50} (extrapolation from DoP) (m s^{-1})**
9 mm glass sphere	n/a	58.9	152.0	145.3
9 mm ceramic sphere	69.1	70.1	n/a	125.7
9 mm steel sphere	35.9	36.2	73.5	85.6

Table 11: V_{50} data for pig thigh impacts with the skin intact and removed

Impacts to the thighs with the skin removed showed significantly lower velocities required to penetrate into the muscle tissue, around 45% of the V_{50} for when the skin was intact (range was between 40% and 56%).

Figure 14 shows the DoP against velocity for all the valid shots conducted.

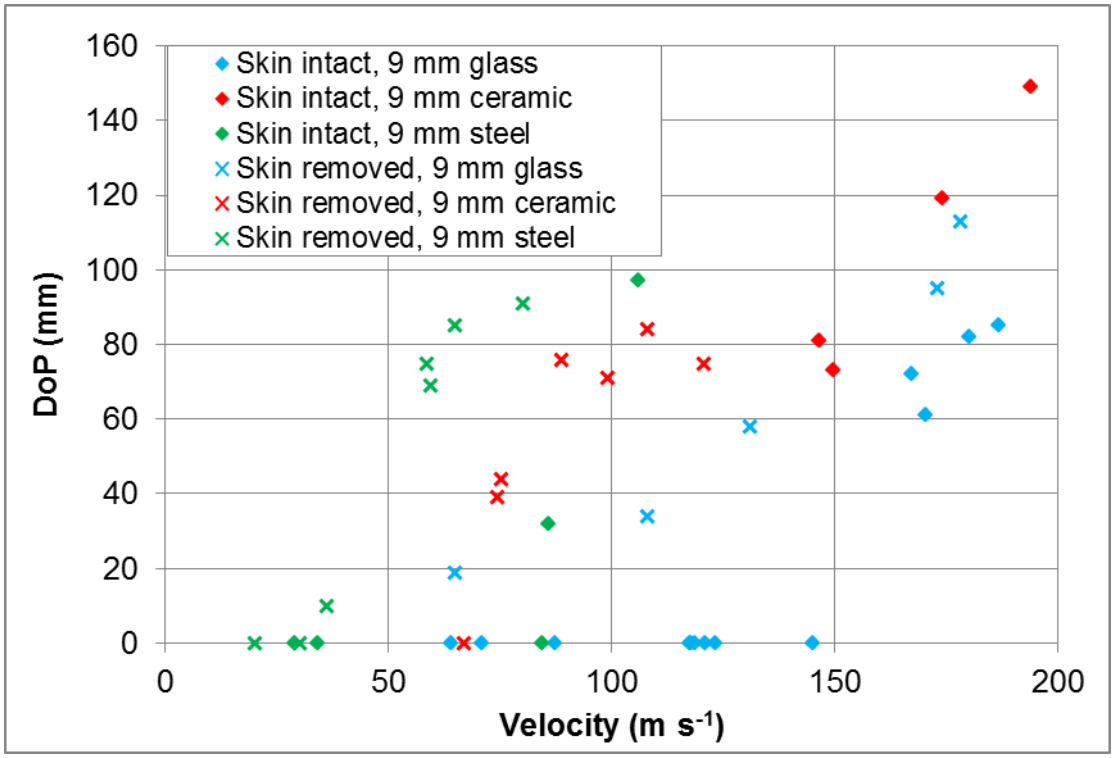

Figure 14: DoP for the 9 mm glass, ceramic and steel spheres into pig thigs with and without skin.

Figure 14 shows that when the projectile penetrated the target, a larger DoP resulted when the skin had been removed. However this comparison is based on limited data for each projectile.

In order to compare equivalent penetration into the targets across all the different projectiles, the DoP was normalised. This normalisation was achieved by dividing the DoP by the projectile diameter and then by the projectile density to give a 'normalised DoP over density' function as described in Section 4.

Normalising the DoP and combing the data provided a clearer and statistical comparison of this data; it has been replotted in Figure 15 with the data for each target type grouped. Linear fits were then applied to only the penetrating or

perforating shots (although the non-penetrating shots are still shown in Figure 15 for information only).

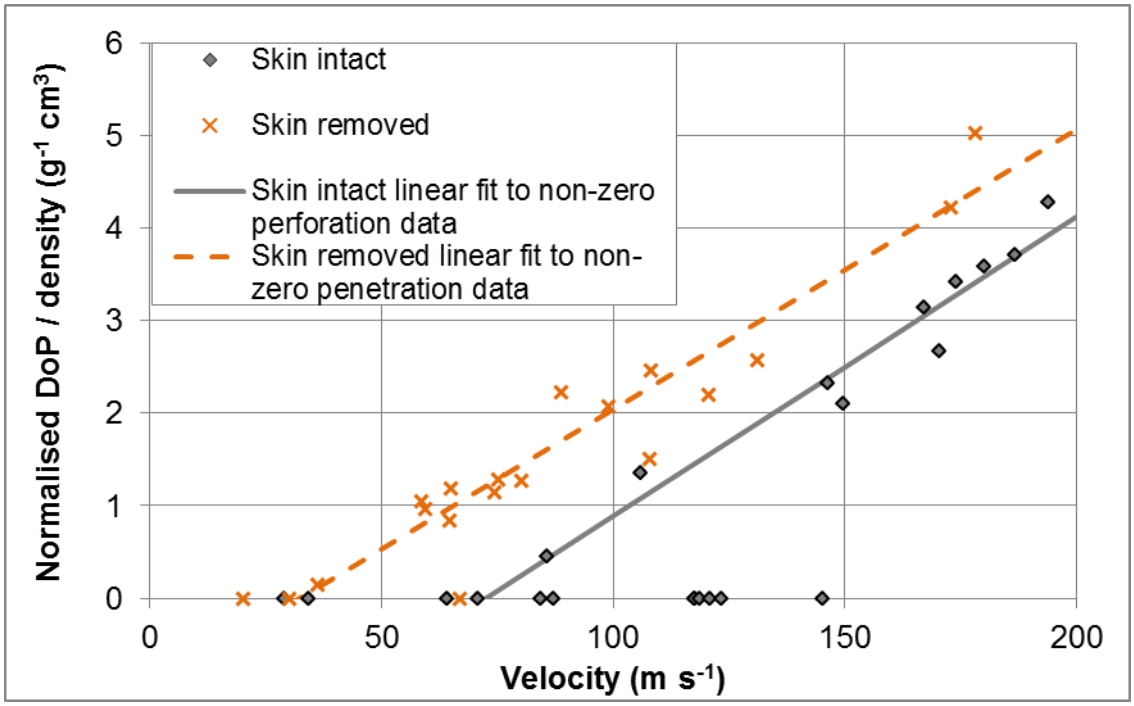

Figure 15: Combined projectile data for the normalised DoP over density into pig thigs with and without skin. All data shown, but fits are only applied to the non-zero DoP data.

The R^2 values for the linear fits shown in in Figure 15 to each of the skin intact and skin removed data (for non-zero DoPs) were 0.948 and 0.922 respectively.

A linear model fitted to the (non-zero) DoP data shown in Figure 15 showed a statistically significant difference at the 95% confidence level for the intercept, but not the gradient between the muscle tissue with skin intact and muscle tissue with skin removed ($p=0.02$ and $p>0.5$ respectively). This shows that the effect of the skin is significant on initiating penetration, but once a projectile has penetrated muscle tissue it follows the same penetration-velocity relationship, just offset according to the velocity required for skin perforation (or surface penetration).

Certainly at low velocities, at least up to 1.6 times the V_{50} (which was the highest velocity with a valid penetration depth in this testing) the skin provides a significant barrier to penetration by ballistic projectiles by reducing the resulting

penetration into muscle tissue. The performance and effect of a skin layer needs to be accounted for in injury models that evaluate the risks of projectiles in this velocity regime.

The conclusions drawn from this testing are based on limited data, for pig skin and at relatively low impact velocities. The influence of the effect of skin on the resulting penetration depth at higher velocities cannot be determined from this data (but is investigated later in Section 9.4 using a virtual model).

5.4 Effect of storage conditions on skin perforation

5.4.1 Background

In a lot of cases, ballistic testing cannot be conducted on fresh tissue. The ability to store tissue (either refrigerated or frozen and then thawed prior to testing) greatly expands the timeframe over which testing can be conducted since death. However, it is not well understood how these different storage conditions affect the skin perforation or muscle tissue penetration response. This is particularly relevant to PMHS testing where tissue storage is normally required.

5.4.2 Aim

A ballistic trial was conducted to determine if there was any significant change in the velocity required by Chisel Nosed (CN) FSPs to perforate the skin of a pig cadaver (and the subsequent depth of penetration into muscle tissue between targets) shot when stored at different conditions after death.

Tests were conducted using two sizes of projectile for three different storage conditions; within an hour after death, after storage at 1°C for 1 week, and after being frozen for 1 month then thawed.

5.4.3 Method

Three recently killed, whole large white pigs were supplied from a separate completed trial that otherwise have been disposed. In addition, there was one supplied a month prior to the trial, which was frozen. They were all females weighing between 55 and 66 kg.

To investigate the effects of storage time and condition on the post mortem targets, three groups of targets with different storage conditions and durations (after death) were defined:

a) Fresh – ballistic testing conducted as soon as practical after death. This was between 20 minutes to 1 hour.

b) Refrigerated – ballistic testing conducted after being refrigerated for 7 days in a non-porous “body bag” at 1°C in a conditioning cabinet.

c) Frozen/thawed storage – ballistic testing conducted after thawing of the target, with it having been frozen as soon as practical after death at -24°C for approximately 1 month.

The refrigerated and frozen-thawed targets were allowed to warm to laboratory temperature (approximately 16°C) prior to testing to avoid any potential effects of the temperature of the tissue influencing the outcomes. Fresh targets were tested as soon as practical after culling and although not measured, would have been above laboratory temperature.

The impact locations used were the muscle mass of the front and rear thighs. To minimise any potential influence from inter and intra-target variability, the same targets were used for the fresh and refrigerated conditions. For the fresh condition, impacts were conducted against the right side of the target, with the corresponding firings for comparison on the refrigerated storage condition completed against the matching location on the left side.

The projectiles used for this testing were the 0.49 g and 1.1 g steel CN FSPs, to Reference [208].

Velocities were measured using 3 sets of the model 57 infra-red Oehler velocity screens [207], with a 0.5 m separation between each pair, connected to an AMOtronics Saturn System 120 series oscilloscope sampling at 3 MHz. The final screen was approximately 0.5 m from the target. No correction for velocity loss due to drag prior to impact was made. Each velocity measurement was saved and incorporated a timestamp for each firing. This timestamp was used as a

reference for the timings throughout the trial. Impacts were viewed using a Phantom Miro M310 high speed camera [209] at 18,000 frames per second and 512x320 pixels.

A minimum of 20 shots were conducted to obtain a V_{50} for each target and projectile combination. These shots were conducted such that one set of 10 shots were performed against one region of one animal. Another 10 shots were then performed on the same region of a different animal with the same storage conditions. This was to minimise time taken to complete the testing against an individual target (and minimise potential aging effects during the testing), as well as average out some of the inter-target variability. The V_{50} shots that perforated the skin also allowed a DoP measurement to facilitate the comparison between storage conditions.

A minimum of 5 shots were also performed at equivalent velocities for each of the projectiles into the fresh and stored targets (nominal 170 m s^{-1} for the 0.49 g FSP and 210 m s^{-1} for the 1.1 g FSP) to compare DoP. Any shots impacting bone were removed from the DoP analysis.

The timings (to the nearest minute) after death and removal from storage for each target are detailed in Table 12.

Target	Storage condition	Time after death into storage (hh:mm)	Duration of storage (hh:mm)	Time after removal from storage to firings commenced (hh:mm)	Subcutaneous temperature at start of firing (°C)	Time after death firing commenced (hh:mm)	Duration of firings (hh:mm)	Time after death firing completed (hh:mm)
1	Fresh	n/a	n/a	n/a	n/a	01:01	03:23	04:24
2	Fresh	n/a	n/a	n/a	n/a	00:20	00:44	01:04
3	Fresh	n/a	n/a	n/a	n/a	00:20	02:54	03:14
1	Refrigerated	04:40	159:59	00:45	Not measured	165:24	03:25	168:49
2	Refrigerated	23:20[61]	139:04	04:27	15.2	166:51	00:56	167:47
3	Refrigerated	04:11	139:16	19:46	15.9	163:13	03:44	166:57
4	Frozen	00:30	843:53	40:20	13.4	884:43	01:37	886:20

Table 12: Storage durations and timings of firings for each target

[61] Of which 20 hours was in a turned off, but chilled (at 1°C) freezer before storage.

5.4.4 Results

A total of 129 fair impacts were conducted across all target types and projectiles. As there was only 1 pig available for the frozen-thawed target, sufficient space was available for only the 1.1 g FSP skin perforation assessment. The skin perforation V_{50} results are given in Table 13 for each target-projectile combination assessed.

Storage Condition	**Mass (g)**	**Sectional density (g cm^{-2})**	**V_{50} (probit) (m s^{-1})**	**± 95% confidence interval (m s^{-1})**	**Percentage difference to fresh (%)**
Fresh	0.49	3.78	140.2	7.0	n/a
Refrigerated	0.49	3.78	127.2	4.3	-9.3
Fresh	1.10	4.80	115.0	12.0	n/a
Refrigerated	1.10	4.80	112.0	17.6	-2.6
Frozen-thawed	1.10	4.80	127.2	8.2	+10.6

Table 13: Skin perforation V_{50}'s for the different projectile and staorge combinations.

The 0.49 g CN FSP had a statistically significant lower skin perforation V_{50} for the refrigerated target than the fresh ($p<0.01$). This was approximately a 10% difference. There was no statistically significant difference at the 95% confidence level for the skin perforation V_{50} between each of the storage conditions for the 1.1g CN FSP.

The percentage differences in skin perforation V_{50} compared to the fresh condition are shown in Figure 16.

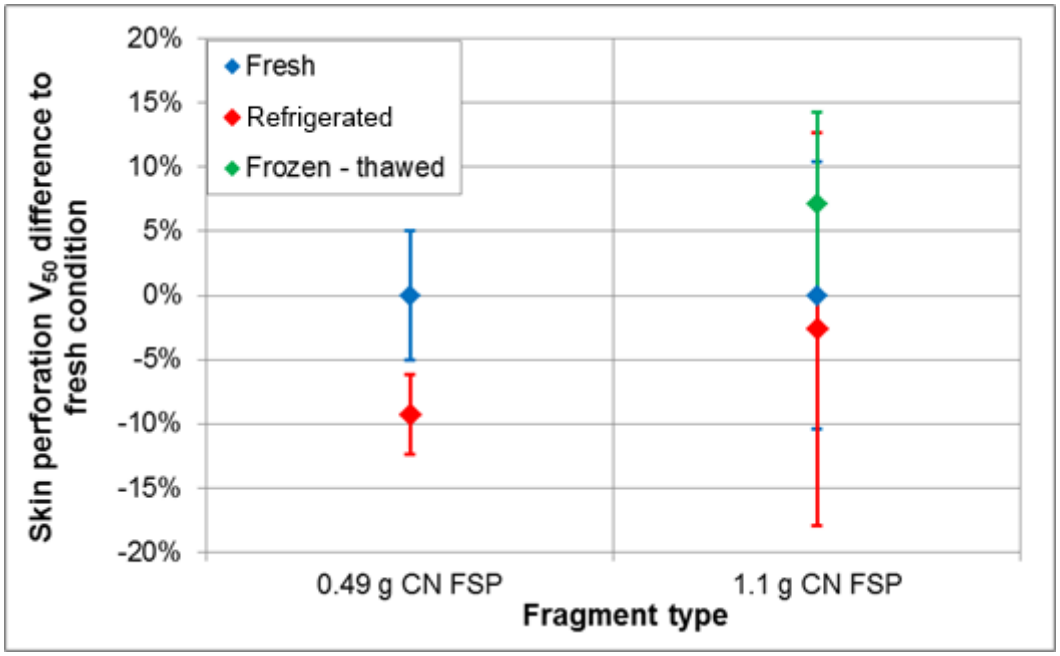

Figure 16: Percentage difference in skin perforation V_{50} compared to the fresh condition. Error bars are the 95% confidence intervals.

Figure 17 shows the comparison of the probability of skin perforation for the 1.1 g CN FSP into the targets with the three different storage conditions.

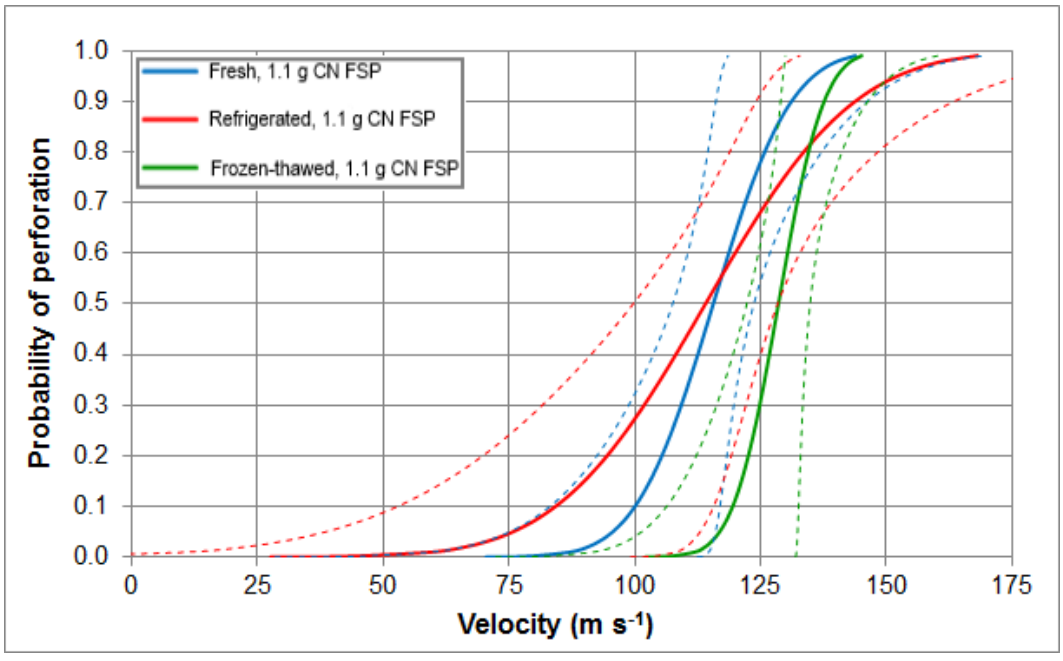

Figure 17: Comparison of the probit curves showing the probability of skin perforation for the 1.1 g CN FSP into the targets with the three different storage conditions. Dashed lines show the 95% confidence interval of the solid curves.

Figure 17 highlights that there are no significant differences present at the 50% probability of perforation, as well as across the other probability levels (indicated by the overlapping 95% confidence intervals on each curve).

For the 1.1 g CN FSP, the slope of the probit curve for the fresh target was significantly different to the refrigerated target, even though the V_{50} values showed no differences ($p<<0.01$). The slope of the probit curve for the fresh target showed no significant difference to the frozen-thawed target ($p=0.10$).

The mean values of the (minimum of) 5 shots performed at equivalent velocities for each FSP are shown in Figure 18 for each storage condition tested.

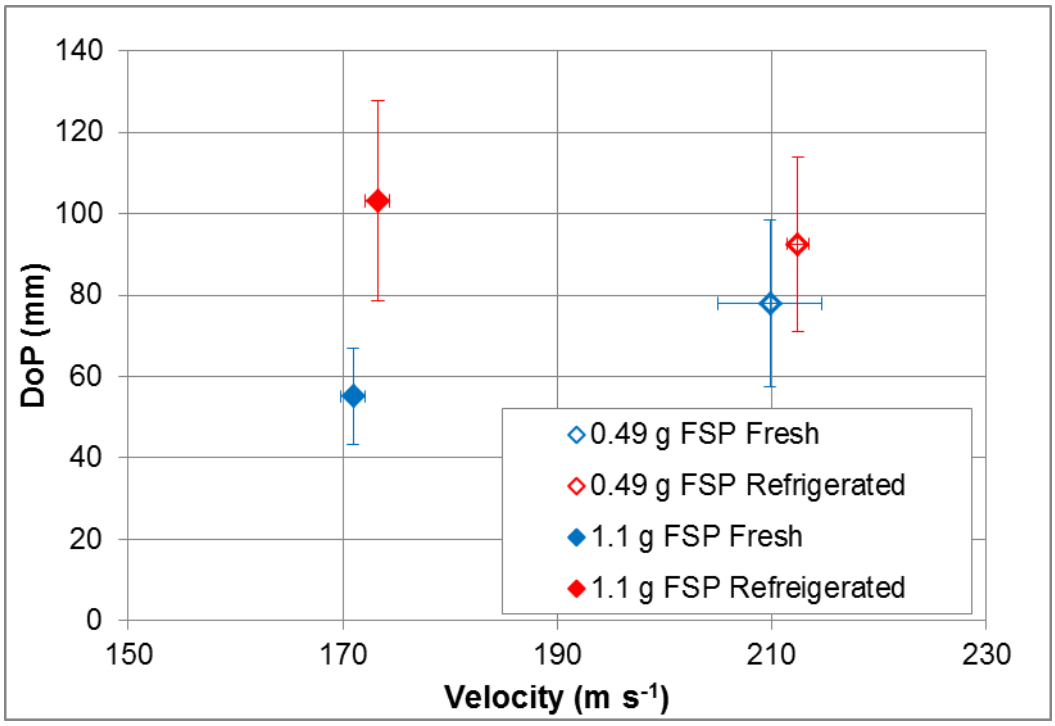

Figure 18: Mean DoP and velocity for each group of fragments and the fresh and refrigerated targets. Error bars show the 95% confidence interval on the mean.

There was no significant difference in the DoP at the 95% confidence level between fresh and refrigerated tissue for the 0.49g CN FSP ($p>0.5$).

The refrigerated tissue was penetrated to significantly greater depths with the 1.1 g CN FSP than the fresh tissue at equivalent velocities ($p<0.01$), average of 52% increase.

This is supported by the comparison of the penetration response with varying velocity for the different projectiles and storage conditions. Figure 19 shows the penetration response for all the 1.1 g CN FSP impacts into the targets for the three different storage conditions. Shots below a certain velocity will always have a zero penetration depth and a non-linear least squares regression model for extrapolation from the DoP equation[62] was used to fit the data.

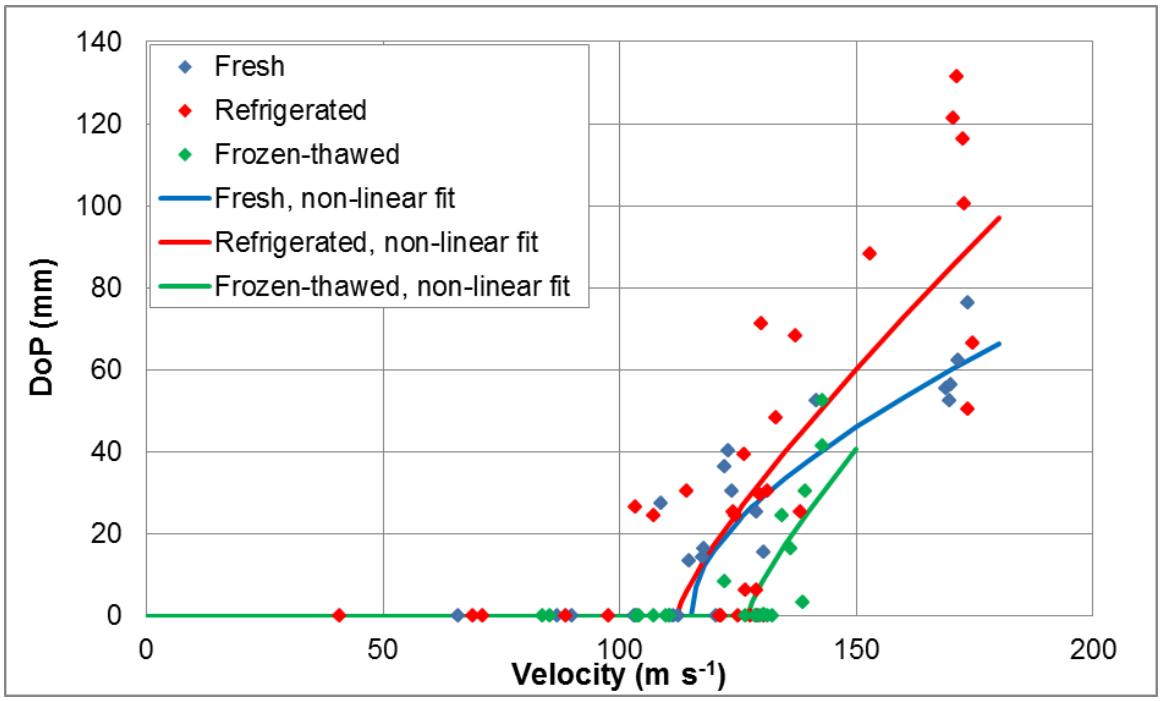

Figure 19: Normalised DoP over density against velocity for the 1.1 g CN FSP into the fresh, refrigerated and frozen-thawed pig tissue.

Figure 19 indicates that the refrigerated targets are penetrated to a greater extent than the fresh target at equivalent velocities for the 1.1 g CN FSP. Due to the limited data and type of fit applied, meaningful statistical comparisons of these fits cannot be conducted.

The non-zero penetration data for the frozen-thawed targets was over a much more limited velocity range than the other groups. From this limited data, once

[62] See Section 9.4, Equation 23 for an explanation and detail of this non-linear least squares regression model for extrapolation from DoP data.

the skin has been perforated, the penetration response of the frozen-thawed muscle tissue appears similar to the fresh and refrigerated targets.

The general indication that refrigerated tissue was penetrated to a greater extent than fresh tissue was also apparent within the data for the 0.49 g CN FSP, shown in Figure 20 (similarly no meaningful statistical comparisons can be made).

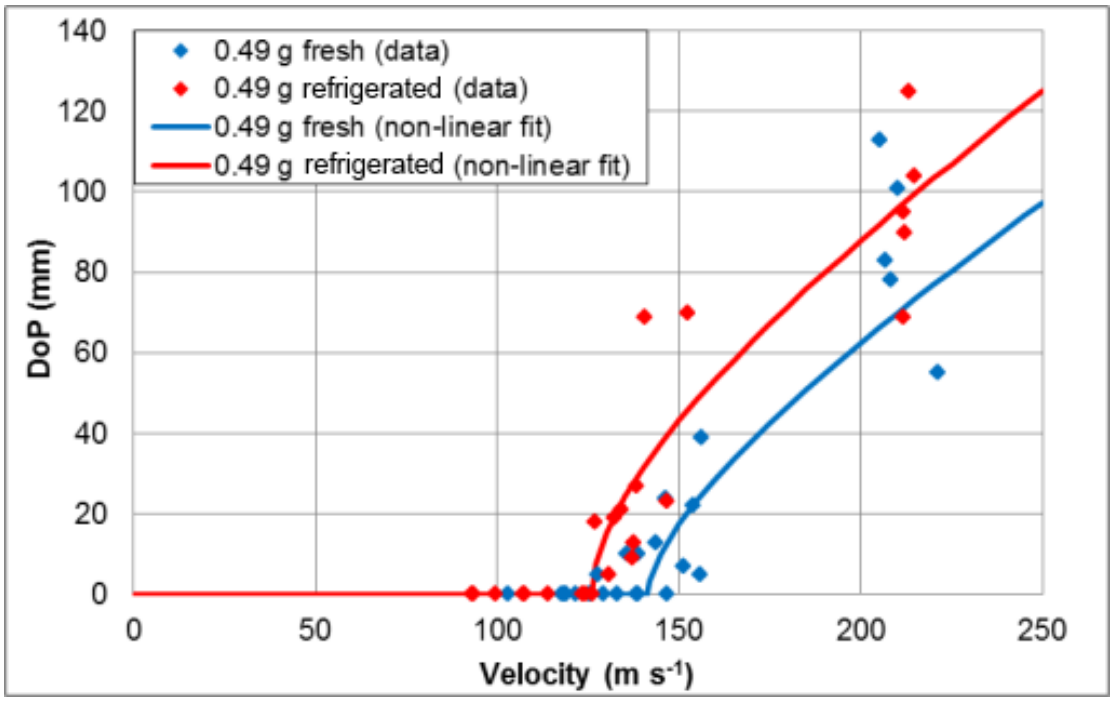

Figure 20: Normalised DoP over density against velocity for the 0.49 g CN FSP into the fresh and refrigerated pig tissue.

In order to conduct a statistical comparison on the penetration into the targets for the different storage conditions, the non-zero penetration data for the two projectiles were pooled. The DoP was converted into the normalised DoP over density function (process described in Section 4). In order to also account for the different skin perforation V_{50} for the different projectiles and storage conditions, the impact velocity (V_s) was scaled by the V_{50}. This effectively doubled the available data on which to make these comparisons due to the two different projectiles and removed influence of the skin response from the comparison. This gave 30 data points for the fresh condition, 37 for refrigerated and 8 for the frozen-thawed tissue.

Linear fits were applied to the data, with intercepts fixed to go through $V_s/V_{50}=1$ at normalised DoP over density=0 (i.e. forced to give a zero penetration at $V_s=V_{50}$). Linear fits were deemed suitable over this limited velocity range and are shown in Figure 21 with the combined data for each of the different storage conditions.

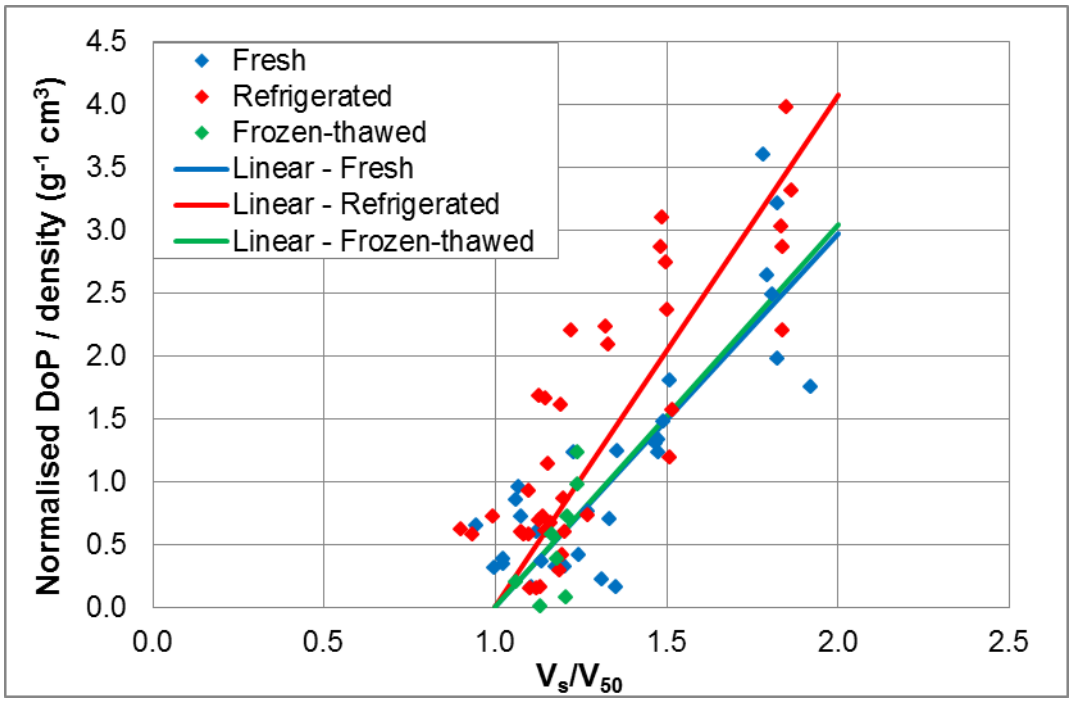

Figure 21: Normalised DoP over density against V_s/V_{50} for the different storage conditions with data for the projectiles pooled.[63]

Figure 21 indicates that the refrigerated targets are penetrated more easily at equivalent velocities to the fresh targets once the skin has been perforated. This is supported by the linear fits: there was a statistically significant difference at the 95% confidence level in the gradient of the linear fits between the fresh and refrigerated group ($P<0.01$). There was no statistically significant difference at the 95% confidence level between the gradients of the linear fits for either the fresh and frozen-thawed or refrigerated and frozen-thawed groups ($p>0.5$ for both).

[63] The linear fit to the frozen-thawed data has been extrapolated past the limits of the data to show the predicted response in comparison to the other storage conditions.

5.4.5 Discussion

The data for the fresh and refrigerated targets were directly comparable as impacts were conducted on matched pairs of legs with the same number of shots against each individual target (i.e. they have the same baseline performance). The data for the frozen-thawed target was on a different individual. It is not known if any potential variation (outside of the storage conditions) between the individual targets may have influenced the response when comparing to the frozen-thawed target. Without testing on additional targets, or conducting the testing on the target fresh, prior to freezing, any inter-individual variation cannot be accounted for.

Rigor mortis was not controlled for during this testing and may have affected the fresh target results. This was not considered within the analysis conducted for this thesis, although all shots conducted were timestamped with reference to the target time of death (the presence/absence of rigor mortis for each shot was not recorded).

The overall conclusions are that (pig) cadavers stored refrigerated for 1 week prior to testing may result in significantly different outcome in terms of a lower skin perforation V_{50} as well as deeper penetration at equivalent velocities to a cadaver tested straight after death. However, these differences could only be statistically observed in half the testing performed[64], or when all data was pooled. The data indicates that storing the targets refrigerated for a week is likely to increase the variability in the response (shallower gradient on the probability of perforation against velocity curve, Figure 17 and lower R^2 value for the linear fit in Figure 21). However, as commonly observed with biological material, even the data for the fresh target showed considerable variability in the penetration response.

[64] The 0.49 g FSP showed statistical difference in skin V_{50} between the fresh and refrigerated conditions, but not in the DoP. The 1.1 g FSP showed statistical difference in DoP between the fresh and refrigerated conditions, but not in the skin V_{50}.

The data for the frozen target was more limited due to only a single target being available for the frozen condition. From the available data, there were no observable differences in the penetration response for the frozen-thawed tissue compared to the other tissue types. Additional data over a wider velocity range may provide more insight into the effect of this storage condition on the penetration response compared to fresh tissue.

Consideration also needs to be given for potential differences in penetration response between a live and recently killed target.

5.5 Comparison of skin perforation and DoP in different targets

5.5.1 Aim

It often not possible to use PMHS for ballistic work and animals are frequently used instead. Goat skin was previously shown to have comparable ballistic performance to PMHS [76; 79] and sheep have been used in other wound ballistic work [78]. The aim of this study was to determine the difference in skin perforation and the resulting DoP into the underlying muscle for PMHS, pig, goat and sheep using 3 steel projectiles.

5.5.2 Method

Three projectiles; the 0.16 g and 0.49 g cylinder FSPs [210] and the 1.1 g CN cylinder FSP [208; 210] shown in Figure 22 were chosen for this comparison due to the existing data for these targets.

Figure 22: Photograph of the FSPs used for this testing. Left to right are the 1.10 g CN FSP (unskirted), 0.49 g cylinder FSP and the 0.16 g cylinder FSP.

New testing was not performed for this comparison. Instead existing data was used and is detailed below:

- All the goat data (for each of the 3 projectiles) was from Reference [79]. This data was for a recently killed target, impacted on the thigh.
- The sheep testing was conducted alongside that described in Reference [79], although not published. The sheep impacts were for a recently killed target, impacted on the thigh, performed using the same methods as for the goat testing [79].
- The PMHS testing was conducted by Wayne State University (WSU) [63] using the 0.49 g cylinder FSP and the 1.1 g CN FSP [208; 210]. A brief overview of this testing are outlined in Section 3.3.1. It should be noted that this testing was performed on the neck region of targets that had been refrigerated (for a maximum of 14 days).
- All the data for the 0.16 g FSP for the pig was from Reference [88]. Data for the 1.1 g CN FSP was also taken from Reference [88] and combined with additional data from Section 5.4. The testing in Reference [88] was for a recently killed pig with a mix of impacts to the neck and thigh regions.

For each study specified above (References [63; 79; 88]), the raw data was obtained (velocity, skin penetration or perforation outcome and resulting DoP) for each shot and the V_{50}s were recaculated in line with the descriptions in Section 3.2.3.

- The remaining pig data for the 0.49 g CN FSP and 1.1 g CN FSP was that generated in Section 5.4, using only the data for fresh storage condition. Instead of the 0.49 g cylinder FSP, this data was for the 0.49 g CN FSP and was included despite being a different geometry used for the other targets. The 1.1 g CN FSP data was available as a direct comparison.

5.5.3 Results

Due to limited data, the only V_{50} calculation method that was able to be calculated consistently was the perforation V_{50} by the average method. An exception to this was the 0.16 g FSP for the pig, which was based on extrapolation from the DoP data due to no non-perforating shots. Table 14 summarises the results.

Projectile	Perforation V_{50}, average method (m s^{-1})			
	PMHS (neck)	Goat (leg)	Sheep (leg)	Pig (leg & neck)
0.16 g FSP	N/A	119.7	135.7	159.6 [65]
0.49 g FSP	99.4	115.8	96.2	140.3 [66]
1.10 g CN FSP	96.2	99.1	101.8	114.0

Table 14: Skin perforation V_{50} (by the average method) for different target types with the three FSPs. Data from References [63; 79; 88] and Section 5.4.

The results in Table 14 are shown in Figure 23 in terms of the percentage difference to PMHS skin (or sheep skin for the 0.16 g FSP as no reference value for PMHS skin was available).

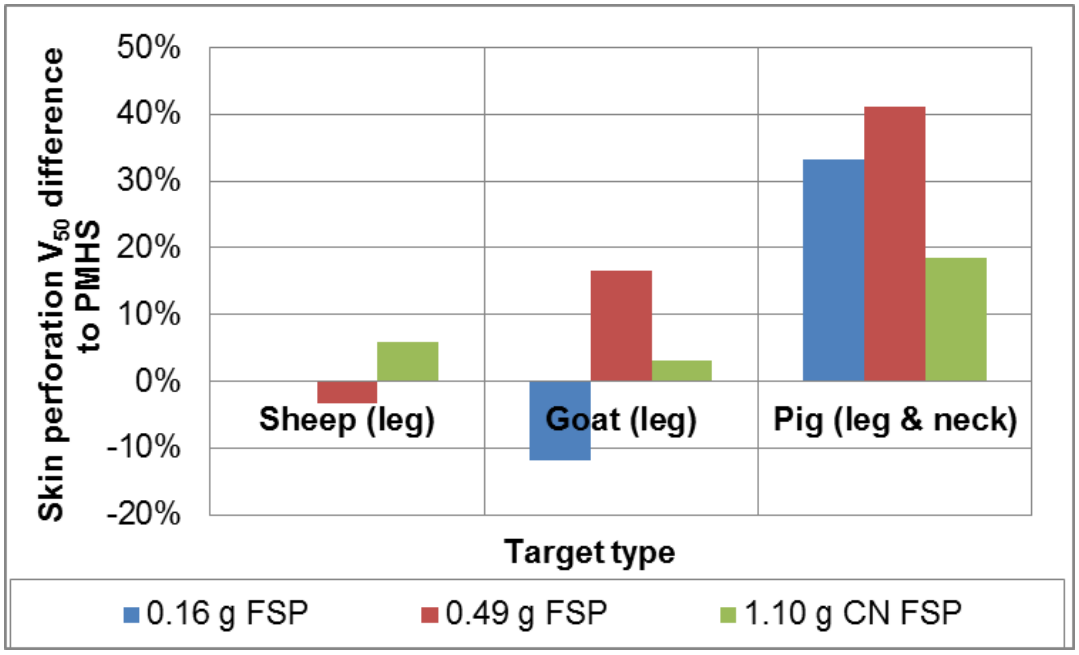

Figure 23: Skin perforation V_{50} percentage difference to PMHS skin (or sheep skin for the 0.16 g FSP). Data from References [63; 79; 88] and Section 5.4.

The data in Figure 23 showed that the goat skin was an average of +10% of the PMHS performance for the 2 projectiles allowing a direct comparison. Sheep skin was an average of +2% of the PMHS performance and pig skin was an average

[65] Different calculation method due to limited data (via extrapolation from DoP).
[66] Data for 0.49 g CN FSP instead of 0.49 g plain cylinder FSP.

of +30% of the PMHS performance. This indicates that the best animal model (of those assessed) for comparison to PMHS skin performance is sheep, followed by goat. Pigs provide a significantly greater resistance to skin perforation compared to PMHS, as have previously indicated [69].

Error bars or confidence intervals in the skin perforation V_{50}s were not given due to the calculation by the average method to maintain consistency across all the targets.

The normalised DoP over density function (to allow comparison across the different projectiles used) was compared across the different targets and is shown in Figure 24.

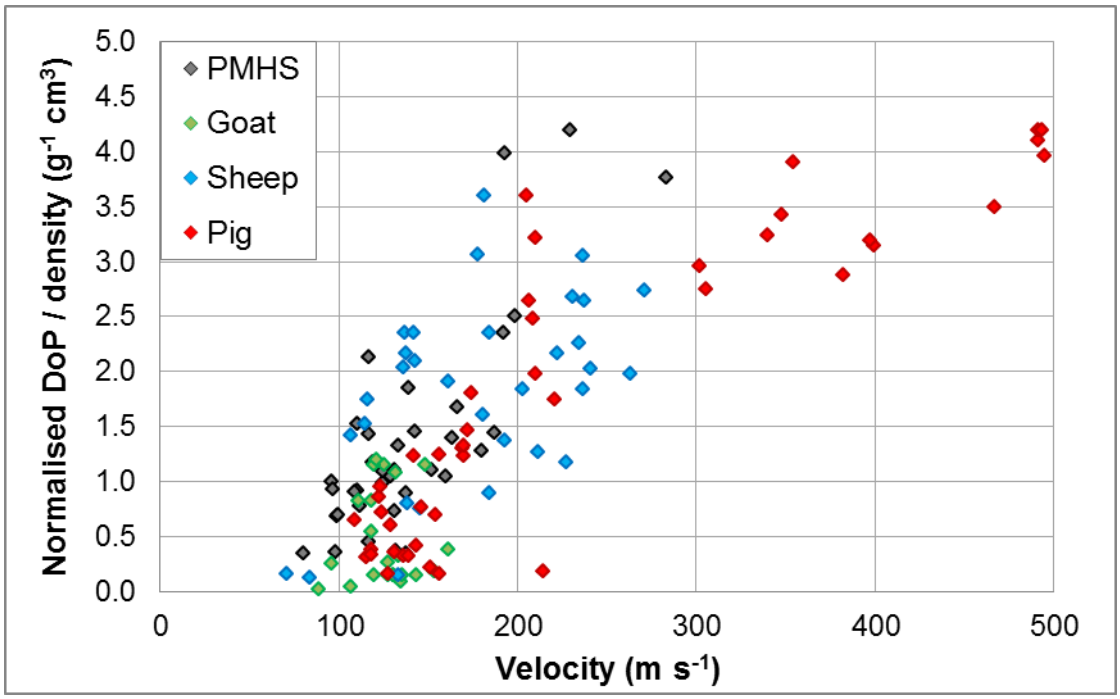

Figure 24: Normalised DoP over density in the different targets for the shots that perforated the skin. Data from References [63; 79; 88] and Section 5.4.

Figure 24 shows that once the skin has been perforated, the penetration response of the muscle tissue across the different targets was very similar. No clear trends between the different targets can be seen, caveated by the goat data limited to velocities close to the skin V_{50} and the outlier point for the pig may be

partially due to the comparatively higher skin V_{50} (214.5 m s^{-1} with the 0.16 g FSP).

Evident across all the targets in Figure 24 is the high scatter in the penetration response, due to variations in the biological tissues (although a small portion of this variation is likely a result of the use of the normalised DoP over density function).

5.5.4 Discussion

All the targets were in a fresh condition, apart from the PMHS which was refrigerated. As discussed in Section 5.4 this may influence the results obtained, but likely to increase the variability rather than raise or lower the skin V_{50}.

Additionally the sheep and goat data was for impacts to the thigh. The PMHS was for impacts to the neck and the pig was a mix of thigh and neck data.

The skin perforation V_{50}s for the 0.16 g and 0.49 g FSP both showed differences between sheep and the goat, although one result for the sheep was higher and one lower than the goat. The data for the 1.1 g FSP showed minimal differences between the sheep and goat skin performance (<3%).

Based on the skin perforation response, the target comparison can be summarised as: sheep (thigh) ≈ goat (thigh) ≈ PMHS (neck) ≠ pig (thigh and neck).

A limitation for the sheep and goat data was due to the fact that only 1 animal of each type was used. For the pigs and PMHS, multiple targets were used to generate the data. The average age of the PMHS from Reference [63] was 58 and targets were stored refrigerated for up to 14 days prior to testing. This may not have provided a good a representation of the (live) human population to be modelled.

The 0.49 g FSP was a different geometry for the pig testing compared to the other targets (chisel-nosed instead of plain cylinder). It would be expected that the chisel-nosed cylinder would have a lower skin perforation V_{50} compared to the blunt cylinder. The fact that the pig skin shows a much higher V_{50} for the 0.49 g

projectile in spite of this reinforces the conclusion that pig skin is more resistant to perforation compared to PMHS skin.

Comparisons in this study were all direct, using the same (or very similar) projectiles. This limits the observations made to the conditions used in the testing. This limitation is addressed for the skin performance in Section 6.1.5 using all the collated skin perforation data for a wide variety of projectiles and target conditions.

The DoP data for the pig (although not broken down into specific body regions in Figure 24) indicated that the muscle in the neck gave a very similar penetration response to the thigh.

6 Empirical equations for skin perforation and eye penetration

6.1 Development of an empirical equation for skin perforation

6.1.1 Requirement

Whilst multiple attempts to produce predictive equations to address the velocity required to penetrate or perforate the skin have been made (Section 3.7), none have accounted for the different factors deemed to be (potentially) significant from the review of the literature.

6.1.2 Simple empirical equation for skin perforation

The majority of references that developed an empirical equation for the V_{th} or V_{50} have based it on the form given in Equation 1 with appropriate constants calculated for each specific case (i.e. intact refrigerated pig skin on the thigh). On a case by case basis Equation 1 can give a good fit to the experimental data.

In order to describe each of the different significant target and projectile factors, multiple equations of the form given in Equation 1 are required. Constants *a* and *b* are specific to a single scenario. If an equation were required to predict the result for a slightly different scenario (such as a different body region or target type) different parameters would be required. This is the approach that has generally been taken previously in the literature [45; 55; 65; 67-69; 71; 75; 76; 80; 81; 84; 100; 104; 105], but it severely limits the applicability of the equation or loses accuracy due to generalisation.

Fitting of Equation 1 to all the data collected is also problematic as much of the data is not directly comparable. Instead, it either needs to be fitted to specific conditions, or the equation expanded to enable it to account for different conditions. To demonstrate this issue, all the available skin penetration and perforation data was combined and plotted together in Figure 25.

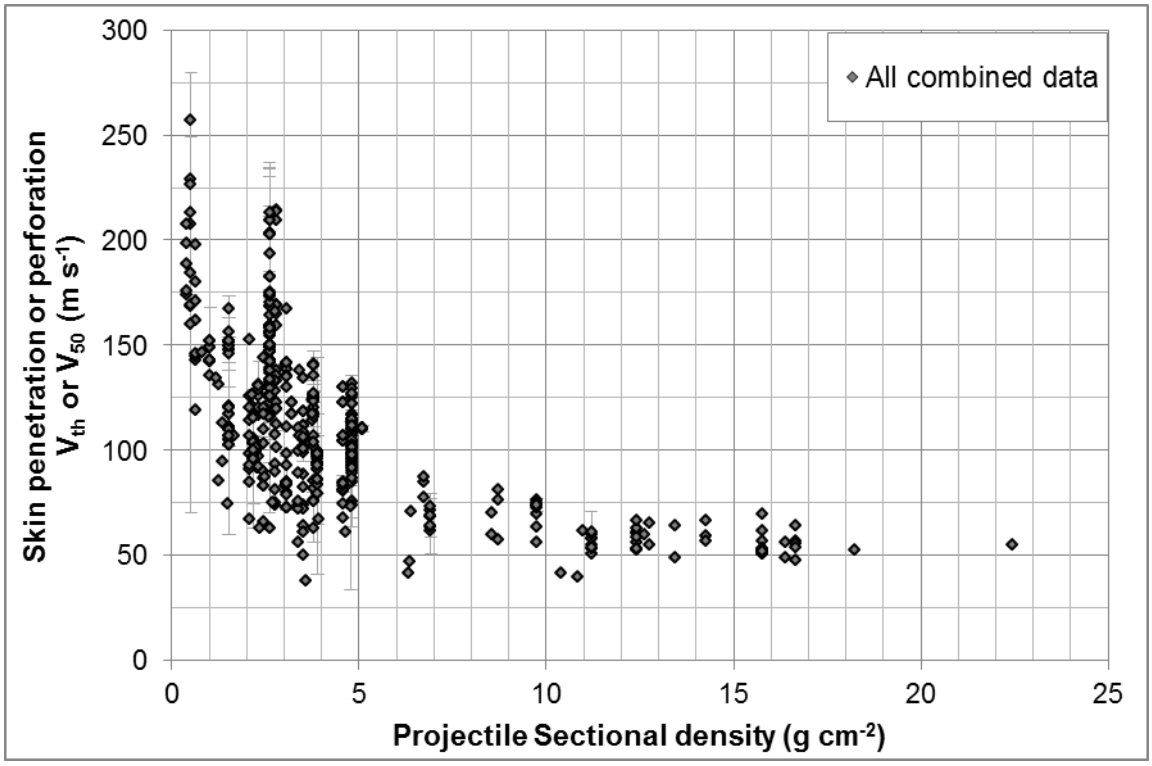

Figure 25: All combined skin penetration and perforation data (V_{th} and V_{50}) for all target and projectile conditions (n=521). Data from References [43; 45; 55-64; 66; 68; 71; 74-76; 79; 83-88; 90]) and the original data generated in Section 5. Error bars show 95% CI on V_{50} probit data.

Figure 25 shows a large degree of scatter in the individual data, considered to be from the mixture of different penetration and perforation calculation methods, target types, target body regions, backing methods, storage conditions and projectile geometries. Data at equivalent projectile sectional densities showed differences in the skin penetration or perforation velocity in excess of 100%.

For this reason, a single, simple empirical equation for skin penetration or perforation was not calculated.

6.1.3 Expanded empirical equation for skin perforation

Generating all the possible combinations of parameters *a* and *b* for Equation 1 would be a tedious process given the number of different combinations of target types and conditions within the data collated. It would also be extremely

challenging to validate each separate equation over the range of conditions of interest.

Even though only a handful of conditions are likely to be useful, the corresponding values may not be able to be directly calculated as there may be insufficient data from these scenarios on which to generate the parameters.

Instead of multiple different equations or a single equation forced to generalise over all target factors, an expanded empirical equation has been generated that can account for all the different projectile and target factors of interest. It is relevant to a wide range of different scenarios and selection of the appropriate parameter values make it specific to that scenario. The benefit of this approach is that predictions can be made for scenarios where there is no existing data, by extrapolation using the entire dataset.

This expanded equation has the same form as Equation 1, but parameters *a* and *b* expanded (denoted by ***a'*** and ***b'***) to describe the different conditions. This is given as Equation 5, Equation 6 and Equation 7 below:

$$v_{50} = a' S^{b'}$$

Equation 5: initial version of the expanded empirical skin perforation equation

$$a' = a(\alpha \gamma_a \delta_a \varepsilon_a \kappa_a \eta_a)$$

Equation 6: Parameter *a'* for expanded empirical skin perforation equation

$$b' = b(\beta \gamma_b \delta_b \varepsilon_b \kappa_b \eta_b)$$

Equation 7: Parameter *b'* for expanded empirical skin perforation equation

Where:

a and *b* are constants as for Equation 1

α and *β* = parameters dependent on penetration/perforation and prediction method; V_{th}, V_{50} by average method, V_{50} by probit method etc.

γ_a and γ_b =parameters dependent on target type; PMHS, pig, goat etc.

δ_a and δ_b = parameters dependent on impact location, e.g. thigh, back etc.

ε_a and ε_b = parameters dependent on if the skin is intact, isolated-backed (and backing type) or completely isolated

κ_a and κ_b = parameters dependent on storage condition, e.g. fresh, refrigerated, frozen

η_a and η_b = parameters dependent projectile type; blunt, pointed or rounded. Projectiles were considered blunt if they had:

- An impact face ≥75% of their full cross sectional area, or
- A radius of curvature > projectile radius

Although the effect of storage condition was deemed to be a less significant factor from the review of the literature, the ability to include these parameters in the expanded model has been retained. Based on the parameters generated, it will be evaluated as to the relative influence (and requirement for inclusion in the equation).

6.1.4 Parameter generation for the expanded empirical equation for skin perforation

To calculate the parameters for the different prediction methods, the skin penetration or perforation velocity by each method was compared to the prediction from the skin perforation V_{50} by the probit method. It was found that there was no correlation in sectional density between the differences in the different V_{50} calculation methods compared to the probit method for skin perforation[67]. The different prediction methods were scaled relative to the skin perforation V_{50} by the probit method using only the parameter α (with β=1).

A least squares regression was subsequently run on the target and projectile parameters across all skin penetration and perforation prediction methods. This allowed the least squares regression to be performed across 521 data points

[67] The result for each prediction method from each test was divided by that for the skin perforation V_{50} by the probit method (where this had been calculated). The resulting ratios were plotted against projectile sectional density, with linear fits giving R^2 values between 0.002 and 0.072 for each of the other V_{th} or V_{50} prediction methods.

rather than the 142 individual tests, as multiple measures for the different prediction methods could be calculated in some cases. The data used is summarised in Table 1 (from References [43; 45; 55-64; 66; 68; 71; 74-76; 79; 83-88; 90]) [68] and the original data generated in Section 5.

A limitation of this approach is that it assumes that differences in the skin at different body regions (i.e. due to mechanical properties that may affect ballistic response, as well as thickness) are comparable both at different specific places within the general location and across the different species, e.g. the difference between the thigh and abdomen response is comparable between PMHS and pig.

Where combined storage conditions were reported, ("fresh and refrigerated" [56; 62], "fresh and frozen-thawed" [71]) and "fresh / refrigerated and frozen" [64]) they were condensed and treated as the "fresh" storage condition.

Although not stated, it is assumed that refrigerated and frozen-thawed targets were allowed to stabilise to room temperature prior to testing. Some of the fresh testing on animal cadavers conducted in Section 5 was initiated within 30 minutes of the animals' euthanasia and would have been at, or close to body temperature at the start of the testing[69]. For the basis of the empirical prediction of skin perforation, it is assumed that there are no residual temperature effects (from the storage conditions) on the resulting skin perforation performance.

Where combined body regions were reported (e.g. "thigh and buttocks" in Reference [60]) these were calculated by averaging the resulting parameters for each of the component body regions.

Unfortunately, some pairs of parameters could not be decoupled. This was the case when the target location or storage condition was not known and the other parameter was unique to that dataset. In these cases, parameters were generated manually by conducting pairwise comparisons between the next best

[68] Data from Reference [89] was not included in the dataset at the time this analysis was completed for parameter generation.
[69] Subcutaneous temperature readings were not taken for the 'fresh' storage condition targets.

data types. For example, data from both Reference [43; 76] were used to determine the parameters for isolated, unbacked skin as 4 identical projectiles were used for tests on intact and isolated, unbacked skin (even though the targets were not completely identical[70]).

Parameters for unknown target storage conditions and unknown target impact areas were left as 1, as they were not specific to a single test series[71]. Backing by 10% or 20% gelatin could not be decoupled from unknown target areas and/or storage conditions, so parameters could not be generated.

Parameters for pointed geometry projectiles could not be reliably calculated by the least squares regression. Pairwise comparisons for the available data showed no observable difference between the resulting V_{50} between round or pointed projectiles based on sectional density (comparison data from References [59; 60; 71; 84]). Following this, the pointed and round projectile parameters were combined, leaving only a distinction to blunt projectiles.

This left 420 data points (from References [58-60; 62-64; 70; 71; 79; 83; 85; 88] and Section 5) for which the parameters could be decoupled or where they had already been calculated from pairwise comparisons. The least squares regression was re-run on only these data, so effects from unknown target area or conditions were removed.

Based on the parameters generated, Equation 5 was simplified by removing unnecessary parameters and constructed such that if all the expanded parameters are set=1, the equation collapses back to the simple form (Equation 1) for the specific case of a PMHS, thigh, intact, perforation V_{50} by probit method and a spherical or pointed projectile. The final version of the expanded empirical skin perforation equation is given by Equation 8.

---

[70] Reference [43] used intact goat skin, but target location and the storage condition was not known. Reference [76] used a mix of PMHS and goat thigh skin, isolated and unbacked, storage condition not known.

[71] Target area was unknown in 6 references; [43; 45; 68; 83; 84; 86]. Target storage condition was unknown in 7 references, the same 6 references as target area [43; 45; 68; 83; 84; 86] and additionally Reference [76].

$$v_{50} = 153.8\left(\alpha\gamma_a\delta_a\varepsilon_a\eta_a\right)S^{-0.354\left(\gamma_b\delta_b\kappa_b\eta_b\right)}$$

Equation 8: The final version of the expanded empirical skin perforation equation

The parameters for Equation 8 are given in Table 15 to Table 17.

Prediction type	$\boldsymbol{\alpha}$
Penetration threshold	0.871
Penetration V_{50} average	0.914
Penetration V_{50} ZMR	0.951
Penetration V_{50} Probit	0.937
Perforation threshold	0.943
Perforation V_{50} extrapolated from DoP data	1.027
Perforation V_{50} average	0.977
Perforation V_{50} ZMR	0.994
Perforation V_{50} Probit	1.000

Table 15: Parameters for different penetration and perforation prediction methods (α) for Equation 8.

The perforation V_{50} based on the probit method was the preferred method as it could statistically account could account for all shots conducted without skewing the outcome.

Target type	$\boldsymbol{\gamma_a}$	$\boldsymbol{\gamma_b}$		**Target location**	$\boldsymbol{\delta_a}$	$\boldsymbol{\delta_b}$
Child PMHS	0.898	1.208		Abdomen	1.788	1.894
Goat	1.053	1.103		Back	1.255	0.813
Pig	1.226	1.029		Buttocks	0.757	0.719
PMHS	1.000	1.000		Buttocks, thigh, calf	0.879	0.860
Sheep	0.972	1.007		Thigh	1.000	1.000
				Thorax	1.256	1.413

Table 16: Parameters for different target types (γ_a and γ_b) and target locations (δ_a and δ_b) for Equation 8.

Backing type	ε_a		Projectile shape	η_a	η_b
Intact	1.000		Blunt	1.345	1.276
Isolated	1.200		Round or pointed	1.000	1.000
Isolated and backed by cork	*0.969*		***Storage Condition****	κ_b	
			Fresh	*1.000*	
Isolated and backed by Mipoplast	*1.189*		*Frozen-thawed*	*1.166*	
			Refrigerated	*0.798*	

Table 17: Parameters for different backing types (ε_a), projectile shapes (η_a and η_b) and target storage conditions* (κ_b) for Equation 8. * Not a significant parameter[72].

Figure 26 shows Equation 8 prediction for all the penetration and perforation data which had valid parameters, with 95% confidence and prediction intervals.

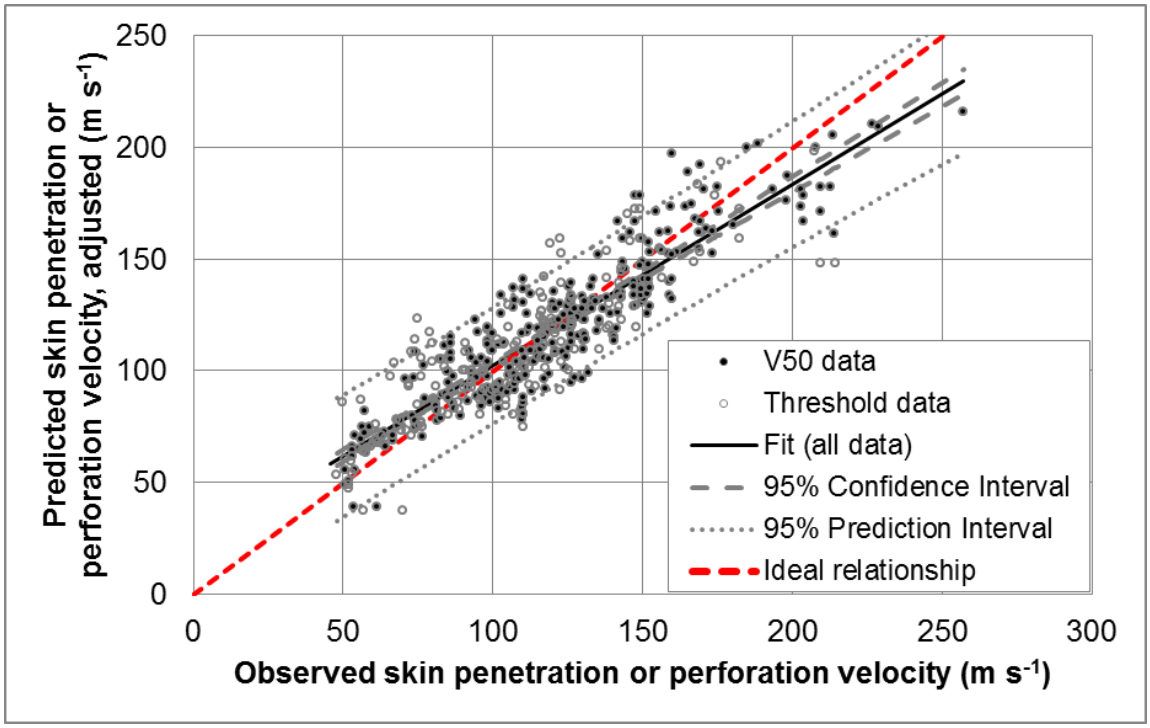

Figure 26: Observed and predicted skin penetration and perforation velocities based on Equation 8, for valid parameters, n=450 from References [58-60; 62-64; 70; 71; 79; 83; 85; 88] and Section 5.

[72] The refrigerated and frozen-thawed storage conditions are not considered significant in terms of reliably predicting the skin perforation response. They are provided to help bound the potential variability observed from testing stored tissue.

Figure 26 shows that in general; Equation 8 gives good predictions at low velocities, but under predicts the required penetration or perforation velocity at higher velocities (>150 m s^{-1}), although the ideal relationship lays within the 95% prediction interval across the full range of velocities. The standard error on the linear fit to all the data was 12.9 m s^{-1}. The higher velocity data is for limited tests, but multiple penetration or perforation calculation methods from each, which may partially explain the skew the relationship at this velocity extreme.

Reliable confidence intervals on the individual parameters in Equation 8 could not be generated.

Pairwise comparisons for the parameters generated by the least squares regression was conducted to verify the values where possible. 'Validation' data for specific cases (e.g. PMHS, thigh, fresh, intact with a rounded projectile) is given in APPENDIX C to show model prediction against actual data sets. Although this is not true validation as it is using data on which the model is built, it does show the model accuracy for specific cases instead of all data grouped together as in Figure 19.

6.1.5 Factors that affect skin perforation using the expanded empirical equation for skin perforation

Figure 27 to Figure 31 show the distinct effect of changing each of the different target and projectile factors individually based on the output of Equation 8: The final version of the expanded empirical skin perforation equation. Figure 32 shows the output of Equation 8 for a limited selection of the different penetration and perforation calculation methods. The baseline case is PMHS, thigh, intact, perforation V_{50} by probit method, rounded or pointed projectile and is shown by a solid black line in each of Figure 27 to Figure 32.

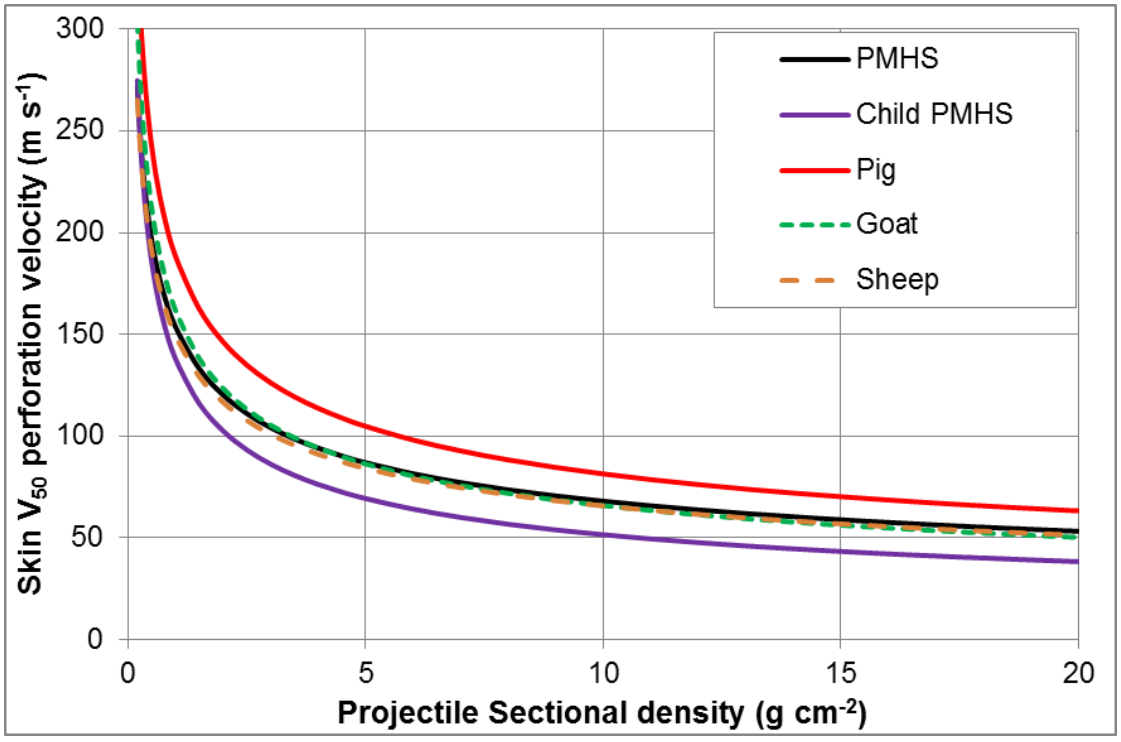

Figure 27: Output of Equation 8: The final version of the expanded empirical skin perforation equation, showing differences due to target type/species

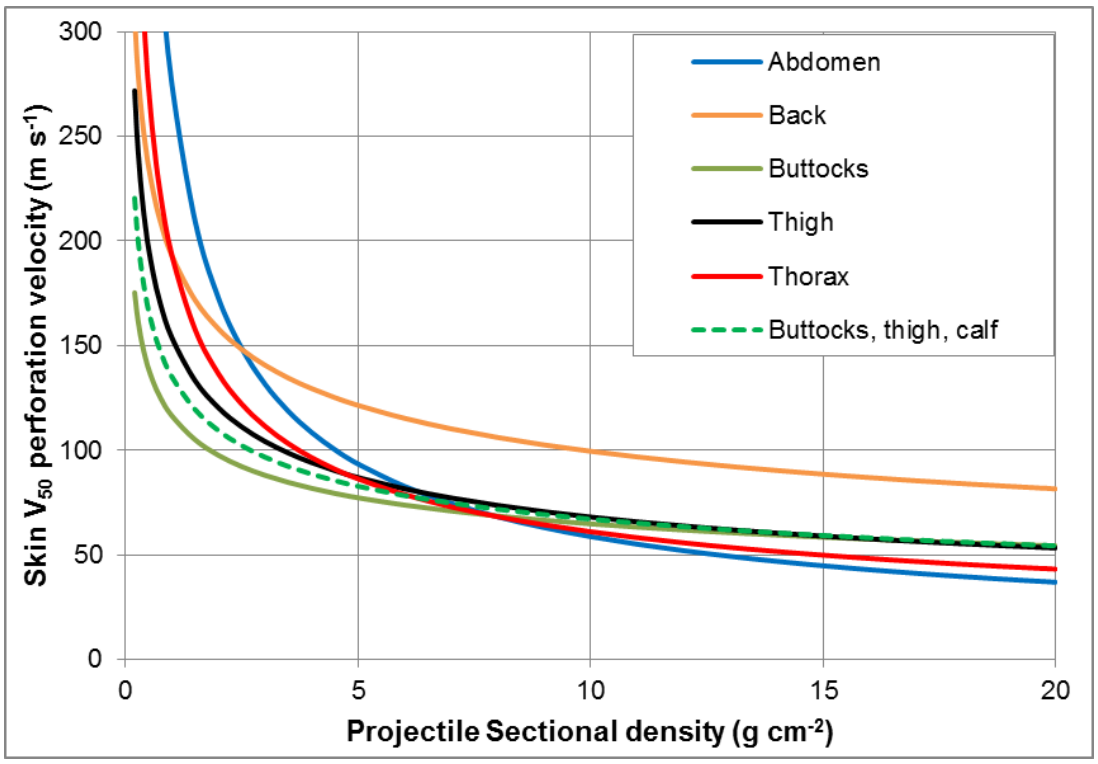

Figure 28: Output of Equation 8: The final version of the expanded empirical skin perforation equation, showing differences due to target area / body region

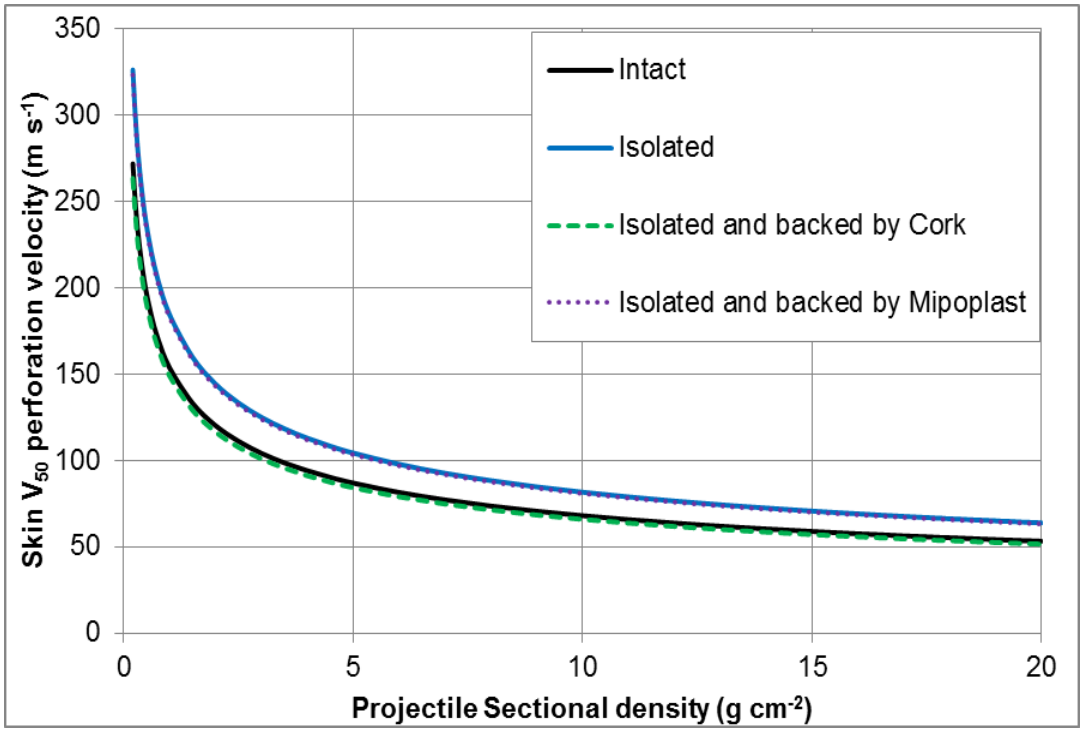

Figure 29: Output of Equation 8: The final version of the expanded empirical skin perforation equation, showing differences due to target backing

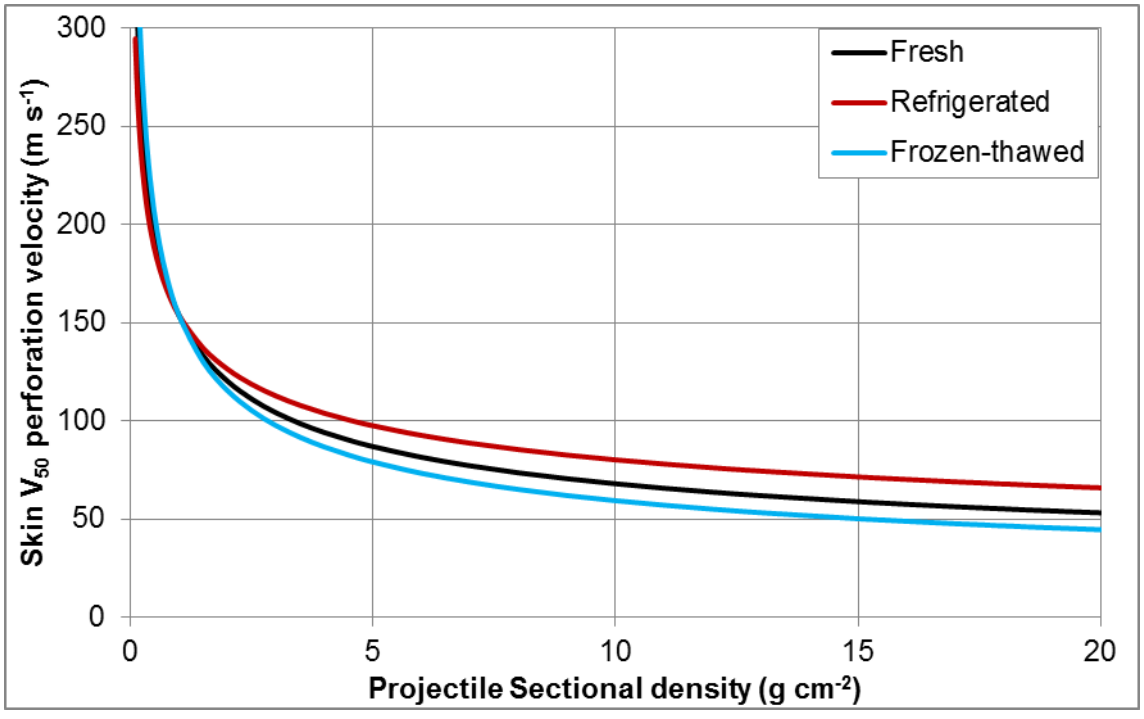

Figure 30: Output of Equation 8: The final version of the expanded empirical skin perforation equation, showing differences due to target storage condition

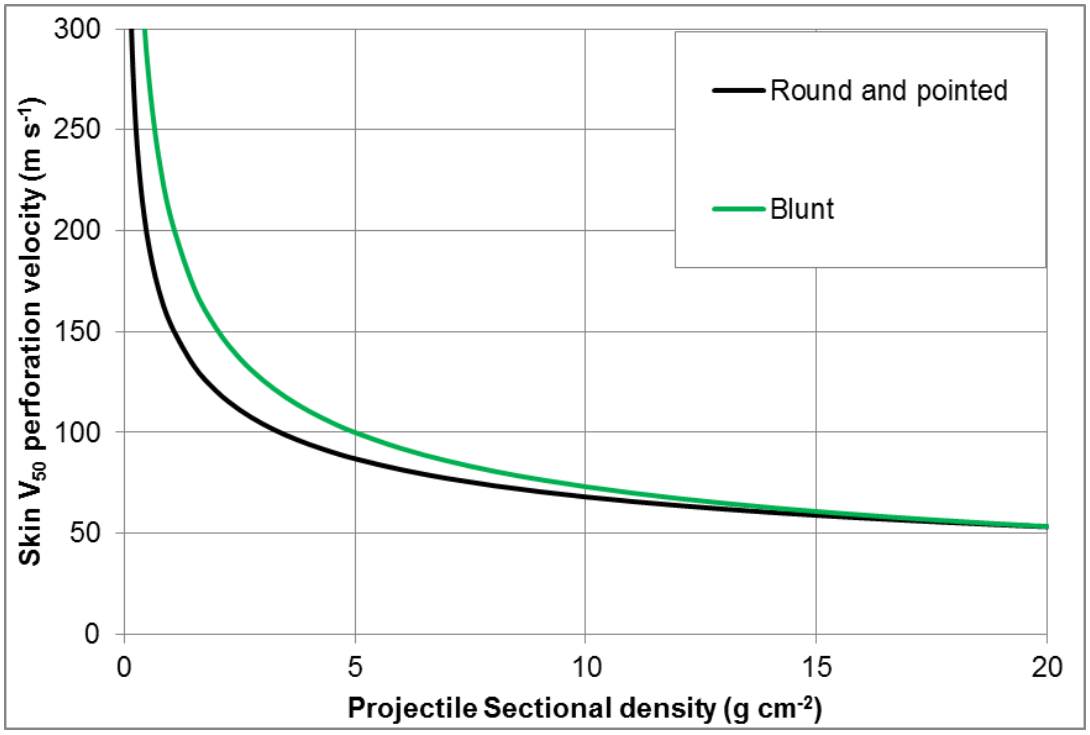

Figure 31: Output of Equation 8: The final version of the expanded empirical skin perforation equation, showing differences due to projectile geometry

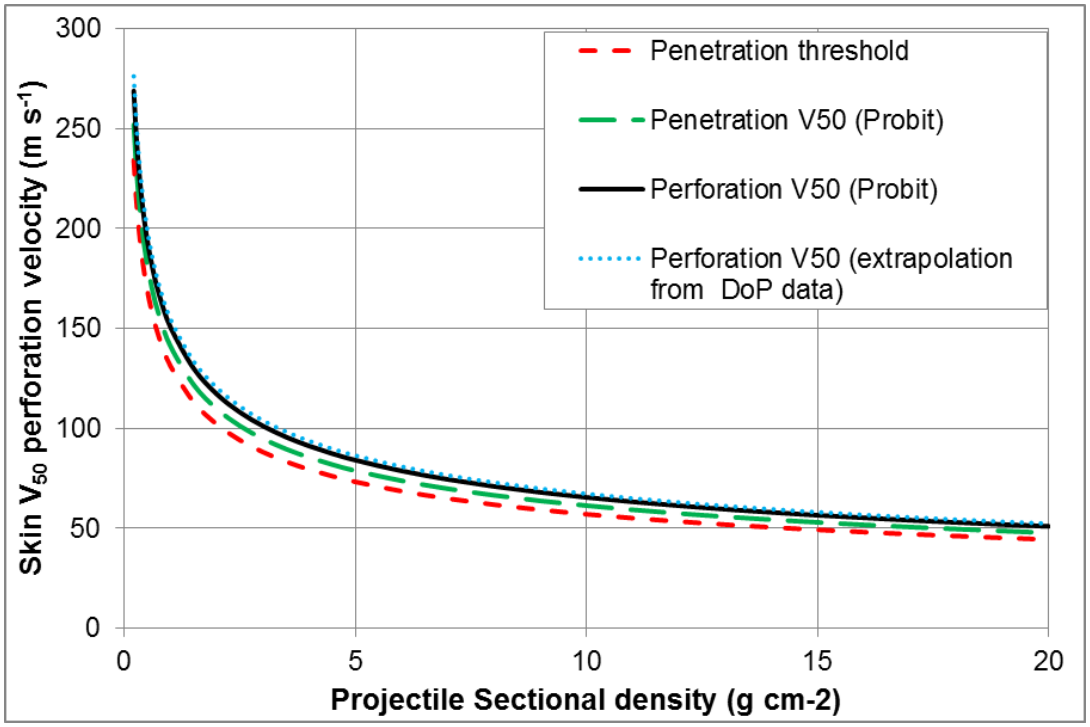

Figure 32: Output of Equation 8: The final version of the expanded empirical skin perforation equation, showing differences due to penetration or perforation prediction method for a sub-selection of methods.

Below is a discussion of notable differences from Figure 27 through Figure 32.

Target types (Figure 27):

- Goat skin ≈ Sheep skin ≈ PMHS skin. The similarity between goat and PMHS skin agrees with previous studies that have reached the same conclusions (Section 5.5 and References [76; 79]).
- Pig skin ≠ PMHS skin. Pig skin requires a higher velocity to perforate compared to PMHS skin (indicated in Reference [69]). This reinforces the outcomes shown in Section 5.5 on the effect of target types, although the target conditions were not directly comparable in that testing.
- Child PMHS skin has the lowest perforation velocity.

Target location (Figure 28):

In general, skin on the back requires the highest velocity to perforate. However, at low sectional densities, abdominal (and thorax) skin is calculated to require the highest velocities to perforate. Target location is assumed to account for the differences in skin mechanical properties and thickness that would be expected.

Target backing (Figure 29):

Isolated (unbacked) skin requires higher velocities to perforate compared to intact skin, by approximately 20% over the range of projectile sectional densities investigated. The backing conditions evaluated can be summarised as:

- Intact skin ≈ isolated and backed by cork < Isolated, unbacked skin ≈ Isolated and backed by Mipoplast[73].

Target storage condition (Figure 30):

The data on which these parameters are based is variable without showing clear trends to increase or decrease the velocity required for skin perforation. The parameters for the frozen-thawed condition could only be completed by pairwise

[73] Mipoplast is a thin, ~0.5 mm plastic film.

comparisons. It cannot be stated with any confidence that the perforation velocity for fresh skin is any different to that when stored refrigerated or frozen and then thawed. The target storage condition is likely to increase the variability of the skin response and this may explain the differences observed. It would be expected that storing the skin for longer periods would result in a decrease in the resulting skin perforation velocity (i.e. fresh skin>refrigerated), but this is not the case from the predictions of Equation 8. Refrigerated skin shows a higher velocity required for skin perforation to fresh skin, whilst frozen-thawed skin, as might be expected, requires a lower velocity. One potential explanation is that refrigerated samples may have been tested cold in some test setups, rather than at room (or body) temperature which may have been enough to affect the resulting performance. Refrigeration and frozen-thawed tissue storage are likely to cause post mortem changes in the tissue due to different mechanisms: Refrigeration due to decomposition, frozen storage due to cell damage from water freezing and expanding.

The storage condition is not considered to be a significant parameter in Equation 8, but is included as it can be used to bound the potentially variable performance from storing skin prior to testing.

Projectile shape (Figure 31):

As would be expected, blunt projectiles require higher velocities to penetrate or perforate compared to rounded or pointed projectiles at equivalent sectional densities. With the available data, no observable difference could be seen between rounded and pointed projectiles and one set of parameters was found to be sufficient to describe both conditions. Interestingly (but as would be expected), the effect of projectile shape on skin perforation velocity is more pronounced at lower projectile sectional densities. At high projectile sectional densities (over approximately 15 g cm^{-2}), Figure 31 indicates minimal difference in the resulting perforation velocity. A different way to describe projectile shape, rather than simple categorisation in broad groups, might show a stronger dependence of projectile shape on perforation velocity.

Prediction methods (Figure 32):

As expected, penetration predictions have comparatively lower velocities than perforations, and thresholds lower than the corresponding V_{50}. However, the differences aren't as large as between target types, body regions or backing methods. For example, a perforation threshold is calculated to give a 6% reduction in skin perforation velocity compared to the probit V_{50} method. The only method which predicts a higher perforation velocity compared to the probit V_{50} method is the extrapolation from DoP method (+3%).

The benefits of this expanded empirical equation for prediction of the risk of skin perforation are that:

- It was based on an extensive range of experimental data to determine both the overall form of the equation and the factors affecting skin perforation, rather than comparing individual V_{50} values (i.e. higher confidence in resulting predictions)
- It is the first equation to explicitly determine, account for, and to demonstrate the degree of influence of each of the significant target (and projectile parameters), across a range of projectile properties. This is in contrast to grouping all data together generically or using multiple equations for specific scenarios.
- It provides the ability to scale results from other testing, e.g.:
    - To estimate the human skin response from pig testing data
    - To estimate the skin performance for vulnerable groups (based on child PMHS parameters) to better support safety cases or collateral damage type assessments.

Limitations remain in this expanded empirical equation for prediction of the risk of skin perforation and are summarised in Section 6.3.

6.1.6 Prediction of the probability of a skin perforation

One of the drawbacks of Equation 1, even with the expanded parameters in Equation 8, is that only predictions of the penetration V_{50}, perforation V_{50} or threshold (V_{th}) velocities are possible. If the probability of a perforation for a given scenario is required, then a different equation is needed. For example in a safety

case assessment, knowing the velocity that equates to a 50% probability of skin perforation is not ideal. Instead the velocity that equates to a given level of risk, i.e. 1% or 5% probability is much more useful[74].

The raw, individual shot data was gathered from each test to give a total of 1258 shots, across the mix of target and projectile factors. This enabled Equation 8 with the parameters already generated to be adapted to predict the probability of a perforation for a given velocity (and vice-versa). The probability of perforation equation is shown in both the simple and expanded forms as Equation 9.

$$P_{skin\ perforation} = \phi\left(C + D\left[\frac{aS^{-b}}{V_s}\right]\right)$$

or;

$$P_{skin\ perforation} = \phi\left(C + D\left[\frac{153.8\left(\alpha\gamma_a\delta_a\varepsilon_a\eta_a\right)S^{-0.354\left(\gamma_b\delta_b\kappa_b\eta_b\right)}}{V_s}\right]\right)$$

Equation 9: Probability of skin perforation (simple and expanded forms)

Where:

$P_{skin\ perforation}$ is the probability of a skin perforation (between 0 and 1).

Φ is the normal distribution function.

C and *D* are curve fitting constants.

V_s is the strike or impact velocity of the projectile (m s^{-1}), not the V_{50} or V_{th}

Equation 9 was based on the raw data (velocity and penetration or perforation outcome for every individual shot) rather than the aggregated V_{50} data. This limits the data used to generate the curve fitting constants for the equation to those studies for which the individual shot data was available [56; 61; 62; 64; 71; 79;

[74] Noting that the estimate from a probit model is less reliable at extreme probability values, $0.2 \geq P \geq 0.8$.

83; 86; 88; 90] as well as that from Section 5. In addition, some raw data from more general penetration studies could also be included [93-95; 114].

The curve fitting constants for Equation 9 were determined by fitting the value in square brackets in Equation 9 for each shot to the outcome (perforation or non-perforation) and using a probit model. The values for the constants in Equation 9 were determined as C=2.95 and D=-2.80.

An example of the implementation of Equation 9 is given in Figure 33 using some of the data generated in Section 5.4 (for the 0.49 g FSP into the refrigerated pig thigh) compared to the predictions from each of Equation 8 and Equation 9.

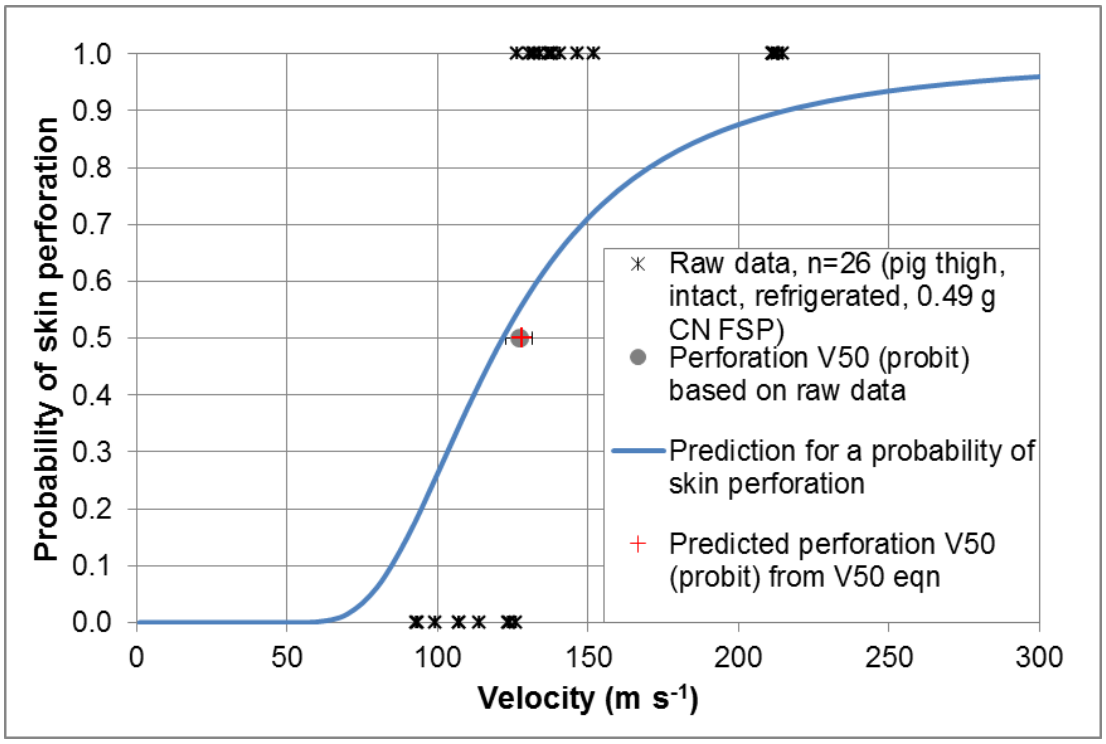

Figure 33: Probability of skin perforation showing raw data and calculated perforation V_{50} for a refrigerated pig thigh (data from Section 5.4) compared to the predictions from each of Equation 8 and Equation 9.

Figure 33 shows how the predicted V_{50} differs between Equation 8 and Equation 9 as well as how Equation 9 describes the perforation probability over the entire impact velocity range compared to the raw data[75].

In Equation 9, when $P_{skin\ perforation}=0.5$, $V_s=V_{50}$. However, Equation 9 is optimised to fit all perforation probabilities, so the V_{50} calculated from Equation 9 not equal to that calculated from Equation 8. When quoting predicted skin perforation velocities it is essential to state which equations were used to produce any predictions, along with the result.

The prediction based on Equation 9 does not follow the standard probit shape with symmetrical tails as the probability calculated is a function of both the velocity and the combination of the target and projectile factors.

The main focus of the empirical skin perforation equations within this thesis has been for Equation 8. More validation (and greater confidence in the outcomes) has been conducted for Equation 8 compared to Equation 9. It is suggested to use Equation 8 for predictions wherever possible.

It has not been possible to generate confidence intervals on the predictions from Equation 9.

6.2 Development of an empirical equation for eye penetration

6.2.1 Prediction of probability of eye penetration

In order to produce an equation for predicting eye penetration, a similar approach to that used to generate Equation 9 was followed. Energy density was found to be the best predictor of penetrating eye injury [171] compared to a combination of sectional density and velocity used for skin perforation. Equation 9 was re-written for eye penetration based on constant energy density and is given by Equation 10.

[75] This is not validation as it has used the same data to generate and check to equations.

$$P_{eye\ penetration} = \phi\left(G + H\left[\frac{E}{A}\right]\right)$$

Equation 10: Probability of eye penetration

Where:

E is the impact energy of the projectile (J)

A is the cross sectional area of the projectile (cm^{-2})

G and *H* are curve fitting constants.

The eye penetration data summarised in Table 7 was used with its energy density value for each shot and outcome (penetration or non-penetration) to run a least squares regression to fit the probit model (Equation 10) for the each target type separately in the dataset. The parameters (*G* and *H*), the number of impacts used in the calculation and the energy density value for the 50% risk of eye penetration are given in Table 18 for different target types.

Target	**Parameter G (standard error)**	**Parameter H (standard error)**	$\left(\frac{E}{A}\right)_{50}$ **(J cm^{-2}) (± 95% CI)**	**Number of data points**
All	-4.439	0.653	6.80	403
Human	-4.412 (0.495)	1.240 (0.134)	3.56 (0.80)	87
Pig	-5.505	0.801	6.87	299

Table 18: Parameter values for Equation 10 for the risk of penetrating eye injury. Values for the standard error or 95% CI on the parameters are given in parenthesis for human eyes.

Parameters for cat eyes (n=17) could not be calculated as the data consisted only of non-penetration impacts.

The curves calculated from Equation 10 are shown in Figure 34 along with previous predictions of eye penetration based on energy density from the literature [171; 197].

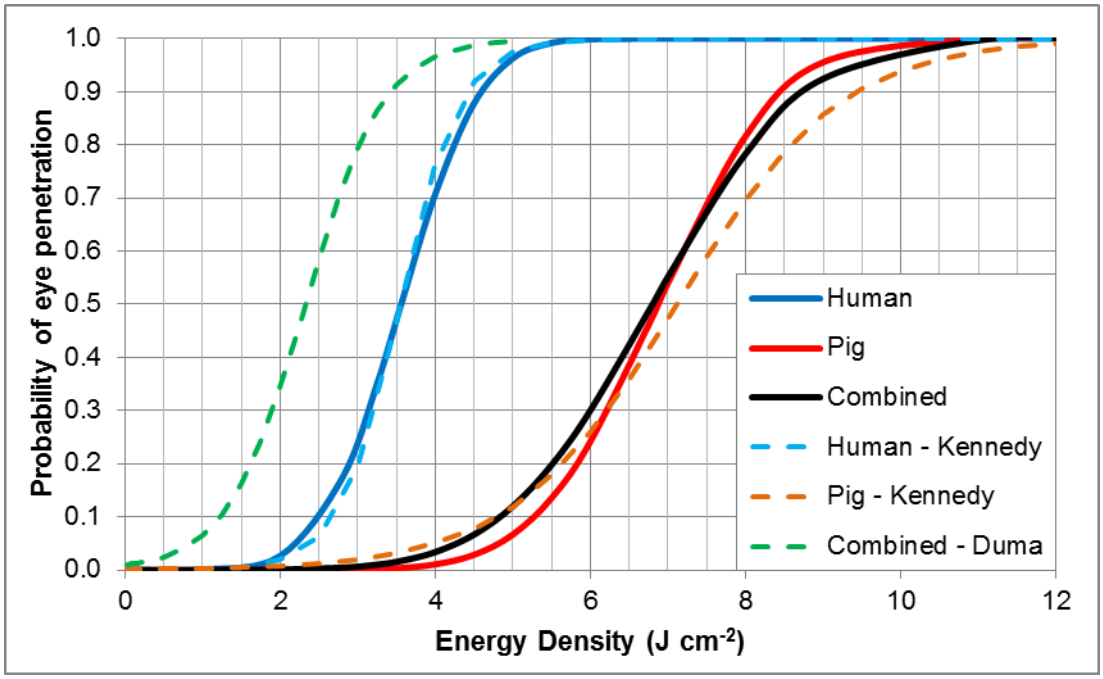

Figure 34: Probability of eye penetration using energy density as a predictor with Equation 10 and existing predictions from the literature [171; 197].

Figure 34 shows that human eyes are considerably more vulnerable to penetration than pig eyes (approximately half the energy density required for a 50% probability of penetration for a typical human eye compared to a typical pig eye).

The curves for the human eye response are very similar to that given by Kennedy in Reference [171], as the dataset was almost identical. The new curve generated for pig eyes also seem extremely similar to that previously generated in Reference [171], despite the current dataset including an additional 199 impacts.

The relationship given by Duma in Reference [197] appears very conservative compared to Reference [171] and the current predictions from Equation 10. Reference [197] used 71 data points to generate the risk function and included data from References [198; 199] which are very heavy projectiles and may result in a blunt rather than penetrating rupture mechanism.

Figure 35 shows the prediction for probability of penetration of human eyes based on Equation 10 and parameters from Table 18 with the associated 95% confidence intervals.

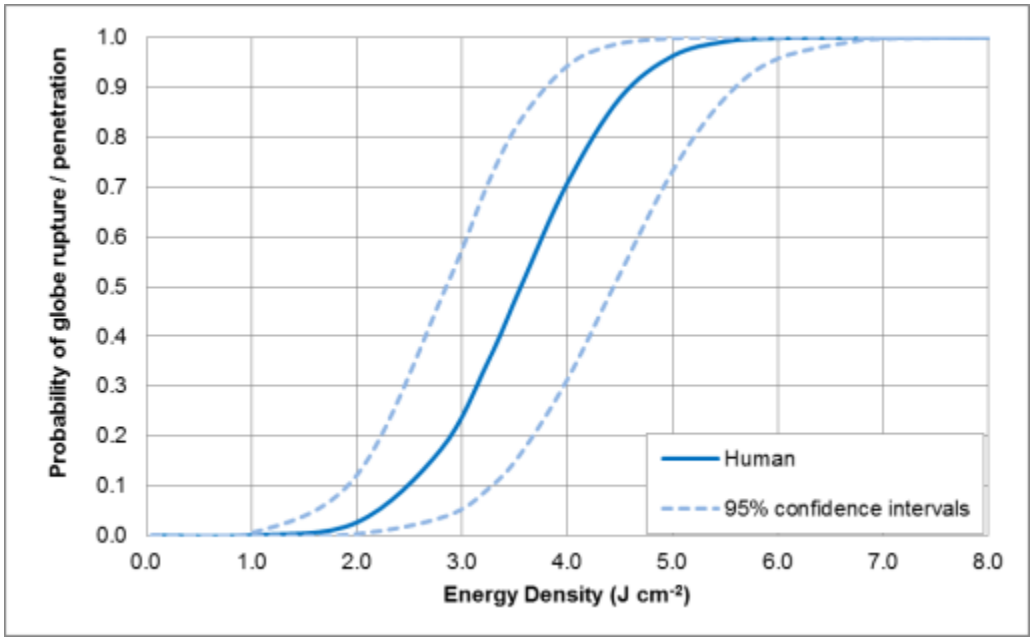

Figure 35: Probability of eye penetration using Equation 10 and parameters from Table 18, showing 95% confidence intervals on the prediction. Note different scale to Figure 34.

6.2.2 Simple empirical equation for eye penetration

To allow selection/ranking of appropriate materials for a physical model of eye penetration, a V_{50} performance criterion (and performance limits) were required. This was generated for the 50% probability case (P_{50}) for probability of penetration of human eyes (Equation 10) calculated with the parameters in Table 18. This gave parameters that could be used in Equation 2 to define the ideal performance for a physical eye model. The parameters generated to be used with Equation 2 are given in Table 19.

	$\left(\frac{E}{A}\right)_{50}$ (J cm^{-2})	a	b
Lower 95% CI	2.76	74.30	-0.5
Ideal performance curve / human eye P_{50}	3.56	84.34	-0.5
Upper 95% CI	4.36	93.38	-0.5

Table 19: Parameters for Equation 2 to predict the ideal performance (average human eye) and 95% CI curves

Substituting the values for the ideal performance curve / human eye P_{50} into Equation 2 gives the relationship defined by Equation 11 and shown in Figure 36.

$$v_{50} = 84.34S^{-0.5}$$

Equation 11: Simple empirical equation for eye penetration

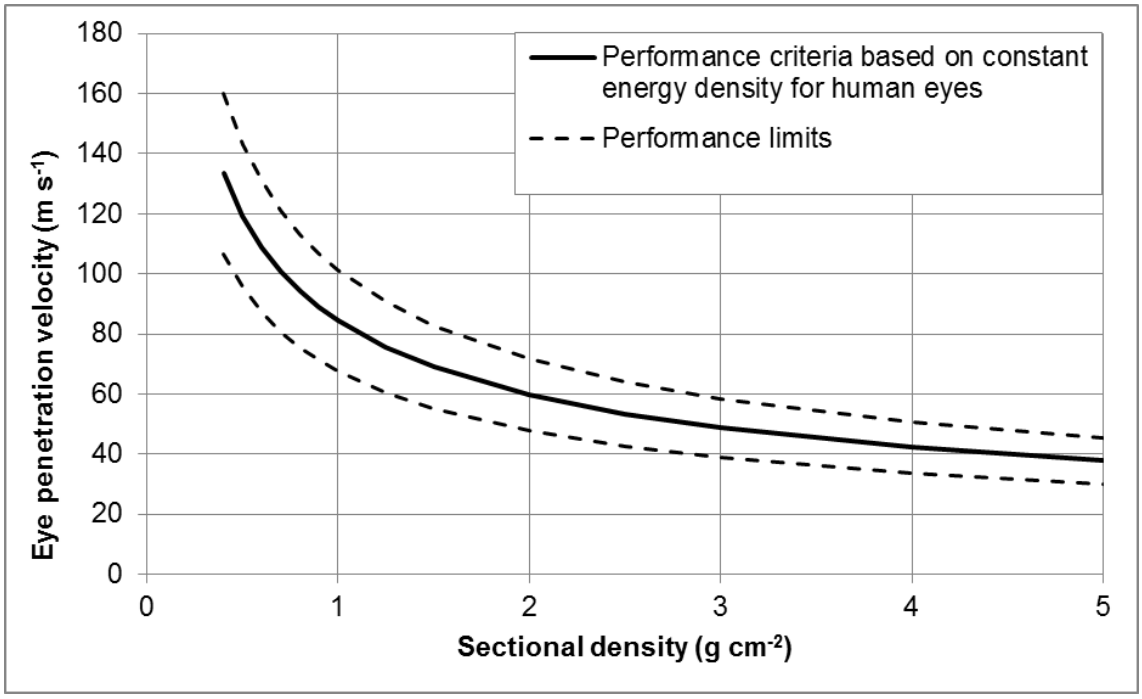

Figure 36: Ideal physical model performance shown by the curve generated from Equation 11 with a constant energy density. Performance limits are based on the 95% confidence intervals of the human eye data.

This ideal performance and limits shown in Figure 36 (Equation 2 with values from Table 19) will be used in Section 10.4 to evaluate a physical model for eye penetration. As discussed in Section 3.10.2, due to the paucity of PHMS eye V_{th} or V_{50} data, the performance criteria given in Figure 36 cannot be compared to existing data to judge the fit.

6.3 Limitations of empirical models for skin perforation and eye penetration

The limitations to the empirical equations are applicable to the skin perforation equations (“Equation 8: The final version of the expanded empirical skin

perforation equation" and "Equation 9: Probability of skin perforation (simple and expanded forms)") and "Equation 11: Simple empirical equation for eye penetration":

- Construction and development of the empirical equations were determined by the available data[76].
- Projectiles must be non-deforming and non-fragmenting.
- There is no ability to account for the effect of clothing in front of the skin.
- Skin perforation predictions are not applicable to glass shard or other "cutting" type projectiles.
- The majority of experimental data is based on PMHS or dead animals. Predictions for a live human target are assumed to be modelled by 'fresh' PMHS;
- The data from PMHS may not represent population they are intended to model. PMHS tend to be older (e.g. the PMHS used in Reference [59] had an average age of 58 and average age of 72 in Reference [61]). Aging will affect the skin mechanical properties [211], but has not been determined to significantly affect ballistic response within the limitations of the experimental studies conducted [59].
- Section 5.4 has highlighted potential differences in the response of the target due to the target storage conditions before testing. Much of the experimental data examined from the literature used mixed storage conditions (e.g. a combination of fresh and frozen-thawed), the details were vague or not given and therefore cannot be fully accounted for;
- The models can account for the following body regions: abdomen, back, buttocks, thigh, thorax, and eyes.

[76] As more data becomes available the range of applicability may be altered, or the confidence limits may be clarified. Similarly the need to revise the model (and associated parameters) may become apparent.

- The consideration of the different properties of skin (such as thickness), that may affect the perforation velocity were constrained by the data that was available. Some aspects were addressed indirectly, for example skin properties such as thickness may be factored in using the parameters for different body regions;
- Unless using Equation 9 for the probability of skin perforation (or Equation 10 for the propability of eye penetration), all impacts below the V_{50} are assumed to be non-perforations, all above the V_{50} are assumed to be perforations. By definition 50% of impacts at the V_{50} velocity are expected to perforate;
- The model(s) address whether the skin has been perforated or not. The size of the perforation and impact on military effectiveness is not addressed.

7 Development of physical models for single projectile impacts

7.1 Overall model structure

It was decided that the physical model should consist of two parts to replicate the gross structure of real skin and muscle tissue: A muscle tissue simulant (addressed in this section) and a skin simulant layer (addressed in Section 8), to maintain manageable Section sizes.

A physical model to assess eye penetration is considered as part of a separate model in Section 10.4 (which can be used for single or multiple projectile impacts).

In order to select a suitable muscle tissue simulant, a number of comparisons to animal muscle tissue have been made. Depending on the requirement, either the permanent DoP and/or the retardation response of a muscle tissue simulant may be required. As these two metrics are independent of each other (i.e. a material can be made to match the DoP response to muscle tissue but not retardation, or vice versa), both metrics were considered separately[77]:

- The permanent DoP over a range of impact conditions (Section 7.2)
- The energy loss in a 100 mm target, to evaluate the retardation response (Section 7.3).

These comparisons were used to select a muscle tissue simulant in Section 7.4.

The diameter and/or volume of the permanent or temporary cavity produced between animal muscle and simulants would be a useful metric to evaluate a simulant, as this could be used to infer the damage in real muscle tissue. However, data for the diameter or volume of the temporary cavity for animal muscle is much more limited due to the requirement for high speed or flash x-ray

[77] This differentiation between the suitability of muscle tissue simulants for DoP or retardation predictions does not appear to be well understood within the wound ballistics literature.

in order to capture cavities in opaque tissue, greatly restricting any comparisons that can be made with this metric.

Instead of attempting to validate the cavity predictions of the tissue simulant against this sparse muscle tissue data, experiments to determine some of the significant factors of temporary cavity formation in the selected muscle tissue simulant have been conducted (Section 7.5).

7.2 Muscle tissue simulants – DoP comparison

7.2.1 Overview of comparison

A variety of different tissue simulants, selected from those used in previous studies and those suggested in the literature, were ballistically impacted with a range of different projectiles at varying velocities. The resulting depth of penetration into the simulant was measured as well as retardation and the maximum cavity produced[78] in some cases. These measures were then compared to similar data obtained from studies of projectile impacts into animal tissue in order to select the tissue simulant that is most representative.

The penetration data was compared using the normalised DoP over density function (Section 4). Unless specifically stated, the effect of projectile shape was ignored.

7.2.2 Tissue simulants assessed

As highlighted in Section 3.9.2, gelatin concentration, usage temperature and mix method can affect the response of the gelatin. Aspects of these factors were investigated by penetration testing. A number of synthetic materials were also assessed. Table 20 provides a summary of the different simulants assessed as part of this original testing.

[78] Maximum temporary cavity in elastic, transparent simulants, the permanent cavity in the opaque/translucent, plastically deformable simulants

Gelatin Based	Non-gelatin based
Dstl 5% at 10°C	Soap 1.06 g cm^{-3} (opaque)
Dstl 10% at 10°C	Soap 1.10 g cm^{-3} (translucent)
Dstl 20% at 10°C	Perma-Gel™
Dstl 20% at 20°C	Paraffin Wax
Dstl 30% at 10°C	Stabili-gel (32.5% SEBS)
Fackler 10% at 4°C	
NATO 20% at 10°C	

Table 20: Materials evaluated as potential muscle tissue simulants.

As shown in Table 20, the gelatin was produced using different mix methods and these are detailed in APPENDIX D.

Testing of the Dstl 10% (as well as the 5% and 30%) gelatin was conducted at the same time as for Dstl 20% gelatin at 10°C, which required all targets to be conditioned to the same temperature. This is instead of the 10% gelatin being tested at the more common 4°C (i.e. in the Fackler mix method). Testing different concentrations at a fixed temperature also allowed the effect of gelatin concentrations to be explicitly assessed.

The specification of ballistic soap used in previous research could not be obtained for this testing, so soap was procured to match the density of muscle tissue (1.06 g cm^{-3}) [118] and also a different mix to provide a more practical translucent simulant.

These materials were compared with data from previously reported penetration studies of these and other muscle tissue simulants identified in Table 6 of Section 3.9.5.

7.2.3 Animal tissue DoP data and comparisons

In order to determine which tissue simulant is most appropriate, DoP data for fragment (i.e. simple geometry, non-tumbling and non-deforming projectile) penetration into animal tissues (all with skin intact) were required with a range of different projectiles. The data highlighted in Table 4 in Section 3.9.4, along with

the data generated in Section 5 were used as the basis for this comparison. Table 21 summarises the additional animal data from Section 5 along with that from Table 4 used for the comparison. All targets had the skin intact over the muscle tissue.

Target type	**Reference(s)**	**Number of shots**	**Shots with non-zero DoP data**
PMHS	[56; 62-64; 71]	284	137
Goat	[79]	41	22
Goat and sheep	Section 5.2 and 5.5	114	63
Pig	[58; 88; 90; 93; 94]	99	95
Pig	Section 5.3	23	11
Pig	Section 5.4	129	75
Total		**690**	**403**

Table 21: Summary of PMHS and animal muscle tissue (with skin) DoP data for comparison to muscle tissue simulants.

The animal and PMHS data in Table 21 were all combined into a single dataset in order to produce a performance curve against which the muscle tissue simulants could be assessed. This dataset comprised of the 403 non-zero DoP shots for projectiles with diameters 2.7-20 mm, masses 0.04-15.92 g, densities 2.5-8.2 g cm^{-3}, different geometries (cylinders, CN cylinders and spheres) and velocities 65-1652 m s^{-1} (but comparisons limited to below the speed of sound in muscle tissue, 1463 m s^{-1} [24]).

For the purposes of this comparison, the data from targets with different storage conditions were combined (a separate comparison of fresh and stored muscle tissue is provided in APPENDIX E).

Often cited as a definitive result for the penetration depth into fresh pig muscle tissue (with the skin intact) is the data from Fackler and Kneubuehl [94]. Due to the frequency that this data is cited in the literature, it is highlighted in red in Figure 37 with all the animal and PMHS muscle tissue data.

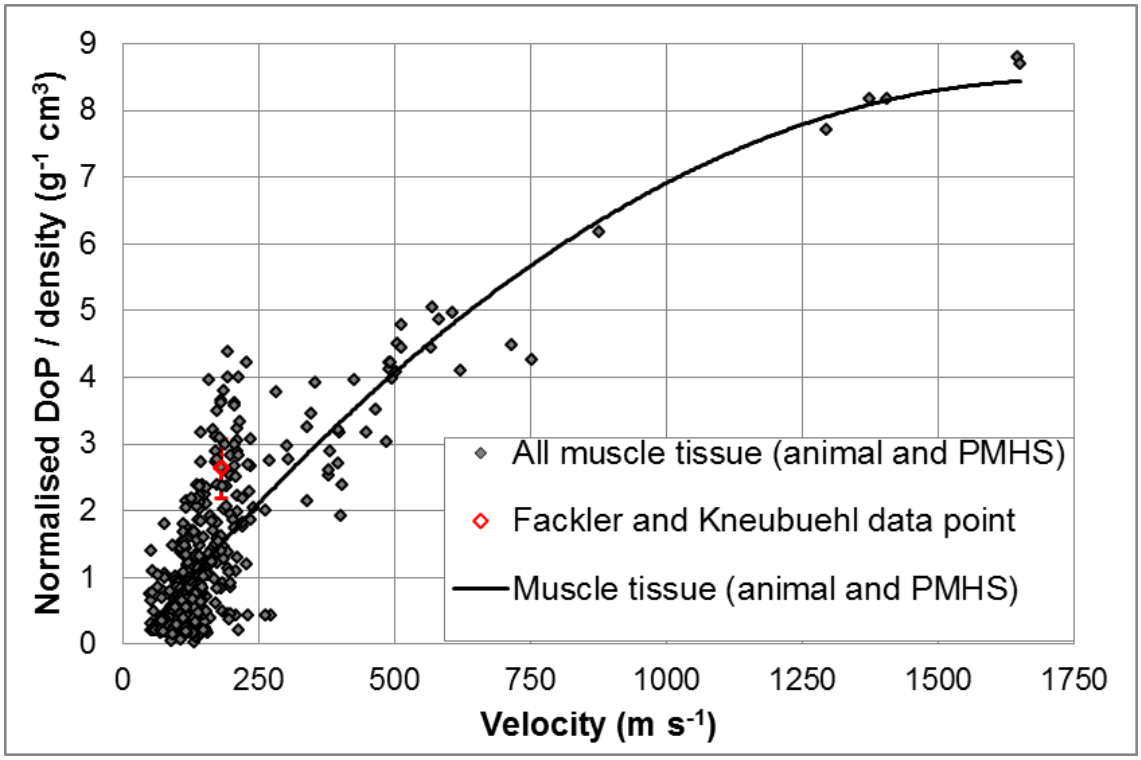

Figure 37: Normalised DoP over density against velocity for all projectiles in animal and PMHS muscle tissue[79]. The error bars show the reported data limits. Data from References [56; 58; 62-64; 71; 79; 88; 90; 93; 94] and Section 5.

Figure 37 shows all the combined animal and PMHS data with the 2nd order polynomial fit that was applied to the data. The data includes all target types and storages conditions. It can be seen that there is large variability in the data (R^2 value is 0.746), but it all follows the same general trend. The variability in biological tissue is one of the key areas on which a tissue simulant can improve. The fit shown in Figure 37 is given by Equation 12.

$$\text{Normalised DoP over density} = -2.84\text{x}10^{-6}v^2 + 0.00999v - 0.213$$

Equation 12: Normalised depth of penetration over density for animal and PMHS muscle tissue (with skin intact), all target types and storage conditions.

[79] Caution should be exercised for the data above 1463 m s^{-1} (the speed of sound in muscle tissue [24]).

Figure 37 shows that there appear to be two trends in the muscle tissue data. One set approximately follows Equation 12 whilst the other shows higher normalised DoP over density values for up to 250 m s^{-1}. This was thought to be due to the different storage conditions of the muscle tissue and is considered further in APPENDIX E.

It can be seen from Figure 37 that the data for fresh pig thigh from Fackler and Kneubuehl [94] sits above the best fit to all the animal and PMHS muscle tissue data (Equation 12), but within the scatter of the other individual data points.

In addition to Equation 12, the penetration response of muscle tissue from the ComputerMan shot line model [30] was extracted from Reference [42]. The data in Reference [42] was for 6 mm steel spheres between approximately 50 and 1000 m s^{-1}. This data was converted to normalised DoP over density and plotted against the raw animal and PMHS muscle tissue data in Figure 37.

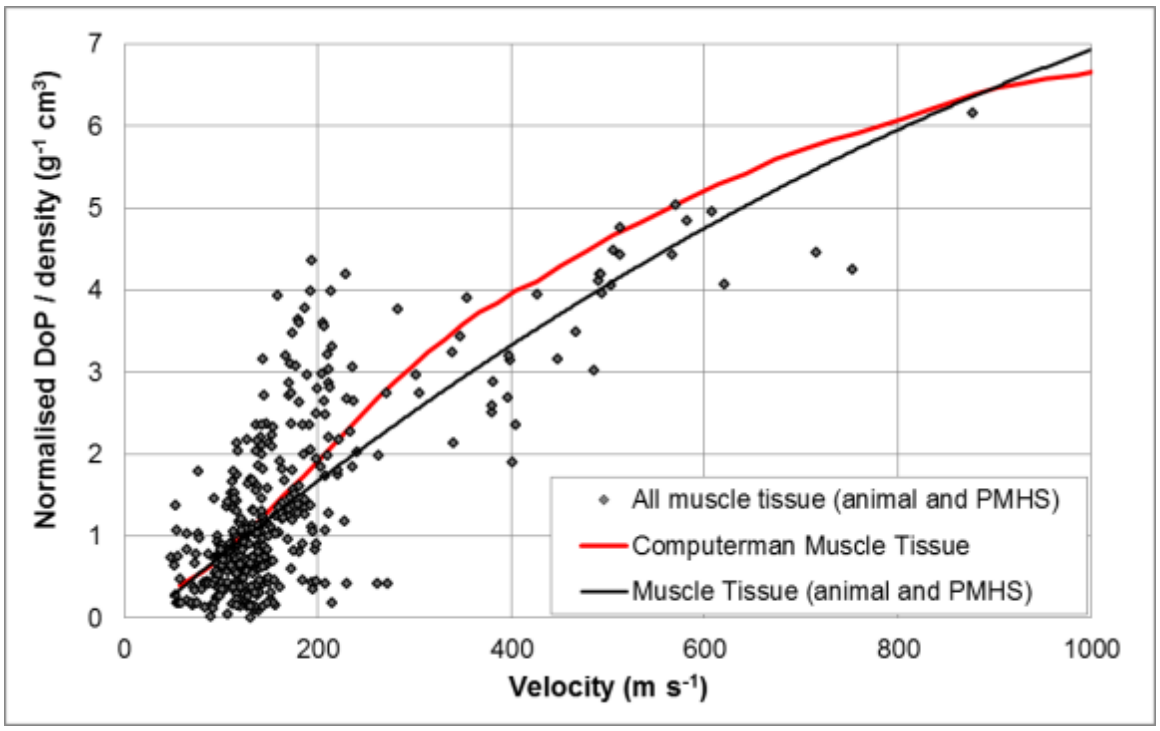

Figure 38: Normalised DoP over density against velocity for all projectiles in animal and PMHS muscle tissue compared to the relationship for muscle tissue in the ComputerMan model. Data from References [42; 56; 58; 62-64; 71; 79; 88; 90; 93; 94] and Section 5.

Figure 38 shows that the ComputerMan muscle tissue penetration response is similar to the curve fit given by Equation 12. The ComputerMan penetration response shown in Figure 37 is approximated by Equation 13.

$$\text{Normalised DoP over density} = -6.28\text{x}10^{-6}v^2 + 0.0133v - 0.425$$

Equation 13: Approximation of the normalised depth of penetration over density for muscle tissue from the ComputerMan model, based on 6 mm steel spheres.

The ComputerMan muscle tissue penetration response is believed to be based on an extensive database of penetration (and/or retardation) in muscle tissue. However, the details of the data used to construct the model and its validation are not openly available. Despite not being able to confirm the validation of this relationship, it is considered to be a reliable model with which multiple countries defence organisations have (openly documented) vulnerability and lethality studies [30; 42; 212].

A number of additional comparisons between different factors within the animal and PMHS tissue penetration data are given in APPENDIX E.

7.2.4 Method – ballistic assessment of tissue simulants

The 11 muscle tissue simulants listed in Table 20 were prepared (where necessary). The gelatin preparation methods used are given in APPENDIX D, including calibration standards. All gelatin used in this work was Type A, 250 bloom. The different concentration Dstl gelatin mixes all followed the Dstl 20% method, but the proportion of gelatin modified accordingly.

Gelatin was tested at its specified use temperature dependent on the manufacture method. Non-gelatin simulants were used at room temperature (20±2°C).

In order to compare the tissue simulants, they were ballistically tested and compared to the polynomial fit to the raw animal and PMHS muscle tissue (Equation 12) and the ComputerMan penetration response (Equation 13) for a number of different projectiles.

7.2.4.1 Tissue simulant testing setup

Testing was conducted over numerous separate trials, with setup varying between each trial depending on available equipment. The typical setup used across these trials is described below.

The HTPH weapon system was used with 37 mm rechargeable compressed Airmunition cartridges or the MPH with blank pyrotechnic charges. Each could be fitted with a range of smooth bore barrels to match the projectile diameter or a rifled barrel with sabot. Details of the weapon systems are given in APPENDIX B.

A Crossmans RepeatAir 1077 CO_2 powered 0.177" air rifle was used to perform the 4.4 mm sphere calibration shots for gelatin.

Typically, two HSV cameras were used to get a view from the side and top of the target (top view via a 45° mirror). These were either a pair of Phantom Miro M310 high speed cameras [209] at 20,000 frames per second and 512x288 pixels, or a pair of Photron SA-Z high speed cameras [206], typically 40,000 frames per second and 1024x512 pixels[80]. For opaque tissue simulants, a single HSV camera was used.

For transparent targets, the HSV was used to track the projectile through the simulant to allow retardation curves for each shot to be generated. Projectile tracking was done by selecting the projectile location in each frame of the HSV (using open source software called Tracker [213]). For the majority of impacts this could be performed automatically by the software after the projectile had been identified in a reference frame. The x-y pixel locations were then converted into their position relative to the impact face of the target. The penetration depth was calculated to account for travel in the x and y plane (but not z plane, towards or away from the camera).

[80] Up to 100,000 frames per second with corresponding resolution of 640x280 pixels were used for some shots.

In addition, the HSV was used to measure the maximum temporary cavity envelope for selected shots using software called MS EKE [214][81].

Impact velocities were recorded using MSI solid state velocity equipment [205] with a 1 m separation between the velocity heads.

Testing of the temperature controlled targets was completed within 30 minutres of their removal from the conditioning cabinet. Multiple shots were conducted into each target, with care taken to ensure zones of permanent damage did not overlap.

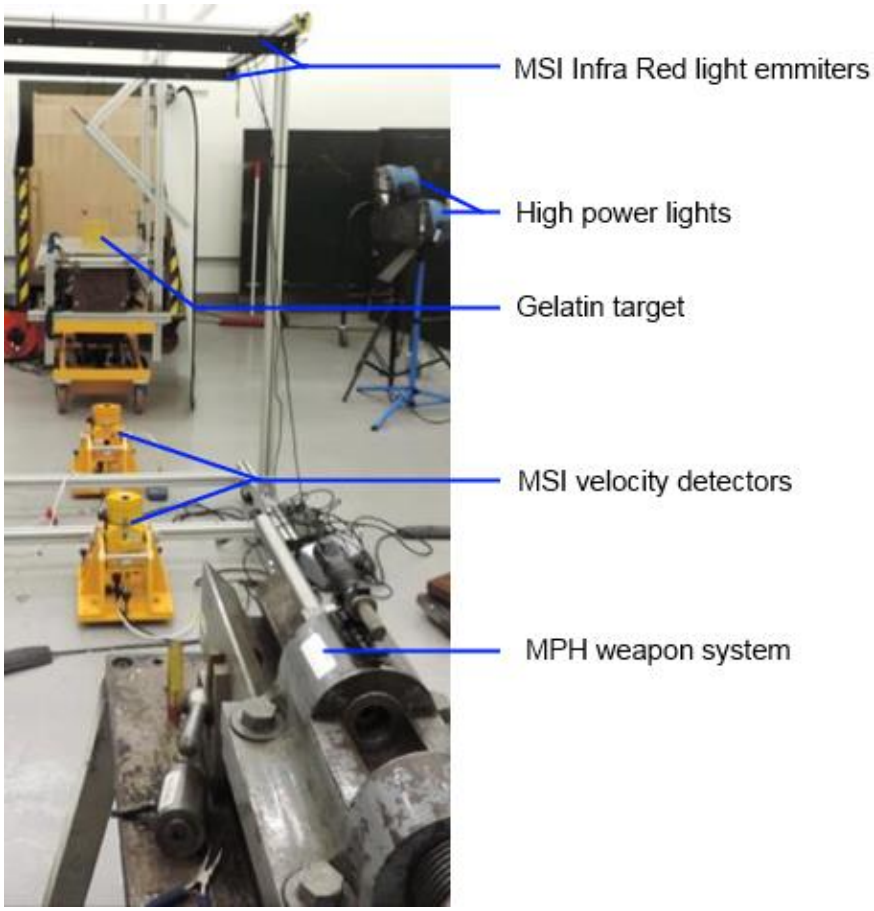

Figure 39: Annotated photograph of setup of tissue simulant testing along the direction of firing with a gelatin block target. The MPH weapon system is shown in this setup.

[81] Projectile tracking could also be performed in this software, but was limited to manual selection of the projectile position in each frame.

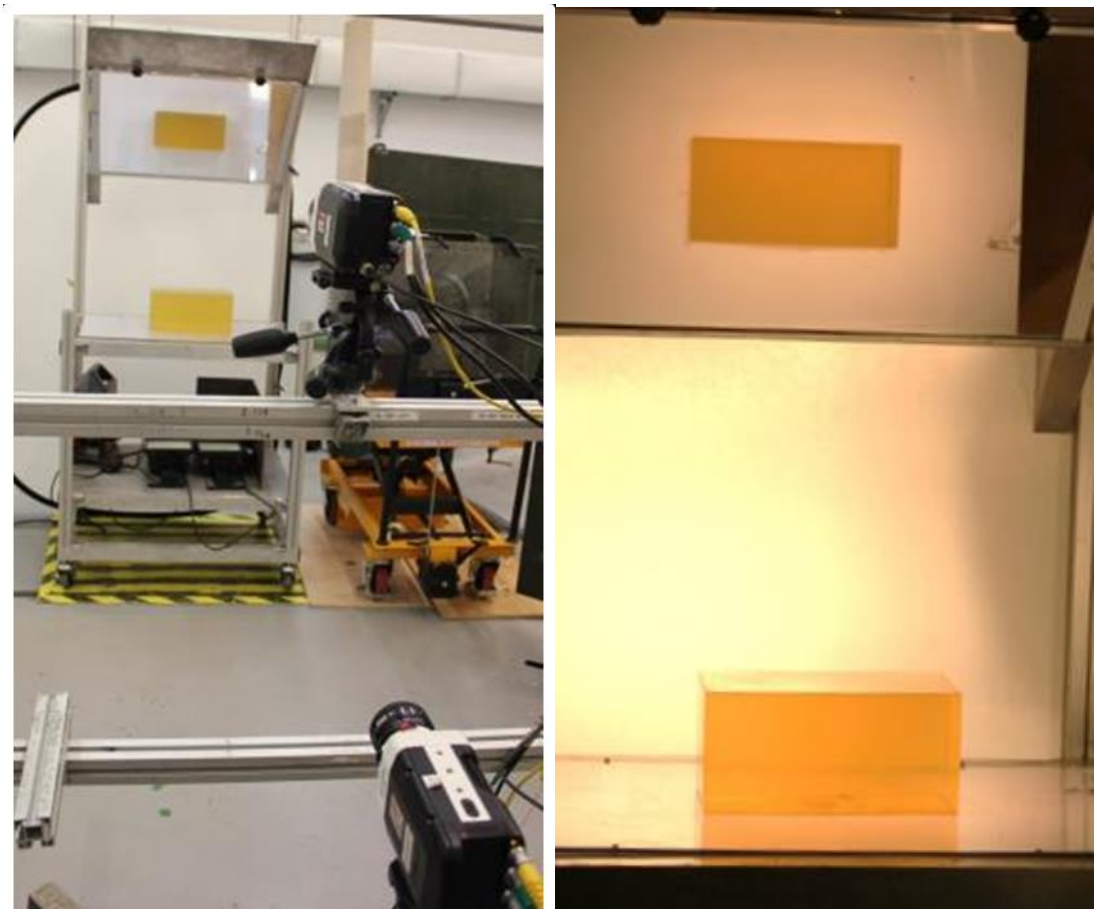

Figure 40: Photograph of setup of tissue simulant testing with a gelatin block target. Left – view from the position of the HSV cameras (two Phantom Miro M310 cameras shown). Right – close up of the gelatin block on the firing table with high power lighting on. The top view of the block can be seen via a 45° mirror.

DoP in the simulant was measured by inserting a stiff rod down the resulting cavity until it contacted the back of the projectile. The projectile length was added to this DoP measurement.

7.2.4.2 Projectiles used for ballistic assessment of tissue simulants

Properties of the projectiles used in the original work are given in Table 22, ordered by geometry and then by mass.

Geometry	Mass (g)	Diameter (mm)	Material	Density (g cm^{-3})	Shots (all simulants)
Sphere	0.04	3	Glass	2.5	16
Sphere	0.05	3	Ceramic	3.8	21
Sphere	0.11	3	Steel	7.85	25
Sphere	0.14	4.8	Glass	2.5	14
Sphere	0.22	4.8	Ceramic	3.8	16
Sphere	0.29	6	Glass	2.5	33
Sphere	0.34	6.4	Glass	2.5	13
Sphere	0.35	4.4	Steel	7.85	239
Sphere	0.43	6	Ceramic	3.8	39
Sphere	0.46	4.8	Steel	7.85	16
Sphere	0.49	4.5	Lead	10.3	15
Sphere	0.52	6.4	Ceramic	3.8	10
Sphere	0.90	6	Steel	7.85	48
Sphere	0.97	9	Glass	2.5	112
Sphere	1.06	6.4	Steel	7.85	11
Sphere	1.47	9	Ceramic	3.8	108
Sphere	3.04	9	Steel	7.85	118
Sphere	10.9	20	Glass	2.5	12
Sphere	16.03	20	Ceramic	3.8	15
Sphere	33.38	20	Steel	7.85	13
Cylinder	0.24	3.3	Steel	7.85	8
Cylinder	0.49	4.1	Steel	7.85	18
CN cylinder	0.53	5.4	Ceramic	3.8	4
CN cylinder	1.10	5.4	Steel	7.85	1
Cube	0.98	5	Steel	7.85	2
Total					**927**

Table 22: Description of projectiles used in tissue simulant DoP comparison[82].

[82] Although these are the projectile properties used to assess all the simulants, each of these (with fewer total shots) were assessed against Dstl 20% gelatin at 10°C. Therefore, Table 22

Spheres were supplied from GMS Ball Co Ltd. to DIN 5401 - Part 1, G100 (or equivalent)[83]. Cylinders, CN cylinders and cubes were manufactured through the Dstl Engineering Capability. Samples of each projectile type given in Table 22 had diameter and mass measurements taken to verify the projectile properties.

7.2.5 Tissue simulant DoP results

7.2.5.1 Data overview

The DoP results from this assessment were combined with those taken from the literature (previously summarised in Table 6) as well as other data that was made available (not conducted by the author) and not previously published[84].

Only targets with at least 4 penetrating shots were included and all non-penetrating shots or those that exited the simulant were excluded. These data are summarised by simulant type in Table 23.

	Number of penetrating shots from each data source				
Target description	**Original**	**Previously un-reported**	**Literature**	**Total**	**Source**
Dstl 5% gelatin at 10°C	7	0	0	7	n/a
(Fackler) 5% gelatin at 4°C	0	0	28	28	[162]
(Fackler) 7.5% gelatin at 4°C	0	0	37	37	[162]
Cranfield 10% gelatin at 4°C	0	0	178	178	[38; 122; 163; 166]
Haag 10% gelatin at 4°C	0	0	11	11	[137]
AzDPS 10% gelatin at 4°C	0	0	9	9	[137]
Guey/ Kieser 10% gelatin at 4°C	0	0	151	151	[158; 160]
Fackler 10% gelatin at 4°C	16	0	63	79	[19; 42; 94; 162]
Dstl 10% gelatin at 10°C	49	0	0	49	n/a

can be used to indicate then projectile validation bounds for Dstl 20% gelatin at 10°C based on the testing described in the following Section.

[83] Which allows ±47.5 µm tolerance on the nominal diameter and ±2.5 µm deviation from spherical.

[84] Data from internal Dstl studies (Mouland and Reeve, 2009).

	Number of penetrating shots from each data source				
Target description	**Original**	**Previously un-reported**	**Literature**	**Total**	**Source**
Haag 10% gelatin at 10°C	0	0	10	10	[137]
Guey/ Kieser 11.25% gelatin at 4°C	0	0	253	253	[158; 160]
ATK Mission Research 15% gelatin at 10°C	0	0	6	6	[165]
(Fackler) 15% gelatin at 4°C	0	0	29	29	[162]
Haag 20% gelatin at 4°C	0	0	7	7	[137]
ATK Mission Research 20% gelatin at 10°C	0	0	29	29	[165]
Cranfield 20% gelatin at 10°C	0	0	70	70	[38; 122]
Dstl 20% gelatin at 10°C	519	22	98	639	[58; 79; 88]
Haag 20% gelatin at 10°C	0	0	21	21	[137]
Haag 20% gelatin at 10°C over heated during mixing	0	0	6	6	[137]
NATO 20% gelatin at 10°C	49	0	32	81	[42]
Guey/ Kieser 20% gelatin at 10°C	0	0	238	238	[158; 160]
20% gelatin at 10°C (method not stated)	0	0	48	48	[91]
20% gelatin at 10°C (method not stated)	0	0	94	94	[161]
Dstl 20% gelatin at 10°C over heated during mixing	4	0	0	4	n/a
Dstl 30% gelatin at 10°C	32	0	0	32	n/a
Paraffin wax	46	0	0	46	n/a
Perma-Gel[85,86]	75	0	155	230	[38; 122; 167]
Soap 1.06 g cm^{-3} (opaque)	29	0	0	29	n/a
Soap 1.1 g cm^{-3} (translucent)	37	0	0	37	n/a

[85] As detailed in Table 6, this includes 'new' and re-melted Perma-Gel data.
[86] Data from Reference [167] was limited to velocities under 1400 m s^{-1}.

	Number of penetrating shots from each data source				
Target description	**Original**	**Previously un-reported**	**Literature**	**Total**	**Source**
Soap (glycerine based, commercial grade)	0	0	44	44	[164]
Stabili-gel (40% SEBS)	0	0	9	9	[155; 159]
Stabili-gel (35% SEBS)	0	0	13	13	[155; 159]
Stabili-gel (32.5% SEBS)	64	0	0	64	n/a
Stabili-gel (30% SEBS)	0	0	14	14	[155; 159]
Stabili-gel (25% SEBS)	0	0	12	12	[155; 159]
Stabili-gel (20% SEBS)	0	0	7	7	[155; 159]
Total	**927**	**22**	**1672**	**2621**	

Table 23: Summary of muscle tissue simulant DoP data from original testing and the literature[87].

Different aspects of the simulants are compared in the following sections. For the gelatin based simulants this includes the effects of: mix method, mix temperature, use temperature, concentration, fragment geometry and mold size.

Some of the testing was performed prior to the adoption of a calibration standard, so a comparison of calibration tests is not available across all simulants assessed.

7.2.5.2 Penetration window comparison to muscle tissue

The best performing and most common muscle tissue simulants were compared to the muscle tissue response in this sub-section. The normalised DoP over density function was used to create ‘penetration windows’ for muscle tissue (both with and without skin) and the selected simulants. The penetration windows are shown in Figure 41 and were based on the limits of the individual data points evaluated for each target. The penetration windows were deemed to provide a

[87] Acronyms in table: AzDPS = Arizona Department of Public Safety, Dstl = Defence Science Technology Laboratory, NATO = North Atlantic Treaty Organisation, SEBS = poly(styrene-b-ethylene-co-butylene-b-styrene).

clearer distinction between the different target responses than using the raw data points (due to the large number of points), or best fit lines to each target.

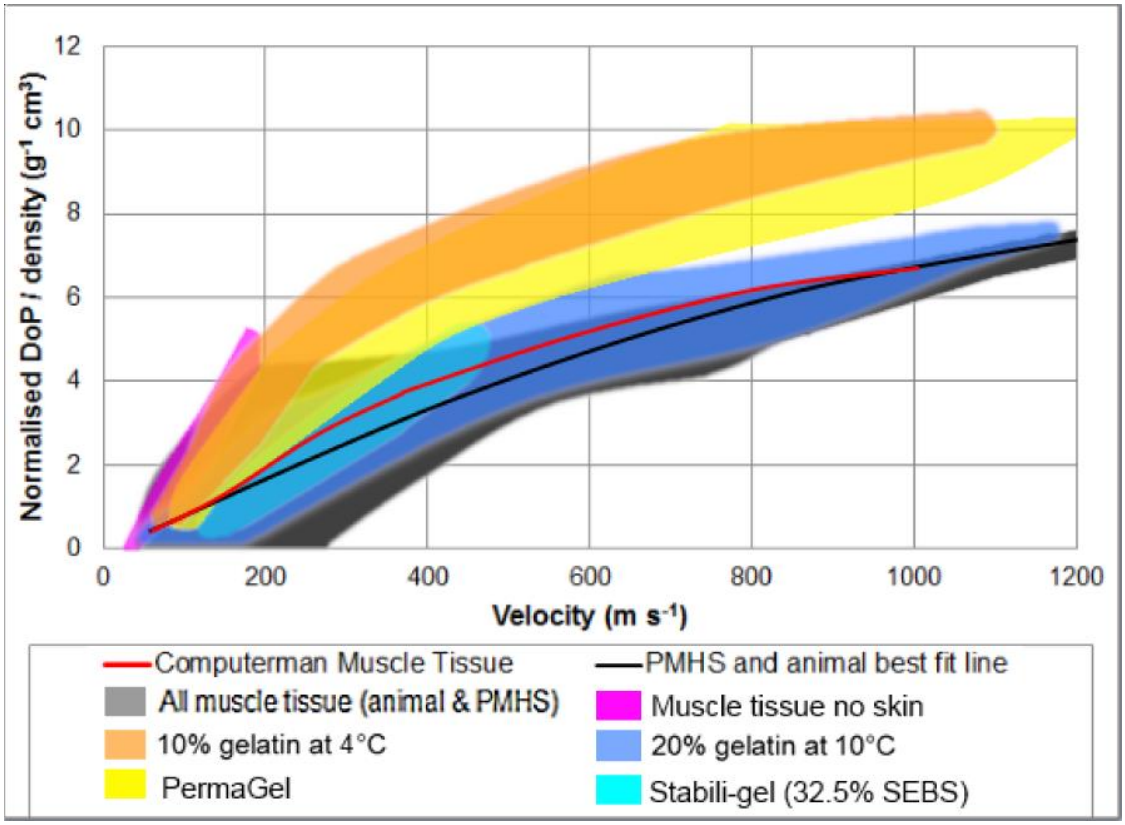

Figure 41: Comparison of penetration windows for muscle tissue (with and without skin), selected muscle tissue simulants and the muscle tissue best fit curves.

Based on permanent DoP alone as a performance metric, the simulant that gave the closest match to real muscle tissue was 20% gelatin at 10°C.

Figure 41 shows the penetration response of 20% gelatin at 10°C gave a good fit to muscle tissue over the velocity range considered, in terms of matching penetration windows, as well as very good match to the ComputerMan and PMHS and animal best fit lines.

The penetration windows for 20% gelatin at 10°C and muscle tissue do not completely overlay one another. This is partially because muscle tissue is more variable in its response, but also different projectiles have been used in the different targets.

The Stabili-gel (32.5% SEBS) provided a reasonable penetration response compared to the real muscle tissue, but was evaluated over a much more limited velocity range (and more limited number of shots). The corresponding performance of Stabili-gel at high velocities is not known.

The 10% gelatin at 4°C and Perma-Gel windows only fall within the muscle tissue response window for certain projectiles and at low velocities. At higher velocities, both these simulants give a very different response to that seen in muscle tissue, where they show much deeper penetrations than muscle tissue. Therefore 10% gelatin at 4°C and Perma-Gel are not deemed suitable muscle tissue simulants.

Often cited as the argument in favour of the use of 10% gelatin at 4°C is the DoP comparison for a 4.3 mm steel sphere at 181 m s^{-1} given by Fackler and Kneubuehl [94] comparing it to the DoP in pig thighs with the skin intact.

The normalised DoP over density value calculated from Fackler and Kneubuehl [94] for pig thighs is 2.63±0.45 g^{-1} cm^3 at 181±4 m s^{-1}. This is show overlaid on the penetration windows for muscle tissue and the two main gelatin mixes in Figure 42.

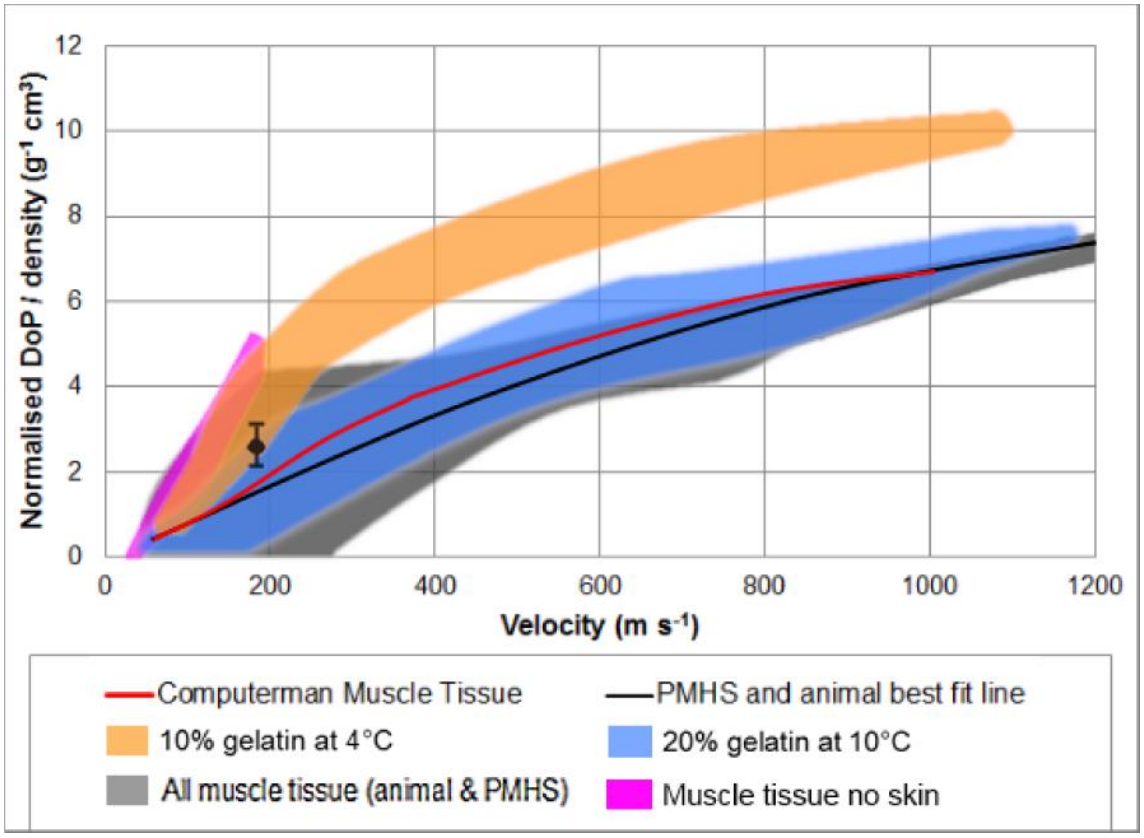

Figure 42: Comparison of penetration windows for muscle tissue (with and without skin), 10% gelatin at 4°C, 20% gelatin at 10°C and muscle tissue best fit curves with the Fackler data point shown in black. The error bars on the Fackler data point are those given in the original reference [94].

Whilst the conclusions in favour of the use of 10% gelatin at 4°C based on the DoP comparison reached in the paper by Fackler and Kneubuehl [94] are justifiable based on the tests with a single projectile at one velocity, the data presented in (Figure 41 and) Figure 42 based on comparisons of the normalised DoP over density with a more extensive and broader dataset contradict these previous findings.

Figure 41 and Figure 42 highlight that one of the issues in the selection of a suitable tissue simulant is the variability in the target response, particularly in real muscle tissue.

Based on Figure 42, 10% gelatin at 4°C appears to follow the general response of the animal muscle tissue without skin, but only up to velocities of 200 m s^{-1}. Comparing the DoP data for animal and PMHS muscle tissue data with skin intact

to the 10% gelatin at 4°C at higher velocities (e.g. >500 m s^{-1}), there are large discrepancies between the two datasets, indicating that 10% gelatin at 4°C is not a suitable simulant for muscle tissue.

7.2.5.3 20% gelatin at 10°C comparison to muscle tissue

20% gelatin at 10°C was shown as the most promising muscle tissue simulant in Figure 41 and Figure 42. The response of this simulant (from combined data for all different 20% mix methods) compared to muscle tissue based on the raw data points is shown in Figure 43, and just the Dstl 20% gelatin at 10°C mix with muscle tissue in Figure 44.

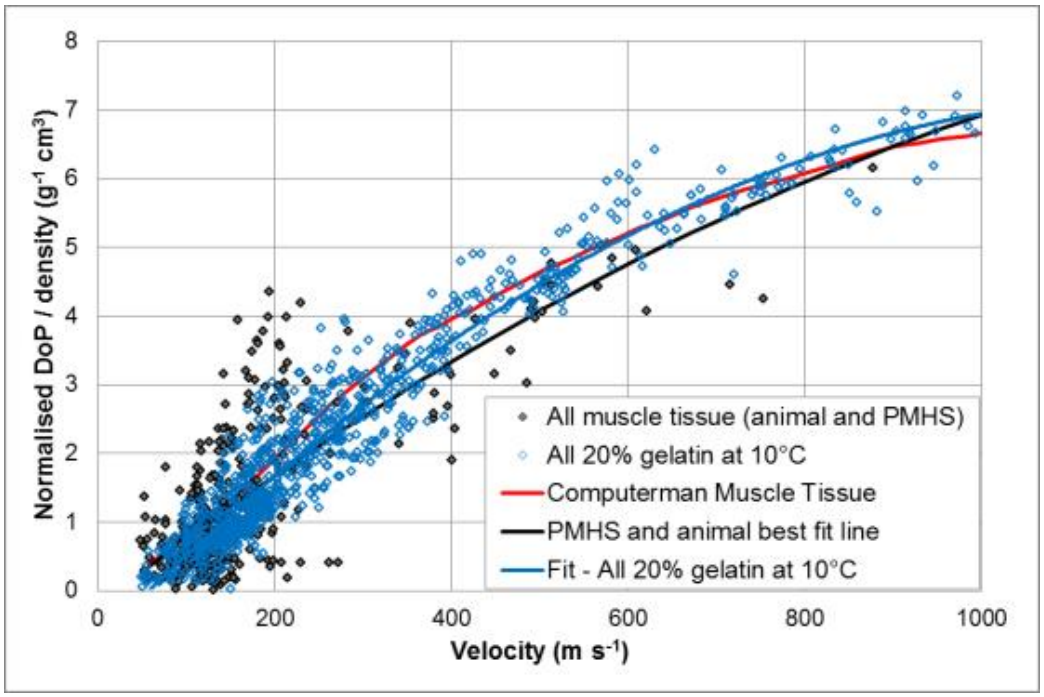

Figure 43: Comparison of penetration in (all different mix methods) 20% gelatin at 10°C to muscle tissue raw data and performance curves. Data from original testing and that summarised in Table 6.

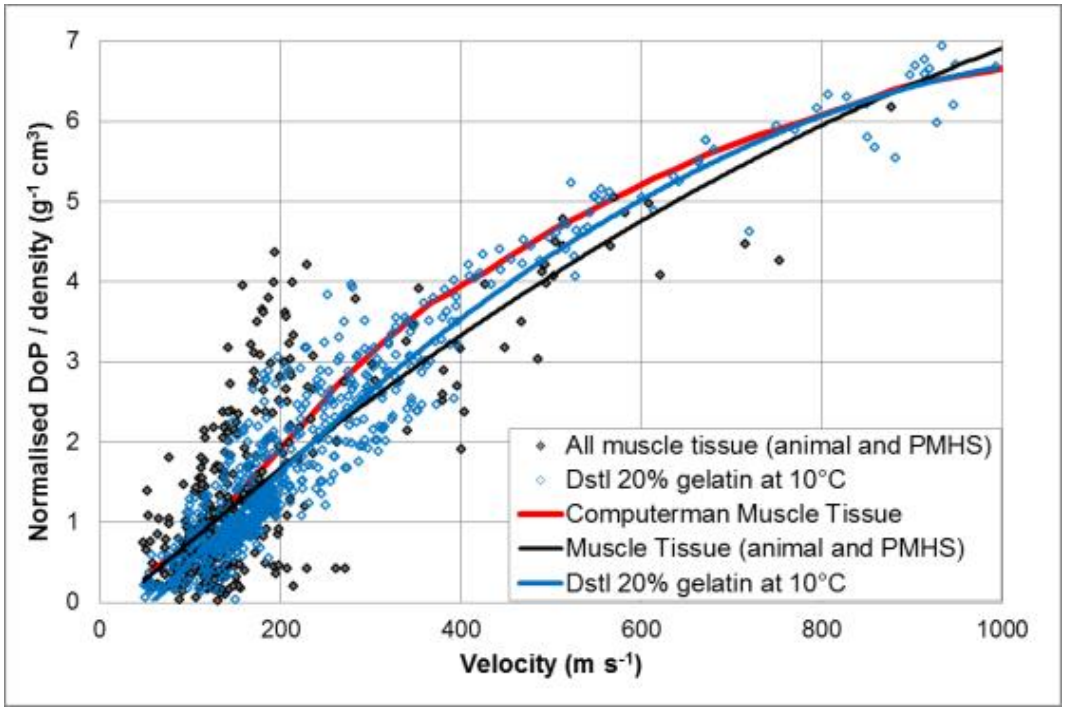

Figure 44: Comparison of penetration in Dstl 20% gelatin at 10°C to muscle tissue data and performance curves. Data from original testing and References [58; 79; 88].

Figure 43 and Figure 44 show the raw data and best fit curves to the 20% gelatin at 10°C data (all mixes and just the Dstl mix respectively). The best fit curves lay very close to the muscle tissue response curves over the entire velocity range assessed (50 m s^{-1} to 1000 m s^{-1}). Despite the Dstl 20% gelatin at 10°C data being conducted for a greater number of different projectiles than the muscle tissue data (that would be expected to contribute to the variability in the data), the simulant response is less variable than muscle tissue.

In the following sub-sections, factors affecting gelatin penetration response are evaluated.

7.2.5.4 Gelatin mix temperature

Gelatin has limited solubility in cold water and therefore is normally heated or mixed with hot water to allow the gelatin powder to dissolve. Different preparation methods specify different temperatures for this, but excessively high temperatures break down the long collagen chains in the gelatin [127].

Different sources recommend different maximum mix temperatures, and not all agree on what these limits should be [111; 128; 129; 137; 215]. It appears that 10% gelatin is more sensitive to excess heat and 20% gelatin is more thermally stable [129].

The standard preparation procedure for Dstl 20% gelatin involves mixing the gelatin powder with water at 70±5°C. During the manufacture of one batch, the gelatin was mixed with water at approximately 80°C and produced a visually different end product. This overheated Dstl 20% gelatin was calibrated at 10˚C with the fixed velocity calibration test for 20% gelatin in APPENDIX D (Section D.5.3) and produced penetration depths three times larger than expected (average 108 mm at an average of 179 m s^{-1}). Based on this, the calibration test appears to be a suitable method to determine where the gelatin has been overheated during preparation.

These data suggest that temperatures in excess of 80°C are likely to affect the gelatin properties of 20% gelatin mixes. 20% gelatin when mixed following the Dstl method at 70±5°C meets the required calibration standard and appears to be a ‘safe’ temperature. The upper temperature limit for 10% gelatin mixes is in the range 60-70°C. Extended exposure to high temperatures will cause breakdown of the long chain collagens and therefore extra caution should be taken when mix methods use water baths or similar to heat the mixture rather than adding gelatin powder to preheated water.

Whilst the Dstl mix method has been used to make 10% (and 5%) gelatin for the comparisons here, it is not advised to use this method to produce 10% gelatin due to these gelatin mix temperature issues.

7.2.5.5 Gelatin concentration

Based on the Dstl mix method and all tested at 10°C, four different gelatin concentrations were evaluated from 5% to 30% gelatin by mass.

The 5% concentration gelatin had difficulty supporting its own weight, with two of the three blocks damaged beyond use just removing them from the mold. It was evident that the lower concentration gelatin mixes were significantly more

transparent, although the 30% was still sufficiently transparent to be practical for high speed video analysis (with block dimensions of 150 mm by 150 mm by 300 mm length).

Figure 45 shows the normalised DoP over density plotted against velocity for each of the 4 concentrations.

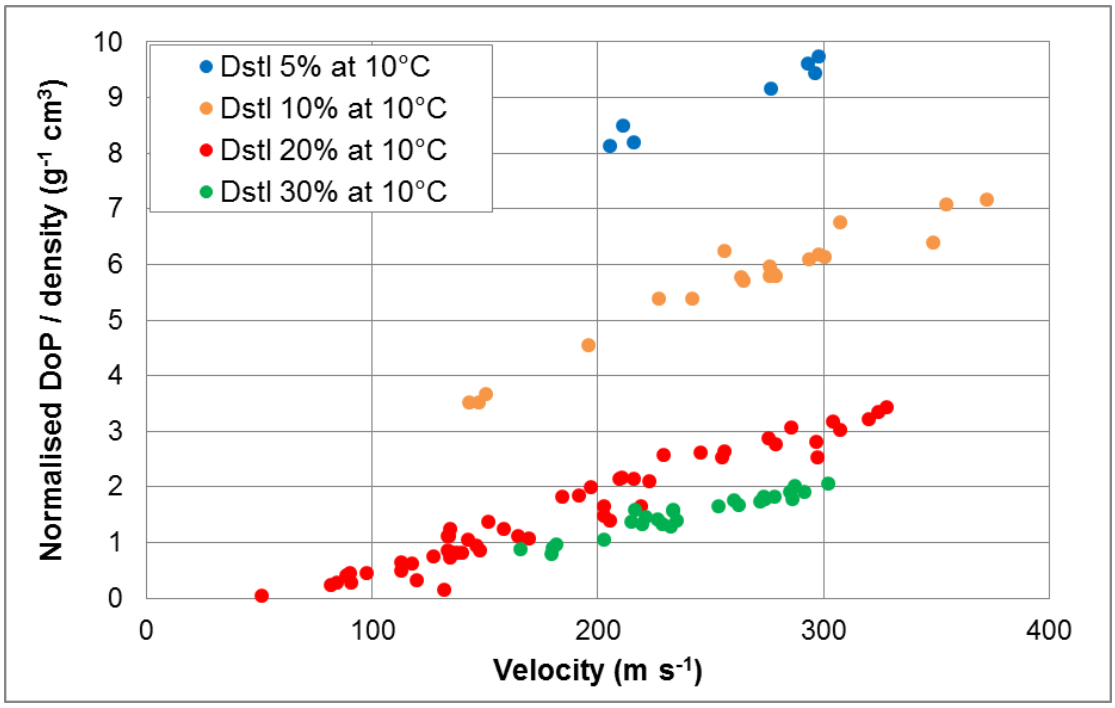

Figure 45: Penetration into different Dstl gelatin concentrations at constant use temperature (9 mm spheres of different densities). Data is from original testing.

As expected in Figure 45, increasing the gelatin concentration decreases the normalised DoP over density of the projectile. The difference between 5% and 10% is similar to the difference between the 10% and 20% concentration, with the difference between 20% and 30% much smaller. These data were replotted in terms of velocity contours required to provide equivalent penetrations at different gelatin concentrations as a way of visualising the effect of gelatin concentration on the results.

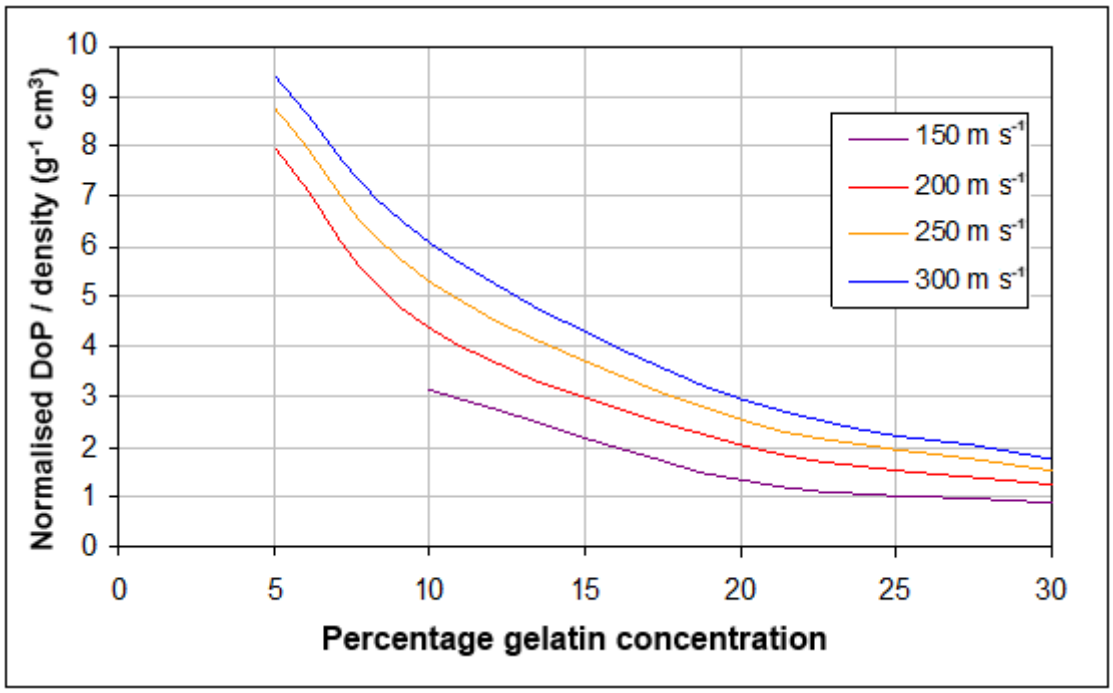

Figure 46: Velocity contours for penetration into different concentration gelatin mixes at 10°C from 9 mm sphere data.

Figure 46 shows average velocity contours for 4 velocities across the range of Dstl gelatin concentrations tested (at 10°C). This gives an indication of the difference in the expected penetration as the gelatin concentration is varied at a constant usage temperature. These velocity contours could be generated for any specific velocity in the range 150 to 300 m s^{-1} based on the raw data. This may have utility in estimating the variation in gelatin concentration that the calibration test (APPENDIX D, D.5.3) may be able to resolve[88].

7.2.5.6 Gelatin preparation method effects on DoP

A comparison between all the data across the different 10% gelatin at 4°C mixes is shown in Figure 47.

[88] Noting the limitations of the normalised DoP over density function described in Section 4.

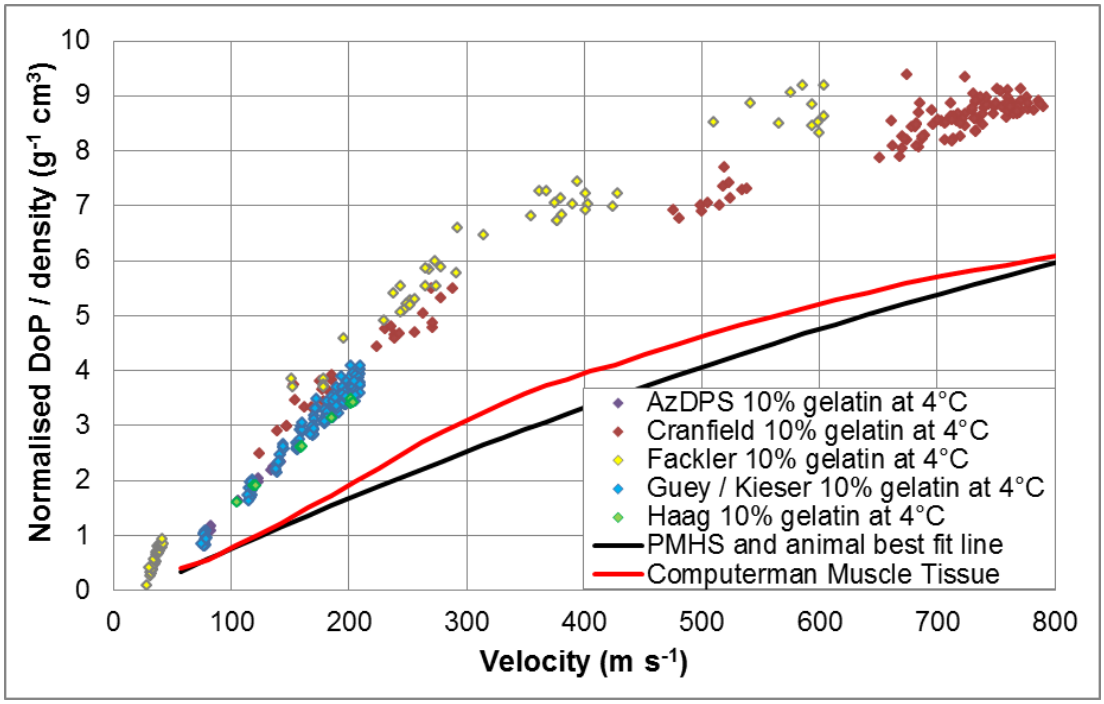

Figure 47: Comparison of penetration in different 10% gelatin at 4°C mix methods. Data from original testing and that summarised in Table 6.

The different 10% gelatin at 4°C mix methods are compared against each other, and to the muscle tissue best fit responses in Figure 47. This clearly demonstrates that 10% gelatin at 4°C is not a suitable muscle tissue simulant for the DoP response over the impact conditions investigated.

In Figure 47, the data for Cranfield 10% gelatin at 4°C has been limited to velocities under 800 m s^{-1} (for comparison to the other mix methods). The data shown in Figure 47 suggests that the Fackler method 10% gelatin at 4°C results in a higher DoP under equivelent impact conditions than the other mix methods. The data for Fackler 10% gelatin at 4°C was from both original testing and published data [42]. Where there is overlap in the data from both sources (in the velocity range 230-376 m s^{-1}), the gelatin showed a very similar response. It is unlikely that the difference in the Fackler mix method to the other methods is an artefact of an error in preparation from one experiment. However, neither the original testing on the Fackler method 10% gelatin at 4°C or that from Reference [42] calibrated the gelatin prior to testing. It is therefore possible that the gelatin was not within specification when tested (e.g. insufficient cure, block temperature

too high, incorrect manufacture etc.), although in a similar manner across the two data sources.

A comparison between all the data across the different 20% gelatin at 10°C mixes is shown in Figure 48.

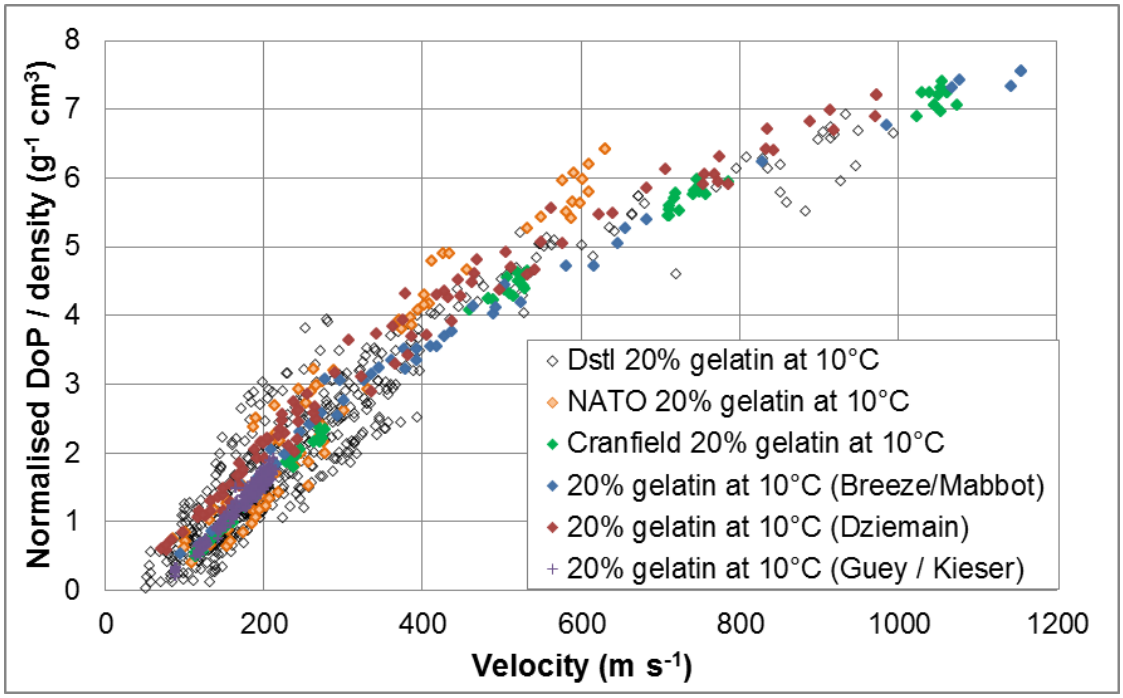

Figure 48: Comparison of penetration in 20% gelatin at 10°C by different manufacture methods (all fragments). Data from original testing and that summarised in Table 6.

There are no clear observable deviations between the different 20% gelatin mix methods based on the trends in Figure 48, apart from the NATO 20% gelatin at 10°C data showing higher penetrations than the other data at velocities around 600 m s^{-1}. A statistical comparison between all the different mix methods was not conducted. The comparisons are complicated by the fact that different projectiles (and a different number and types of projectiles) were used for the different mixes. This manifests in additional variability in the normalised DoP over density response, particularly evident in the Dstl 20% gelatin at 10°C data.

The Dstl 20% gelatin at 10°C variability was not due to less consistent material[89]. Figure 48 also shows the DoP normalisation (by projectile diameter and density) is not ideal (i.e. there is no account made for projectile geometry).

To show the consistency or reliability in the target response, Figure 49 shows the penetration into Dstl 20% gelatin at 10°C with 6 mm steel spheres for a single fragment type (a 6 mm steel sphere).

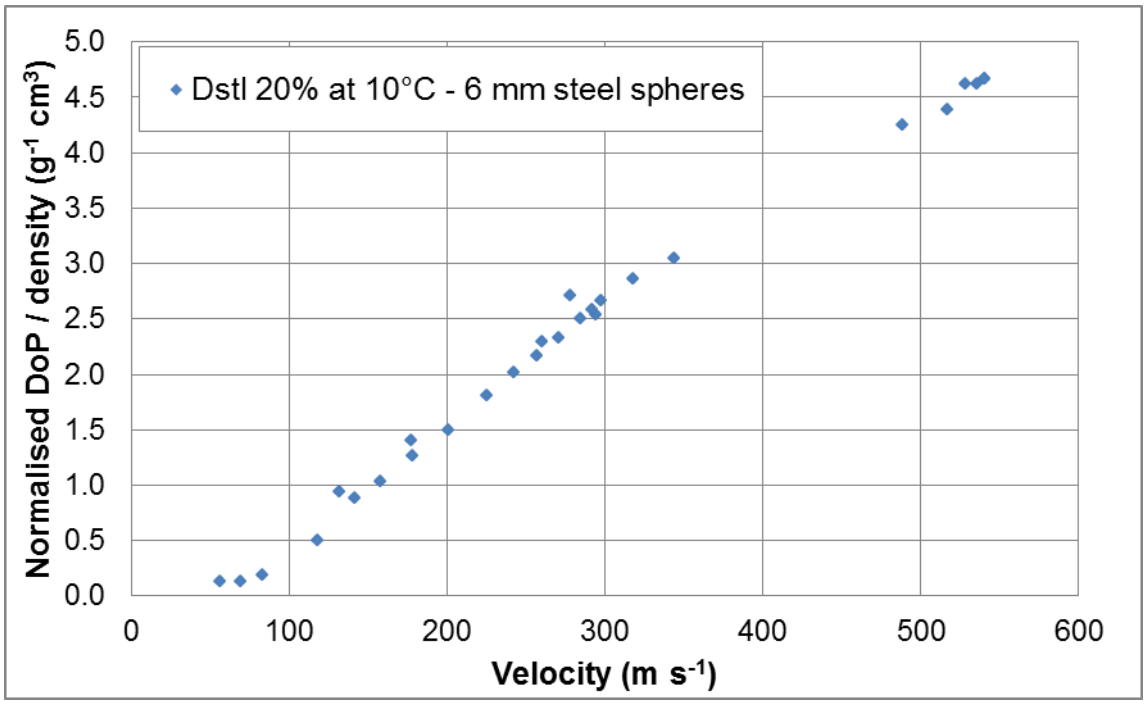

Figure 49: Penetration in Dstl 20% gelatin at 10°C with a single projectile type (6 mm steel sphere). Data is from original testing.

Similarly to Figure 49, the consistency in the target response for some of the other 20% gelatin at 10°C mixes can be compared if the data are limited to steel spheres between 4 mm and 12 mm diameter. This comparison is shown in Figure 50.

[89] Although approximately half the data for Dstl 20% gelatin at 10°C was collected before a calibration standard was available and used for 20% gelatin. Of all the other 20% gelatin at 10°C data shown, only that from Reference [158; 160] was tested with the 4.4 or 4.5 mm sphere used in the gelatin calibration standard(s), APPENDIX D, D.5.3.

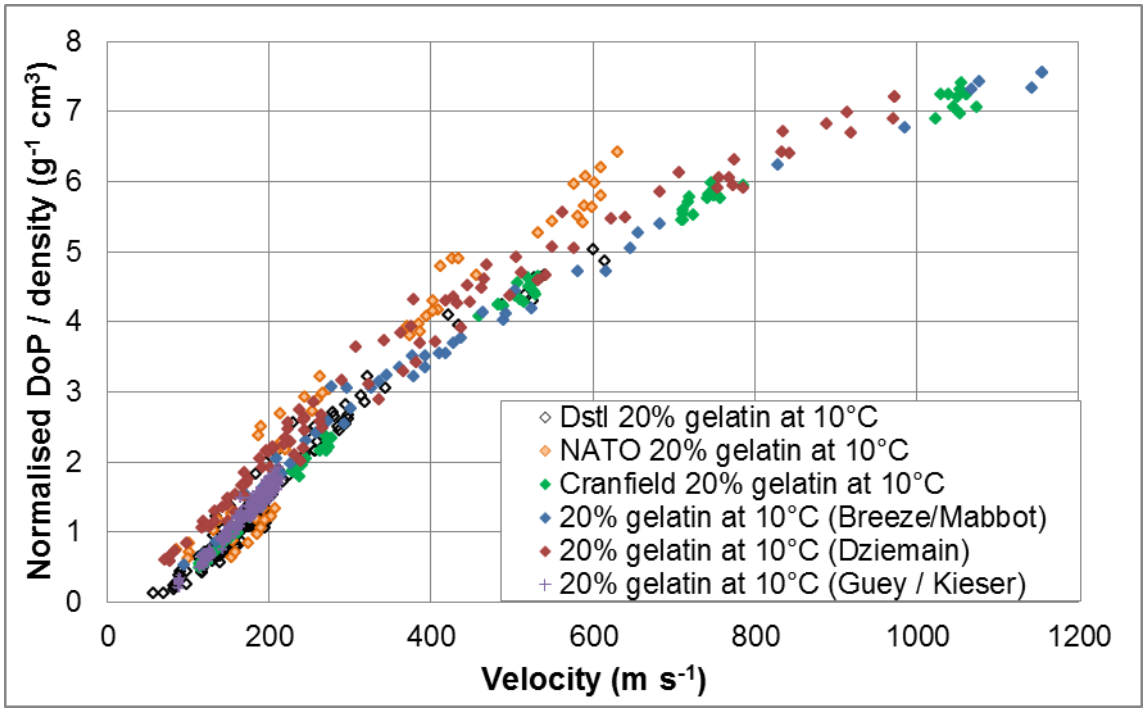

Figure 50: Comparison of penetration in 20% gelatin at 10°C by different manufacture methods for steel spheres, 4-12 mm diameter. Data from original testing and that summarised in Table 6.

Whilst the focus of gelatin testing in the remainder of this thesis is on Dstl 20% gelatin at 10°C, the data in Figure 48 and Figure 50 would suggest that many of these other 20% gelatin preparation methods provide a similar DoP response (the response of the NATO mix to the other methods is questionable for high velocities with the available data). However, the different mix methods have not been validated against each other (it has not been determined if the Cranfield mix method could be used in place of the Dstl mix method for example).

7.2.5.7 Other factors for gelatin not explicitly investigated

Although not planned to be investigated, it was observed during the original testing conducted that gelatin of the same type and from the same supplier took different durations to reach full cure, determined by the time required to meet the calibration DoP test. This was evidenced when two batches of Dstl 20% gelatin at 10°C were prepared side by side. Both were supplied by VWR International Ltd, from the manufacturer Gelita AG. They were both labelled as “Gelita ®

Ballistic 3 Gelatine"; one was supplied in a 25 kg bag, the other in a 15 kg bag[90]. Both were well within their stated best before dates.

The gelatin blocks produced from the 25 kg bag met the calibration standard after conditioning at 10°C, 65% RH for approximately 18 hours[91]. The gelatin blocks produced from the 15 kg bag initially failed the calibration test (DoP too deep[92]) after approximately 18 hours conditioning[91] at 10°C, 65% RH. The same blocks met the calibration test after approximately 42 hours of conditioning[91]. All blocks were tested less than 5 minutes after removal from the conditioning cabinet.

This highlights the importance of the calibration test in verification of the gelatin produced, as well as planning time into any practical testing to mitigate issues such as this. The Dstl 20% gelatin at 10°C mix method (APPENDIX D, D.1) allows storage of the gelatin for up to 5 days prior to testing.

Data extracted from Reference [137] shows how the gelatin usage temperature effects 20% gelatin penetration response, shown in Figure 51.

[90] 25 kg bag lot number 073750. 15 kg bag with lot number 073602.
[91] Conditioning started within approximately 30 minutes of pouring the gelatin into the molds, with the molds pre-conditioned to 10°C. Both batches were made, poured and conditioned at the same time and were conditioned in the same cabinet.
[92] 4 shots were conducted, each being 1 or 2 mm greater than the DoP limits of Equation 14: New calibration standard developed for Dstl 20% gelatin at 10°C.

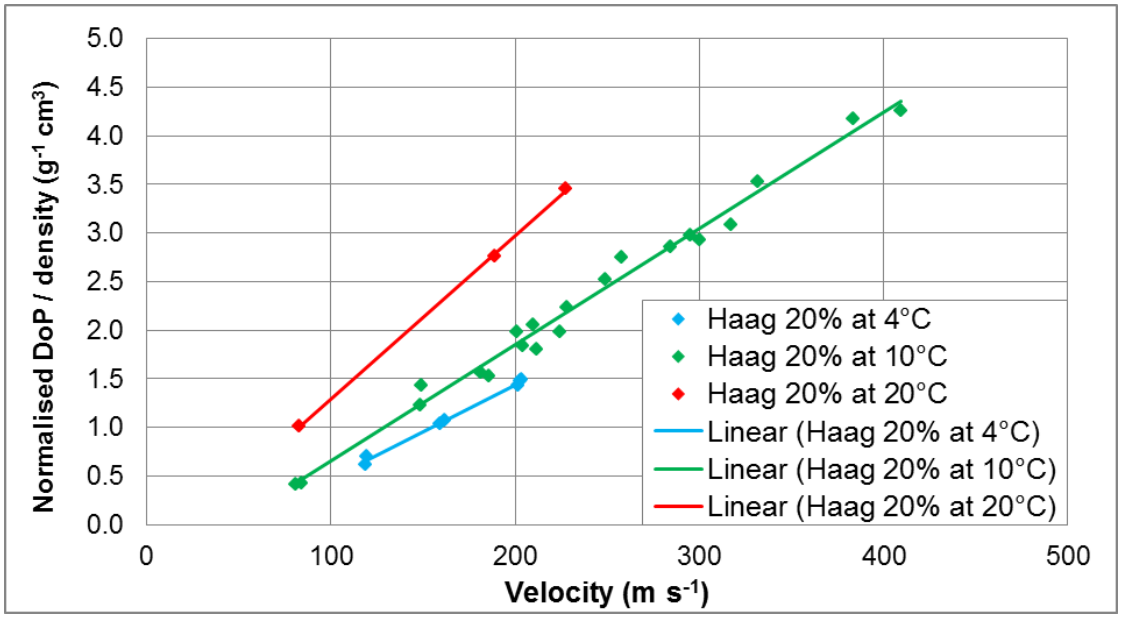

Figure 51: Comparison of penetration in Haag 20% gelatin at different usage temperatures. Data from Reference [137].

Reference [94] showed that penetration depths increased by 82% when the use temperature of 20% gelatin was raised from 4°C to 10°C and 20°C.

Although raw data is not available, Reference [215] showed DoP was dependent on the gelatin usage temperature (between 3°C and 8°C), which had a weaker dependence with higher gelatin concentrations.

These data show the importance of ensuring the gelatin at the correct usage temperature (which calibration can be used to verify) and that the gelatin is used within a set timeframe after removal from the fridge / cabinet to minimise (bulk) heating of the block that may alter the penetration response.

7.2.5.8 Non-gelatin tissue simulants

Based on the compositions evaluated in Reference [155], 32.5% polymer SEBS (67.5% mineral oil) was selected to give the best SEBS concentration to represent animal muscle tissue and 20% gelatin at 10°C. This SEBS formulation and the other non-gelatin muscle tissue simulants assessed are shown in Figure 52 compared to the muscle tissue best fit line (Equation 12).

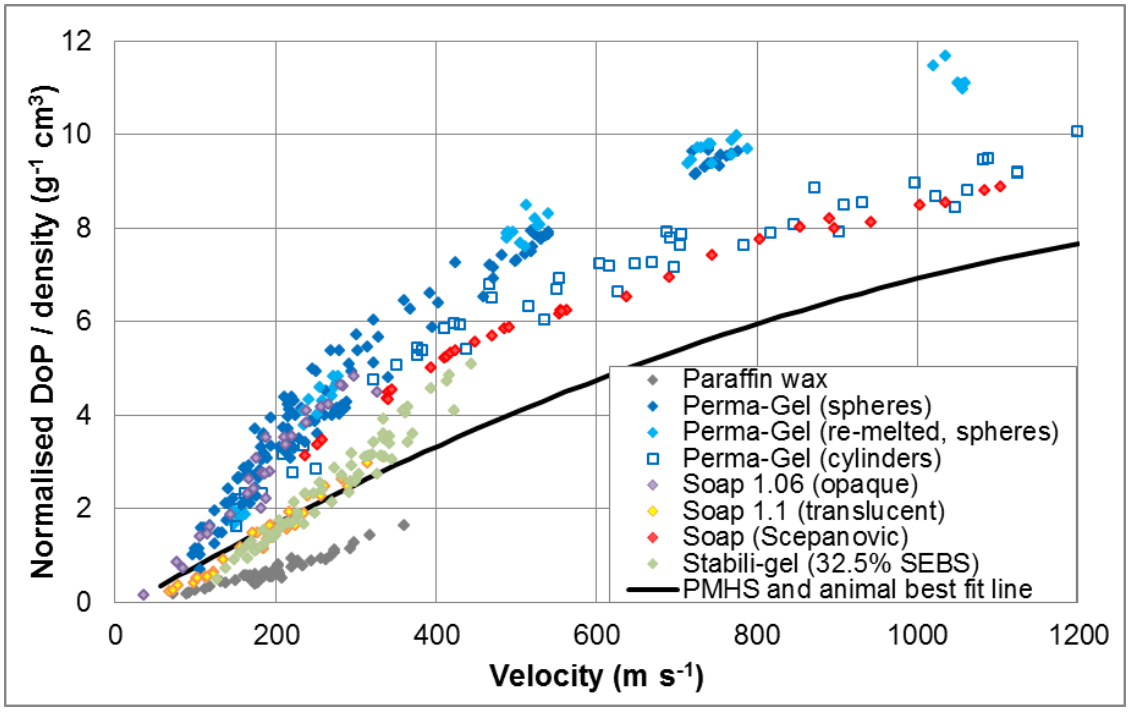

Figure 52: Comparison of penetration into non-gelatin tissue simulants to the muscle tissue best fit. Data from original testing and that Reference [38].

Of the synthetic (non-gelatin) simulants shown in Figure 52, the 1.10 g.cm^{-3} density soap gave the best match to the average animal tissue fit (Equation 12).

Whilst the permanent DoP response of the Stabili-gel (32.5% SEBS) was similar to the muscle tissue response curve[93] for velocities up to approximately 300 m s^{-1}, it was observed to have large elastic recoil of the projectile from its maximum temporary to permanent penetration depth, compared to gelatin.

The Perma-Gel data from References [167; 168] was included in Figure 52, but displayed separately as it was the only non-gelatin simulant tested with cylinders. As discussed, the normalised DoP over density function cannot account for geometry and therefore is best limited to projectiles of the same geometry.

[93] Although not as good match as 20% gelatin at 10°C in Figure 41, Figure 43 and Figure 44.

References [38; 122] indicated that Perma-Gel DoP performance changed when re-melted[94]. Perma-Gel is marketed as being reusable, however, it is not known if these changes will stabilise after additional melting and reuse cycles. As Perma-Gel has been designed to replicate 10% gelatin at 4°C [38; 122], the focus on its performance was likely focused on its ability to pass the 10% gelatin calibration test (APPENDIX D, Section D.5.2), not its ability to correctly model muscle tissue response.

Whilst Reference [126] used handgun bullets to evaluate (the 10% gelatin alternative) Clear Ballistics Gel® in comparison to 10% gelatin at 4°C, some of the findings are general and can be applied to other projectile types. It was found that the retarding force (calculated from the projectile retardation history) was significantly different to the 10% gelatin, and projectiles expanded to a smaller degree in the Clear Ballistics Gel®. The conclusion was that Clear Ballistics Gel® has utility in down selection of potential candidate projectiles, but further testing would require the use of gelatin [126].

Similar (although stated that it was not statistically significant) differences were observed in Reference [125] comparing 10% gelatin at 4°C, 20% gelatin at 10°C, Perma-Gel and Clear Ballistics Gel® in both the 10% and 20% mixes using 9 mm and 380 Auto pistol bullets. Differences were observed in both the energy absorbed with depth, as well as cavitation in each of the different simulants.

The requirement for a muscle tissue simulant outlined in Section 3.9.3[95] favoured a transparent material and one that gave elastic rather than plastic response. Apart from potentially the Stabili-gel (32.5% SEBS), none of the other synthetic (non-gelatin) simulants were deemed suitable as muscle tissue simulants. The data was limited to lower velocities for most simulants, so the high velocity

[94] These differences aren't obvious in Figure 52, which contains additional original test data for velocities up to 471 m s^{-1}.

[95] Ability to measure permanent DoP, retardation, temporary cavity dimensions and tumbling for bullets.

response cannot be determined, where potential rate sensitive effects may be more evident.

The synthetic simulant comparison does show that if there are not requirements for an elastic, rather than plastic response of the simulant, it is possible to have a ballistic soap that matches the penetration response of muscle tissue. Unfortunately the soaps used in the original testing (referred to by their densities) were not the formulations used and reported on previously in the literature [146; 148; 150; 164].

To investigate the potential of the Stabili-gel, further analysis was conducted: comparison of the different ratio SEBS formulations from References [155; 159] and original data for 32.5% SEBS are shown in Figure 53, in comparison to the muscle tissue fit curves.

It should be noted that different projectiles were used for the original evaluation of 32.5% (4.4 mm steel, 9 mm glass, ceramic and steel spheres) to that in Reference [155] (5.56 mm steel spheres).

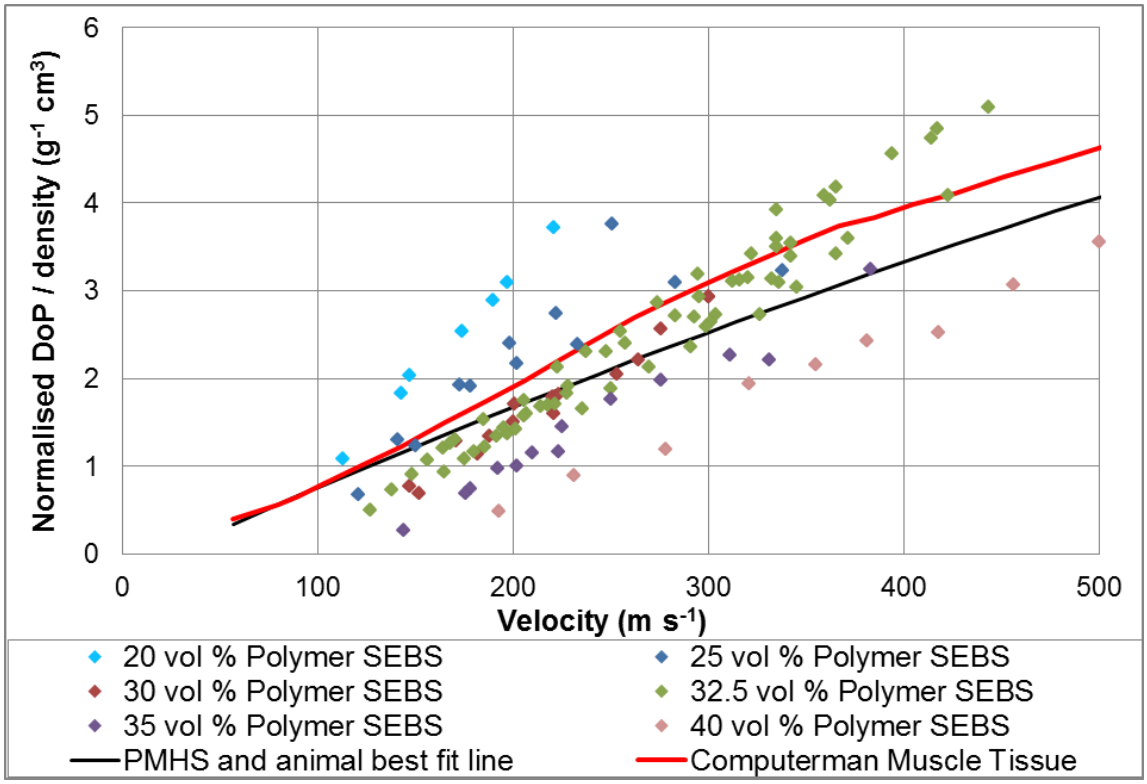

Figure 53: Comparison of penetration in various concentration SEBS (Stabili-gel) simulants to muscle tissue performance curves. 32.5% SEBS is original data, the remainder is from References [155; 159].

Figure 53 shows that whilst there is some scatter within the data for each concentration SEBS, the 32.5% SEBS gave a reasonable match to the ComputerMan and muscle tissue best fit curves. The 32.5% SEBS appears to slightly under-predict the penetration response at low velocities (<200 m s^{-1}) and over-predict the penetration response at higher velocities (<400 m s^{-1}). However, these differences may be (partially) due to the different projectiles used in the testing compared to the response curves. The comparison is also limited by the absence of high velocity data for the Stabili-gel.

The Stabili-gel with 32.5% SEBS showed un-anticipated behaviour during ballistic testing, where within certain velocity windows, the projectiles did not penetrate as deep as expected. This is more clearly demonstrated with data for a single projectile type, shown for the 4.4 mm steel sphere in Figure 54.

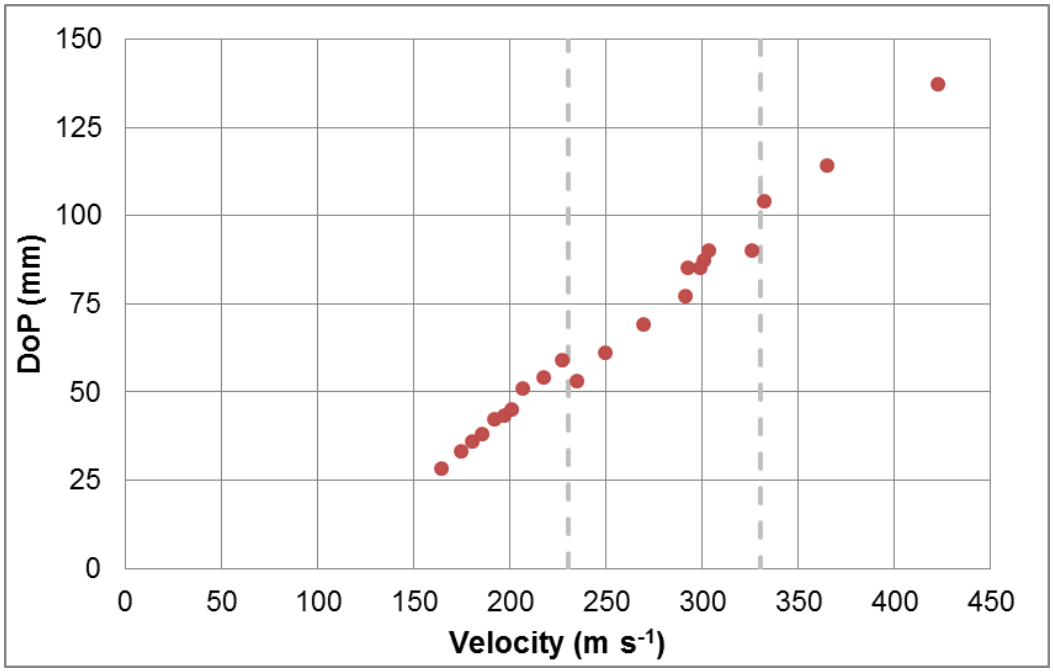

Figure 54: Depth of penetration in Stabili-gel (32.5% SEBS) with a 4.4 mm steel sphere. Data is original testing.

Figure 54 shows that between impact velocities of approximately 230 m s^{-1} and 330 m s^{-1} a discontinuity in response was observed in the simulant (between the grey dash lines). This was thought to be the way in which the temporary cavity collapsed whilst the projectile rebounded from its maximum temporary penetration depth, which may be related to the response frequency of the Stabili-gel. In this 'different' region, the projectile plugged the permanent cavity, trapping air in front of the projectile. At faster and slower velocities, this air was able to escape. The results of this phenomenon can be seen in Figure 55.

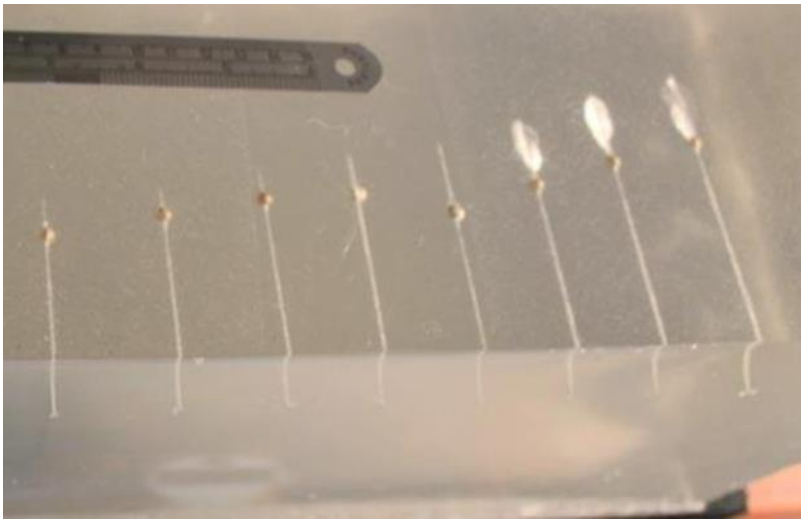

Figure 55: Photograph of 4.4 mm steel sphere DoP in Stabili-gel (32.5% SEBS) after shooting. Projectiles had increasing impact velocity from left to right (207 to 326 m s^{-1}).

Figure 55 shows the trapped air in front of the projectile in the 3 shots on the far right. It was also present in the fourth from the right, but escaped during subsequent shots, prior to this photograph being taken. The air escaping in this way did not cause the projectile to move from its previously measured position in this case. However, it was noted that the penetration depth did change for similar shots with the 4.4 mm steel sphere in this discontinuous response region.

Figure 55 also shows how far the projectile rebounded from the end of the permanent cavity. The maximum temporary penetration depth was much greater than the depth to which the permanent cavity extended.

The discontinuity in penetration response was seen in 3 of the 4 projectiles evaluated with Stabili-gel (32.5% SEBS) within the velocity ranges considered. The remaining projectile (9 mm glass) was found to fracture in the simulant at higher velocities; it is assumed that the velocity regime for the ‘trapped air’ behaviour was not reached for the velocities where the projectile remained intact.

References [125; 126] indicate that Clear Ballistics Gel® in both the 10% and 20% mixes are unsuitable as direct replacements or alternatives to ‘standard’ 10% gelatin at 4°C or 20% gelatin at 10°C. Whilst References [125; 126] do not indicate if Clear Ballistics Gel® designed to replicate 20% gelatin would match

real muscle tissue, the differences observed to 20% gelatin at 10°C within References [125; 126] imply that it is unlikely to be suitable. DoP testing (with spheres) in line with the other muscle tissue simulant data for the Clear Ballistics Gel® would allow these apparent discrepancies to be quantified in relation to real muscle tissue.

The normalised DoP over density function provides a method to enable the comparison of a large number of different tests with different projectiles and over a wide velocity range, which has not been performed in the literature previously. This avoids the potential pitfalls of selecting a muscle tissue simulant on limited data.

The normalised DoP over density function is not a perfect comparison tool as the resulting penetration windows are still quite wide (i.e. it does not account for all the projectile variables that would collapse the data onto a single curve, even when only considering spherical projectiles). Other sources of variability include the simulant response as well as that no account is taken of projectile geometry. The projectile geometry (for example combining data for spheres and cylinders) greatly increases the width of the corresponding penetration windows. This limitation of the normalised DoP over density function for different projectile geometries is demonstrated in Figure 52 for the Perma-Gel data, which is shown separately for spheres and cylinders, where the fundamental simulant response is considered to be quite repeatable.

This limitation extends to the best fit line for the PMHS and animal muscle tissue (Equation 12), where impacts over 700 m s^{-1} were exclusively for steel cylinders ≤0.2 g. Target thickness will always limit the DoP data that can be generated at higher velocities, particularly for heavier projectiles (>0.2 g). This limitation is addressed by considering the muscle tissue simulant response in terms of retardation or energy loss in Section 7.3, where the projectile is allowed to fully perforate the target.

7.2.6 20% gelatin at 10°C calibration development

There is no openly available calibration test for general 20% gelatin at 10°C, including no calibration associated with NATO 20% gelatin at 10°C [130].

To provide verification of the gelatin produced for ballistic testing, an existing (but not openly published) 'fixed velocity' calibration standard [216] was implemented part way through the testing described within this thesis.

This fixed velocity calibration will be referred to as method 1 calibration and required firing a 0.35 g steel sphere at a velocity of 180±5 m s^{-1} to generate a DoP of 38±6 mm (measured to the shallowest part of the projectile).

Due to the weapon systems used for ballistic testing (see APPENDIX B for the systems used within this thesis), achieving velocities within the required limits was not always practical.

After it was implemented, this fixed velocity calibration was performed for all the testing conducted against Dstl 20% gelatin at 10°C. The results for the batches that passed the calibration were collated, even those outside the allowed velocity limits. Any data for batches that failed calibration were discarded for the purposes of this analysis. This enabled a new calibration method to be generated, based on a wider impact velocity range.

The collated data was for a total of 166 shots from approximately 36 different gelatin batches. The resulting data is given in Figure 56, with the proposed wider impact velocity range calibration (method 2) and the previous fixed velocity calibration (method 1).

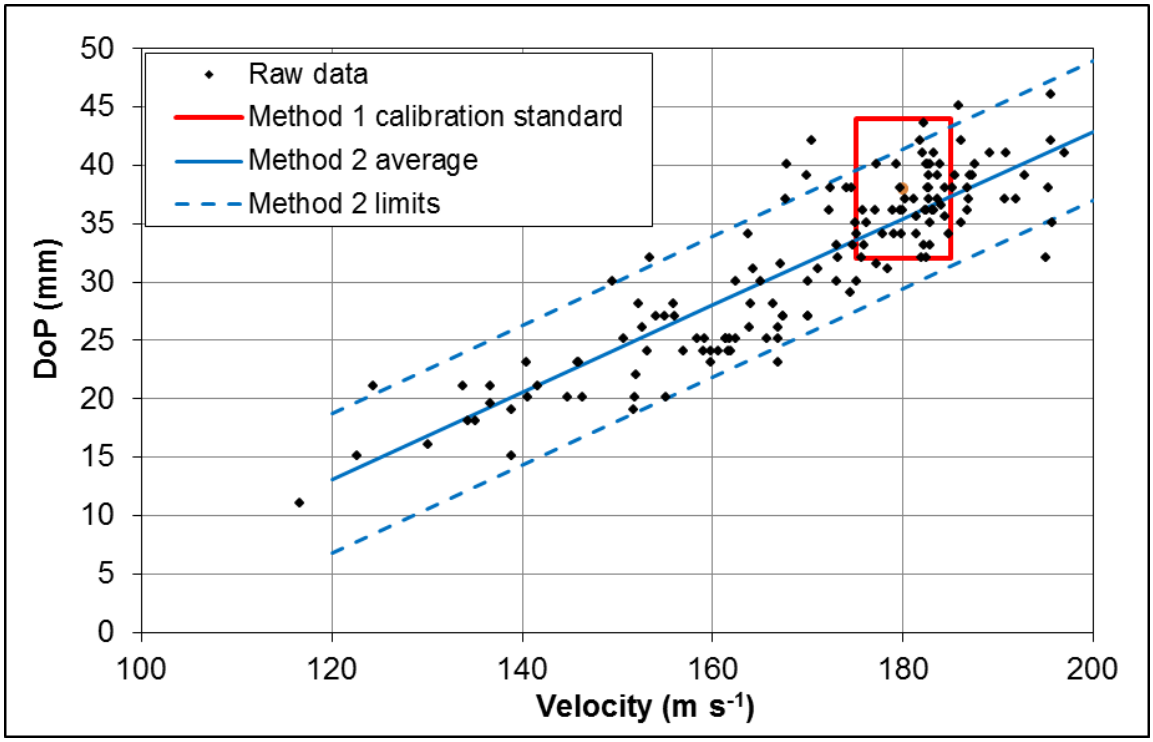

Figure 56: Calibration standards and data for Dstl 20% gelatin at 10°C. Data is original testing.

The proposed wider impact velocity range calibration (method 2) was based around the calculated 90% prediction interval of the linear fit to the raw data. The 90% prediction interval gave (average) limits of ±5.8 mm from the best fit line, which was rounded to ±6 mm for practicality. These limits were chosen to provide a balance between ensuring consistency and minimising the risk of rejecting a good batch. The wider impact velocity range calibration (method 2) shown in Figure 56 is given by Equation 14:

$$DoP = 0.378v - 32.6 \pm 6$$

Equation 14: New calibration standard developed for Dstl 20% gelatin at 10°C.

Where:

DoP is in mm (measured to the shallowest part of the projectile)

v is the impact velocity in m s^{-1}, within the velocity limits $120 \leq v \leq 200$ m s^{-1}.

There is potential for disagreement between the 20% gelatin existing standard (method 1) calibration [216] and Equation 14 (method 2). Equation 14 does not include the entire DoP range of the allowed method 1 ‘fixed velocity’ standard. Equation 14 should be adopted as the calibration standard for Dstl 20% gelatin at 10°C to ease practicality of achieving the required impact velocities.

91% of the data falls within the limits given by Equation 14. Given that the gelatin data used to produce this new calibration standard had already passed the method 1 calibration, the following guidance is suggested to reduce the risk of rejecting a good batch:

One result that is in calibration is required per batch (or per block if calibrating each block individually). If the first shot is at a valid velocity, but the resulting DoP is not within Equation 14, conduct an additional shot at a valid velocity. This second shot must then pass the calibration. If both fail, the batch should be rejected. It is suggested to report all calibration results (impact velocity and resulting DoP) with the studies in which it was generated to provide assurance on the gelatin verification.

The fixed velocity (method 1) and wider velocity range (method 2) calibration tests are detailed in APPENDIX D, Sub-Section D.5.3.

7.3 Muscle tissue simulants – energy loss comparison

7.3.1 Introduction

As a different metric to the DoP comparison, the energy lost by the projectile within muscle tissue to the simulant was also compared. This energy loss evaluates the simulant in terms of its retardation response compared to muscle tissue (e.g. the transient or temporary response, rather than the permanent one). This aspect of a muscle tissue simulant is critical for (and will dictate the validity of) assessment of projectiles such as bullets where behaviours such as tumbling or deformation may need to be measured or evaluated.

It is also critical for validating the muscle tissue simulant response for DoP predictions where the projectile may tumble, deform or fragment.

The retardation response dictates the deceleration experienced by the projectile and therefore the force acting upon it. In order to observe the correct projectile response(s) as in real muscle tissue and at the correct depths in the target, the retardation of the simulant must match real tissue.

The energy lost by the projectile in this comparison is one way of expressing the retardation response of the muscle tissue and simulants. It is an approach that has been used to do this type of comparison previously in the literature [107-109; 111; 123; 217], but with drawbacks previously detailed in Section 3.9.2.

An added benefit of this comparison is that typically when this type of testing is reported in the literature the animals have been kept alive, but terminally anesthetised. Although this means there may not be a realistic muscle tone, there is blood flow and it is likely to be more representative of a live person than using animal cadavers.

Data for animal tissue was sourced from the literature, apart from one series of testing, which is described in APPENDIX E, E.2. The original aim of this comparison was just to compare the data discussed in APPENDIX E, E.2 with the testing replicated in muscle tissue simulants. After investigation of available data from the literature, a much wider range of valid impact energy data was collated, enabling a broader comparison to be made.

The majority of the data for tissue simulants were produced as part of the testing described in Section 7.2, apart from some of the high energy impacts for Dstl 10% and 20% gelatin at 10°C, which are described in Section 7.3.2.

Available muscle tissue and simulant energy loss data was collated from the literature. Valid data for animal targets had:

- The skin intact over the muscle
- A nominal 100 mm wound track (100 mm -20/+50 mm were allowed[96]).

[96] Data from Reference [95] showed no differences to the relationship between impact energy and energy loss per 100 mm in live pig thighs until track lengths equal to or greater than

Valid data for muscle tissue simulant targets had:

- A nominal 100 mm wound track (100±10 mm were allowed), or the remaining energy at a nominal 100 mm penetration depth was measured (i.e. from HSV).

Only non-tumbling, non-deforming fragments were allowed (not bullets). Energy loss was normalised to a 100 mm target size to account for variation within the comparison.

The energy loss per mm may be a more common or digestible format, however, maintaining the reference back to the 100 mm target thickness should help avoid this data being compared to other data where different target thicknesses were used. This is important as using thinner or thicker targets will cause the energy loss per unit length to be different[97]:

- For thicker samples, the average energy loss per unit length will be lower
- For thinner samples, the average energy loss per unit length will be higher

7.3.2 Method for additional data

Previous work completed for the Combat Casualty Care programme in Dstl (and its predecessor organisations) investigated the efficacy of recombinant Factor VIIa (rFVIIa) for improving the survival rate in live, terminally anesthetised large white pigs that had been subjected to a ballistic penetrating injury on the muscle mass of the thigh to produce a repeatable ballistic injury.

This rFVIIa ballistic testing had not been previously published, but setup details and raw ballistic data were made available [96], to enable the testing to be recreated with tissue simulants. The testing details and results are provided in APPENDIX E, E.2.

150 mm were included. The data from Reference [95] included track lengths from 91 mm up to 210 mm.

[97] This can be highlighted with the FREM of projectile retardation in muscle tissue or gelatin in Section 9.3.

The rFVIIa data provided valuable validation for the muscle tissue simulants and was recreated using targets of Dstl 10% and 20% gelatin at 10°C[98]. Impact velocities were measured with 2 MSI 858 optical detectors [205] spaced 1000±1 mm apart and centred at 2500±10 mm from the target, connected to an 817 timing unit and a 570 computer interface, with processing by MSI Ballistics DB software. The tolerance on velocity measurement was calculated to be <±0.3%.

Exit velocities were measured using two Photron SA-Z high speed cameras [206], running at 80,000 frames per second and a resolution of 768 by 304 pixels. One camera was looking directly at the block, perpendicular to the shot line and the other a top down view via a mirror at 45°. The top camera was placed such that both cameras had a similar distance to the shot line (±10 mm). The gelatin was lit from behind and from underneath through diffusers, using multiple halogen flood lights. The lights were turned on remotely just prior to firing to reduce heating of the target. The setup is shown in Figure 57.

[98] Testing of the Dstl 10% gelatin was conducted at the same time as for Dstl 20%gelatin at 10°C, therefore requiring all targets to be conditioned to the same temperature.

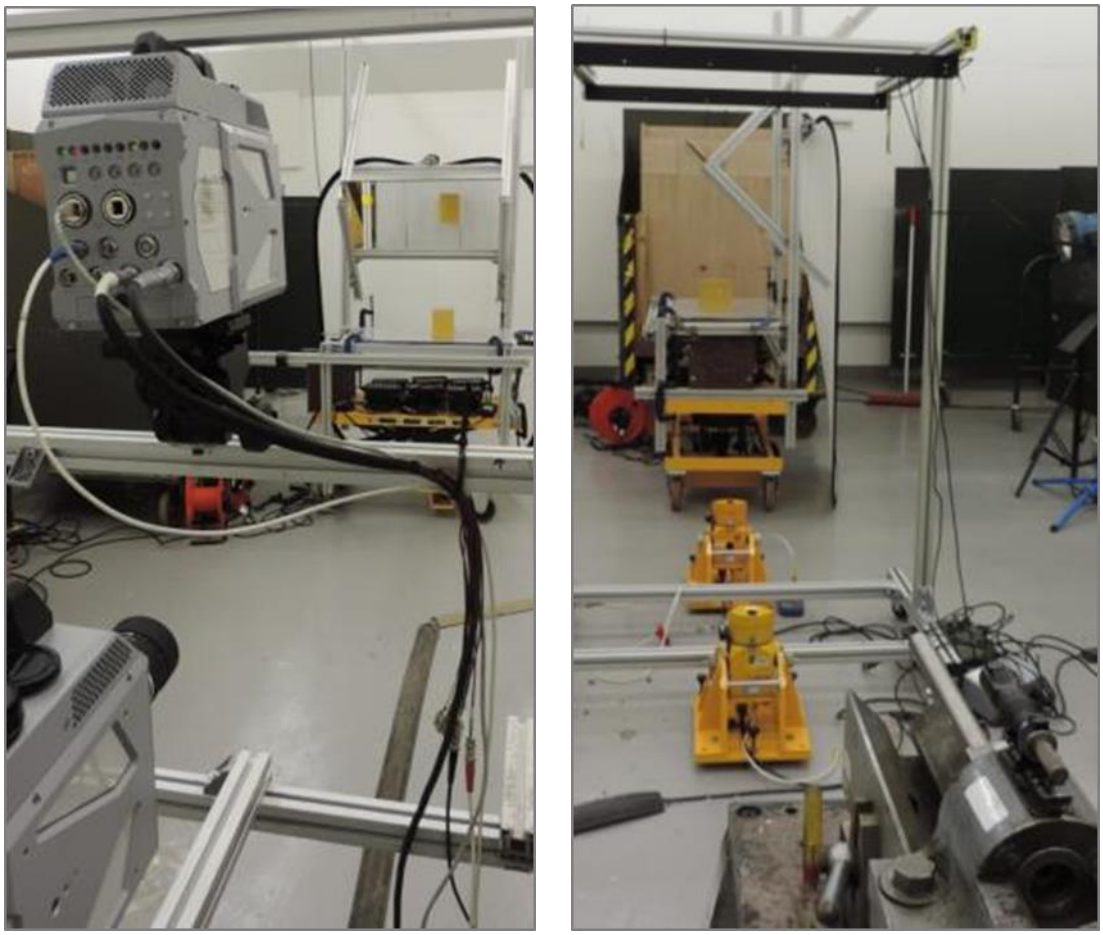

Figure 57: Left - HSV views of the target, with top camera via a 45° mirror. Right: view from weapon showing MSI velocity equipment and target table.

Exit velocities were calculated from the HSV using tracking software (Tracker [213]) over a distance of 300 mm after exiting the gelatin. The tolerance on velocity measurement for this method was calculated to be <±1.5%.

The gelatin blocks were approximately 100 mm in length, the actual length of the track of the projectile was measured after impact with a stiff rod.

7.3.3 Results overview

The data sourced from the literature listed in Table 5 were combined with the data described in Section 7.3.2 and other data from the previous DoP comparison into muscle tissue simulants (Section 7.2).

Some data given in Table 5 was excluded (as the wound track lengths were not within the allowed bounds):

- 11 shots from Reference [95] with wound track lengths > 150 mm
- References [58; 109] into dead pig thighs (wound track lengths between 20 and 30 mm).
- Reference [157] into live anesthetised dog thighs (averages of grouped wound track lengths were 48 to 56 mm).

Additionally, the high impact energy outlier (1870 J) for live, anesthetised pig thighs from Reference [96] was excluded from further analysis as it was at a much higher energy than any of the other muscle tissue or simulant data.

The data on energy loss per 100 mm suitable for the comparison is summarised in Table 24 for animal muscle tissue (with skin intact) and Table 25 for muscle tissue simulants.

Reference	**Target type**	**Number of data points**	**Impact energy range (J)**
Eason [95]	Live anesthetised pig thigh	37	96-1056
APPENDIX E, E.2 [96]	Live anesthetised pig thigh	17 (+1 outlier)	970-1175 (182)
Dahlgren [113]	Live anesthetised pig thigh	3[99]	~440
Jin [123]	Live anesthetised pig thigh	1[100]	298
Total		59	96-1175

Table 24: Summary of animal muscle tissue energy loss data from steel sphere impacts.

The combined data for live, anesthetised pig thighs gave 59 data points all with steel spheres of diameters between 4.8 and 9.525 mm.

[99] Grouped data, average of 10 shots per group.
[100] Based on the fitted model retardation equation generated from 14 shots.

All simulants assessed were original firings within this work. To match the animal muscle tissue data in Table 24, the simulant data has been limited to spheres. As detailed in Section 7.2.2, the Dstl 10% gelatin was assessed at the same time as the Dstl 20% gelatin at 10°C, requiring both simulants to be conditioned together at 10°C. The Fackler 10% gelatin at 4°C assessment was performed at a different time to the Dstl 20% gelatin, allowing it to be conditioned to 4°C (but only assessed at lower impact energies). The available muscle tissue simulant data for this comparison is summarised in Table 25.

Target type	**Number of shots**	**Impact energy range (J)**
Dstl 10% gelatin at 10°C	43 3	5-90 940-1330
Dstl 20% gelatin at 10°C	163	30-1256
Fackler 10% gelatin at 4°C	17	8-105
Perma-Gel	26	5-63
Totals	252	5-1330

Table 25: Summary of muscle tissue simulant energy loss data from sphere impacts (from original work).

Energy loss data for 44 shots with cylinder and CN cylinder projectiles in Dstl 20% gelatin at 10°C were excluded due to the different projectile geometry to the available pig data (impact energies in the range 36-1256 J).

The muscle tissue simulant data summarised in Table 25 used a range of different spheres with diameters 4.5 to 20 mm and different materials (glass, ceramic, steel and lead[101]).

[101] Lead projectile impacts were all low energy, such that there was no deformation of the projectile.

7.3.4 Results for energy loss comparison

There are some severe limitations on the comparisons that can be made for all but Dstl 10% and 20% gelatin with animal data due to lower energies for the other simulants. Perma-Gel has no overlap in the data with muscle tissue; the Fackler 10% gelatin at 4°C has only 1 data point. Given these limitations and the conclusions from Section 7.2, the energy loss comparison is focused around the suitability and validation of 20% gelatin at 10°C as a muscle tissue simulant.

The data for all spheres in muscle tissue and simulants are shown in Figure 58.

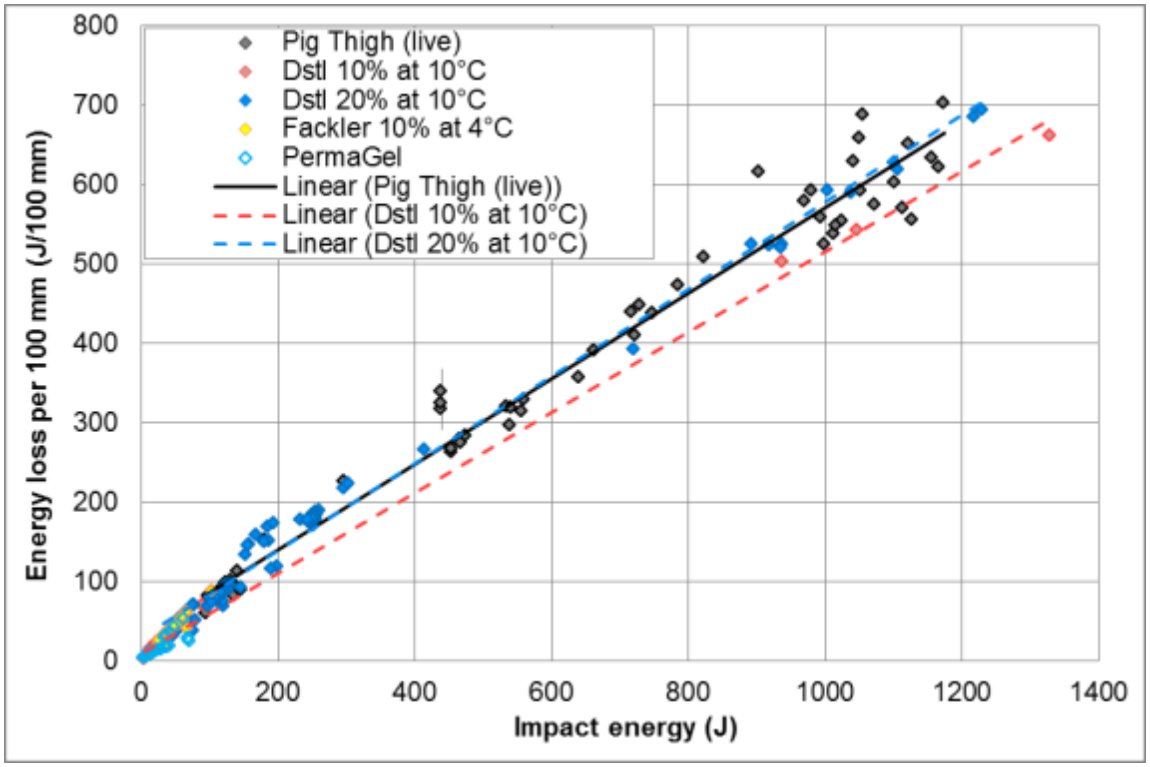

Figure 58: Energy loss per 100 mm in live pig thighs and muscle tissue simulants for spheres of different diameters and densities. Pig data from References [95; 96; 113; 123]. Tissue simulant data is from original testing.

The scatter in the data shown in Figure 58, particularly evident in the Dstl 20% gelatin at 10°C data, is due to the results being from a combination of spheres of different diameters and densities. This scatter is expected for different diameter

projectiles even of the same density[102]. Larger diameter projectiles of the same density are expected to lose less energy per unit length at equivalent impact energies (i.e. do not retard as quickly).

Condensing the data to just steel spheres up to 9.525 mm diameter reduces the scatter for the tissue simulants, but does not exclude any of the animal tissue data. This simplifies the comparison between the pig data and simulants and the steel sphere comparison is shown in Figure 59.

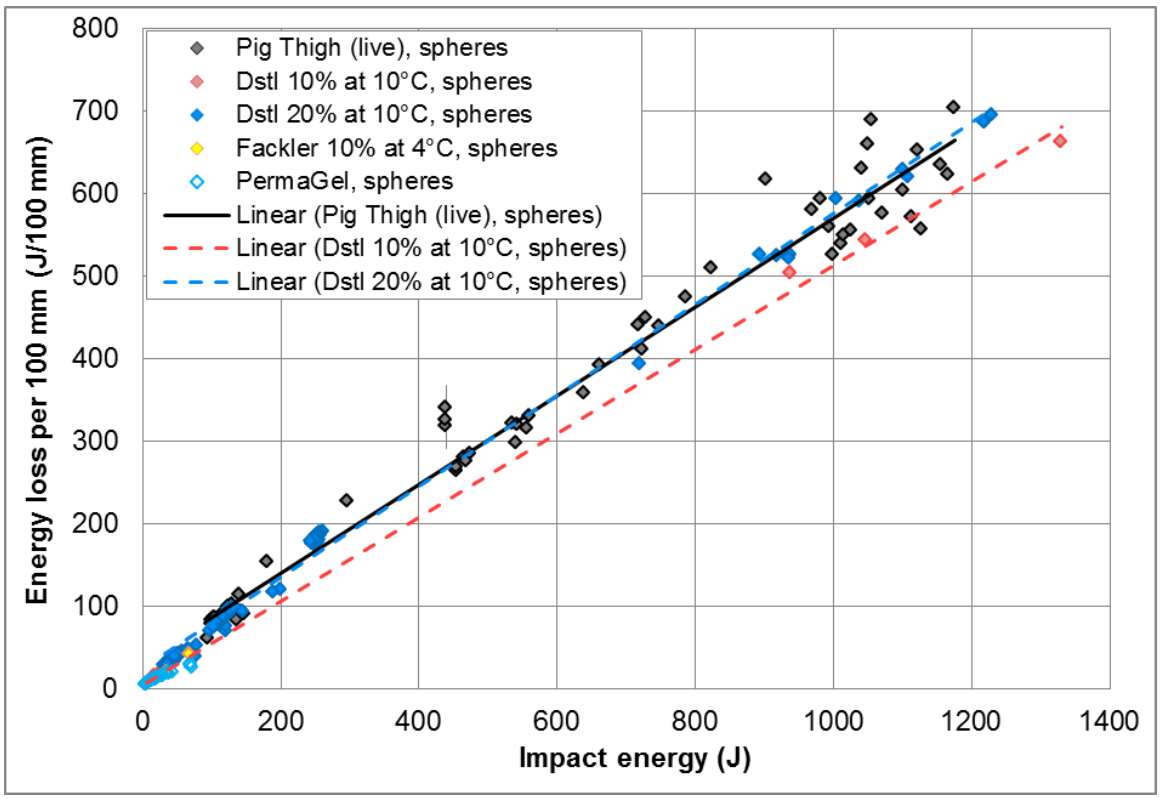

Figure 59: Energy loss per 100 mm in live pig thighs and muscle tissue simulants for steel spheres up to 9.525 mm diameter. Pig data from References [95; 96; 113; 123]. Tissue simulant data is from original testing.

Figure 59 shows that the Dstl 20% gelatin at 10°C gives the same performance as live pig thighs, in terms of energy loss through a 100 mm target across the range of impact energies assessed. A linear fit showed no significant difference

[102] This can be demonstrated with the predictions of the FREM for projectile retardation in muscle tissue or gelatin given in Section 9.3.

at the 95% confidence level in either the intercept or gradient between Dstl 20% gelatin at 10°C and the live pig thighs (p=0.107 and p=0.218 respectively). Figure 59 also shows that the Dstl 20% gelatin at 10°C response is less variable than the live pig thighs.

The fit applied to the 10% gelatin at 10°C data in Figure 59 shows that projectiles lose less energy in that target compared to live pig thighs; however it is based on more limited data. A linear fit showed a significant difference at the 95% confidence level in the intercept but not the gradient between Dstl 10% gelatin at 10°C and the live pig thighs (p=0.033 and p=0.158 respectively). It would be expected that a projectile would lose less energy in a given target thickness of 10% gelatin at 10°C compared to 20% gelatin at 10°C, based on the DoP data (Figure 45 and Figure 46).

For reference, a typical high-velocity rifle bullet energy at the muzzle would be in the region of 1.8 kJ to 3.5 kJ (depending on calibre and barrel lengths) and will decrease with increasing range to the target.

There is insufficient data for the other tissue simulants at higher impact energies in order to compare the energy loss in a 100 mm thick target to that in live pig thighs. This limitation is addressed (at least partially, as there are still some data limitations) in Section 9.10, where a different comparison approach between simulants and muscle tissue is employed.

All the pig data was for muscle tissue with the skin intact. The muscle tissue simulant data was ‘bare’. The effect of a skin simulant in conjunction with a muscle tissue simulant is considered using this pig data in Section 8.7.

7.3.5 Energy loss in tissue and simulants using bullets

Using energy loss from bullets to compare tissue and tissue simulants is more challenging, as there are many more factors introduced by using bullets compared to a simpler geometry projectile. For example bullets will tumble, may deform and/or fragment in tissue or a simulant, which will add significant scatter to any data and shots under nominally the same impact conditions may provide significantly different outcomes due to these bullet behaviours.

For example, using data from Reference [111]; for a 5.56x45 mm SS92 bullet with nominally the same impact conditions there was a difference of a factor of 4.5 between the smallest and largest energy loss in pig thighs and a factor of 3.2 in 20% gelatin at 20°C.

The use of bullets to select a suitable tissue simulant by comparison to the effects in tissue should be avoided (apart from potentially as a validation exercise), even though it may be desired end use of the simulant and more data may be available in the literature for comparison (see Reference [112] for a review of available pig muscle tissue data).

7.3.6 Discussion and limitations of energy loss comparison

Comparisons of simulants to live (muscle) tissue are infrequent, but can yield highly valuable data. In order to maximise the amount of live animal data that could be utilised, it was critical to use metrics that were independent or accounted for the different projectiles and impact conditions used as far as possible. Impact energy against the energy loss[103] in (or normalised to) a 100 mm target was found to meet these requirements (i.e. energy loss $\propto$ impact energy).

Previous comparisons of energy loss in tissue and tissue simulants (References [107; 108; 124; 217]) have normalised the energy loss to the target thickness, but not to the impact velocity or energy of the projectile. This limitation means that comparisons are only valid at equivalent impact velocities. Grouping data into (wide) impact velocity bins may increase the apparent variability in the targets which could (at least partially) be explained using the current comparison methodology.

For the comparisons of energy loss using spheres:

- Gelatin is more repeatable than muscle tissue. The scatter in the results is less than pig data (R^2=0.989 for Dstl 20% gelatin at 10°C, compared to

[103] Energy loss was based only on changes to kinetic energy of the projectile.

R^2=0.975 for live pig thigh). Some of the scatter seen in Dstl 20% gelatin at 10°C can be attributed to the use of a greater range of projectile types.

- For live pig thighs, there is still significant scatter in the energy loss, even with the same projectile (see APPENDIX E, E.3 for energy loss per 100 mm graphs for individual projectiles).

Limitations of this comparison method are:

- The comparison used a mix of projectiles. Only data for steel spheres could be properly evaluated in the muscle tissue simulants
    - The different diameters of the steel spheres used introduced some additional variability in the results. This makes it challenging to establish the target variability in relation to the projectile induced variability with the figures presented. To mitigate this limitation, projectile specific comparisons are given in APPENDIX E, E.3.
    - Available data on projectiles of other densities and geometries were excluded.
- It assumed that live, terminally anesthetised pigs shot in the thighs are a good model for live human (thigh) muscle tissue in order to base the selection of an appropriate muscle tissue simulant. Effects from a higher skin perforation V_{50} in pigs were not considered to affect the results[104].
- In all these experiments (References [95; 96; 111; 113; 123]) the pig was supine, with the leg elevated. The muscle tone to support the animals' weight would not have been present and it is unknown how any differences in muscle tone may affect these results.
- The Dstl 10% gelatin at 10°C data was limited to low and high impact energies with a large gap in the data between 90-940 J. The relationship

[104] The impacts were all greater than 3 times the V_{50}, see Section 9.4. The potential effect of skin on exit was not considered.

defined on the data available was assumed to hold over the entire impact energy range.

- Data for additional muscle tissue simulants other than Dstl 20% gelatin at 10°C and Dstl 10% gelatin at 10°C were not available over the required impact energy range to enable a comparison of their performance to the available pig data. This is recognised as a limitation for those researchers interested in the performance of 10% gelatin at 4°C compared to muscle tissue. However, additional analysis is presented in Section 9.10 and in conjunction with the outcomes from Section 7.2 it is not considered a significant limitation of this thesis.
- All the data was limited to comparisons in a nominal 100 mm thick target. Similar tissue or simulant thicknesses were required as the energy loss is dependent on the target thickness. This target thickness may not always be practical to achieve and excludes the use of other valuable data to aid in the comparison.

A method to enable comparisons of tissue and tissue simulants that is independent of target thickness would be to scale the DoP from experiments to that predicted using a mathematical (virtual) model that could account for the impact conditions. This would allow the use of other existing data to validate the tissue and tissue simulant response, including that for different density and geometry projectiles. This method is explored further in Section 9, sub section 9.10.

Although the comparison detailed in Section 9.10 is directly relevant to the selection of an appropriate muscle tissue simulant, it is predicated on a Fast Running Engineering Model of projectile retardation in muscle tissue that first needs to be introduced and validated, so cannot be given in this Section.

7.4 Selection of a suitable muscle tissue simulant for a physical model of single projectile impacts

As stated, the best performing simulant from the DoP comparison was the 20% gelatin at 10°C. All the 20% gelatin at 10°C mixes showed a similar DoP response

to the animal and PMHS muscle tissue data. The Dstl 20% gelatin at 10°C also showed good agreement to the energy loss per 100 mm to the animal muscle tissue data.

Dstl 20% gelatin at 10°C was selected as the muscle tissue simulant for a physical model based on the DoP comparison, the energy loss per 100 mm comparison and an extensive data set with availability of HSV (from which retardation and temporary cavities could be measured).

The soap (1.10 g cm^{-3}) was also found to give a similar DoP to animal tissue. The gelatin allows a dynamic assessment of the temporary cavity formation, whereas the soap is permanently deformed, and so gives a picture of the maximum cavity produced over the whole penetration.

In reference back to the original requirements of a muscle tissue simulant (Section 3.9.2), in addition to providing a similar penetration and retardation response to real muscle tissue, the ability to measure permanent DoP, retardation, temporary cavity dimensions and tumbling for bullets were required. Dstl 20% gelatin at 10°C meets these requirements and was taken forward as the basis for the muscle tissue simulant aspect of this model.

The data presented in this Section was sufficient to enable the selection of Dstl 20% gelatin at 10°C as a suitable muscle tissue simulant. Additional comparisons in Section 9.10 are used to further reinforce this selection.

A common approach to analysing the penetration or retardation in different targets across the wound ballistics literature would greatly increase the utility and exploitability of the data created.

7.5 Tissue simulant cavitation

7.5.1 Introduction

With the selection of Dstl 20% gelatin at 10°C as a suitable muscle tissue simulant, based on DoP and retardation, there remains questions regarding the ability to represent the maximum temporary (or permanent) cavity within muscle tissue.

Along with the DoP or retardation of a projectile, the size (i.e. radius or diameter) of the maximum temporary cavity is a useful measure of the injury potential of the projectile at different depths within the muscle tissue (simulant).

Due to the technical difficulties in measuring temporary cavitation in real muscle tissue (requiring flash or high speed x-ray or similar techniques), there is a paucity of data for comparison with the simulants; particularly for simple projectiles that are more straightforward for modelling.

The data that is available (and suitable) will be utilised within Section 9 for the development of a FREM of penetration, retardation and cavitation within 20% gelatin at 10°C and muscle tissue. In this section, consideration is given to some factors that influence the resulting temporary cavity produced and therefore require special consideration whenever gelatin (or any tissue simulant) is used to provide outputs related to cavity sizes.

These factors that are thought to affect the temporary cavity produced are: the target (lateral) size, target edge effects (constraint); shot placement[105] and the (minimum) block size required to enable temporary cavity measurements [143; 218-220].

Despite the potential of these factors to influence the resulting cavities (or permanent cracks as a proxy to the temporary cavity size) that are experimentally measured, very few sources in the literature have considered these first two effects (quantitatively) previously [143; 218-220].

Jussila in Reference [143] noted that "*the simulant does not expand evenly in all radial directions*" and "*the cavitation suppressing effect of surrounding tissue is to some extent missing*". It was then suggested "*The problems can be averted if large enough simulant blocks are used"* [143].

The outcome of one study where the gelatin was confined within 6.35 mm wall thickness fibre-glass tubes is quoted below:

[105] This could be considered as a sub-case of the target size, with an asymmetrical target about the shot line.

"It should be noted that microsecond X-rays, of gelatin blocks shot with the ¼-inch spheres show that temporary cavity formation is almost completely suppressed in confined cylinders, as in the case of cylinders shot with APM2 and calibre 0.22" Hornet bullets." [220]

The (minimum) block size required to enable valid temporary cavity measurements is not prescribed within this thesis, as too many factors are involved to be able to bound the issue (particularly for tumbling bullets with divergent shot lines). Additionally, the user need statement or requirement for use of the model (the gelatin block) may dictate the target size required, related to how the outputs are needed. Instead, the issue is illustrated and consequences discussed.

7.5.2 Block minimum size

The NATO gelatin standard [130] specifies a 300 mm x 150 mm x 150 mm size gelatin block for testing. Small arms testing conducted by the author, but not detailed within this thesis, has shown that the NATO size 20% gelatin block at 10°C can tear due to the cavitation from off centre impacts and some larger calibre bullets (7.62 mm or greater). The resulting maximum temporary cavity cannot be measured meaningfully if the block ruptures due to the expansion of the cavity. An example of this tearing is given in Figure 60.

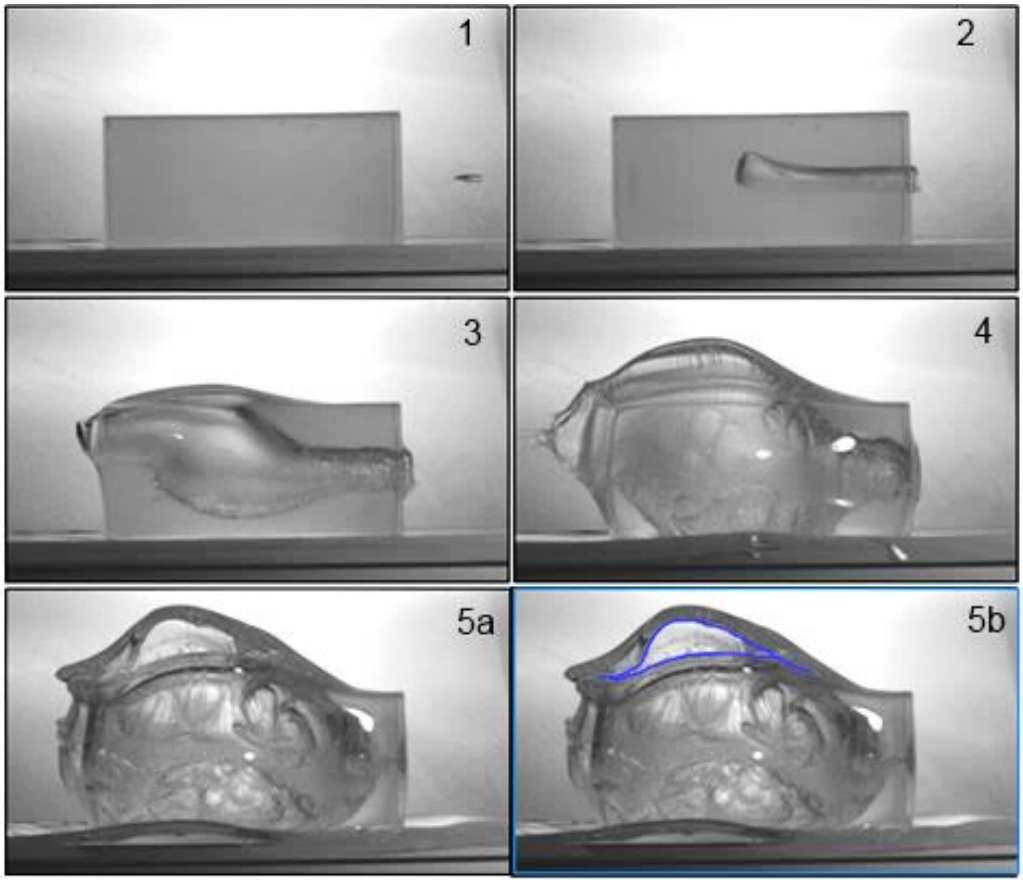

Figure 60: 1-5(a) - Series of frames from HSV of 300 mm x 150 mm x 150 mm size 20% gelatin at 10°C block being penetrated by a 7.62x51 mm round. Image 5b shows the tear in the block outlined in blue.

As can be seen in Figure 60, this tearing occurs after the exit of the projectile from the block (approximately 2 ms after it has exited the block in this case).

Also evident from Figure 60 is that the bullet hit centrally in the vertical plane, but exited very close to the top of the block, despite the bullet traveling along the centre line of the target pre-impact.

This issue has been noted and discussed previously in relation to the use of permanent cracks in (10%) gelatin as a measure of the temporary cavity [24; 38; 143].

It has been demonstrated that the temporary cavity (or permanent cracks/fissures) produced within 10% gelatin at 4°C are larger than in 20% gelatin

at 10°C for equivalent impacts [38]. This means the suggested block sizes for 20% gelatin at 10°C are not applicable to 10% gelatin at 4°C (and vice-versa).

7.5.3 Gelatin block size and confinement test method

Noting the difference in the experimental temporary cavities in gelatin related to potential confinement [220], as well as issues related to tearing of gelatin from the expansion of large cavities from ‘severe’ threats, an additional series of testing was conducted.

This testing was aimed at investigating the response of the temporary cavity in gelatin when:

- The cross sectional (lateral) size of the target was altered
- The target was confined
- A combination of these effects.

In order to investigate these potential effects on the resulting cavity, a 6 mm steel sphere at a nominal 750 m s^{-1} was chosen as the threat projectile, impacted into the centre of a Dstl 20% gelatin block at 10°C. Each block was used only once.

The gelatin was made to the Dstl 20% at 10°C method (APPENDIX D, D.1, including calibration to the fixed velocity method in D.5.3). The gelatin was cast into one of 4 lateral sizes (square section, nominal 250 mm length):

- 50 mm x 50 mm
- 75 mm x 75 mm
- 100 mm x 100 mm
- 150 mm x 150 mm

Each of the four different sized gelatin blocks were tested in an unconstrained (or free) and constrained configuration:

- ‘Unconstrained’ – laid on a polycarbonate table (the base of block was constrained by table, all other faces ‘free’)

- Constrained – the gelatin block was cast and shot within a 4 mm polycarbonate mold (superglued at the joins and sealed with silicone sealant). The impact and exit faces were unconstrained.

This gave 8 target configurations. An average of 4 repeats were conducted on each target configuration and additionally the 150x150 mm impact face blocks were impacted at a nominal 500 m s^{-1} (for the both constrained and unconstrained configurations).

The MPH weapon system at 5 m from the target, with blank pyrotechnic charges (0.38” or 5.56x45 mm) and a 6.05 mm smooth bore barrel was used to fire the 6 mm steel spheres at the required velocities. Details of the weapon system are given in APPENDIX B.

The blocks were viewed using two Photron SA-Z high speed cameras [206], running at 40,000 frames per second and a resolution of 1024 by 488 pixels. One camera was looking directly at the block, perpendicular to the shot line and the other a top down view via a mirror at 45°. The top camera was placed such that both cameras had a similar distance to the shot line (±10 mm). The gelatin was lit from behind and from underneath through diffusers, using multiple halogen flood lights. The lights were turned on remotely just prior to firing to reduce heating of the target[106].

Impact velocities were measured with 2 MSI 858 optical detectors [205] spaced 1000±1 mm apart and centred at 2500±10 mm from the target, connected to an 817 timing unit and a 570 computer interface, with processing by MSI Ballistics DB software. The tolerance on velocity measurement was calculated to be <±0.3%.

After the firings were completed, the HSV was analysed to measure the maximum temporary cavity outline over all time, using the method described in APPENDIX

[106] The setup was similar to that described in Section 7.3.2 with the test setup shown in Figure 57.

G, for each of the side and top view of the target. The data from the repeats on each target configuration were combined, and 4th order polynomial fits were applied to the cavity radius with penetration depth, separately for each view and cavity direction (cavity projecting top, bottom, left and right from the shot line).

The impact position of the projectile from the centre of the target was also measured using the HSV in both planes.

The results of this testing are given in relation to the effect of shot impact location on the temporary cavity in Section 7.5.5, block confinement in Section 7.5.6, block size in Section 7.5.7 and then combined effects from block size and confinement in Section 7.5.8.

7.5.4 General results applicable to all testing

The gelatin was made and cast in one batch with the subsequent testing conducted over two days. One block was calibrated at the start of each firing day. The calibration results obtained were:

- Firing day 1; impact velocity 176.0 m s^{-1}, DoP 33 mm
- Firing day 2; impact velocity 179.2 m s^{-1}, DoP 34 mm

Both results confirmed the gelatin was in calibration on each day. Additional calibration shots were conducted but were outside the velocity limits specified for the fixed velocity method. The wider velocity method (Equation 14) had not been introduced at the time of this testing.

A total of 39 valid shots were conducted for the 6 mm steel spheres. 32 at nominal 750 m s^{-1} impact velocity and 7 at nominal 500 m s^{-1} impact velocity.

For the nominal 750 m s^{-1} impacts, the average impact velocity recorded was 748.5 m s^{-1} with a standard deviation of 5.1 m s^{-1}. For the nominal 500 m s^{-1} impacts, the average impact velocity recorded was 498.1 m s^{-1} with a standard deviation of 3.7 m s^{-1}.

An issue with the constrained targets was that the polycarbonate constraining mold broke during firing, so it did not provide as rigid a constraint as desired. This

in itself did not cause a problem with the outcomes of the testing, only that the constraint provided to the block should be considered as 'partial constraint' and does not represent the full potential extent of cavity suppression that could be achieved with a more rigid boundary condition.

An example of the mold failure, photographed immediately after the shot is shown in Figure 61.

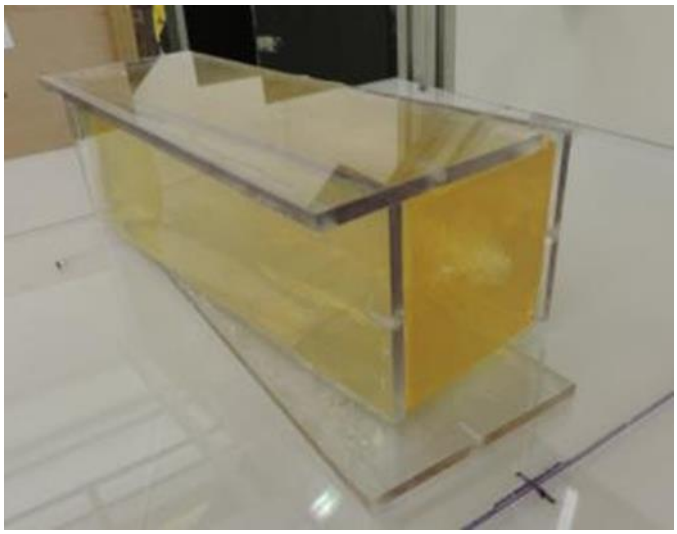

Figure 61: Photograph of a gelatin block in polycarbonate mold which has failed at the edges during cavity formation.

The accuracy of the weapon system was not as good as anticipated, even at 5 m range[107]. This resulted in impacts up to 30 mm from the point of aim on the centre of the block. The point of impact was an average of 6.9 mm off from the point of aim in each plane. In relation to the different sized targets used this was an average of 7.5% of the block width from the point of aim in each plane. All shots impacted within the central third of the block face.

The potential effect of off centre impacts has not been accounted for within the results and is considered a potentially significant limitation of the testing conducted.

[107] This was later found to be related to issues in overtightening the breech onto the back of the cartridge case, rather than inherent inaccuracy of the barrel used.

In all the testing the gelatin contained the temporary cavity without splitting or tearing.

7.5.5 Effect of shot placement (off-centre impacts) on the temporary cavity

Despite not normalising for the shot location within the results, some simple observations were made by comparison of shots close to, and more distant from, the point of aim.

This can be demonstrated by two firings into the 75 mm x 75 mm free gelatin target. One shot was 3 mm below the point of aim; the other was 26 mm below (but both less than 5 mm off centre in the horizontal plane). The cavity radius from the shot line was adjusted such that the shot line followed the y-axis[108]. This allowed the differences in radius to be easily compared and is given in Figure 62.

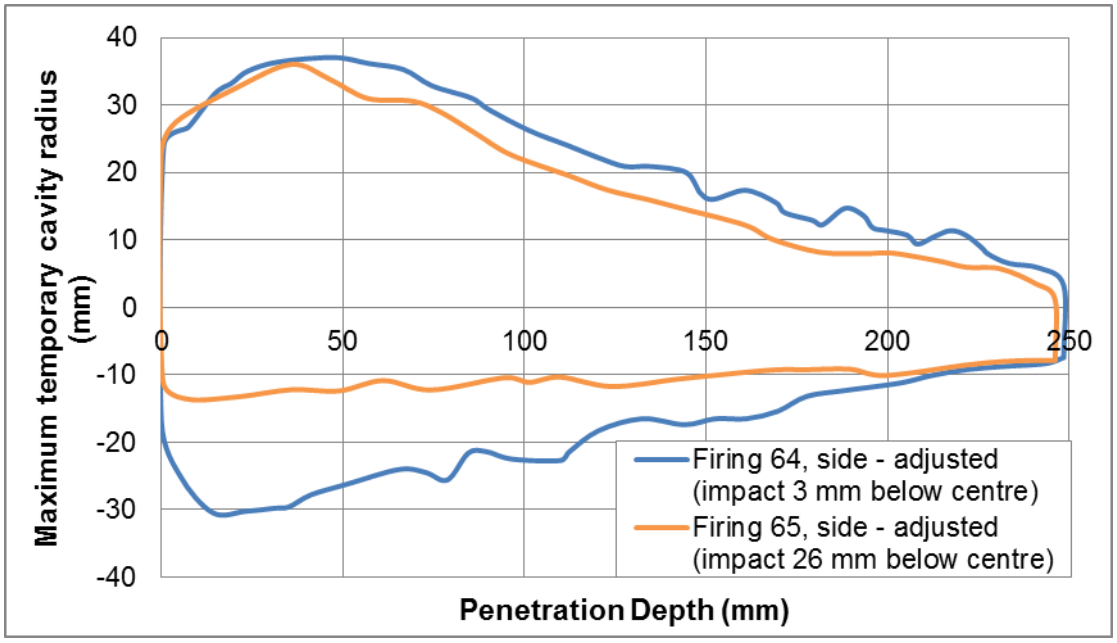

Figure 62: Two firings into the 75 mm x 75 mm free gelatin block target showing the different cavity outlines measured in relation to the shot line (side adjusted=adjusted so point of impact is y=0) when different points of impact were obtained.

[108] When the x or y-axis are referred to, this is in respect to the plane of the figure, not in relation to the path of the projectile.

Figure 62 demonstrates how, for an off centre impact below the intended point of aim (but otherwise under the same conditions[109]), both the top half and bottom half of the resulting measured cavity were affected. The top half of the cavity shows a slightly reduced cavity radius across the majority of the length of the target by a few millimetres. The bottom half of the cavity shows a large reduction in cavity size due to constraint from the table on which it was placed. The cavity outline of the bottom half of the cavity approximately followed the base of the gelatin block along the majority of the length of the target.

7.5.6 Effect of block confinement on the temporary cavity

The top half of the temporary cavity from the side view was chosen to be used to compare across target configurations. This was so as not to introduce unwanted confinement effects from the table in the bottom half of the cavity (although not shown, similar results were observed when taking the cavities measured from the top camera view).

The average cavity radii with depth for the 150 mm x 150 mm free and constrained targets (using the top half of the temporary cavity from the side view) is given in Figure 63 at both impact velocities.

[109] Measured velocities were within 0.1 m s^{-1} for these shots, and both were in the same size, free target.

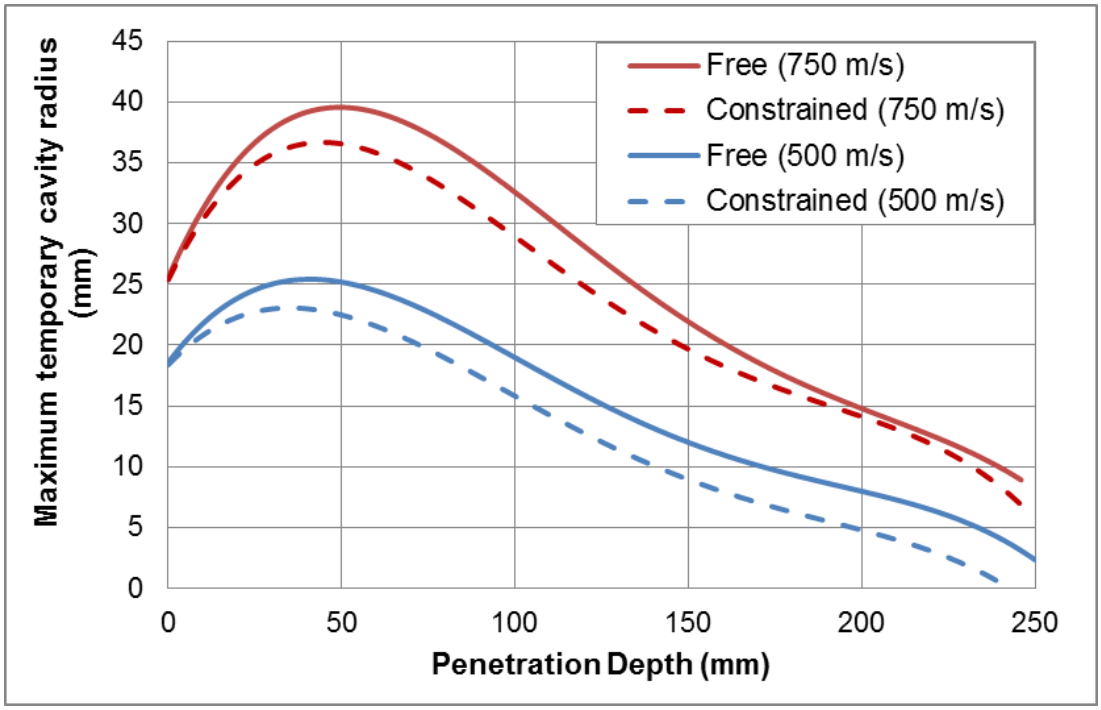

Figure 63: Average MTC radius with depth for a 150 mm by 150 mm impact face gelatin block, showing effect of (partial) constraint at 2 impact velocities for a 6 mm steel sphere.

Figure 63 shows that the (partial) constraint in the gelatin block decreased the temporary cavity radius at both impact velocities across all depths in the block, apart from immediately on impact. The total temporary cavity volume will also be reduced in the constrained configuration.

The constrained cavities show an almost constant offset in radius from approximately 25 mm depth, apart from between 175 mm and 225 mm in the 750 m s^{-1} targets. The average difference between the free and constrained radius across all penetration depths was 2.2 mm and 2.8 mm for the 750 m s^{-1} and 500 m s^{-1} impacts respectively.

The deviation from the expected cavity shape for the 750 m s^{-1} constrained target between 175 mm and 225 mm depth is believed to be due to the aggregation of data where one shot, which showed a similar cavity diameters at corresponding depths to the others, but appeared to be shifted vertically in relation to the shot

line by approximately 5 mm[110]. The result of this was the radius of the top half of the cavity from the shot line appeared greater. This may have been due to the failure of the constraining mold at a different time or location to the other shots, but cannot be confirmed.

The smaller cavities in constrained targets are not due to different amounts of energy absorbed. Energy is absorbed by strain in the constraining material. The polycarbonate is very stiff in comparison to the gelatin so has very small displacements (prior to the mold failing) which are not easily observable.

7.5.7 Effect of gelatin block size on the temporary cavity

The effect of block lateral size on the resulting temporary cavity for the free targets is demonstrated in Figure 64 at 750 m s^{-1} impact velocity.

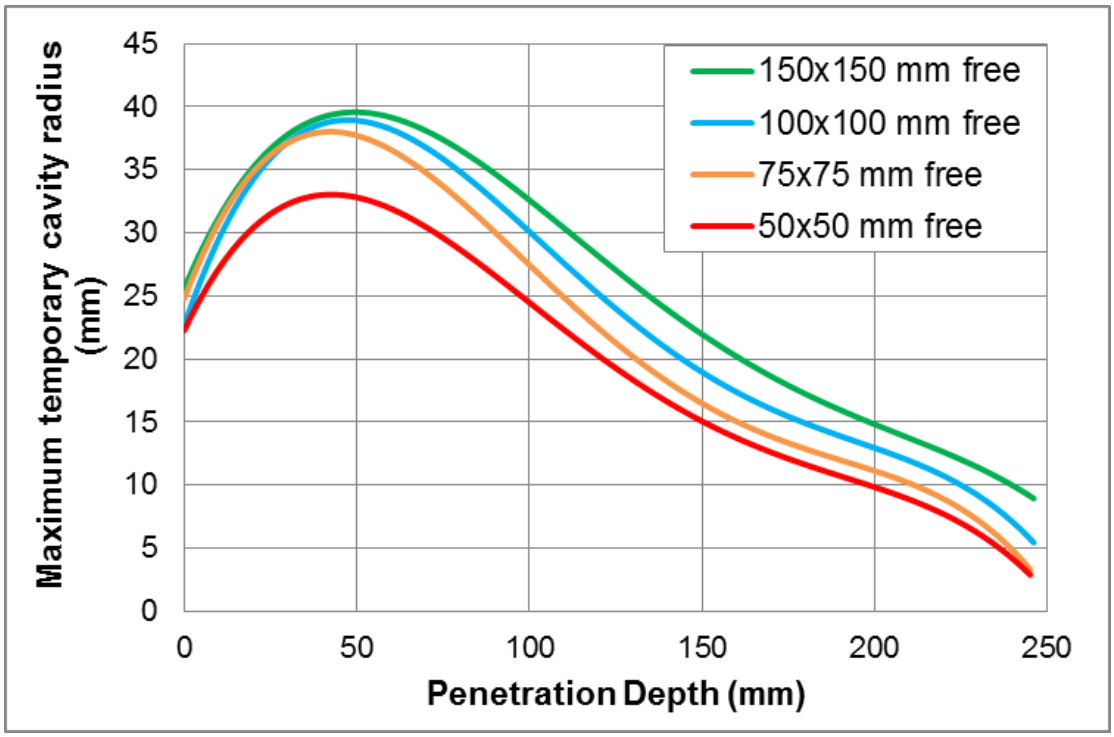

Figure 64: Average MTC radius with depth for a free gelatin blocks, showing effect of varying block impact face dimensions for a 6 mm steel sphere at 750 m s^{-1}.

[110] This shot fell within the scatter in terms of point of impact in relation to the point of aim, compared to the other shots against this target configuration.

Figure 64 shows that increasing the lateral dimension of the gelatin impact face increased the (average) cavity radius at all penetration depths in the target.

In the smaller size blocks (50 mm x 50 mm and 75 mm x 75 mm) the maximum temporary cavity extends past the original dimensions of the gelatin block.

Figure 64 was based on the average (curve fitted) cavity outline for each configuration and some scatter was observed on individual tests under the same conditions. Quantitative comparisons of the effects are demonstrated in the following section.

7.5.8 Combined effects of gelatin block size and constraint on cavity formation

To allow quantitative and statistical comparison of the combined effects of gelatin block size and constraint on the temporary cavity formation, three metrics were used to describe the temporary cavity. These were the maximum diameter of the MTC, the total volume of the MTC and the depth at which the maximum diameter of the MTC was observed.

The maximum temporary cavity diameter for all target configurations is shown in Figure 65.

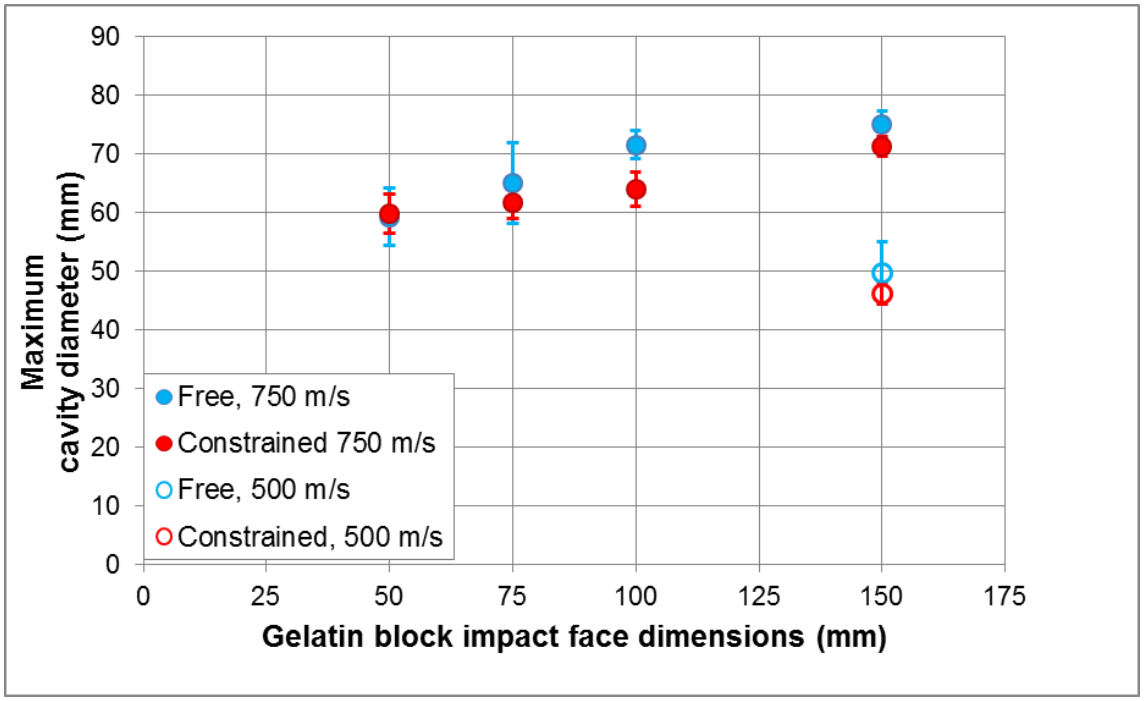

Figure 65: The maximum temporary cavity diameter with block impact size and (partial) constraint for the two different impact velocities. Error bars are the 95% CI.

Figure 65 shows that increasing the lateral dimension of the gelatin impact face (linearly) increased the maximum temporary cavity diameter, for both free and constrained targets.

The 100 mm x 100 mm and 150 mm x 150 mm at 750 m s^{-1} targets showed statistically significantly larger maximum temporary cavity diameters in free targets, compared to constrained, at the 95% confidence level ($p<0.001$ and $p=0.008$ respectively).

For the 50 mm x 50 mm, 75 mm x 75 mm and 150 mm x 150 mm at 500 m s^{-1} blocks, the effect of (partial) constraint did not have a statistically significant effect on the resulting MTC maximum diameter ($p>0.5$, $p=0.333$ and $p=0.123$ respectively).

Reducing the impact velocity from 750 m s^{-1} to 500 m s^{-1} showed a 34% and 39% reduction in the maximum temporary cavity diameter for the free and constrained targets respectively.

The 100 mm x 100 mm size target showed the biggest difference in the maximum temporary cavity diameter between free and constrained targets. The approximately linear increase in the maximum temporary cavity diameter (and volume, Figure 66) with target lateral dimensions is not considered to hold for larger target sizes than those evaluated. There will be a target size at which it could be treated as semi-infinite in terms of the cavity response: increasing the target size past this point or applying lateral constraint won't affect the size of the temporary cavity. Extrapolating the current data suggests this may be for a block with lateral dimensions as small as 200 mm by 200 mm. However, this is based on impacts in the order of 250 J, whereas typical small arms rifle bullet muzzle energies may be up to 3.5 kJ depending on calibre, etc.. Finite Element Analysis may be a more pragmatic approach to investigate this, including the effect across a wider variety of projectile impact conditions.

The maximum temporary cavity volume for all target configurations is shown in Figure 66.

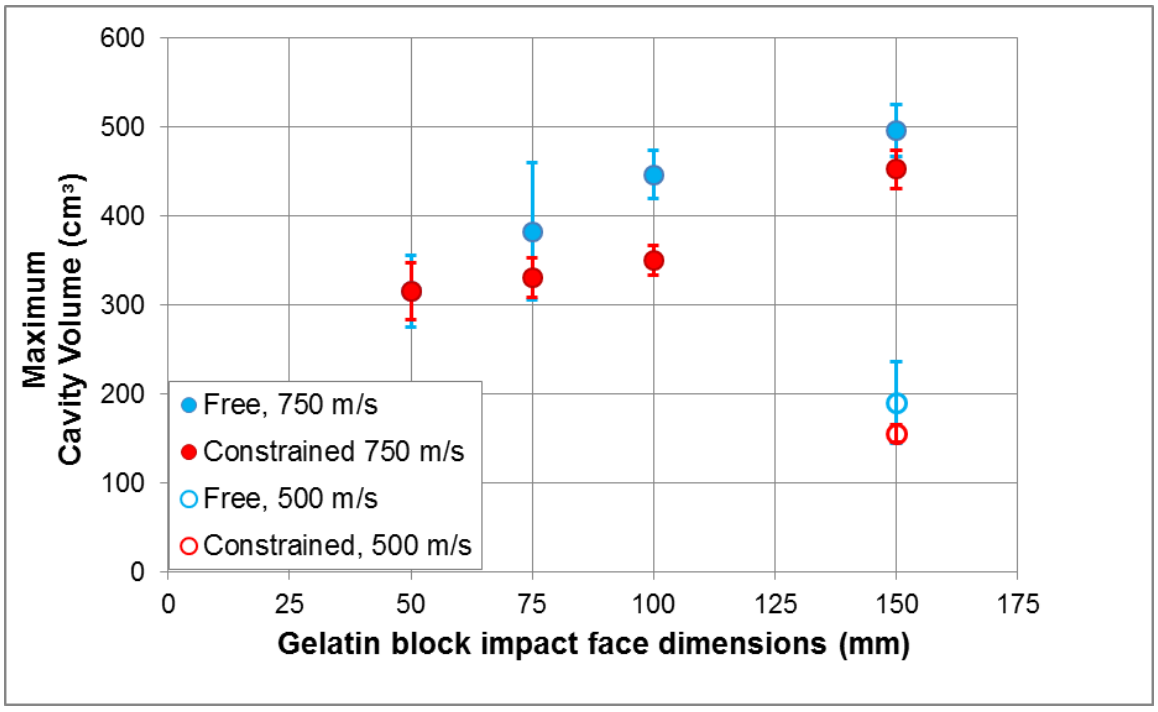

Figure 66: The maximum temporary cavity volume with block impact size and (partial) constraint for the two different impact velocities. Error bars are the 95% CI.

Figure 66 shows a very similar response of the maximum temporary cavity volume with target size and constraint as seen for the maximum cavity diameter in Figure 65. This is due to a consistent cavity shape across all targets, just the magnitudes of the cavity radii scaled.

Correspondingly, the same targets showed statistically significant differences in the maximum cavity volume as for the maximum diameter. The 100 mm x 100 mm and 150 mm x 150 mm at 750 m s^{-1} targets had $p<0.001$ and $p=0.014$ respectively. The 50 mm x 50 mm, 75 mm x 75 mm and 150 mm x 150 mm at 500 m s^{-1} targets had $p>0.5$, $p=0.162$ and $p=0.089$ respectively.

The depth of the maximum diameter of the temporary cavity for all target configurations is shown in Figure 67.

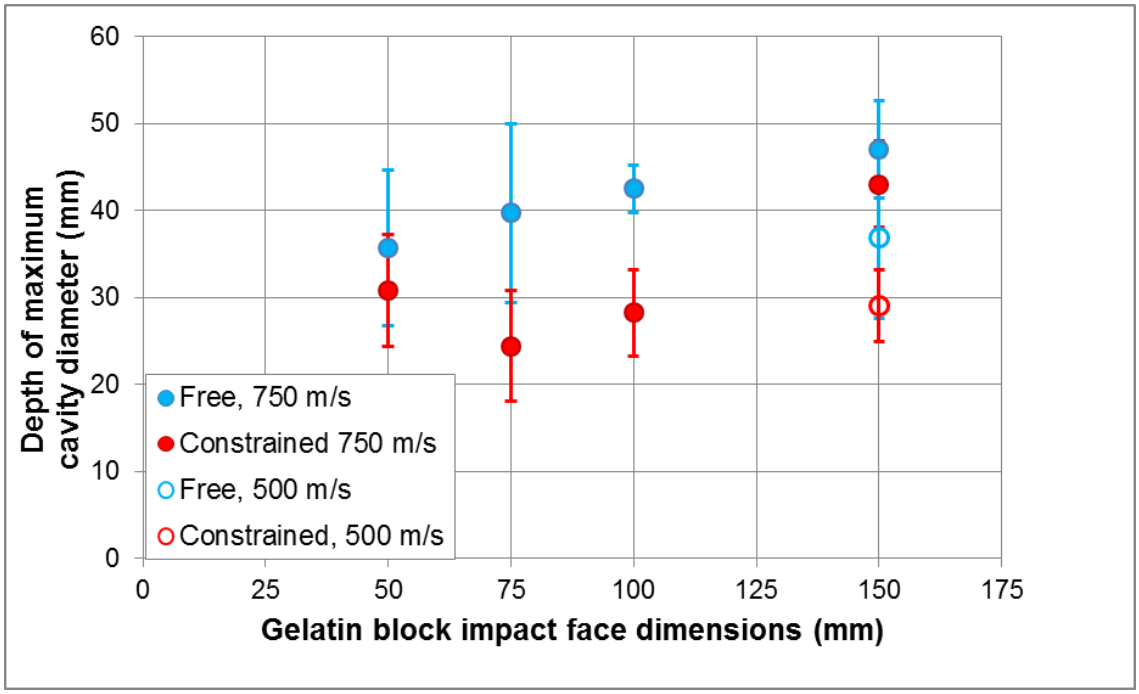

Figure 67: The depth of maximum temporary cavity diameter with block impact size and (partial) constraint for the two different impact velocities. Error bars are the 95% CI.

Figure 67 shows that when the target is free, increasing the block size increases the depth at which the maximum temporary cavity diameter is observed (again, following an approximately linear relationship). The data for constrained targets is more variable when considered in relation to target size. This may be due to

failure of the constraining mold at different points within the cavity expansion process for the different sized targets. In all cases, constraining the target showed a shallower depth of the maximum temporary cavity diameter compared to free targets. This difference was only statistically significant at the 95% confidence level for the 75 mm x 75 mm and 100 mm x 100 mm targets ($p=0.012$ and $p<0.001$ respectively).

The difference in the depth of the maximum temporary cavity diameter is due to the flow of the gelatin in direction of firing. Larger cavities, formed in the larger targets, take a longer time to form and therefore more lateral flow has occurred by the point at which the cavity is maximal, meaning it occurs deeper. Applying constraint to the gelatin also appears to restrict the ability of the gelatin to flow in the direction of firing.

Figure 67 highlights an important point that is not normally considered: the maximum diameter of the temporary cavity is heavily dependent on the size of the target and this maximum diameter does not equate to the depth of maximum energy deposited[111]. It should at least be valid as a comparison metric, but only as long as block size and the projectile position in relation to the block edges are consistent throughout the testing. The alternative would be to use the average depth at which the maximum cavity radius was measured in each direction from the shot line (which could be non-linear if the projectile diverged from the shot line, commonly observed for military rifle bullets).

Based on a linear model for each of the datasets, target size was a significant predictor at the 95% confidence level for each metric (maximum cavity diameter, volume and depth of the maximum diameter) for both free and constrained targets ($p<0.002$ across all conditions).

The main limitations of this testing are considered to be: the off-centre impacts which have not been corrected for and the failure of the polycarbonate molds during the expansion of the temporary cavity. If the work was to be repeated, one

[111] The retardation of the projectile in these different targets is independent of target size and constraint, which is shown in APPENDIX I, I.1.

piece, circular cross section molds could be used that are less likely to fail. Using a circular cross section target would complicate the cavity measurement as refraction effects would be significant. It is likely that permanent crack measurement as a proxy for the size of the temporary cavity [143] would have to be used (at suitable step sizes in penetration depth). Circular cross section targets would also ensure better symmetry about the shot line (assuming accurate shot placement).

The effect of refraction (or 'lensing') on the measured size of the cavity in gelatin was not considered. Refraction effects due to the curved surface of the gelatin block when the temporary cavity has formed will distort the passage of light through the block, changing the apparent size of the cavity measured. For smaller size blocks, the distortion is likely to br greater (smaller radius of curvature) in order to allow the cavity to form, increasing the optical distortion and the apparent size of the cavity. The 'true' cavity will be smaller than the apparent measured cavity. Accounting for any refraction effect will likely increase the differences observed between different gelatin block sizes.

7.5.9 Discussion of gelatin block (lateral) size

A (20% at 10°C) gelatin block of a specific size will only give a cavity prediction comparable to cavities produced within the same sized gelatin block. The optimum sized gelatin block to accurately represent (bulk) muscle tissue cannot currently be determined.

Although a potentially inefficient process, it would be useful to determine the lateral target size at which the target could be considered semi-infinite in terms of its cavity response. It should then be determined if that holds for higher energy impacts, or is also a function of the projectile impact properties. Determination of the target size that replicates the response of a semi-infinite target and assessing if this is beyond what would be considered practical in typical wound ballistics research would be useful.

The HSV data collected as part of this study could be analysed in terms of investigating the rate (or initial velocity) of the temporary cavity expansion. This

would aid understanding of the mechanisms involved across the different target sizes and constraint.

A calibration test that also accounts for cavity size may allow results to be reported in a dimensionless form or scaled to other block sizes, to aid comparison of data between institutions[112]. This could also enable block sizes to be tailored to the threat (saving resources), whilst still allowing read-across between them.

Although a suitable method has not been generated as part of this work, cavity sizes could be normalised to a specific calibration scenario (a specific projectile and velocity combination). For example the maximum temporary cavity in a given size gelatin block measured for a 6 mm steel sphere at a nominal 750 m s^{-1}.

This type of calibration could allow scaling or comparison across different block sizes or translation between other muscle tissue simulants.

Current calibration standards (APPENDIX D, Section D.5) are solely focused on ensuring the DoP is consistent, but no account is given to any effects on the measured temporary cavitation. Additional calibration testing for the cavity formation may also differentiate between factors such as gelatin surface hardening[113] which may not be evident in the current DoP calibration test, but may affect the (apparent) gelatin constraint and therefore resulting cavity measurements.

The effect of block size and constraint on cavity formation in gelatin raises some key considerations. The size of gelatin block suitable for terminal effects work depends on the threat being considered:

- Too small a block for the given threat will cause the block to split and invalidate cavity results (see Figure 60);

[112] There is no accepted standard gelatin block size across the wound ballistics community. As shown by Figure 60, the NATO sized gelatin block is too small for some common military bullets.
[113] Surface hardening is attempted to be minimised by the specified storage conditions and durations within the appropriate gelatin manufacture method.

- Cavities produced in different size blocks are not directly comparable (as block size affects the cavity formed). This will cause issues for sharing of data between institutions or nations and comparison to legacy data if different sized blocks are used;
- Too large a block will:
    - Degrade the quality of imaging (as there is more material for light to pass through);
    - Add additional materials costs; and
    - Potentially cause practical or manual handling issues.

Using the measured maximum temporary cavity (or permanent crack lengths) in gelatin as a metric for injury:

- The distance from the projectile to the block edge may be an issue for bullets, particularly with divergent shot lines[114] (and accuracy limitations if conducted at real range).
- The second half of a cavity (from the point the bullet has reached 90° yaw and significantly diverges from the original shot line) may be 'misrepresented' or 'misinterpreted' due to varying distance from the projectile to the block edge.
- The bottom half of the temporary cavity, viewed from the side, may need to be treated differently to the top half.
- Best practice for irregular or tumbling projectiles (such as bullets when the temporary cavity is being considered) is to additionally view the target from above. Doing this as standard or instead of a side view for 'simple' projectiles would remove issues due to confinement effects from the base on which the gelatin is placed.

Some institutions have performed testing with a cut out in the table underneath the gelatin, to allow unconstrained expansion. However, sufficient material is required to maintain the support to the perimeter of the block and this may be

[114] Analysis of 60 shots with 3 different military small arms rounds at a variety of typical engagement ranges fired into Dstl 20% gelatin at 10°C gave an average deviation of 20 mm from the original pre-impact shot line (maximum deviation was 52 mm).

enough to still influence the cavity formation. Pre-stressing or distorting the gelatin by spanning a cut-out in the table may also have an effect.

Viewing the gelatin from the side is generally a more experimentally practical approach as the camera can be placed on a tripod and is easily accessed. Viewing the target from above requires either an angled mirror (the approach used within this thesis)[115], or having the camera high above the target, which prevents easy adjustment such as focusing.

The outcomes of this testing have been directly applied within Dstl in the following ways:

- A better understanding of some of the potential factors that can influence the gelatin cavity measurements and therefore more considered control of these variables within the experimental setups and analysis. In particular this includes specifying 'fair shot' conditions, one of which requires impacts to be within the central third of the target impact face (including when testing weapon systems at real engagement ranges).
- A new 'standard' gelatin block target size[116] (200 mm by 200 mm impact face and 300 mm length) has been adopted to replace the 150 mm by 150 mm impact face NATO block and a 205 mm wide by 230 mm tall and 300 mm length mold.
- Terminal effects testing on gelatin where cavity formation is measured uses 2 HSV cameras (one from the side and one from above) regardless of the projectile geometry and propensity to tumble in the target.
- When testing bullets with divergent shot lines, the bullet centre of gravity is tracked in each frame of the HSV whilst it is within the target[117]. This can be used to determine the degree to which it has diverged from the original

[115] But can get dirty, be easily damaged, cause ghost reflections unless front silvered mirrors are used which are more susceptible to damage and more expensive, etc.
[116] This has also been designed to pour the liquid gelatin in the exit face of the block, rather than a side face, so that the sides remain clear and bubble free for HSV.
[117] The bullet centre of gravity is calculated from 3 points: the tip of the bullet and each side of the base. The ratio of the centre of gravity from the tip of the bullet to its overall length from engineering drawings is used to locate the centre of gravity in the image to account for shortening of the projectile if it is yawing in the plane of view.

shot line and indicate where this may affect temporary cavity measurements.

- Considering the ability to account for diverging shot lines within the vulnerability and lethality shot-line models used to assess bullets (see Section 9.11).
- Investigating other output metrics from gelatin testing that could be used to correlate to ‘injury’ that are less dependent on target size.
- Investigating the effect of gelatin block size and constraint on cavity formation in circular cross section gelatin targets
- Investigating the potential of a new type of Personal Protective Equipment (PPE) specifically designed to constrain cavity formation in muscle tissue and therefore reduce subsequent injury from fragments and bullets.

8 Physical model for skin perforation

8.1 Requirement for a physical skin simulant

The testing performed in Section 5.3 on the effect of the presence of skin on the resulting penetration showed the significant effect skin has of preventing penetrations into the muscle tissue, or reducing their overall DoP, particularly at low velocities, close to the skin V_{50}.

Whilst Dstl 20% gelatin at 10°C was selected in Section 7 as the best performing muscle tissue simulant, penetration at low velocities may not match that in muscle tissue with skin. The expanded empirical model of skin perforation (Equation 8) was used to show the desired performance of PMHS, intact, fresh thigh skin compared to the approximate penetration V_{50} of Dstl 20% gelatin at 10°C for a range of projectiles. The data for Dstl 20% gelatin at 10°C was from the original data used in Section 7 and was not optimised for evaluating the penetration V_{50}. Therefore the V_{50} velocities given are based on limited shots and are should be treated as ‘indication only’. Figure 68 shows the comparison of the predicted performance of PMHS skin to Dstl 20% gelatin at 10°C.

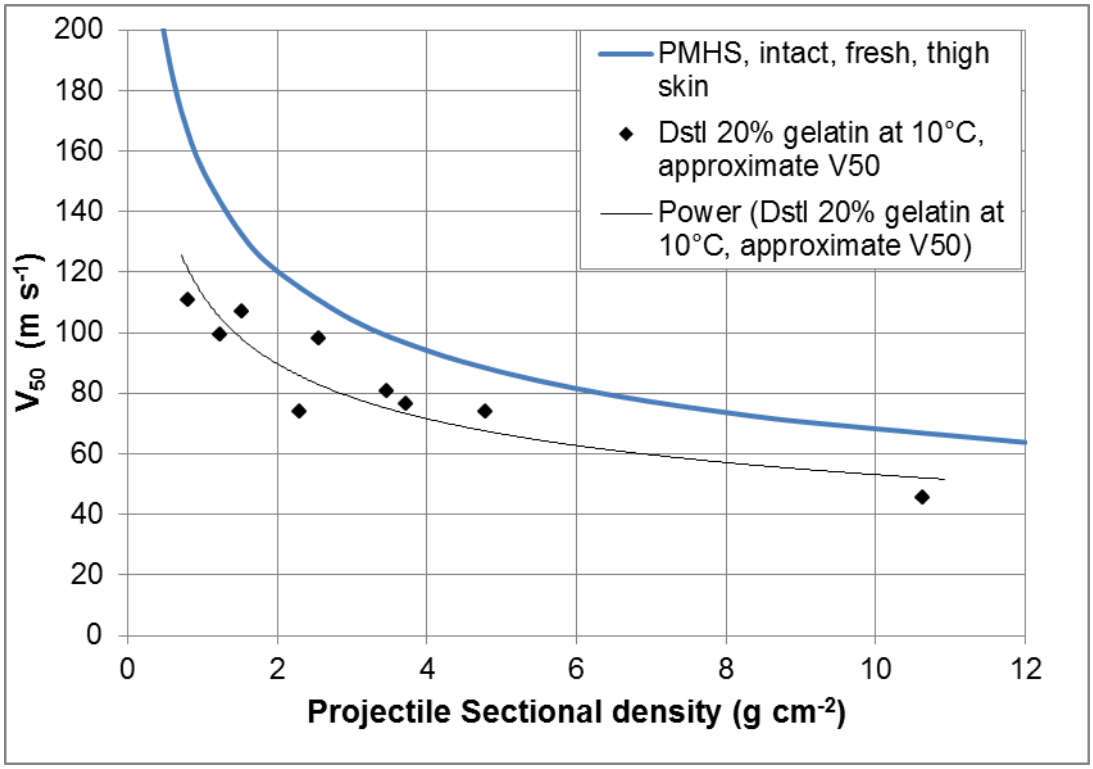

Figure 68: Predicted PMHS, intact, fresh thigh skin perforation performance using Equation 8 compared to approximate penetration V_{50} of Dstl 20% gelatin at 10°C for a variety of projectiles (data from Section 7).

Figure 68 shows that Dstl 20% gelatin at 10°C consistently under-predicts the required velocity for initial penetration across the range of projectile sectional densities compared to the desired PMHS, intact, fresh thigh skin performance using Equation 8. It is also expected that for low velocity impacts, the DoP in gelatin may under predict the desired DoP in muscle tissue with skin.

In order to allow accurate assessment of the potential injury risks of penetrating projectiles at low velocities, a physical skin simulant is required that can be used in conjunction with the (Dstl) 20% gelatin at 10°C muscle simulant. This would then allow both skin perforation V_{50} determinations (or risk of skin perforation) during physical testing, in addition to the normal DoP and cavitation effects that gelatin is traditionally used for.

Based on the skin structure and thickness (as discussed in Section 3.2.2), a skin thickness of 2.0±0.5 mm was set as an objective for a simulant to give a general

representation, independent of body location. This thickness would then allow DoP measurements to be directly comparable to real skin and muscle.

A skin simulant material does not necessarily have to replicate this different layered structure, only the (approximate) overall thickness and ballistic performance.

8.2 Review of materials for a skin simulant

The best skin simulants (of PMHS skin) evaluated for small projectile perforation are animal skin such as goat (when backed by the subcutaneous tissue and muscle). When used in this manner the location of the skin and age of the animal have to be carefully controlled to give the correct properties.

Some previous studies showed pigskin (fresh and 6 days old stored refrigerated) was a good simulant to PMHS data when backed by 10% gelatin at 4°C [87]. This shows an alternative to using the skin intact on the animal, but still is not particularly practical. There are a number of issues with using animals and biological materials, such as; ethics, storage, supply, control and variability. Variability is one of the major factors that need addressing to produce a suitable physical skin perforation model.

An ideal skin simulant has specifiable mechanical properties, with well-defined tolerances on them. This should ensure repeatability in testing and the material properties should be insensitive to environmental conditions during the test (for example variations in test site temperature and humidity). Also consistency in supply over time is desired, as manufacturers may update materials to better match their intended purpose (which is unlikely to be a ballistic skin simulant).

Consideration of materials for a skin simulant in the literature has focused on man-made materials like rubbers and synthetic leathers, or imposing strict limits and controls on the biological materials to use.

1.6 mm neoprene rubber backed by gelatin (30% gelatin for outdoor stability) was identified as a potential skin simulant, but slightly underestimated the number of penetrations from a buried Anti-Personnel Mine (APM) in gravel, compared to pig

tissue and it overestimated the area damaged [221]. Reference [221] also investigated the suitability of 1.6 mm thick vinyl nitrile rubber and found that it greatly over estimated the number of penetrations and the total area damaged. However, due to the nature of the experiment, no indication of the threshold or V_{50} velocities for any of the materials could be obtained.

Jussila [102] investigated a number of materials and suggested a 'cowhide, semi-finished chrome tanned upholstery crust, not treated to final softness', 0.9 to 1.1 mm thick and a natural rubber 1.0 mm thick [102]. Jussila commented on the variability of the properties of the tanned cowhide, but found the natural rubber to have a slightly low penetration velocity. The testing of these materials was done with a 10% gelatin tissue simulant backing.

Cowhide has been used for assessing BB gun safety/injury risk [222]. 6 mm plastic and steel spheres were impacted into the skin simulant (backed by 10% gelatin at 4°C) and the V_{50} perforation velocity determined. No comparison was made within Reference [222] to actual skin performance values. However, comparison of their results to Equation 8 shows the plastic sphere was close to the expected PMHS performance, but the steel sphere required 60% higher velocities to perforate the cowhide than predicted for PMHS.

12% gelatin has also been suggested as a skin simulant, based on experiments with micron scale particles for transdermal pharmaceutical delivery [223]. Due to the scale of the projectiles in these experiments, extrapolation of the thickness required for millimetre scale projectiles would require a gelatin thickness of approximately 50 mm which is not practical.

Some studies have looked at modifying gelatin mixes to better represent the skin. This involves adding chopped fibres (1-5 mm) to represent collagen and diols (e.g. ethandiol) or triols (e.g. glycerol) to the gelatin to strengthen it [224]. The simulants that did undergo mechanical testing were not sufficiently close to the properties of skin to warrant ballistic testing [224]. Gelatin diol/triol mixes (with or without added fibres) may produce a good simulant, that could offer better performance to human skin compared to synthetic leathers, but would require significant development work [224].

Butyl rubber car tyre inner tubes [103; 225] and aviation tyre inner tubes [83] have also been previously recommended as skin simulants since they have been shown to have similar ballistic performance to the PMHS data.

RTV 428 silicone rubber [226], used to manufacture the elements for the UK MOD BABT rig [227], may also be a suitable skin simulant, based on indications of the penetration threshold from unpublished ballistic testing within Dstl.

Silicone rubber is often suggested as a skin simulant, for fragment type impacts [106] as well as for knife/stab and blunt injuries [228-233]. The suggested properties of silicone for this purpose range from 1.5 mm to 12 mm thickness and from Shore Hardness A of 40 to 80. The ballistic skin simulant proposed as part of an initial torso surrogate in Reference [106] used a combination of silicone of 1.6 mm thick, Shore Hardness A of 50, as the an epidermal layer and a 6.35 mm thick neoprene foam as dermal layer (total thickness of 7.95 mm). These materials showed a reasonable match to their skin perforation response corridors presented, but is not deemed suitable for the requirement in this thesis of having a skin simulant (of 2.0±0.5 mm thickness) to cover the front of a Dstl 20% gelatin block at 10°C.

Additionally dental silicones have been suggested as a potential skin simulants for blunt impact testing on the head [234], based on mechanical testing compared to pig skin.

Polyurethane is also suggested in the literature as a skin simulant for different applications. A 3 mm thick, 33 Shore Hardness A polyurethane sheet was shown to have similar performance to skin perforation data from References [56; 84] for a 4.4 mm diameter steel ball bearing [235]. A different study also evaluated 0.8 mm thick polyurethane for NLW impact round skin assessments [236].

Polyurethane has also been shown to have a similar stress/strain response to human skin, with sheets of Shore A hardness values up to 60. The suggested thickness ranged between 2.25 mm and 4 mm for a skin simulant for stab applications [231; 237; 238].

NATO has suggested a ‘standard’ skin simulant for blunt trauma type impacts for evaluating NLW [239]. It is based on a single layer of (dry) natural chamois (1.39 mm optimal thickness) backed by a 6 mm closed cell foam held onto 20% gelatin at 10°C [240]. The foam’s mechanical properties are unknown and it is not available outside the US, so a substitute foam backing may be required. Due to the overall thickness of this skin simulant (7.39 mm) it may not be suitable if depth of penetration assessments are required when the skin is perforated.

This synthetic chamois (but without the foam layer) was used in Reference [241] to investigate the penetration and deformation of different types of air rifle pellets into 10% gelatin with and without a skin simulant layer.

A similar 1.3 mm chamois backed by 10% gelatin has been investigated using a 4.5 mm sphere and compared quite well to pig skin [83]. Reference [236] attempted to replicate the simulant in Reference [239], instead using real leather and a 6 mm closed cell foam.

Materials for a stab skin simulant have been suggested based on synthetic chamois, 1 layer thick, either soaked in water or dry [233]. These materials were assessed by stress/strain tests and it was found that their strength was around four times less than pig skin.

Table 26 summarises all these suggested materials along with the type of testing (if any) that has been performed on the material in the literature to support its use as a skin simulant. Blunt impact describes the type of impacts from larger LLW type impactors, to differentiate from ballistic impacts with smaller diameter bullets and fragments.

	Previous testing performed				
Material	**Qualitative**	**Mechanical**	**Stab**	**Blunt impact**	**Ballistic**
Neoprene rubber	X				X
Vinyl nitrile	X				X
Cowhide		X			X

Material	Previous testing performed				
	Qualitative	**Mechanical**	**Stab**	**Blunt impact**	**Ballistic**
Natural rubber		X			X
Butyl rubber					X
RTV 428					X
Silicone rubber		X	X	X	X
Polyurethane		X	X		X
12% gelatin slab					X
Chopped fibre and diol/triol gelatin		X			
Chamois + closed cell foam				X	
Real chamois			X	X	
Synthetic Chamois (wet and dry)		X	X	X	X

Table 26: Skin simulant materials and their respective degree of testing in the literature.

The majority of simulants that have been ballistically assessed have only used one projectile, so the performance across other projectile sectional densities is unknown.

Reference [106] is an exception to this, which conducted ballistic testing with four projectiles purposefully to identify the performance over a wider sectional density range.

Supporting (shoring) the skin simulant with a backing has a significant effect on the perforation velocity or V_{50}. Reference [83] found that stretched, un-backed skin simulants required a higher velocity to perforate by approximately 30% (for a 1.3 mm chamois) compared to those tested with the same projectile backed by 10% gelatin. The skin simulants backed by gelatin tested in Reference [83]

agreed with the reported skin penetration data much better than the stretched, un-backed simulants.

8.3 Skin simulants selected for evaluation

12 simulants were selected for mechanical and ballistic testing to assess their performance as skin simulants (some simulants were variations of the same material under different conditions). Table 27 shows some of the properties of the materials (where known) to allow comparison to PMHS skin. The values for PMHS skin are for a variety of genders, ages, body regions, strain rates (increasing strain rate corresponds to higher tensile strengths [48]) and strain directions in relation to the main orientation of collagen fibres. This results in a wide spread of reported mechanical properties for PHMS skin. Where the number of layers is given for a particular material, this is for the ballistic testing. The mechanical testing always used a single layer of the material.

Material	**Thickness (mm)**	**Density (g cm^{-3})**	**Hardness (Shore A)**	**Engineering strain**	**UTS (MPa)**
PMHS skin	1.5 - 2.5	1.18	(12-45 Shore 00)	0.4 – 1.7 (3 outlier)	1 - 42
Neoprene rubber	1.5	1.41	70	2	6.9
Natural rubber	1.0	1.04	40	6	17
Polyurethane rubber	3.0	1.04	30-35	14	2.6
Silicone rubber	2.0	1.15	50	2.5-7[119]	7-10[119]
Silicone rubber	2.0	1.19	80	3.5[119]	7-9[119]
Car inner tube (butyl rubber)	1.2	0.92	50	4[119]	8[119]
Aircraft inner tube (butyl rubber)	1.5	0.92	55	4[118]	8[119]

[118] Properties not available for actual product used. Instead they have been estimated from specifications of similar products.

Material	Thickness (mm)	Density (g cm^{-3})	Hardness (Shore A)	Engineering strain	UTS (MPa)
Synthetic chamois (dry) 2 layers	2.5		(35)	1.2-1.8[119]	3-4[119]
Synthetic chamois (wet) 2 layers	2.5			1.3-1.9[119]	3.6-4.0[119]
Real chamois soaked in 20% gelatin, 3 layers	1.5				
Real chamois dry, 3 layers	1.5				
RTV 428 rubber	2.0	1.30	28	4.5	3.2

Table 27: Skin simulant materials selected for ballistic testing with their quoted properties where known [102; 221; 226; 229; 235; 242-244]. Also shown are available properties of PMHS skin for comparison [48; 50; 245; 246]. UTS = Ultimate Tensile Strength.

All the synthetic materials had tight tolerances on their thicknesses and other mechanical properties (as quoted by the manufacturers). The real chamois were highly variable in thickness, between different examples (0.5 ± 0.3 mm) and to a lesser extent on the same chamois leather (± 0.1 mm). For the purposes of the skin simulant testing, real chamois leathers of measured thicknesses of 0.50 ± 0.05 mm were selected.

8.4 Skin simulant mechanical testing

8.4.1 Mechanical testing method

Six of the twelve simulants in Table 27 underwent tensile testing. Also tested was a surgical skin simulant[119] (this material was not available for the corresponding ballistic evaluation in Section 8.5) and a neoprene foam (used in the model

[119] Supplied by Adam Rouilly Ltd, part number MX01, sundry items AR products

detailed in Section 10). The butyl rubber tested was from the aircraft inner tube (1.5 mm thickness) detailed in Table 27.

References [247] or [248] were followed for conducting the tensile testing where possible. Dumb bell type test pieces were used with a test length of 85 mm and width of 10 mm due to limitations in the available die cutters. This specimen test length is between the standard and large sizes specified within Reference [247]. References [248] specifies specimen test lengths of 20 or 25 mm (due to larger strain of rubbers).

Sample thicknesses ranged between 1 and 4 mm depending on the material. All samples were conditioned to 23°C, 50% relative humidity for a minimum of 12 hours prior to testing.

An Instron model 5567 universal test machine (30 kN load cell) was used with pneumatic grips and constant extension speed of 100 mm min^{-1} which corresponded to a 0.02 s^{-1} strain rate. Load and extension measurements were taken via the displacement cell on the cross-head of the Instron machine with Instron Bluehill® software [249].

Additionally, 2D Digital Image Correlation (DIC)[120] was employed, independently using a Phantom v641 (2560x124 pixels and 10 frames per second) and FLIR Systems, Inc. (formerly Point Grey) Flea 3 (1928x350 pixels and 15 frames per second) cameras. Both cameras were oriented to give the maximum resolution in the direction of the applied strain. A random spot pattern was applied onto each sample prior to testing for the DIC analysis.

A sample of the synthetic chamois with the spot pattern in the pneumatic grips is shown in Figure 69 alongside an overview of the tensile test setup (no specimen).

[120] DIC is a full-field optical strain measurement technique which uses image registration to measure the 2D or 3D deformation of a material [250].

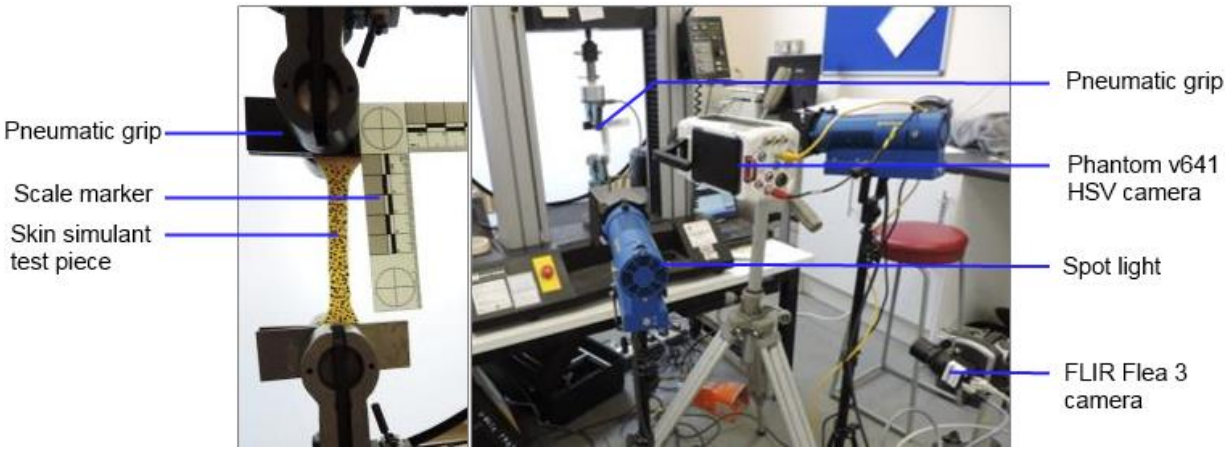

Figure 69: Left - a synthetic chamois sample in the pneumatic grips with DIC pattern. Right - overview of the tensile test setup (no specimen) showing the two cameras and lighting.

An average of 8 repeats were conducted for each material. The results for each material were averaged across all the repeats performed.

8.4.2 Mechanical testing results and discussion

Not all samples failed within the maximum ~500% elongation achievable. Therefore ultimate tensile strength cannot be determined for all samples.

The results of the ultimate tensile strength and strain are detailed in Table 28 for the materials evaluated. Also shown are the PMHS skin properties as detailed in Table 27.

Material	Engineering strain at failure	UTS (MPa)	Manufacturer strain at failure	Manufacturer UTS (MPa)
PMHS skin	0.4-1.7	1-42		
Butyl rubber	>4.84	>5.65	4[119]	8[119]
Natural rubber	>4.84	>4.79	6	17
Neoprene Rubber	2.11	7.10	2	6.9
Polyurethane	>4.84	>1.44	14	2.6
Real Chamois	0.61	1.25	n/a	n/a
Surgical simulant	>4.84	1.69	n/a	n/a

Material	Engineering strain at failure	UTS (MPa)	Manufacturer strain at failure	Manufacturer UTS (MPa)
Synthetic chamois	0.35	3.16	1.2-1.8[119]	3-4[119]
Neoprene foam	*1.01*	*0.56*	*1*	*0.5*

Table 28: Ultimate stress strain values from the mechanical testing of skin simulants compared to manufacturers reported values[119] and PMHS skin [48; 245; 246]. Results for neoprene foam (italics) are given for information in relation to the model in Section 10.

In order to compare the skin simulants to PMHS skin which have a wide spread of reported mechanical properties, an example stress-strain response for PMHS skin from Reference [250] was used. This was for a comparable strain rate of 0.012 s^{-1} and is shown in Figure 70 along with the results for the skin simulants.

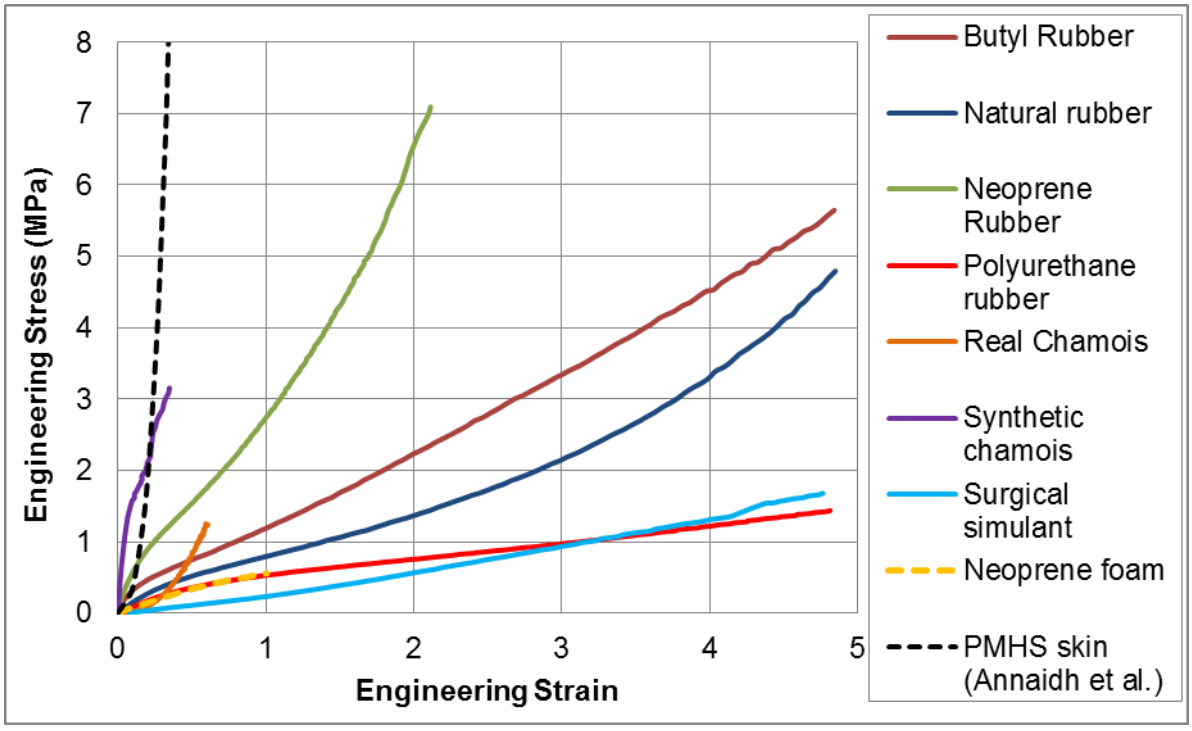

Figure 70: Average tensile test reuslts for the skin simulants. Also shown by the dashed black line is the result for a typical stress strain response of PMHS back skin from Reference [250]. The stress axis was limited to 8 MPa, with the PMHS skin example curve failing at approximately 21 MPa.

Figure 70 shows that the synthetic chamois gives a reasonable match to the PMHS stress strain curve, until it fails at much lower UTS.

All the materials evaluated either showed failure strains in excess of what was achievable with the setup used (>5), or much lower UTS than the PMHS skin reference performance.

The butyl rubber gave a very similar response compared to the PMHS skin for low strains (<0.1). After this it had much greater extensions for similar stress.

The real chamois showed the same characteristic shape of the stress-strain curve to PMHS skin as described in Reference [48]: initially "*collagen fibres are still wavy and elastin fibres are the load-bearing components*", then "*the collagen fibres are … aligned and contribute to load-bearing*", until "*all the collagen fibres are aligned and the tissue has its highest stiffness*." [48]

Despite the real chamois showing the same characteristic shape of the stress-strain curve as PMHS skin, the stress was approximately an order of magnitude lower than in the PMHS skin for equivalent strains.

Of the skin simulants assessed, only the real chamois showed stress and strains at failure within the PMHS skin performance windows from Table 27. Based on PMHS skin data in Table 27, the 54% failure strain used for the PMHS skin stress-strain response (from Reference [250]) shown in Figure 70 is at the lower end of the performance window.

It is unknown how many of the simulants would perform at higher strain rates, comparable to those in ballistic impacts, or if the mechanical testing at representative strain rates would allow better evaluation of potential ballistic skin simulant materials.

Unsurprisingly, at these low strain rates, where manufacturer's data was available for the materials tested the results agreed well with the stated performance values.

Whilst the mechanical testing itself has not produced clear outcomes in terms of suitable skin simulant materials, the potential materials have been characterised.

This will allow similar performing materials to be used in their place in the subsequent models developed, should the original materials change specification or no longer be available.

Some of the limitations identified from this testing were:

- Not all materials that were ballistically tested could be mechanically tested.
- The samples were cut based on the available cutters; it was not to the leathers or rubbers test standard
- This limited the maximum strain achievable (<5 engineering strain).
- The displacement via the cross head on the tensile test machine was used rather than DIC.
- The tensile performance of human skin is extremely variable [48; 50; 245; 246] and therefore the reference performance may not be ideal as an objective performance for the simulants.

Due to the facilities available and focus of this thesis, it was deemed a better use of resources and more practical to conduct ballistic testing to evaluate the potential simulant materials under suitable ballistic test conditions instead of additional mechanical testing (at higher strain rates) or full analysis of the strain from DIC measurements.

8.5 Skin simulant ballistic testing

Part of the ballistic testing detailed in this Section was conducted by the author prior to the start of this PhD registration and has previously been published in Reference [251]. As part of this thesis, additional data has been generated (n=69) and the combined previous raw and new data re-analysed using updated V_{50} performance calculation methods (Section 3.2.3) and updated performance metrics (Section 8.5.1)[121] for the skin simulant response.

[121] In the previously published reference, evaluation of the skin simulant response was based on the average perforation performance of mixed animal and PMHS skin, both intact and isolated, different storage conditions and body regions [251].

8.5.1 Skin simulant performance metric

Depending on the application of the physical model, 2 separate performance metrics were used to represent the risk of skin perforation based on Equation 8 for different scenarios:

- V_{50} performance curve for skin perforation of PMHS adult thigh, skin intact and fresh. This could be taken to represent a reasonable 'most likely case' for an adult population or military personnel.
- V_{50} performance curve for skin perforation of PMHS child thigh, skin intact and fresh. This could be taken to represent the 'worst likely case' civilian or vulnerable group population and may be most suitable for situations where the risk does not want to be under-predicted, i.e. a collateral damage type prediction for a vulnerable population or general public[122].

It is desired that a skin simulant can closely match at least one of these performance metrics, without requiring (consistently) higher velocities to perforate it. If higher velocities are required to perforate the skin simulant, then there is potential that assessments using the skin simulant could determine particular impact conditions to be 'safe' when there is still a significant residual risk of skin perforation. Therefore it is always desired (for safety case type assessments) that models slightly over-predict injury or vulnerability, to err on the side of caution[123].

Skin simulants tested with a particular backing will only be valid when used in combination with that specific backing, in this case Dstl 20% gelatin at 10°C.

[122] The thigh was not determined to be the most vulnerable body region in Section 6.1.5. However, the thigh region was chosen as Equation 8 has been validated against this specific case (see APPENDIX C). The performance of child PMHS skin on the buttocks region (the most vulnerable body region seen in adult PMHS) cannot be stated with the same levels of confidence, as no other body regions were tested for the child PMHS skin.
[123] Both in terms of not wanting to put anyone inadvertently at risk/harm, but also from a potential legal/litigation standpoint, determining a scenario to be 'safe' which later turns out not to be.

8.5.2 Selected projectiles for skin simulant testing

The projectiles shown in Table 29 were chosen to allow evaluation of each target material over the applicable sectional density range, so that the skin simulant can be used for a wide range of projectiles. Projectiles were supplied from GMS Ball Co Ltd. to DIN 5401 - Part 1, G100 (or equivalent)[124]. Table 29 gives the optimal performance in terms of V_{50} of the projectiles, to aid the assessment of the skin simulants, calculated from Equation 8[125].

		Predicted skin perforation V_{50} (m s^{-1})	
Projectile	**Sectional density (g cm^{-2})**	**Adult PMHS (thigh)**	**Child PMHS (thigh)**
3 mm glass sphere	0.51	195.2	184.2
6 mm glass sphere	1.03	152.2	136.4
9 mm glass sphere	1.53	132.3	115.1
4.4 mm steel sphere	2.30	114.5	96.7
9 mm ceramic sphere	2.32	114.2	96.4
6 mm steel sphere	3.19	102.0	84.1
9 mm steel sphere	4.79	88.5	70.8
20 mm steel sphere	10.63	66.6	50.3

Table 29: Projectiles for assessment of skin simulants. Predicted V_{50} values were calculated from Equation 8.

Examples of the projectiles used are shown in Figure 71.

[124] Which allows ±47.5 µm tolerance on the nominal diameter and ±2.5 µm deviation from spherical.
[125] These data in Table 29 can also be used as verification data for Equation 8.

Figure 71: Examples of the steel, ceramic and glass spheres used in the assessment. From left to right 20 mm, 9 mm, 6 mm, 4.4 mm and 3 mm spheres.

Due to the number of shots required for the V_{50} assessment and the numerous target materials, the skin simulants were evaluated in stages. All simulants were tested with a 9 mm steel sphere to give a V_{50} for a central projectile sectional density. Promising materials were then additionally tested with a 6 mm glass sphere and 9 mm glass sphere. This evaluated the material at the lower range of sectional densities.

If a skin simulant was shown to be in close agreement with the skin perforation performance metric, further testing was done with a selection of 3 mm glass 4.4 mm steel, 6 mm steel, 9 mm ceramic and 20 mm steel spheres.

8.5.3 Method

Details of the testing conducted are given here, which includes both the previous [251] and new testing. All materials were backed by a Dstl 20% gelatin block (manufactured according to the specification in Section D.1).

The simulants were held in close contact with the gelatin by a single thin sheet of PVC cling film to one of the long sides of the 300 mm by 150 mm by 150 mm block. It was not expected that this single layer of film significantly affected the resulting perforation of fragments [102], however, this layer is included as an integral part of the model. Projectile impacts were normal to the target. All firings were performed with the simulants stored at 22°C and 45% relative humidity for

a minimum of 24 hours prior to testing when they were applied to the front face of the gelatin block, immediately prior to firing. Gelatin blocks at 10°C were used within a 20 minute window from removal from a conditioning cabinet.

Figure 72 shows a photograph of one of the skin simulant materials attached to the gelatin block with cling film, ready to test.

Figure 72: Photograph of the polyurethane skin simulant attached to the long face of the 20% gelatin block using PVC film.

Projectiles were fired using the Honed Tube Pressure Housing weapon system, with a separate smooth bore barrel for each different diameter projectile. The projectiles were propelled using rechargeable 37 mm compressed Airmunition cartridges. For the low velocities required for the 6 mm glass sphere against some materials, 0.32” blank cartridges were used (see APPENDIX B for weapon system details).

Projectile velocities were measured using Oehler Model 57 Infrared ballistic screens [207] with 0.8 m separation, connected to a Nicolet Sigma 10 oscilloscope.

The statistical package R [52] (with a bias reduced generalized linear model, brglm [53]) was used to calculate the value for the skin V_{50} perforation velocity for each fragment with a 95% confidence interval on the V_{50} velocity.

8.5.4 Results

A total of 40 V_{50} assessments were conducted across the 12 materials and 8 projectiles. Tabulated data is provided in Table 46 in APPENDIX F.

Figure 73 shows the V_{50} performance of all the skin simulant materials with the different projectiles.

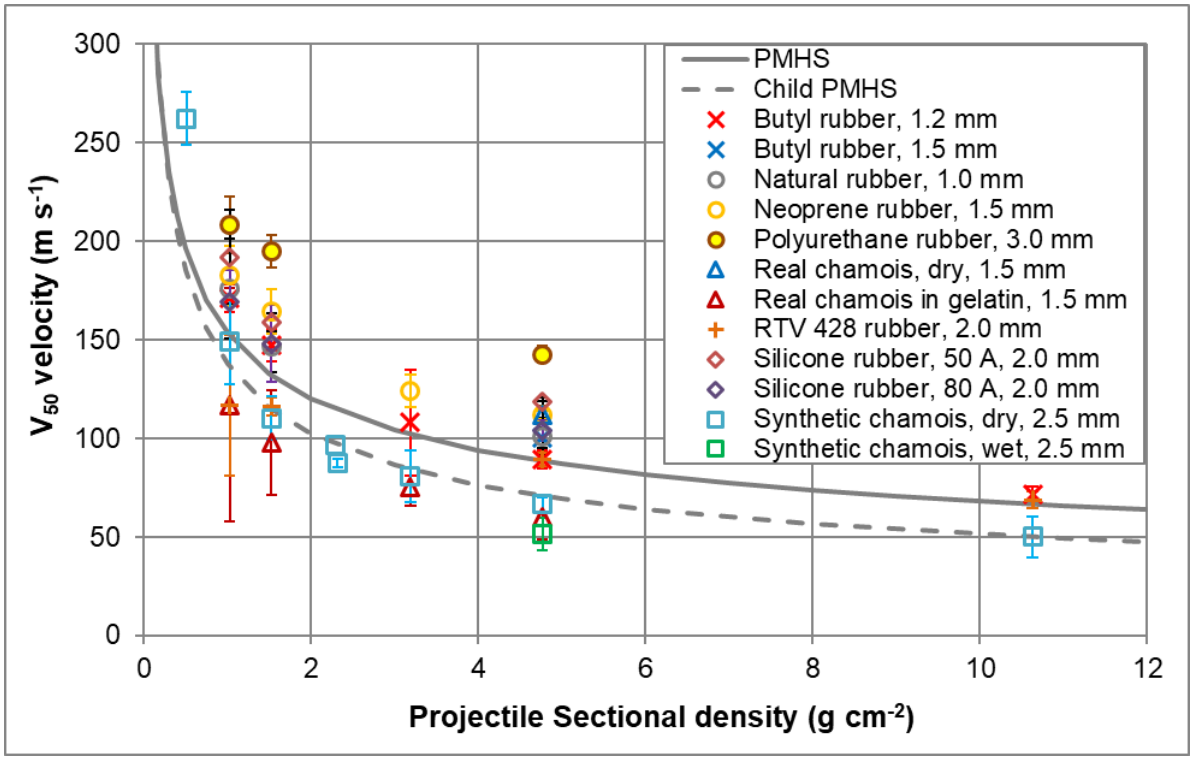

Figure 73: V_{50} Performance of the skin simulant materials backed by Dstl 20% gelatin at 10°C. (Some raw data was from Reference [251] with additional original data and V_{50}s recalculated in line with Section 3.2.3.) The error bars show the ±95% confidence interval.

It can be seen that all the materials tested with V_{50}s calculated follow the general trend of lower perforation velocity with increasing sectional density of the projectile, although different simulant materials show a wide spread in performance at equivalent projectile sectional densities.

For clarity, Figure 73 is replotted with just the 4 best performing simulants in Figure 74.

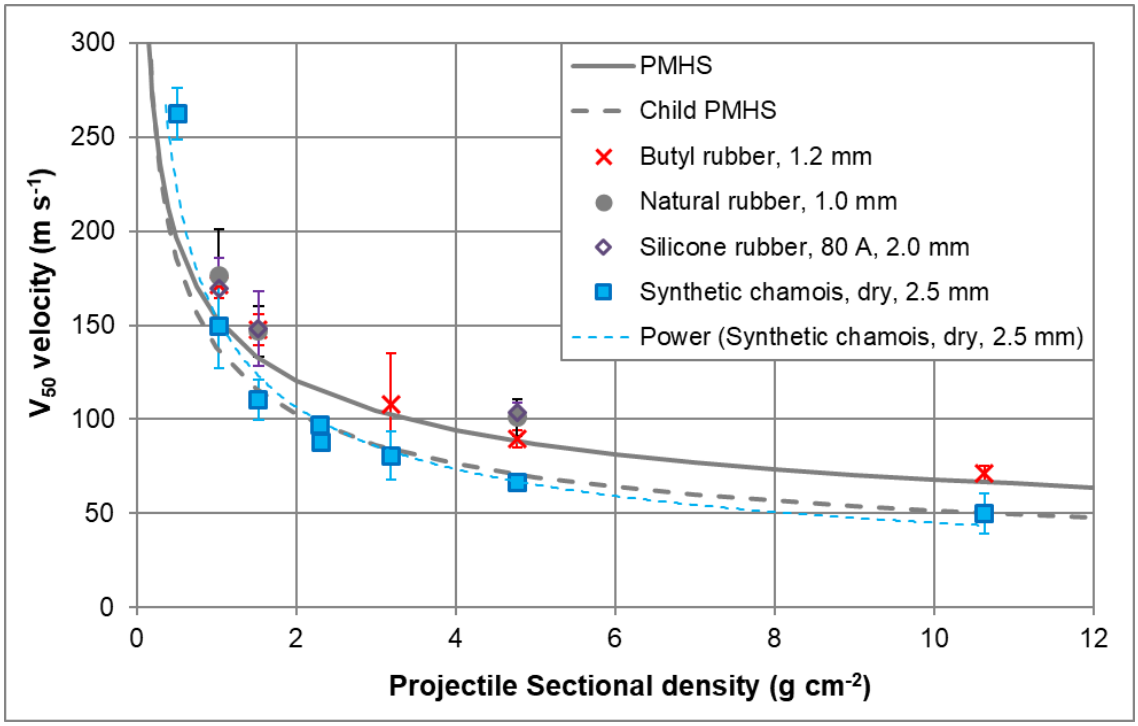

Figure 74: V_{50} Performance of the 4 best performing skin simulant materials backed by Dstl 20% gelatin at 10°C. (Some raw data was from Reference [251] with additional original data and V_{50}s recalculated in line with Section 3.2.3.) The error bars show the ±95% confidence interval.

The simulant which performed closest to the optimal performance curve (Equation 8) without requiring (consistently) higher velocities to perforate was the 2.5 mm thick (2 layers) synthetic chamois. This material was assessed with eight different projectiles. The synthetic chamois required a higher velocity to perforate compared to the desired performance at very low projectile sectional densities (<1 g cm^{-2}). The other materials assessed showed a tendency to under-predict the risk at a greater range of projectile sectional densities.

The next best performing material was the 1.2 mm thick butyl rubber (car inner tube), assessed with 5 projectiles. The 1.2 mm butyl rubber closely matched the PMHS performance, but required consistently higher velocities to perforate (particularly evident below projectile sectional densities of approximately 3 g cm^{-2}) and as such would under-estimate the skin perforation risk.

Both the synthetic chamois and butyl car inner tube are from commercial off the shelf products and there is a risk their specification may change or they may be discontinued without notice.

Although the 2.5 mm thick synthetic chamois closely matches the perforation (V_{50}) performance of child PMHS skin, it did not produce similar types of damage on impact[126]. It was believed that using wet synthetic chamois may make the resulting damage more representative of real skin. However, it was found that soaking the synthetic chamois in water reduced the velocity required to cause perforation, resulting in a poorer fit to the optimal performance curve.

The real chamois soaked in 20% gelatin (3 layers thick) appeared to produce damage that was more similar to the damage expected with impacts into real skin; however, its performance was not as close a match to the desired performance as the synthetic chamois. Additionally, the real chamois was highly variable in thickness, required preparation and cannot be stored (prepared) for longer than 24 hours. Testing of 3 layers of real chamois when dry (not soaked in gelatin) increased the velocity required for perforation, over the desired performance limits.

The silicone (50A and 80A) and butyl rubber (car and aircraft inner tube) materials all showed a significant degree of plastic deformation at velocities slightly under that required for perforation. This deformation was up to a projectile diameter, an example of this can be seen in Figure 75.

[126] The synthetic chamois tended to rip and tear when perforated by large projectiles such as the 20 mm steel sphere and showed pencilling with the 3 mm glass sphere. This is not consistent with the failure mechanism seen real skin.

Figure 75: Back face of the butyl car inner tube showing deformation after impacts with the 9 mm steel sphere.

The synthetic chamois (2 layers, ~2.5 mm thickness) was selected as a skin simulant when backed by Dstl 20% gelatin at 10°C. For use with Equation 8 (and other equations later in this thesis), values for target type (γ_a and γ_b) for the synthetic chamois are 1.009 and 1.469 respectively (all other expanded parameters set=1).

The validation range for the physical skin simulant model[127] was for non-deforming spheres with sectional densities between 0.5 and 10.6 g cm^{-2}.

The 2 layers of dry synthetic chamois has only been assessed when backed by 20% gelatin at 10°C and its performance may change significantly if backed by a different material. If used with a different backing, it would require re-validation.

Should the synthetic chamois no longer be available (or a skin simulant required to match adult PMHS performance rather than child PMHS), a butyl rubber with thickness between 1.0-1.2 mm and approximately 50 A Shore Hardness backed by Dstl 20% gelatin at 10°C would be a good starting point as a potential alternative.

8.6 Skin perforation model calibration

In order to have a verification or calibration test in line with the standard calibration tests for 10% and 20% gelatin (APPENDIX D, D.5), original testing of the synthetic chamois and 20% gelatin at 10°C was conducted. This was

[127] The thin PVC film layer used to hold the skin simulant to the face of the gelatin block is an integral part of the model and has been accounted for in the validation.

determined to be more practical than conducting a V_{50} test against the skin simulant model and should enable verification of the complete model. The model was impacted with the 4.4 mm steel ball bearing weighing 0.35 g at a range of velocities and the corresponding DoP measured.

This allowed a calibration or verification test to be defined, based on the 90% prediction interval of the linear fit to the velocity – DoP data. The raw data (n=16) and resulting fits are shown in Figure 76.

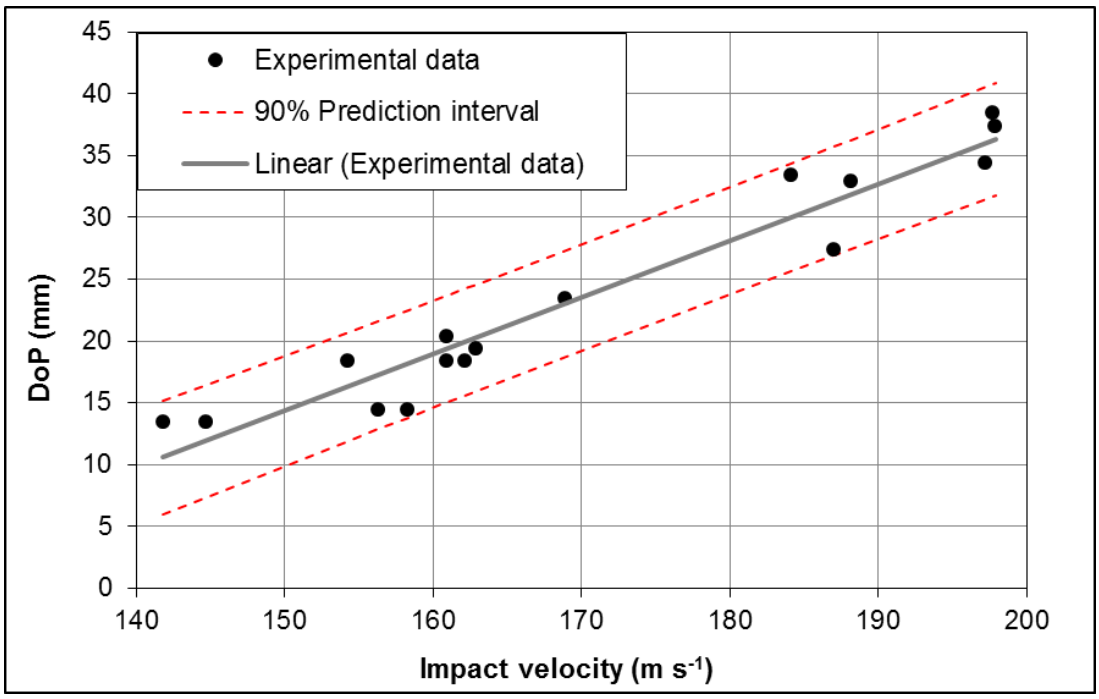

Figure 76: Calibration data and limits for the physical skin perforation model (2 layer synthetic chamois on Dstl 20% gelatin at 10°C).

The calibration limits as described by the 90% prediction interval in Figure 76 are given by Equation 15:

$$DoP = 0.458v - 54.4 \pm 4.5$$

Equation 15: Calibration test for the physical skin perforation model.

Where:

DoP is in mm (measured to the shallowest part of the projectile)

v is the impact velocity in m s^{-1} (velocity limits $145 \leq v \leq 200$ m s^{-1}).

As for the gelatin calibration in Section 7.2.6, one result that is in calibration is required per batch (or per model if calibrating each individually). If the first shot is at a valid velocity, but the resulting DoP is not within the limitations of Equation 15, conduct an additional shot at a valid velocity. This second shot must then pass the calibration. If both fail, the batch should be rejected. It is recommended to report all calibration results (impact velocity and resulting DoP) with the studies in which it was generated to provide assurance on the model verification.

8.7 Additional validation of physical model for skin perforation

The physical model for skin perforation has been well characterised against the desired skin V_{50} performance within Section 8.5. To additionally validate the model, the energy loss per 100 mm in live pig thighs data described in Section 7.3.2 and APPENDIX E, E.2 was used to compare to the gelatin and skin simulant model. As for the (bare) Dstl 20% gelatin at 10°C, the impacts were recreated against the physical model for skin perforation (synthetic skin simulant and Dstl 20% gelatin at 10°C). The 2 layer synthetic chamois was applied to both the impact and exit face of a nominal 95 mm Dstl 20% gelatin at 10°C block (so that with the skin simulant applied, total nominal thickness was 100 mm).

The testing was conducted at the same time as the bare Dstl 20% gelatin at 10°C impacts described in Section 7.3.2. A 9.525 mm (3/8”) steel sphere (nominal mass 3.55 g) was impacted into the model at a nominal impact velocity of 775 m s^{-1}. The exit velocity of the projectile was measured following the perforation, and so was the total thickness of target (skin and gelatin) penetrated by the projectile. A total of 10 shots for the physical skin perforation model were conducted and the residual velocity compared to both the bare Dstl 20% gelatin at 10°C and live pig thigh data.

The raw data of impact velocity and velocity loss per mm for each shot is shown in Figure 77.

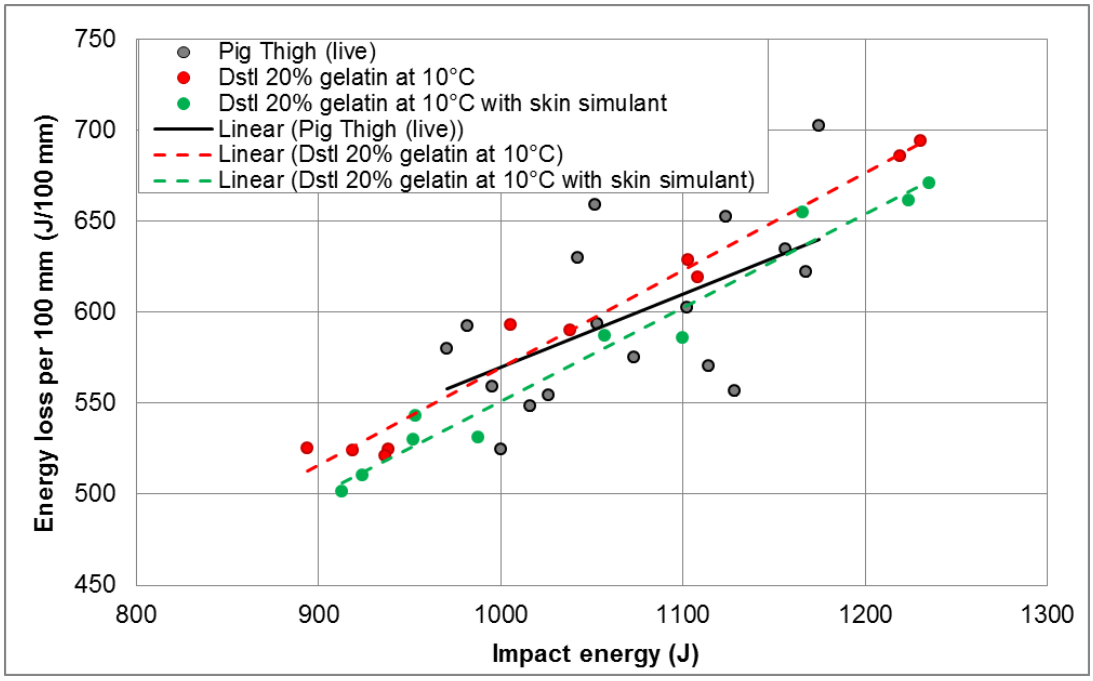

Figure 77: Energy loss per 100 mm in live pig thighs and muscle tissue simulants for 9.525 mm steel spheres. Pig data is from Reference [96].

Figure 77 shows that both the bare 20% gelatin at 10°C and that with the skin simulant on its impact and exit face provided a similar energy loss to the live pig data. No statistically significant difference at the 95% confidence level was detected in the average energy loss per 100 mm between the pig thighs and the skin perforation model (p=0.175).

Figure 77 shows that the projectiles passing through the gelatin with skin simulant lost slightly less energy per 100 mm than in the bare gelatin. This difference was approximately 20 J/100 mm and was statistically significant at the 95% confidence level (p=0.012)[128].

[128] This outcome for gelatin and the skin simulant contradicts the expected response for muscle tissue and real skin, based on the ComputerMan tissue retardation curves, see Section 9.9.

9 Equations for tissue (simulant) penetration, projectile retardation and cavitation

9.1 Review of penetration equations

An equation (or set of equations) to accurately predict the depth of penetration and retardation in gelatin or tissue could aid injury assessments, generate a Fast Running Engineering Model (FREM) and feed human vulnerability shot line models.

Ideally a suitable equation for (live) muscle tissue would be evaluated or produced. However, due to the numerous limitations of using real muscle (Section 3.9.3), a muscle tissue simulant may be preferable.

A number of (closed form) equations were reviewed that could be implemented in Microsoft® Excel® to investigate how they fitted the experimental data for Dstl 20% gelatin at 10°C, which was selected as the most appropriate muscle tissue simulant. In order to be considered, equations needed the following input and outputs given in Table 30.

Minimum inputs	**Additional desired inputs**	**Minimum outputs**	**Additional desired outputs**
Projectile impact velocity	Projectile density	Permanent DoP	Retardation profile (i.e. remaining velocity prediction at any given penetration depth)
Projectile diameter or cross sectional area	Projectile geometry or drag coefficient		
Projectile mass[129]			

Table 30: Desired input and outputs for a Fast Running Engineering Model (FREM) of gelatin penetration.

The additional desired inputs would allow the previous test data generated in Section 5 to be modelled by the equation(s).

[129] Or as a function of diameter and/or density

Equations specific to other materials, other than those for muscle tissue, were not included. For example those for 10% gelatin at 4°C or for 20% gelatin at other usage temperatures were discounted.

The equations considered are given in Table 31[130]. Unless stated otherwise the DoP is the maximum permanent depth of penetration. Where necessary, equations were rearranged from their original form to give DoP as a function of velocity.

[130] Note that the symbols used in Table 31 are those used in the original references and may not align with those used through this thesis. The symbols in Table 31 are not specifically defined in the LIST OF SYMBOLS.

Equation name and Source	Equation(s)	Application range
Dstl 20% gelatin at 10°C empirical fit Based on data in Section 7.2	$DoP = \rho_p d(-5.42x10^{-6}v^2 + 0.0128v - 0.729)$ **Equation 16: Dstl 20% gelatin at 10°C empirical fit**	$2.5 \leq \rho_p \leq 10.3$ g cm^{-3} $2.7 \leq d \leq 20$ mm $v \leq 1000$ m s^{-1} Geometry= cylinder, CN cylinder, sphere
Animal tissue empirical fit Equation 12	$DoP = \rho_p d(-2.940\text{x}10^{-6}v^2 + 0.01008\text{v} - 0.2139)$	$2.5 \leq \rho_p \leq 8.0$ g cm^{-3} $2.7 \leq d \leq 20$ mm $v \leq 1680$ m s^{-1} Geometry= cylinder, CN cylinder, sphere
ComputerMan muscle tissue, Equation 13 [42]	$DoP = \rho_p d(-6.275\text{x}10^{-6}v^2 + 0.01326\text{v} - 0.4246)$	6 mm steel spheres, but generalised for other diameters and densities
Based on Peters [252-254]	$DoP = 10\left(\frac{m}{\rho_T A C_D}\right)\ln\left[\left(\frac{V_S}{U\left[0.74e^{-(18C_D{}^4)} + 1.2\right]}\right)^2 + 1\right]$ $U = U_6\left(\frac{d}{d_6}\right)^{-1/3}$	Not stated in original reference

Equation name and Source	Equation(s)	Application range
Sturdivan [255]	$$DoP = \frac{m}{C_I \rho_T A} ln\left(1 + V_0\left(\frac{C_I \rho_T b}{C_v \mu}\right)\right)$$ $$V_0 = \frac{V_s}{1 + \frac{a}{\rho_p} e^{V_s/c}}$$ DoP is the maximum temporary depth in cm and velocity in cm s^{-1} C_I=0.1 for spheres and 0.175 for cylinders, cubes and fragments $\frac{C_v \mu}{b} = 3000$, a=0.295 g cm^{-3}, c=82000 cm s^{-1}	v≤1500 m s^{-1} Geometry= Spheres, cubes, cylinders, fragments (Developed on data for: $7.0 \leq \rho_p \leq 16.8$ g cm^{-3} 1.4≤d≤12.4 mm 0.03≤m≤14.7 g)
Dziemian, as given in Reference [161]	$$DoP = \left(\frac{M}{A}\right)^{1.21}\left[\frac{{V_c}^2}{\alpha {V_c}^2 + \beta V_c + \gamma} + \frac{\beta}{\alpha\sqrt{4\alpha\gamma - \beta^2}}\left(tan^{-1}\frac{2\alpha V_c + \beta}{\sqrt{4\alpha\gamma - \beta^2}} - tan^{-1}\frac{2\alpha V_0 + \beta}{\sqrt{4\alpha\gamma - \beta^2}}\right) - \frac{1}{2\alpha} ln\frac{\alpha {V_c}^2 + \beta V_c + \gamma}{\alpha {V_0}^2 + \beta V_0 + \gamma}\right]$$ α = 20.207, β = 1925, γ = 333,000 and V_c = 20 m s^{-1} DoP in m, M = mass of sphere in kg and A = cross sectional area of sphere in m^2	Spheres, implementation could not be verified
Curve fit to Dziemian [161] $\frac{DoP}{\left(\frac{m}{A}\right)^{1.21}}$ scaling	$$DoP = \left(\frac{m}{A}\right)^{1.21}(-5.50x10^{-5}v^2 + 0.144v - 3.97)$$ DoP in mm, mass in g, A in cm^2	Spheres

Equation name and Source	Equation(s)	Application range
Segletes [200] (corrected)[131]	$DoP = \frac{4\rho_P D}{3\rho_T b(2-\alpha)} ln\left[1 + b\left(\frac{D}{D_c}\right)^{\alpha}\left(\frac{V_0}{V_c}\right)^{2-\alpha}\right]$ DoP is the maximum temporary depth (mm)	Spheres
Harvey [116]	$DoP = 23.15dln\left(\frac{V}{84}\right)$	Muscle tissue, steel spheres
Tausch [71]	$Dop = \frac{89.69m}{\rho_T A e^{0.629\sqrt{m}}} ln\left(\frac{V}{277.7e^{-0.482\sqrt{S}}}\right)$	Muscle tissue, steel spheres
Kneubuehl [69]	$DoP = \frac{1}{R}\ln\left(\frac{V_0 - V_{ds}}{V_{stk}}\right)$ $R = C_D \rho_T \frac{A}{2m}$ V_{ds}=28.7 m s^{-1} and V_{stk}=14.0 m s^{-1}. ρ_T in kg m^{-3}, A in m^2, mass assumed in g to give DoP in mm.	Spheres, implementation could not be verified

Table 31: Equations considered for modelling the maximum penetration into 20% gelatin at 10°C (or muscle tissue).

[131] The equation given in Reference [200] used a log function and verification showed an issue due to poor fit to the data. Replacing it with a natural logarithm was found to fit the data as expected. The form that has been verified to fit the data is presented and used in this thesis.

The Kneubuehl equation [69] was implemented but verification against Dstl 20% gelatin at 10°C showed a very poor fit to the data. Verification data or example implementation was not provided within Reference [69] and therefore this may be a theoretical relationship. As this equation could not be verified, it was not considered further.

The Dziemian equation [161] could not be implemented and verified for the general case. However, the implementation of the projectile specific cases (3/16" and 1/4" steel sphere) were verified against the data points from Reference [161], as well as original gelatin data for these 2 projectiles. The projectile specific fits show good fit to the data, as expected from Reference [161]. Instead of the general case of the Dziemian equation, an empirical fit was made to the scaled DoP over $(m/A)^{1.21}$, the same scaling as applied in Reference [161]. This empirical fit (which ignored the low velocity correction in Dziemians original equation [161]) provided a good fit to the sphere data (of all densities).

Each equation from Table 31 that was implemented was compared to the Dstl 20% gelatin at 10°C experimental data[132] to determine how well the model fit the experimental data. Figure 78 compares the predicted versus experimental measured permanent DoP in Dstl 20% gelatin at 10°C for the five of the predictive models given in Table 31. Individual graphs showing the predicted against experimental measured DoP for each equation are given in APPENDIX H.

[132] Experimental data used is given in in Table 23 in terms of the breakdown of original data by the author, that from other-unpublished work (not by the author) and that previously published. This same data is used for validation of the equations throughout Section 9.

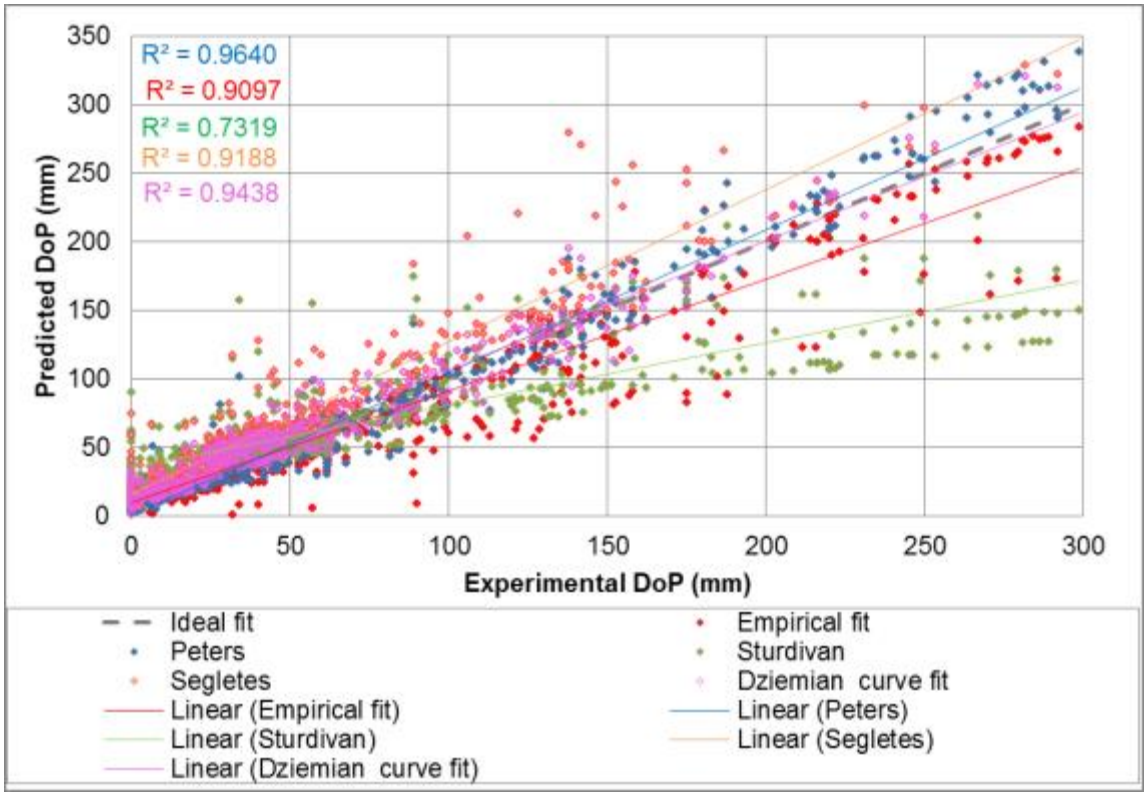

Figure 78: Predicted versus experimental measured permanent DoP in Dstl 20% gelatin at 10°C for different predictive models [161; 200; 252; 255] and Equation 16. The fit to all projectiles valid for each equation is shown (n≤659 from Section 7.2).

The equation based on Peters [252] showed the best predictive ability of the Dstl 20% gelatin at 10°C experimental data, shown in Figure 78. Additionally it has the ability to account for the desired, as well as minimum inputs detailed in Table 30. Retardation can be predicted using a different variant of the equation and will be considered separately (Section 9.3). The Peters equation was chosen to use as the basis of the FREM for gelatin penetration.

The next best ranked equations by Dziemian [161] and Segletes [200] respectively were only applicable to spheres.

Figure 79 compares the Peters equation [252] to experimental results for predictions of the permanent DoP in 20% gelatin at 10°C for a variety of projectiles.

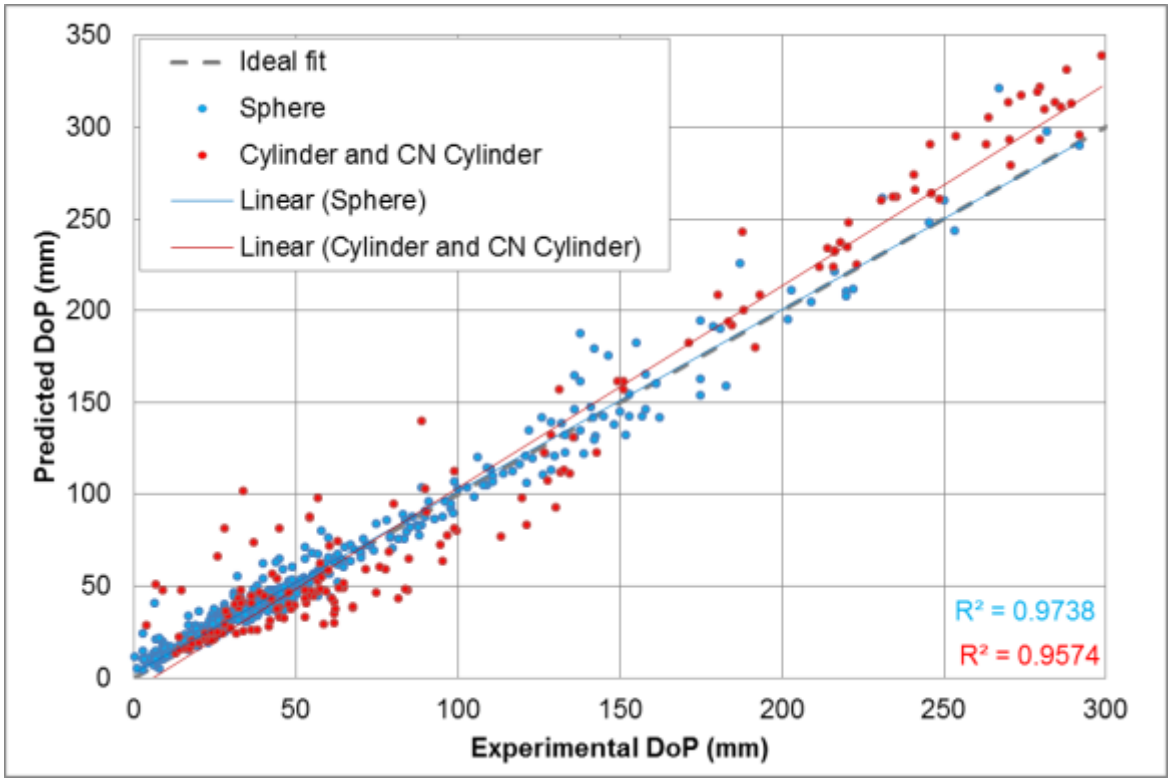

Figure 79: Comparison of the experimental and predicted permanent DoP in Dstl 20% gelatin at 10˚C using the Peters equation [252], with a range of different density, diameter and geometry projectiles (n=659 from Section 7.2)

Figure 79 shows good agreement of the prediction to the experimental results for the projectile geometries shown. The projectiles included spheres, cylinders and CN cylinders, in a range of diameters (2.7 to 20 mm), densities (2.5 to 10.3 g cm^{-3}), masses (0.04 to 54 g) and velocities (28 to 994 m s^{-1}). All shots were conducted on a 300 mm length gelatin block.

9.2 Tissue (simulant) penetration depth

9.2.1 Permanent DoP prediction

The equation from Peters [252] was found to give the best fit to the data for predicting the permanent DoP and has a wide application range to account for different projectile properties. It is given below in Equation 17.

$$DoP = 10\left(\frac{m}{\rho_T A C_D}\right)\ln\left[\left(\frac{V_S}{U\left[0.74e^{-\left(18{C_D}^4\right)}+1.2\right]}\right)^2+1\right]$$

Equation 17: Permanent penetration depth in muscle tissue or 20% gelatin at 10°C (based on Reference [252])

With:

$$U = U_6\left(\frac{d}{d_6}\right)^{-1/3}$$

Equation 18: Rupture modulus[133] scaling for gelatin or tissue [252]

Where:

V_S is the strike or impact velocity of the projectile (m s^{-1}).

DoP is the penetration depth (mm).

ρ_T is the density of the target (taken to be 1.06 g cm^{-3} for 20% gelatin at 10°C and muscle tissue).

A is the cross sectional area of the projectile (cm^2). Units are consistent with the skin perforation and eye penetration equations (Equation 1 to Equation 11). The cross sectional area for a cube should be taken as the area of one face, despite the fact it may be tumbling.

C_D is the (velocity independent) drag coefficient.

e is base of the natural logarithm.

U is the velocity related to the rupture modulus[134] of the target as a function of the diameter of the projectile (m s^{-1}).

[133] The 'rupture modulus', *U*, approximates the velocity at which the projectile will start penetrating gelatin (even though Equation 17 will always predict a DoP>0 for V_S>0).

U_6 is the reference rupture modulus for a 6 mm diameter projectile. For predictions of permanent penetration depth, U_6 for 20% gelatin at 10°C= 98 m s^{-1}, animal tissue= 90 m s^{-1}.

d is diameter of the projectile (mm).

d_6 is the reference value for a 6 mm diameter projectile (d_6=6 mm).

The drag coefficient values in muscle tissue or 20% gelatin at 10°C for a selection of common fragment geometries used in this thesis are listed in Table 32 (assumed to be velocity independent over the velocity ranges of interest [69; 200]).

Projectile geometry	**C_D**
Sphere	0.33
Chisel nosed cylinder (CN face on)[134]	0.55
Cube (random orientation)	0.74
Cylinder (face on)	0.80

Table 32: Drag for some common fragment geometries used within this thesis in muscle tissue and 20% gelatin at 10°C.

Equation 17 was used to plot the predicted DoP for four different geometry projectiles. All the projectiles had an equal mass and presented area to show only the effect of the geometry on penetration into gelatin or tissue. The resulting velocity against DoP predictions are shown in Figure 80.

[134] The chisel nosed cylinder had 35° nose angle conforming to Reference [208].

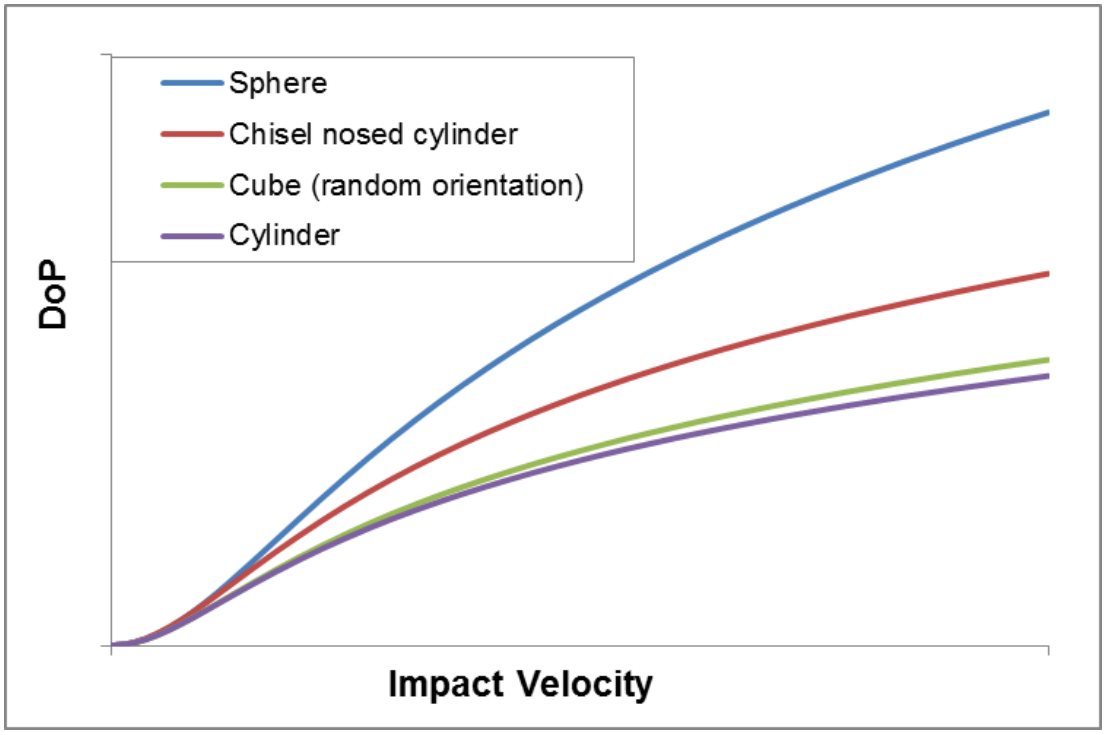

Figure 80: Predicted DoP with velocity for 4 different fragment geometries, all of equal mass and presented area in 20% gelatin at 10°C.

As shown in Figure 80, projectiles with lower drag coefficients are predicted to give higher DoP at equivalent depths. Axis values in Figure 80 are left blank as projectile size (maintaining equal cross sectional area and mass across each geometry) is independent of the shape of the DoP – velocity curve (assuming all velocities are subsonic in tissue).

The difference in DoP between the choice of the U_6 value for muscle tissue or 20% gelatin at 10°C is shown in Figure 81.

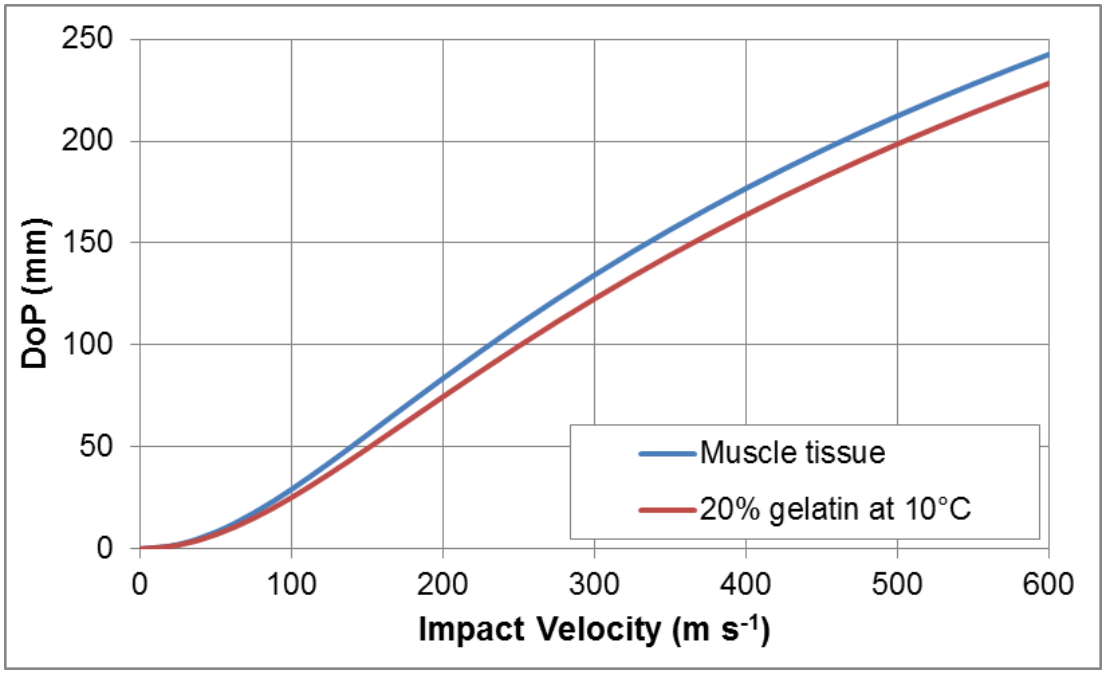

Figure 81: Predicted permanent DoP with velocity for a 6 mm steel sphere showing difference in choice of U_6 values for muscle tissue or 20% gelatin at 10°C, based on Equation 17.

Figure 81 shows that muscle tissue is predicted to be penetrated to a slightly greater extent than 20% gelatin at 10°C using Equation 17. It is suggested that the value of U_6 chosen for use in Equation 17 represents the conditions being simulated. For example predictions in gelatin should use U_6=96 m s^{-1} and those in for tissue should use U_6=90 m s^{-1}. There are specific cases described later where the equations require a specific value of U_6 in order to provide valid outputs.

9.2.2 Validation of permanent DoP prediction

Validation of Equation 17 for the permanent DoP in 20% gelatin at 10°C has already been shown as part of the FREM selection in Figure 79. Equation 17 showed very good agreement to the experimental penetration data for spheres, but slightly more scatter for cylinder and CN cylinder projectiles.

Whilst Figure 79 shows good agreement of the predictions for a wide range of projectiles, it may be more useful to consider a single projectile type across a range of velocities. Data for 6 mm steel spheres in Dstl 20% gelatin at 10°C were

used as the validation case (this was the projectile with the most individual shots, spanning a reasonable velocity range). The experimental data against the prediction is given in Figure 82.

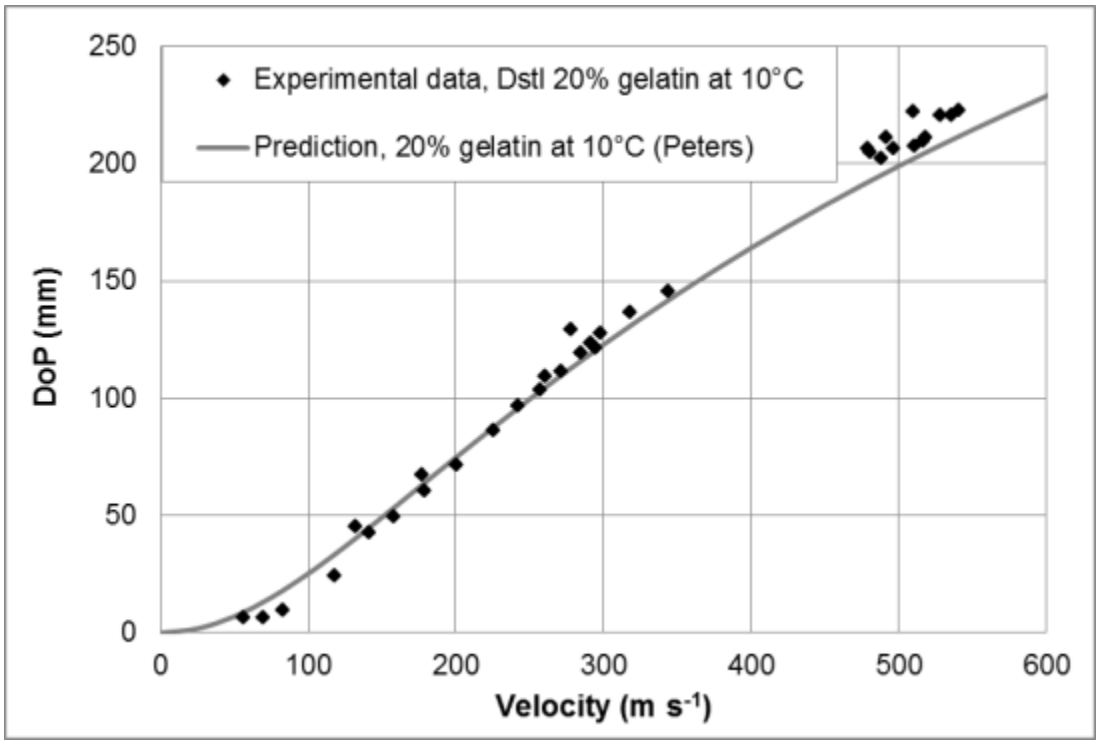

Figure 82: Predicted permanent DoP (Equation 17) for a 6 mm steel sphere compared to experimental data in Dstl 20% gelatin at 10°C (n=34 from Section 7.2).

Figure 82 shows a good agreement of Equation 17 to the experimental data for 6 mm steel spheres. Equation 17 slightly under-predicts the DoP compared to the experimental data, which is more evident at higher velocities (>350 m s^{-1}). The under-prediction at high velocities is specific to certain projectile properties (i.e. Equation 17 does not generally over-predict DoP at high velocities). Although not evident in Figure 82, the predictions at low velocities (around the experimental penetration threshold velocity required to start penetrating the gelatin) are less reliable. This limitation is considered separately in Section 9.4.

In order to determine the suitability Equation 17 for irregular fragments, 14 shots were attempted into Dstl 20% gelatin at 10°C with nominal 0.5 g natural limestone fragments. However, the limestone fragments did not separate from the sabots properly at lower velocities, or broke up and lost mass on impact with the gelatin

at the higher velocities (tested in the range 160 to 700 m s^{-1}) [135]. This prevented the data being suitable for validation of Equation 17 (projectiles must be non-deforming and non-fragmenting).

As another method to validate the predictions from Equation 17, it was compared to the ComputerMan muscle tissue and animal best fit lines from Section 7.2.3 (Equation 12 and Equation 13). The normalised DoP over density curve for PMHS and animal muscle tissue data was converted into a DoP for a 6 mm steel sphere to match the ComputerMan curve (which was based on a 6 mm steel sphere from Reference [42]). Predictions for muscle tissue and 20% gelatin at 10°C were made for the 6 mm steel sphere using Equation 17. Figure 83 shows the predictions from Equation 17 for both 20% gelatin at 10°C and muscle tissue plotted against the other two muscle tissue DoP curves.

[135] Granite gravel was subsequently obtained to repeat this testing, but could not be completed. Granite is expected to remain intact under these impact conditions and would provide a method to determine the suitability Equation 17 for irregular fragments.

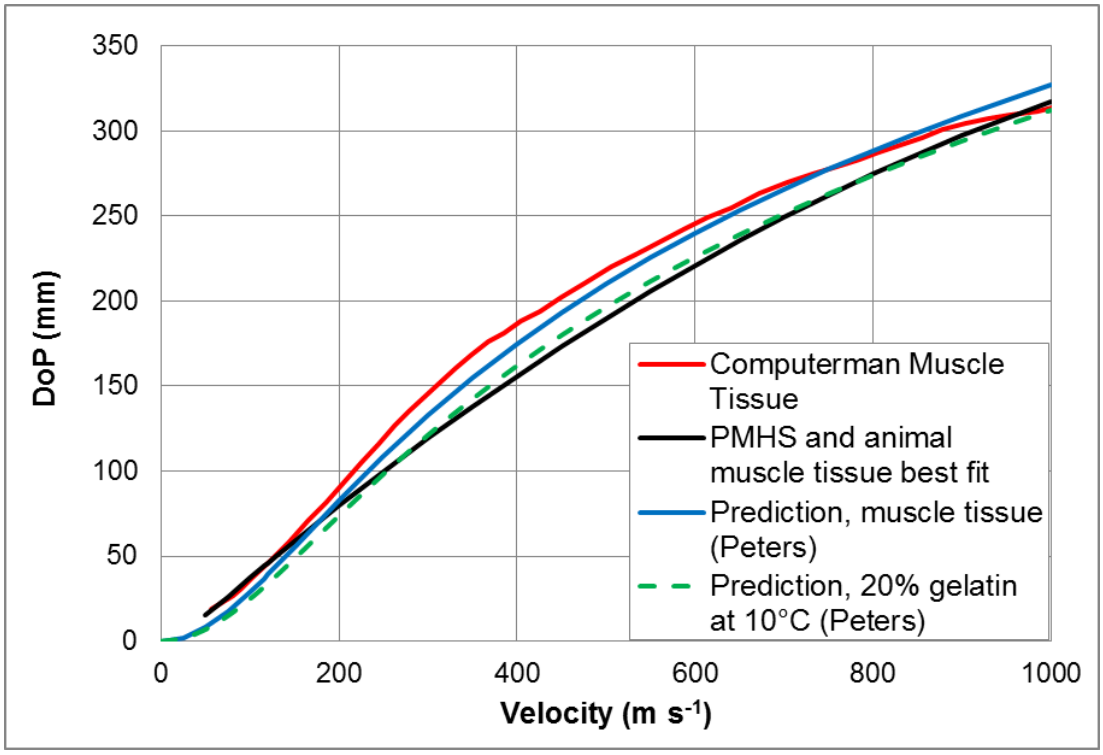

Figure 83: Predicted permanent DoP (from Equation 17) of a 6 mm steel sphere compared to the ComputerMan muscle tissue curve and the combined PMHS and animal muscle tissue fit.

Figure 83 shows that Equation 17 provides a very similar prediction for 6 mm steel spheres to both the ComputerMan muscle tissue and animal best fit lines from Section 7.2.3 (Equation 12 and Equation 13).

As previously discussed, the model fitness for purpose must be based against the particular requirement or user need statement. It is down to the model end user to utilise the validation shown within this thesis to determine the model validity for their particular application. However, Equation 17 is considered suitable for most applications predicting DoP in gelatin or muscle tissue for non-deforming and non-tumbling projectiles within the limits discussed for Figure 79.

9.2.3 Maximum temporary DoP

Equation 17 predicts the permanent DoP in 20% gelatin at 10°C or muscle tissue. If the maximum temporary DoP is required to be estimated (or the permanent DoP estimated from the maximum temporary DoP) an empirical scaling equation has been developed. This scaling equation was based on comparison of

experimental data using the permanent DoP and maximum temporary DoP for 128 firings with a range of different projectiles in Dstl 20% gelatin at 10°C (cylinders and spheres made of steel, ceramic and glass, diameters from 3 mm to 20 mm). Equation 19 gives the estimated maximum temporary DoP based on the permanent measured DoP.

$$DoP_{maxT} = 1.06DoP + 2d$$

Equation 19: Permanent DoP to maximum temporary DoP empirical scaling for Dstl 20% gelatin at 10°C.

Where:

DoP_{maxT} is the maximum temporary DoP

The resulting measured versus predicted maximum temporary DoP based on Equation 19 is shown in Figure 84.

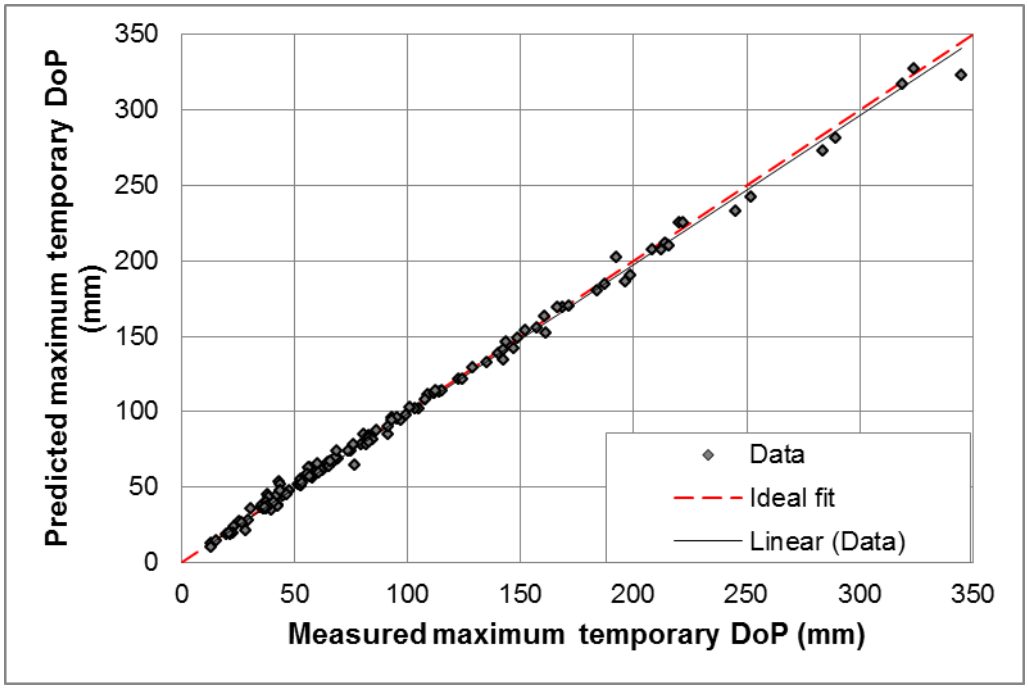

Figure 84: Measured versus predicted maximum temporary DoP based on Equation 19 for Dstl 20% gelatin at 10°C. Data from Section 7.2

As shown by Figure 84, Equation 19 gives a good fit to the experimental measured maximum temporary DoP for the range of projectiles considered, with

an R^2 value of 0.996. Equation 19 is valid only for Dstl 20% gelatin at 10°C. Data to compare the maximum temporary and permanent DoP in muscle tissue was not available and Equation 19 should not be used for muscle tissue.

9.3 Projectile retardation

9.3.1 Prediction of the Projectile retardation

Equation 17 can be reworked to predict the retardation of a projectile with depth in gelatin or muscle tissue. The change in instantaneous velocity, *v*, with depth is given by Equation 20, re-arranged for *v* from Reference [252]:

$$v = V_s \sqrt{e^{-\frac{\rho A C_D DoP}{10m}} \left[1 + \left(\frac{U\left(0.74e^{-18{C_D}^4} + 1.2\right)}{V_s}\right)^2\right] - \left(\frac{U\left(0.74e^{-18{C_D}^4} + 1.2\right)}{V_s}\right)^2}$$

Equation 20: Retardation of a projectile with depth in 20% gelatin at 10°C or muscle tissue [252]

Where:

DoP is the instantaneous penetration depth (mm)

U_6 values of 80 m s^{-1} should be used for retardation predictions for both 20% gelatin at 10°C and muscle tissue (in Equation 18).

The value of U_6 for retardation calculations is based on optimisation conducted within this thesis against the available data (see following section on validation). Examples of implementation of Equation 20 are given in the following section.

9.3.2 Validation of projectile retardation equations

9.3.2.1 Drag coefficient

Equation 17 and Equation 20 use a velocity independent drag coefficient, but this is not representative of reality. However, for modelling purposes at subsonic velocities in tissue or tissue simulants, a velocity independent drag coefficient is frequently used [69; 200].

The speed of sound in gelatin or muscle tissue is given as 1463 m s^{-1} [24]. The value of the drag coefficient is expected to sharply increase when velocities are supersonic [138] and will start to be effected at velocities over approximately 1100 m s^{-1} [252]. A velocity dependent drag coefficient has not been considered within this thesis for the following reasons:

- The majority of applications for the FREM of retardation in gelatin or tissue do not require a consideration of transonic or supersonic velocities in gelatin or tissue[136].
- At high velocities, solid steel projectiles will deform (or even fragment) and therefore consideration of changing mass, cross sectional area and drag coefficient of the projectile also needs to be considered. Reference [133] showed deformation of steel cylinders at velocities over 1300 m s^{-1} and steel spheres at velocities over 1530 m s^{-1} when penetrating 10% gelatin at 4°C.
- Equipment constraints on firing projectiles over 1200 m s^{-1} mean that original experimental data could not be generated and existing data in the literature is extremely limited. This would prevent adequate validation of the transonic and supersonic aspect of the model.

The drag coefficients (and validation of the equations that use them) in this thesis are based on the assumption that all impact velocities are below the speed of sound in gelatin or muscle tissue and projectiles do not deform or fragment.

9.3.2.2 Validation against live pig data with steel spheres

Equation 20 was used to predict the remaining velocity and then energy loss for each of the live pig data points from Section 7.3. The sphere mass, diameter, impact velocity and target thickness were used as inputs to Equation 20. The energy loss in the target was then scaled to 100 mm as was done for the data in

[136] Fragments approaching, or over 1100 m s^{-1} are likely only in very close proximity (within a few metres) to the explosive device from which they originate (initial velocities in the region of 1800 m s^{-1}). Therefore anyone hit is likely to sustain multiple impacts from these very high velocity fragments [93]. An injury assessment is unlikely to be required, as even for individuals wearing body armour, multiple impacts would likely occur to the unprotected regions and still be lethal.

Section 7.3. The same filters on the data used in Section 7.3 were applied (target thickness 100 mm -20/+50 mm). A comparison of the measured against predicted energy loss per 100 mm in live pig thigh muscle is given in Figure 85.

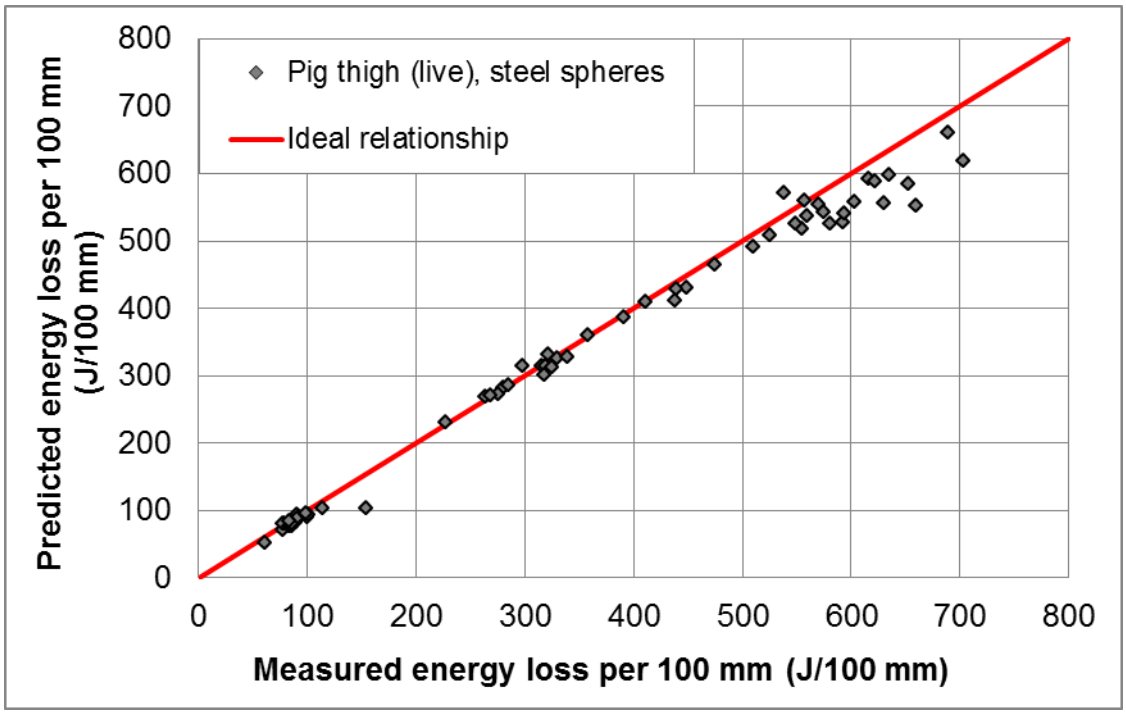

Figure 85: Comparison of measured against predicted energy loss per 100 mm in live pig thighs with steel spheres. Prediction is using Equation 20. Data from References [95; 96; 113; 123]

As shown in Figure 85, there is good agreement between the measured and predicted energy loss per 100 mm in live pig thighs using Equation 20. Some scatter is expected in the measured versus predicted plot due to natural variations from the pig tissue and experimental error.

There is a tendency for Equation 20 to slightly under predict the energy lost (or retardation) at high values of energy loss per 100 mm (>550 J per 100 mm), equivalent to impact energies >900 J.

This validation was based on 59 shots with steel spheres, 6.0 mm to 9.5 mm diameter, impact energies ~100 to 1200 J, with all impact velocities less than 1463 m s^{-1} (the speed of sound in muscle tissue [24]).

9.3.2.3 Validation against live and dead muscle tissue

The validation of Equation 20 in Section 9.3.2.2 was repeated, but additional data included:

- Additional data from Reference [95] was included for impacts with track lengths over 150 mm, previously excluded (additional 11 data points from this source).
- Data from Reference [57; 58] which contained impacts to dead pig thighs subject to different storage conditions and with a mixture of sphere and CN cylinder projectiles (n=18). The data were previously discounted due to the small target size (thickness range 21 – 38 mm).
- Also included was data from Reference [157] for live dog thighs using 6 mm steel spheres with aggregated shots at 3 velocity groups (n=53).

Data from References [109; 124] was not included as it used muscle tissue with the skin removed. For direct comparison to the live muscle tissue data which had the skin intact, this data was not included for validation (although not shown, was observed to fall within the scatter of the other dead pig muscle tissue data with intact skin).

Validation was based on the exit velocity for an equivalent thickness of muscle tissue, so explicitly accounts for target thickness, expanding the data on which validation can be based (as well as for an additional geometry projectile in real tissue).

Equation 20 was used to predict the remaining velocity (with U_6=80 m s^{-1} and C_D values from Table 32) replicating each of the data points (projectile geometry, mass, diameter, impact velocity and target thickness as inputs). No account was taken of the different target storage conditions. The resulting measured against predicted exit velocities are given in Figure 86.

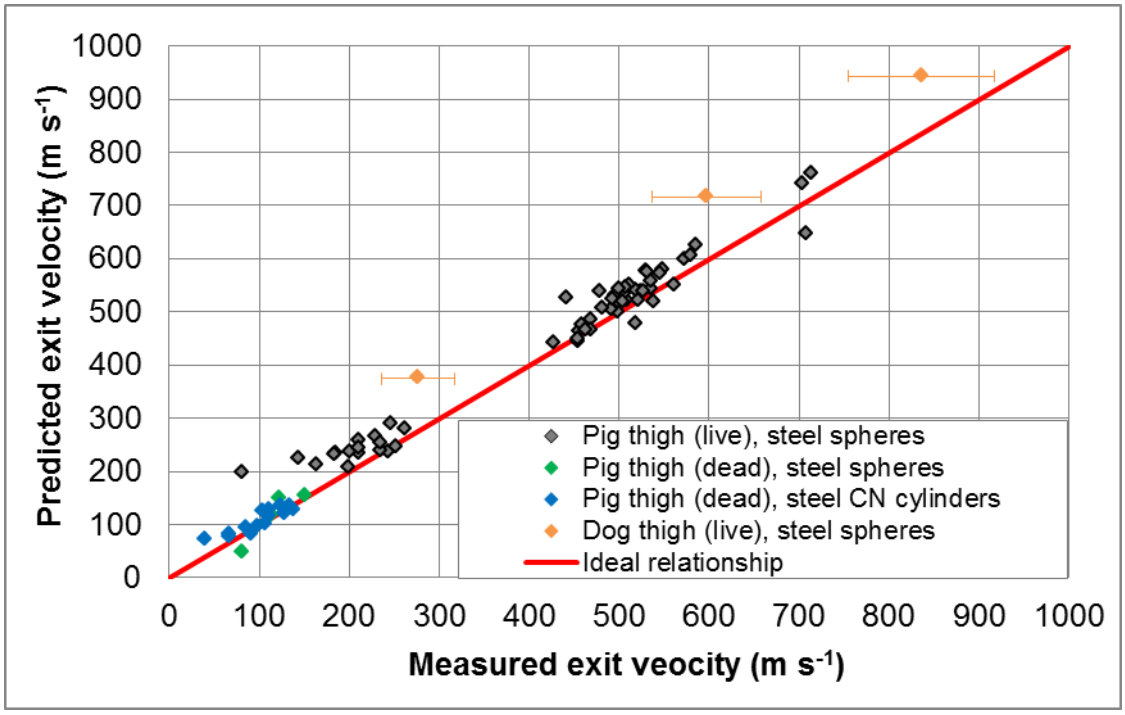

Figure 86: Comparison of measured against predicted exit velocity in live and dead pig thighs and live dog thighs. Prediction is using Equation 20. Data from References [57; 58; 95; 96; 113; 123; 157]

Figure 86 shows there is good agreement between the measured and predicted exit velocities in live and dead muscle tissue, for all but the dog data. There is a tendency for Equation 20 to slightly over predict the remaining projectile velocity (across the range of exit velocities and conditions considered).

Figure 86 shows Equation 20 provides a good prediction for both the live and dead muscle tissue. The data for the live and dead muscle tissue do not cover similar impact or exit conditions, meaning a direct comparison is not possible, however there no observable difference in their respective response (to each other or Equation 20) based on Equation 20.

This validation was based 77 (+3 for the dog data) shots with steel spheres and CN cylinders, 4.1 mm to 9.5 mm diameter, impact energies 3 to 1200 J, with all impact velocities less than the speed of sound in muscle tissue. There was no account for skin effects (on entry or exit).

Within Reference [157], a value for the drag coefficient of 0.50 was suggested for spheres in dog muscle tissue (compared to C_D=0.33 for spheres in (pig) muscle tissue and 20% gelatin at 10°C). Implementing this drag coefficient for just the dog data from Reference [157] moves those data points much closer to the ideal relationship between measured and predicted exit velocities and is shown in Figure 87.

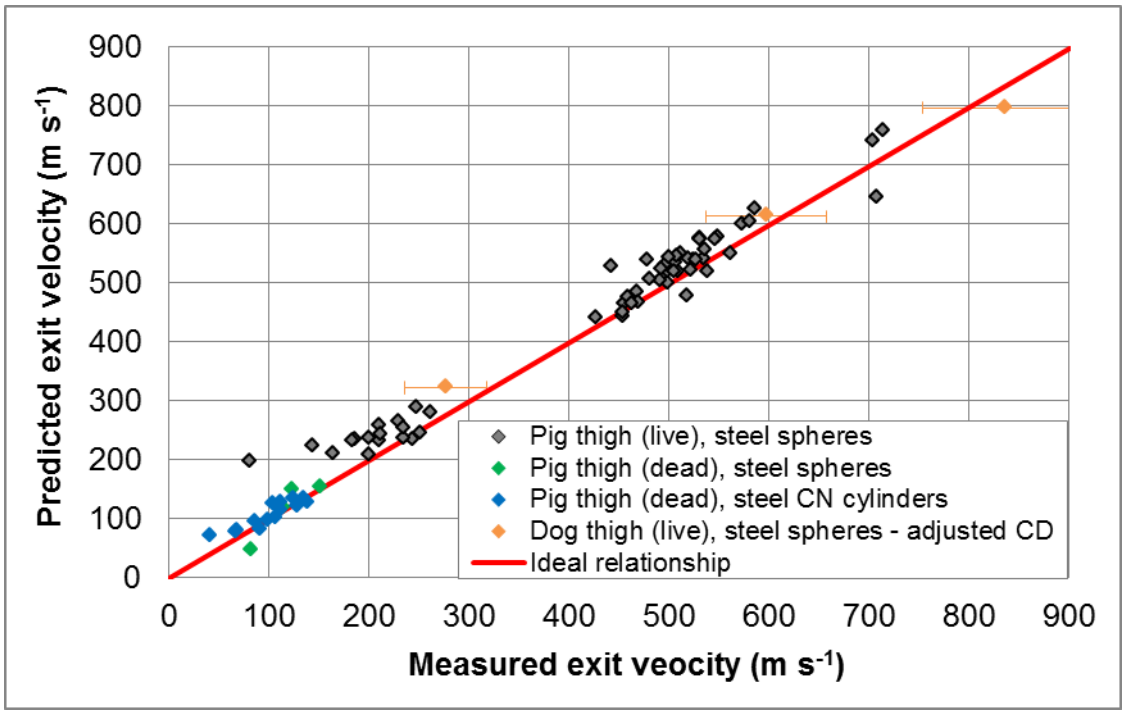

Figure 87: Comparison of measured against predicted exit velocity in live and dead pig thighs and live dog thighs. Prediction is using Equation 20, dog data used adjusted C_D. Data from References [58; 95; 96; 109; 113; 123; 157]

Figure 87 indicates that muscle tissue (including skin) from different animals' causes different drag on the projectile: dog muscle tissue retards the projectile more than pig muscle tissue. Similarly, Reference [116] gives a value of C_D=0.45 for spheres in live cat muscle[137].

[137] These C_D values were calculated from shots with impact velocities many times greater than the skin perforation velocity. However, the skin on exit may still affect the residual velocity. The differences are likely (but not certain) to be due to the differences in retardation of the muscle tissue, rather than influence of the skin (see Section 9.5)

Whilst these differences in retardation in muscle tissue from different animals can be accounted for when sufficient data is available for the drag coefficient to be characterised for the projectile in question, it does not indicate which provides to closest match to human muscle tissue.

Figure 161 and Figure 163 in APPENDIX E provide a comparison of penetration in PMHS muscle tissue to animal muscle tissue. Discounting effects due to the higher skin V_{50} for pig skin compared to PMHS skin; PMHS and animal (pig, sheep and goat) muscle tissue data showed a comparable degree of penetration at equivalent velocities, suggesting that both retard projectiles to a similar degree (i.e. have similar drag coefficients). This strongly suggests that differences in the penetration response of muscle tissue between PMHS and pigs (at low velocities) are due to the different performance of the skin.

At low impact (and exit velocities), the prediction using Equation 20 is likely to become less accurate compared to experimental data for intact animal thighs, as retardation effects of the skin (on entry and exit) will become more important. This aspect is considered within Sections 9.4 and 9.5.

The U_6 value of 80 m s^{-1} selected here for use within Equation 20 is shown to be suitable given the validation against live and dead pig muscle tissue as well as Dstl 20% gelatin at 10°C.

9.3.2.4 Validation against Dstl 20% gelatin at 10°C using remaining velocity after 100 mm of penetration

As the available Dstl 20% gelatin at 10°C data had been analysed to determine the remaining projectile velocity at 100 mm depth in gelatin, this was used as a metric to provide validation of Equation 20 for a range of projectiles in the same way as that in Section 9.3.2.2 and 9.3.2.3. Equation 20 (with U_6=80 m s^{-1}) predictions for the 20% gelatin data is given in Figure 88.

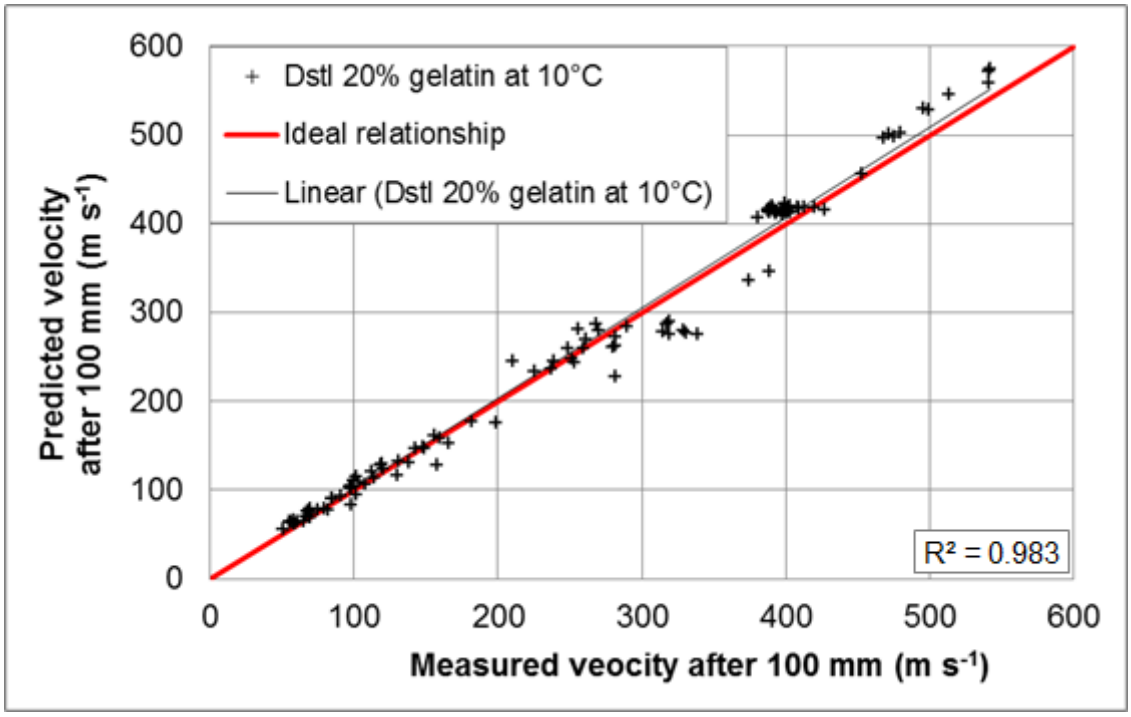

Figure 88: Comparison of measured against predicted velocity using Equation 20 after 100 mm of penetration in Dstl 20% gelatin at 10°C. Data from Section 7.2.

Figure 88 shows a very good agreement between the measured and predicted remaining velocity after 100 mm of penetration in Dstl 20% gelatin at 10°C.

This validation was based 163 shots with spheres and CN cylinders, made from glass ceramic and steel, 5.4 mm to 20.0 mm diameter, impact energies 30 to 1256 J, with all impact velocities less than the speed of sound in gelatin.

9.3.2.5 Validation against Dstl 20% gelatin at 10°C using retardation history

Data for 132 shots into Dstl 20% gelatin at 10°C for projectiles with a range of velocities, diameters and material types were analysed using tracking software (MaxTRAQ M2 [256] or Tracker [213]) to output the penetration time history as discrete points from which velocities could be calculated.

Figure 89 shows an example of a 6 mm steel sphere at 540 m s^{-1} impact velocity in Dstl 20% gelatin at 10°C with position tracked automatically with Tracker software [213] from HSV compared to the prediction using Equation 20.

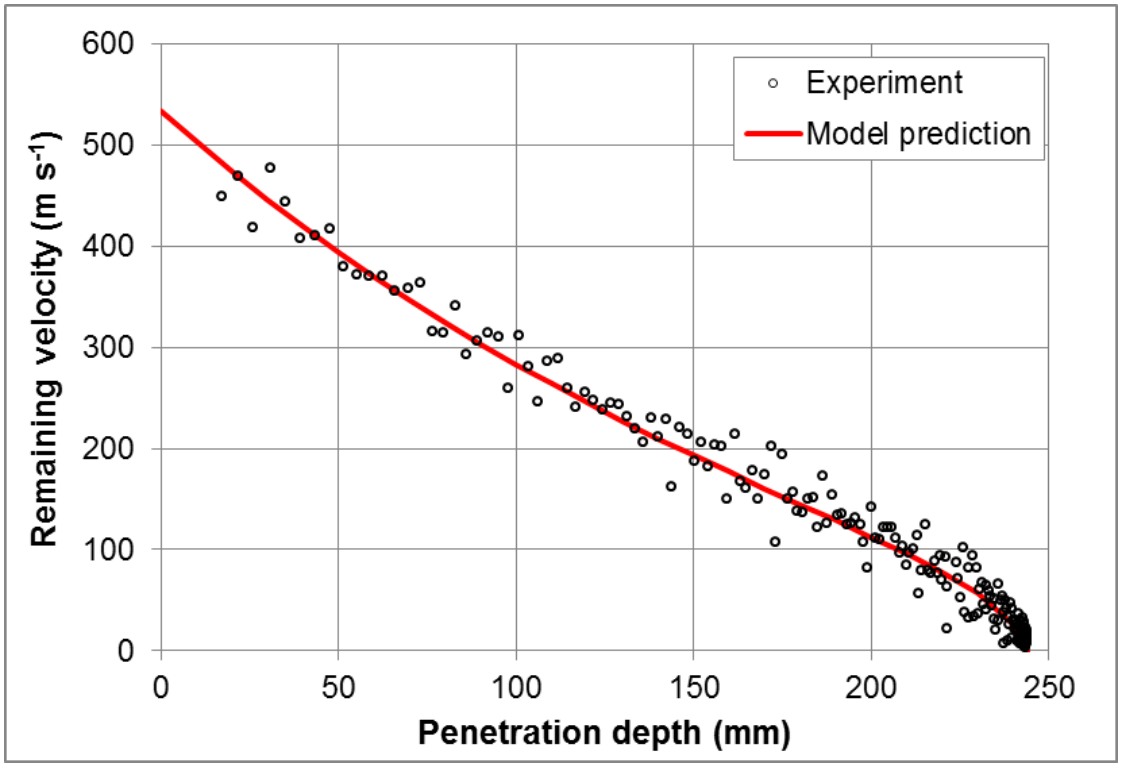

Figure 89: Retardation of 6 mm steel sphere at 540 m s^{-1} impact velocity in Dstl 20% gelatin at 10°C showing measured data at 100,000 frames per second compared to the prediction. Data from Section 7.2

The available data for the retardation history validation was for spheres with a range of diameters from 3 mm to 20 mm, masses 0.11 to 33 g, velocities of 50 to 950 m s^{-1}, made from glass, ceramic and steel. Each tracked shot was compared individually to the retardation prediction (Equation 20) to determine how well it matched (R^2 value and offset in penetration depth of the model prediction form the experimental data).

Equation 20 gave a good fit to the analysed sphere data for all these 132 cases with an average R^2 value of 0.936. The prediction always followed the trend of the data, sometimes with a minor offset. The predictions were offset by average -1.6 mm with a standard deviation 9.1 mm (68% of the data was within an offset of -10.7 mm to 7.5 mm and 95% within an offset of -19.8 mm to 16.6 mm).

The accuracy in retardation aspect of the FREM (Equation 20) for Dstl 20% gelatin at 10°C is within 20 mm (-20.0/+16.5 mm) at the 95% confidence level for all the projectile parameters considered.

Additional validation of the retardation prediction using Equation 20 is given in APPENDIX I for:

- Retardation with different block sizes and edge constraint
    - This includes a number of repeats under nominally identical impact conditions
- 1 mm steel spheres
- Different geometry projectiles (cylinders and cubes).

9.3.2.6 Summary of retardation validation

Equation 20 with a velocity independent drag coefficient and a single value for U_6 of 80 m s^{-1} has been shown to provide good predictions of retardation for a wide variety of non-deforming, non-tumbling projectiles in:

- Live pig muscle tissue;
- Dead pig muscle tissue;
- Live dog muscle tissue (with adjusted drag coefficients); and
- Dstl 20% gelatin at 10°C.

Based on the Dstl 20% gelatin at 10°C data, the accuracy in the penetration depth predictions for a given instantaneous velocity (Equation 20) is within 20 mm (-20.0/+16.5 mm) at the 95% confidence level across all the projectile parameters considered.

9.4 Accounting for the effect of skin on projectile penetration depth and residual velocity skin

‘Equation 17: Permanent penetration depth in muscle tissue or 20% gelatin at 10°C (based on Reference [253])’ will predict a non-zero DoP at any non-zero velocity. In reality a minimum velocity is required to penetrate gelatin, as with

skin[138]. Figure 90 shows the log velocity against log DoP relationship predicted for a 6 mm steel sphere using Equation 17.

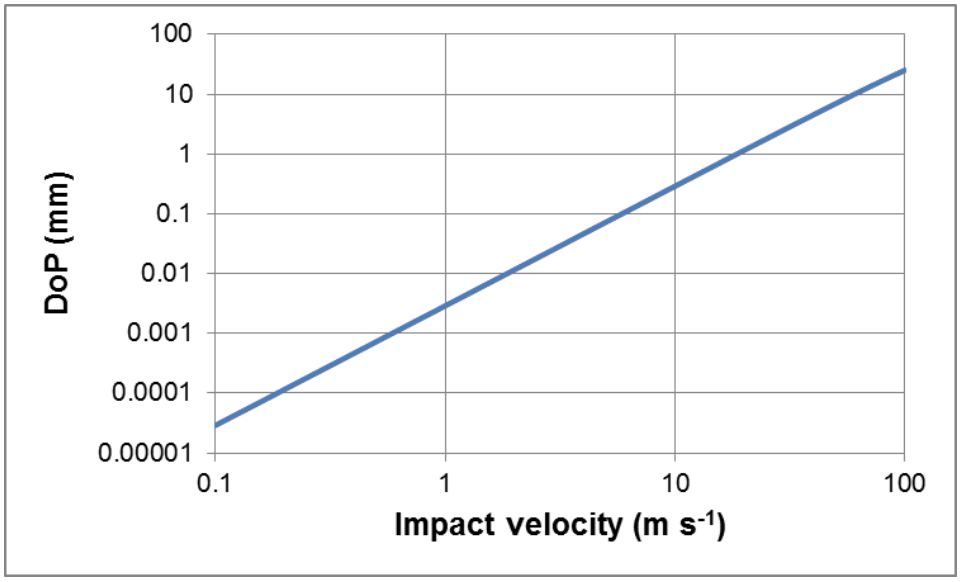

Figure 90: Log-log graph of impact velocity against DoP for a 6 mm steel sphere using Equation 17, highlighting low velocity DoP prediction issue.

Figure 90 shows that even at very low impact velocities, a non-zero DoP is predicted (albeit very small). In order to be able to account for the effect of skin on projectile penetration depth and residual velocity, the penetration and retardation equations require further development.

Limited previous attempts have been found in the literature to calculate or characterise the reduction in projectile velocity or DoP due to the presence of skin, which could then be used to modify existing penetration equations.

Macpherson [84] provides a model in which residual velocity (or penetration depth) following skin perforation can be estimated. However this was based on using skin perforation threshold velocities and excised pig skin overlying 10% gelatin, so has limited application to the models considered here. However, Reference [84] used the model to show the effect of skin is projectile and velocity dependent (smaller velocity loss due to skin at higher impact velocities) as well

[138] Figure 68 shows this comparison for experimental data with Dstl 20% gelatin at 10°C and skin predictions using Equation 8.

as giving some figures for expected velocity loss for certain conditions. For example, an impact at 183 m s^{-1} with a 'light bullet' resulted in a velocity loss of 2.4 m s^{-1}, whereas a 'heavy bullet' at the same impact velocity results in a velocity loss of 1.2 m s^{-1}.

A separate experimental study in the literature used 9 mm handgun bullets penetrating pig skin on 10% gelatin at 300 m s^{-1} (5 times the threshold perforation velocity), where the overall permanent penetration of the projectile was reduced by around 3.5% [83; 92].

Based on initial visual comparisons between the experimental data collected within this thesis and Equation 17 used to predict DoP, the reduction in DoP is substantial for impacts at, or near to, the V_{50}, but becomes less significant as the impact velocity increases above the V_{50}.

Experimental data for muscle tissue with and without skin (Reference [90] and Section 5.3) and Dstl 20% gelatin at 10°C with and without a skin simulant (Section 7 and 8) was collated. Preliminary analysis showed there was not a fixed amount or proportion of velocity or energy that was lost during the skin (simulant) penetration process, but was related to the impact velocity.

The first attempt to adapt the FREM to account for the reduction in DoP due to the retardation from the skin was based on comparing the normalised DoP over density function scaled by $(V_S/V_{50})^n$. However, with the parameters generated, independent verification of the equations showed it predicted an illogical increase in DoP for some projectiles when accounting for the effect of the skin layer, compared to the existing prediction without skin [257].

Following this, a different approach was taken: the FREM was adapted to account for velocity loss due to the skin by fitting to the experimental data using a non-linear regression equation based on a generalised version of the conservation of energy [54].

The application of this method is described below in respect to calculations from a single set of experimental data with one projectile.

The penetration depths of all fair shots[139] were plotted against the impact velocity. This method required multiple perforating shots with a spread in velocities where their associated penetration depths into tissue or a validated tissue simulant were recorded. The V_{50} perforation value was that extrapolated or interpolated value calculated by a non-linear regression model[140].

This non-linear regression model was based on a broader version of the conservation of energy equation (assuming no change in mass of the projectile). This is frequently applied to testing of armour materials where the impact and residual velocity of the projectile are recorded.

The conservation of energy equation is given below, assuming a constant projectile mass:

$$V_R = \left(V_s{}^2 - V_{50}{}^2\right)^{1/2}$$

Equation 21: Conservation of energy, assuming a constant mass.

Where:

V_S is the strike or impact velocity (m s^{-1})

For amour testing where there is no backing, multiple shots are performed and the V_R and V_S data are graphed. Equation 21 is then used to calculate the V_{50} value.

Reference [54] adapted Equation 21 into a more generic empirical form, by generalising the squared and square root terms to a variable, λ and $1/\lambda$. This is given by Equation 22[141].

[139] Those that hit bone etc. must be removed. Non-perforations are given a DoP of zero and are included in the analysis.
[140] Equation 8 for predicting the skin perforation V_{50} was not used for this aspect of the model development. However, it is used in the final version of the model (Equation 24).
[141] Symbols changed from original reference to avoid confusion with constants already used here.

$$V_R = \begin{cases} 0, V_s \leq V_{50} \\ \mu\left({V_s}^{\lambda} - {V_{50}}^{\lambda}\right)^{1/\lambda}, V_s > V_{50} \end{cases}$$

Equation 22: Generic, non-linear least squares regression form of conservation of energy, assuming a constant projectile mass [54]

Where:

μ and λ are parameters bounded by: $0<\mu<1$ and $\lambda>1$ [54].

Equation 22, the generic version of the model was further modified by substituting residual velocity for the DoP (as experimental residual velocities were not recorded when the skin was intact or backed), on the assumption that DoP $\propto$ residual velocity.

$$DoP = \begin{cases} 0, V_s \leq V_{50} \\ \mu\left({V_s}^{\lambda} - {V_{50}}^{\lambda}\right)^{1/\lambda}, V_s > V_{50} \end{cases}$$

Equation 23: Non-linear least squares regression model for DoP (constant projectile mass)

Equation 23 can be used for extrapolation or interpolation of the V_{50} from experimental DoP data[142]. This moves the model away from its dimensionally correct form. An example of this method (Equation 23) applied to actual data is given in Figure 91.

[142] Where μ and λ are calculated specifically for each projectile and skin type.

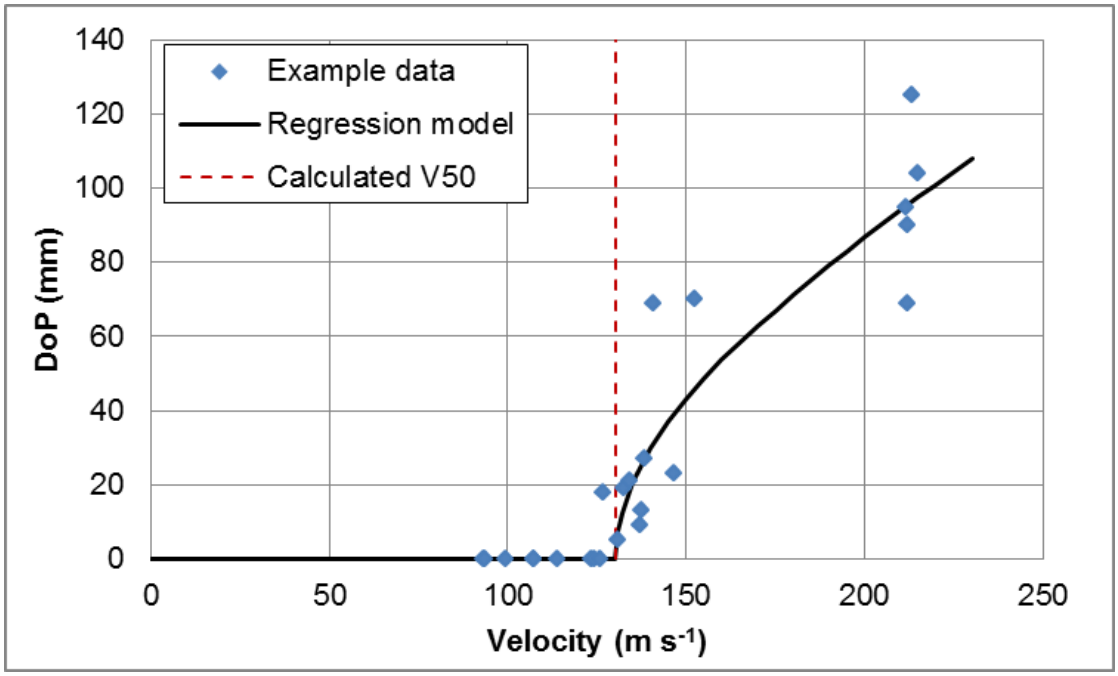

Figure 91: Non-linear least squares regression model (Equation 23) plotted for an example data set; the 0.49 g CN FSP into refrigerated pig tissue from Section 5.4.

Equation 17 was adapted to account for the reduced penetration depth (*DoP'*) due to perforating skin by substituting the predicted residual velocity (V_R) from Equation 22, in place of the impact velocity (V_s). This amended equation was applied to all skin and muscle tissue (animal and PMHS, Table 4 and Table 21) and 20% gelatin at 10°C with skin simulant (Section 8) DoP data in order to generate constants μ and λ. This data included spheres, cylinders, chisel nosed cylinders, air rifle pellets and handgun bullets for a range of diameters and densities. Data for different target types (animal species or PMHS) as well as impact location of the body were all combined for this analysis. This combination of all the data was deemed appropriate as the model was fitted to the V_S/V_{50} relationship, so target factors affecting the V_{50} were already accounted for by this normalisation to the V_{50}.

The final amended equation with fitted constants (found to be μ=1 and λ=3.45)[143] is given by Equation 24.

[143] Using Equation 21, the dimensionally correct form (μ=1 and λ=2), gave a much poorer fit to the data and is compared to the optimised fitted constants.

$$DoP' = \begin{cases} 0, V_s \leq V_{50} \\ 10\left(\frac{m}{\rho A C_D}\right) \ln\left[\left(\frac{V_{50}\left[\left(\frac{v_s}{v_{50}}\right)^{3.45} - 1\right]^{1/3.45}}{U\left[0.74e^{-\left(18{C_D}^4\right)} + 1.2\right]}\right)^2 + 1\right], V_s > V_{50} \end{cases}$$

Equation 24: Modified DoP prediction accounting for the effect of the skin layer

Where:

DoP' is the modified depth of penetration, accounting for the effect of the skin (mm)

The V_{50} can either be calculated using Equation 8[144] or using a 'known' value from experimental testing of the relevant target conditions and projectile of interest.

Equation 24 gives a zero predicted DoP for all velocities below the V_{50}. Above the V_{50} the penetration depth is reduced due to the retardation from the skin layer. For application specifically to bare gelatin penetrations, the penetration V_{50} for gelatin could be used (if available).

The effect on the DoP or residual velocity when accounting for the skin layer with Equation 24 diminishes as V_S/V_{50} increases from 1. The effect of the skin layer on reducing the residual velocity can be considered to be negligible when $V_S/V_{50} \geq 3$ ($V_R/V_S > 99\%$). Some values of V_R/V_S related to the impact velocity are shown in Table 33.

V_S/V_{50}	V_R/V_S
1.001	0.193
1.1	0.692
1.25	0.835
1.5	0.921
2.0	0.973

[144] Parameters for Equation 8 for the synthetic chamois on 20% gelatin at 10°C as the physical skin simulant model are given in Section 8.5.4.

V_S/V_{50}	V_R/V_S
2.5	0.988
3.0	0.993
5.0	0.999

Table 33: V_R/V_S values showing the degree to which the skin affects the velocity of the projectile at different impact velocities.

Equation 24 shows good agreement to the few cases where sufficient experimental data is available across a range of impact velocities in proximity to the V_{50}.

Comparisons between the existing 'original' predictions (Equation 17) and amended equation to account for the effect of skin (Equation 24) with examples of the raw data are given in Figure 92 and Figure 93. Also included in Figure 92 is Equation 24 in the dimensionally correct form (μ=1 and λ=2), to show the comparison of this fit.

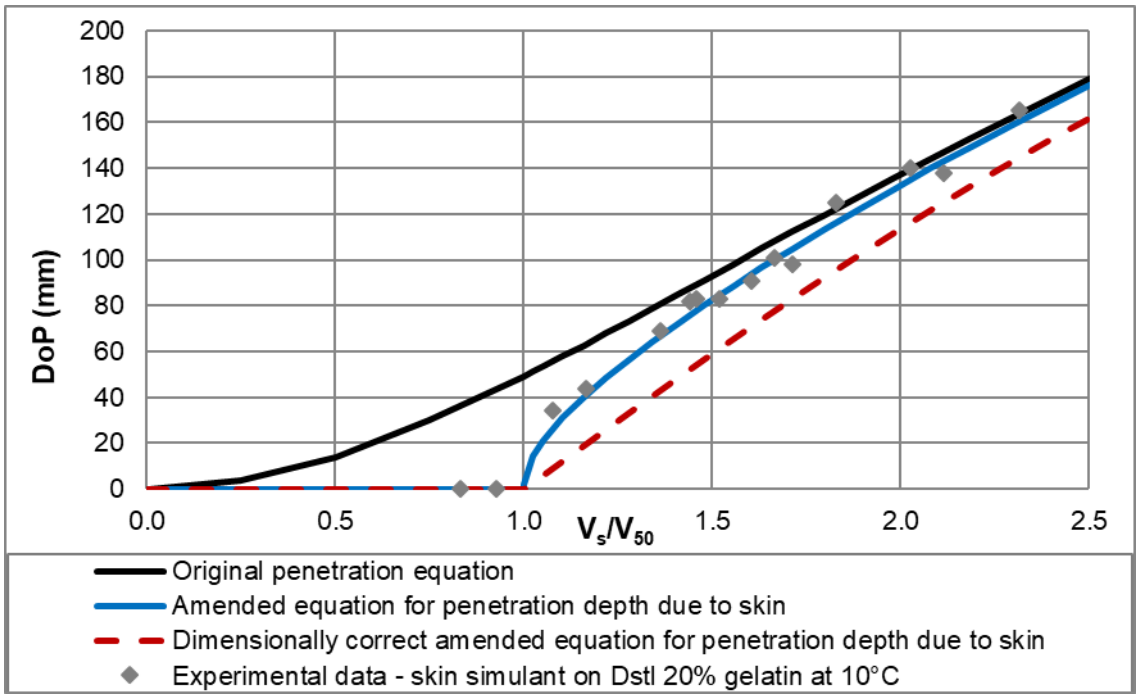

Figure 92: Comparison between the original prediction (Equation 17) and the amended equation to account for the effect of skin (Equation 24) with original experimental data for a 9 mm steel sphere. Data is from Section 8.5.

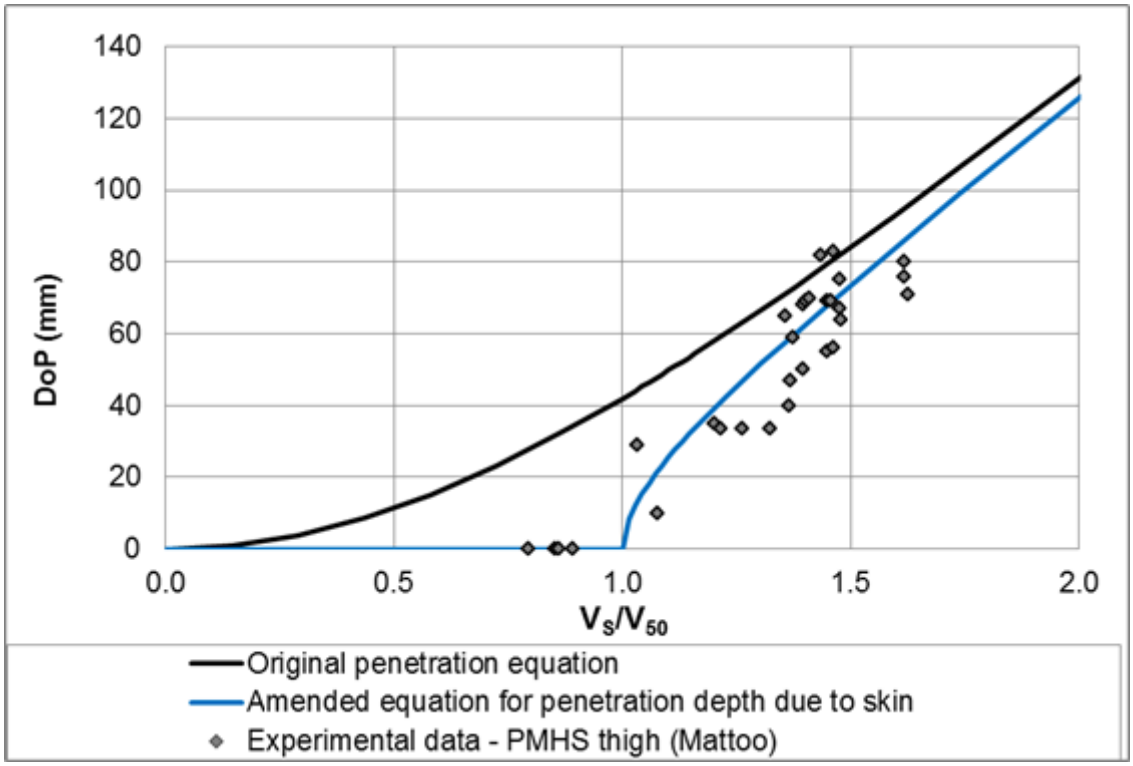

Figure 93: Comparison between the original prediction (Equation 17) and amended equation to account for the effect of skin (Equation 24) with experimental data for a 9.14 mm lead sphere into PMHS thigh skin and muscle from Reference [64].

Figure 92 and Figure 93 show good general agreement of the experimental data to the prediction using Equation 24. As expected, minimal variation is seen in the skin simulant on 20% gelatin at 10°C experimental data (Figure 92) in comparison to real PMHS skin and muscle tissue (Figure 93).

Experimental testing on real skin and muscle tissue is hampered in terms of the upper limit of velocities (V_S/V_{50}) that can be achieved with the projectile remaining within the target, meaning validation at higher V_S/V_{50} is challenging unless projectiles are specially selected that slow quickly in tissue (which may not be representative of the desired projectiles) or simulants are used.

Equation 24 is considered more representative of the outcomes compared to Equation 17. For high velocity fragments (and typical rifle bullets), the effect of the skin layer is unlikely to influence the resulting DoP ($V_S/V_{50}>>3$).

Equation 24 is further compared to real skin and muscle tissue data in Section 9.9.5.

9.5 Retardation in tissue accounting for velocity loss due to the skin

The retardation equation (Equation 20) can be modified to enable calculation of the projectile retardation accounting for the effect of the skin layer by substituting Equation 22 for the residual velocity following skin perforation, V_R, into Equation 20 in place of the strike velocity, to give Equation 25.

$$v = \begin{cases} 0, V_s \leq V_{50} \\ V_R \sqrt{e^{-\frac{\rho A C_D D o P}{10m}} \left[1 + \left(\frac{U\left(0.74e^{-18{C_D}^4} + 1.2\right)}{v_R}\right)^2\right] - \left(\frac{U\left(0.74e^{-18{C_D}^4} + 1.2\right)}{v_R}\right)^2}, V_s > V_{50} \end{cases}$$

Equation 25: Retardation in tissue accounting for velocity loss due to the skin

Where:

$$V_R = V_{50}\left[\left(\frac{V_s}{V_{50}}\right)^{3.45} - 1\right]^{1/3.45}$$

Equation 26: Residual velocity of the projectile after perforating skin.

The skin layer is treated as infinitely thin and any retardation effects are considered to happen instantaneously on impact. Implementation of Equation 25 compared to Equation 20 at different impact velocities, shown as multiples of the skin perforation V_{50} velocity are given in Figure 94, to highlight the effect of the skin layer on the projectile retardation. The outputs have been generalised by dividing the strike velocity by the V_{50} and penetration depth is given in arbitrary units.

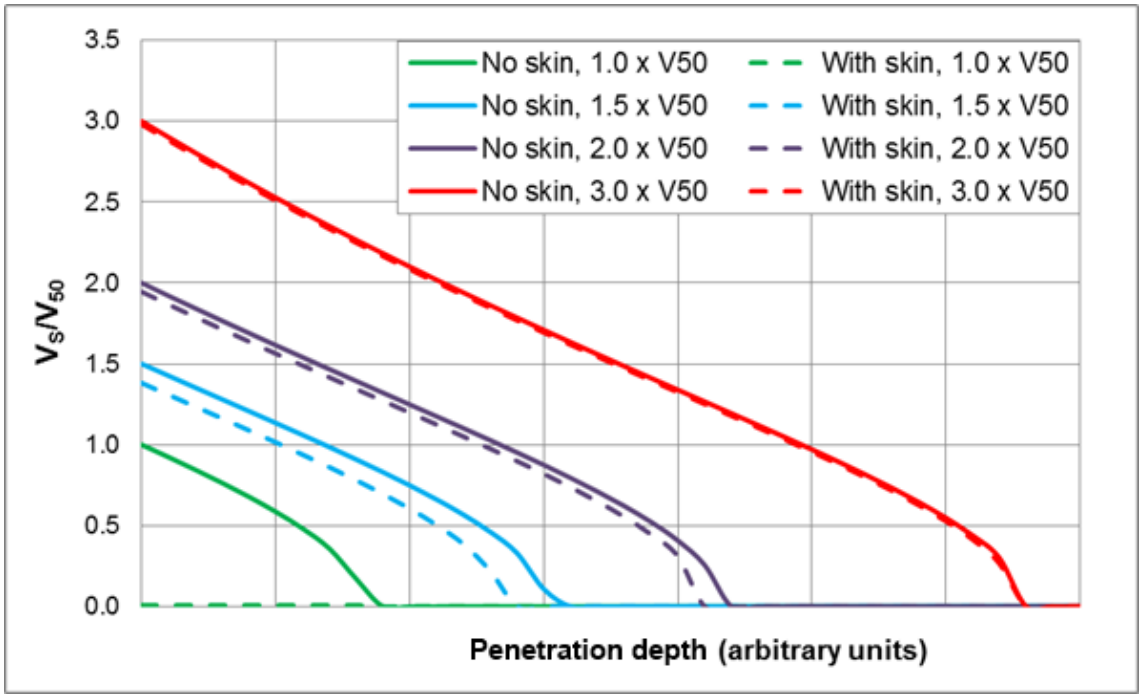

Figure 94: Generalised retardation profiles at 4 multiples of the skin perforation V_{50} velocity in 20% gelatin at 10°C, showing the difference between accounting for the skin (dashed lines, Equation 25) to the 'standard' retardation equation (solid lines, Equation 20).

Figure 94 shows that as the strike velocity (in multiples of V_S/V_{50}) increases, the effect of the skin on the residual velocity (Equation 25) is reduced, as for the modified depth of penetration accounting for the effect of the skin (Equation 24).

The model only considers the effect of skin on the projectiles velocity entering the body, not on exit.

Equation 25 is validated against both live and dead skin and muscle tissue data in Section 9.9.5. This validation is possible as retardation data were not used to generate the model(s).

9.6 Temporary cavity predictions

9.6.1 General equations for temporary cavity prediction

The retardation profile (Equation 20 or Equation 25) can be used to calculate the projectile instantaneous velocity which is needed to estimate the radius of the Maximum Temporary Cavity (MTC) in 20% gelatin at 10°C or muscle tissue with

penetration depth. The MTC calculated here is the maximum radius at each depth, not the instantaneous MTC envelope, as would be observed experimentally with HSV in gelatin. The MTC outline calculated by this method is assumed symmetrical about the shot line and is comparable to the cavity that would remain in an inelastic solid after penetration (such as soap), or to the MTC in gelatin over all time (See APPENDIX I for more detail).

Unless stated otherwise, all figures shown in the remainder of Section 9 use the predictions ignoring the effects of the skin and base support[145]. This is so that the equations can be easily validated against bare gelatin, which is a more typical experimental test setup when testing against tissue simulants.

The following equations can be used to predict the maximum radius of the temporary cavity with penetration depth. The cavity is assumed to be symmetrical about the shot line[146].

$$r_{MTC} = 10\left(\frac{A_c}{\pi}\right)^{0.5}$$

Equation 27: Radius of the maximum temporary cavity in 20% gelatin at 10°C.

Where:

r_{MTC} is the radius of the MTC at a given depth (in 20% gelatin at 10°C)[146] (mm).

A_c is the local cross sectional area of the MTC (cm^2).

$$A_c = \begin{cases} 0, v = 0 \\ A\left(1 + \overline{g}_{\infty}\overline{g}\overline{A}C_D\left(\frac{d}{d_6}\right)^{-2/3}\left[\left(\frac{v}{U}\right)^2 + \left(0.74e^{-18C_D{}^4} + 1.2\right)^2\right]\right), v > 0 \end{cases}$$

Equation 28: The local cross sectional area of the MTC in 20% gelatin at 10°C [253].

---

[145] As shown in Section 7.5, constraint on the block affects cavity formation. This includes the effect from the table on which the gelatin is placed.

[146] $r_{MTCtissue}$ will be used to denote the radius of the MTC in tissue. If not explicitly stated, MTCs are assumed to be those for gelatin.

Where:

$\bar{g}$ is a temporary cavity formation parameter.

$\bar{g}_\infty$ is the asymptotic value of g at large *v/U,* related to the lateral dimensions of the target[147].

$\bar{A}$ is the entrance region attenuation factor.

The temporary cavity predictions assume symmetry about the shot line. However, as noted in Reference [258], the orientation of an inhomogeneous muscle can affect the resulting cavities. The orientation of the (rectus femoris) muscle in goats was found to significantly affect the mean central diameter of the temporary cavities (at the 95% confidence level) when shot with a .30 cal (7.62 mm) solid steel bullet at 415 and 849 m s^{-1}, but not at 1279 m s^{-1} [258].

9.6.2 Validation of cavity predictions

The validation of the cavity predictions were conducted based on Dstl 20% gelatin at 10°C due to practical difficulties in extracting the required measurements from opaque muscle tissue.

As discussed in Section 7.5, the (maximum) temporary cavity is related to the target size and constraint. All data used for validation within this section were based on impacts to the approximate centre of a 150 mm x 150 mm impact face, unconstrained target, away from any previous damage and where the target completely contained the MTC without splitting at the edges[148].

Suitable data for Dstl 20% gelatin at 10°C (a subset of that summarised in Table 23), were analysed to measure the maximum temporary cavity diameter with penetration depth over all time, using the method described in APPENDIX G.

---

[147] $\bar{g}_\infty$ =14 was validated for a 150x150 mm impact face target. This value has been used for the calculations and figures shown here, unless otherwise stated.

[148] As noted in Section 7.5, larger blocks (200 mm x 200 mm impact face) are now recommended to provide consistency between testing and allow evaluation of typical high velocity rifle bullets without the cavity splitting the block. Updates to the cavity predictions for blocks other than 150 mm x 150 mm impact face is considered in Section 9.6.3.

This cavity analysis was completed for 137 shots with spheres and cylinders, 4 mm to 20 mm diameter, densities 2.5 to 10.3 g cm^{-3} and impact velocities 56 to 950 m s^{-1}. Impacts with lead spheres (10.3 g cm^{-3}) were <200 m s^{-1} and were not observed to plastically deform. The resulting predicted versus measured maximum diameter of the maximum temporary cavity in Dstl 20% gelatin at 10°C is given in Figure 95.

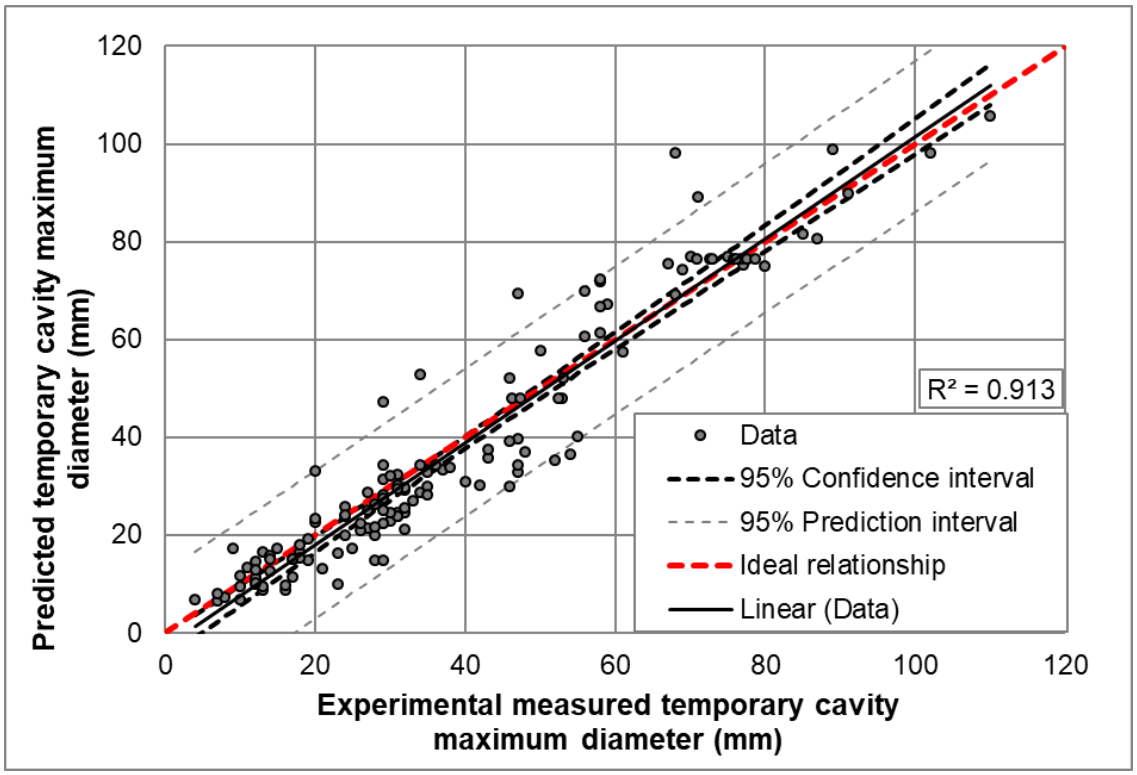

Figure 95: Validation of maximum diameter of the MTC predictions in 150x150 mm impact face Dstl 20% gelatin at 10°C blocks for data from Section 7.2. 95% confidence and prediction intervals are shown based on the methods from Reference [259].

Figure 95 shows a comparison between the experimentally measured and predicted maximum diameter (viewed from the side) of the temporary cavity in Dstl 20% gelatin at 10°C. The standard deviation of the data, σ, was 7.5 mm and the R^2 of the linear fit shown in Figure 95 was 0.913, which very closely follows the ideal relationship (red dashed line).

Some of the scatter in the fit may be due to:

- Not all the impacts for the experimental shots were ideally centred on the gelatin, although they were all for the same size block. Apart from the testing described in Section 7.5, the projectile impact location on the gelatin was not measured during testing[149].

- Measurement errors: distortion of the true MTC in the HSV image due to refraction, velocity measurement, HSV scaling (pixel to distance), human error in the selection of the points that form the outline of the MTC during the analysis, etc..

It could be expected that the maximum temporary cavity diameter could be used to predict the volume of the maximum temporary cavity for a given projectile geometry and size of gelatin block[150]. Equation 27 predicts that the maximum temporary cavity will be the same shape for the same geometry projectiles, just stretched in width and depth according to the projectile impact conditions. The same shots used for the validation in Figure 95 are shown in Figure 96 in terms of the measured maximum diameter and volume of the maximum temporary cavity.

[149] It is likely, although cannot be confirmed, that outliers in the predicted versus measured plot of maximum cavity diameter in Figure 95 are due to shots away from the centre of the impact face that caused the resulting cavity size to be affected (see Section 7.5 for discussion of this issue).
[150] Noting observations on shot impact location and constraint on the base of the block.

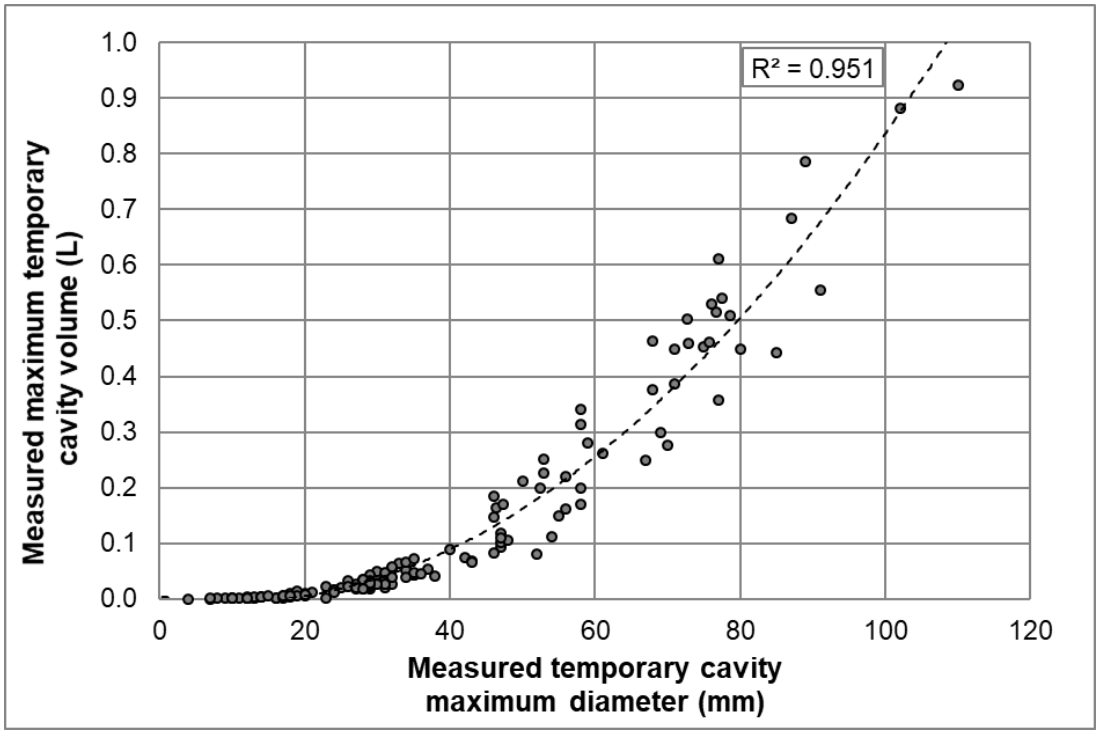

Figure 96: Measured maximum temporary cavity maximum diameter against the volume of the for a 150x150 mm impact face, Dstl 20% gelatin at 10°C target for data from Section 7.2

Figure 96 shows that MTC volume can be reasonably predicted from the measured maximum diameter of the MTC for spheres and cylinders (R^2=0.951). This may be a worthwhile approximation to minimise the burden of analysis of HSV of a large number of shots, for some applications. This relationship is not expected to hold for bullets or other projectiles which tumble or deform or where the edge effects (constraint conditions) on the block change.

The shape of the maximum temporary cavity outline (i.e. diameter or radius with penetration depth) was compared between the prediction and experimental data. This was done for a variety of projectiles. The outcomes for a 6 mm steel sphere at (nominal) 750 m s^{-1} were chosen for validation as four repeats under the same conditions were performed[151].

[151] The data is from original testing conducted for Section 7.5.7.

Equation 28 was used to predict the local cross sectional area of the MTC for the 6 mm steel sphere at 750 m s^{-1} impact velocity, using the predicted retardation from Equation 20. The predicted local cross sectional area of the MTC was then converted to a diameter as this metric was directly measured from the experimental HSV.

The superimposed measured cavity diameters with penetration depth for the 4 shots with the prediction (Equation 20 and Equation 28) are given in Figure 97 (with the target viewed from the side).

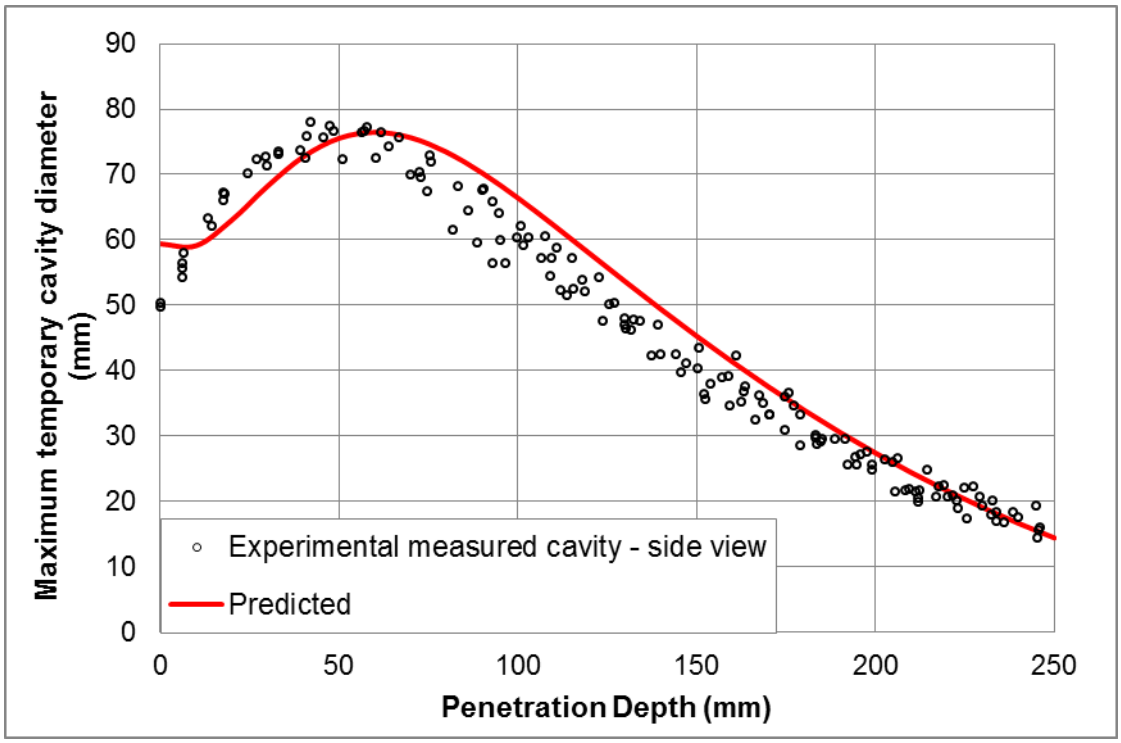

Figure 97: Superimposed measured cavity diameters with penetration depth for the 4 shots with 6 mm steel spheres at 750 m s^{-1}. The corresponding cavity prediction (Equation 18 and Equation 27) is also shown. Data from Section 7.5.

Figure 97 shows that the maximum temporary cavity predictions give a good estimate of the cavity diameter with depth and match the shape of the cavity seen in the experimental testing. The cavity diameter is slightly over-predicted in this example by up to 5 mm (9%) compared to the experimental measurements (and this over-prediction is more pronounced for penetration depths in the region 75 mm to 200 mm).

However, there is asymmetry in the gelatin block due to support underneath the block (i.e. the table on which it is placed, discussed in Section 7.5). If instead of the cavity diameter, the cavity radius from the shot line is considered, a slightly different response is observed in the experimental testing. A comparison of measured and predicted cavity radii is given in Figure 98 for the 4 repeats. All shots were within ±11 mm of centre point (y=0).

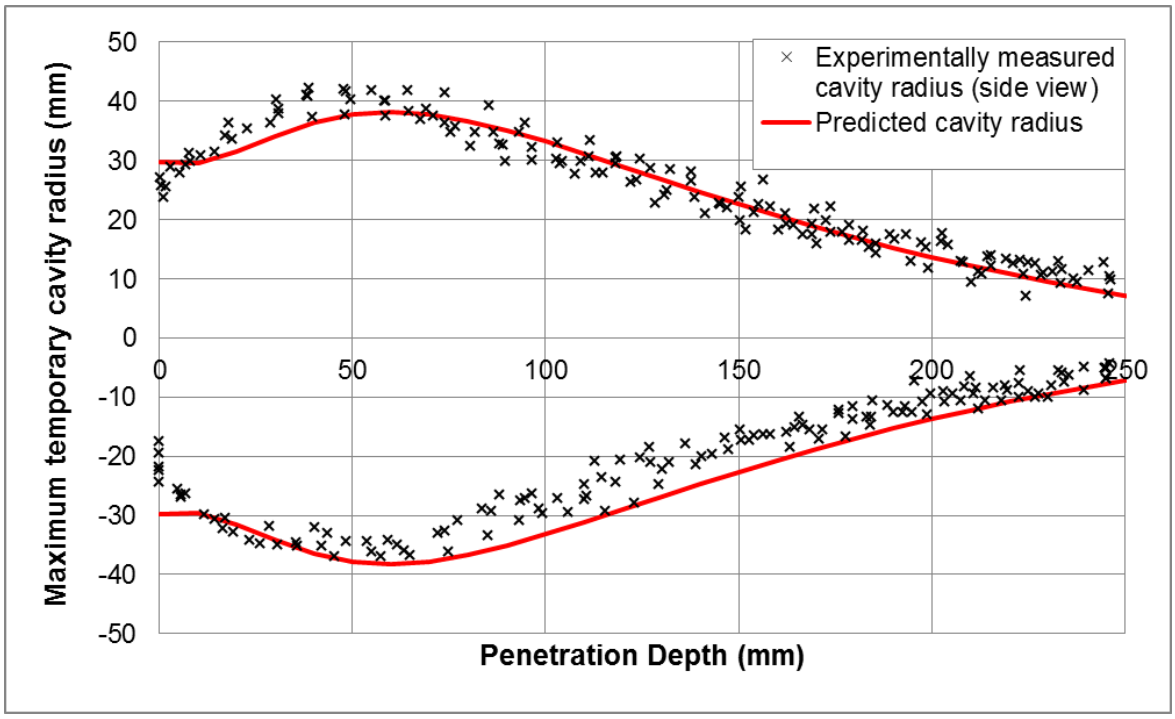

Figure 98: Comparison of experimentally measured maximum temporary cavity radius with depth for side view of 4 shots using a 6 mm steel sphere at 750 m s^{-1} in a 150x150 mm block of Dstl 20% gelatin at 10°C and predicted radius using Equation 20 and Equation 27. Data from Section 7.5.

Equation 27 gives a very good prediction of the upper half of the maximum temporary cavity radius shown in Figure 98, but appears to over-predict the maximum temporary cavity radius for the lower half of the cavity, which is slightly suppressed in the experimental testing due to confinement from the table on which the gelatin is placed.

Figure 98 also shows that the experimental measurements taken across the 4 repeat shots are quite consistent. Although not shown in Figure 98, the experimental data showing the largest radii in the top half of the cavity showed

the smallest in the lower half and vice-versa, i.e. similar diameters, but shifted vertically. This is assumed to be due to the differences in impact location on the front of the block (impacts within ±11 mm of centre point, y=0 in Figure 98).

All predictions using Equation 27 assume symmetry about the shot line, which is not the case for this 150 mm x 150 mm lateral sized gelatin block if viewing from the side, even for spheres. The radius of the maximum temporary cavity is not simply half the diameter (or vice-versa). It is dependent on the direction in which the measurement is taken and any constraints on the gelatin block.

This needs to be considered, when conducting experiments with gelatin, analysing the results and when using the data to inform or validate modelling.

The temporary cavity predictions in this thesis have been validated against the response of Dstl 20% gelatin at 10°C and not muscle tissue. Therefore, the reliability of using these equations to model muscle tissue is unknown.

9.6.3 Updates to cavity predictions accounting for target lateral dimensions

The testing detailed within Section 7.5 was planned to enable the ability to develop the predictions using Equation 27 to be able to account for target size using the parameter $\bar{g}_\infty$. However, due to the limitations in the practical testing of the accuracy of the impact of the projectile from the desired point of aim, the analysis of the data were more complicated than anticipated.

It was found that the parameter $\bar{g}_\infty$ (the asymptotic value of g at large *v/U*) is not linearly proportional to the target lateral dimension. When the asymptotic value of g at large v/U was set to the lateral target size (in cm), Equation 27 was found to give a reasonable prediction of the cavity, but only for penetration depths over 125 mm. For penetration depths below 125 mm the experimental cavities were significantly under-predicted. This is shown for the curve fits to the 100 mm x 100 mm, 75 mm x 75 mm and 50 mm x 50 mm blocks and corresponding predictions in Figure 99.

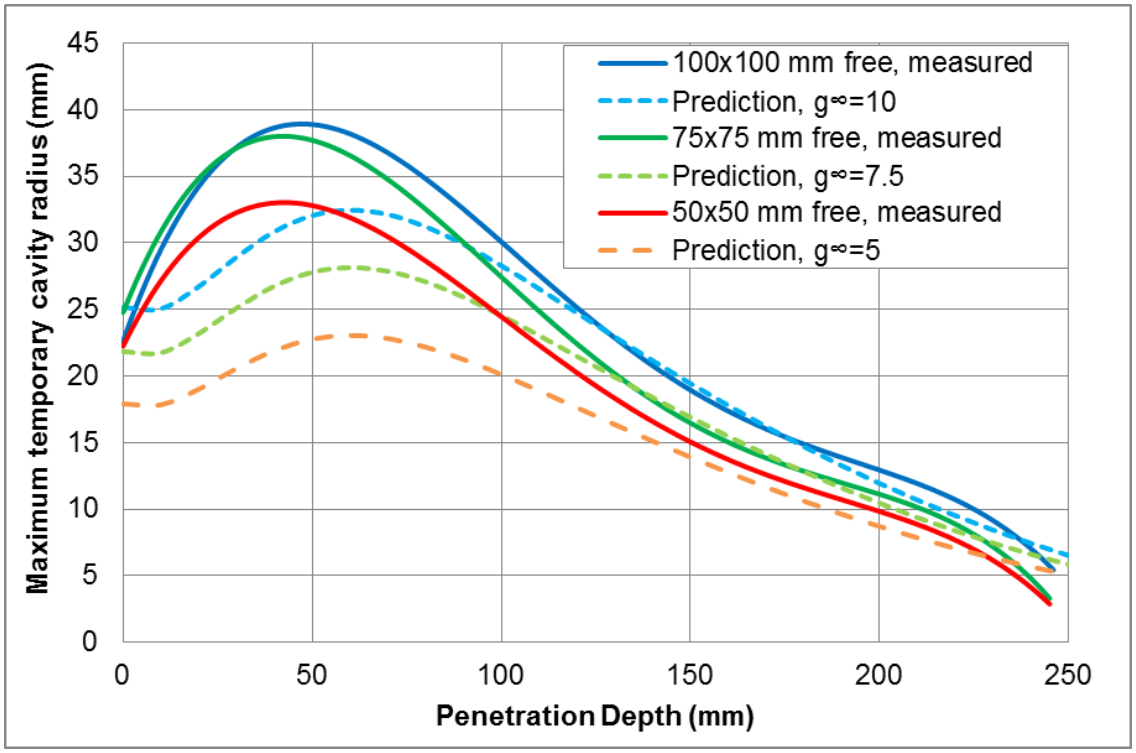

Figure 99: Maximum temporary cavity radius (curve fits) for the 100 mm x 100 mm, 75 mm x 75 mm and 50 mm x 50 mm Dstl 20% gelatin at 10°C blocks and corresponding predictions using Equation 27 by altering $\bar{g}_\infty$. Data from Section 7.5.

This suggests that other modifications to Equation 27 are required, possibly making $\bar{g}_\infty$ a function of both target lateral size and penetration depth.

Further development of the model (Equation 27) was not completed and cannot be used for predictions in other sized targets, apart from 150 mm x 150 mm.

9.7 Permanent cavity prediction

9.7.1 Radius of the permanent cavity in muscle tissue

The permanent cavity (PC) prediction in muscle tissue uses a simple empirical relationship that has been based on experimental observations (based on the average value from experiments detailed in References [95; 220; 260-262]). It is simply a scaled version of the MTC in tissue.

$$r_{PC} = 0.28 r_{MTCtissue}$$

Equation 29: Radius of the permanent cavity in muscle tissue.

For prediction of the PC radius (which is only valid in bulk muscle tissue and cannot be used for gelatin), the parameters related to retardation in tissue should be used. The r_{PC} should be calculated from the $r_{MTCtissue}$, rather than predicting it from the radius of the MTC in gelatin.

An example of the calculated permanent and maximum temporary cavity in muscle tissue is shown by Figure 100.

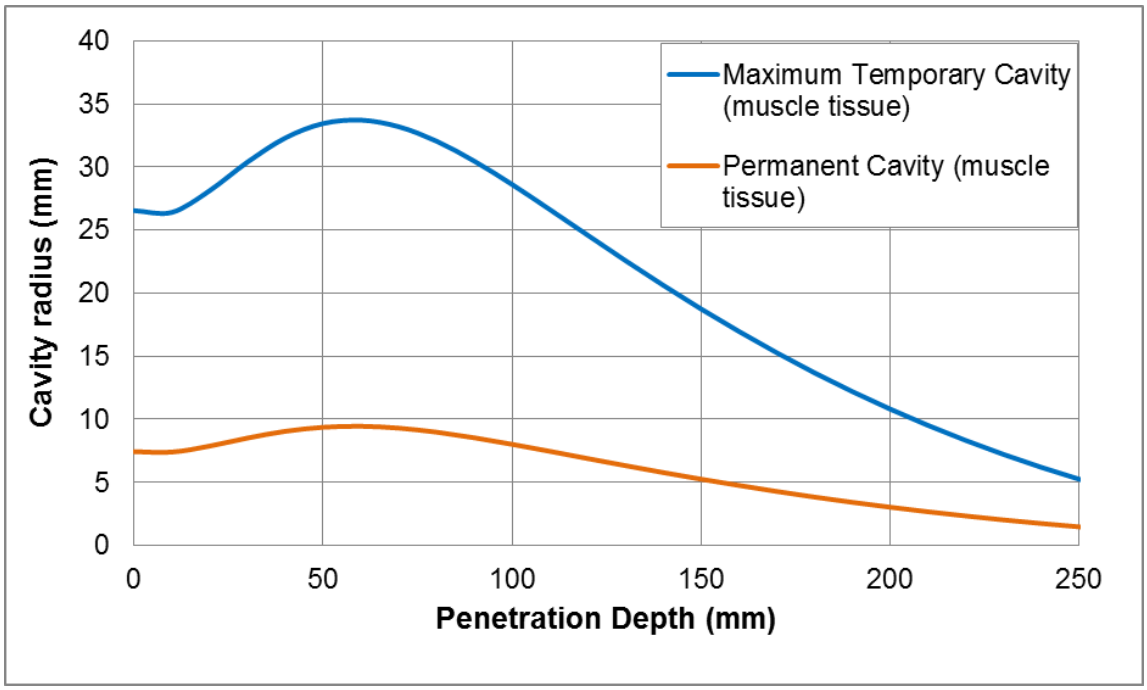

Figure 100: Calculated permanent and maximum temporary cavity radius in muscle tissue for a 6 mm steel sphere at 750 m s^{-1}.

Equation 29 predicts that the permanent cavity diameter in muscle tissue will collapse down to less than the projectile diameter at deep penetration depths (Figure 101 shows this more clearly than Figure 100). Based on experimental observations of testing muscle tissue from Section 5, this seems reasonable: The projectile was always partially obscured by the surrounding tissues when viewed down the permanent cavity, albeit these impacts were all relatively low velocity.

9.7.2 Variation in the predicted PC

The relationship between the PC and MTC was based on average values from a number of different experiments [95; 220; 260-262]. This factor of 0.28 may benefit from further refinement and validation. The range of the average values from each separate source was 0.20 to 0.40. The standard deviation (SD) on the average PC radius[152] (σ_{rPC}) was ±0.09. The variation in PC radius with penetration depth in tissue with ± 1 SD is shown in Figure 101.

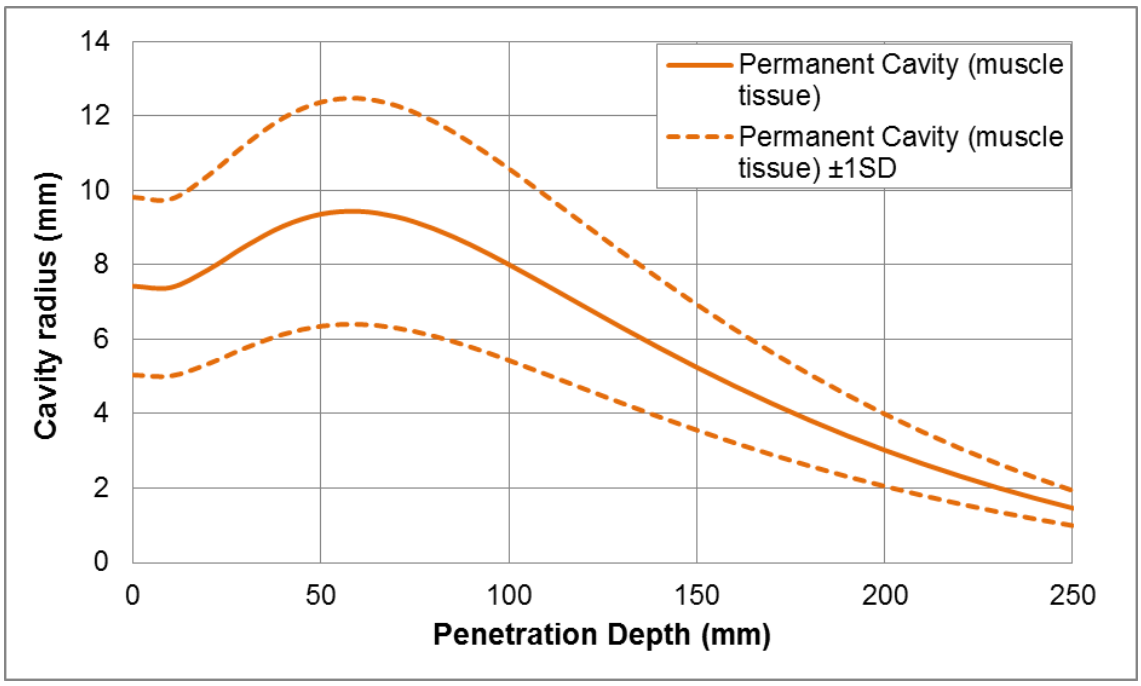

Figure 101: Calculated permanent cavity radius for a 6 mm steel sphere at 750 m s^{-1} in muscle tissue showing ±1 standard deviation on the prediction.

There was no data available in order to validate the permanent cavity radius predictions, other than that on which the model is based.

9.8 Damaged muscle tissue

The mechanisms of muscle tissue damage are described in Section 3.9.2. The zone of damaged tissue is bounded by the permanent and temporary cavities.

[152] Ideally the average value and SD should be revised based on re-examination of the original data, rather than has been done here on the already averaged data.

Equation 28 and Equation 29 can therefore be used to provide a comparative measure of ‘damage’ between different impact conditions.

The available data in the literature for muscle tissue damage was predominantly for bullets [112]. There are existing relationships to estimate the mass of damaged tissue based on the mass of surgically debrided tissue (e.g. Reference [112]), however, they are based on the total energy dissipated in a given wound length. This has then been used to provide the average energy dissipated per unit length prediction.

Due to the data based on bullets that tumbled and deformed; the resulting relationship from Reference [112] had a relatively low R^2 correlation value (R^2=0.293). It is considered that the available data is not sufficiently detailed, in terms of damage at different depths along the shot line (related to the actual or predicted energy loss at corresponding depths) to enable reliable predictions. It is for this reason that an equation or prediction is not provided to estimate the radius of damaged muscle tissue within this thesis.

There are implications related to the radius of damaged tissue that can be considered without a direct mathematical prediction.

According to Reference [253], the amount of damaged muscle tissue is from a combination of prompt damage; “*compression, shearing and stretching of tissue in the immediate vicinity of the projectile*” [253] and temporary cavity damage.

Within Reference [218], pig legs were shot with and without a plaster cast to restrict temporary cavitation. The outcomes from this testing clearly demonstrated that there was less muscle tissue damaged (based on the mass of surgically debrided tissue), by almost 40%, in the legs that were constrained within the plaster cast molds.

As pointed out by Fackler [219], due to the orientation of the constraint in relation to the shot line within the testing of Reference [218], the temporary cavity (and its contribution to the subsequent damaged tissue) will not be fully suppressed along the long axis of the limb. Therefore, it is considered that the contribution of

the damage from the temporary cavity mechanism is a minimum of 40% of the total damaged muscle tissue.

There is no suitable data available for confinement of temporary cavity formation in muscle tissue (and resulting 'damage' measures) that could be used to validate this assumption or generate an equation.

From the predictions of cavity sizes (Sections 9.6 and 9.7) and results in Section 7.5 on the confinement of gelatin on the resulting temporary cavity, it can be assumed, and has been demonstrated [218], that this confinement effect would translate to real muscle tissue. The implications in terms of the role of cavities on the resulting injury are:

- Results from wound studies on tissues tested in isolation should be treated with caution (as boundary conditions would not be accurate). Retardation studies of the projectile would not be affected. A simple solution may be to embed tissue into gelatin for the purposes of wound studies[153].
- Wounds from ballistic projectiles could be reduced in severity by PPE designed to restrict the formation of a temporary cavity in the body, for tissues in which the temporary cavity contributes significantly to the overall wounding effect. This would apply to muscle tissue and this type of PPE may be practical for the extremities. Experiments such as those in Reference [218] have shown that muscle constraint by plaster cast reduced the mass of debrided muscle tissue by almost 40%. It may be feasible to use a strain rate dependent material that adds minimal restriction to normal movement given the timescale of the tissue response during cavity formation (few milliseconds from formation to collapse) compared to the timescales over which normal movement occurs.

[153] But not suggested as a hybrid tissue penetration model due to the variables introduced. A simpler and more exploitable method for non-deforming, non-tumbling projectiles is to use homogeneous gelatin and equate penetration in gelatin to other tissue types during the analysis, see Section 9.9.

9.9 Accounting for other tissue types (penetration and retardation only)

9.9.1 Tissue thickness equivalence scaling

Whilst the previous equations detailed in Section 9 allow predictions of penetration and retardation for muscle tissue or muscle tissue simulants (potentially accounting for skin), treating a human as entirely muscle is not an accurate representation.

Possible solutions to this could be:

- Repeating the generation of a (complex) set of equations for different tissue types of interest;
- Having a complex physical model (i.e. with simulants for skin, muscle, bone, blood vessels and all the other tissue types required) that provides an accurate representation, but is specific to that scenario and very sensitive to small variations in impact conditions; or
- Scale the outputs from those calculated for muscle tissue, or a homogeneous muscle tissue simulant, to different tissue types.

The latter route was followed, as discussed in Section 2.6. Reference [42] gives details of the relative muscle tissue thickness required to achieve the same deceleration for other tissues. This is a velocity dependent relationship, but is independent of fragment size, geometry and density. Whilst the equation(s) in Reference [42] cannot be reproduced as the parameter values were not detailed, an abstracted version of this relationship has been generated by digitising the relevant data which is reproduced in Figure 102.

To obtain abstracted data fits, the x-y co-ordinates at multiple points along each curve were extracted using ImageJ [263]. These were then converted into the corresponding values for each co-ordinate. The LINEST function in Microsoft® Excel® was used to generate the parameters for a 3rd order polynomial fit to half of the data from 50 m s^{-1} to a crossover velocity. An additional 3rd order polynomial fit was then calculated in the same manner for the remaining points up to 1400 m s^{-1}. A single curve fit across the entire velocity range could not be

accurately determined. The crossover point in velocity between these two curves was determined for each tissue type separately by looking at when the R^2 value of the polynomial fits started dropping and no longer gave a good representation of the data[154]. The resulting curves are shown in Figure 102.

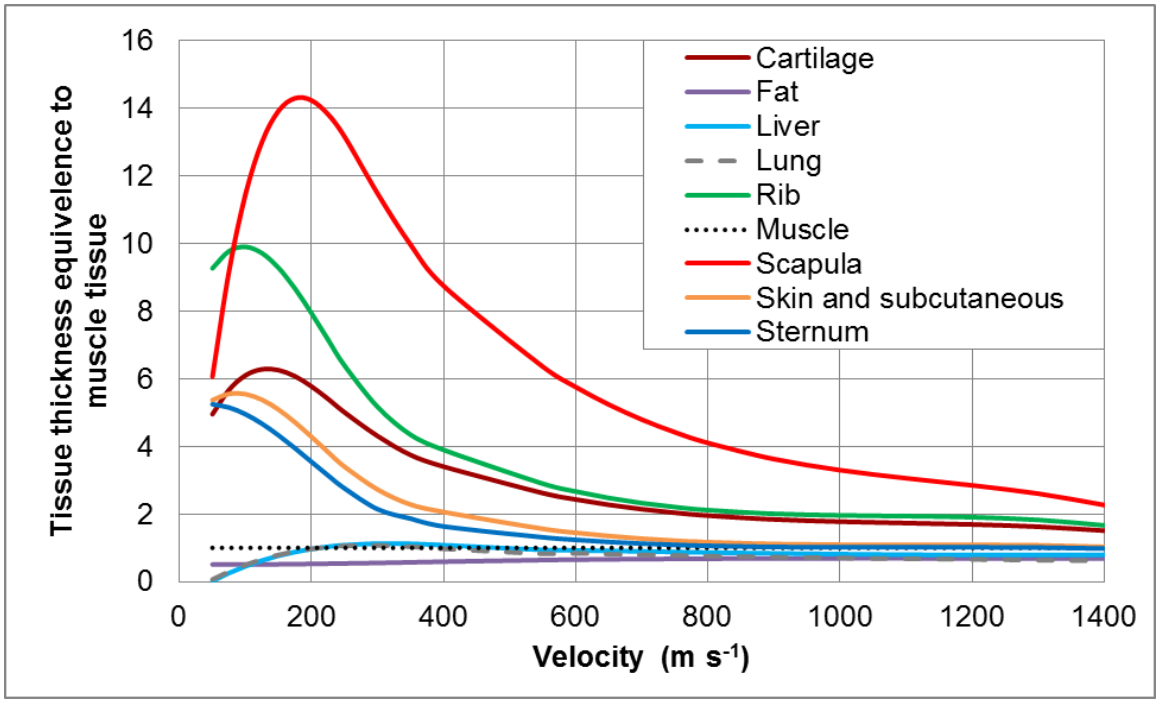

Figure 102: The relative tissue thickness required to achieve the same deceleration as for muscle tissue. Reproduced from the data extracted from Reference [42].

The parameters used to produce Figure 102 using Equation 30 are given in Table 34.

$$Eqiv\ thickness = T_a v^3 + T_b v^2 + T_c v + T_d$$

Equation 30: Equivalent tissue thickness required to achieve the same deceleration as for muscle tissue

Where T_a – T_d are parameters for the different tissue types

[154] R^2 values of >0.9 were achieved for the 3rd order polynomial fits, most cases with R^2>0.98.

It should be noted that due to the abstraction of the data from Reference [42], Equation 30 and the values in Table 34 are only valid in the velocity range 50 to 1400 m s^{-1}.

In ComputerMan, the various tissues are modelled by one of these ‘parent’ tissue types. Reference [215] gives a different list of tissue groups that do not match those from Reference [42]. Reference [215] does not give the information required to produce the parameters for the equivalent tissue thickness required to achieve the same deceleration as for muscle tissue.

The equivalent tissue thickness scaling from ComputerMan are based on experiments using animal tissues to determine the relationships [42]. How these various animal tissues (likely goat [76]) match those of human tissue is unknown, other than as previously discussed for skin in Section 3, 5.5 and 6.1.5.

	Low velocity parameters				High velocity parameters				
Tissue	T_a ($\times 10^{-9}$)	T_b ($\times 10^{-6}$)	T_c ($\times 10^{-4}$)	T_d	T_a ($\times 10^{-9}$)	T_b ($\times 10^{-6}$)	T_c ($\times 10^{-4}$)	T_d	**Switch velocity (m s^{-1})**
Cartilage	471.26	-339.91	657.22	2.46	-4.13	13.60	-153.28	7.62	330
Fat	-1.20	1.38	-1.62	0.51	0.19	-0.70	8.46	0.35	570
Liver	25.37	-32.97	132.47	-0.57	0.23	-0.41	-0.67	1.06	475
Lung	29.04	-36.16	135.63	-0.53	-0.26	0.95	-13.35	1.35	580
Muscle	0.00	0.00	0.00	1.00	0.00	0.00	0.00	1.00	1
Rib	700.83	-460.79	695.27	6.86	-6.03	19.38	-209.54	9.56	330
Scapula	1032.53	-896.19	2243.54	-3.04	-10.20	35.07	-422.71	20.70	360
Skin and subcutaneous	372.97	-238.44	327.73	4.28	-2.73	9.10	-100.83	4.81	330
Sternum	221.34	-132.24	100.70	5.05	-1.80	5.99	-66.06	3.43	360

Table 34: Parameter values for Equation 30, the relative tissue thickness required to achieve the same deceleration as for muscle tissue.

9.9.2 Example implementation (verification) of hybrid tissue type retardation

To demonstrate the implementation of the relative tissue thickness for different tissues, an example shot line through the abdomen will be considered. Figure 103 shows a cross section of the abdomen from a CT scan. Overlaid onto this is a red arrow indicating the example shot line. This shot line was taken to be 204 mm from entry to exit and passes through skin, muscle, fat, liver and ribs.

Figure 103: Cross section of the abdomen from CT scan [264] showing an overlaid hypothetical shot line (red) through different tissue types. Image reproduced under the GNU General Public License.

Using Figure 103 and tissue identification tools within the digital CT scans from Reference [264], the distances of the different tissues along the shot line were approximated and are given in Table 35.

Distance along shot line (mm)	Tissue type
0-9	Skin and subcutaneous tissue
9-40	Muscle
40-44	Fat
44-177	Liver
177-186	Fat
186-196	Rib
196-200	Muscle
200-204	Skin and subcutaneous tissue

Table 35: Distance along an example shot line showing the depth of the different tissue types.

The equivalent penetration depths in muscle tissue at three different impact velocities (300, 600 and 900 m s^{-1}) were calculated using Equation 20, Equation 30 and values from Table 34 for a 6 mm steel sphere. Retardation into the hybrid tissues using the equivalent depth in muscle tissue scaling are plotted in Figure 104, also showing the equivalent retardation in muscle tissue.

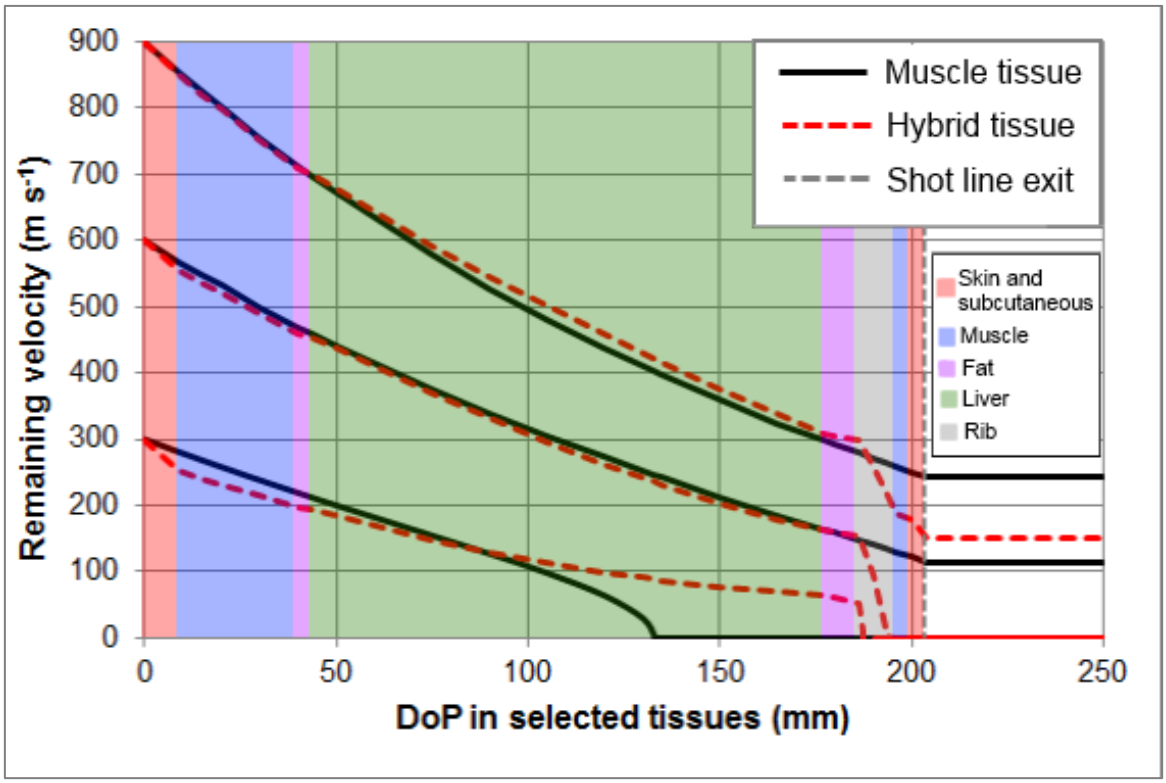

Figure 104: Comparison of retardation for muscle tissue compared to hybrid tissue types for the example shot line for 3 different impact velocities of a 6 mm steel sphere.

Figure 104 shows how the retardation of the projectile depends on the remaining velocity as well as the tissue type for a comparative retardation to muscle tissue. It also shows that depending on the impact velocity, the resulting permanent DoP or exit velocity may be greater for predictions in muscle tissue, or in hybrid tissues.

It is also possible to implement this equivalent depth in muscle tissue scaling for permanent DoP predictions (based on Equation 17).

9.9.3 Additional tissue types, parameter generation for equivalent depth in muscle tissue scaling

9.9.3.1 Background for bones embedded in gelatin

A trial was conducted in order to generate data to use for additional parameters for different tissue types and initial validation of an existing tissue type for the equivalent depth in muscle tissue scaling. Three different bone types were used:

- Long bone mid-shaft (Red Deer Tibia)
- Long bone proximal end (Red Deer Tibia)
- Flat bone sample (cut from Bovine Scapula)

The red deer tibia were chosen to give a generic long bone of similar dimensions to humans, with sufficient size to enable mid shaft and proximal sections to be taken from the same bone. Bones were from mature individuals where tibia lengths were between 300 mm and 400 mm[155]. Red deer femurs have previously been suggested as a good model to human femurs due to similar morphology in place of that from pigs or sheep [265].

Similarly fallow deer thighs and femurs have been used for ballistic studies as a more biofidelic alternative to pigs [166].

The bovine scapula was chosen to give a generic flat bone and has previously been used as a model for the temporal-parietal region of the human skull (having similar thickness and geometry) [266].

The two different tibia sections were used to generate new parameters for the equivalent depth in muscle tissue scaling (in the following sub-sections). The scapula was used to provide initial validation of Equation 30 with the values from Table 34 (discussed in Section 9.9.4).

9.9.3.2 Method for bones embedded in gelatin

Bone sections were embedded into Dstl 20% gelatin at 10°C. The bones were embedded in gelatin so that the tissue scaling model could be applied to hybrid tissue types as well as to ensure the fracture/damage response would be more realistic, however, bone damage is not accounted for in this model.

The bone sections and indicative impact locations are shown diagrammatically in Figure 105.

[155]Deer tibias were obtained in January, this avoided potential low bone density issues due to osteoporosis in males growing antlers.

Long bone shaft	Long bone proximal end	Flat bone section
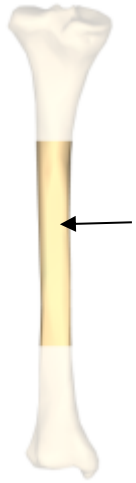		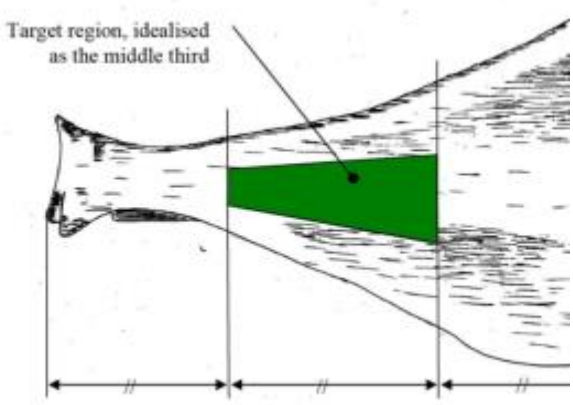

Figure 105: Diagrams of bone sections and impact locations. Bovine scapula original artwork by Andrew Sedman, used with permission.

Bone sections were supplied from the food chain and stored frozen. Bones were collated by suppliers up to a maximum of 6 weeks prior to the commencement of the trial (the quantity of bones required meant the bones could not be supplied and shot fresh). Red deer tibias came from carcasses that were aged for 1 week prior to butchering, at which point the meat was removed from the bones and then the bones frozen.

Bones were hand sawn into the required sections whilst frozen. Bovine scapula samples were cut to be less than 150 mm width to ensure they would fit into the gelatin molds. The distal end on the tibia was left intact on the tibia mid-section samples to reduce the amount of target preparation required.

The bones were defrosted by immersion in room temperature Hartmann's solution[156] for a minimum of 12 hours before inserting into the gelatin to ensure they did not dehydrate.

[156] Hartmann's solution is a mixture of sodium chloride, sodium lactate, potassium chloride, and calcium chloride in water.

Gelatin was manufactured to the Dstl mix method (APPENDIX D, D.1) with calibration on additional blocks without any embedded bones, following the fixed velocity method for 20% gelatin in APPENDIX D, D.5.3.

Gelatin was poured into molds (cubes of 150 mm side length) and then the defrosted bone sections were inserted, held in position by frames or clamps whilst the gelatin set. A red deer tibia mid shaft embedded in Dstl 20% gelatin ready for shooting is shown in Figure 106.

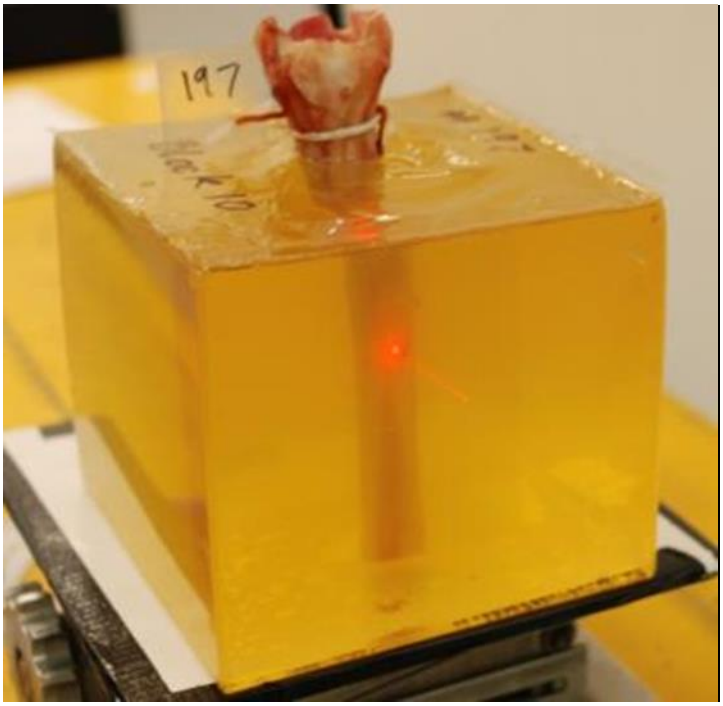

Figure 106: Photograph of the red deer tibia mid shaft embedded in Dstl 20% gelatin with point of aim shown by a red laser.

For the flat bone (bovine scapula sections), the bone was inserted into the gelatin to give a 0° angle of incidence to the shot line (normal obliquity) or 30° angle of incidence.

Projectiles were 3, 6 and 9 mm steel spheres, fired from the MPH (APPENDIX B, B.2) using smooth bore barrels for each size projectile, propelled by blank pyrotechnic charges.

Impact velocities were recorded using 3 sets of MSI solid state velocity equipment [205], each with a 0.5 m separation between the velocity heads and the last head was 0.38 m to the target.

Testing was completed within 30 minutres of removal of targets from the conditioning cabinet to ensure the gelatin was at the correct usage temperature of 10°C.

HSV was used to get a view of the target orthoganal to the shot line to enable measurement of projectile retardation. The HSV cameras used were a Photron SA-Z [206] recording at 100,000 frames a second with a resolution of 640x280 pixels or a Phantom V710 [209] recording at 60,000 frames a second with a resolution of 320x256 pixels (a single camera was not avilable for the entire duration of the trial). Additionally, a Phantom Miro M-310 recording at 24,000 frames a second with a resolution of 512x240 pixels was used throughout to give an additional view of the target at slower frame rate.

The velocity at impact with the bone was extraoplated from the projectile tracking by HSV (using the higher frame rate cameras and tracking software Tracker [213]), as was the projectile exit velocity from the bone. Impact velocities to the gelatin block were all less than 1400 m s^{-1} to avoid any transonic effects in gelatin and remain within the limitations of Equation 20. This limited the maximum bone impact velocities achieved, as sufficient distance in gelatin was needed prior to bone impact in order to track the projectile to enable a bone impact velocity to be estimated.

9.9.3.3 Results - bones embedded in gelatin

The 3 mm steel spheres couldn't be fired fast enough to enable full perforations of any of the embedded bones with the setup used. For the 3 mm steel spheres, maximum velocities achieved were 615 m s^{-1} impacting the gelatin and 314 m s^{-1} impacting the bone.

A total of 80 fair impacts with the 6 mm and 9 mm steel spheres were conducted. Table 36 summarises these fair impacts for each bone type.

Bone type	Bone thickness at impact location (mm) [157]	Bone impact velocity (m s^{-1})	Number of fair impacts
Tibia mid shaft	18.0 – 22.2	225 – 750	26
Tibia proximal end	25.0 – 56.0	160 – 800	18
Bovine scapula (0° impacts)	2.6 – 9.2	115 – 650	22
Bovine scapula (30° impacts)	2.5 – 10.9	275 – 775	14

Table 36: Summary of impacts to the bones embedded in Dstl 20% gelatin at 10°C.

In order to provide a retardation estimate for use in the equivalent muscle tissue thickness scaling, the experimental data was analysed to produce muscle tissue equivalent scaling values for the deer tibia mid shaft and proximal end.

The velocity lost by the projectile within the bone, calculated from the HSV projectile tracking (extrapolated to the bone surface) and the bone thickness at the point of impact were used to predict what thickness of muscle tissue would be required to create an equivalent velocity loss in muscle tissue using Equation 20. The thickness of muscle tissue required to provide an equivalent velocity loss was found to be independent of bone impact velocity over the velocity range investigated for the mid tibia (a linear fit to the data showed the gradient was not significant at the 95% confidence level, p=0.795).

An average value for the scaling factor for the mid tibia was found to be 6.94 times the thickness of muscle tissue (i.e. for Equation 30, T_a, T_b and T_c=0, T_d=6.94). The 95% confidence interval on this value was ±0.52 (with σ=1.28).

Using these parameter values for Equation 30 for the deer tibia mid shaft and Equation 20, the retardation of a 6 mm steel sphere through the Dstl 20% gelatin at 10°C and deer mid tibia was compared to experimental data from one of the firings in Figure 107. When the projectile is in air, there is no predicted retardation (i.e. air drag is not considered).

[157] This is the traversed bone thickness accounting for the angle for the 30° impacts.

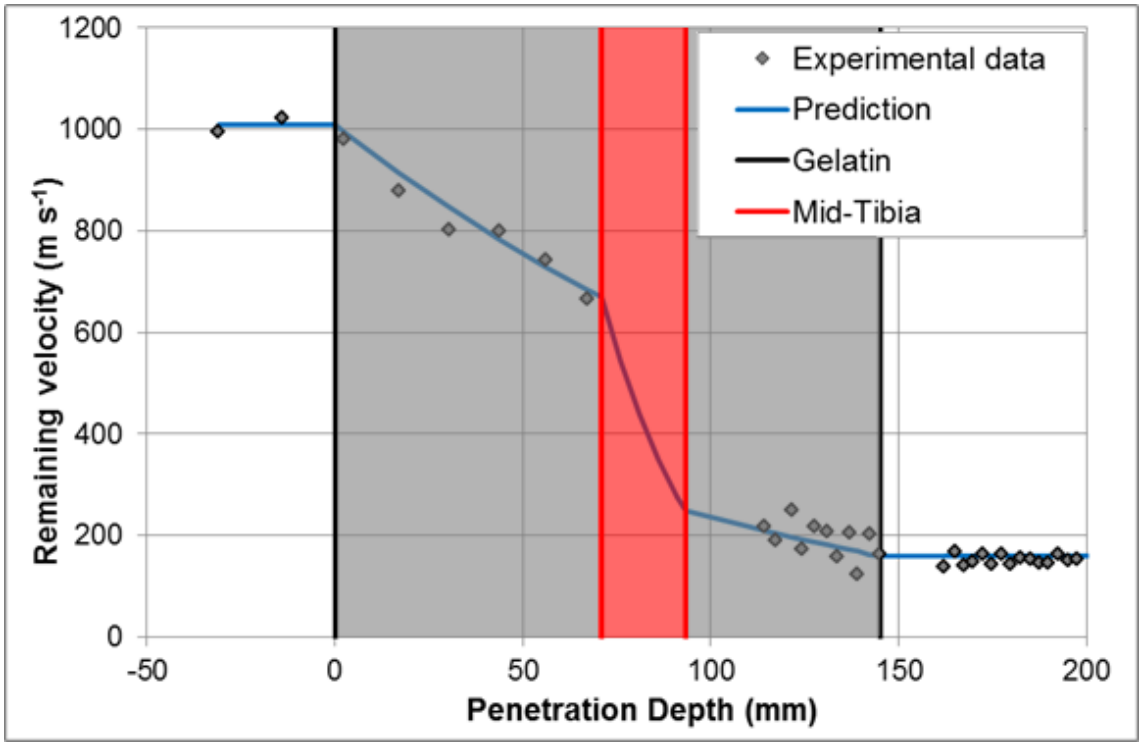

Figure 107: Comparison of experimental data for 6 mm steel sphere penetrating the deer mid tibia in gelatin target compared to Equation 20 and Equation 30 using the newly determined mid-tibia parameters.

Figure 107 shows that whilst this equivalent muscle tissue thickness scaling for the deer tibia can be seen to agree well to the experimental data (for the firing conditions shown), the parameter generation is over a more limited velocity range than the other tissue types given in Figure 102 and Table 34. Therefore it is suggested to be treated as an indicative value only.

Analysis was repeated for the red deer proximal tibia impacts. Unlike the tibia mid shaft, the muscle tissue thickness equivalence scaling was found to be dependent on the bone impact velocity for the proximal end. The calculated parameters for Equation 30 were T_a=0 T_b=0, T_c=-0.0014 and T_d=3.71. The experimental data and linear fits for both the tibia mid shaft and proximal end are shown in Figure 108, along with 95% confidence intervals on the linear fits.

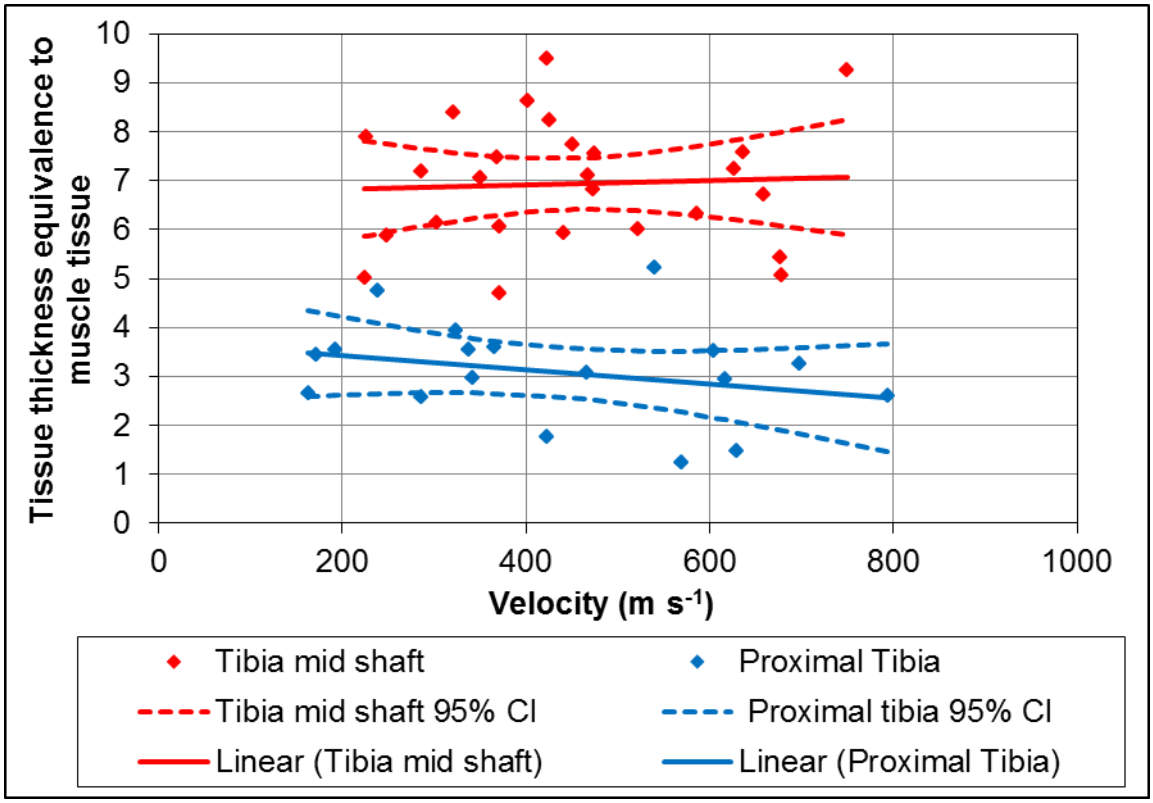

Figure 108: Comparison of scaled muscle tissue thickness based on the experimental data for the red deer tibia mid shaft and proximal end (in gelatin).

Figure 108 shows the scaled muscle tissue thickness for the red deer tibia mid shaft and proximal end. As with a lot of biological targets, the results are typified by high degrees of scatter. It is noted that the peak in the scaled muscle tissue thickness seen for many of the other tissues in Figure 102 is not seen in the fits applied to the deer tibia mid shaft and proximal end shown in Figure 108. This may be due to lack of data at lower velocities where this peak is expected to occur.

Using the parameter values for Equation 30 from the linear fit to the data shown in Figure 108 for the deer proximal tibia and Equation 20, the retardation of a 6 mm steel sphere through the Dstl 20% gelatin at 10°C and deer mid tibia was compared to experimental data from one of the firings and is shown in Figure 109.

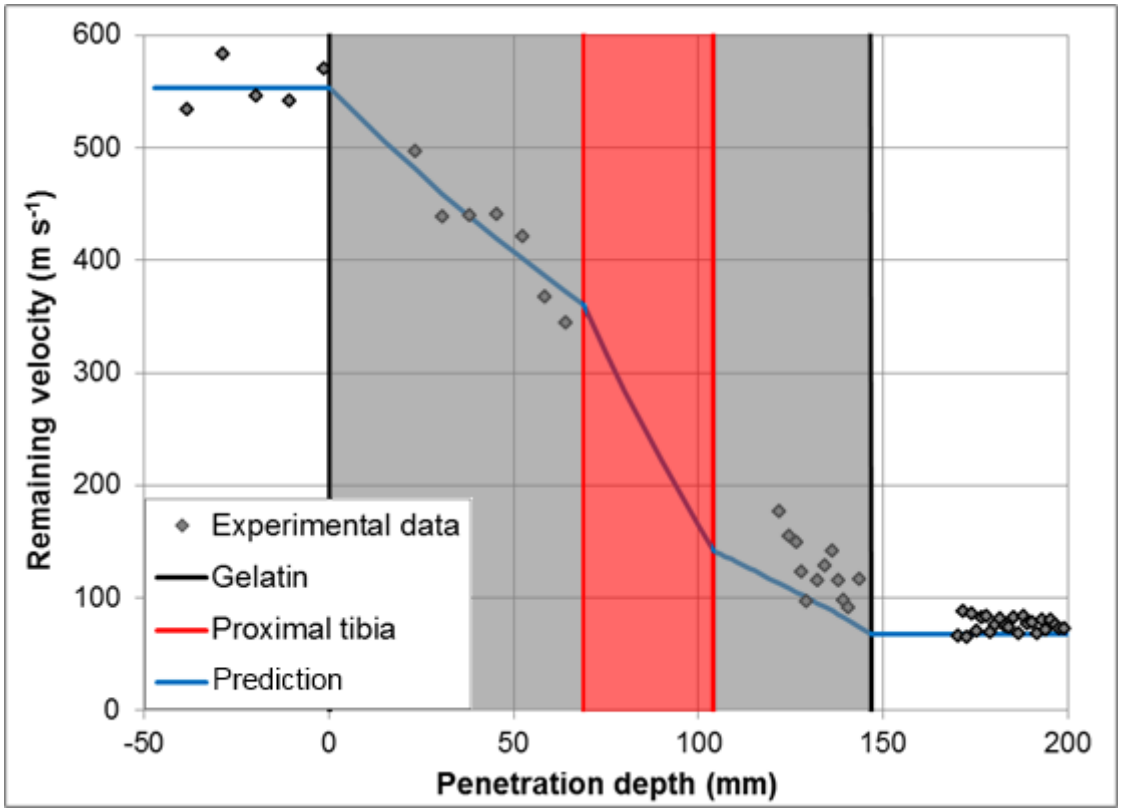

Figure 109: Comparison of experimental data for 6 mm steel sphere penetrating the deer proximal tibia in gelatin target compared to Equation 20 and Equation 30 using the newly determined proximal-tibia parameters.

Figure 109 shows how the scaled muscle tissue thickness equations and parameters can be used to predict the retardation through the gelatin and deer proximal tibia. High scatter is seen in the residual velocity data obtained from the HSV following the projectile exit from the bone. This is due to bone fragments distorting a clear view of the projectile.

9.9.4 Initial validation of tissue type scaling for bones embedded in gelatin

The same analysis process discussed in Section 9.9.3 for generating parameters for new tissue types was used for the initial validation for scapula embedded in gelatin.

Analysis of impacts into bovine scapula (at normal obliquity and at 30°) embedded in Dstl 20% gelatin at 10°C showed highly variable results in terms of equivalent muscle tissue thickness ratios. Despite the considerable scatter in the

data, the curve fit to the calculated equivalent muscle tissue thickness scaling for the scapula agreed with that from the ComputerMan abstraction (Figure 102 and Table 34). The comparison of the experimental data for both impact angles compared to the ComputerMan scaled muscle tissue thickness is shown in Figure 110.

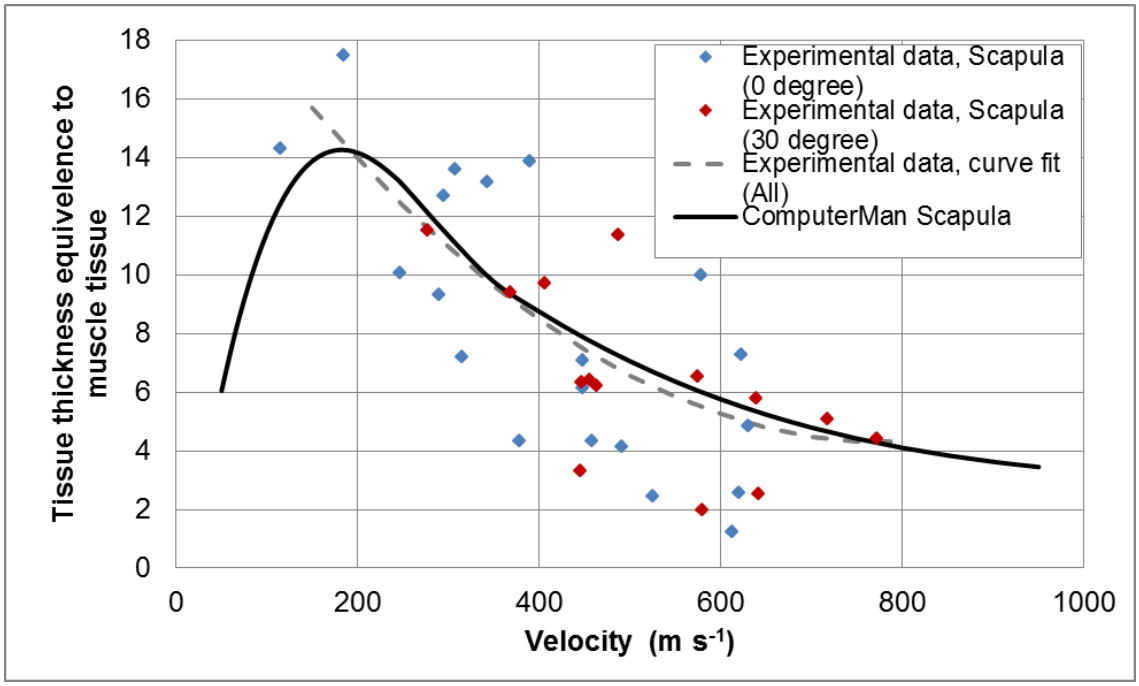

Figure 110: Comparison of experimental data for the scapula (in gelatin) scaled muscle tissue thickness compared to the ComputerMan relationship.

Figure 110 shows that the curve fit to the experimental data (combined 0° and 30° impacts) gives very good agreement to the existing ComputerMan Scapula relationship. However, there is a large degree of variability in the raw data; similar to the tibia mid shaft and proximal end raw data.

Potential sources of variability may be due to:

- Biological variation;
- Different thickness ratios of cortical to cancellous bone in the scapula;
- Different mechanical properties of the bones due to the age of the animals from which the bones came;

- Different mechanical properties of the bones due to the time from death to storage and/or use;
- Storage conditions affecting mechanical properties (bones were frozen and defrosted prior to inserting into warm gelatin).

The predicted retardation of a 6 mm steel sphere through the Dstl 20% gelatin at 10°C and bovine scapula target was compared to experimental data from one of the firings (using the scapula parameters in Table 34) and is shown in Figure 111.

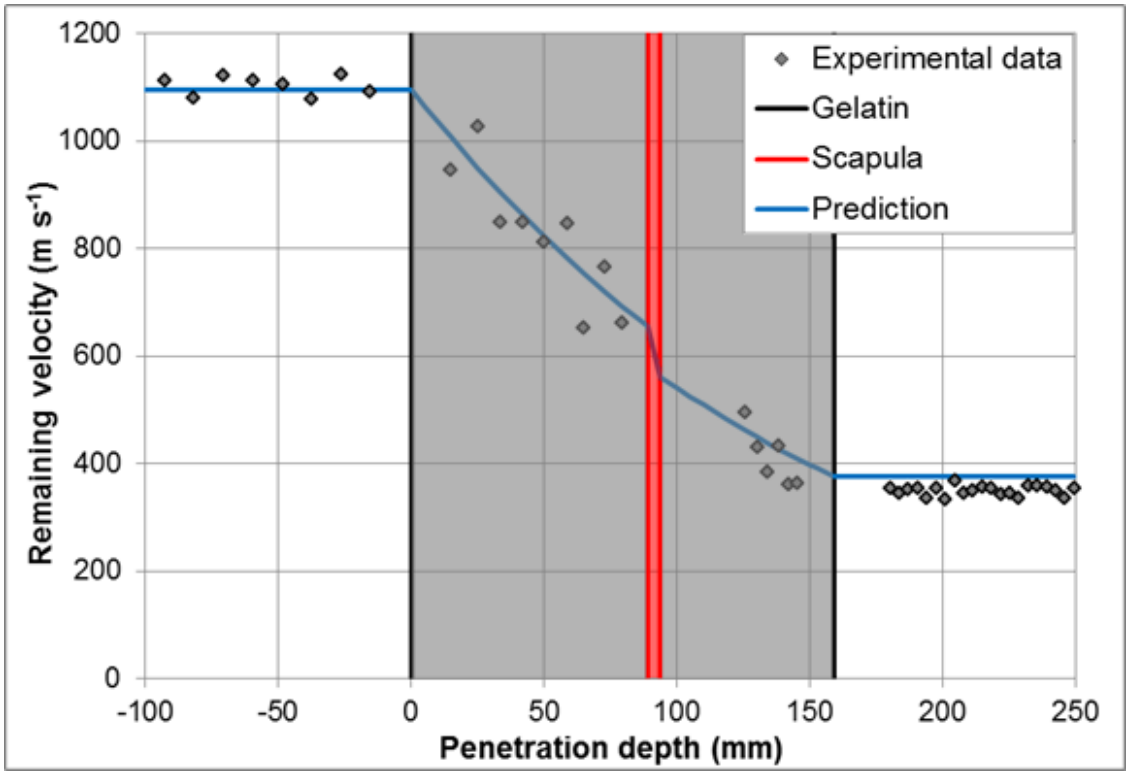

Figure 111: Comparison of experimental data for 6 mm steel sphere penetrating the bovine scapula in gelatin target compared to the prediction using Equation 20 and Equation 30.

Figure 111 shows that for the shot modelled using Equation 20 and Equation 30, the predicted retardation through the different parts of the physical model provide a good match to the experimentally measured values. However, the high variability of the data in Figure 110 means that if a different shot is chosen to be modelled, the predictions may not be as accurate for that particular case.

Published data for other tissue types was also compared to the predictions using Equation 20 and Equation 30. Data from References [95; 107; 217] were used for the liver and lung. Data from Reference [95] were individual raw data points for the liver (target thickness, impact and exit velocities reported for each shot, n=20). Data from References [107; 217] for the liver and lung were grouped, averaged data (between 5 and 24 shots for each group with a spread of impact and exit velocities and target thicknesses. Grouped data for liver; n=7, lung; n=6). Data from Reference [124] were identified, but not used as impact velocities were not reported for each individual shot. The resulting comparison of the experimental data for lung and liver compared to the ComputerMan scaled muscle tissue thickness is shown in Figure 112.

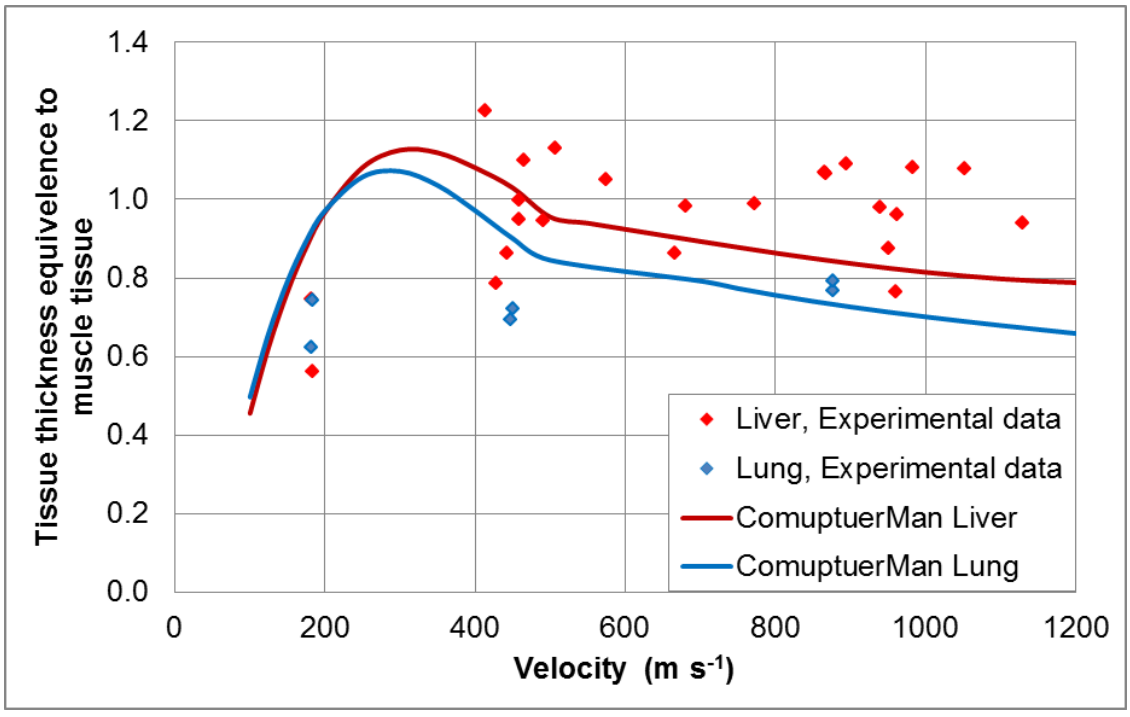

Figure 112: Comparison of experimental data for liver and lung scaled muscle tissue thickness compared to the ComputerMan relationships. Experimental data from References [95; 107; 217]

Figure 112 shows that for the liver, the ComputerMan scaled muscle tissue thickness gives a reasonable fit to the data. Equation 30 with parameters in Table 34 appear to under-predict the equivalent muscle tissue thickness for liver at higher velocities (>700 m s^{-1}). However, it is unknown how much of this is due to

the grouping of data in References [107; 217]. The raw data (at least 79 raw data points) from References [107; 217] was not available, so this was based on the average / binned data that was reported.

Similarly, the limited grouped lung data from References [107; 217] shows good agreement in Figure 112 with the ComputerMan scaled muscle tissue thickness for lung, although over-predicting the equivalent muscle tissue thickness below approximately 500 m s^{-1}. However, without comparison to the raw data (68 shots) where all the factors can be properly accounted for, more complete validation of Equation 30 and values from Table 34 cannot be conducted.

Additional ballistic data is given in References [107; 108; 124; 217] for the heart and kidney (as well as for spleen, fat and aorta, limited to a nominal low velocity). Table 34 does not include the heart and kidney as distinct tissue types for the ComputerMan scaled muscle tissue thickness. If the raw data from References [107; 108; 124; 217] were avialable, it could be used to determine, which, if any of the existing tissue types could be used to represent the heart and kidney, or to generate an initial set of paramaters that could be used with Equation 30.

Additional shots were conducted against isolated deer mid and proximal tibia, as well as bovine mid-tibia as part of the testing described for Section 9.9.3, but have not been analysed. These isolated bone data could be used as validation data.

Limitations of the additional tissue type parameter generation and initial validation (Sections 9.9.3 and 9.9.4) are considered to be:

The predictions using Equation 30 represent the projectile response in an ‘average’ target and there is a need to be able to account for the potential variability seen in the response of real tissues (addressed in Section 9.9.5).

It has been assumed that red deer tibia (mid shaft and proximal end) is a suitable model of human long bone [265; 267] and that the bovine scapula was a suitable model for human scapula or a generic flat bone [266]. It was also assumed the process and preparation of bones did not adversely affect their ballistic response compared to live bones.

The variances in bone structure (such as wall thickness or ratios of different bone types) were not considered. The outside diameter or thickness of the bone was used as the reference measurement, which was measured post-impact (as exact impact location couldn't be determined prior to molding the bones in gelatin). The bone was frequently destroyed around the impact point and therefore measurement of bone thickness had to be made adjacent to the impact point, on the closest complete section of bone.

Tissue damage was not considered as part of this model.

9.9.5 Tissue variability

As noted many times previously in this thesis when discussing penetration and retardation in real tissue, there is inevitably scatter or variability in the results. Equation 30 provides a route through which the variability in different tissues can be bounded (i.e. by modification of the parameters in Table 34 to describe (for example) the standard deviation in the response for the given tissue). Data for muscle tissue and skin was analysed to determine the variability in response in this manner.

Data for live pig thighs and dead muscle tissue with skin (PMHS, pig, sheep and goat) from the literature and the data generated in this thesis was collated. In order to remove some of the high variability in the target response for velocities very close to the predicted V_{50} (see Section 9.4), filtering of the data was conducted for DoP≥ 20 mm and V_s/V_{50}≥1.1. After filtering, this yielded n=329 data points for 22 different projectile types:

- n=244 data points for DoP in dead muscle tissue with skin (PMHS, pig, sheep and goat (subset of the data detailed in Table 21 from References [56; 58; 62-64; 71; 79; 88; 90; 93; 94] and Section 5, all for DoP≥ 20 mm).

- n = 68 data points[158] for live pig thighs based on retardation (data detailed in Table 24, but including data excluded from use in Section 7.3 due to long track lengths, References [95; 96; 113; 123]).
- n =17 data points for dead pig thighs based on retardation, References [57; 58].

For shots where a permanent DoP was measured, “Equation 24: Modified DoP prediction accounting for the effect of the skin layer” was used to predict the permanent DoP in muscle tissue with skin using the corresponding projectile impact conditions[159]. The measured DoP was divided by this predicted DoP to get the DoP ratio predicted in muscle tissue (with skin). A ratio>1 indicates a smaller measured DoP to that predicted in muscle tissue (with skin), a ratio<1 indicates a larger measured DoP in the tissue or simulant than expected.

For shots that fully perforated the target, “Equation 25: Retardation in tissue accounting for velocity loss due to the skin” was used to predict the thickness of muscle tissue with skin required to give the same exit velocity with the corresponding projectile impact conditions[160]. As for the DoP, the measured thickness over predicted thickness was calculated to give a retardation ratio compared to the predicted value in muscle tissue and skin[161]. The retardation ratio data for live and dead muscle tissue were combined (the dead muscle tissue was all for impact velocities below 215 m s^{-1} and live muscle tissue all above 429 m s^{-1}).

The resulting ratio for the measured over predicted DoP or retardation in muscle tissue is shown in Figure 113.

[158] Includes 3 data points which are grouped, with an average of 10 shots per group [113] and one based on the fitted model retardation equation generated from 14 shots [123]. The total shots for live pig thighs = 108.
[159] U_6=90 m s^{-1}. The V_{50} was calculated for each projectile using Equation 8 with the inputs for all the expanded parameters set=1.
[160] U_6=80 m s^{-1}. The V_{50} was calculated for each projectile using Equation 8 with the inputs for all the expanded parameters set=1.
[161] Only the effect of the skin on the projectile retardation at impact was considered, not on exit.

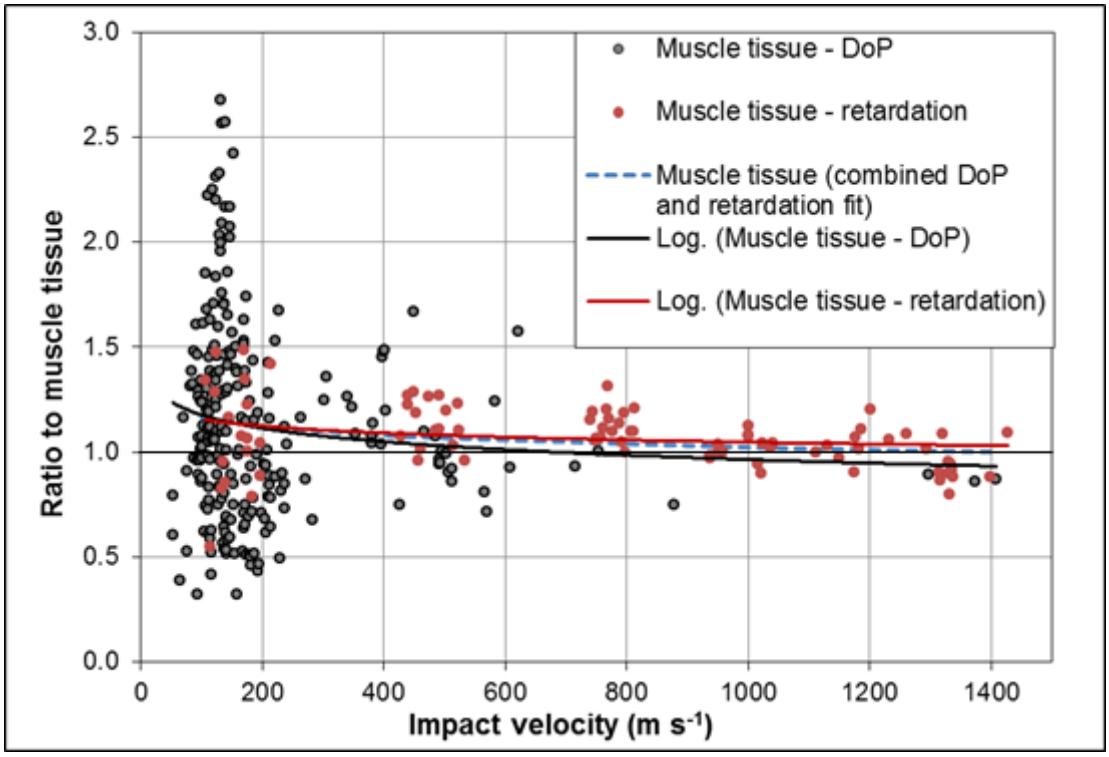

Figure 113: The ratio for the measured over predicted DoP or retardation in muscle tissue for combined live and dead tissue (using Equation 24 and Equation 25). Raw data from References [56-58; 62-64; 71; 79; 88; 90; 93-96; 113; 123] and Section 5.

Figure 113 shows:

- High variability in the individual calculated points, especially at low velocity (<250 m s^{-1}) and for the DoP data.
- Based on the fits to the data, the average ratios were between:
    - 117.5% and 93.0% at 100 and 1400 m s^{-1} respectively for the muscle tissue DoP data.
    - 115.6% and 102.9% at 100 and 1400 m s^{-1} respectively for the muscle tissue retardation data.
- Validation of Equation 24 and Equation 25. Both equations provide a good (average) prediction of DoP and retardation in live and dead muscle tissue across the velocity range 250-1400 m s^{-1}, slightly over predicting the DoP or retardation at the lower velocities. This is shown by the blue dashed fit to all the DoP and retardation data in Figure 113.

A linear model was applied to the combined data for DoP and retardation ratios and showed that the gradient was not significant at the 95% confidence level (p=0.628). Assuming this velocity independent relationship, the standard deviation on all the combined muscle tissue DoP and retardation data was 0.37, with standard error of 0.02. These values can be used to adjust the penetration or retardation calculations for skin and muscle tissue (Equation 24 and Equation 25) to account for the variability of the biological targets. It is also assumed that this approach would be suitable for Equation 17 or Equation 20 when $V_S/V_{50} \geq 3$.

The muscle tissue scaling for the scapula data from Section 9.9.4 was further analysed to generate the standard deviation on the fit to the data[162]. The muscle tissue scaling for the scapula is heavily dependent on velocity and the standard error on the scaling ratio can be approximated by Equation 31.

$$\boldsymbol{SE = 6.90 * 10^{-6} v^2 - 6.29 * 10^{-3} v + 1.99}$$

Equation 31: Approximation of the Standard Error on the ratio of the muscle tissue scaling for the scapula.

Using Equation 31 and based on the data collected for the scapula (n=34), the standard deviation can be estimated by the SE multiplied by 5.83 and the 95% confidence intervals can be calculated by SE multiplied by 2.04.

The variability of the scaling parameters for the mid tibia were stated in Section 9.9.3 (95% CI= 0.52, with σ=1.28), where the ratio to muscle tissue was assumed to be velocity independent.

For the proximal tibia, Standard Error (SE) on the scaling ratio can be approximated by Equation 32.

[162] Due to limitations on calculating confidence intervals (or standard error intervals) on the second order polynomial fit, the magnitude of the error related to velocity was approximated using a linear fit to the data. The error margins (±SE) from the linear fit were then assumed to provide an approximation of the standard error on the mean prediction of the polynomial fit shown in Figure 110.

$$SE = 2.23 * 10^{-6}v^2 - 1.94 * 10^{-3}v + 0.670$$

Equation 32: Approximation of the standard error on the ratio of the muscle tissue scaling for the red deer proximal tibia.

Using Equation 32 and based on the data collected for the proximal tibia (n=18), the standard deviation can be estimated by the SE multiplied by 4.24 and the 95% confidence intervals can be calculated by SE multiplied by 2.12.

To show implementation of accounting for the variability in the retardation response using the muscle tissue scaling (Equation 30) the retardation profile for a shot through a gelatin-mid tibia physical model was calculated. For consistency with the variation in the predicted permanent cavities (Section 9.7.2), the variation on the retardation profile plotted was ±1 SD and is shown in Figure 114.

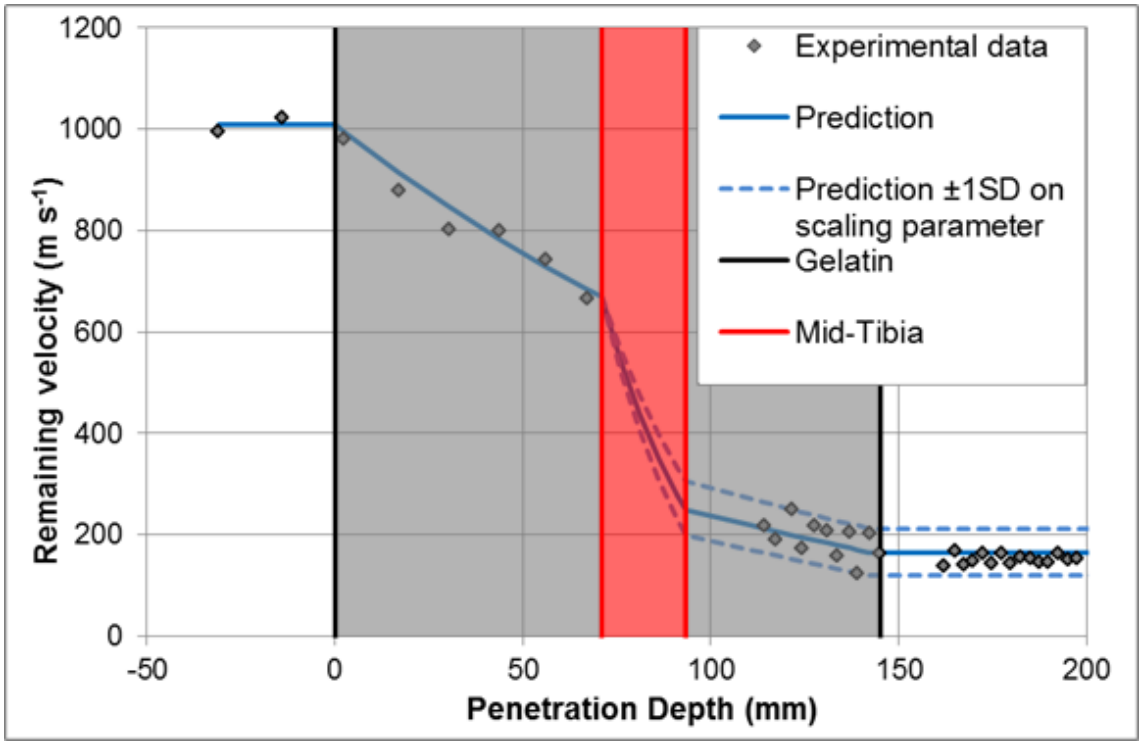

Figure 114: Comparison of experimental data for single impact with a 6 mm steel sphere penetrating the deer mid tibia in gelatin target compared to the average prediction and prediction ±1 SD on the scaling factor.

Figure 114 shows the retardation prediction through gelatin (assuming no variation) and the deer mid tibia, using ±1 SD on the scaling factor. The upper and lower bounds of the predicted exit velocity from the gelatin can be seen to be quite large in this particular example (± 47 m s^{-1}), despite the comparatively thin tibia (22 mm).

Using ±1 standard deviation to scale the muscle tissue thickness equivalence ratio may not be the best metirc to use. However, due to lack of data for predicting the variability in the permanent cavity, the standard deviation has been used to maintain consistancy.

Where the muscle tissue thickness equivelence ratio (and variability on it) are velocity dependent, both these values need to be caluclated in terms of the instantanious velocity (e.g. in a step wise manner). Appropriate choice of step size will be dependent on the instantanious velocity as well as the magnitude of the scaling factor (e.g. tissues with larger scaling factors may require smaller step sizes for an accurate prediction as the instantanious velocity will change more quickly).

Additional data to further characterise the variability of these and other tissue types in terms of the muscle tissue thickness equivelence ratio would allow the variability of all the tissues to be accounted for in the hybrid tissue model. This would allow better representation of the penetration and retardation process within shot-line models, where thousands of runs can be programmed and run to simulate the range of variables of interest.

Further limitations of these comparisons are discussed in conjunction with the comparison to muscle tissue simulants in the following section.

9.10 Penetration and retardation in tissue simulants using equivalent muscle tissue thickness scaling

9.10.1 Introduction and method

Different tissues as well as tissue simulants show different depths of penetration or retardation under otherwise equivalent impacts. In order to better understand

the suitability of different muscle tissue simulants, the simulants with sufficient experimental data available were re-analysed. This included 10% gelatin at 4°C, 20% gelatin at 10°C, Perma-Gel and Stabili-gel. The existing data detailed in Section 7 was used (Table 23 and Table 25[163]).

The DoP and retardation aspects of the muscle tissue simulant response were considered separately. This was because it would be possible for a simulant to have very large elastic recoil from its maximum temporary penetration depth, but match the required DoP behaviour. In this case the retardation behaviour would not match the desired response. Similarly, if a muscle tissue simulant was required for assessing bullets, typically only the temporary response is needed, so the permanent DoP response would not matter, as long as the retardation matched actual muscle tissue.

The same analysis procedures used for the muscle tissue variability in Section 9.9.5 were used for the tissue simulants. “Equation 24: Modified DoP prediction accounting for the effect of the skin layer” was able to specifically account for projectile geometry, making a more accurate prediction than the previous DoP comparison in Section 7.2 (using the normalised DoP over density function).

Projectiles of different densities and geometries could be used for the retardation comparison as these differences in impact conditions could be accounted for within “Equation 25: Retardation in tissue accounting for velocity loss due to the skin” (in contrast to the energy loss comparison in Section 7.3). This expanded the amount of data available on which this comparison could be based.

For ease of analysis and direct comparison to Section 7.3, the velocity loss between impact and approximately 100 mm depth were measured in the tissue simulants for the retardation comparison. The actual depth at which the residual velocity was measured was accounted for within Equation 25. This reduced the need to interpolate between frames of the HSV.

[163] The majority of the data given in Table 25 was from shots in which the permanent DoP was also measured (and detailed in Table 23).

The data for the DoP and retardation comparisons for the muscle tissue simulants is summarised in Table 37.

	DoP comparison			Retardation comparison		
Simulant	**Data points**	**Projectile types**	**Data sources**	**Data points**	**Projectile types**	**Data sources**
(Dstl) 20% gelatin at 10°C[164]	851	n=33, spheres, cylinders and CN cylinders	Section 7 and [38; 42; 58; 79; 88; 91; 122; 158; 160; 161; 165]	167	n=14, spheres, cylinders and CN cylinders	Section 7
10% gelatin at 4°C	360	n=7, all spheres	Section 7 and [19; 38; 42; 94; 122; 137; 158; 160; 162; 163; 166]	18	n=6, all spheres	Section 7 and [268]
Perma-Gel	228	n=13, spheres and cylinders	Section 7 and [38; 122; 167]	29	n=6, all spheres	Section 7
Stabili-gel (32.5% SEBS)	64	n=4, all spheres	Section 7	24	n=3, all spheres	Section 7

Table 37: Summary of the number of data points, number of different projectile types and data sources for the muscle tissue simulant comparison for DoP and retardation using the equivalent tissue thickness scaling.

9.10.2 DoP equivalent muscle tissue thickness scaling results

The data for the DoP ratios to muscle tissue for each of the 4 muscle tissue simulants are shown in Figure 115.

[164] For the DoP comparison, this is a combination of different mix methods. For the retardation comparison it is solely Dstl 20% gelatin at 10°C.

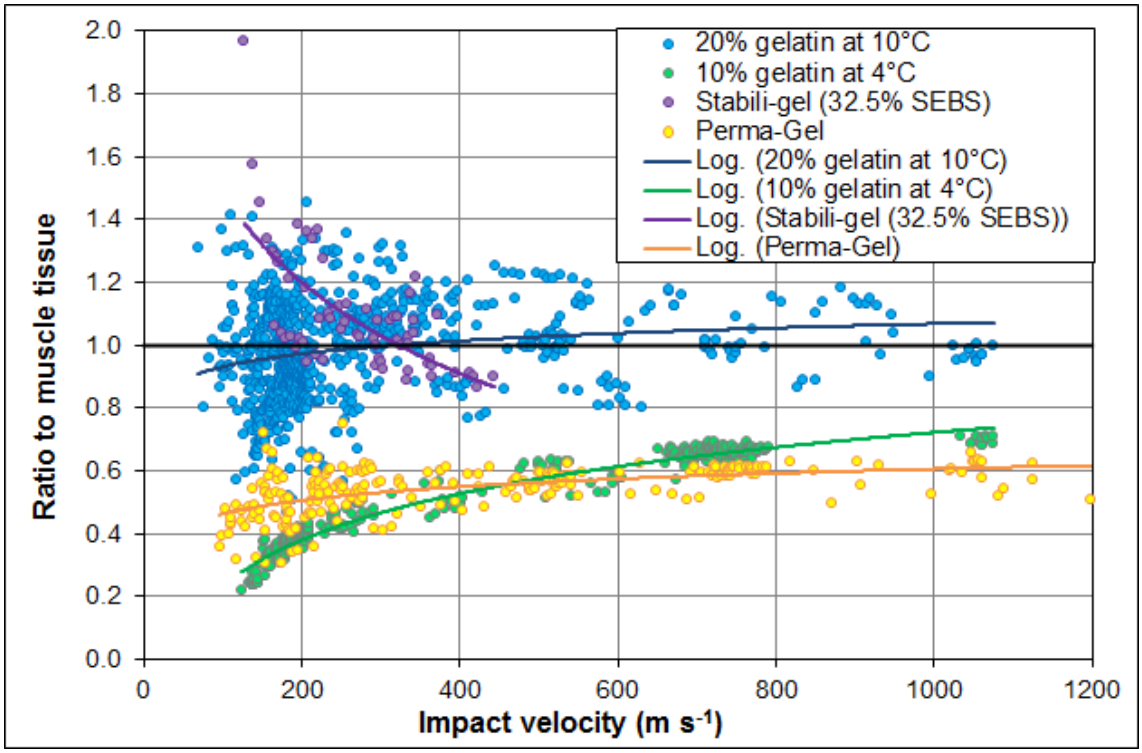

Figure 115: The DoP ratio to the prediction in muscle tissue (Equation 24) for selected muscle tissue simulants. Raw data for each simulant is summarised in Table 37.

It was found that logarithmic fits to the different target data provided the best model over the velocity ranges considered[165] and are shown in Figure 115. Based on these log fits, the average ratios in the velocity range 125–1075 m s^{-1} (the range for which there is data for most targets) for each target is given below:

- 20% gelatin at 10°C (combined mix methods) equates to between 94.4% and 107.2% equivalent thickness of muscle tissue
- 10% gelatin at 4°C (combined mix methods) equates to between 27.9% and 73.5% equivalent thickness of muscle tissue
- Perma-Gel equates to between 47.4% and 62.7% equivalent thickness of muscle tissue

[165] All fits to 20% gelatin at 10°C were poor due to there being no difference in the rate dependence to muscle tissue. For consistency, a logarithmic fit is shown in Figure 115 and the 20% gelatin at 10°C data additionally considered in terms of this rate independence.

- The Stabili-gel best fit curve is not considered reliable to make the equivalent thickness of muscle tissue comparisons due to the limited velocity range over which the data was collected. However, apart from a few data points that show high muscle tissue equivalence ratios at the lowest velocities, the Stabili-Gel DoP response is considered similar to that of 20% gelatin at 10°C in the velocity range 150-450 m s^{-1}.

Figure 115 shows that by comparing the DoP in the simulants to that predicted in muscle tissue, any rate dependence of the simulants in relation to muscle tissue is observed (e.g. deviations from a ratio of 1). The 20% gelatin at 10°C showed no rate dependence across the velocity range investigated (gradient≈0)[166], apart from very low velocities (<200 m s^{-1}) which are likely to be dominated by skin penetration effects.

In contrast, 10% gelatin at 4°C and Perma-Gel show a different rate dependence to that predicted in muscle tissue (gradient>0). The rate dependence difference between muscle tissue and 10% gelatin at 4°C is more pronounced than in Perma-Gel. This means that whilst the equivalent DoP in 10% gelatin at 4°C could be scaled to muscle tissue for simple projectiles, consideration of the impact velocity is required in order to do this.

As the 20% gelatin at 10°C showed no rate dependence, the equivalent thickness of muscle tissue for the DoP response can be expressed as 0.981±0.010 at the 95% confidence level (or 98.1±1.0% as a percentage).

The data and fit for Stabili-Gel is skewed by the few data points giving high ratios at low velocities and limited by no data above 445 m s^{-1}. It is unclear based on this limited data for Stabili-gel, how its DoP performance relates to muscle tissue over the required impact conditions.

The 20% gelatin at 10°C showed less variability than the other materials when the target response was compared to muscle tissue, despite using a much

[166] A linear fit to the 20% gelatin at 10°C showed that the gradient was significant at the 95% confidence level (P<0.01), however, the value of the gradient was only 0.0001.

greater variety of projectile types. Some of this scatter is due to the different projectiles used for each target, so is not a direct comparison.

A better representation of the variability in the target response can be seen if a single projectile type is used. The most data was available for the Cranfield 10% and 20% gelatin mixes with a 5.5 mm steel sphere [38; 122; 163; 166] and is plotted in Figure 116.

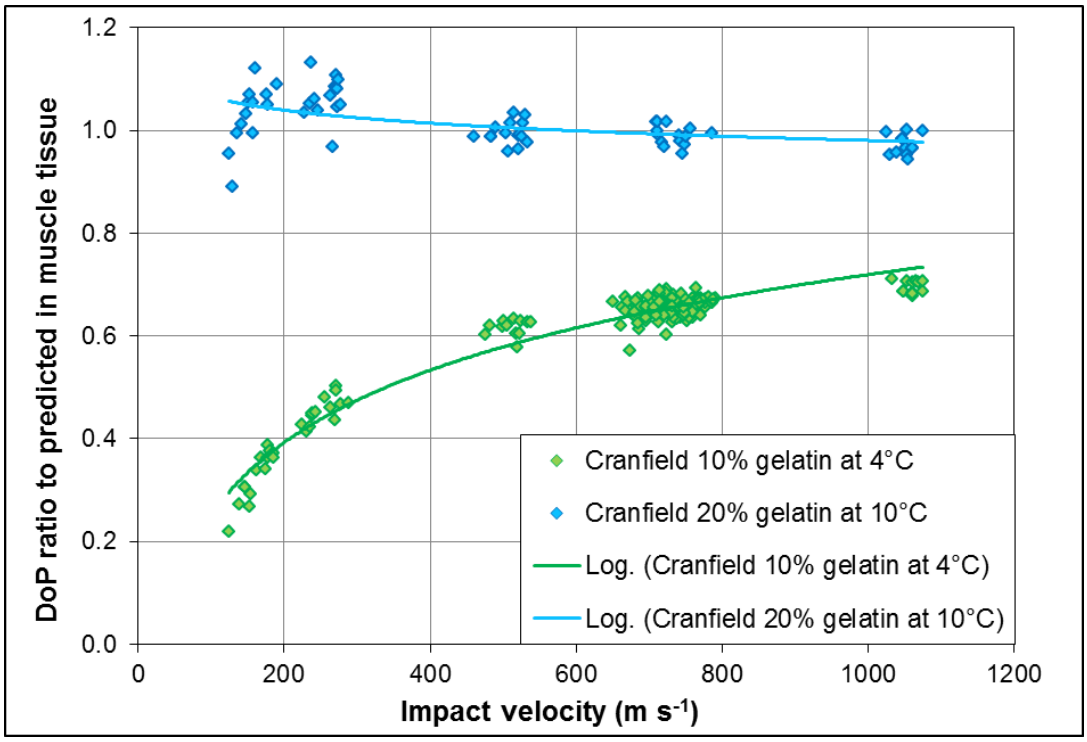

Figure 116: DoP ratio compared to muscle tissue for Cranfield 10% gelatin at 4°C, Cranfield 20% gelatin at 10°C with 5.5 mm steel spheres. Raw data was from References [38; 122; 163; 166].

Figure 116 shows low variability in both gelatin targets when the projectile related variables are minimised.

9.10.3 Retardation equivalent muscle tissue thickness scaling results

The data for the retardation ratios to muscle tissue for each of the 4 muscle tissue simulants are shown Figure 117.

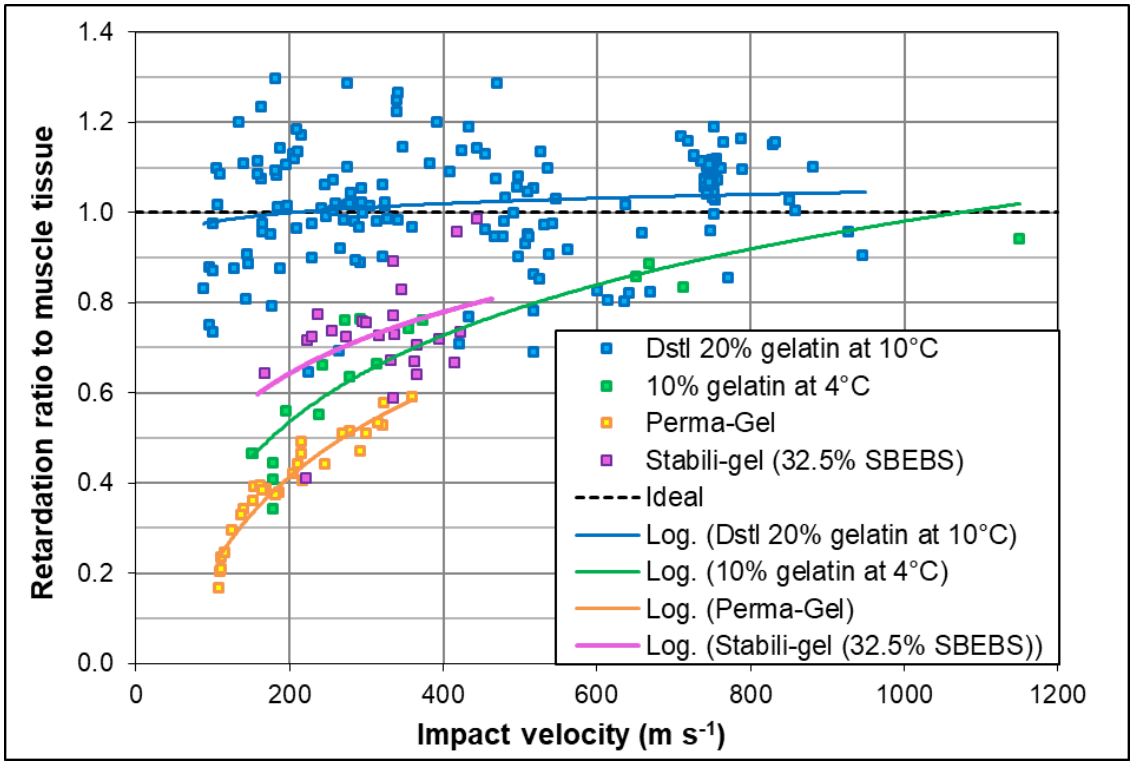

Figure 117: Retardation ratio compared to muscle tissue for Dstl 20% gelatin at 10°C, 10% gelatin at 4°C, Perma-Gel and Stabili-gel.

Figure 117 shows that Dstl 20% gelatin at 10°C provides an average response close to 1 for the retardation ratio compared to muscle tissue, across the entire velocity range. The scatter in the Dstl 20% gelatin at 10°C data appears greater than the other two simulants. This is likely due to the much greater range of projectiles used for the Dstl 20% gelatin at 10°C (see Table 37).

As for the DoP comparison in Figure 115, 10% gelatin at 4°C and Perma-Gel both greatly under-estimate the retardation predicted in muscle tissue. Additionally, the Stabili-gel greatly under-estimates the retardation predicted in muscle tissue even though it approximated the DoP response.

The comparison for the Perma-Gel and Stabili-gel response are limited by the data available (velocities up to 360 m s^{-1} and 445 m s^{-1} respectively). It should be noted that the retardation ratio for the Stabili-gel was collected with a sub-optimal experimental setup; therefore the scatter in the resulting data is considered more likely to be from experimental error in accurately tracking the projectiles in the HSV, rather than inherent variability of the Stabili-gel itself.

At very high velocities (approximately 1000 m s^{-1}) the retardation ratio for the 10% gelatin at 4°C approaches 1. However, the fit is being driven by very limited data point at those high velocities, so does not provide much confidence in the outcome.

A log fit was applied to the Dstl 20% gelatin at 10°C data in Figure 117 for consistency to the other simulants and to Figure 115. However, as with the 20% gelatin at 10°C DoP data, there was no difference in rate dependence to that predicted in muscle tissue. A linear model showed that the gradient was not significant at the 95% confidence interval (p=0.083) and the relationship can be treated as velocity independent. The retardation ratio of Dstl 20% gelatin at 10°C compared to muscle tissue can be given as 1.018±0.019 at the 95% confidence level (or 101.8±1.9% as a percentage).

9.10.4 Discussion of equivalent muscle tissue thickness scaling for muscle tissue simulants

In order to compare the DoP and retardation ratios side-by side for real muscle tissue and the tissue simulants, the best fit curves from Figure 113, Figure 115 and Figure 117 have been plotted in Figure 118.

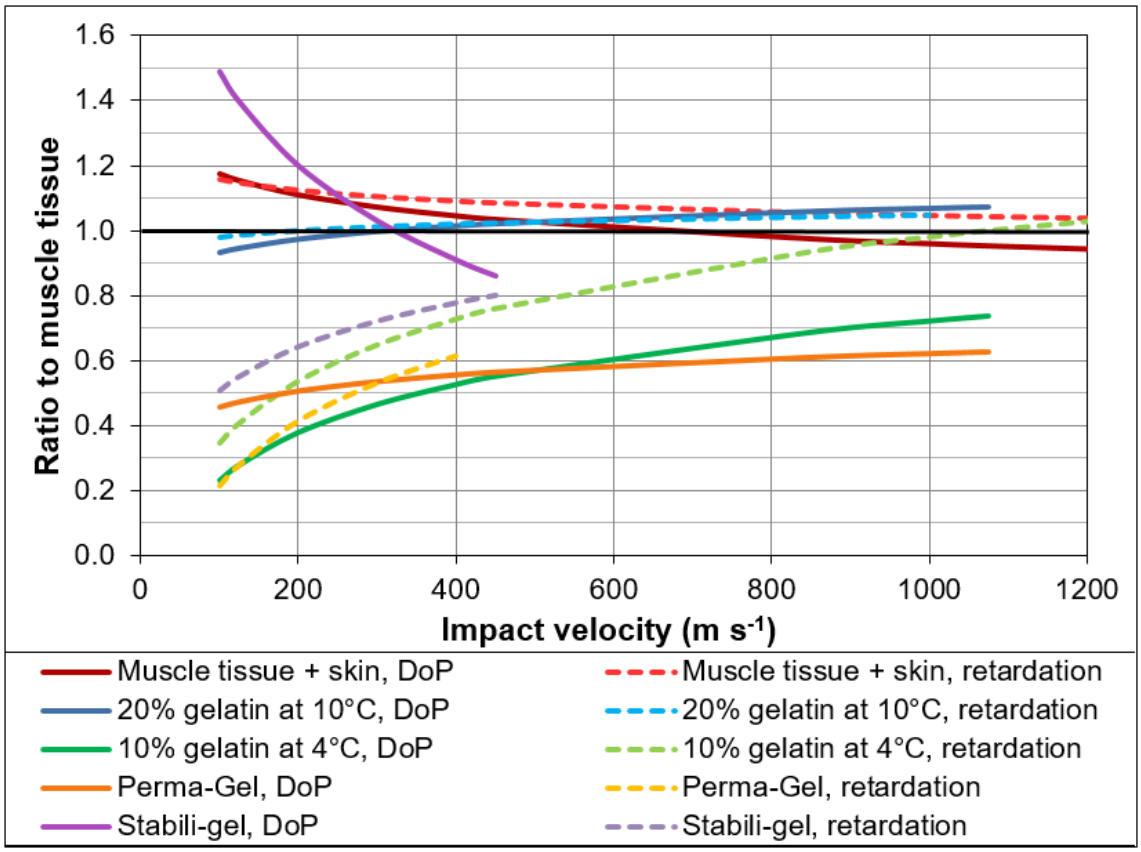

Figure 118: Best fit lines for the DoP and retardation ratios compared to the predictions for skin and muscle tissue (Equation 24 and Equation 25). Targets shown are real muscle tissue (with skin, live and dead), 20% gelatin at 10°C, 10% gelatin at 4°C, Perma-Gel and Stabili-gel (32.5% SEBS).

The black line in Figure 118 for the ratio to muscle tissue=1 shows the ideal predicted response of muscle tissue with skin.

Evident from Figure 118 is that (Dstl) 20% gelatin at 10°C[165] provides a very good response for both DoP and retardation ratios across the entire velocity range considered.

Figure 118 also shows that Equation 24 and Equation 25 provide a good, but not ideal prediction for the penetration or retardation in muscle tissue and skin. At low velocities this discrepancy is largest, where (on average) muscle tissue is not penetrated or does not retard projectiles as much as is predicted. Part of this discrepancy may be due to the scatter in the experimental data and practical limitations with DoP testing at high velocities (due to target thickness limitations).

Figure 118 shows that the 10% gelatin at 4°C and Perma-Gel ratios have reversed between the DoP and retardation responses compared to each other. The elastic response of the Perma-Gel and Stabili-gel shows the importance of assessing the simulants with respect to their end use: DoP and/or retardation response, as well as at a representative velocity.

For a projectile of constant mass and given impact velocity, then the retarding force on the projectile will be directly proportional to the deceleration in the target (force equals mass times acceleration).

Differences in the retarding force may dictate different projectile responses. For bullets this may mean differences to the tumbling, deformation or fragmentation behaviour. Consideration of how these forces differ in muscle tissue and simulants must be considered. Projectiles with an impact velocity in the range 100 - 1000 m s^{-1} in (Dstl) 20% gelatin at 10°C are likely to give a response representative of the (predicted or average) behaviour of muscle tissue for both DoP and retardation, but not if using 10% gelatin at 4°C.

For assessing low velocity impacts (e.g. below 200 m s^{-1}), a physical tissue and skin simulant would be better suited to achieve the correct response of muscle tissue with skin (as per Section 8), rather than a bare muscle tissue simulant.

These issues can be applied when considering the scaling to other tissue types (Section 9.9). The projectile response needs to be considered before simply applying the scaling laws for the different tissue types. This will be most pronounced for tissues with very different retardation to muscle tissue, such as bone.

Combining the DoP and retardation data, the ratio of 20% gelatin at 10°C compared to muscle tissue was 0.987±0.009 at the 95% confidence level (or 98.7±0.9% as a percentage), based on a velocity independent relationship (for n=1018 shots). Table 22 in Section 7 provides details of the variety of projectile properties used for Dstl 20% gelatin at 10°C that can be used to define the validation bounds of this assessment.

Whilst these outcomes on the suitability of the tissue simulants agree with the permanent DoP comparison (using the normalised DoP over density function) in Section 7.2 and the energy loss comparison in Section 7.3 (although limited for 10% gelatin at 4°C), the main benefit of the comparison in Figure 115 is that the tissue simulant performance is given as a direct function of the (validated) average muscle tissue (and skin) response. It allows the force on the projectile to be estimated in comparison to what would be expected in muscle tissue. This method can account for different projectile properties as well as shots that are retained in the target or fully perforate, for any target thickness, as long as the exit velocity is known and the projectile does not deform or tumble. This maximises the available data on which to base comparisons of tissues and tissue simulants.

The limitations of the comparisons (and the equivalent in Figure 113 for the real muscle tissue data) are:

- Residual velocity measurements were made at nominal 100 mm depths in the simulants and the ratios related back to the impact velocity. A more accurate representation for calculation of the retardation ratios may be to use instantaneous velocity.
    - The velocity loss over small penetration distances throughout the target thickness may be a more logical approach to maximise the data available from each target account for the instantaneous velocity. However, as the (Dstl) 20% gelatin at 10°C showed the same rate dependence as muscle tissue, it is unlikely that this different analysis approach would alter the conclusions drawn around the suitability or validation of the 20% gelatin at 10°C.
- Skin perforation V_{50}s for the muscle tissue data were based on a simplified prediction (all expanded parameters in Equation 8 set to 1). This may partially explain some of the scatter in the muscle tissue DoP and retardation data at the lower velocities.
- Retardation ratios for real muscle tissue and skin only accounted for the effects of skin on impact, not on exit.

- The DoP data in Figure 113 for impacts over 700 m s^{-1} was exclusively for steel cylinders ≤0.2 g. Target thickness will always limit the DoP data that can be generated at higher velocities, particularly for more massive projectiles of the types considered here.
- It cannot account for projectiles that tumble, deform or fragment: data for bullets cannot be included.
- Data were combined from different mix methods for both the 10% gelatin at 4°C and the 20% gelatin at 10°C. This may influence the local precision of any result, but not the overall comparison and conclusions, apart from potentially adding to the variability.

9.11 Exploitation of FREMs

All of the equations (or variants of them) in Sections 9.2 through 9.8 to describe penetration, retardation, cavity formation and tissue damage have been implemented in the UK MOD V/L shot line model; the Human Vulnerability Tool within the Weapon Target Interaction (WTI) architecture [32].

The Human Vulnerability Tool is used "*to provide the evidence base for decision making … for dismounted infantry, vehicle crew and mounted troops… required by the UK Ministry of Defence to inform policy, procurements, operational risk and thereby improve the survivability of personnel*" [32].

An example of the representation of the human geometry within the WTI shot-line model is shown in Figure 119 and an example of the grid output of injury severity from a number of runs through the model is given in Figure 120.

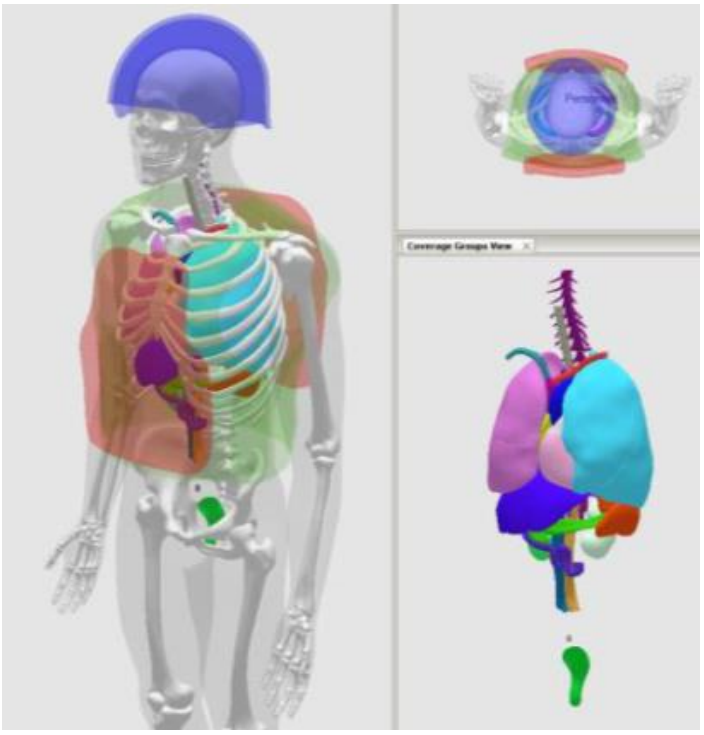

Figure 119: Representation of the human geometry within WTI with selected internal organs and body armour shown. Images from Reference [32]

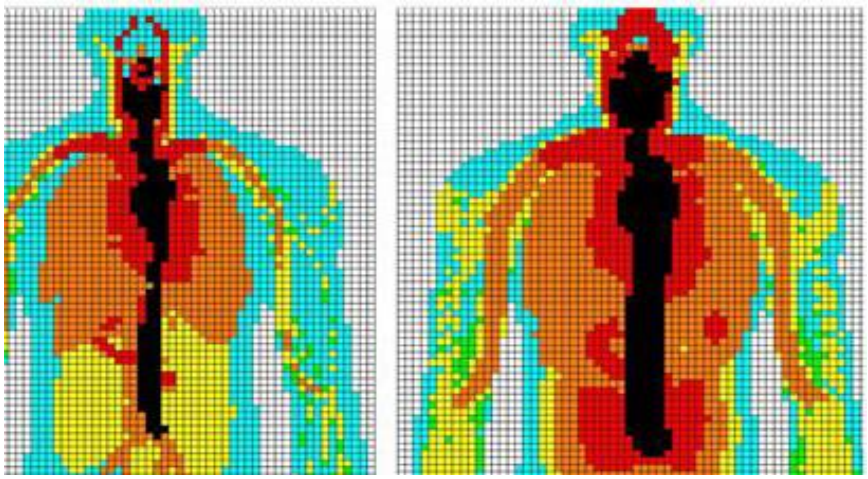

Figure 120: Example grid output from a large number of runs through the WTI model for 2 different impact conditions. Different colours indicate different predicted injury states (blue=lower severity, black=maximal severity). Image from Reference [32]

The hybrid tissue retardation model could also be implemented into shot line models, such as WTI, to enable vulnerability or lethality assessments. This would aid comparison or optimisation of PPE. However, how the hybrid tissue

retardation model could be applied to tumbling or deforming projectiles requires careful consideration. Implementation of these equations within shot-line models is outside the scope of the thesis, but shown only to illustrate potential applications of the models developed.

Simplified versions of the retardation equations from Section 9.3[167] as well as the probability of eye penetration and skin perforation equations (Equation 1, Equation 9 and Equation 11) have been implemented in the UK MOD Collateral Damage Model (CDM). The CDM is used during operations to aid commanders' decisions on the potential collateral damage from indirect fire and air-dropped weapons. These equations enable the CDM to provide casualty estimates based on the onset of likely penetrating injury from fragments.

As well as direct exploitation of the FREMs, a number of softer exploitations have also been realised, based on the improved understanding of the penetration process through these equations and associated physical testing. As this improved understanding and exploitation has come from a combination of different sections within the thesis, they are brought together and summarised in the Discussion section.

[167] Simplified to the specific scenarios being considered within the Collateral Damage Model to optimise fast run time of the model.

10 Development of a physical model for penetrating injury by multiple discrete projectiles

10.1 Multiple Discrete Fragment Physical Injury Model (MDFPIM)

10.1.1 Model requirement

For (outdoor) trials involving explosive threats producing fragmentation there may be a requirement to assess the injury potential of the fragments generated. Using the typical muscle tissue simulants such as gelatin in these scenarios is often impractical. This is due to the fact that often large areas need to be assessed, multiple fragments are generated and simple analysis is required. On top of this temperature dependence of gelatin further restricts its practicality for this type of application.

Instead of a gelatin-like tissue simulant, layered fragment witness packs are used instead. These witness packs capture the fragments and then analysis of the number of layers perforated, along with fragment mass can be used to back calculate impact velocities. Different fragment witness packs are available for different types of fragment, however it has been found that the existing witness packs are unsuitable for non-metallic (and/or low density) and low energy fragments (i.e. typical secondary fragments).

The development of the witness pack in this thesis was initiated following attempts to use other materials and models to investigate the risk of fragments from buried explosive devices were unsuccessful. Short descriptions of each of these attempts are given below.

Limited success was shown using 20 layer strawboard packs at 1 m from buried anti-personnel mines, comprising of 50 to 500 g of high explosive. "*The stones break up during an impact so it is not relevant to measure their depth of penetration. An alternative is to measure the maximum depth over which the strawboard is permanently deformed*" [269].

Five layer strawboard packs (each layer nominal thickness 3.81 mm) were used to try to observe penetrations by fragments generated from buried Home-Made Explosive (HME) devices. Packs were placed 2 m from a 10 kg device, which was buried 300 mm in the soil. Two firings were conducted and in both cases, the packs showed evidence of being impacted, but there were no embedded fragments and no perforations of the first strawboard layer. At the location of these strawboard packs, subject matter expert opinion was that an unprotected person standing at that location would have suffered severe soft tissue injury.

Metal spaced witness packs, constructed to Reference [270], have also been used for similar applications, but with the material specifications changed to:

- 1 mm aluminium BS EN 485-2 [271] 1050A, 1050 Aluminium Vinyl Coated, temper H14, Thickness tolerance ± 2%.
- 1.5 mm Mild steel CR4 to BS 1449-1.1:1991 [272], Thickness tolerance ± 2%.
- 25 mm Polystyrene to BS 3837-1:2004 [273].

In this case, a pack 2 m tall and 0.5 m wide was placed at 1.5 m from a 5 kg HME device buried to 300 mm. After the blast, the pack showed evidence of impacts and some dents, but no perforations of even the first aluminium layer. Again, subject matter expert opinion was that an unprotected person standing at that location would have suffered severe soft tissue injury.

In an attempt to have a material that could be easily penetrated, a witness pack based on expanded polystyrene was used for a range of buried HME tests. This pack was constructed from 10 layers of 10 mm polystyrene-divinyl benzene (SDVB) at a density of 15 kg m^{-3}, backed with two layers of 1 mm aluminium 1050A, each separated by 10 mm SDVB. Whilst it was penetrated by the fragments, there were several major issues with this pack: it was overly easy to penetrate, was frangible and was frequently massively disrupted during the blast, preventing meaningful analysis.

A comparison of the velocities required to perforate the first layer of these models[168] to PMHS skin (Equation 8[169]) and PMHS eyes (Equation 11) is given in Figure 121.

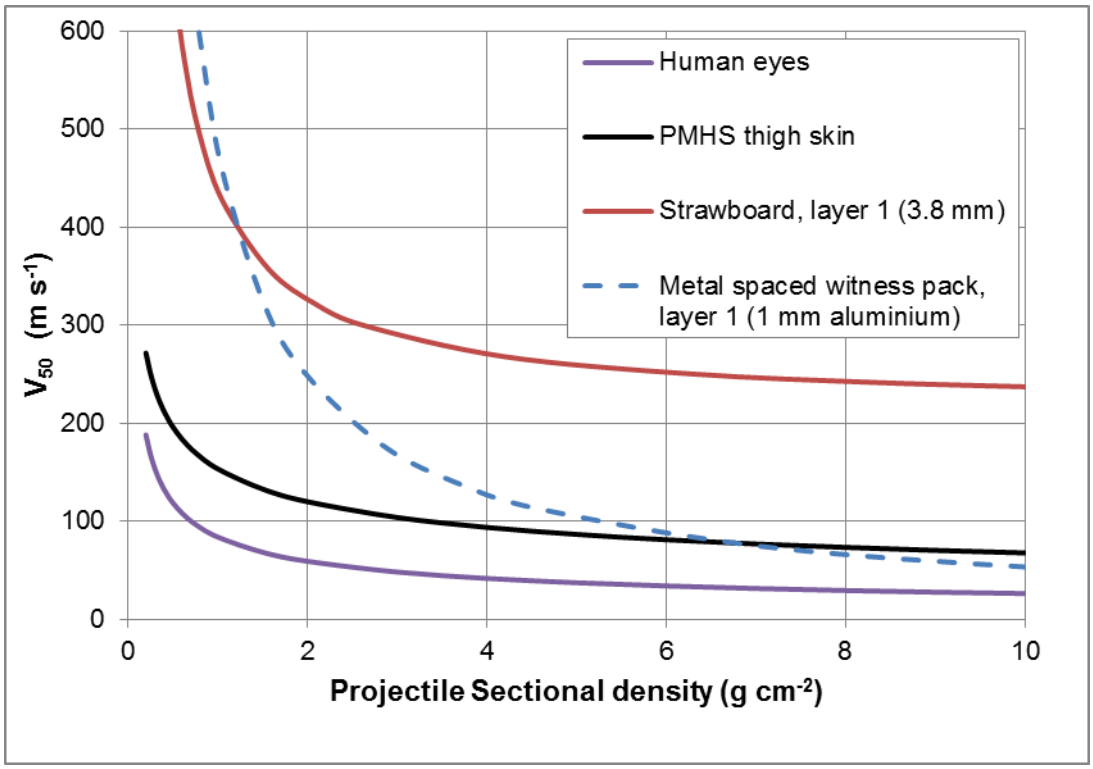

Figure 121: Comparison of the predicted perforation velocities for strawboard layer 1, metal spaced witness pack layer 1, PMHS eyes and skin.

Figure 121 shows the regions where strawboard (Reference [274] type D, 3.8 mm thick) or the metal spaced witness pack [270] will not allow assessment of potentially injurious fragments. Layer 1 of strawboard requires approximately 3 times the velocity required to perforate skin before it is perforated. The metal spaced witness pack is very dependent on the fragment sectional density as to whether the velocity to perforate layer 1 is much higher, or similar to that required to perforate PMHS skin.

[168] Strawboard was to Reference [274] type D. The metal spaced witness pack (layer 1) velocities were based on Reference [270].
[169] PMHS skin on the thigh, intact, perforation V_{50} by probit method and a spherical or pointed projectile

10.1.2 Model definition

A new model, the Multiple Discrete Fragment Physical Injury Model (MDFPIM) was designed to allow a prediction of injury risk from multiple projectiles that are spatially separated (i.e. where the mechanical damage caused by each fragment is independent of the others). This fragment pattern, that provides a more realistic testing regime than the use of a single FSP, could be generated within a ballistic range or arena style tests.

This model was developed to address the gap for non-metallic projectiles (considered particularly relevant to secondary fragments from IEDs; applicable to both the military and from terrorist incidents) and low velocity metallic projectiles.

The model was based on a layered pack system where the number of layers perforated along with the mass of the projectile allows the impact velocity to be estimated for each penetrating projectile.

The model was required to have a penetration response similar to, or providing deeper penetration depths to muscle tissue such that any potentially injurious penetrating projectiles would not be artificially discounted by the model.

It was intended that this model could also be used as a backing during PPE testing, such that penetrating injuries resulting from the overmatch or failure of the protection can be assessed.

The initial development of the MDFPIM V1.0 and V1.1 was conducted by the author prior to the registration of this PhD. The details of the development of the MDFPIM V1.0 and 1.1 are included for background information to the current MDFPIM V2.0, 2.1 and 2.2.

10.2 MDFPIM V1.0

10.2.1 Model development and material selection

Following the use of the polystyrene witness pack in arena trials that fractured during blast test, other, non-frangible materials were considered with an additional aim of providing a similar penetration response to animal muscle tissue data.

The Home Office Scientific Development Branch / Centre for Applied Science and Technology knife stab test composite backing pack [275; 276] (consisting of different thickness and density foam and rubber layers) was not considered for this application due to its composite structure which would not be expected to provide a linear DoP response.

Nine different material combinations were evaluated, including a selection of low, medium and high density SDVB, a cast silicone and a selection of foams. The materials used, along with basic properties are given in Table 38.

Retarding material	**Layer thickness (mm)**	**Nominal density (kg m^{-3})**
Low Density (LD) SDVB	15	10
Medium Density (MD) SDVB	10	15
Medium Density (MD) SDVB	15	15
High Density (HD) SDVB	10	20
High Density (HD) SDVB	15	20
Closed cell neoprene foam	9.5	160
Closed cell silicone foam	10	200
Closed cell polyethylene foam (Plastazote)	10	45
Cast silicone sheet (Dragon Skin®)	10	1080

Table 38: Materials for initial pack down selection

All packs were constructed to 300 mm width, 500 mm height and used between 4 and 10 layers of the selected retarding material, with 62.5 µm (250 gauge) thick polythene sheeting between each layer to act as a witness.

The packs were impacted with individual fragments (3, 6 and 9 mm steel spheres and 3, 6.35 and 20 mm glass spheres) over the velocity range 30 to 500 m s^{-1}. Impacts were conducted into each pack, ensuring the impact location was distant from previous shots. A pack of each material was also simultaneously impacted by 20 g of 3 mm steel spheres (approximately 175 in number) at an average of 115 m s^{-1} to ensure it would hold up against simultaneous penetrations and the pack could be subsequently analysed.

Projectiles were fired using the Honed Tube Pressure Housing weapon system, with a separate smooth bore barrel for each different diameter projectile. The projectiles were propelled using rechargeable 37 mm compressed Airmunition cartridges [277], with pressures of 3 to 20 MPa.

Projectile velocities were measured using two pairs of Oehler Model 57 Infrared Ballistic Screens [207], with 1 m separation within each pair, connected to an AMOtronics Saturn System 120 series oscilloscope at 3 MHz sample rate.

Analysis of the number of layers of the polythene sheeting perforated for each shot was converted into a discrete DoP into the pack (number of layers perforated times individual layer thickness). That was then converted into the Normalised DoP over density function (described in Section 4). This enabled comparison to existing animal perforation data (Section 7.2.3, Equation 12).

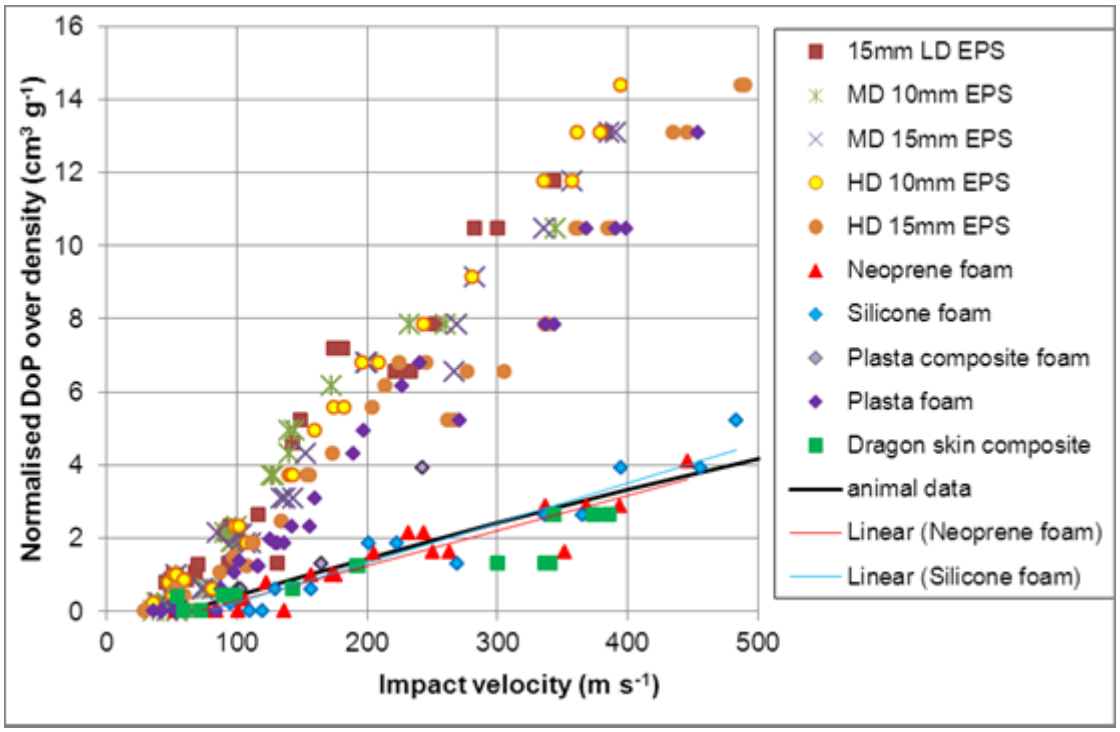

Figure 122: Raw penetration data for the materials[170] evaluated in comparison to the averaged animal data. Animal data performance based on Equation 12.

[170] LD – Low density. MD – Medium Density. HD – High Density. EPS – Expanded PolyStyrene

Three materials were found to give a good match to the animal penetration data (from Section 3.9), as shown in Figure 122. One of these was dismissed due to production time and thickness variability of the material (the cast silicone Dragon Skin®).

Out of the two remaining materials (neoprene and silicone closed cell foams), both were found to have no statistically significant difference to the animal perforation data at the 95% confidence level (in terms of a comparison of their best fit lines over the velocity range investigated).

The closed cell neoprene foam was chosen as there was more data from this initial testing and the material was readily available and specifiable (in terms of its mechanical properties).

10.2.2 Model construction

The MDFPIM V1.0 is based on 10 mm thick neoprene closed cell foam sheets (mechanical properties are in APPENDIX J) inter-wound with 62.5 µm (250 gauge) polythene sheeting, with a double layer on the front. The diagram below shows the layer numbering for the polythene sheeting and the black rectangles represent the neoprene foam.

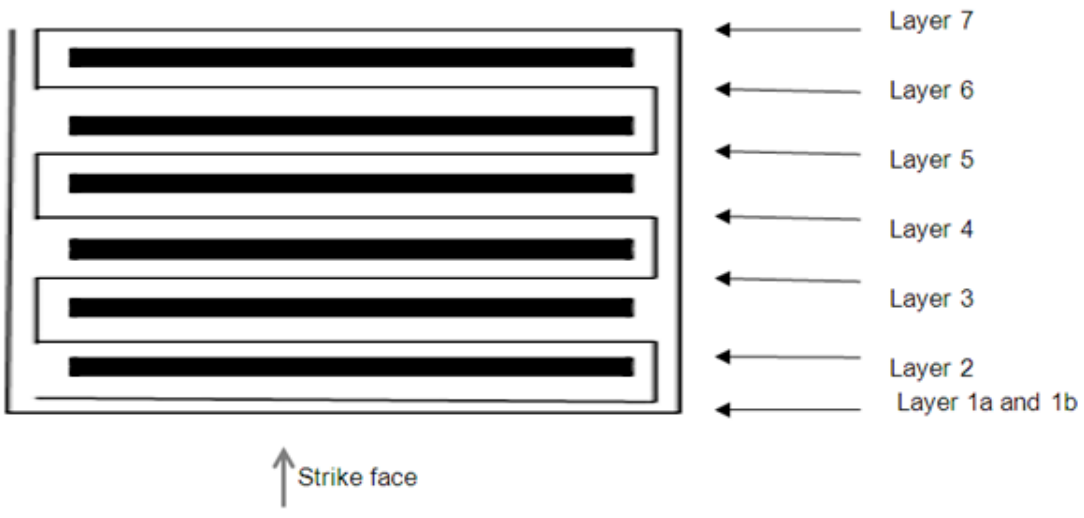

Figure 123: Diagram of MDFPIM V1.0 construction showing numbered layering of the polythene between the neoprene foam layers (not to scale).

10.2.3 Calibration of MDFPIM V1.0

Calibration was conducted on a pack with 6 layers of the neoprene foam and polythene sheeting.

The calibration was conducted with 3, 6 and 9 mm steel spheres, 3 mm and 6.35 mm glass spheres over the velocity range required to bracket no penetration up to full penetration of the pack, with an average of 25 shots for each projectile. A total of 132 valid shots were completed, allowing calculation of 27 V_{50} velocities for different fragment and layer combinations. A V_{50} calculation gives a better statistical representation of the penetration data, which would otherwise be very sensitive to the velocities of the shots conducted during the experiment if raw data was used to construct the calibration relationship (and would appear to have steps in velocity at higher normalised DoP over density values).

The model was calibrated whilst backed 25 mm around its periphery (e.g. as a frame). Figure 124 below shows the V_{50} velocity required to perforate each layer, converted into the normalised DoP over density. All the points agree well to a linear fit with an R^2 of 0.970.

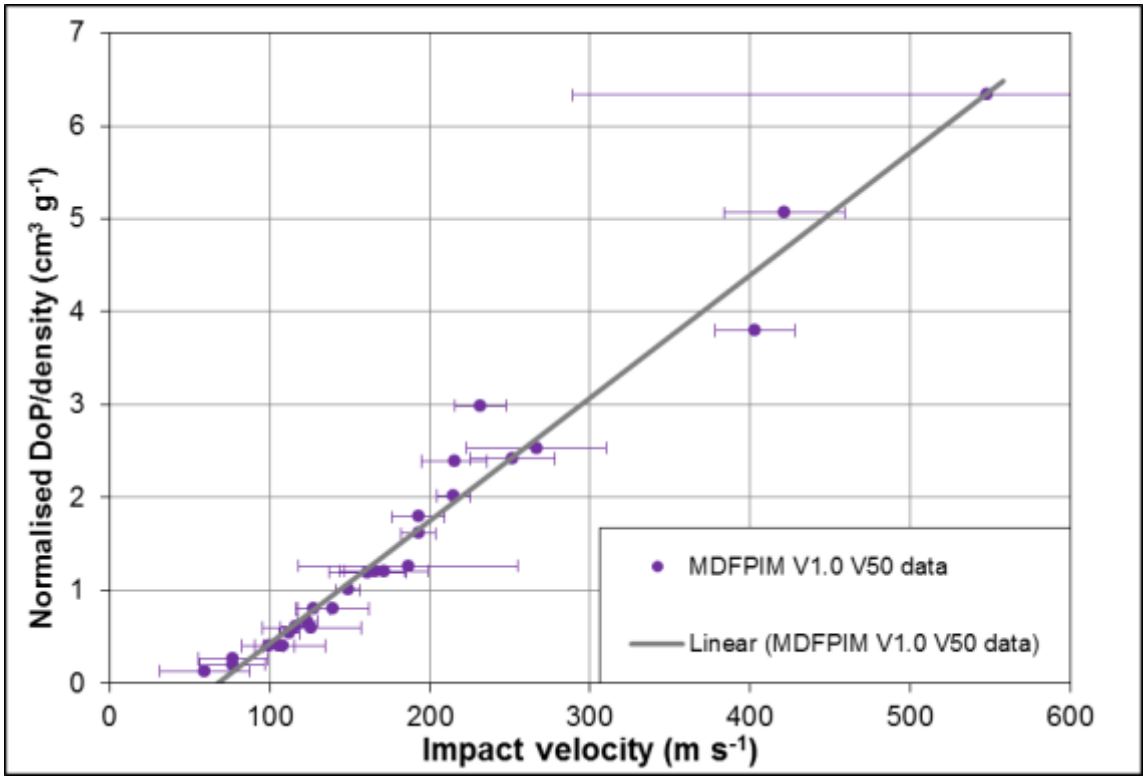

Figure 124: Calibration of the MDFPIM V1.0 showing the V_{50} velocity against normalised DoP over density using 3, 6 and 9 mm steel spheres and 3 and 6.35 mm glass spheres.

The large confidence interval on the highest V_{50} shown in Figure 124 was due to it being at the limit of the weapon capability, not allowing the desired velocities to be achieved in order to improve the confidence interval, rather than large variability in that data point.

The velocity required to perforate layer 2 of the MDFPIM was found to be within the scatter of the skin perforation data for PMHS, goat and sheep values, over the range of projectiles used in the calibration. This means any projectiles not perforating through layer 2 are not likely to be injurious and can be ignored. The model is unlikely to miss capturing any injurious projectiles that hit the pack.

10.3 Development of MDFPIM Version 1.1

10.3.1 Introduction

The MDFPIM V1.0 was used in some blast trials and showed instances where the pack had been fully perforated[171]. The MDFPIM was modified (to version 1.1) to ensure that the new V1.1 model was less likely to be overmatched compared to the V1.0, when deployed in a variety of different blast trials.

A ballistic trial was conducted to calibrate a thicker version of the MDFPIM (designated V1.1), such that it could capture higher velocity fragments without being completely perforated, compared to the previous version (V1.0). If the model was completely perforated, the impact velocity estimation cannot be performed, as the necessary information is not captured. An additional change was to use a rigid backing for improved practicality.

10.3.2 Model overview: MDFPIM V1.1

The following changes were made to the model:

- The number of neoprene layers increased from 6 to 9.
- The last neoprene layer had an additional piece of strawboard[172] in front of the neoprene.
- The completed model was held in contact with a rigid backing during the testing.

The MDFPIM V1.1 construction is shown in Figure 125, with the polythene sheet interleaved between each neoprene foam layer and the strawboard layer shown in grey. As shown in Figure 125, the layer numbering is based on the polythene sheeting.

[171] Given that the pack was perforated, the fragment was not retained and therefore the corresponding impact velocity could not be estimated. It is not known what degree of overmatch occurred.

[172] Conforming to Reference [274] type D

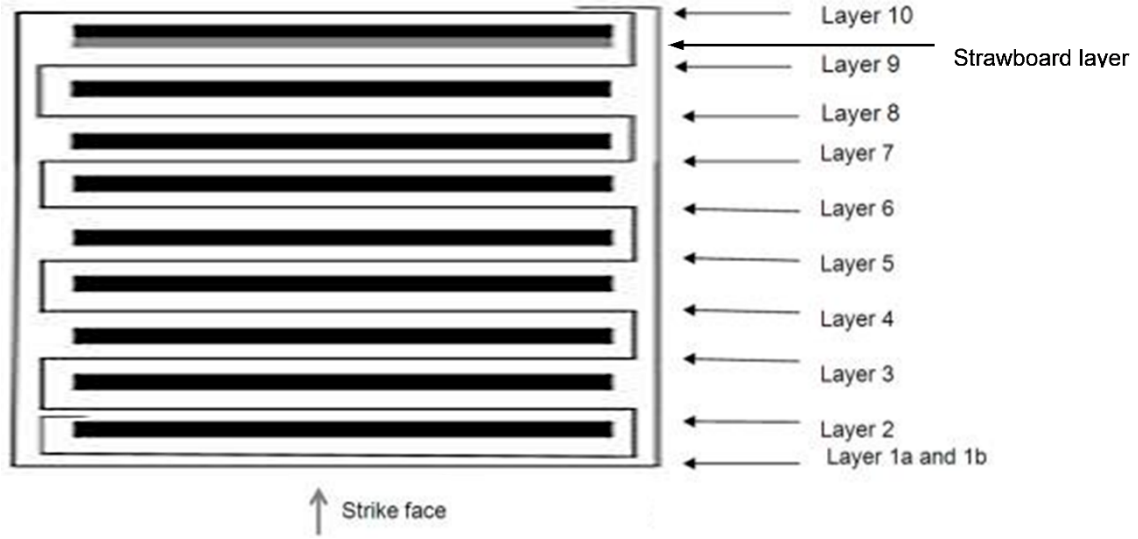

Figure 125: Diagram of MDFPIM V1.1 construction (not to scale).

The last neoprene-strawboard layer should help retain some of the faster projectiles, allowing their recovery and comparative analysis.

10.3.3 Calibration method for MDFPIM V1.1

The same projectiles used to calibrate the MDFPIM V1.0 were used for the calibration of the MDFPIM V1.1[173], with the addition of a 1 mm steel sphere (0.004 g).

All projectiles except the 1 mm steel spheres were fired using the Honed Tube Pressure Housing weapon system, with a separate smooth bore barrel for each different diameter projectile. The projectiles were propelled using rechargeable 37 mm compressed Airmunition cartridges [277], with pressures of 3 to 20 MPa.

The 1 mm steel spheres were fired using the Sabre Ballistics gas gun using sabots in a 7.62 mm calibre rifled barrel, and propelled using compressed helium up to pressures of 30 MPa. Details of both weapon systems are given in APPENDIX B.

[173] A 6 mm glass sphere was used in place of the 6.35 mm glass sphere.

Projectile velocities were measured using two pairs of Oehler Model 57 Infrared Ballistic Screens [207], with 1 m separation within each pair, connected to an AMOtronics Saturn System 120 series oscilloscope at 3 MHz sample rate.

Projectiles were fired one at a time with at least 50 mm spacing between impact locations. Impacts were conducted over a range of velocities for each projectile type, from as slow as possible as was achievable with the system, up to full perforation of the pack (or the maximum velocity achievable if full perforation could not be achieved). After the firings had been completed, the MDFPIM V1.1 was dismantled, and the maximum number of layers perforated was recorded for each shot.

10.3.4 Calibration results for MDFPIM V1.1

To allow comparison of the penetration of the MDFPIM V1.1 for all the projectiles used, the layers of the pack perforated were converted to the normalised DoP over density. Only perforations up to and including layer 8 for the MDFPIM V1.1 have been included (due the step change in materials and use of a rigid backing).

A total of 131 shots were completed across 6 projectiles, allowing 28 V_{50} velocities for different fragment and layer combinations to be calculated.

The normalised DoP over density against velocity graph is plotted for all the results for the MDFPIM V1.1 calibration in Figure 126.

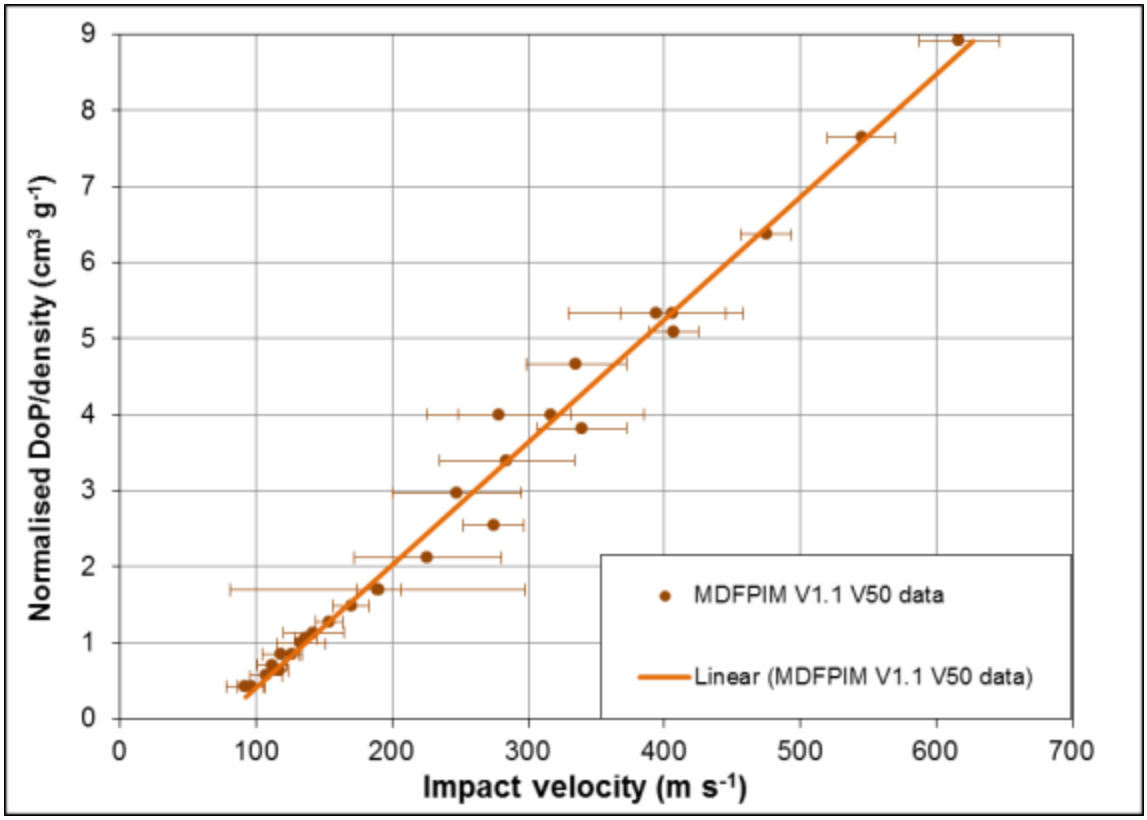

Figure 126: MDFPIM V1.1 normalised DoP over density calibration.

When all the projectiles are plotted with a linear regression line as shown in Figure 126, it gave an R^2 value of 0.988.

The changes to the MDFPIM V1.1 make the model easier to use in a blast trial, due to the thicker pack and option for a rigid mounting method.

10.4 Development of MDFPIM Version 2.0, 2.1 and 2.2

10.4.1 Introduction

Limitations of the MDFPIM V1.0 and 1.1 included that all injury assessments required back calculation of fragment velocities from their DoP and recovered mass. This restricted the results that could be determined immediately following a test as the analysis process could be resource intensive.

The MDFPIM was modified to allow direct estimations of the risk of eye injury (corneal abrasion and eye penetration) and skin perforation in addition to (as for

the V1.0 and V1.1) estimating impact velocities based on fragment mass and penetration depths into the pack.

10.4.2 Modifications to the physical model

The MDFPIM V1.1 was modified, with the construction detailed below and shown in Figure 127.

- 9 layers of neoprene closed cell foam, each 10 mm thick, density 160 ± 10 kg m^{-3}. The specification for the foam is given in APPENDIX J.
- The last neoprene layer had an additional piece of strawboard, conforming to Reference [274] type D, in front of the neoprene[174].
- 62.5 µm (250 gauge) thick polythene sheeting is placed between each layer to act as a witness, with a double layer over the impact face[175].
- A layer of layer of 23 ± 2 µm polyester-film, with polyacrylate adhesive on both sides of the film[176], applied directly to the strike face.

This modified version of the MDFPIM was referred to as the MDFPIM V2.0.

[174] This is to give the pack some extra rigidity and to stop some fragments that would otherwise completely perforate the entire pack and therefore be lost. For all development work, a nominal 3.75 mm thickness strawboard was used.
[175] Can be black or transparent as required by the user and analysis process used
[176] Product ‘gudy 802’, supplied by Neschen AG, Germany

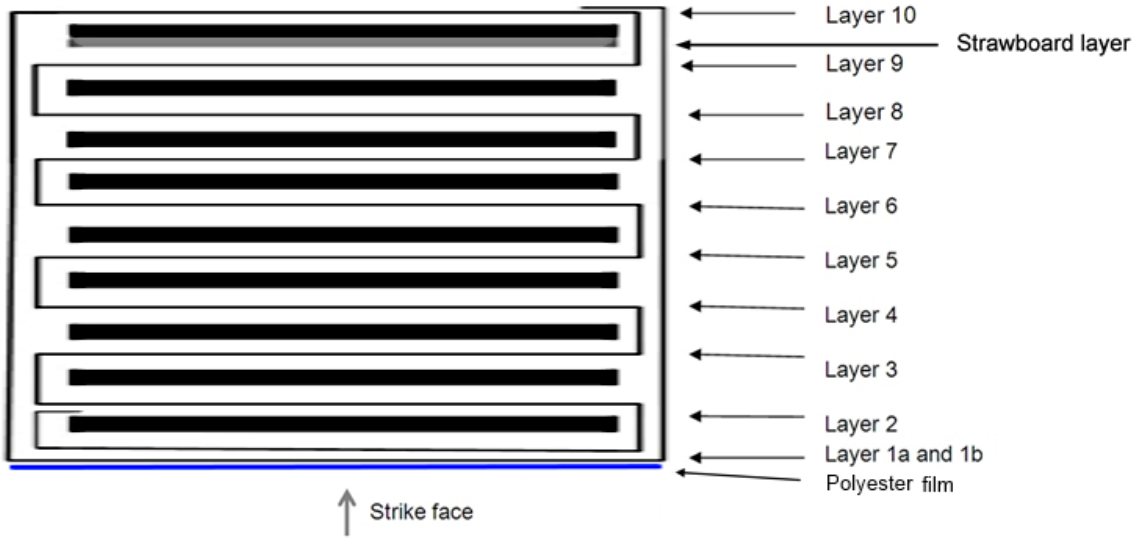

Figure 127: MDFPIM V2.0 construction (not to scale).

The MDFPIM V1.0 and V1.1 were designed to allow injury assessment or back calculation of velocity following an impact from a penetrating fragment. The multiple layers used in the pack to allow these calculations and this aspect is retained. For assessment of eye injuries, the additional layers may not always be required, depending on the requirements of the testing, but are integral to the MDFPIM V2.0 and calibration.

A second model variant was based on a thin version of the MDFPIM V2.0 described above. This was to allow a model to be used where only eye penetration or skin perforation assessments are required, but still providing the same model response and reducing material requirements. The thin version (named MDFPIM V2.1) had 3 layers of the neoprene foam, with 62.5 µm (250 gauge) thick polythene sheeting between each layer with a double layer over the impact face. The 23 ± 2 µm polyester-film was also applied directly to the strike face. MDFPIM V2.1 is shown in Figure 128.

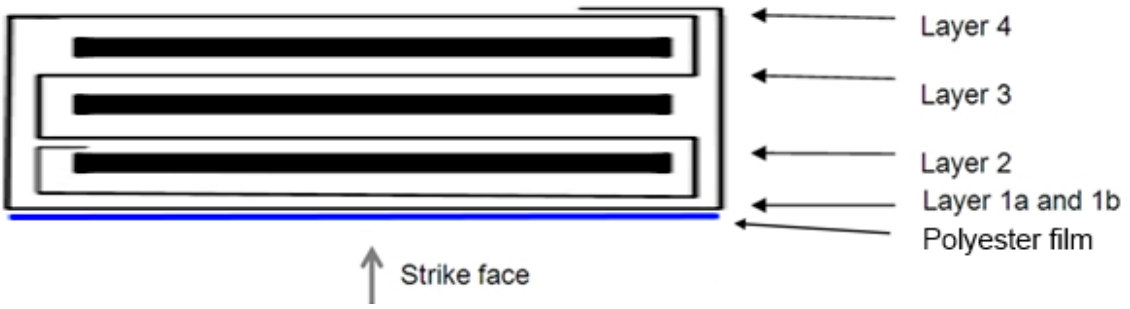

Figure 128: 'Thin' MDFPIM construction, MDFPIM V2.1 (not to scale).

Corneal abrasion is a very low level injury as discussed in Section 3.10.1. For applications where corneal abrasion injuries are of interest, a separate model version, MDFPIM V2.2 has been specified. V2.2 is identical to V2.1; apart from the polythene layer that encases the impact face is transparent and the remainder of the polythene is black. All the polythene is to the same grade and changing its colour is only to assist with the analysis process. The MDFPIM V2.2 also allows assessment of eye penetration or skin perforation risk. The construction of the MDFPIM V2.2 is shown in Figure 129.

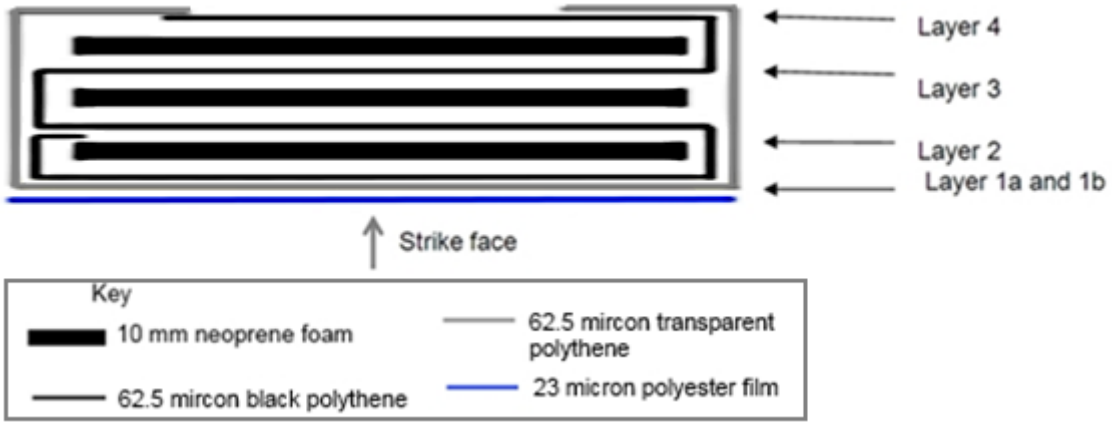

Figure 129: MDFPIM V2.2 construction for applications where assessing corneal abrasion injuries are required (not to scale).

All layer numbering for the MDFPIM is based on the polythene sheet layer numbers.

For assessment of corneal abrasion injuries, any particles adhering to the polyester film after testing indicate a potential abrasion risk[177].

The MDFPIM V2.0 and V2.1 were tested to determine how their penetration response related to penetrating eye injury performance (from Equation 11), skin perforation (from Equation 8) and to generate a calibration curve for penetrations deeper into the model. MDFPIM V2.2 was not specifically tested as it was assumed that there was no performance difference between the different colours of the polythene sheeting[178].

10.4.3 Projectiles used for MDFPIM V2.0 ballistic testing

Ballistic testing of the MDFPIM V2.0 for the eye penetration response, skin perforation response and penetration depth calibration deeper into the model used many of the same projectiles. Table 39 gives these projectiles and their properties (listed in order of increasing mass), identifying which were used in each of the eye penetration, skin perforation and DoP calibration assessments for the MDFPIM V2.0 (and V2.1).

Geometry	Diameter (mm)	Material	Mass (g)	Density (g cm^{-3})	Eye	Skin	DoP
Sphere	1.6	Acrylic	0.003	1.24	X		
Sphere	1.0	Steel	0.004	7.85	X	X	X
Sphere	4.2	HDPE	0.03	0.95		X	X
Sphere	3.0	Glass	0.04	2.50	X	X	X
Sphere	3.2	Aluminium	0.05	2.70		X	X
Sphere	5.0	Cellulose acetate	0.08	1.30		X	X
Sphere	5.7	HDPE	0.09	0.95		X	X
Sphere	3.0	Steel	0.11	7.85	X	X[179]	X

[177] Assessment of corneal abrasion injuries can be completed with MDFPIM V2.0 and V2.1, but particles adhering to the polyester film may be more challenging to identify against a black background of the polythene sheeting.
[178] Testing of the MDFPIM V2.0 was performed with a mix of models using either black or transparent polythene. Although not specifically assessed, no differences were observed in the penetration responses of the models with different colour polythene.
[179] Additionally for the skin perforation assessment of the MDFPIM V2.1

Geometry	Diameter (mm)	Material	Mass (g)	Density (g cm^{-3})	Eye	Skin	DoP
Sphere	3.0	Tungsten carbide	0.22	15.63		X	X
Sphere	6.0	Glass	0.29	2.50	X	X	X
Sphere	6.4	Glass	0.34	2.50			X
Sphere	4.4	Steel	0.35	7.85	X	X	X
Cube	4.0	Steel	0.50	7.85		X	X
Irregular	7.5	Limestone	0.50	2.30			X
Sphere	6.0	Steel	0.89	7.85	X	X	X
Sphere	9.0	Glass	0.95	2.50	X	X	X
CN FSP	5.4	Steel	1.10	7.85			X
Sphere	9.0	Ceramic	1.45	3.80	X	X[181]	X
Cube	6.0	Steel	1.68	7.85		X	X
Sphere	9.0	Steel	3.02	7.85	X	X	X
Cube	8.0	Steel	3.97	7.85			X
Cube	12.7	Aluminium	5.44	2.70		X	X
Sphere	12.7	Steel	8.30	7.85	X	X	X
Sphere	20.0	Glass	10.50	2.50		X	X

Table 39: Projectiles and properties used to assess the MDFPIM V2.0 for each of the eye penetration, skin perforation and DoP calibration tests.

10.4.4 MDFPIM V2.0 eye penetration response

All targets were rigidly backed. Projectiles identified in Table 39 were used for the eye penetration testing and were fired using the Honed Tube Pressure Housing weapon system, with a separate smooth bore barrel for each different diameter projectile. To achieve very low velocities, some projectiles were fired from oversized barrels. The projectiles were propelled using rechargeable 37 mm compressed Airmunition cartridges, using pressures of 5 to 20 MPa. See APPENDIX B for additional weapon system details.

Two MSI 858 optical detectors [205] spaced 1000 ±1 mm apart were connected to an MSI 817 timing unit and an MSI 570 computer interface, with processing by MSI Ballistics DB software. For the majority of testing, the MSI light gates were

centred at 0.403 m from the target, with a muzzle to target distance of 1.876 m. The tolerance on the MSI velocities was calculated to be < ±0.3%.

A Phantom Miro M310 high speed video camera [209] was used to confirm the impact point on the target and as a secondary velocity measurement system. Images were captured at 640 by 240 pixels, 20,000 frames per second and 5 μs shutter speed, with a view that included the 440 mm prior to impact with the target. The tolerance on the high speed video velocities was calculated to be <±0.8%.

After the firings had been completed on each pack, analysis of the number of layers (of the polythene sheeting) perforated for each shot was recorded. The V_{50}'s were calculated using the statistical program R [52] (using a bias reduced generalized linear model, brglm [53]). This enabled the V_{50} to be calculated, along with 95% confidence intervals on the measurement.

10.4.5 MDFPIM eye penetration ballistic testing results

A total of 504 fair shots were completed across the different targets and eleven different projectiles (all spheres). This included repeating the 3 mm steel sphere and 9 mm ceramic sphere testing against the MDFPIM V2.1.

The V_{50} data is shown graphically in Figure 130, compared to the ideal model performance and 95% confidence limits on the ideal performance (from Figure 36). The error bars on the V_{50} data are the 95% confidence intervals.

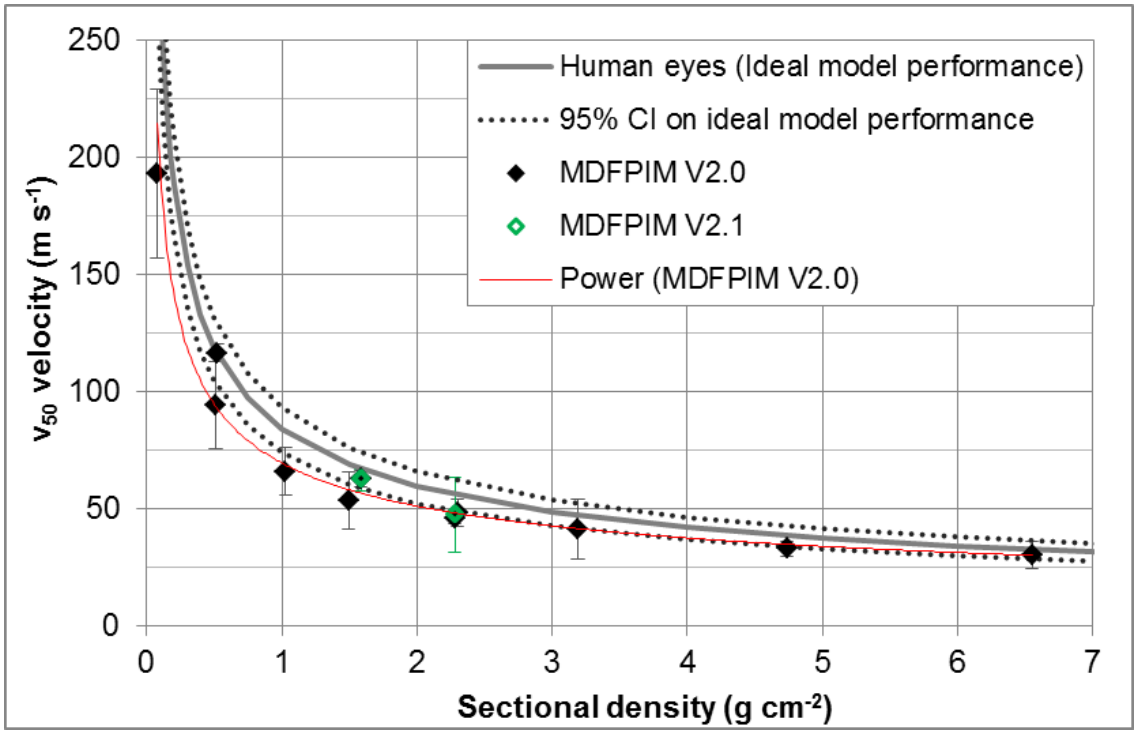

Figure 130: MDFPIM V2.0 and V2.1 layer 1b V_{50}s compared to the ideal model performance and 95% confidence limits.

Figure 130 shows that for the 11 projectiles tested for the MDFPIM V2.0 over the sectional density range 0.08 to 6.55 g cm^{-2} and the two projectiles for the MDFPIM V2.1, the physical model performed very close to the ideal performance curve (indicating a 50% risk of human eye penetration).

A power fit applied to the MDFPIM V2.0 layer 1b data (see Figure 127 for layer numbering) sat just below the ideal human eye performance (and below the lower 95% confidence interval line for projectile sectional densities <3 g cm^{-2}). Although this indicates the MDFPIM V2.0 (and V2.1) slightly overestimate the risk of eye penetration (i.e. the MDFPIM V2.0 layer 1b will be perforated at slightly lower velocities than average human eyes), this is the desired way round for an injury model that could be applied to safety cases. The model needs to ensure that if it determines a scenario to be 'safe', then the residual risk of being incorrect is minimised.

Users of the model therefore do not need to be overly cautious about the interpretation of the predicted penetrating eye injury risk for most applications.

Due to this general requirement to err on the side of caution for application to safety case type assessments and that the model performed within the human eye ideal performance 95% CI for projectile sectional densities >3 g cm^{-2}, it was not deemed necessary to modify the MDFPIM V2.0 to attempt to obtain a better fit to the human eye ideal performance.

There was no statistically significant difference at the 95% confidence level between the performance of the model V2.0 and V2.1[180] for eye penetration assessments for the 2 projectiles that were evaluated against both models ($p>0.5$).

10.4.6 MDFPIM V2.0, V2.1 and V2.2 validation for skin perforation

The V_{50} response of layer 2 of the MDFPIM V2.0 and V2.1 was also determined (see Figure 127 and Figure 128 for layer numbering). Perforation of layer 2 was taken to indicate a 50% risk of skin perforation.

The same methods and analysis procedures were used as detailed for the eye penetration assessment of the MDFPIM (Section 10.4.5). 19 different projectiles were used to assess the skin perforation performance of the model, with the projectile details listed in Table 39.

Performance metrics to compare the performance of the physical models were taken from Equation 8: The final version of the expanded empirical skin perforation equation. Two separate performance metrics were used to bound the risk of skin perforation for different scenarios, which could be applied to the MDFPIM V2.0:

- V_{50} performance curve for skin perforation of PMHS adult thigh, skin intact and fresh. This could be taken to represent a reasonable ‘most likely case’ for an adult population or military personnel and may be most suitable for situations where the risk does not want to be over-predicted, i.e. lethality or effectiveness prediction on a military population.

[180] MDFPIM V2.2 is assumed to be identical to V2.1.

- V_{50} performance curve for skin perforation of PMHS child thigh, skin intact and fresh. This could be taken to represent the 'worst likely case' civilian or vulnerable group population and may be most suitable for situations where the risk does not want to be under-predicted, i.e. a safety case or collateral damage type prediction for a vulnerable population or the general public[181].

The V_{50} values calculated from the experimental data for each of the MDFPIM versions are shown in in Figure 131 compared to the performance metrics detailed above (16 V_{50}s for the MDFPIM V2.0 with spheres, 3 V_{50}s with cubes and 2 V_{50}s with spheres for the MDFPIM V2.1).

As previously noted, the cross sectional area of a cube is taken as the area of one face, even if the cube is randomly orientated.

[181] The thigh was not determined to be the most vulnerable body region in Section 6.1.5. However, the thigh region was chosen for the "vulnerable civilian population", based on the child PMHS skin perforation performance, as Equation 8 has been 'validated' against this specific case (see APPENDIX C). The performance of child PMHS skin on the back region (the most vulnerable body region seen in adult PMHS) cannot be stated with the same levels of confidence, as no other body regions were tested for the child PMHS skin.

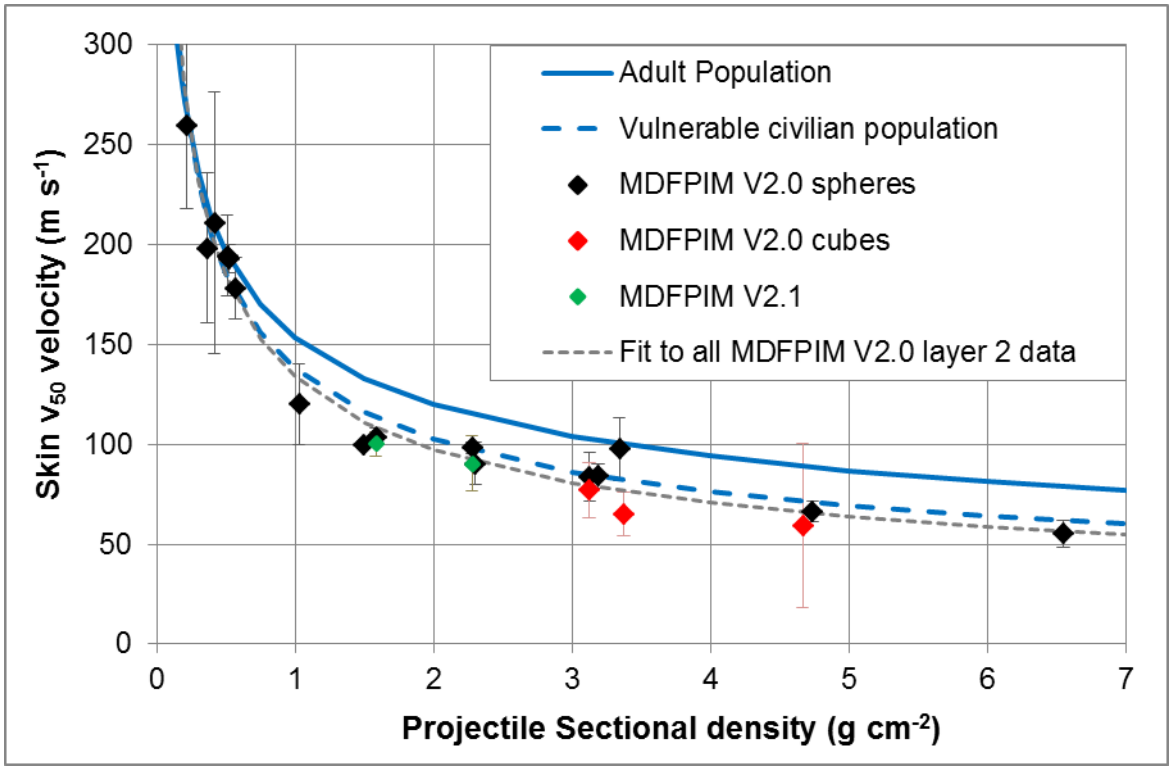

Figure 131: MDFPIM V2.0 and V2.1 layer 2 V_{50}s compared to skin perforation performance metrics (Equation 8). Error bars represent the 95% CI on the V_{50}s.

Figure 131 shows that for the 19 projectiles tested for the MDFPIM V2.0 over the sectional density range 0.22 to 6.55 g cm^{-2} and the two projectiles for the MDFPIM V2.1; layer 2 of the physical model performs very closely to the 'vulnerable civilian population' skin performance curve calculated from Equation 8. A power fit to the combined sphere and cube MDFPIM V2.0 data (R^2=0.964) provides a very good match (within 5.5 m s^{-1} for the projectile sectional densities tested) to the performance curve for the vulnerable civilian population.

The physical models may slightly over-estimate the risk of skin perforation for an adult population. For a vulnerable civilian / worst case general population, the physical models give a good prediction of the (50%) risk of skin perforation.

Given the inherent variability in the animal and PMHS skin data on which the ideal performance was based, coupled to the scatter in the MDFPIM V2.0 individual V_{50} data points, the MDFPIM V2.0 layer 2 performance is within the desired performance range and is less variable than actual biological tissue.

A selection of other materials were obtained prior to this testing as potential alternatives to the 23 µm sticky polyester film to go on the front of the MDFPIM to modify its penetration response. The polyester film was the first material evaluated and gave good agreement to the required eye and skin penetration response as detailed above, with the additional benefit of allowing assessment of potential for corneal abrasion. Further testing on alternative materials was not needed (and would not have enabled assessment of corneal abrasion risk). The alternative materials procured for the testing are listed below and were chosen based on matching material properties to the human cornea:

- 0.125 mm thick silicone elastomer film
- 0.45 mm thick silicone elastomer film
- 0.5 mm thick silicone elastomer film
- 0.6 mm thick silicone elastomer film
- Silicone Sheet - 30 shore A, 1 mm thick
- Silicone Sheet - 40 shore A, 1 mm thick
- Silicone Sheet - 50 shore A, 0.5 mm thick

Also tested was a version of the MDFPIM V2.0 (with the 23 µm sticky polyester film) using 125 µm (500 gauge) polythene sheeting instead of the 62.5 µm, impacted with the 3 mm steel sphere. This was found to raise the penetration response of layer 1 above the upper limit of the eye penetration performance corridor and the V_{50} for layer 2 above the military population skin performance. Due to this, the 125 µm polythene was discounted for use in the model.

10.4.7 MDFPIM V2.0 calibration curve

The MDFPIM V2.0 was calibrated by firing a variety of different projectiles at the model over a range of velocities. As was done for model versions 1.0 and 1.1, velocities were from as slow as possible as was achievable with the weapon system, up to full perforation of the pack (or the maximum velocity achievable if

full perforation could not be achieved). Not all projectiles were evaluated over this entire velocity range.

After the firings had been completed, the MDFPIM V2.0 was dismantled and the maximum number of layers perforated was recorded for each shot.

This calibration testing was all performed at ambient test temperatures (24±3°C)[182] on the MDFPIM V2.0 constructed from foam from the same batch[183]. The foam used to construct the models had been stored for 1 year since production, prior to this testing.

23 different projectiles were used with details listed in Table 39. A total of 728 valid shots were conducted against the model. This includes shots conducted as part of the eye and skin layer performance assessment of the MDFPIM (Sections 10.4.5 and 10.4.6). From this, the V_{50} for each layer of the pack was calculated (where sufficient data was available), resulting in 112 separate V_{50}s. Of these, some were for layers 1 and 10, which have been excluded from the calibration curve, leaving 101 valid V_{50}s. Layer 1 V_{50}s were discounted as they had a 0 depth of penetration and would have skewed the calibration fit (different projectiles will have a different velocity required to perforate layer 1, see Figure 130). Layer 10 V_{50}s were discounted due to the strawboard layer and discontinuity in material types in the model.

The number of layers perforated for each V_{50} were used to calculate the Normalised DoP over density and plotted against the corresponding V_{50}. The calibration curve for the MDFPIM V2.0 is shown in Figure 132. Error bars are the 95% confidence intervals on the individual V_{50} assessments.

Confidence and prediction intervals on the linear fit for all projectiles were calculated using the equations in Reference [259] (based on the V_{50} values). These are shown with the MDFPIM V2.0 V_{50} values in Figure 132.

[182] The actual ambient temperature was recorded every few hours over the course of the testing.
[183] Referred to as MDFPIM V2.0 reference performance in Table 41, Section 10.4.10.

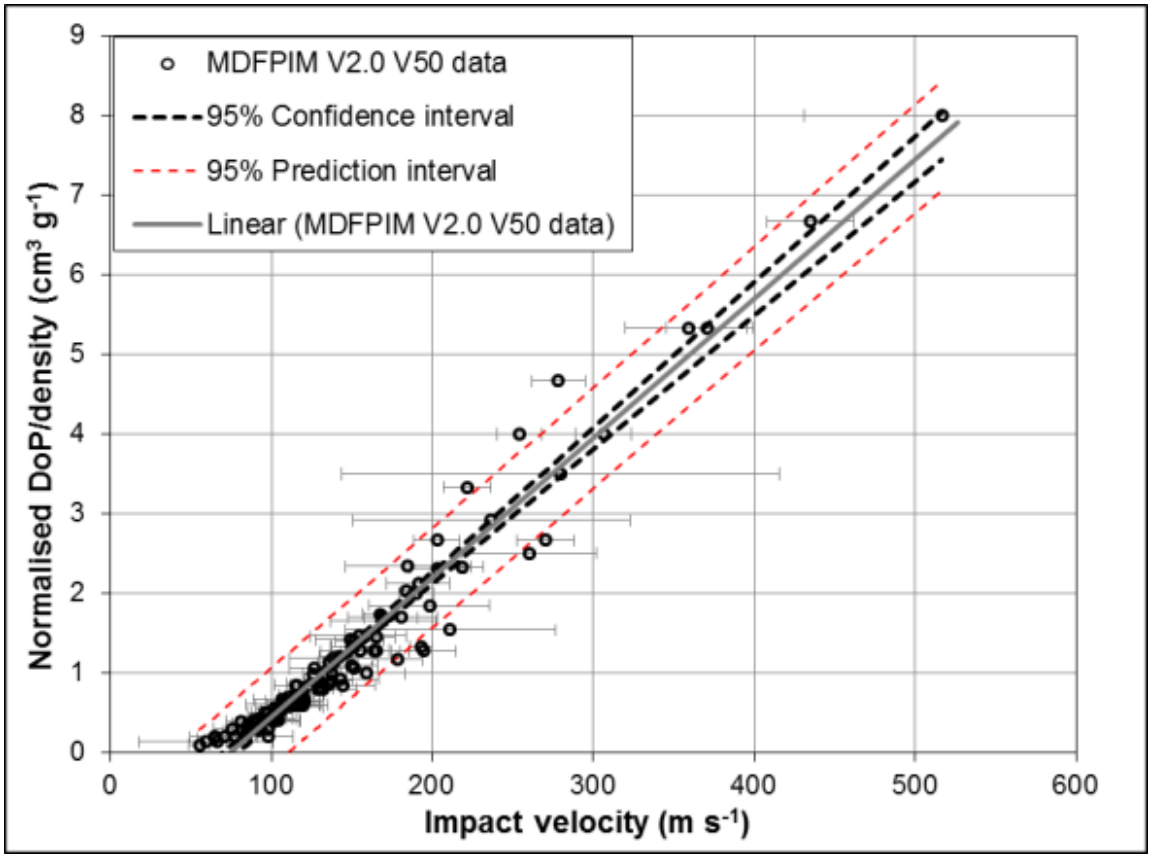

Figure 132: MDFPIM V2.0 normalised DoP over density calibration curve, showing 95% confidence and prediction intervals on the linear fit.

The MDFPIM V2.0 calibration curve is given by Equation 33 (with an R^2 value of 0.952).

$$\frac{Normalised\ DoP}{\rho} = 0.0175v - 1.312$$

Equation 33: MDFPIM V2.0 generic calibration equation

Where:

ρ is the projectile density (g cm^{-3})

v is the impact velocity (m s^{-1})

The residuals of the linear regression of Equation 33 are normally distributed. Curves representing the 95% confidence intervals can be approximated by Equation 34 and Equation 35.

$$\frac{Normalised\ DoP}{\rho} = -1.91 \times 10^{-6} v^2 + 0.018v - 1.42$$

Equation 34: Lower 95% confidence interval for the MDFPIM V2.0 generic calibration equation

$$\frac{Normalised\ DoP}{\rho} = 1.91 \times 10^{-6} v^2 + 0.017v - 1.12$$

Equation 35: Upper 95% confidence interval for the MDFPIM V2.0 generic calibration equation

The curves representing the 95% prediction intervals can be approximated by Equation 36 and Equation 37.

$$\frac{Normalised\ DoP}{\rho} = -4.90 \times 10^{-7} v^2 + 0.018v - 1.94$$

Equation 36: Lower 95% prediction interval for the MDFPIM V2.0 generic calibration equation

$$\frac{Normalised\ DoP}{\rho} = 4.90 \times 10^{-7} v^2 + 0.017v - 0.680$$

Equation 37: Upper 95% prediction interval for the MDFPIM V2.0 generic calibration equation

Where:

$$Normalised\ DoP = \frac{10(L-1)}{d}$$

Equation 38: Normalised DoP related to MDFPIM layer number, where each layer is nominally 10 mm thick

d = projectile diameter (mm). For cubes, the average projected length in 3D is used (given by Equation 4). For irregular fragments, the diameter of an equivalent mass and density sphere is used.

L = layer number of the MDFPIM polythene sheeting (see Figure 127).

If the layer thickness for a given batch of foam used in the MDFPIM is measured (and within the allowed limits of 10±1 mm), the actual layer thickness can be used in Equation 38 in place of the constant 10.

The MDFPIM V2.0 calibration curve given by Equation 33 can be used to estimate impact velocities within the validation limits stated in Table 40, where the maximum layer perforated by the projectile and its mass are known[184]. This normally requires removal and weighing of each fragment with its associated deepest perforation in the model.

	Mass (g)	**Diameter (mm)**	**Density (g cm^{-3})**	**Geometry**	**Velocity (m s^{-1})**	**Deformation**
Min	0.004	1	0.95	Cylinder, cube, sphere (irregular). Length/ diameter~1	Fragment dependent [185]	Non-deforming, non-fragmenting
Max	10.5	20	15.6			

Table 40: Validation limits for projectiles in the MDFPIM V2.0

Due to the discrete nature of the DoP measurements (related to the nominal 10 mm layer thickness), the predicted impact velocities from the model based on a perforation to layer n (L_n) can be easily bounded by the predicted impact velocity for the layer before and after ($L_{n\pm1}$).

When quoting predicted velocities, it is advised that the bounding velocity for the layer before and after also be given. This can be achieved by rearranging Equation 33 for velocity:

$$v = \frac{571.43(L-1)}{\rho d} + 74.5$$

Equation 39: Predicted impact velocity to the MDFPIM V2.0, rearranged from Equation 33.

[184] This assumes the foam batch has first been verified against Equation 33.
[185] Fragment must not perforate deeper than layer 9 of the model in order to provide a valid impact velocity estimate.

Where L≥2.

When using the MDFPIM V2.0 for trials where the properties of the impacting fragment aren't known prior to the testing, the fragment properties have to be determined by recovering them from the model. In these cases, it is likely to be more practical to use the fragment mass and density. Equation 39 can be modified using the fragment (average) diameter estimated based on the measured fragment mass and (assumed) density, for a spherical geometry fragment, using Equation 40:

$$d = 20\left(\frac{3m}{4\pi\rho}\right)^{1/3}$$

Equation 40: Estimated diameter of a spherical fragment based on mass and density.

Combining Equation 39 and Equation 40, the mass and (assumed) density of each fragment can be used to predict the impact velocity, using Equation 41:

$$v = \frac{46.06(L-1)}{m^{1/3}\rho^{2/3}} + 74.49$$

Equation 41: Predicted impact velocity to the MDFPIM V2.0, based on recovered fragment mass, (assumed) density and maximum layer perforated.

Where L≥2.

Equation 39 or Equation 41 can also be used to estimate the maximum velocity of a given fragment to remain analysable within the MDFPIM V2.0 (the velocity which equates to perforations up to layer 9).

As with other fragment packs using discrete layers, off axis penetrations will result in an underestimate of fragment velocity due to underestimating the thickness of material penetrated.

10.4.8 Accounting for different projectile geometries with the MDFPIM V2.0

The calibration equation for the MDFPIMV2.0 (Equation 33) using the normalised DoP over density function already accounts for projectiles of different diameters and densities and can be used to collapse data onto a single curve with velocity. However, there is no explicit way to deal with different geometry fragments.

The V_{50} used for the calibration of the MDFPIM V2.0 (perforating at least layer 2, up to layer 9) were reanalysed accounting for projectile geometry. For comparison to spheres, the following projectiles were used and examples of each are shown in Figure 133:

- Cubes of 4, 6 and 8 mm side length made of steel and one of 12.7 mm side length made of aluminium.
- Irregular stones, nominal 0.5 g (limestone gravel).
- 1.1 g steel CN FSP

Figure 133: Left: 4, 6 and 8 mm steel cubes. Centre: example of 2 of the irregular 0.5 g limestone fragments. Right: 1.1 g CN FSP. Not to sale.

The V_{50} data for spheres were compared to these other projectile geometries in Figure 134 using the normalised DoP over density function.

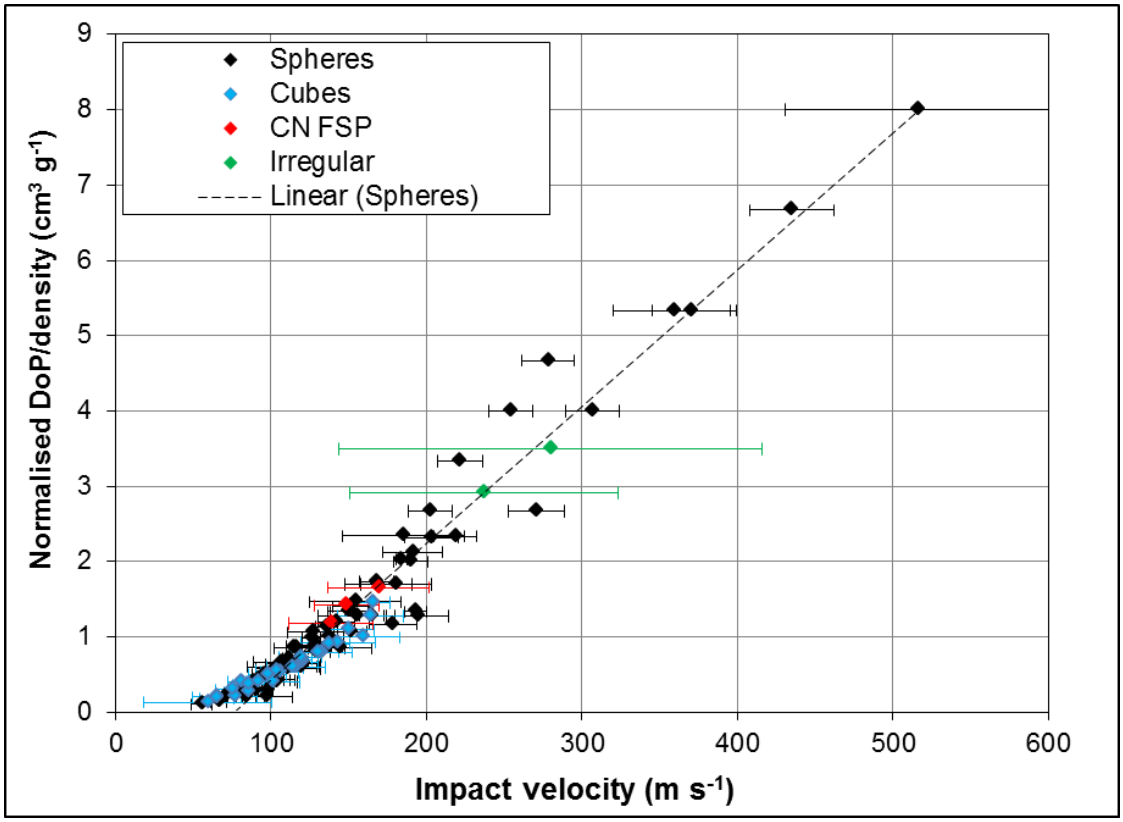

Figure 134: MDFPIM V2.0 normalised DoP over density calibration, showing different projectile geometries.

Figure 134 shows that all the different geometry projectiles tested follow the same relationship as for the spheres. The cube data collapses onto the sphere data when the cube's average projected length in 3D is used (Equation 4).

The large confidence intervals for the CN FSP and irregular fragment data in Figure 134 are due to a very limited number of shots on which the V_{50} predictions are based.

For 'chunky' projectiles, those with length to diameter ratios of approximately 1, there is no need to explicitly consider the projectile geometry as long as the 'equivalent' projectile diameter is properly accounted for:

- For spheres and cylinders (including chisel-nosed), this is the diameter
- For cubes, the average projected length in 3D is used (Equation 4).
- For irregular fragments, the diameter of an equivalent mass and density sphere is used.

The analysis process for the MDFPIM is detailed in APPENDIX K and image analysis process (where the fragment geometry may not be known) is given in APPENDIX L.

The impact velocity predictions from the MDFPIM V2.0 calibration equation are considered less reliable when the length to diameter ratios of the projectile diverges from 1.

10.4.9 MDFPIM V2.0 temperature dependence testing

The MDFPIM V2.0 was envisaged to be able to be deployed to arena style blast trials which may take place worldwide, at any time of year. This means that the model should be able to provide valid predictions given a potentially large variation in temperatures in which the model may be used.

The MDFPIM is enclosed in polythene and the foam is closed cell so the resulting MDFPIM is effectively waterproof. The effect of humidity or rain on the model penetration performance is assumed not to be significant.

In order to determine if there is any temperature dependence on the penetration response of the MDFPIM V2.0, ballistic testing was conducted at selected ‘hot’ and ‘cold’ temperatures (with models conditioned for a minimum of 12 hours prior to testing):

- Cold condition: -10°C (40% relative humidity), representative of the midpoint, near-extreme (daytime) C0 (mild cold) category meteorological condition from DEF STAN 00-35 [278].
- Hot condition: +40°C (22% relative humidity), representative of midpoint, near-extreme category A2 (hot dry) meteorological condition from DEF STAN 00-35 [278].

The temperature range from -10°C to +40°C was deemed suitable to represent the vast majority of conditions under which the model may be deployed. As for any model, additional validation may be required for specific applications. The cold test temperature of -10°C is also well away from the glass transition temperature of neoprene foam of -45°C.

The conditioning cabinet used for this testing was not able to control the relative humidity; the humidity values stated are those measured during the testing.

3 mm glass spheres and 6 mm steel spheres were impacted into the MDFPIM at a range of velocities with the model remaining within the conditioning cabinet at the required temperature. An opening in the side of the cabinet allowed the projectiles to enter and this hole was plugged with a rubber bung when firings were not taking place. The cabinet was able to maintain the set temperature for the short periods (1-3 minutes) taken for each shot when the rubber bung was removed. A steel plate with a circular aperture was used in front of the conditioning cabinet to prevent stray projectiles damaging the equipment.

Projectiles were fired using the HTPH with 37 mm rechargeable Airmunition cartridges. Impact velocities were recorded using MSI solid state velocity equipment [205] with a 1 m separation between the velocity heads. Figure 135 shows a photograph of the setup used.

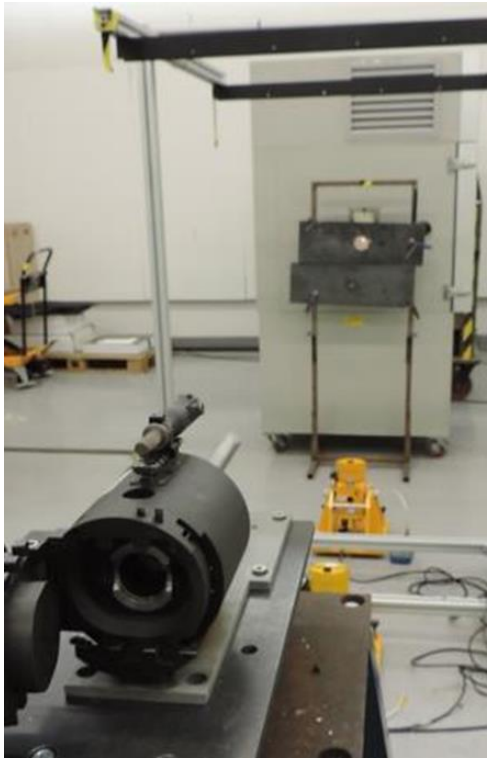

Figure 135: Photograph of the setup used for the temperature dependence testing of the MDFPIM V2.0. The cabinet is shown with the hole plugged through which the projectile passed.

On the completion of testing, the packs were dismantled and the maximum layer of the MDFPIM V2.0 perforated was recorded for each shot.

A total of 63 fair impacts were conducted for testing at high and low temperatures with the two projectile types (minimum of 15 impacts for each target condition and fragment type).

The maximum layer perforated for each fragment and its corresponding velocity were used to calculate V_{50}s for each layer, fragment and temperature combination. Due to the data collected, not all combinations could be calculated. This resulted in 20 V_{50}'s across the hot and cold testing conditions.

The linear fit to the V_{50}s for each condition was compared to existing data for the MDFPIM V2.0 when tested at 24±3°C. This comparison is shown in Figure 136.

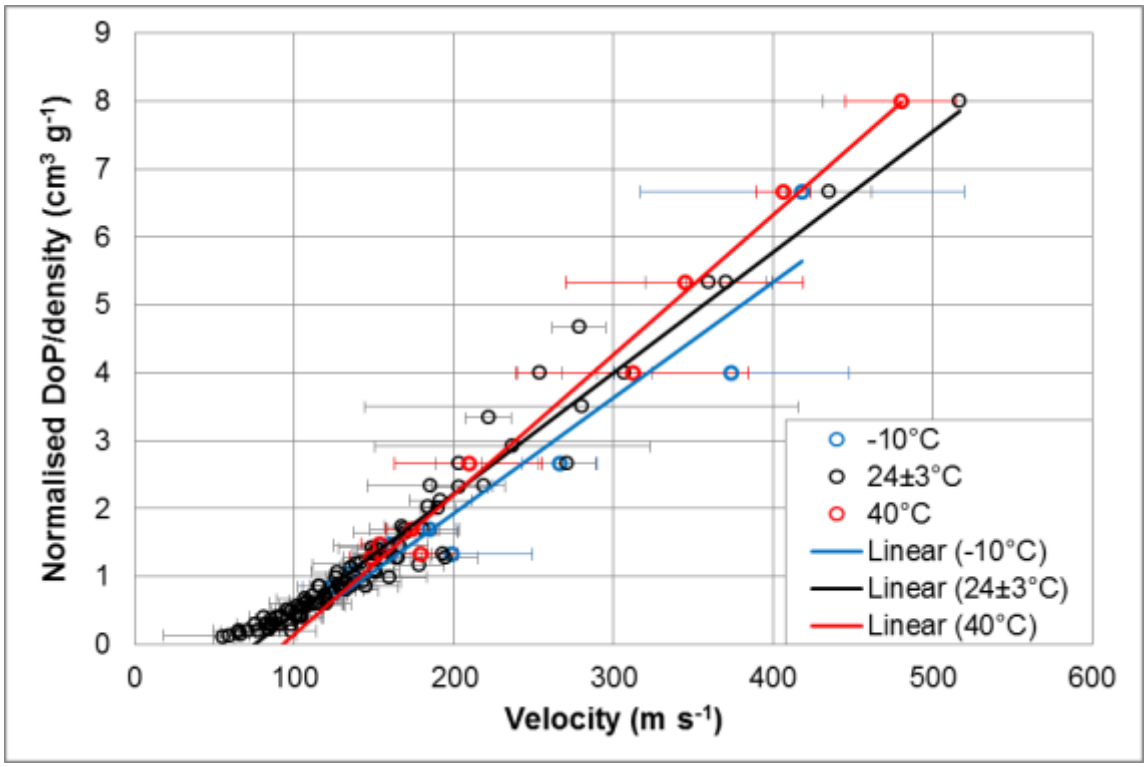

Figure 136: MDFPIM V2.0 normalised DoP over density calibration for model at different temperatures.

As shown in Figure 136, linear fits were applied to hot and cold testing and had a statistically significant difference in the gradients at the 95% confidence level to the normal testing condition (p=0.004 and 0.013 respectively). This was despite

there being no significant difference between some of the individual V_{50}s for the same layer for the hot, cold and normal condition.

The raw data for 'normal' test conditions was conducted without the MDFPIM V2.0 at a controlled temperature; rather the ambient temperature was monitored regularly during the testing. Each V_{50} data point is therefore based on testing at 24±3°C. This may be expected to introduce additional scatter into the results. Given the accuracy of the prediction based on Equation 33, it is not expected to adversely affect the MDFPIM V2.0 use or performance.

The calibration equation for 'normal' test conditions (Equation 33) was expanded to account for the test temperature in both the gradient and constant terms. The gradients and constants of the fits from each temperature test range shown in Figure 136 were calculated and plotted against temperature in Figure 137.

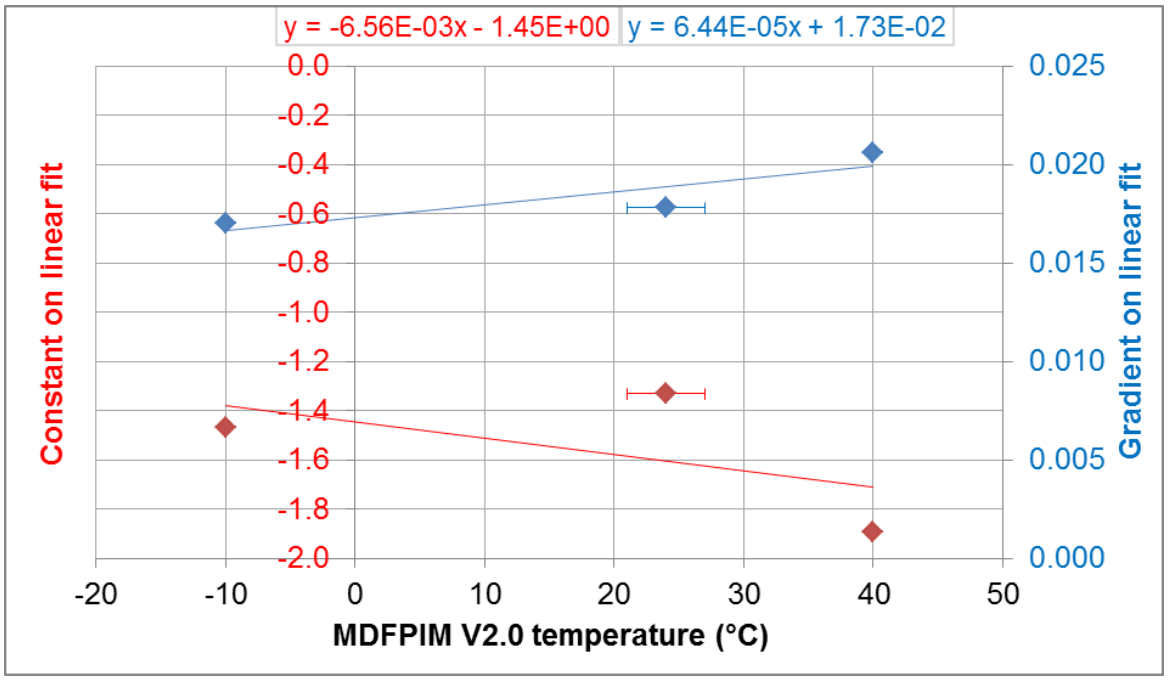

Figure 137: gradients and constants on each of the linear fit to the MDFPIM V2.0 temperature dependent V_{50} data.

The parameters of the linear fits shown in Figure 137 were used to expand Equation 33 to additionally account temperature, resulting in Equation 42:

$$\frac{Normalised\ DoP}{\rho} = (6.44x10^{-5}T + 0.0173)v - 0.00656T - 1.45$$

Equation 42: MDFPIM V2.0 temperature dependent calibration equation

Where

T is the temperature of the MDFPIM (°C).

Equation 42 is based on multiple linear fits to the data; it does not collapse back to "Equation 33: MDFPIM V2.0 generic calibration equation". Attempts to calculate parameters for Equation 42 based on least squares residual fits to the V_{50} data were not able to produce a practical solution; neither was using parameters in Equation 42 based on polynomial fits to the data in Figure 137.

Equation 42 was used to calculate the predicted penetration relationship for the MDFPIM V2.0 at 10°C increments in temperature in order to visualise the temperature dependence. This is shown in Figure 138 within the valid range of test temperatures.

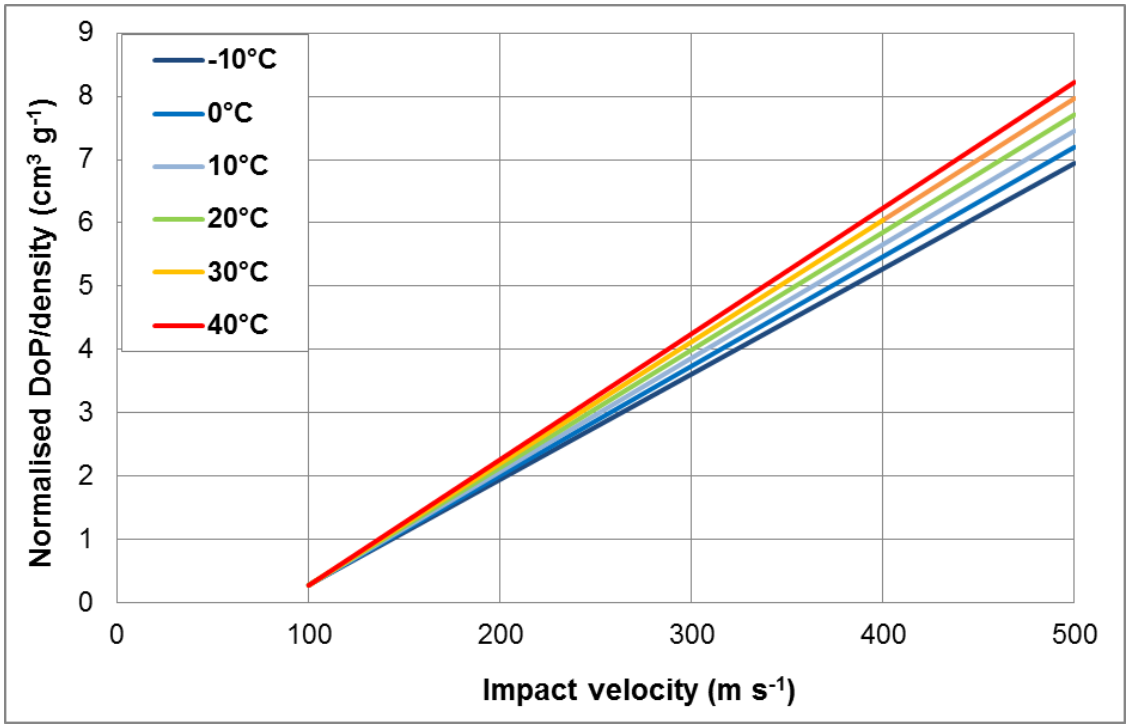

Figure 138: Predicted temperature dependence of the penetration of MDFPIM V2.0, showing temperature contours at 10°C increments from -10°C to +40°C.

An example of what this means in terms of difference to the DoP for a 6 mm glass sphere at -10, 20 and +40°C is given based on predictions from Equation 42: For a perforation of layer 8 (DoP=70 mm, Normalised DoP over density=4.67 $cm^3\ g^{-1}$), the impact velocity at +20°C is predicted to be 332.9 m s^{-1}. At -10°C the predicted impact velocity is 363.3 m s^{-1} (+9%) and at +40°C, 320.9 m s^{-1} (-3.6%).

The predicted impact velocity at the temperature extremes of -10°C and +40°C based on predictions from Equation 42 are within ±10% of that at +20°C. The variation in the maximum layer perforated may not be evident at temperature extremes for all impact conditions due to the discrete layers in the model.

Due to the fact that Equation 42 for the temperature dependence of the penetration of the MDFPIM V2.0 does not collapse back to the normal calibration equation (Equation 33), if testing is conducted in the range 24±3°C, it is suggested to use Equation 33 as standard. There are different options for interpreting the MDFPIM V2.0 penetration response, the equations used for any analysis should be reported with the model output for traceability.

A V_{50} for each of layer 1 (representing penetrating eye injury) and layer 2 (representing skin perforation injury) of the MDFPIM V2.0 were calculated at -10°C and +40°C with at least one of the fragments. Although this testing was not optimised for a V_{50} assessment of these front layers, the results showed no apparent difference between the different temperatures (-10°C, +24°C and +40°C) for either the eye or skin layer. This is supported by the predictions in Figure 138, where the impact velocity prediction converges at low values of normalised DoP over density.

The hot and cold data for skin and eye penetration matched the ‘normal’ test data and desired performance criteria for the eye and skin, shown in Figure 139.

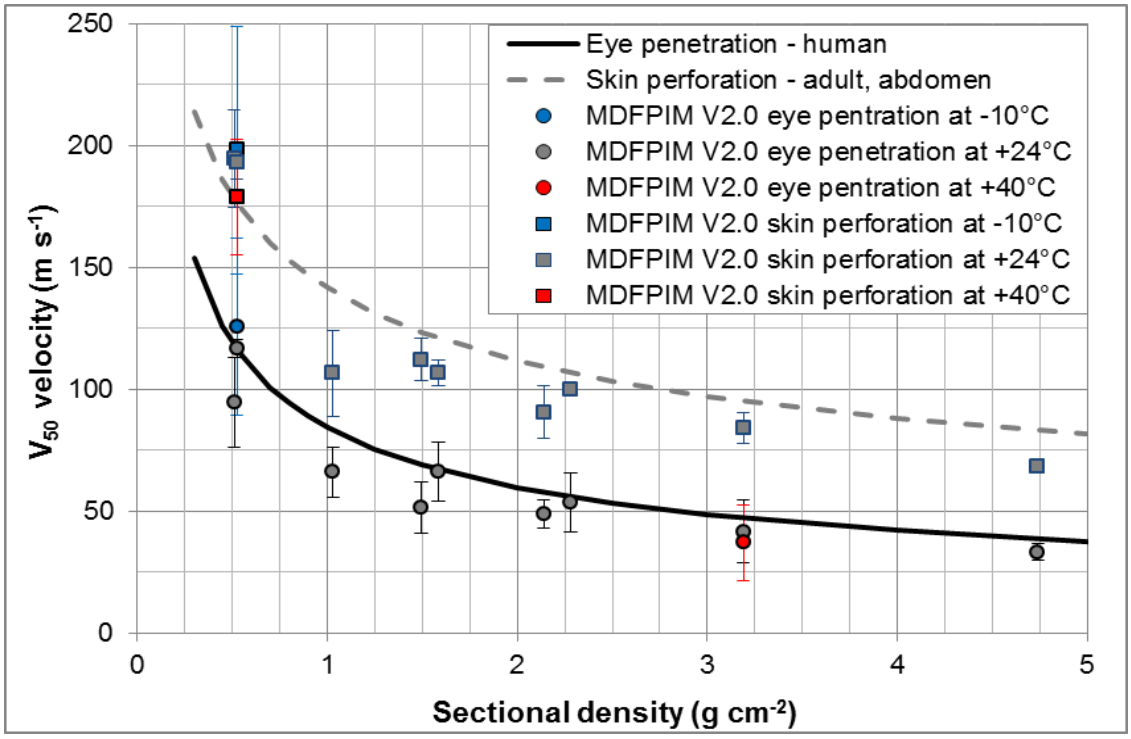

Figure 139: V_{50} of eye and skin injury levels of the MDFPIM V2.0 for different temperature conditions compared to ideal performance curves. Circles represent eye data (layer 1) and squares represent skin data (layer 2). Error bars are the 95% CI on the V_{50}.

This data suggests that if the MDFPIM V2.0 (or V2.1 or V2.2) were used solely to determine the risk of penetrating eye injury and/or skin perforation, consideration of the ambient temperature does not need to be accounted for within the range of -10°C to +40°C.

10.4.10 MDFPIM V2.0 batch variation

10.4.10.1 Foam batches and tests

The performance of the foam in the MDFPIM V2.0 from different batches supplied over a 5 year period was investigated using mechanical and ballistic testing.

All foam was closed cell neoprene to the specification given in Table 47 in APPENDIX J, provided by the same supplier over a 5 year period.

For the ballistic testing, complete MDFPIM V2.0 were used with the performance compared to existing 6 mm steel sphere data from the development of the V2.0 of the model (shown in Figure 132).

Foam from the same batch, but stored for different periods prior to ballistic testing was also compared to look at the shelf life of the model.

Mechanical testing (compression deflection and ball drop testing) was performed on foam from different batches to determine if a simple verification or calibration test could be created.

Table 41 provides details of the different batch names, storage durations and estimated storage conditions.

.Batch ID	Manufacture date	Storage duration(s) prior to testing	Estimated storage temperature range (°C)
MDFPIM V2.0 reference performance	August 2015	1 year	+10°C to +25°C
Batch 1	October 2014	2.5 years 4 years	-5°C to +30°C
Batch 2	October/November 2016	2 years	+10°C to +45°C
Batch 3	February 2017	2 months 1.5 years	+10°C to +25°C
Batch 4	December 2017	10 months	-5°C to +30°C
Batch 5	January 2019	2 months	+10°C to +25°C

Table 41: Details of the different foam batches used in the batch comparison tests.

10.4.10.2 MDFPIM V2.0 batch ballistic testing

MDFPIM V2.0 were constructed from a given batch of foam (labelled 1-5). Apart from the tests conducted on batch 1 stored for 2.5 years and batch 3 stored for 2 months, the polythene sheeting and polyester film were from the same batch.

The thickness of the foam was measured on 20 samples per batch (across 4 different layers of foam). The average layer thickness (given for each batch in

Table 42) was used within the normalised DoP over density calculation performed once testing was complete.

Testing was conducted by firing 6 mm steel spheres at the complete models using the Sabre gas gun (APPENDIX B, Section B.3) at velocities from 45 to 200 m s^{-1}. A minimum of 20 shots were conducted for each batch at each of the storage durations indicated in Table 41.

On the completion of testing, the packs were dismantled and the maximum layer of the MDFPIM V2.0 perforated was recorded for each shot. The V_{50} for perforation of each layer of the layer of the MDFPIM (from layer 2 to 9) was calculated using R [52] as previously described (Section 10.4.7).

A total of 162 valid shots were completed allowing calculation of 54 V_{50}s across the different batches.

A linear model was applied to the normalised DoP over density against velocity data for each batch and storage duration. The intercept and slope of the model were compared back to the MDFPIM V2.0 reference performance (6 V_{50}s for the 6 mm steel sphere), and is shown in Figure 140.

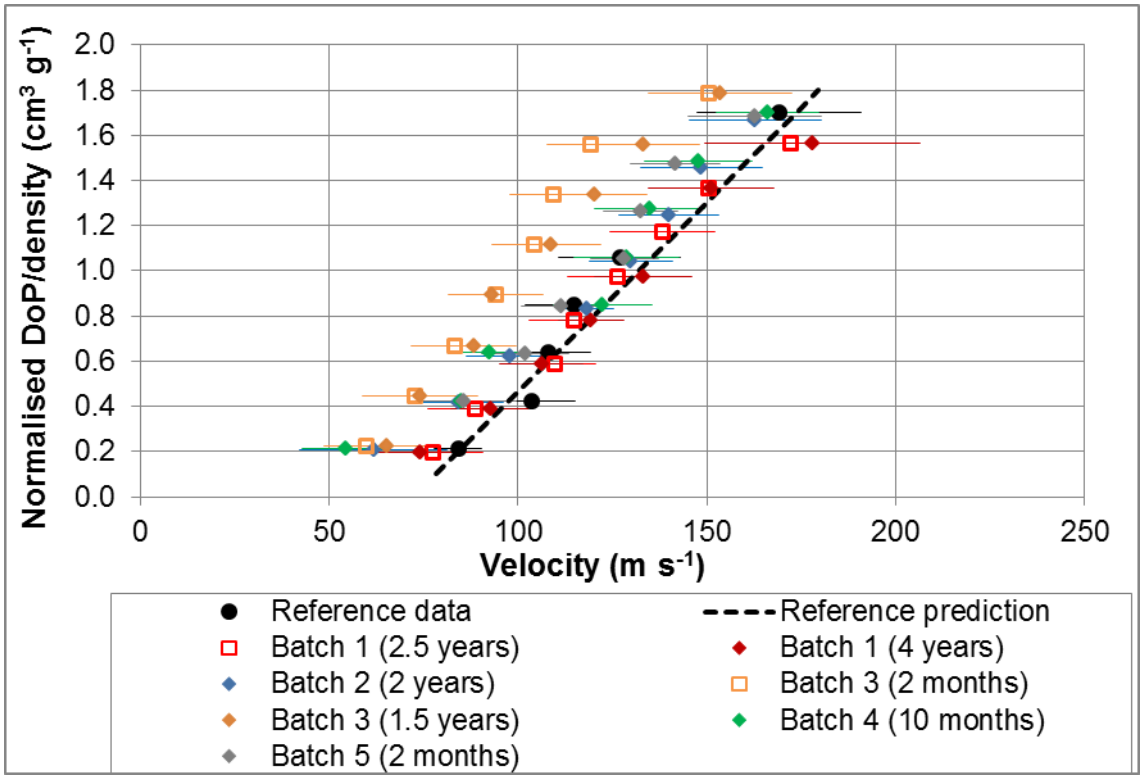

Figure 140: Penetration response of MDFPIM V2.0 for 6 mm steel spheres using foam from different batches.

Of all the batches compared to the reference data, only Batch 3 (both the 2 month and 1.5 year stored) showed a statistically significant difference at the 95% confidence interval between the intercepts on the linear fit (p=0.036 and 0.037). There was no statistically significant difference at the 95% confidence interval between the gradients of any of the batches with the reference data performance.

A linear model was fitted to the normalised DoP/density and velocity data for the different storage durations of batch 1 foam and is shown in Figure 141.

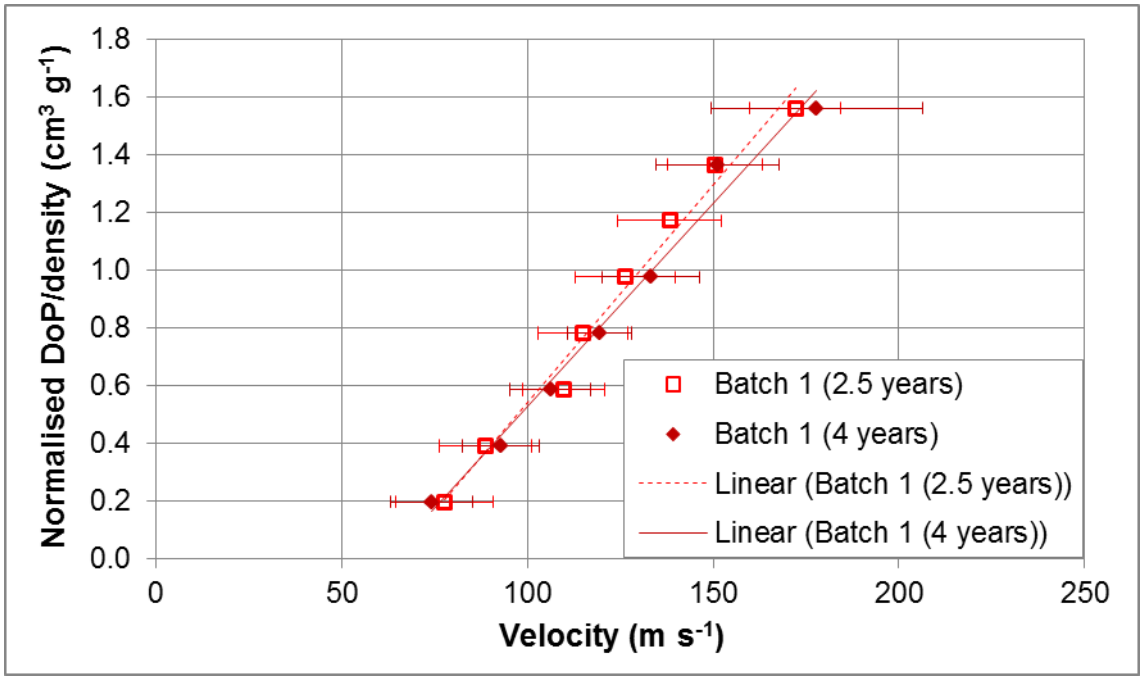

Figure 141: Penetration response of MDFPIM V2.0 for 6 mm steel spheres using foam from the same batch (batch 1), but different storage durations.

Comparing the foam from the same batch, but different storage durations in Figure 141, there was no statistically significant difference at the 95% confidence interval between the intercepts or gradients for the 2.5 years stored foam compared to the 4 year stored foam ($p>0.5$ for the intercept and $p=0.335$ for the gradient).

Similarly for batch 3 foam shown in Figure 142, there was no statistically significant difference at the 95% confidence interval between the intercepts or gradients for the 2 month stored foam compared to the 1.5 year stored foam using a linear model ($p>0.5$ for the intercept and gradient).

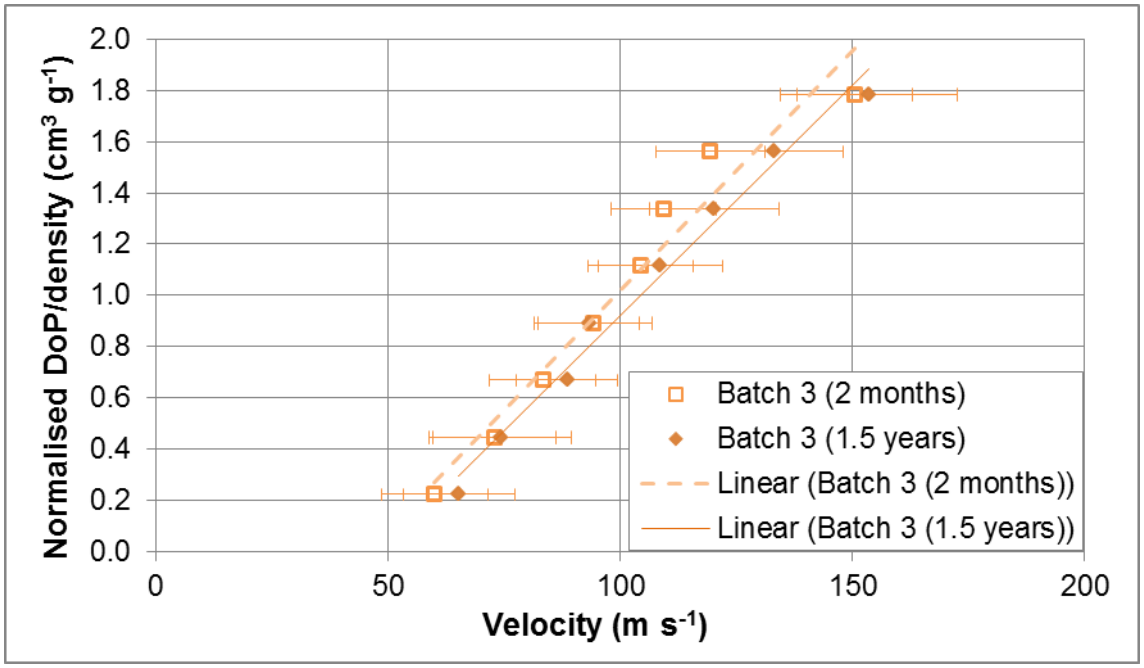

Figure 142: Penetration response of MDFPIM V2.0 for 6 mm steel spheres using foam from the same batch (batch 3), but different storage durations.

The comparisons of different foam batches in Figure 140 to Figure 142 show that long term storage[186] of the foam in the MDFPIM is unlikely to significantly affect the model response. However, it is important to understand the performance of each individual batch, as batch to batch variation of the foam can lead to significant differences in the foam penetration response.

10.4.10.3 MDFPIM V2.0 batch mechanical testing

The foam used in the mechanical testing is detailed in Table 41, but different storage durations of the same batch were not investigated. Only the longer of the storage durations in Table 41 were evaluated where 2 durations are given. The foam from the MDFPIM V2.0 reference performance was no longer available when the mechanical testing was performed.

Compression deflection testing was conducted to ASTM D 1056 [279]. A 28 mm diameter sample of the foam, nominally 10 mm thick, was compressed between two patterns at 50 mm minute^{-1}. Each sample had its thickness measured and

[186] Up to 4 years, estimated between -5°C and +45°C

the Hounsfield universal test machine (model 5 kN/704227) set to perform compression to 25% of the sample thickness. The test was repeated until the load measured varied less than 5%. 5 samples were taken from each of 4 different layers of foam from each batch (20 samples per batch). This was performed for each of the batches 1-5. Testing was performed with the foam at 24±1°C.

Ball drop testing nominally followed [275; 276]: A 63.5±0.05 mm steel sphere of 1.043±0.005 kg mass was dropped from a height of 1.000±0.002 m using an electromagnet onto 5 layers of foam (nominal layer thickness 10 mm). Drop spacing was 75 mm from an edge and 100 mm from previous drop locations. The maximum rebound height was measured using a calibrated HSV at 100 frames per second and 1280x400 pixels. A minimum of 10 drops were conducted for each of the 5 different foam batches. Testing was performed with the foam at 24±1°C.

The results are given in Table 42 and Figure 143. All the foam tested had measured thickness in the range 10.0±1.0 mm.

Batch ID	Layer thickness (mm)		Rebound height (mm)		Pressure for 25% compression deflection (kPa)	
	Average	SD	Average	SD	Average	SD
1	9.21	0.09	423.4	19.9	45.2	1.1
2	9.84	0.34	463.6	17.1	44.9	4.3
3	10.47	0.30	493.8	21.3	36.2	1.0
4	9.96	0.17	580.4	15.3	28.2	1.6
5	9.91	0.31	572.7	10.0	29.8	1.9

Table 42: Results from the compression and ball drop testing for the different foam batches.

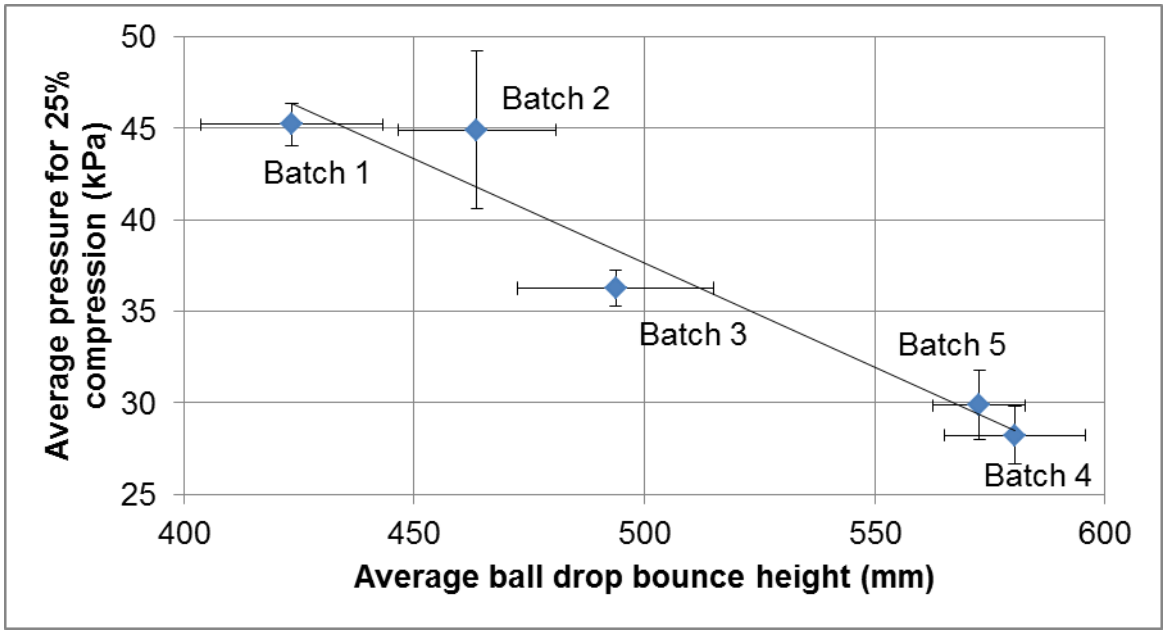

Figure 143: Comparison of the compression and ball drop test results for the different foam batches

Figure 143 shows there was a strong correlation between the ball drop results and compression deflection tests for each batch (R^2=0.939). The ball drop test was a statistically significant predictor of the compression deflection tests (p=0.04). Therefore, if useful as a discrimination or verification test for different foam batches, either test could be used.

However, neither the compression deflection test nor ball drop test were statistically significant predictors of ballistic performance (p≥0.5 in both cases).

Instead of using the height reached by the ball following the drop, the coefficient if restitution could be used. This is a more widely accepted format to present the outcomes, but would not affect the conclusions drawn.

10.4.10.4 Batch testing outcomes

From the batch testing conducted, storage of the foam in the model prior to use (for up to 4 years, estimated between -5°C and +45°C) doesn't appear to affect the model ballistic response. However, batch to batch variation was shown to cause variability in both the foam mechanical properties and affect the ballistic

response in some cases and needs to be assessed against the model reference performance (i.e. verification or calibration).

Neither the compression deflection test nor ball drop test were statistically significant predictors of ballistic performance. A limitation was that the reference MDFPIM V2.0 foam was not available for mechanical testing.

Batch 3 was more easily penetrated than the MDFPIM V2.0 reference performance, but had the median outcomes for both the ball drop and compression deflection tests. Batch 3 was the thickest of the foam samples tested (average 10.47 mm), but this was accounted for within the method for both the ballistic testing and compression testing.

A suitable verification or calibration test could not be developed. The 6 mm steel sphere used for the ballistic testing may not have been an ideal choice of projectile as it did not allow clear discrimination between batches. A lower sectional density projectile[187] that allows characterisation of the model over wider velocity (and normalised DoP over density) ranges would be preferable.

In place of a specific calibration test for the MDFPIM, ballistic calibration against “Equation 33: MDFPIM V2.0 generic calibration equation” with the 95% prediction intervals to give the upper and lower limits (Equation 36 and Equation 37) should be used. This requires sufficient shots to be conducted to calculate a V_{50} for a given layer. It is suggested that the model response be characterised by V_{50}s for multiple layers of the pack. The use of the MDFPIM calibration equations for this purpose allows the user to select a suitable projectile for the testing. It is suggested that if practical, a projectile is selected that closely matches the (expected) fragment properties that will be generated in the actual testing for which the MDFPIM will be used.

There was no calibration test developed for the MDFPIM V2.1 or V2.2. If either of these models are required to be used, calibration should be conducted by

[187] A 4.4 mm glass sphere is suggested as this would enable calibration testing with the existing weapon systems used for gelatin calibration (APPENDIX D, D.5).

constructing (at least) one MDFPIM V2.0 on which the above calibration procedure can be conducted.

Batch testing was only conducted on the foam part of the MDFPIM. There is the potential that the polythene sheeting or polyester adhesive film could vary between batches and affect the results. This was minimised as far as possible within this batch testing, but the potential effect of this at the time the testing was conducted on the reference MDFPIM V2.0 performance (described in Sections 10.4.5 to 10.4.9) was not considered and cannot be accounted for. Calibration of packs prior to use should overcome this issue.

Only the foam from the reference performance batch for the MDFPIM V2.0 was used to construct models and collect data that was used to develop the MDFPIM V2.0 (e.g. data shown in Figure 130, Figure 131 and Figure 132).

10.4.11 MDFPIM V2.0 resolution of predictions

The resolution of the MDFPIM V2.0 impact velocity predictions is determined by the neoprene foam layer thickness (nominal 10 mm). Only perforations to discrete layers are assessed, using the polythene sheeting as a witness layer. As discussed in Section 10.4.7, the predicted impact velocities from the model based on a perforation to layer n (L_n) can be easily bounded by the predicted impact velocity for the layer before and after ($L_{n\pm1}$). This will help highlight the resolution limitation and discrete nature of the MDFPIM V2.0 predictions. This can be done prior to testing if the projectile properties are known and can be used to help assess the model fitness for purpose.

The design of the MDFPIM was such that the model should be similar to, but at least as easy to penetrate as muscle tissue, such that any potentially injurious penetrating projectiles would not be artificially discounted by the model.

By using the MDFPIM V2.0 calibration data from Section 10.4.7 as inputs to predict the DoP in muscle tissue using Equation 17, the equivalent depth in

muscle tissue could be estimated at each V_{50} and DoP of the MDFPIM[188]. The difference in estimated DoP in muscle tissue between successive layers of the MDFPIM V2.0 was used to determine a measure of the resolution of the MDFPIM. This equivalent muscle tissue thickness appears to be velocity dependent for the MDFPIM V2.0 and is shown in Figure 144.

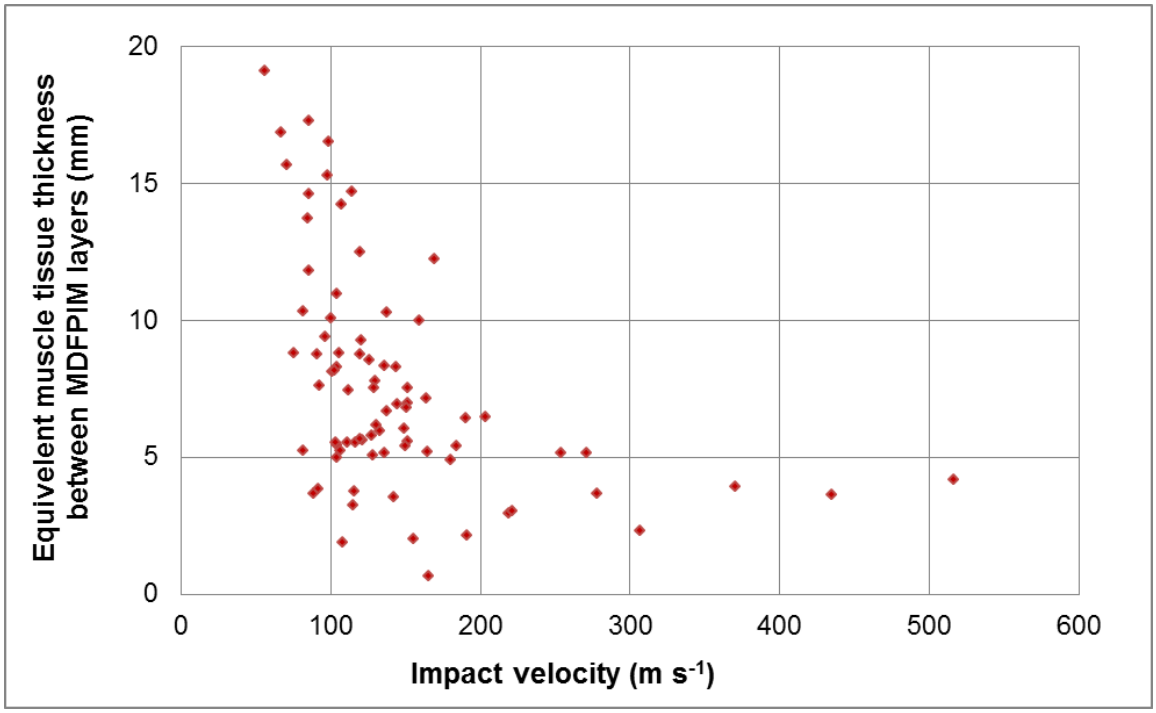

Figure 144: Resolution in terms of equivalent muscle tissue thickness between successive layers of the MDFPIM V2.0, based on measured V_{50} velocities.

Figure 144 shows that the resolution between layers of the MDFPIM V2.0 improves as impact velocity increases. Based on the equivalent thickness of muscle tissue; below 100 m s^{-1}, resolution is between 4 mm and 19 mm. At velocities over 200 m s^{-1}, resolution is approximately equivalent to 5 mm in muscle tissue for the projectiles assessed as part of the MDFPIM V2.0 calibration (see Table 39).

[188] This was a similar approach to muscle tissue simulant DoP comparison in Section 9.10, apart from here the MDFPIM V2.0 layer thickness is fixed at 10 mm and is not designed to match the muscle tissue penetration response.
Equation 17 (no account for effect of the skin) was used rather than Equation 24 which accounts for the effect of the skin on the subsequent DoP. This was because the analysis in this section was completed prior to the finalisation of Equation 24 (and Equation 8).

Compared to strawboard packs (Reference [274] type D) of 3.8 mm layer thickness and the metal spaced witness pack [270], the MDFPIM V2.0 has approximately 2.5 times better resolution in terms of impact velocity predictions for the projectiles used as part of the MDFPIM V2.0 calibration[189].

Increasing the resolution of the MDFPIM V2.0 would require reducing the foam layer thickness (and re-calibration of the model). This would also add significant additional burden to post-test analysis of the model where fragments have to be identified and recovered from the model to obtain the maximum layer perforated and fragment mass.

Prediction of eye penetration risk is independent of the foam layer thickness and prediction of skin perforation risk is only dependent on the 10 mm thickness of the first layer of foam in the model, allowing the performance to be matched to human skin.

Unless automated or semi-automated analysis methods, such as CT scanning, are utilised that do not require deconstruction of the MDFPIM, additional development of the MDFPIM V2.0 to increase the resolution of the model is not recommended.

In some of the trials in which the MDFPIM has been used (see Section 10.6), spatial distributions of impacts to the packs have been over 20,000 fragments per m^2. Decreasing the layer thickness to increase resolution in model predictions, whilst still maintaining the same overall model thickness, would not have been practical in these situations.

It should be noted that in these trials with very high fragments per unit area, semi-automated image analysis was used to identify perforations to each layer of the MDFPIM, as the mass of the projectiles were known prior to testing or could be estimated from the hole size left in the polythene sheeting. This greatly reduced

[189] Metal spaced witness pack velocities were based on the difference between layer 1 and 2. Velocity differences between layers for the metal spaced witness pack will increase with increasing layer number.

the time required to analyse the model. APPENDIX K provides an overview of the MDFPIM analysis, with the image analysis process in APPENDIX L.

Whether the MDFPIM V2.0 is a suitable model should be assessed, as with the use of any model, in this context based on the threat being assessed in terms of likely projectile properties and velocities impacting the model.

10.5 Benefits and limitations of MDFPIM

The main benefits and limitations of the MDFPIM are summarised in Table 43.

Benefits	**Limitations**
Allows assessment of potentially injurious projectiles that would not be analysable using 'legacy' models.	Can be prone to disruption in blast tests with associated loss of data (or quality of data) if positioned too close to device, or from fire.
Simple and quick interpretation of risk of eye and skin penetration valid across wide range of projectiles.	Limited accuracy of back calculation of impact velocities to perforate layer 2 for some projectiles (Equation 39 will always predict velocities ≥74.5 m s^{-1}. The estimate of skin perforation risk from the physical model (L2) is not affected).
Long shelf life (validated for at least 4 years)	Batch to batch variation for the neoprene foam. This is a potential issue for V2.0 (specification allows 160±10 kg m^{-3}).
Calibrated for velocity estimate for wide range of projectiles (geometries, diameters, masses and densities).	Material sourcing (polythene grades may not be easily available in other countries).
Analysis can be semi-automated using image analysis of holes in polythene layers if fragment densities are known (and approximately spherical geometry).	If overmatched, data is lost on the overmatch fragment resulting in underestimate of injury potential.
Can tile multiple small packs to cover large or complex areas (models have been deployed inside platforms and covering large walls).	Resource intensive analysis requires physical recovery of fragments from pack and their masses.
Can be used to back protective materials to look at overmatch or compare to unprotected case.	May influence measured performance of protective materials when used as a backing

Benefits	Limitations
Has been deployed extensively within UK and with other nations	Planar geometry – may not allow easy mounting of all PPE systems (but good for flat or flexible panels).
A reduced thickness version is available for scenarios where only the potential for corneal abrasions, risk of penetrating eye injury and/or risk of skin perforation are required	Temperature dependence of penetration response. However, can be corrected for if ambient testing conditions known (limitation is less severe than for gelatin).
Relatively inexpensive materials. Approximately £40 per MDFPIM V2.0 and £15 per MDFPIM V2.1/2.2 (500 x 500 mm) depending on material order quantities.[190]	Multiple models may be needed to assess the full range of fragment injury (i.e. MDFPIM V2.0 for lower energy fragments and strawboard or spaced metal witness packs for higher energy fragments).
Polythene outer layer is waterproof and the foam is closed cell so water proof. Not affected by rain or damp when used outdoors. Ease of storage.	Directional – off axis penetrations will result in underestimate of fragment velocity.
Can be calibrated or verified against MDFPIM V2.0 calibration curve (Equation 33) prior to use	Non-ballistic calibration or verification test might be easier to implement.
Comparatively lightweight pack (~2.4 kg for MDFPIM V2.0 500 x 500 mm impact face) aiding ease of deployment during trials, particularly at height or in confined spaces.	Disposal: Materials are generally not recyclable compared to ‘legacy’ models.
The MDFPIM V2.0 and V2.1 slightly overestimate the risk of eye penetration and skin perforation (for an adult population). This means that users of the model do not need to be overly cautious about the interpretation of the predicted penetrating eye injury or skin perforation risk for most applications.	
The resolution in terms of impact velocity predictions of the MDFPIM V2.0 may be considered a limitation, but is a significant improvement over existing models. Resolution of the model is a trade-off between the burden of analysis from the multiple layers and layer thickness.	

Table 43: Benefits and limitations of MDFPIM (V2.0, V2.1 and V2.2).

[190] There will be additional (man power) cost associated with model construction from the raw materials.

Many of the limitations of the MDFPIM are linked to the materials used in the model. Modifying the materials used in the construction would require re-validation of the model which would require significant resource.

The potentially severe issue of blast damage preventing (or limiting) analysis of the MDFPIM can be reduced by:

- Consideration of fit for purpose.
- Trial design.

Analysis could be conducted by CT scanning to reduce resource required to recover all fragments. However, if this was a consistently available analysis route, a monolithic fragment pack would likely prove more practical.

Other feedback that has been received on the MDFPIM with respect to its benefits and limitations was:

- "D*ata collection when manually performed is very time consuming. Recommend using CT or another automated procedure.*
- *Witness pack appears to be able to capture fragments in a unique velocity zone that was not captured by ballistic gelatin.*
- *In close proximity to the buried threat, witness packs can be overmatched by the blast and not collect data.*" [280]

"*It was noted at that time that the 10 mm foam layers did not provide sufficient granularity for the smallest fragments*" [281].

10.6 MDFPIM use / exploitation

The injury prediction to use for the MDFPIM depends on the requirements of the testing being performed. The most appropriate method to take the MDFPIM V2.0 outputs and convert to an injury output should be determined on a case by case basis.

In addition to the direct assessment of the risk of penetrating eye injuries and skin perforations, there are a number of output routes shown in the model linkage

diagram in Figure 2 for the MDFPIM V2.0. The projectile properties and predicted impact velocity from the MDFPIM V2.0 can be used to:

- Calculate the DoP or retardation profile in muscle tissue or hybrid tissue types as discussed in Section 9.9.
- Input into an injury algorithm, such as the Sperrazza and Kokinakis (S&K) incapacitation criteria [43].
- Input into a shot line model.

The MDFPIM analysis procedure and an example of the S&K incapacitation criteria [43] for generating an injury prediction are detailed in APPENDIX K.

The MDFPIM (all versions) are known to have been used in at least 23 separate trials within UK and with other nations. Individual trials have used up to 150 models each (such as that described in APPENDIX K, K.2). The type of trials in which the MDFPIM has been used includes:

- Safety assessments of;
    - Explosive devices, such as IEDs and Active Integrated Protection Systems
    - Explosive Methods of Entry
    - Door breaching (ballistic)
    - Render Safe Procedures
    - Ricochet of small arms rounds
    - Behind barrier effects, including within vehicles and structures
- Lethality / effectiveness assessments
- PPE/ballistic material performance assessments

Due to sensitivities of many of the trials on which the MDFPIM has been used, full descriptions of its exploitation are not given in this thesis.

Some photographs of the MDFPIM deployed in a selection of different trial setups are given in APPENDIX M.

An open source description of the use of the MDFPIM is in Reference [282].

A presentation on the development and potential applications of the MDFPIM V2.0 was given to the Group Of Experts in Mitigation Systems (GEMS) [283]. The slides from this presentation are given in ANNEX A.

Use of the MDFPIM V2.0 in a Dstl trial has resulted in a Chief Scientific Advisor (CSA) Commendation on 4th April 2019 at MOD Main Building, winning the 'Excellent Science or Engineering' category (high quality, novel, significant and impactful science or engineering which delivers an exceptional contribution to UK Defence and Security). The MDFPIM and author were critical to meet the trial objectives.

Additionally, this same work was recognised by the Dstl Annual Awards Celebration 2019 (26th September 2019 held at Tidworth Garrison).

This commendation shows that whilst it has not been possible to describe many of the exploitation situations of the MDFPIM due security constraints, peer review at a high level has been conducted of its use in supporting practical, real world assessments. These assessments would not have been possible without the use of this model to the required accuracy/confidence.

A patent has been applied for covering the MDFPIM [284].

11 Discussion

11.1 Background and approach taken

Understanding how different projectiles penetrate tissue and perforate the skin is critical for a number of applications. This includes understanding the injury potential of different threats (such as primary and secondary fragments from explosions, air rifle pellets and other sporting equipment), models to inform safety cases, development of predictive models of penetration and for casualty prediction models. The existing models used for these applications have a number of limitations which has led to their suitability being questioned for a range of scenarios (Section 3.9.3). To address these issues, the primary aim of this thesis was to "develop (a suite of complementary) models that facilitate the assessment of injury from penetrating ballistic projectiles, in both a physical and virtual environment".

Modelling real tissue is complicated due to its high variability in response to ballistic penetration. This is due to biological variation, which occurs both within and between individual targets, making comparison or validation of models (both virtual and physical) challenging. Variability of the threat projectile may compound this issue.

To mitigate the variability of the data from real tissue, the approach taken within this thesis was to use a large number of shots (from different targets) to determine an average response. These data collected (to use as performance metrics or for model development) were much more extensive (greater number of shots) and broader (in terms of velocity range, projectile densities, projectile geometries, etc.)[191] than previously assessed in a single source in the literature.

There was also a paucity of data for skin perforation, real muscle tissue penetration and retardation and tissue simulant penetration and retardation

[191] But still within the bounds of what would be considered valid for these aims: projectiles would be expected to causing penetrating (and not blunt) injuries, projectiles were non-deforming, non-tumbling, etc., targets were suitable (e.g. data for cows, horses and chicken discounted), etc..

related to non-metallic fragments (i.e. typical secondary fragments) from the literature. The above approach also addressed this issue and allowed the validation of the models to address the additional objectives defined in Section 1.2.2, to “be applicable to a broad a range of input parameters to enable their use over a wide variety of scenarios” and to “determine the model accuracy and reliability compared to experimental data (to allow potential model users to make a sound judgement on model ‘fitness for purpose’)”.

(Muscle) tissue simulant selection is not practical using bullets due to their variable response, even under the same setup conditions. The projectile data were limited to non-deforming, non-tumbling projectiles so that the projectile responses were consistent and repeatable. Whilst the intended end use of muscle tissue simulants is often for bullet assessments, the selection and validation using non-tumbling and non-deforming projectiles is not considered to hinder the applicability of the models for these applications. However, additional considerations for bullets in muscle tissue simulants are required and are discussed (Section 11.5).

There are limitations associated with the data for real muscle tissue collated. The data from PMHS may not represent population they are intended to model (the average ages of PMHS were 58 and 72 from References [59; 61]). Despite this, it is assumed that the data from the PMHS studies can be taken to represent a general adult population (unless indicated otherwise). The suitability of different animal models to represent humans has been considered and validated for skin perforation and muscle tissue penetration against this PMHS response within this thesis (but had not been performed adequately in the literature).

Data for retardation through live animal tissues has also been used in this thesis to validate the models and was compared with dead tissue and FREM predictions (Sections 9.3.2 and 9.10). This provided confidence that the predictions made are likely to be accurate for live human muscle tissue, even though this cannot be directly assessed.

11.2 Discussion of the literature review outcomes

The literature review of skin perforation testing (Section 3) showed that impact velocity and projectile sectional density were key projectile parameters for predicting skin perforation. These properties in isolation have been used to provide skin perforation predictions in the literature, but ignore the other factors that were determined to be (potentially) significant from the literature review: species (i.e. human, goat, pig, etc.), age distinction in terms of child / adult, target body region, and the backing method (intact, isolated backed or isolated) and projectile geometry.

As pigs are one of the most popular targets for wound ballistics, much of the available data is for shots against pig skin. However, this leads to inaccurate skin perforation predictions when data is combined and target type is not accounted for.

A considerable number of references confused the definitions of penetration and perforation, either miss-reporting data or combining data of mixed types. As for the other factors that were considered to be significant in influencing skin perforation, failure to account for the penetration or perforation calculation type has led to inaccurate predictions in the literature.

None of the currently available empirical predictions for skin perforation in the literature were deemed suitable due to their inability to account for these different factors considered to be significant in determining skin perforation.

In order to have suitable data on which to construct the eye penetration empirical model, the focus was on the collation of individual raw shot data from eye penetration studies. These contained many more impacts against PMHS eyes, such that the response of human eyes could be confidently determined.

It was quite surprising that no previous attempts were found to collate muscle tissue DoP data from across the literature for comparison to simulants. Analysis of collated muscle tissue data has been performed in the literature for other purposes (such as Reference [112] for tissue devitalisation), but not DoP comparison.

Most of the DoP data collated from the literature in this thesis were from the same references that provided skin perforation data, as it is a logical extension to the testing to also measure DoP for any shots that perforate the skin[192]. The testing in the references given in Table 1 are likely to have been primarily focused on the skin perforation aspect, with DoP measurements secondary. This has resulted in the majority of the DoP data being for relatively low penetration depths, close to the skin V_{50} and presented some limitations for comparisons to the muscle tissue simulant data that are discussed in Section 11.5.

Muscle tissue simulants (such as gelatin, soap and synthetic 'gelatin alternatives') offer many advantages to testing on real tissue. The suitability of a given simulant depends on the requirement. In order to determine 'fitness for purpose' of a muscle tissue simulant, first a user needs statement or requirement is defined. In this thesis, this requirement was defined as: "the ability to measure and provide the same permanent DoP, retardation, temporary cavity dimensions and tumbling for bullets as expected in muscle tissue". This directed the selection of a muscle tissue simulant towards a transparent material to allow HSV analysis.

There was a no suitable data in the literature for low density, non-metallic fragments (that could be considered representative of secondary fragmentation from an explosive device) for penetration or retardation in real muscle tissue or muscle tissue simulants.

No previous literature was found that could suitably validate any of the muscle tissue simulants over the required range of impact conditions and requirements defined. Consideration of "fitness for purpose" and validation does not appear to be common practice in the wound ballistics literature. Verification is more common, but far from universal (at least for muscle tissue simulants, by means of a depth of penetration test; e.g. APPENDIX D, D.5). The lack of validation of muscle tissue simulants questions the reliability of the outcomes of some studies reported in the literature. Implications are discussed for comparative and predictive uses of muscle tissue simulants in Section 11.5.

[192] See the references given within Table 1 and Table 4.

11.3 Discussion of skin perforation and DoP comparisons from Section 5

From the testing performed on pig legs, with and without skin (Section 5.3), the presence of the skin was significant on initiating penetration. However, once a projectile had penetrated into the muscle tissue it followed the same penetration-velocity relationship as bare muscle tissue, just offset according to the velocity required for skin perforation (or surface penetration). This allowed the reduction in DoP due to the skin to be quantified; showing that the performance and effect of a skin layer needs to be accounted for within injury models that evaluate the risks of projectiles in the velocity regime at least up to 1.6 times the skin V_{50}.

These data also show that in order for an injury model (e.g. tissue simulant) to be applicable across a range of velocities, it needs to match (or otherwise account for) the combination of skin and muscle tissue. A muscle tissue simulant designed to match the response of bare muscle tissue will over-estimate the degree of penetration if used in isolation (i.e. without an additional skin simulant layer).

Based on the skin perforation response in Sections 5.2 and 5.5, direct comparison of skin perforation V_{50} across 4 different targets was summarised as: sheep (thigh) ≈ goat (thigh) ≈ PMHS (neck) ≠ pig (thigh and neck). These outcomes validate the use of goat and sheep impacted on the thigh as models for PMHS skin perforation studies[193]. The use of animal models in place of PMHS provides benefits in terms of ease of supply, ethics, etc..

The outcomes from the skin perforation target comparison also showed the dissimilarity between PMHS skin and pig skin, where pig skin had an average V_{50} 30% greater than the PMHS performance. Whilst pigs are commonly used for skin perforation assessments, the results cannot be directly applied to humans, or the skin perforation risk will be significantly under-estimated. This could have major implications if pigs (or pig skin) are used to assess the safety of a given

[193] Supported by the outcomes from Equation 8: The final version of the expanded empirical skin perforation equation.

scenario or provide collateral damage assessments, where it is important that the risk is not under-estimated (i.e. determining the scenario safe when it is not).

As for the selection of a suitable muscle tissue simulant in the literature, the choice of a given animal model for skin perforation studies has often not been validated. It is recognised that skin perforation studies are non-trivial, but there has been ample data available in the literature to use as the baseline PMHS performance against which animal models could be validated. Although not a direct aim or objective, the validation of specific animal models for ballistic skin perforation (and muscle tissue) studies has been specifically addressed within this thesis[194].

The testing detailed in Section 5.4 was intended to characterise the effect of different storage conditions of pig tissue on the subsequent skin perforation and DoP response. Despite a large number of shots across 4 targets, the effect of storage was not distinct. Statistical differences between the fresh and refrigerated pigs were only observed for half of the conditions tested. This indicated that whilst storing targets refrigerated for 1 week prior to testing can cause a reduction in the skin perforation V_{50} or deeper penetration at equivalent velocities to a fresh pig, it is likely due to an increase in the variability of the response after targets had been stored.

The data for the frozen targets were much more limited, and did not show any differences to the fresh tissue. However, the frozen target might be expected to have the same consequences as for the refrigerated targets of increasing the variability in the target response. Differences in the way the cells are damaged through each storage process could lead to variation in how the resulting ballistic performance of the tissue is changed relative to fresh (or live) tissue. In refrigeration cell damage is due to decomposition and in frozen storage it is due water freezing and expanding. In both cases it would be expected that cell

[194] The fitness for purpose of a given model depends on the requirement, consequently the validity of any model needs to be confirmed for the given scenario or application. It cannot be stated that a given model (in this case goats or sheep as models for PMHS for ballistic skin perforation assessments) are ‘universally valid’.

damage would lead to some degree of lowering of the skin perforation V_{50} and an increase in DoP. It is expected that minimising the severity of storage (i.e. refrigeration over freezing is preferable) and reducing the duration of storage as far as possible will help to minimise these potential effects.

Original DoP data was generated from the skin perforation testing within Section 5 (n=149 for non-zero penetration depths) to add to the existing muscle tissue penetration dataset from the literature (n=254). This has greatly increased the available data used to aid the selection of suitable muscle tissue simulants. Whilst this additional data is still clustered at velocities near the skin perforation V_{50} (already discussed as one of the limitations in the DoP data form the literature), it does help to provide additional confidence in the average muscle tissue response due to the significant variability of the biological tissue. The original DoP and skin perforation data generated provided an extended range of projectile properties compared to that already collated from the literature (for example the glass and ceramic spheres, 3-20 mm diameter to increase the understanding on the effect of secondary fragments). This extended range of data helps to "validate the models over a broad range of input parameters", one of the secondary objectives from Section 1.2.2.

11.4 Discussion of skin perforation and eye penetration empirical predictions

A simple empirical equation for prediction of the risk of skin perforation was considered based on projectile sectional density and velocity of the form of the majority of the equations from the literature (Section 3.7). However, this failed to take account of the potentially significant factors identified from the literature review that may influence skin perforation (Section 3.8). Use of a simple equation of this form would not have produced accurate or reliable skin perforation predictions (for example approximately 30% of the available skin perforation data was from tests on pigs, which would cause any predictions based on a combined dataset to over-estimate the risk of skin perforation).

The expanded empirical equation; "Equation 8: The final version of the expanded empirical skin perforation equation" was generated to account for the different

impact conditions to provide accurate and reliable predictions of the skin penetration or perforation outcome. The factors affecting skin perforation included in Equation 8 were the skin perforation prediction method, target type, body region, backing of skin and projectile geometry.

Despite some of the outcomes of Equation 8 appearing obvious, such as a pointed projectile will perforate skin at lower velocities compared to an equivalent blunt projectile, these effects had only been characterised from pairwise comparisons in the literature. Their predicted affect for other impact conditions had not been previously established. The benefits of this equation over other existing methods were considered to be:

- An extensive range of experimental data (142 separate tests, producing 521 data points for the different skin penetration and perforation calculation methods) were used to determine the factors affecting skin perforation, rather than comparing individual V_{50} values. This means Equation 8 is “applicable to a broad a range of input parameters to enable its use over a wide variety of scenarios”, addressing the secondary objectives from Section 1.2.2.
- It is the first approach to explicitly determine, account for, and to demonstrate the degree of influence of each of the significant target and projectile parameters, across a range of projectile properties. This is in contrast to using just the velocity and projectile sectional density[195] and either grouping all data together generically (which results in inaccurate predictions), or using multiple equations for specific scenarios (which adds complexity and reduces the range of input parameters over which the equations are applicable or valid).
- It provides the ability to scale results from other testing, which is not possible with the other approaches identified in the literature. For example Equation 8 can be used to estimate:

[195] Or other measure of projectile mass and/or area.

    - The human skin response from pig testing data (enabling physical testing to be conducted against the more practical pig target, but outcomes scaled so as they do not over-predict the response of human skin).
    - The skin performance for vulnerable groups (based on child PMHS parameters), given test data on other targets or estimated directly from the projectile properties. This can then be used to better support safety cases or collateral damage type assessments providing a metric with lower residual risk in the outcomes.
    - Estimation of the response of skin under target conditions which have not been experimentally investigated (within the applicability range of the model). This is possible as the target parameter values are calculated across all the data accounting for the different factors. For example the dataset did not contain any experiments for pig skin tested completely isolated (unbacked), but this is considered within the applicable range of Equation 8 and could be estimated using the parameters in Section 6.1.4.
- Should data for additional conditions within any of the different factors be identified (e.g. testing conducted on a different body region) it may be possible to add an extra parameter value for this condition without effecting the existing equation. This reduces the resource required to update the equation and means that once updated (given the same input conditions) the equation will maintain consistency, providing the same output as prior to any updates.

Although different parameters were generated for Equation 8 for different storage conditions (fresh, refrigerated and frozen-thawed), low confidence was placed in the resulting parameter values. This (in combination with the studies on skin and penetration into muscle tissue for different storage conditions in Section 5.4 and the velocity loss in muscle tissue validation for live and dead tissue in Section 9.3.2.3) has led to the conclusion that the effect of storage conditions on the resulting skin perforation velocity is not significant, other than to increase the variability of the target response.

The practical testing on different storage conditions (discussed in Section 11.3) indicated that storage (of any type) compared to fresh tissue is likely to reduce the resulting skin perforation V_{50}, however, Equation 8 predicts a higher skin V_{50} for refrigerated compared to fresh targets at sectional densities over 1.5 g cm^{-2}. This may be attributed to the variability of the individual V_{50} values on which the equation was generated or possible oedema in the tissues. The parameters for Equation 8 for storage conditions are given to help bound the potentially variable performance from storing skin prior to testing. To predict the skin perforation V_{50} velocity for stored tissue, Equation 8 should be used with the fresh parameter value. An indication of the upper and lower average variability from the different storage conditions can then be estimated by recalculating the output from Equation 8 with each of the refrigerated and frozen-thawed parameter values regardless of the actual storage condition desired to be modelled.

An assumption made when using Equation 8 is that the skin is perforated when $V_s > V_{50}$; even though some perforations are expected below this velocity and some non-perforations above this. Predictions using Equation 8 related to safety assessments should consider adding additional safety margins into the outcome because of this. An alternative solution is to use “Equation 9: Probability of skin perforation (simple and expanded forms)” to predict the velocity corresponding to the desired level of residual risk (for example this may be the 5% risk, instead of the 50% risk from Equation 8)[196].

As noted in Section 6.1.6, the V_{50} predictions between Equation 8 and Equation 9 differ for identical input conditions which could lead to discrepancies. Whilst Equation 9 has advantages in being able to predict the any probability of skin perforation, the equation has only been verified and not properly validated. It was also assumed that the parameter values used for Equation 8 were suitable for Equation 9. Due to the need for individual shot data to generate the curve fitting constants, Equation 9 uses a different base dataset to Equation 8 and is therefore likely that the parameters are not optimised for Equation 9. It was considered that

[196] Noting that estimates from a probit model are less reliable at extreme probability values.

Equation 8 would be sufficient for most applications and to avoid confusion and additional complexity, these same parameters were left unchanged for Equation 9.

An empirical equation for eye penetration was based on a probit fit to the raw shot eye penetration data, rather than the V_{50} data as performed for the skin perforation equations. This was due to the very limited V_{50} data for PMHS eyes and would have provided inaccurate predictions. Sufficient raw shot data was available for PMHS eyes on which an equation to predict the probability of an eye penetration could be based (Equation 10).

In contrast to the skin perforation data, the only factors considered for the resulting risk of eye penetration were the energy density of the projectile (which accounted for the projectile velocity, mass and cross sectional area) and target species (PMHS or pig). It may be possible to determine additional factors that influence the risk of eye penetration such as storage condition and projectile geometry, as for skin perforation or the mounting type (left intact in the head or removed and embedded in gelatin, etc.). The need to account for additional factors was not considered necessary due to the response of eyes showing high potential variability in performance (a difference in velocity of 25% was recorded between the highest non-penetration and lowest penetration impact from a single series of testing with otherwise identical conditions [188]). It is likely that inclusion of additional parameters into Equation 10 would not improve its performance sufficiently to warrant the additional complexity.

An existing empirical equation for eye penetration in the literature [171] based on the probability of eye penetration was found to give a very similar prediction to Equation 10 developed within this thesis. This was despite the development of Equation 10 based on including an additional 199 impacts. This showed that despite a dataset almost double the size used here, the risk of eye penetration has been well characterised and modelled in the literature. This is likely due to the high potential morbidity associated with severe eye penetrating injuries, their relative vulnerability to penetration and interest for a range of different

applications: in the automotive industry for car crash testing, for recreational activities (airsoft, paintball and air rifle shooting), as well as military applications.

Equation 10 (and those from Kennedy [171]) considered the difference between the response of pig and PMHS eyes, showing PMHS eyes were predicted to be penetrated at approximately half the energy density compared to pigs. This shows that as for skin perforation, pig eyes are not a suitable model for human eyes unless the outcomes are appropriately scaled. Consequently and due to the majority of data used to construct Equation 10 based on the performance of pig eyes; a combined target dataset use to predict the risk of human eye penetration would greatly under-estimate the risk.

In order to generate a performance metric that could be applied more easily to the development of a physical eye penetration model (the MDFPIM V2.0 detailed in Section 10.4 and discussed in Section 11.8), the energy density corresponding to a 50% risk, $\left(\frac{E}{A}\right)_{50}$, of human eye penetration was used. The resulting prediction (Equation 11) was able to provide accurate predictions of human eye penetration performance which could not be obtained by generating this response directly from the V_{th} and V_{50} dataset.

11.5 Discussion of physical model for muscle tissue

11.5.1 Discussion of methods for the muscle tissue simulant comparisons

The selection of an appropriate muscle tissue simulant is a topic of huge debate within the wound ballistics literature. As discussed in Section 3.9.3, no suitable validation of muscle tissue simulants has been conducted in the available literature.

The permanent DoP and retardation response of a muscle tissue simulant are independent of each other: a material can be made to match the DoP response to muscle tissue but not retardation, or vice versa. Consequently both metrics were validated separately. This differentiation between DoP and retardation validation does not appear to be well understood within the wound ballistics

literature and has led to researchers using simulants for retardation studies of bullets based on (limited) DoP validation between the simulants and real muscle tissue. The implications of this inappropriate assumption are discussed later in this section.

In order to consider both the DoP and retardation response of the simulants, three different comparison methods to real muscle tissue (with skin) were utilised:

- Normalised DoP over density with velocity compared to dead PMHS and animal muscle tissue with skin (Section 7.2).
- Energy loss (retardation) in 100 mm thick targets compared to that in live pig thighs (Section 7.3) based on steel spheres.
- Penetration and retardation using equivalent muscle tissue thickness scaling (Section 9.10).

Each comparison method had its own benefits and limitations. Of these three methods, only energy loss comparisons have been conducted in the literature to assess tissue or to validate simulants. The use of the normalised DoP over density function as well as the equivalent muscle tissue thickness scaling are considered novel for this application and provide many benefits over the previous methods[197].

The use of the normalised DoP over density function overcame the major drawback of using a single projectile to compare between muscle tissue and simulants. This had been one of the major limitations to validating muscle tissue simulants over the required range of projectile impact conditions, without the need for matched pairs of data (i.e. the same projectile and velocity range in muscle tissue and each simulant). The use of the normalised DoP over density function enabled some of the effects of the projectile properties on the resulting penetration response to be accounted for; projectile diameter and density (and

[197] Previous comparison methods have been simple DoP comparisons between matched projectiles, or normalised DoP (which is the DoP divided by projectile diameter) for projectiles all of the same density.

therefore mass), greatly increasing the dataset for which comparisons could be made.

Limitations of the normalised DoP over density comparison were that the real muscle tissue data were exclusively for dead tissue, some of which had been stored (refrigerated or frozen - thawed) prior to testing. This is not ideal for modelling the response in a live human as storing of tissue prior to testing has been observed to increase the variability in its response (Sections 5.4 and 6.1.5), so is a less reliable model.

The normalised DoP over density function does not fully account for all the projectile variables that would collapse the data onto a single curve, even when considering only spherical projectiles (Section 4). Reference [200] suggests that this is due to strain rate behaviour in the target, which itself is dependent on the projectile diameter (based on a virtual model to describe penetration into 20% gelatin at 10°C).

The combined data for different projectile geometries in the normalised DoP over density comparison increased the variability of the data, but was considered a justifiable compromise in order to extend the velocity range over which the comparison could be made[198].

The inclusion of cylinder and CN cylinders reduced the normalised DoP over density value compared to spheres at corresponding velocities (as they have higher drag co-efficients). The data presented in the normalised DoP over density comparison do not indicate which data points relate to which geometry projectile, meaning the degree of this shift cannot be judged. This is addressed within the 'penetration and retardation using equivalent muscle tissue thickness scaling' comparison which can be viewed to supersede the normalised DoP over density comparison (as well as supersede the energy loss in 100 mm thick targets comparison).

[198] The data for 20% gelatin at 10°C, Perma-Gel and real muscle tissue each used a mix of different geometry projectiles.

It is possible that with inclusion of the correct metric, effects related to projectile geometry could be accounted for within a modified version of the normalised DoP over density function. The normalised DoP over density function was considered fit for purpose for the situations in which it was applied and limitations were addressed by other comparison methods.

The energy loss (retardation) in 100 mm thick target comparison had the main benefit of being able to validate the muscle tissue simulant response against live animal tissue. Energy loss in a tissue simulant has been used to do this type of comparison previously in the literature [107-109; 111; 123; 217], but with limitations. For example, whilst testing has been performed at different impact velocities or energies, results were only analysed in relation to a given impact velocity group, rather than the relationship across the impact velocity (or impact energy) range being determined. This also meant that variability in the impact velocity from the practical testing could not be accounted for, but could be tested for significance between different targets.

The determination in Section 7.3 that the energy loss in the nominal 100 mm targets was directly proportional to the impact energy for steel spheres meant that the suitability of muscle tissue simulants could be assessed continuously across this range of impact conditions.

The equivalent muscle tissue thickness scaling comparison is based on the premise that the underlying FREMs used to calculate the scaling ratios are valid (the FREMs are discussed in Section 11.7).

The equivalent muscle tissue thickness scaling comparison is considered to be a powerful technique for the validation of different simulants because it has the ability to account for DoP and retardation data, all projectile properties considered significant, as well as the target thickness. This avoids many of the limitations of both the normalised DoP over density and energy loss comparisons. Figure 118 (which showed only the best fit lines for the different targets for each of the DoP and retardation comparisons) provided clear indications of the accuracy and validity of each of the targets for DoP and retardation predictions across the range of velocities assessed. The equivalent muscle tissue thickness scaling is

recommended as the method to use for comparing or validating ballistic muscle tissue simulant performance.

11.5.2 Discussion of outcomes from the muscle tissue simulant comparisons

Based on the equivalent muscle tissue thickness comparison for the combined DoP and retardation data (Section 9.10), the average ratio of (Dstl) 20% gelatin at 10°C compared to (that predicted in) muscle tissue was 0.987±0.009 at the 95% confidence level (or 98.7±0.9% as a percentage). This was shown to be a velocity independent relationship and validated between 100-1075 m s^{-1}. This validation shows the suitability of (Dstl) 20% gelatin at 10°C for both DoP and retardation studies and addresses (aspects of) each of the two aims of this thesis in Section 1.2.1.

Both the 10% gelatin at 4°C and Perma-Gel showed velocity dependence for the predicted equivalent muscle tissue thickness, in both the DoP and retardation responses. Whilst these simulants were shown to provide a poor match to the (predicted) muscle tissue response, it did demonstrate that it is critical to ensure tissue simulants are validated at the intended velocities where the model(s) will be used. An air rifle calibration test at approximately 180 m s^{-1} does not provide validation or confidence in the simulant response for bullet impacts which may be up to 4 or 5 times greater velocities.

Dstl 20% gelatin at 10°C provided comparable equivalent muscle tissue thickness for the retardation data and therefore matches the forces on the projectile compared to those in muscle tissue. Projectile behaviours such as retardation, deformation, fragmentation, tumbling, as well as the extent and depths at which these occur in Dstl 20% gelatin at 10°C should match muscle tissue.

In certain situations (i.e. non-deforming, non-tumbling projectiles), the use of other muscle tissue simulants may be suitable for comparative studies. Comparisons between projectiles with different damage mechanisms, e.g. non-tumbling projectiles to bullets that are designed to tumble, deform or expand are unlikely to be valid if conducted in 10% gelatin at 4°C (or Perma-Gel). The extent

and depths at which these occur may differ as the forces on the projectile will be lower compared to muscle tissue and different mechanisms may dominate. For example at extreme cases (e.g. longer engagement ranges), this may indicate that expanding bullets do not expand in 10% gelatin at 4°C when in muscle tissue or 20% gelatin at 10°C they would under the same impact conditions.

If predictive studies are required, the outputs are required to be scaled to the tissue(s) of interest. For 10% gelatin at 4°C and Perma-Gel this scaling is velocity dependent. Predictive scaling from 10% gelatin at 4°C or Perma-Gel to muscle tissue would only be possible for non-deforming, non-tumbling projectiles without further development of the FREMs. This limitation rules out the ability of a large proportion of studies using bullets in 10% gelatin at 4°C to provide predictive outcomes. Misleading conclusions are likely if the outcomes of testing in 10% gelatin at 4°C are taken as a direct measure to real muscle tissue.

The use of projectiles that were non-tumbling, non-fragmenting and non-deforming for the comparisons in this thesis eliminated the issues faced by previous comparisons using bullets. In spite of this, the validation of (Dstl) 20% gelatin at 10°C was such that it is expected to be a valid muscle tissue simulant for DoP and retardation studies: for ballistic projectiles less 1000 m s^{-1} and between 2.7-20 mm diameter. This covers the vast majority of military and civilian small arms bullets (both handgun and rifle). The reliability of (Dstl) 20% gelatin at 10°C is reduced at velocities close to[199] the skin V_{50} where 20% gelatin at 10°C is likely to over-predict the DoP (under-predict retardation) compared to muscle tissue and skin. This limitation can be addressed:

- During physical testing, with the use of a physical skin simulant on the front impact face of the 20% gelatin at 10°C (Section 8 and Discussion Section 11.6).

[199] Based on the FREMs in Section 9.4, the effect of the skin on the resulting DoP was shown to rapidly diminish as V_S/V_{50} increases from 1. The effect of the skin layer on reducing the residual velocity following skin perforation can be considered to be negligible when $V_S/V_{50} \geq 3$ ($V_S/V_R < 1\%$).

- During analysis of test data for 20% gelatin at 10°C using the FREMs to adjust the measured DoP or retardation by accounting for the effect a skin layer would have had (Sections 9.4 and 9.5).

To avoid breakdown of collagen fibres due to excessive heat when making 20% gelatin, water temperature should not exceed 75°C. If water baths or similar methods are used that maintain the gelatin temperature for extended periods, maximum temperatures should be reduced.

Calibration of a muscle tissue simulant is considered essential. Some researchers have modified the air rifle based calibration test by using a higher velocity projectile [38; 91; 163]. The drawback is that (depending on the projectile chosen) higher velocity impacts are likely to cause more damage to the target, reducing the usable volume of the target for the actual testing (as noted in Reference [158]). This could be avoided by performing calibration tests on a separate block to those used for actual testing; however, this can be wasteful and (depending on the requirement) it may be necessary to calibrate every block rather than a single example from the each batch.

Considering the purpose of the calibration test; as a method to verify the correct response of the gelatin (or other simulant) under controlled input conditions, high velocity calibration is not required. The calibration test is performed to verify (as far as reasonably practicable) that the gelatin has been made properly to the stated method (i.e. correct concentration and not overheated during mixing), has reached full cure and has been tested at the correct usage temperature. Validation for a given application should have been confirmed or conducted prior to verification.

The calibration standards given in APPENDIX D (D.5.2 and D.5.3) use easily obtainable air rifles and projectiles. This allows calibration to be conducted by users who may not have access to more tightly controlled firearms and ammunition or at locations where high velocity fragment impacts using bespoke pyrotechnic charges to achieve the desired velocities may be less practical.

There may be scenarios where a muscle tissue simulant other than 20% gelatin block at 10°C may be preferable. For example a potential exploitation for the synthetic gelatin alternatives (Perma-Gel, Clear Ballistics Gel® and Stabili-gel) would be for molding complex geometries, to enable the assessment of PPE 'dressed' onto a human geometry target, in outdoor blast trials. However, these materials have other limitations, most notably their dissimilarity to penetration and/or retardation response of real muscle tissue.

Stabili-Gel (32.5% SEBS) was observed to give a similar penetration (DoP) response to muscle tissue and although it has long shelf life and (may be) reusable, there remain issues:

- Discontinuities were observed in the penetration response within certain velocity windows (these velocities appeared projectile dependent). This also shows a potential benefit of conducing impacts at a variety of impact velocities, rather than at pre-defined velocity groups which is unlikely to have detected this response.
- The simulant was more elastic than 20% gelatin at 10°C (therefore assumed to be more elastic than muscle tissue). Whilst the permanent DoP response *may* make it a suitable muscle tissue simulant, the retardation response (and therefore tumbling, etc. of a projectile) are unlikely to be suitable as it provides lower retardation than in muscle tissue.

11.5.3 Discussion of muscle tissue simulant cavitation experiments

The testing of Dstl 20% gelatin at 10°C in four different lateral size targets, with and without constraint (Section 7.5), provided insight into the factors that are essential to consider when using the maximum temporary cavity as a metric for injury.

The size of the gelatin block did not (nor is it expected to) affect projectile response (i.e. DoP or retardation). The size of the gelatin block does significantly affect the temporary cavity formation. Therefore, if experiments are conducted only to investigate the projectile response, target size and impact location do not

matter. Multiple shots can be conducted against a single target as long as the projectile path does not intersect previous damage. Projectile response testing will remain valid even if the block ruptures during testing from the cavity formation, as this will be at a later time to the passage of the projectile.

The constraint applied to the gelatin blocks in the testing in Section 7.5 (4 mm polycarbonate mold superglued at the joins with the impact and exit faces unconstrained) were far from ideal for their intended purpose as they failed part way through the cavity formation process. Although differences in the cavities produced between free and the constrained targets were observed, the constraint condition should be considered more of a 'partial constraint'.

If the constraint had not failed, the resulting temporary cavities are likely to be further reduced. It is unlikely in the setup in Section 7.5 that the temporary cavities would have been completely suppressed along the entire length of the target. Firstly, the 4 mm polycarbonate is likely to flex to some degree and therefore will not provide a perfectly rigid edge condition. Additionally, the different size targets showed differences in the depth at which the maximum diameter of the temporary cavity was observed. This suggested the gelatin flowed in the direction of firing. A feature of gelatin testing observed on HSV is also the temporary displacement of gelatin in the direction of the weapon system. This means that as the impact and end faces of the target were unconstrained, the gelatin at each of the ends of the target would be under different constraint conditions to gelatin in the middle of the target. The distance over which these end effects occur is unknown and cannot be determined form the current testing.

The point of impact on the gelatin block was observed to influence the resulting cavity formed as this was effectively the same as changing the lateral dimensions of the target from the point of view of the projectile.

Using the measured maximum temporary cavity in gelatin as a metric for injury requires the following considerations[200]:

[200] These conditions are a condensed version of the issues discussed in Section 7.5.9.

- The size of gelatin block suitable for terminal effects work depends on the threat being considered:
    - Too small a block for the given threat will cause the block to split and invalidate cavity results;
    - Cavities produced in different size blocks (or off centre impacts) are not directly comparable with potential to cause issues for sharing of data;
    - Too large a block will degrade the quality of imaging;
- The results from wound studies on tissues tested in isolation should be treated with caution.
- The distance from the projectile to the block edge will change during the penetration process for most military bullets due to divergent shot lines. The cavity may be 'misrepresented' or 'misinterpreted' due to varying distance from the projectile to the block edge.
- The bottom half of the temporary cavity, viewed from the side, may need to be treated differently to the top half due to constraint on the cavity due to the table on which the gelatin is placed.
- HSV of the target from above for non-tumbling projectiles would remove issues due to confinement effects from the base on which the gelatin is placed compared to the side HSV view.
- The maximum diameter of the temporary cavity (and depth at which it occurs) is heavily dependent on the size of the target:
    - The depth of the maximum diameter is not analogous to the depth of maximum energy deposited
    - To ensure consistency (particularly for analysis of bullets) the average depth at which the maximum cavity radius was measured in each direction from the shot line should be used (where the actual shot line through the gelatin may not be straight).

All the testing within this thesis has been conducted on cuboidal targets, generally with a square impact face. As target size (and/or point of impact) affect the cavity response, it is reasonable to assume that for a sphere where a symmetrical cavity in all directions perpendicular to the shot line would be expected, the cavity in the

direction of the corner of the block would be different to that along the shortest distance to the block edge. With HSV analysis of the temporary cavity this cannot be seen as the camera needs to view through a flat face so as not to distort the observed cavities. It may be possible to investigate using the permanent crack length measurement technique [143] as a proxy for estimating the maximum temporary cavity volume and would be interesting to compare the difference between the same diameter/width square and circular cross section targets.

Use of cylindrical gelatin targets for cavity measurement is not considered practical due to refraction of light through the target distorting the measured cavity sizes from HSV.

The outcomes and understanding obtained from the testing have been used to influence the practical gelatin testing conducted and analysis methods used within Dstl (which are listed in Section 7.5.9). These changes aim to make the gelatin testing more consistent and reliable. The net result is that greater confidence can be placed in the outcomes of the testing. In relation to the gelatin testing conducted by Dstl, this means that equipment for UK Armed Forces and police can be better optimised.

A metric of ‘damage’ that can be extracted from 20% gelatin at 10°C that is independent of block size, constraint and impact location on the block would be ideal. The projectile response is independent of these target factors, but the target response metrics considered within this thesis are not. It may only be through development and validation of the FREMs in Section 9 and discussed in 11.7 (or other virtual models) that the projectile response from physical testing may be interpreted in terms of a predicted ‘standardised target’ response, therefore independent of the target size used during the practical testing.

11.6 Discussion of physical skin simulant model

The physical skin simulant was required to have a thickness similar to average human skin (in the range 2.0±0.5 mm), so that subsequent penetration into the muscle tissue simulant would not be affected by an unrealistic skin thickness. Some skin simulants from the literature used skin simulants between 7-8 mm

thick [106; 239], which if used for DoP assessments for a combined skin and muscle simulant model would result in incorrect DoP measurements compared to real skin and muscle tissue.

Up to eight different projectiles were chosen to allow evaluation of the different skin simulants over a wide range of projectile sectional densities. The use of a single projectile had been a significant limitation of the majority of skin simulants ballistically assessed in the literature. The performance at one projectile sectional density does not indicate its accuracy or validity under other conditions.

The simulant selected as the basis for the physical skin simulant model, which performed closest to the optimal performance curve, was the 2.5 mm thick (2 layer) synthetic chamois. The synthetic chamois provided good representation of to the skin perforation (V_{50}) performance of child PMHS skin (based on Equation 8) apart from at very low projectile sectional densities (<1 g cm^{-2}) where it required a higher velocity to perforate compared to the desired performance.

The child PMHS skin performance (and therefore physical skin model based on the synthetic chamois and gelatin) was taken to represent the 'worst likely case' civilian or vulnerable group population and is suitable for situations where the risk does not want to be under-predicted, i.e. a collateral damage type prediction. This means there is low residual risk of the model incorrectly predicting a scenario to be safe when it is not, apart from where projectile sectional densities are 0.5 g cm^{-2} (the lower validation limit) to approximately 1.0 g cm^{-2}. At the 0.5 g cm^{-2} projectile sectional density extreme, this under-prediction could be up to 20% of the corresponding velocity compared to child PMHS skin.

If it is known or reasonably expected that fragments with low sectional densities require assessment for a given scenario, then it is suggested to use the MDFPIM V2.0 (or V2.1 / V2.2), either in addition to, or in place of the chamois and gelatin based skin simulant. The MDFPIM V2.0 has been validated for skin perforation with projectile sectional densities between 0.22 to 6.55 g cm^{-2} and provides a very close match to child PMHS skin without under-predicting the skin perforation risk (see Section 10.4.6). The average response of the MDFPIM V2.0 was within

5.5 m s^{-1} of the child PMHS performance from Equation 8 over the entire range of projectile sectional densities tested.

A verification test (calibration) has been developed for the physical model of skin perforation. This provides confidence to future users of the model through simple tests that the materials used to construct the model will provide the desired response in terms of skin perforation risks.

The physical model of skin perforation is only valid when the synthetic chamois is backed by 20% gelatin at 10°C. There is no specified thickness of gelatin required for this backing. In the testing conducted, the gelatin backing was 150 mm, but it is presumed this could be reduced to at least 50 mm depending on the projectiles being evaluated. Projectiles with lower skin perforation velocities (higher sectional densities) would require thicker gelatin backing, as the skin simulant and gelatin are likely to deform to a greater degree before rupturing. Any contact with a rigid backing after the gelatin, if the gelatin is not thick enough, is likely to alter the skin simulant perforation response.

A thin gelatin backing would make the model more practical where larger areas are required to be assessed, however would also limit the time at which the gelatin could maintain 10±2°C (its required usage temperature).

It is anticipated that the physical skin simulant model has the best potential for exploitation where there is also a requirement to determine additional transient or projectile deformation effects within gelatin (if the skin simulant is perforated) or when explicitly considering the effect of the skin on penetration into muscle tissue.

For physical skin perforation assessments the MDPFPIM V2.1 or V2.2 may be more suitable models. Where there is a requirement to assess skin perforation and obtain DoP measurements, the MDFPIM V2.0 is likely to be a more suitable model (the FREMs in Section 9 could be used to estimate the equivalent penetration in real tissue from the predicted MDFPIM outputs). An example of the use of the MDFPIM V2.2 in this context was an assessment conducted (and supported by the author) in the same ballistic range used for the entire gelatin

testing conducted in this thesis. The ricochet hazard (in terms of skin perforation) from small arms rounds after impacting a steel plate was required, along with an indication of the degree of overmatch if skin perforation was indicated as a risk. The MDFPIM V2.2 was selected as the most suitable model for this purpose, as the resulting fragments were considered to be potentially very small[201].

The synthetic chamois is a commercial off the shelf product, subject to change or may be discontinued without notice. It is not ideal as the basis of a material for use in an injury model as future supply cannot be guaranteed. Any materials used as a skin simulant should be verified using the calibration procedure developed for the model (Section 8.6), or validated against Equation 8.

11.7 Discussion of virtual models (FREMs) for muscle tissue and gelatin

A number of virtual models were identified and assessed for their ability to predict DoP in 20% gelatin at 10°C or muscle tissue. Up to 659 experimental shots in Dstl 20% gelatin at 10°C (from Section 7.2) were used to select a suitable predictive model. The number of shots used for each equation depended on the validity of the projectile parameters for that equation (for example, some were only valid for spheres). This was an extensive (large number of shots) and broad (in terms of projectile properties) dataset against which the suitability of the different equations were judged. This broad range of input parameters helped determine the fitness for purpose of the equations assessed over a wide variety of scenarios.

The models based on Peters [252-254] for 20% gelatin at 10°C and muscle tissue were taken as the basis for the FREMs within Section 9. The equations have been described, developed and validated which allow a wide range of outcomes to be generated for both 20% gelatin at 10°C as well as multiple different tissue types. These equations are considered to provide a significant capability for

[201] Figure 200 in APPENDIX M shows the setup for this assessment.

virtual modelling over a wide range of input conditions. Whilst many of the equations are not new, adequate validation had not been previously presented. This would have prevented their use in many applications as the reliability or confidence in the predictions was not known or could not be quantified.

Validation of the FREMs has been conducted along with characterisation of each model's reliability or confidence based on the variation in the underlying data. This enables the underlying potential variability from each prediction to be combined. Due to the inherent variability of real tissues, the overall model predictions can be significantly affected if the variability is accounted for and therefore consideration of this aspect is critical.

Whilst the average case of these predictions are frequently used to demonstrate the FREM predictions within this thesis, predictions based on the upper and/or lower error bounds could also be used. For example, for a safety case or collateral damage type assessment, the upper bound that corresponds to the most severe risk could be used, so as not to under-estimate the potential hazard. For a lethality or effectiveness type assessment, the lower bound that corresponds to the least severe risk could be used, to provide confidence that the projectile will deliver the desired effect.

The (aspects of the) FREMs in Section 9 that are considered novel to the wound ballistics literature (in addition to the validation already discussed) are:

- The ability to account for the effect of skin on the subsequent DoP or retardation in gelatin or muscle tissue (Equation 24 and Equation 25).
- The consideration of target size on the target response (Section 9.6.3).
- An applied hybrid tissue retardation model (Section 9.9).

The effect of skin has been shown to be important for impact velocities close to the skin V_{50} so as the resulting DoP or retardation is not over-estimated. It can also be used to estimate the effect of skin from testing using bare gelatin without having to repeat the physical tests (discussed in Discussion section 11.5.2).

The effect of target size on temporary cavity formation could not be accounted for within the FREM using the Dstl 20% gelatin at 10°C data from Section 7.5. This was partially due to the fact that the point of impact on the target in the experiments was not as tightly controlled as desired. It was originally anticipated that the parameter $\bar{g}_\infty$ within Equation 27 could be used to simply account for the target size. However, this was not the case and predictions using this technique greatly under-estimated the size of the maximum temporary cavity at shallower penetration depths (<125 mm).

A FREM to account for target size (or off centre impacts) would enable better use and sharing of practical test data that is often limited in terms of the number of shots that can be achieved.

The temporary cavity predictions in this thesis have been validated against the response of Dstl 20% gelatin at 10°C and not muscle tissue. Therefore the implications of using these equations to model either bulk muscle tissue, or specific muscle groups on the body is unknown.

The hybrid tissue model allows impacts to be considered in terms of realistic retardation in a specified tissue. Penetration through the body could be accurately modelled based on specific impact locations and based on the different tissue types traversed. This is in contrast to considering the retardation response of all tissues to be approximated by muscle tissue or a single tissue simulant. Depending on the tissue type and projectile velocity, the deceleration on the projectile can be increased or decreased compared to muscle tissue. Consequently the depths in the body at which energy is deposited by the projectile and therefore the pattern of tissue damage with depth will be re-distributed compared to single tissue (simulant) based predictions. This could mean the expected severity of injuries from a given projectile are altered as the energy deposited based on the hybrid tissue model could be predicted to move either closer to, or more distant from vital organs.

Whilst the parameters for the different tissues originate from the ComputerMan model, the equations are not openly available and require a validated equation for retardation in muscle tissue in order to apply them.

There remain limitations with the hybrid tissue model in that only the parameters for a small selection of different tissue types are available and validation is limited to a sub-set of these tissue types. Obtaining raw rather than averaged data from studies given in the literature [107; 108; 124; 217] may provide sufficient information on which to verify additional tissue types within the hybrid tissue model (e.g. liver, lung, heart and kidney).

Based on considerations from the constrained gelatin testing (Section 7.5) and the relationship for tissue damage due to temporary cavity expansion (Section 9.8), wounds from ballistic projectiles could be reduced in severity by clothing or PPE designed to restrict the formation of a temporary cavity in the body. Practically this may only be possible in the extremities and the role of temporary cavity damage has only been shown for muscle tissue within this thesis. A material to provide this constraint without hindering movement may be feasible given the timescale of the tissue response during cavity formation (few milliseconds from formation to collapse) compared to the timescales over which normal movement occurs.

This type of PPE could potentially reduce the mass of damaged muscle tissue by up to 40% (based on pig thigh plaster cast experiments), for minimal burden, especially compared to traditional materials used to mitigate bullet injuries. The implications of up to a 40% reduction in the mass of damaged muscle tissue in the extremities has not been considered in terms of its clinical significance (resulting injury severity or medical management) within this thesis.

An additional benefit of a constraining PPE would be that it would not be ‘overmatched’ in the traditional manner. The reverse is likely true (up to the failure of the constraining material); the more severe the threat, the greater the contribution of the temporary cavity damage mechanism to overall muscle tissue damage and therefore the more benefit the PPE should provide.

This constraining PPE would also likely reduce the probability or magnitude of other effects, such as:

- Distant or remote effects, e.g. non-contact bone fracture (smaller cavities would mean the shot would have to be closer to the bone to create a corresponding loading onto the bone).
- Infection: the volume of the temporary cavity would be reduced, therefore so would the magnitude of the sub-atmospheric pressure within the temporary cavity, reducing the amount of foreign material sucked into the wound.

The ability of the FREMs to predict other projectile responses, such as tumbling, deformation or expansion, both in gelatin as well as in different tissues needs to be considered and is a limitation of the current models. This prevents their use for assessment of any bullets, which is a key focus of the wound ballistics community.

The implementation of the equations within the UK MOD V/L model; the Human Vulnerability Tool within the Weapon Target Interaction (WTI) architecture [32] and the UK MOD Collateral Damage Model (CDM) allows 'real world' injury predictions to be made. This enables design, optimisation or ranking of different PPE measures, assessment of potential threats, as well as enabling the quick running tools that are used to during operations to support Commanders' decision making.

Without the FREMs developed within this thesis, the predictions would still be required and would have to be based on other models. The predictions would then be less accurate, have lower associated confidence, require bespoke physical testing for each different scenario or rely on slower running models (e.g. FEA) that may not meet the required timeframes for a prediction.

11.8 Discussion of the physical model for penetrating injury by multiple discrete projectiles

Trials involving explosive threats may involve a requirement to assess the injury potential of the fragments generated. There was a lack of suitable models available to be able to use in this type of scenario, especially for low density and low energy fragments. The previously available models such as strawboard and

spaced metal witness packs miss capturing potentially injurious projectiles as they each require higher velocities to perforate their first layer than is needed for human eye penetration and skin perforation. Using either of these models in safety cases or collateral damage assessments could lead to erroneous conclusions on the safety of the scenario.

Development of the MDFPIM to the current version 2.0 (as well as versions 2.1 and 2.2) was performed in order to enable direct estimates for the risk of eye penetration and skin perforation from the model. This provided unambiguous and simple outputs from the models against thresholds that are commonly used to define the limits of acceptability of a system or scenario. For example, a hypothetical requirement may be that 'device "A" must not generate fragments that have the ability to perforate bare human skin at a distance of "X" metres'.

The MDFPIM V2.0 (and V2.1, V2.2) is considered novel and fills a capability gap as no other models have been deemed suitable to assess either the risk of skin perforation or eye penetration for scenarios generating multiple fragments that are expected to impact simultaneously[202,203]. Additionally, the MDFPIM V2.0 provides the capability to predict the impact velocity of projectiles that perforate the skin assessment layer. These outputs can then be used with other injury models to determine an injury severity or outcome form the testing, in the same manner as the outputs of the current models such as strawboard and spaced metal witness packs.

The MDFPIM V2.0 captures and can assess projectiles that have the ability to penetrate the eye or perforate the skin, therefore the risk of missing potentially injurious fragments is greatly minimised. Additionally, due to the design focused around low density and low energy penetrating fragments, the MDFPIM provides

[202] Simultaneously in this context means over a short timescale, e.g. a few micro or milliseconds.
[203] Other than the physical model for skin perforation and the skin simulants discussed in Section 8.2 which all have severe limitations in terms of their suitability, practicality and/or validation.

superior resolution in the velocity predictions compared to strawboard packs of 3.8 mm layer thickness and the metal spaced witness pack[204].

As with the other models developed within this thesis, an emphasis was placed on validating the MDFPIM with a large dataset containing a wide range of projectile impact conditions. This has provided a strong practical foundation that has enabled the MDFPIM to be exploited in a wide variety of scenarios. Due to the extensive characterisation, a high degree of reliability is associated with the model outputs. The consideration of factors that may affect the model response and predictions is considered to be superior to other fragment packs in many situations. For example the effects of ambient temperature (between -10°C to +40°C), long term storage of the foam (for at least 4 years, between -5°C and +45°C) and foam batch to batch variations have all been characterised (and accounted for within the model).

The generic applicability and wide dataset on which the calibration equations for the MDFPIM V2.0 were developed removes the requirement for bespoke calibration for each different type of fragment generated in every different scenario, as long as the projectiles are within the validation bounds of the model (Table 40).

Whilst the MDFPIM V2.0 temperature dependent penetration response is not ideal, the fact it has been characterised and can be accounted for in an expanded version of the calibration equation provides greater confidence in its predictions, particularly for outdoor testing where temperatures cannot be controlled. The fact that the model response is validated in the temperature range -10°C to +40°C means it is likely to be suitable for the vast majority of scenarios. This type of temperature dependent validation has not been considered for other fragment packs in the literature, which could lead to a significant source of error in their predictions.

[204] The MDFPIM V2.0 has approximately 2.5 times better resolution in terms of impact velocity predictions for the projectiles used as part of the MDFPIM V2.0 calibration. However, the maximum impact velocity that can be assessed with the MDFPIM V2.0 is much lower.

A power fit applied to each of the eye penetration and skin perforation responses of the MDFPIM V2.0 sat just below the objective performance curves over the majority of the projectile sectional density range assessed for each metric (Sections 10.4.5 and 10.4.6). The MDFPIM V2.0 (and V2.1) slightly overestimates the risk of eye penetration and skin perforation for an adult population.

This is the desired way round for an injury model that could be applied to safety cases. If the model is used to determine a scenario to be ‘safe’, then the residual risk of being incorrect is minimised. Users of the model do not need to be overly cautious about the interpretation of the predicted penetrating eye injury or skin perforation risk.

9 layers of 10 mm thick neoprene foam are used in the MDFPIM V2.0. Whilst some applications may require finer resolution in terms of the resulting velocity estimates, decreasing the layer thickness would require complete re-calibration of the model. The retardation of the projectile is affected by a combination of both the polythene layer and the foam layer. Altering the foam thickness or ratio of the foam to polythene will alter the penetration response of the model. The current layer thickness and number of layers are considered a good balance between the resolution and resource requirements for analysis.

A recurring limitation of MDFPIM V2.0 when deployed in blast trials was its susceptibility to severe damage, limiting the analysis that was possible. The model was designed to assess eye penetrations and skin perforation which limit the degree to which the model can be more robustly engineered to withstand blast conditions.

Mitigation of MDFPIM V2.0 overmatch or destruction, which limits the subsequent analysis, can be achieved by:

- Using image analysis to estimate fragment masses from the polythene hole size where fragment density is known or can be estimated if the physical fragments have not been retained in the model[205].
- Using a suite of models (for example MDFPIM V2.0 to assess lower severity injuries and strawboard or spaced metal witness packs to assess higher severity injuries).
- Deploying them at different distances from the device.

A 6 mm steel sphere was chosen for MDFPIM V2.0 batch calibration testing as it had been a common choice of projectile (with simple geometry) used in this thesis and the literature for tissue and tissue simulant testing. However, the use of a 6 mm steel sphere for the MDFPIM V2.0 batch testing provided limited resolution between different batches which showed significantly different mechanical properties. This may either be because the projectile was a sub-optimal choice, or the mechanical testing outcomes did not correlate to ballistic testing. Future MDFPIM V2.0 verification or batch comparison by ballistic testing would benefit from using a lower sectional density projectile. A 4.4 mm glass sphere may be suitable, which can then be fired from the same weapon systems as used for gelatin calibration testing.

The MDFPIM (all versions) are known to have been used in at least 23 separate trials within UK and with other nations. Individual trials have used up to 150 models each (such as that described in APPENDIX K, K.2). The type of trials in which the MDFPIM has been used includes:

- Safety assessments of;
    - Explosive devices, such as IEDs and Active Integrated Protection Systems

[205] Trials with the MDFPIM against buried explosives (an example of this exploitation is given in APPENDIX M) showed that the polythene sheeting remained intact in a continuous length, even when it appeared at first glance that the model had been completely destroyed and all foam (and embedded fragments) ejected.

    - Explosive Methods of Entry
    - Door breaching (ballistic)
    - Render Safe Procedures
    - Ricochet of small arms rounds
    - Behind barrier effects, including within vehicles and structures
- Lethality / effectiveness assessments
- PPE/ballistic material performance assessments

12 Conclusions

12.1 Development of models for the assessment of injury from penetrating ballistic projectiles

The primary aim of the work within this thesis was to “Develop (a suite of complementary) models that facilitate the assessment of injury from penetrating ballistic projectiles, in both a physical and virtual environment”.

A variety of models have been developed to meet this primary aim. The physical models developed (or enhanced) were:

- 20% gelatin at 10°C as a muscle tissue simulant (Section 7).
- Synthetic chamois backed by 20% gelatin at 10°C as a skin perforation model (Section 8).
- The MDFPIM for multiple projectile impacts (Section 10):
    - Version 2.0 to assess eye penetration, skin perforation and predict the impact velocity of the projectile.
    - Versions 2.1 and 2.2 to assess eye penetration and skin perforation.

The key virtual models developed to meet this aim were:

- The expanded empirical model of skin perforation (Section 6.1).
- The empirical equation(s) for eye penetration (Section 6.2).
- The suite of Fast Running Engineering Models (Section 9) for:
    - Predictions of penetration and retardation in a variety of tissue types and 20% gelatin at 10°C.
    - Cavitation in muscle tissue and 20% gelatin at 10°C.

The outcome of developing a “suite of complementary models” within the primary aim is demonstrated by the overview of model linkages, Figure 2.

The secondary aim of the work in this thesis was to “use the models to further the understanding of the penetration process, access the validity and limitations of the models developed”. The conclusions related to this secondary aim are described for each model in the following sub-sections. The limitations of each model have been detailed and described in the relevant section of the main body of this thesis.

12.2 Review of existing data for skin perforation, eye penetration and penetration into muscle tissue and simulants

Skin can be highly variable in its response to penetration or perforation, even with all conditions controlled as far as possible during practical testing.

The following factors were deemed to be potentially significant for determinations of skin perforation:

- V_{50} penetration and perforation prediction method.
- Projectile properties;
    - Sectional density correlated with perforation V_{50}
    - Shape/ geometry
- Target properties;
    - Species
    - Broad age distinction in terms of child / adult
    - Target area
    - Backing method

The factors above could not be properly accounted for within the empirical equations identified from the literature. This led to inaccurate predictions or equations with limited applicability.

There was extremely limited data in the literature for skin perforation or muscle tissue and simulant penetration with low density, non-metallic fragments that could be considered representative of secondary fragmentation from an explosive device.

There had been no suitable validation of any of the potential muscle tissue simulants conducted in the literature.

Consideration of “fitness for purpose” and validation of muscle tissue simulants is not common practice in the wound ballistics literature.

12.3 Studies based on the outcomes from the review of existing data

A series of studies were performed to address the limitations from the review of existing data.

Data were generated (7 V_{50}s) with low density / non-metallic projectiles, which are more representative of secondary fragments from explosive events, on freshly killed sheep and goat targets. This helped populate the lower projectile density spectrum of the skin perforation dataset.

At low velocities, at least up to 1.6 times the V_{50}, the skin provided a significant barrier to penetration by ballistic projectiles by reducing the resulting penetration depth into muscle tissue.

Different storage conditions were assessed for their effect on both skin perforation and DoP, but the effects were not distinct. Where statistical differences were observed, this was to reduce the skin perforation V_{50} or increase the DoP in the stored tissue, compared to fresh tissue.

A direct comparison of skin perforation V_{50} across 4 different targets showed that sheep and goat skin gave a comparable response to PMHS. Pig skin on the thigh and neck had an average V_{50} 30% greater than the PMHS performance.

12.4 Empirical equations for eye penetration and skin perforation

An expanded empirical equation to predict skin perforation was generated (Equation 8) that accounted for the different projectile and target factors determined to be significant from the literature review.

The benefits of this equation over existing methods were:

- It was based on an extensive and broad range of experimental data to determine both the overall form of the equation and the factors affecting skin perforation.
- It was the first equation to explicitly determine, account for, and to demonstrate the degree of influence of each of the significant target and projectile parameters, across a range of projectile properties.
- The predictions are considered more accurate, reliable and/or with a wider range of applicability than existing empirical equations.
- It provided the ability to scale results from practical testing to other conditions.
- It is straightforward to incorporate into other virtual models.

The model was used to show that pig skin gave a predicted 20-25% increase in skin perforation V_{50} compared to PMHS skin under equivalent conditions.

A probit model using raw shot data was developed for the probability of penetration for human eyes.

The model showed that pig eyes required approximately double the energy density to penetrate compared to PMHS eyes.

12.5 Physical model for single projectile impacts to muscle tissue

The permanent DoP and retardation response of a tissue simulant are independent of each other in relation to modelling real tissue and must be considered separately.

Three different comparison methods were used to account for the permanent DoP and retardation responses of a variety of muscle tissue simulants compared to real tissue and showed that Dstl 20% gelatin at 10°C provided the best match to muscle tissue in each of the DoP and retardation responses, confirmed by each of the three comparison methods employed.

Dstl 20% gelatin at 10°C provided equivalent retardation and therefore forces on the projectile to both live and dead muscle tissue.

The validity of 20% gelatin at 10°C is considered to hold when extrapolated to other projectiles (e.g. bullets).

Studies using 10% gelatin at 4°C may not be valid for representing the projectile response in real muscle tissue, particularly for tumbling or deforming projectiles, or when applying the outcomes directly to predictions on a person.

In spite of limitations identified with the synthetic gelatin alternatives, they are considered to have utility for certain scenarios.

The size, constraint and shot placement for a Dstl 20% gelatin at 10°C block affected the temporary cavity formed, but not the projectile response (i.e. DoP or retardation).

The outcomes and understanding obtained from the testing have been used to influence the practical gelatin testing conducted and analysis methods used within Dstl (detailed in Section 7.5.9).

12.6 Physical skin perforation model

The simulant selected as the basis for the physical skin simulant model was a 2.5 mm thick (2 layer) synthetic chamois backed by Dstl 20% gelatin at 10°C. It provided a good representation of the skin perforation performance of child PMHS skin over the range of projectile sectional densities considered, based on Equation 8: The final version of the expanded empirical skin perforation equation.

As with the other models developed within this thesis, the physical skin simulant model was validated over a range of projectile impact conditions to ensure its applicability over a wide variety of scenarios.

12.7 FREMs for predictions of penetration and cavitation in muscle tissue and tissue simulants

A range of FREMs have been developed and validated[206] for predicting penetration, retardation and cavitation in muscle tissue or 20% gelatin at 10°C.

These FREMS are available for use and have already been exploited by UK MOD within the following models:

- The Human Vulnerability Tool within the Weapon Target Interaction (WTI) architecture to enable design, optimisation or ranking of different PPE measures and assessment of potential threats.
- The Collateral Damage Model (CDM), which is used to during operations to support Commanders' decision making on the potential collateral damage from indirect fire and air-dropped weapons.

The scaling of the penetration or retardation through different tissues has been presented and validated for a selection of tissue types. This enables direct predictions, or results from physical testing with tissue simulants, to be interpreted in terms of a given shot line through the human body.

Failure to account for the different penetration or retardation response of different tissues could dramatically alter any resulting injury predictions.

12.8 Physical model for multiple simultaneous projectile impacts

The MDFPIM V2.0 was developed to assess the hazard from low density and low energy fragments by predicting:

- The risk of corneal abrasion.
- The risk of eye penetration.
- The risk of skin perforation.

[206] It was not possible to validate all of the FREMs due to use of the data in the model development or data availability.

- The impact velocity of fragments based on their penetration depth in the model.

The MDFPIM provided approximately 2.5 times better resolution in the velocity predictions compared to existing models.

The MDFPIM was validated against a large dataset containing a wide range of projectile impact conditions. Unlike previous work, the MDFPIM accounts for:

- Ambient temperature (between -10°C to +40°C).
- Long term storage of the foam (at least 4 years, between -5°C and +45°C).
- Material batch to batch variations.

12.9 Exploitation of models

The models developed within this thesis have been exploited in a variety of real world applications.

- Without these models, the conclusions from these applications would not have been possible to the required accuracy, consistency and/or confidence.
- The use of these models has led to improvements in tactics, techniques, and procedures and equipment for UK Armed Forces and police.
- Ultimately, these models have directly supported UK MOD, wider UK government and international defence organisations to reduce injuries and save lives.

The exploitation of the MDFPIM V2.0 for one of these applications has been recognised by a Chief Scientific Advisor Commendation, winning the ‘Excellent Science or Engineering’ category (high quality, novel, significant and impactful science or engineering which delivers an exceptional contribution to UK Defence and Security).

12.10 Overarching conclusions

Through the proper validation of appropriate tissue simulants and supporting models shown within this thesis, the requirement for the use of animals and/or animal tissue for ballistic studies should be reduced.

The aim to “use these models to further the understanding of the penetration process” can be clearly demonstrated to be met with the following examples:

- Demonstration of the degree of influence of each of the significant target and projectile parameters on skin perforation, across a range of projectile properties.
- Demonstrating the requirement for, and validation of, muscle tissue simulants for both their permanent DoP and retardation response to real tissue.
- The effect of cavity constraint to:
    - Influence how practical gelatin testing is conducted by Dstl.
    - Inspire a new concept of PPE designed to mitigate muscle tissue injury by constraining the temporary cavity formed.

13 Further work

The lack of data relating to secondary fragments may be related to the fact that their contribution to injury in real events is not well understood or consistently documented. It is also possible that since conventional threats are characterised in the nature of their fragment outputs under ‘laboratory’ conditions, secondary fragments are simply not considered as having an effect. Therefore, events that cause casualties in either a military or civilian setting, where the threat needs to be better understood, should attempt to categorise and analyse the types and properties of fragments that have caused injuries. This threat modelling will then help guide the requirements of model development so that more suitable or applicable models are available in the future.

Further investigation of the reasons for the changes observed in the skin perforation V_{50} and muscle tissue DoP affected by storage conditions (such as refrigeration and freezing compared to fresh or live tissue) would guide storage requirements of tissue used in practical testing. This would allow the variability observed in the resulting data to be better controlled.

There was no account for clothing within the empirical equation for skin perforation (Equation 8). A simple development of the current model would be to follow the method (and data used) by Hudgins [68] to provide a way to account for different amounts of clothing on the resulting skin perforation velocity. Based on this approach, it would likely be limited to uniform fabric type materials, rather than protective fabrics (armour materials) due to the available data to construct the model [43; 76; 80].

Finite Element Analysis could be used to examine the effect of gelatin block size and varying degrees of constraint on the resulting cavity. This may be a more feasible approach to understanding these effects due to the complexities involved with extracting the required data in physical testing. As part of this study, or by using physical testing, it may be useful to determine the target lateral size of gelatin (20% at 10°C) at which the target could be considered semi-infinite in terms of its temporary cavity response.

Additional data or understanding of these cavity effects could address the ability of the FREM for temporary cavity formation to account for target size (and shot placement). This would be particularly useful as the recommendations from this thesis have meant that the size of the gelatin block used for testing within Dstl has moved away from the size that has been validated within the FREM.

There are a number of areas where the FREMs could be improved that would improve the utility, accuracy or validation of the predictions:

- Generation and/or refinement of drag co-efficients:
    - For non-spherical projectiles.
    - For Irregular projectiles. As noted in Section 9.2.2, granite gravel may be one potential option as a projectile to ensure it does not fragment or deform during penetration, staying within the limitations required of the FREMs.
- References [252; 253] provide additional equations to the FREMs described within this thesis that could be used to expand the applicability of (aspects of) the predictions to bullets, but consideration of how to scale the tumbling in different tissues would be required.
- The current validation of the models could be extended to consider velocities supersonic in tissue. In the current work, this aspect was limited partly by equipment capability. It has been demonstrated that the drag coefficient rises sharply when the projectile is supersonic [138] (and may start to be effected at velocities over approximately 1100 m s^{-1} [252]) which would significantly affect predictions in this velocity regime.
- The velocity loss due to skin on exiting a target could be considered to more accurately predict residual velocities in applications where fragments may need to be modelled through multiple targets (i.e. terrorist incidents with high crowd densities).
- It is considered that the contribution of the damage from the temporary cavity mechanism may be (significantly) underestimated within the

literature (as pointed out by Fackler [219]). Additional testing on constrained tissue would help refine this model and may support the concept of PPE to mitigate muscle tissue injury based on cavity constraint.

- Development and/or validation of the hybrid tissue model for a wider range of tissues. The priority order in which to generate data to populate this model could be based on a number of different approaches:
    - Tissues where there is already suitable validation data (e.g. raw data from References [107; 108; 124; 217] or the isolated bone data performed as part of testing described in 9.9.3, but not used for the parameter generation).
    - Tissues which may result in the most severe injuries.
    - Tissues that are more susceptible to damage.
    - Tissues that are likely to have the most extreme equivalent muscle tissue scaling factors.
    - Tissue that take up the largest volume of the body.

There is a considerable lack of suitable data on the extent of tissue damage which restricts the generation and validation of predictive models. An objective metric on (muscle) tissue damage would help to reduce the variability in measurement of the tissue response.

Muscle tissue damage data from ballistic impacts has been based on subjective surgical opinion (and limited to a few surgeons) on the mass of debrided muscle tissue required to leave viable tissue. The radius of damaged tissue could be based instead on tissue staining to determine cell death (at different radii from the shot line and different times from wounding) to produce a quantitative, objective measurement. A review of modern histological and experimental techniques would assist in guiding this recommendation. The drawback (as with the debrided muscle mass) is that it would require live tissue. However, this does not necessarily mean a requirement for live animals: procedures such as those developed for organ (limb) transplantation could be utilised [285] to provide tissue

that is maintained ‘as live’ for a 24 hour period, for example. This would greatly simplify the ethical and practical considerations associated with generating this data, in turn, enabling more targets to be used and generating a larger set of data on which to validate the existing models or develop a revised model.

A severe limitation of the models in this thesis, as well as the wider literature, is the focus on muscle tissue. Some tissues are more susceptible to the strain damage from temporary cavitation, such as the liver, whilst others are less, such as intestines [26]. For accurate predictions, particularly in shot line models; damage metrics specific to different tissues are required.

Studies to investigate the damage in tissue need to ensure suitable boundary conditions or constraint so that damage produced is comparable to what it would be with the tissue in-situ in the body. Studies based on isolated tissues may not be representative.

Stabili-gel has been suggested to have utility in some scenarios in place of gelatin or fragment packs. There is potential to tune the response of these synthetic gelatin alternatives to better represent the DoP and retardation response of real muscle tissue. This is recommended before widespread use of this ballistic medium.

Alternative analysis methods (e.g. CT scanning) of the MDFPIM may reduce the burden of analysis from physical trials. However, if CT scanning is a consistently available analysis technique, there would be no need for a layered pack. A homogeneous material could be used instead: a synthetic gelatin alternative (with further development to better match real muscle tissue response) may be suitable for ballistic and blast studies.

REFERENCES

[1] Deputy Head of Defence Statistics (Health). Types of injuries sustained by UK service personnel on operations in Afghanistan (Op Herrick) 1 April 2006 to 30 November 2014, 2016.

[2] Kelly, J., Ritenour, A., McLaughlin, D., Bagg, K., Apodaca, A., Mallak, C., Pearse, L., Lawnick, M., Champion, H., Wade, C., and Holcomb, J. Injury Severity and Causes of Death From Operation Iraqi Freedom and Operation Enduring Freedom: 2003–2004 Versus 2006. *Journal of Trauma and Acute Care Surgery*, 2008, Vol 64(2), pp S21-S27.

[3] Brady, C. An Analysis of Wound Statistics in Relation to Personal Ballistic Protection, Australia, *DSTO-TN-0510,* 2003.

[4] Owens, B.D., Kragh Jr, J.F., Macaitis, J., Svoboda, S.J., and Wenke, J.C. Characterization of extremity wounds in operation Iraqi Freedom and Operation Enduring Freedom. *Journal of orthopaedic trauma*, 2007, Vol 21(4), pp 254-257.

[5] Carey, M. Analysis of wounds incurred by US Army Seventh Corps personnel treated in Corps hospitals during Operation Desert Storm, February 20 to March 10, 1991. *Journal of Trauma-Injury, Infection, and Critical Care*, 1996, Vol 40(3S), pp 165S-169S.

[6] Champion, H., Bellamy, R., Roberts, P., and Leppaniemi, A. A profile of combat injury. *Journal of Trauma-Injury, Infection, and Critical Care*, 2003, Vol 54(5), pp S13-S19.

[7] Matheson, J. Missile wounds since the second world war. *Journal of the Royal Army Medical Corps*, 1968, Vol 114(1), pp 11-23.

[8] Mabry, R., Holcomb, J., Baker, A., Cloonan, C., Uhorchak, J., Perkins, D., Canfield, A., and Hagmann, J. United States Army Rangers in Somalia: an analysis of combat casualties on an urban battlefield. *Journal of Trauma-Injury, Infection, and Critical Care*, 2000, Vol 49(3), pp 515-529.

[9] Owens, B.D., Kragh Jr, J.F., Wenke, J.C., Macaitis, J., Wade, C.E., and Holcomb, J.B. Combat wounds in operation Iraqi Freedom and Operation Enduring Freedom. *Journal of Trauma and Acute Care Surgery*, 2008, Vol 64(2), pp 295-299.

[10] Penn-Barwell, J.G., Roberts, S.A., Midwinter, M.J., and Bishop, J.R. Improved survival in UK combat casualties from Iraq and Afghanistan: 2003–2012. *Journal of trauma and acute care surgery*, 2015, Vol 78(5), pp 1014-1020.

[11] Schreiber, M., Zink, K., Underwood, S., Sullenberger, L., Kelly, M., and Holcomb, J. A Comparison Between Patients Treated at a Combat Support Hospital in Iraq and a Level I Trauma Center in the United States. *Journal of Trauma and Acute Care Surgery*, 2008, Vol 64(2), pp S118-S122.

[12] Ramasamy, A., Harrisson, S., Lasrado, I., and Stewart, M. A review of casualties during the Iraqi insurgency 2006–a British field hospital experience. *Injury*, 2009, Vol 40(5), pp 493-497.

[13] Bowyer, G. Fragment Wounds of Modern Warfare: Aspects of Their Treatment (PhD). University of Cambridge. 1998.

[14] Frykberg, E. and Tepas 3rd, J. Terrorist bombings. Lessons learned from Belfast to Beirut. *Annals of surgery*, 1988, Vol 208(5), pp 569.
[15] Peleg, K., Aharonson-Daniel, L., Michael, M., and Shapira, S. Patterns of injury in hospitalized terrorist victims. *The American journal of emergency medicine*, 2003, Vol 21(4), pp 258-262.
[16] Yasin, M., Nasreen, G., and Malik, S. Injury pattern of suicide bomb attacks in Pakistan. *European Journal of Trauma and Emergency Surgery*, 2012, Vol 38(2), pp 119-127.
[17] US Department of Defense. Medical Research for Prevention, Mitigation, and Treatment of Blast Injuries, *Directive Number 6025.21E. 2006(Incorporating Change 1, October 15, 2018),*
[18] Wightman, G., Cochrane, R., Gray, R., and Linton, M. A contribution to the discussion on the safety of air weapons. *Science & Justice*, 2013, Vol 53(3), pp 343-349.
[19] Ogunc, G.I., Ozer, M.T., Eryilmaz, M., Karakus, O., and Uzar, A.I. The wounding potential and legal situations of air guns–experimental study. *Australian Journal of Forensic Sciences*, 2014, Vol 46(1), pp 39-52.
[20] Hsiao, Y.-T. and Meng, H.-H. Evaluation of wounding potential of airguns using aluminium witness plates. *Australian Journal of Forensic Sciences*, 2018, Vol, pp 1-11.
[21] Godinho, F. Air weapon lethality study how dangerous are low power air weapons (MSc). Cranfield University, Cranfield. 2011.
[22] Ministry of Defence. A Generic Process for the Verification & Validation of Modelling and Simulation & Synthetic Environments Systems, *DEF STAN 03-44 Issue 2,* 2008.
[23] Bir, C., Viano, D., and King, A. Development of biomechanical response corridors of the thorax to blunt ballistic impacts. *Journal of Biomechanics*, 2004, Vol 37(1), pp 73-79.
[24] Fackler, M. and Malinowski, J. The wound profile: a visual method for quantifying gunshot wound components. *The Journal of trauma*, 1985, Vol 25(6), pp 522-529.
[25] Fackler, M.L. Wound ballistics research of the past twenty years: a giant step backwards, Insitute report No. 447. 1990
[26] Fackler, M.L. Wounding patterns of military rifle bullets. *International Defense Revie*, 1989, Vol, pp 59-64.
[27] Fackler, M. Wound ballistics: A review of common misconceptions. *The Journal of American Medical Association*, 1988, Vol 259(18), pp 2730-2736.
[28] Rohne, H. Schießlehre für Infanterie unter besonderer Berücksichtigung des Gewehr 88 und der Schießvorschrift für die Infanterie. Ernst Siegfried Mittler und Sohn, Berlin 1986.
[29] Rettinger, G. The “80 Joule criterion” reconsidered today. *Forensic science international*, 2017, Vol 276, pp 64-70.
[30] Stanley, C. and Brown, M. A Computer Man Anatomical Model, *ARBRL-TR-02060,* 1978.
[31] Eberius, N. and Gillich, P. Survivability Analysis for the Evaluation of Personnel in Body Armor, ARL-RP-304. 2010

[32] Fryer, R., Breeze, J., and James, G. Development of a personnel vulnerability numerical model. *Personal Armour Systems Symposium (PASS), Amsterdam, Netherlands,* 2016.
[33] Macpherson, N. Review of quality assurance of Government analytical models: final report*,* 2013.
[34] HM Treasury. The Aqua Book: guidance on producing quality analysis for government*,* 2015.
[35] Blattnig, S.R., Luckring, J.M., Morrison, J.H., Sylvester, A.J., Tripathi, R.K., and Zang, T.A. NASA standard for models and simulations: Philosophy and requirements overview*. Journal of Aircraft*, 2012, Vol 50(1), pp 20-28.
[36] Balci, O. Verification, validation, and accreditation. *1998 Winter Simulation Conference. Proceedings (Cat. No. 98CH36274),* IEEE, 1998. 41-48.
[37] Moss, L. Validation Procedures for Equations, Algorithms, and Submodels, *ARL-TN-245,* 2005.
[38] Mabbott, A. The overmatching of UK police body armour (PhD). Cranfield University, Cranfield Defence and Security. 2016.
[39] Nguyen, T.-T.N., Tear, G.R., Masouros, S.D., and Proud, W.G. Fragment penetrating injury to long bones. *AIP Conference Proceedings 1979, 090011 (2018),* 2018.
[40] Bolliger, S.A., Poschmann, S.A., Thali, M.J., and Eggert, S. A fully synthetic lung model for wound-ballistic experiments—First results*. Forensic Science International*, 2017, Vol 275, pp 254-259.
[41] Rodrigues, S., Guey, J., Plummer, T., Pullen, A., Shaw, B., and Kieser, D. Influence of rib impact on thoracic gunshot trauma*. Journal of the Royal Army Medical Corps*, 2018, Vol 164(6), pp 405-409.
[42] Bourget, D., Dumas, S., and Bouamoul, A. Preliminary estimate for injury criterion to immediate incapacitation by projectile penetration. *Personal Armour Systems Symposium,, Nuremberg, Germany,* 2012. pp. 449-456.
[43] Kokinakis, W. and Sperrazza, J. Criteria for Incapacitating Soldiers with Fragments and Flechettes, Aberdeen Proving Ground, MD 2101, *Ballistic research laboratory Report No 1269,* 1965.
[44] Tawell, M. Kinetic energy less lethal weapons and their associated blunt trauma injuries (PhD). Cranfield University, Engineering Systems Department. 2007.
[45] Journée, C. Rapport entre la force vive des balles et la gravité des blessures qu'elles peuvent causer*. Revue d'Artillerie*, 1907, Vol 70(1), pp 81-120.
[46] Grocock, C., McCarthy, R., and Williams, D. Ball bearing (BB) guns, ease of purchase and potential for significant injury*. Annals of the Royal College of Surgeons of England*, 2006, Vol 88(4), pp 402.
[47] Bensouilah, J. and Buck, P. Aromadermatology: aromatherapy in the treatment and care of common skin conditions. Radcliffe Publishing, 2006.
[48] Joodaki, H. and Panzer, M.B. Skin mechanical properties and modeling: a review*. Proceedings of the Institution of Mechanical Engineers, Part H: Journal of Engineering in Medicine*, 2018, Vol 232(4), pp 323-343.

[49] Introduction to Structure and Function of Skin. Provided by: Lumen Learning. License: CC BY: Attribution.
[50] Bottigioli, D., Dahel, K., Goujon, C., Hennino, A., Laurent, A., Laurent P, E., Mistretta, F., and Nicolas, J.F. Echographic measurement of skin thickness in adults by high frequency ultrasound to assess the appropriate microneedle length for intradermal delivery of vaccines. *Vaccine*, 2007, Vol 25, pp 6423–6430.
[51] Mascianica, F., Ballistic testing methodology. *In:* Laible, R., Ed. *Ballistic materials and penetration mechanics.* Elsevier, 1980, 41-71.
[52] R Core Team. R: A language and environment for statistical computing. V2.15.2. Vienna, Austria. R Foundation for Statistical Computing, 2012.
[53] Kosmidis, I. brglm: Bias reduction in binary-response GLMs. (R package). 2007.
[54] Lambert, J. and Jonas, G. Towards standardization in terminal ballistics testing: velocity representation, Aberdeen Proving Ground, Maryland, *Ballistics Research Laboritory, Report no. 1852,* 1976.
[55] Translation from French of Journée, C. Rapport entre la force vive des balles et la gravité des blessures qu'elles peuvent causer [Relationship between the kinetic energy of bullets and the severity of injuries they inflict]. *Revue d'Artillerie*, (original 1907), Vol 70(1), pp 81-120. Supplied by Ballistic Research Archives.
[56] DiMaio, V., Copeland, M., Besant-Matthews, P., Fletcher, L., and Jones, A. Minimal Velocities Necessary for Perforation of Skin by Air Gun Pellets and Bullets. *Journal of Forensic Sciences*, 1982, Vol 27(4), pp 894-898.
[57] Breeze, J., Carr, D., Mabbott, A., Beckett, S., and Clasper, J. Refrigeration and freezing of porcine tissue does not affect the retardation of fragment simulating projectiles. *Journal of forensic and legal medicine*, 2015, Vol 32, pp 77-83.
[58] Breeze, J. Design validation of future ballistic neck protection through the development of novel injury models (PhD). University of Birmingham, School of Clinical and Experimental Medicine, College of Medical and Dental Sciences. 2015.
[59] Missliwetz, J. Zur Grenzgeschwindigkeit bei der Haut.(Eine experimentelle ballistische Untersuchung mit Geschossen vom Kaliber 4 mm und 4.5 mm) [The limit velocity to the skin (An experimental investigation with ballistic projectiles calibre 4 mm and 4.5 mm)]. *Beitr Gerichtl Med*, 1987, Vol 65, pp 411-432.
[60] Rathman, G. The effect of shape on BB and pellet penetration. *AFTE Journal*, 1987, Vol 19(4), pp 426-431.
[61] Bir, C., Stewart, S., and Wilhelm, M. Skin penetration assessment of less lethal kinetic energy munitions. *Journal of Forensic Sciences*, 2005, Vol 50(6), pp 1426-1429.
[62] Stewart, S. Assessment of Penetration of Less-Lethal Munitions (PhD). Wayne State University, Department of Biomedical Engineering.
[63] Andrecovich, C., Bir, C., and Cavanaugh, J. *Contract 1000076989*. [Personal Communication to Sedman, A.] Wayne State University. 30 June 2015.

[64] Mattoo, B., Wani, A., and Asgekar, M. Casualty criteria for wounds from firearms with special reference to shot penetration. II*. Journal of Forensic Sciences*, 1974, Vol 19(3), pp 585-589.
[65] Breeze, J. and Clasper, J. Determining the velocity required for skin perforation by fragment simulating projectiles: a systematic review*. Journal of the Royal Army Medical Corps*, 2013, Vol 159, pp 265-270.
[66] DiMaio, V. Penetration and perforation of skin by bullets and missiles. A review of the literature*. American Journal of Forensic Medicine and Pathology*, 1981, Vol 2(2), pp 107-110.
[67] Mattoo, B. Discussion of "Minimal velocities necessary for perforation of skin by air gun pellets and bullets"*. Journal of Forensic Sciences*, 1984, Vol 29(3), pp 700-703.
[68] Hudgins, H. Estimating Ballistic Limits of Skin and Clothing for Projectiles. *40th Annual Armament Systems: Guns - Ammunition - Rockets - Missiles (GARM) Conference,* 2005.
[69] Kneubuehl, B., Coupland, R., Rothschild, M., and Thali, M. Wound Ballistics Basics and Applications. Berlin Heidelberg New York: Springer-Verlag 2011.
[70] Marshall, J., Dahlstrom, D., and Powley, K. Minimum Velocity Necessary for Nonconventional Projectiles to Penetrate the Eye: An Experimental Study Using Pig Eyes*. American Journal of Forensic Medicine and Pathology*, 2011, Vol 32, pp 100-103.
[71] Tausch, D., Sattler, W., Wehrfritz, G., and Wagner, H.-J. Experiments on the penetration Power of Various Bullets into Skin and Muscle Tissue*. Journal of Legal Medicine*, 1978, Vol 81(4), pp 309-328.
[72] Dammermann, W. Anmerkungen zur Arbeit von D. Tausch et al. *Z. Rechtsmed*, 1979, Vol 83, pp 149.
[73] Grundfest, H., Korr, I., McMillen, J., and Butler, E. Ballistics of the Penetration of Human Skin by Small Spheres, *Missile Casualties Report No. 11,* 1945.
[74] French, R. and Callender, G. Ballistic characteristics of wounding agents. Washington DC. Office of the Surgeon General, Department of the Army, II, 92-141, 1962.
[75] Sellier, K., Kneubuehl, B., Rufer, R., and Hawley, J. Wound ballistics and the scientific background. Elsevier Amsterdam, 1994.
[76] Sperrazza, J. and Kokinakis, W. Ballistic limits of tissue and clothing*. Annals of the New York Academy of Sciences*, 1968, Vol 152(1), pp 163-167.
[77] Eardley, W., Watts, S., and Clasper, J. Modelling for conflict: the legacy of ballistic research and current extremity in vivo modelling*. Journal of the Royal Army Medical Corps*, 2013, Vol 159, pp 73-83.
[78] Schantz, B. Aspects on the choice of experimental animals when reproducing missile trauma*. Acta Chirurgica Scandinavica. Supplementum*, 1979, Vol 489, pp 121-130.
[79] Breeze, J., James, G., and Hepper, A. Perforation of fragment simulating projectiles into goat skin and muscle*. Journal of the Royal Army Medical Corps*, 2013, Vol 159(2), pp 84-89.

[80] Lewis, J., Coon, P., Clare, V., and Sturdivan, L. An Empirical/Mathematical Model to Estimate the Probability of Skin Penetration by Various Projectiles, Aberdeen Proving Ground, MD 21010, *Technical Report ARCSL-TR-78004,* 1978.
[81] Neades, D. and Rudolph, R. An Examination of Injury Criteria for Potential Application to Explosive Safety Studies, Aberdeen Proving Ground, MD, *Prepared for presentation to the Explosive Safety Board (DDESB) in 1983-84.,* 1983.
[82] Haag, L. BB Perforation of Fresh Pig Skin Over Ballistic Gelatin*. International Wound Ballistics Association (IWBA) Review* 1995, Vol 2(1), pp 50-51.
[83] Haag, M. and Haag, L. Skin Perforation and Skin Simulants*. AFTE Journal*, 2002, Vol 34(3), pp 268-286.
[84] MacPherson, D. Bullet Penetration: Modeling the Dynamics & the Incapacitation Resulting from Wound Trauma El Segundo, CA: Ballistic Publications 1994.
[85] McKenzie, H., Coil, J., and Ankney, R. Experimental Thoracoabdominal Airgun Wounds in a Porcine Model*. Journal of Trauma-Injury Infection & Critical Care*, 1995, Vol 39(6), pp 1164-1167.
[86] Dahlstrom, D., Powley, K., and Penk, D. 12 gauge bean bag ammunition penetration*. Journal of the International Wound Ballistics Association*, 1999, Vol 3(3), pp 38-41.
[87] Haag, L. Standard steel bb perforation of fresh pigskin over standard ordnance gelatin*. AFTE Journal*, 2010, Vol 42(1), pp 56-60.
[88] Breeze, J., Hunt, N., Gibb, I., James, G., Hepper, A., and Clasper, J. Experimental penetration of fragment simulating projectiles into porcine tissues compared with simulants*. Journal of Forensic and Legal Medicine*, 2013, Vol 20(4), pp 296-299.
[89] Dain, S.J., Huang, R., Tiao, A., and Ralph Chou, B. When is protection from impact needed for the face as well as the eyes in occupational environments? *Clinical and Experimental Optometry*, 2017, Vol, pp.
[90] Bowyer, G., Cooper, G., and Rice, P. Small fragment wounds: biophysics and pathophysiology*. Journal of Trauma-Injury, Infection, and Critical Care*, 1996, Vol 40(3S), pp 159S-164S.
[91] Breeze, J., Mabbott, A., and Carr, D. Experimental penetration of 5mm spherical fragment simulating projectiles into 20% gelatin. *Personal Armour Systems Symposium (PASS), Robinson Colledge, Cambridge, UK,* 2014.
[92] Salziger, B. and Strobele, M. Eindringtiefe von 9mm luger geschossen in gelatine*. Der Auswerfer*, 1999, Vol, pp 29-31.
[93] Fackler, M., Bellamy, R., and Malinowski, J. A Reconsideration of the Wounding Mechanism of Very High Velocity Projectiles-Importance of Projectile Shape*. Journal of Trauma-Injury Infection & Critical Care*, 1988, Vol 28(1), pp.
[94] Fackler, M. and Kneubuehl, B. Applied wound ballistics, what's new and what's true*. Journal of Trauma (China)*, 1990, Vol 6(suppl), pp 32-37.
[95] Eason, R., Pryor, W., and Adams, J. Wound Studies in Porcine Skin, Muscle and Liver as Related to Variation of Velocities of Spherical

Missiles, Camp Lejeune NC, *U.S. Naval Medical Field research Laboratory,* 1975.
[96] Hepper, A. *Legacy data*. [Email to James, G.] Platform Systems Division, Dstl. Mon 09/05/2016 16:11.
[97] Dahlstrom, D., Powley, K., and Fackler, M. Drag-stabalized (bulb with tail) 12 gauge shotgun bean bag projectile*. Journal of the International Wound Ballistics Association*, 2001, Vol 5(1), pp 8-12.
[98] Bowen, I., Richmond, D., Wetherbe, M., and White, C. Biological Effects of Blast from Bombs. Glass Fragments as Penetrating Missiles and Some of the Biological Implications of Glass Fragmented by Atomic Explosions, Albuquerque, New Mexico, *Lovlace Foundation for Medical Education and Research. AECU-3350,* 1956.
[99] Fletcher, E., Richmond, D., and Yelverton, J. Glass Fragment Hazard from Windows Broken by Airblast, Albuquerque NM, *Lovelace Biomedical and Environmental Research Institute. DNA 5593T,* 1980.
[100] Sellier, K. Effectiveness of small calibre ammunition*. Acta chirurgica Scandinavica. Supplementum* 1979, Vol 489, pp 13-26.
[101] Warlow, T. Firearms, the law, and forensic ballistics. CRC press, 2004.
[102] Jussila, J., Leppaniemi, A., Paronen, M., and Kulomaki, E. Ballistic skin simulant*. Forensic Science International*, 2005, Vol 150, pp 63-71.
[103] Keone, B., Id-Boufker, F., and Papy, A. Kinetic Non-Lethal Weapons*,* 2008.
[104] Feinstein, D. Fragment Hazard criteria, Alexandria, VA, *Department of Defense Explosives Safetyboard, AD-A265 238,* 1993.
[105] Feinstein, D., Haugel, W., Kardatzke, M., and Weinstock, A. Personnel Casualty Study, Illinois, *Illinois Institute of Technology, Research Institute Project No J6067. AD842573,* 1968.
[106] Ouellet, S. and Pageau, G. Development of a Simplified Torso Surrogate based on Selected Biofidelity Corridors for the Assessment of the Ballistic Performance of Soft Body Armor. *IRCOBI conference,* 2018, (IRC-18-110).
[107] Humphrey, C., Henneberg, M., Wachsberger, C., and Kumaratilake, J. The deceleration of a spherical projectile passing through porcine organs at laboratory temperature (16°C) and core body temperature (37°C)*. Journal of forensic and legal medicine*, 2018, Vol 53, pp 46-50.
[108] Humphrey, C., Henneberg, M., Wachsberger, C., and Kumaratilake, J. Comparison of porcine organs and commonly used ballistic simulants when subjected to impact from steel spheres fired at supersonic velocities*. Forensic Science International*, 2018, Vol, pp.
[109] Maiden, N.R. The assessment of bullet wound trauma dynamics and the potential role of anatomical models (PhD). University of Adelaide, School of Medical Sciences. 2014.
[110] Scully, R., Artz, C., and Sako, Y. An evaluation of the surgeon's criteria for determining the viability of muscle during débridement*. AMA archives of surgery*, 1956, Vol 73(6), pp 1031-1035.
[111] Berlin, R., Janzon, B., Rybeck, B., Sandegärd, J., and Seeman, T. Local effects of assault rifle bullets in live tissues. Part II. Further studies in live

tissues and relations to some simulant media. *Acta chirurgica Scandinavica. Supplementum*, 1977, Vol 477, pp 5.
[112] Jussila, J., Kjellstromb, T., and Leppaniemi, A. Ballistic variables and tissue devitalisation in penetrating injury - establishing relationship through meta-analysis of a number of pig tests. *Injury. International Journal of the Care of the Injured*, 2004, Vol 36, pp 282-292.
[113] Dahlgren, B., Berlin, R., Janzon, B., Nordstrom, G., Nylof, U., Rybeck, B., Schantz, B., and Seeman, T. The Extent of Muscle Tissue damage Following Missile Trauma One, Six and Twelve Hours After the Infliction of Trauma, Studied by the Current Method of Debridement. *Acta chirurgica Scandinavica. Supplementum*, 1979, Vol 489, pp 137-144.
[114] Mendelson, J. and Glover, J. Sphere and shell fragment wounds of soft tissues: Experimental study. *Journal of Trauma-Injury, Infection, and Critical Care*, 1967, Vol 7(6), pp 889-914.
[115] Maiden, N. Ballistics reviews: mechanisms of bullet wound trauma. *Forensic science, medicine, and pathology*, 2009, Vol 5(3), pp 204-209.
[116] Harvey, E., McMillen, H., Butler, E.G., and Puckett, W. Mechanism of Wounding. Washington DC. Office of the Surgeon General, Department of the Army, III, 1962.
[117] Fackler, M. Gunshot Wound Review. *Annals of Emergency Medicine*, 1996, Vol 28(2), pp 194-203.
[118] Janzon, B. High Energy Missile Trauma - A Study of the Mechanisms of Wounding of Muscle Tissue. Department of Surgery II, University of Goteborg, Sweden: University of Goteborg, Sweden, 1983.
[119] Kieser, D.C., Carr, D.J., Leclair, S., Horsfall, I., Theis, J., Swain, M., and Kieser, J. Gunshot induced indirect femoral fracture: mechanism of injury and fracture morphology. *Journal of the Royal Army Medical Corps*, 2013, Vol 159(4), pp 294-299.
[120] Chen, J., Zhang, B., Chen, W., Kang, J.-y., Chen, K.-j., Wang, A.-m., and Wang, J.-m. Local and distant trauma after hypervelocity ballistic impact to the pig hind limb. *SpringerPlus*, 2016, Vol 5(1), pp 1497.
[121] Health and Safety Executive (HSE). BSE Occupational guidance, 2007.
[122] Mabbott, A., Carr, D., Champion, S., Malbon, C., and Tichler, C. Comparison of 10 % gelatine, 20 % gelatine and PermaGel™ for ballistic testing. *27th International Symposium on Ballistics, Freiberg, Germany,* 2013.
[123] Jin, Y., Mai, R., Wu, C., Han, R., and Li, B. Comparison of ballistic impact effects between biological tissue and gelatin. *Journal of the mechanical behavior of biomedical materials*, 2018, Vol 78, pp 292-297.
[124] Maiden, N.R., Musgrave, I., Fisk, W., and Byard, R.W. Pig organ energy loss comparison experiments using BBs. *Journal of forensic sciences*, 2016, Vol 61(3), pp 679-686.
[125] Bir, C., Villata, R., and Bodo, M. Comparison of Various Gelatine Surrogates for Wound Track Assessmenet. *Personal Armour Systems Symposium (PASS), Washinton, DC,* 2018.
[126] Courtney, E., Courtney, A., Andruiv, L., and Courtney, M. Clear Ballistics Gel®: High Speed Retarding Force Analysis of Paraffin-Based

Alternative to Gelatin-based Testing of Lead-Free Pistol Bullets. *30th International Symposium on Ballistics,* 2017.
[127] Colloids, C. Gelfax - a series of useful facts on all aspects of gelatin quality, Chesire, England.
[128] Jussila, J. Preparing ballistic gelatine—review and proposal for a standard method*. Forensic science international*, 2004, Vol 141(2), pp 91-98.
[129] Fackler, M. and Malinowski, J. Ordnance gelatin for ballistic studies. Detrimental effect of excess heat used in gelatin preparation*. The American journal of forensic medicine and pathology*, 1988, Vol 9(3), pp 218-219.
[130] Specific tests for kinetic munition, Section 4.1. Personnel vulnerability to small arms fire, *AC/225(LG/3-SG1)D14,*
[131] Fackler, M., Surinchak, J., Malinowski, J., and Bowen, R. Wounding potential of the Russian AK-74 assault rifle*. Journal of Trauma-Injury, Infection, and Critical Care*, 1984, Vol 24(3), pp 263-266.
[132] Fackler, M., Surinchak, J., Malinowski, J.A., and Bowen, R. Bullet fragmentation: a major cause of tissue disruption*. Journal of Trauma-Injury, Infection, and Critical Care*, 1984, Vol 24(1), pp 35-39.
[133] Fackler, M., Bellamy, R., and Malinowski, J. Wounding mechanism of projectiles striking at more than 1.5 km/sec*. Journal of Trauma-Injury, Infection, and Critical Care*, 1986, Vol 26(3), pp 250-254.
[134] Fackler, M. What's wrong with the wound ballistics literature, and why, Division of Military Trauma Research, *Institute Report No. 239,* 1987.
[135] Fackler, M., Woychesin, S., Malinowski, J., Dougherty, P., and Loveday, T. Determination of shooting distance from deformation of the recovered bullet*. Journal of Forensic Sciences*, 1987, Vol 32(4), pp 1131-1135.
[136] Hollerman, J.J., Fackler, M., Coldwell, D., and Ben-Menachem, Y. Gunshot wounds: 1. Bullets, ballistics, and mechanisms of injury*. AJR. American journal of roentgenology*, 1990, Vol 155(4), pp 685-690.
[137] Haag, L.C. Ballistic gelatin: controlling variances in preparation and a suggested method for the calibration of gelatin blocks*. AFTE Journal*, 1989, Vol 21(3), pp 483-489.
[138] Charters, A.I. and Charters, A. Wounding mechanism of very high velocity projectiles*. Journal of Trauma-Injury, Infection, and Critical Care*, 1976, Vol 16(6), pp 464-470.
[139] Dubin, H. A cavitation model for kinetic energy projectiles penetrating gelatin*. Bal. Res. Lab Memo. Rept*, 1974, Vol 2423, pp.
[140] Maiden, N.R., Fisk, W., Wachsberger, C., and Byard, R.W. Ballistics ordnance gelatine–How different concentrations, temperatures and curing times affect calibration results*. Journal of forensic and legal medicine*, 2015, Vol 34, pp 145-150.
[141] Cronin, D. and Falzon, C. Characterization of 10% Ballistic Gelatin to Evaluate Temperature, Aging and Strain Rate Effects*. Experimental Mechanics*, 2011, Vol 51(7), pp 1197-1206.
[142] Nicholas, N. and Welsch, J. Insitute for Non-Lethal Defense Technologies Report: Ballistic Gelatin. Penn State Applied Research Laboratory. Penn State Applied Research Laboratory, 2004.

[143] Jussila, J. Measurement of kinetic energy dissipation with gelatine fissure formation with special reference to gelatine validation. *Forensic Science International*, 2005, Vol 150(1), pp 53-62.
[144] Berlin, R., Janzon, B., Rybeck, B., Schantz, B., and Seeman, T. A proposed standard methodology for estimating the wounding capacity of small calibre projectiles or other missiles. *Acta Chir Scand Suppl*, 1982, Vol, pp 11-28.
[145] Janzon, B. Edge, size and temperature effects in soft soap block simulant targets used for wound ballistic studies. *Acta chirurgica Scandinavica. Supplementum*, 1981, Vol 508, pp 105-122.
[146] Janzon, B. Soft soap as a tissue simulant medium for wound ballistic studies investigated by comparative firings with assault rifles Ak 4 and M16A1 into live, anesthetized animals. *Acta chirurgica Scandinavica. Supplementum*, 1982, Vol 508, pp 79-88.
[147] Scepanovic, D., Alberht, M., and Erdeljan, D. A method for predicting effects of military rifles. *Acta Chir Scand Suppl*, 1982, Vol, pp 29-37.
[148] Janzon, B., Berlin, R., Nordstrand, I., Rybeck, B., and Schantz, B. Drag and Tumbling Behaviour of Small Calibre Projectiles in Tissue Simulant. *Acta chirurgica Scandinavica. Supplementum*, 1979, Vol 489, pp 57-70.
[149] Nordstrand, I., Janzon, B., and Rybeck, B. Break-up behaviour of some small calibre projectiles when penetrating a dense medium. *Acta chirurgica Scandinavica. Supplementum*, 1978, Vol 489, pp 81-90.
[150] Pirlot, M., Dyckmans, G., and Bastin, I. Soap and Gelatine for simulating human body tissue: an experimental and numerical evaluation. *19th International Symposium of Ballistics,* 2001. 1011-1017.
[151] Uzar, A., Dakak, M., Ozer, T., Oğünç, G., Yiğit, T., Kayahan, C., Oner, K., and Sen, D. A new ballistic simulant "transparent gel candle"(experimental study). *Ulusal travma ve acil cerrahi dergisi= Turkish journal of trauma & emergency surgery: TJTES*, 2003, Vol 9(2), pp 104-106.
[152] Moy, P., Weerasooriya, T., Juliano, T.F., VanLandingham, M.R., and Chen, W. Dynamic response of an alternative tissue simulant, physically associating gels (PAG), ARL-RP-136. 2006
[153] Ryckman, R.A., Powell, D.A., and Lew, A. Ballistic penetration of Perma-gel. *AIP conference proceedings,* AIP, 2012. 143-148.
[154] Clear Ballistics LLC. *https://www.clearballistics.com/product-category/ballistic-gelatin/.* 2017. [Online] Available from: [Accessed 8th January 2019].
[155] Mrozek, R.A., Leighliter, B., Gold, C.S., Beringer, I.R., Jian, H.Y., VanLandingham, M.R., Moy, P., Foster, M.H., and Lenhart, J.L. The relationship between mechanical properties and ballistic penetration depth in a viscoelastic gel. *Journal of the mechanical behavior of biomedical materials*, 2015, Vol 44, pp 109-120.
[156] DuBois, E.K. Validation of experimental approaches in Forensic Science: a case study of the tissue fragments created during an explosive event (PhD). UCL (University College London), Department of Security and Crime Science. 2018.

[157] Rybeck, B. and Janzon, B. Absorption of missile energy in soft tissue. *Acta chirurgica Scandinavica*, 1976, Vol 142(3), pp 201-207.
[158] Guey, J., Rodrigues, S., Pullen, A., Shaw, B., and Kieser, D.C. Effect of ageing on the calibration of ballistic gelatin. *Journal of the Royal Army Medical Corps*, 2018, Vol, pp.
[159] Mrozek, R. [Personal Communication to James, G.] Tue 29/01/2019 23:10.
[160] Kieser, D. *Re: Effect of ageing on the calibration of ballistic gelatin*. [Personal Communication to James, G.] Tue 16/04/2019 20:58.
[161] Dziemian, A. The Penetration of Steel Spheres Into Tissue Models, *Chemical Warfare Laboratories, CWLR 2226,* 1958.
[162] Swaina, M., Kieserc, D., Shahd, S., and Kieser, J. Projectile penetration into ballistic gelatin. *Journal of the Mechanical Behavior of Biomedical Materials*, 2014, Vol 26, pp 385-392.
[163] Mahoney, P.F. Development of a Synthetic Bone and Tissue Model to Simulate Overmatch Military Ballistic Head Injury (PhD). Cranfield University, Cranfield Defence and Security. 2018.
[164] Scepanovic, D. Steel Ball Effect - Investigation of Shooting at Blocks of Soap. *Acta chirurgica Scandinavica. Supplementum*, 1979, Vol (489), pp 71-80.
[165] Eisler, R., Chatterjee, A., Stone, S., and El-Raheb, M. Analytic Simulation of Tissue Damage from Penetrating Wounds to the Heart, *W81XWH-04-C-0084,* 2006.
[166] Stevenson, T. Ballistic Extremity Wounding: Quantifying tissue damage associated with military fireams (PhD). Cranfield University, Cranfield Defence and Security. 2019.
[167] Freitas, C., Grimm, M., and Mackiewicz, J. High Resolution Simulation of Armor Perforation and Penetrating Injury. *Personal Armour Systems Symposium, Amsterdam, Netherlands,*2016.
[168] Freitas, C., Grimm, M., Bigger, R., and Mackiewicz, J. Injury Characterization of Fragmenting Projectiles Perforating Soft Armor. *Personal Armour Systems Symposium, Robinson College, Cambridge, UK,* 2014.
[169] Blanch, R., Bindra, M., Jacks, A., and Scott, R.A. Ophthalmic injuries in British armed forces in Iraq and Afghanistan. *Eye*, 2011, Vol 25(2), pp 218-223.
[170] Ari, A. Eye injuries on the battlefields of Iraq and Afghanistan: Public health implications. *Optometry - Journal of the American Optometric Association*, 2006, Vol 77(7), pp 329-339.
[171] Kennedy, E.A., Ng, T.P., McNally, C., Stitzel, J.D., and Duma, S.M. Risk functions for human and porcine eye rupture based on projectile characteristics of blunt objects. *Strapp Car Crash Journal*, 2006, Vol 50, pp 651.
[172] McCORMACK, P. Penetrating injury of the eye. *The British journal of ophthalmology*, 1999, Vol 83(10), pp 1101.
[173] Kratz, A., Levy, J., Cheles, D., Ashkenazy, Z., Tsumi, E., and Lifshitz, T. Airsoft gun–related ocular injuries: novel findings, ballistics investigation,

and histopathologic study. *American journal of ophthalmology*, 2010, Vol 149(1), pp 37-44. e32.
[174] Sponsel, W.E., Gray, W., Scribbick, F.W., Stern, A.R., Weiss, C.E., Groth, S.L., and Walker, J.D. Blunt eye trauma: empirical histopathologic paintball impact thresholds in fresh mounted porcine eyes. *Investigative ophthalmology & visual science*, 2011, Vol 52(8), pp 5157-5166.
[175] Farr, A.K. and Fekrat, S. Eye injuries associated with paintball guns. *International ophthalmology*, 1998, Vol 22(3), pp 169-173.
[176] Kennedy, E.A., Stitzel, J.D., and Duma, S.M. Matched experimental and computational simulations of paintball eye impacts. *Biomedical sciences instrumentation*, 2007, Vol 44, pp 243-248.
[177] Taban, M., Taban, M., and Sears, J.E. Ocular findings following trauma from paintball sports. *Eye*, 2007, Vol 22(7), pp 930-934.
[178] Thach, A.B., Ward, T.P., Hollifield, R.D., Dugel, P.U., Sipperley, J.O., Marx, J.L., Abrams, D.A., Wroblewski, K.J., Sonkin, P.L., and Birdsong, R.H. Ocular injuries from paintball pellets. *Ophthalmology*, 1999, Vol 106(3), pp 533-537.
[179] Fineman, M.S. Ocular paintball injuries. *Current opinion in ophthalmology*, 2001, Vol 12(3), pp 186-190.
[180] Bullock, J.D., Johnson, D.A., Ballal, D., and Bullock, R.J. Ocular and orbital trauma from water balloon slingshots: a clinical, epidemiological, experimental, and theoretical study. *Transactions of the American Ophthalmological Society*, 1996, Vol 94, pp 105.
[181] Stitzel, J.D., Duma, S.M., Cormier, J.M., and Herring, I.P. A nonlinear finite element model of the eye with experimental validation for the prediction of globe rupture. *Strapp Car Crash Journal*, 2002, Vol, pp.
[182] Tasman, W. Peripheral retinal changes following blunt trauma. *Transactions of the American Ophthalmological Society*, 1972, Vol 70, pp 190.
[183] Kroll, M.W., Ritter, M.B., Kennedy, E.A., Siegal, N.K., Shinder, R., Brave, M.A., and Williams, H.E. Eye injury from electrical weapon probes: Mechanisms and treatment. *The American Journal of Emergency Medicine*, 2018, Vol, pp.
[184] Pieramici, D.J., Sternberg, P., Aaberg, T.M., Bridges, W., Capone, A., Cardillo, J.A., De Juan, E., Kuhn, F., Meredith, T.A., and Mieler, W.F. A system for classifying mechanical injuries of the eye (globe). *American journal of ophthalmology*, 1997, Vol 123(6), pp 820-831.
[185] Kuhn, F., Morris, R., and Witherspoon, C.D. Birmingham Eye Trauma Terminology (BETT): terminology and classification of mechanical eye injuries. *Ophthalmology Clinics of North America*, 2002, Vol 15(2), pp 139-143, v.
[186] Schmidt, G., Broman, A., Hindman, H., and Grant, M.P. Vision survival after open globe injury predicted by classification and regression tree analysis. *Ophthalmology*, 2008, Vol 115(1), pp 202-209.
[187] *Abbreviated Injury Scale Update 2015.* 2015.
[188] Powley, K., Dahlstrom, D., Atkins, V., and Fackler, M. Velocity necessary for a BB to penetrate the eye: an experimental study using pig eyes.

American Journal of Forensic Medicine and Pathology, 2004, Vol 25(4), pp 273-275.
[189] Williams, R. and Stewart, G. Ballistic studies in eye protection. *Am J Ophthalmol*, 1964, Vol 58, pp 453-464.
[190] Williams, R. and Stewart, G. Ballistic studies in eye protection, Edgewood Arsenal, *Chemical Research and Development Laboratories Technical Reoprt, CRDLR 3194,* 1963.
[191] Tillett, C., Rose, H., and Herget, C. High speed photographic study of perforating ocular injury by the BB. *American journal of ophthalmology*, 1962, Vol 54(4), pp 675-688.
[192] Galler, E., Umlas, J., Vinger, P., and Wu, H. Ocular integrity after quantitated trauma following photorefractive keratectomy and automated lamellar keratectomy. *Investigative Ophthalmology & Visual Science,* 1995, 36(4). S580-S580.
[193] Alphonse, V. Injury Biomechanics of the Human Eye During Blunt and Blast Loading (MSc). Virginia Polytechnic Institute and State University. 2012.
[194] Scott, W.R.M., Lloyd, W.C., Benedict, J.V., and Meredith, R. Ocular injuries due to projectile impacts. *Annual Proceedings/Association for the Advancement of Automotive Medicine,* Association for the Advancement of Automotive Medicine, 2000. Volume 44, pp 205.
[195] McKnight, S., Fitz, J., and Giangiacomo, J. Corneal rupture following radial keratotomy in cats subjected to BB gun injury. *Ophthalmic surgery*, 1988, Vol 19(3), pp 165-167.
[196] Weidenthal, D. and Schepens, C. Peripheral fundus changes associated with ocular contusion. *American journal of ophthalmology*, 1966, Vol 62(3), pp 465-477.
[197] Duma, S.M., Ng, T.P., Kennedy, E.A., Stitzel, J.D., Herring, I.P., and Kuhn, F. Determination of significant parameters for eye injury risk from projectiles. *Journal of Trauma and Acute Care Surgery*, 2005, Vol 59(4), pp 960-964.
[198] Green Jr, R., Peters, D., Shore, J., Fanton, J., and Davis, H. Force necessary to fracture the orbital floor. *Ophthalmic Plastic & Reconstructive Surgery*, 1990, Vol 6(3), pp 211-217.
[199] Weidenthal, D. Experimental ocular contusion. *Archives of ophthalmology*, 1964, Vol 71(1), pp 77-81.
[200] Segletes, S. Modeling the Penetration Behavior of Rigid Spheres Into Ballistic Gelatin, *Army Research Laboratory, ARL-TR-4393,* 2008.
[201] Cunniff, P.M. A Method to Describe the Statistical Aspects of Armor Penetration, Human Vulnerability and Lethality due to Fragmenting Munitions. *28th International Symposium on Ballistics, Atlanta, USA,* 2014.
[202] Pavlyk, O. Wolfram. *A "Trivial" Probability Problem - Wolfram Blog.* 2013. [Online] Available from: https://blog.wolfram.com/2013/06/03/a-trivial-probability-problem/ [Accessed 5th March 2019].
[203] James, G. and Hepper, A. Ballistic simulation of fragmentation from buried improvised explosive devices. *Personal Armour Systems Symposium, Robinson College, Cambridge, UK,* 2014.

[204] Lewis, E.A., Pigott, M., Randall, A., and Hepper, A. The development and introduction of ballistic protection of the external genitalia and perineum. *Journal of the Royal Army Medical Corps*, 2013, Vol 159(suppl 1), pp i15-i17.
[205] *MS Instruments.* 2018. [Online] Available from: https://msinstruments.co.uk/ [Accessed 21/08/2019].
[206] *Photron High Speed Cameras for Slow Motion Analysis.* [Online] Available from: https://photron.com/ [Accessed 21/08/2019].
[207] Oehler Research Inc. *Oehler-Research: Home.* 2019. [Online] Available from: https://oehler-research.com/ [Accessed 21/08/2019].
[208] Defence Clothing Textiles Agency. Fragment Simulating Projectile - Engineering drawing. Stores and Clothing R&D establishment, DCTA/A3/6723 Issue 4.
[209] Vision Research Inc. *Phantom High Speed.* 2019. [Online] Available from: https://www.phantomhighspeed.com/ [Accessed 21/08/2019].
[210] Eriksen, J. NATO Standardization Agreement (STANAG 2920): Ballistic Test Method For Personal Armour Materials and Combat Clothing 2003.
[211] Krueger, N., Luebberding, S., Oltmer, M., Streker, M., and Kerscher, M. Age-related changes in skin mechanical properties a quantitative evaluation of 120 female subjects. *Skin Research and Technology*, 2011, Vol 17, pp 141-148.
[212] Verhagen, T.L., Kemper, R., Huisjes, H., Knijnenburg, S., Pronk, A., and Van Klink, M. Witnessman: The software tool to design, analyse and assess a witness pack with respect to military and medical effects on an (UN) protected (DIS) mounted soldier, 2006.
[213] Open Source Physics. Tracker 4.93. Video Analysis and Modelling Tool.
[214] Mathshop Ltd. MS EKE (V4.0.13). 2016.
[215] Eisler, R., Chatterjee, A., Burghart, G., and O'Keefe IV, J. Casualty assessments of penetrating wounds from ballistic trauma. 2001
[216] Ehlers, T. and Magness, L. *RE: 20% ballistic gelatin calibration* [Personal Communication to Reeve, S.] ARL/WMRD. 05 April 2011 19:18.
[217] Humphrey, C., Henneberg, M., Wachsberger, C., Maiden, N., and Kumaratilake, J. Effects of Re-heating Tissue Samples to Core Body Temperature on High-Velocity Ballistic Projectile–tissue Interactions. *Journal of Forensic Sciences*, 2017, Vol 62(6), pp 1466-1471.
[218] Janzon, B. and Seeman, T. Muscle devitalization in high-energy missile wounds, and its dependence on energy transfer. *Journal of trauma and acute care surgery*, 1985, Vol 25(2), pp 136-144.
[219] Fackler, M. Muscle devitalization in high-energy missile wounds, and its dependence on energy transfer, Letter to the Editor. *The Journal of trauma*, 1986, Vol 26(3), pp 297-297.
[220] Krauss, M. and Miller, J. Studies in Wound Ballistics: Temporary Cavities and Permanent Tracts produced by High-Velocity Projectiles in Gelatin, *CWLR 2340,* 1960.
[221] Mah, J., Anctil, B., and Keown, M. Damage caused by soil debris ejected from buried anit-personnel mines. *Personal Armour Systems Symposium,* 2006.

[222] Jin, Y., Haitao, L., Cheng, W., Wang, X., Han, R., Li, R., and Dong, D. The experimental and numerical investigation on the ballistic limit of BB—Gun pellet versus skin simulant. *Forensic Science International*, 2019, Vol 298, pp 393-397.
[223] Guha, R., Shear, N., and Papini, M. Ballistic impact of single particles into gelatin: Experiments and modelling with application to transdermal pharmaceutical delivery. *Journal of Biomechanical Engineering*, 2010, Vol 132, pp.
[224] Hole, L. Anatomical models based on gelatin and the influence of garments on impact damage, Shoe & Allied Trades Research Association, project no. 76/16080. 1980
[225] Haag, M.G. and Haag, L.C. Shooting incident reconstruction. Academic Press, 2011.
[226] Momentive Performance Materials Inc. Versatile, high strength, low viscosity mould making materials - RTV410, RTV420, RTV428 Technical Data Sheet. 2007.
[227] Cannon, L. Behind armour blunt trauma-an emerging problem. *Journal of the Royal Army Medical Corps*, 2001, Vol 147(1), pp 87-96.
[228] Kieser, J., Whittle, K., Wong, B., Waddell, J.N., Ichim, I., Swain, M., Taylor, M., and Nicholson, H., Understanding craniofacial blunt force injury: a biomechanical perspective. *In: Forensic Pathology Reviews.* Springer, 2009, 39-51.
[229] Shergold, O. and Fleck, N. Experimental investigation into the deep penetration of soft solids by sharp and blunt punches. *Journal of Biomechanical Engineering*, 2005, Vol, pp.
[230] Whittle, K., Kieser, J., Ichim, I., Swain, M., Waddell, N., Livingstone, V., and Taylor, M. The biomechanical modelling of non-ballistic skin wounding: blunt-force injury. *Forensic science, medicine, and pathology*, 2008, Vol 4(1), pp 33-39.
[231] Biermann, P.J., Roberts, J.C., Cain, R.P., Carkhuff, B.G., and Kleinberger, M. Instrumented torso model. Google Patents, 2004.
[232] Parry, D. and Parry, D. Wearable wound simulant. Google Patents, 2013.
[233] Ankersen, J., Birkbeck, A.E., Thomson, R.D., and Vanezis, P. Puncture resistance and tensile strength of skin simulants. *Proceedings of the Institution of Mechanical Engineers Part H- Journal of Engineering in Medicine*, 1999, Vol 213(H6), pp 493-501.
[234] Falland-Cheung, L., Pittar, N., Tong, D., and Waddell, J.N. Investigation of dental materials as skin simulants for forensic skin/skull/brain model impact testing. *Forensic science, medicine, and pathology*, 2015, Vol 11(4), pp 552-557.
[235] Jones, D.J. Skin and tissue simulant for munitions testing. Google Patents, 2007.
[236] Fenton, L. Investigating The Rupture Response Of Skin Penetration Models (MSc). Cranfield University, Cranfield Defence and Security. 2011.
[237] Gilchrist, M., Keenan, S., Curtis, M., Cassidy, M., Byrne, G., and Destrade, M. Measuring knife stab penetration into skin simulant using a

novel biaxial tension device. *Forensic Science International*, 2008, Vol 177, pp 52–65.
[238] McCarthy, C., Ní Annaidh, A., and Gilchrist, M. On the sharpness of straight edge blades in cutting soft solids: Part II – Analysis of blade geometry. *Engineering Fracture Mechanics*, 2010, Vol 70, pp 437–451.
[239] North Atlantic Treaty Organization (NATO). *NATO Standard AEP-94 skin penetration assessment of non-lethal projectiles, Edition A, Version 1*. [Personal Communication to James, G.].
[240] Tam, W. *Notes from LCG/9, DAT11*. [Personal Communication to James, G.].
[241] Werner, R., Schultz, B., Bockholdt, B., Ekkernkamp, A., and Frank, M. Energy-dependent expansion of. 177 caliber hollow-point air gun projectiles. *International journal of legal medicine*, 2017, Vol 131(3), pp 685-690.
[242] Trelleborg. *IIR - Butyl Rubber Sheeting.* [Online] Available from: https://www.trelleborg.com/en/fluidhandling/products--and--solutions/sheeting/iir--butyl [Accessed 17th July 2019].
[243] Advanced Materials Ltd. *General Purpose Grades: GP40 - 80. General purpose silicone rubber applications.* [Online] Available from: https://www.siliconerubberextrusions.co.uk/technical-information/data-sheets/gp [Accessed 17th July 2019].
[244] Ankersen, J., Birkbeck, A.E., Thompson, R., and Vanezis, P. Puncture resistance and tensile strength of skin simulants. *Proceedings of the Institution of Mechanical Engineers part H*, 1999, Vol 213(6), pp 493-501.
[245] Choh, C., Wall, M., Brown, M., Nicolson, A., and Simms, M. Use of durometry in assessment of venous disease. *Phlebology*, 2010, Vol 25, pp 94-99.
[246] Kissin, E.Y., Schiller, A.M., Gelbard, R.B., Anderson, J.J., Falanga, V., Simms, R.W., Korn, J.H., and Merkel, P.A. Durometry for the assessment of skin disease in systemic sclerosis. *Arthritis Care & Research: Official Journal of the American College of Rheumatology*, 2006, Vol 55(4), pp 603-609.
[247] *BS EN ISO 3376:2011 Leather. Physical and mechanical tests. Determination of tensile strength and percentage extension.* 2012.
[248] *Draft BS ISO 37. Rubber, vulcanized or thermoplastic. Determination of tensile stress-strain properties.* 2015.
[249] Instron. Bluehill(R) 2 Materials Testing Software.
[250] Ní Annaidh, A., Bruyère, K., Destrade, M., Gilchrist, M.D., and Otténio, M. Characterization of the anisotropic mechanical properties of excised human skin. *Journal of the Mechanical Behavior of Biomedical Materials*, 2012, Vol 5(1), pp 139-148.
[251] Google Patents. *Skin and tissue simulant.* Inventor: James, G. Application: PCT/GB2013/000221. Patent: WO2013171444 A1.
[252] Peters, C.E., Sebourn, C.L., and Crowder, H.L. Wound ballistics of unstable projectiles. Part I: projectile yaw growth and retardation. *Journal of Trauma-Injury, Infection, and Critical Care*, 1996, Vol 40(3S), pp 10S-15S.

[253] Peters, C.E. and Sebourn, C.L. Wound ballistics of unstable projectiles. Part II: temporary cavity formation and tissue damage. *Journal of Trauma-Injury, Infection, and Critical Care*, 1996, Vol 40(3S), pp 16S-21S.
[254] Peters, C. A mathematical-physical model of wound ballistics. *J Trauma (China)*, 1990, Vol 6(2 Supplement), pp 308-318.
[255] Sturdivan, L.M. A mathematical model of penetration of chunky projectiles in a gelatin tissue simulant. 1978
[256] Innovision Systems Inc. MaxTRAQ 2D M2.
[257] Ouellet, S. *RE: References wrt soft tissu penetration* [Personal Communication to James, G to James, G.] 30/11/2016.
[258] Krauss, M. and Miller, J. Comparison of permanent and temporary cavities produced by high-velocity rifle bullets in soft tissue, *Chemical Warfare Laboratories, Report No. 2144,* 1957.
[259] Young, M. and Merkl, B. Physics Department, Colorado School of Mines. *Confidence interval of a line spreadsheet.* 2001. [Online] Available from: http://inside.mines.edu/~mmyoung/CIofLine.xls [Accessed 06/08/2013].
[260] French, R. and Callender, G. Ballistic Characteristics of Wounding Agents. Washington DC. Office of the Surgeon General, Department of the Army, II, 143-235, 1962.
[261] Liu, Y., Chen, X., Li, S., Chen, X., Guo, R., Wang, D., Fu, X., Jiang, S., and Xu, G. Wounding effects of small fragments of different shapes at different velocities on soft tissues of dogs. *Journal of Trauma-Injury, Infection, and Critical Care*, 1988, Vol 28(S1), pp S95-S98.
[262] Krauss, M. and Miller, J. Studies in wound ballistics: temporary cavities and permanent tracts produced by high velocity projectiles in gelatin, USA, *CWLR 2340,* 1960.
[263] *ImageJ. An open platform for scientific image analysis.* [Online] Available from: https://imagej.net/Welcome [Accessed 29/08/2017].
[264] Talos, I.-F., Jakab, M., and Kikinis, R. *SPL Abdominal Atlas.* 2015. [Online] Available from: https://sectional-anatomy.org/ct-abdomen/ [Accessed 26th June 2018].
[265] Kieser, D.C., Kanade, S., Waddell, N.J., Kieser, J.A., Theis, J.-C., and Swain, M.V. The deer femur–a morphological and biomechanical animal model of the human femur. *Bio-medical materials and engineering*, 2014, Vol 24(4), pp 1693-1703.
[266] Allanson-Bailey, L. Improved cranial fracture metrics for assessing the protective benefits of helmet systems (PhD). The Open University. 2016.
[267] Kieser, D.C., Carr, D.J., Leclair, S.C., Horsfall, I., Theis, J.-C., Swain, M.V., and Kieser, J.A. Remote ballistic fractures in a gelatine model-aetiology and surgical implications. *Journal of orthopaedic surgery and research*, 2013, Vol 8(1), pp 15.
[268] Stevenson, T. *Gelatin calibration data*. [Exchange of high speed video files to James, G.] 12th July 2019.
[269] Couldrick, C., Trevor, A., Gotts, P., and Iremonger, M. Assessment of secondary fragments from buried AP blast mines. *Personal Armour Systems Symposium, TNO, Rijswijk, the Netherlands,* 2004.

[270] Verlome, J., Szymczak, M., and Broos, J. Metallic witness packs for behind-armour debris characterization. *International Journal of Impact Engineering*, 1999, Vol 22, pp 693-705.
[271] British Standards Institution. *BS EN 485-2:2016 Aluminium and aluminium alloys. Sheet, strip and plate. Mechanical properties.* 2016.
[272] British Standards Institution. *BS 1449-1.1:1991 Steel plate, sheet and strip. Carbon and carbon-manganese plate, sheet and strip. General properties.* 1991.
[273] British Standards Institution. *BS 3837-1:2004 Expanded polystyrene boards. Boards and blocks manufactured from expandable beads. Requirements and test methods.* 2004.
[274] Defence Standard 93-59. Chipboard (For Use at Proof and Experimental Establishments), *DEF STAN 93-59 Issue 3,* 2005.
[275] Croft, J. and Longhurst, D. HOSDB Body Armour Standards for UK Police (2007). Part 3: Knife and Spike Resistance, Publication No. 39/07/C. 2007
[276] Payne, T., O'Rourke, S., and Malbon, C. Body Armour Standard (2017), *CAST Publication number: 012/17,* 2017.
[277] *37 mm Airmunition cartridge.* [Online] Available from: http://www.airmunition.info/37mm_e.html [Accessed 04/04/2016].
[278] Ministry of Defence. Environmental Handbook for Defence Materiel - Part 4. Natural Environments, *DEF STAN 00-35 Part 4 Issue 4,* 2006.
[279] *ASTM D1056 Standard Specification for Flexible Cellular Materials—Sponge or Expanded Rubber.* 2000.
[280] Gillich, P. *Frag report*. [Personal Communication to Weir, J.] 11 February 2019 05:37.
[281] Mahoney, M. *Frag report*. [Personal Communication to Weir, J.] Defence Science and Technology Group, Australia. 11 February 2019 06:48.
[282] Duvall, P. Experimental Setup to Assess Blast and Penetration-Induced Secondary Debris in a Military Operations in Urban Terrain (MOUT) Environment, Army Research Laboratory, *ARL-TN-0714,* 2015.
[283] James, G. A new witness pack appropriate for non-metallic fragments. Dstl/PUB099788. *Group of Experts on Mitigation Systems (GEMS) 18th Annual Meeting, Defence Academy of the United Kingdom at Shrivenham,* 2017.
[284] *WITNESS PACK.* Inventor: James, G. Application: GB1918144.5.
[285] Stone, J., Amin, K., Kerr, J., Geraghty, A., Shaw, M., Wong, J., Dabare, D., and Fildes, J.E. The development of a porcine ex-vivo trauma research tool that does not require laboratory animals (Poster). 2019.
[286] Jussila, J. Wound ballistic simulation: Assessment of legitimacy of law enforcement firearms ammunition by means of wound ballistic simulation (PhD). University of Helsinki, The Second Department of Surgery and Police Technical Centre. 2005.
[287] *Draft Procedures for the evaluation and classification of personal armour. Bullet and fragmentation threats*. [Personal Communication to James, G.] NATO Standardisation Agency (NSA).

[288] Sydor technologies. *Ballistic/Impact Testing | Sydor Technologies.* 2017. [Online] Available from: https://sydortechnologies.com/sabreballistics/ [Accessed 21/08/2019].
[289] James, G. Preparation of Gelatin Targets, *DSTL/DOC89719. LOP/PR046 Issue Number 03,* 2015.
[290] James, G. Preparation of Gelatin Targets, *DSTL/DOC89719. LOP/PR046 Issue Number 04,* 2018.
[291] HP White Laboratories. Test Procedure, Ballistic Gelatin Blocks. HPW-TP-0601.02. 1998
[292] *Ed Harris 10 % Gelatin.* 1996. [Online] Available from: http://yarchive.net/gun/ammo/ballistic_gelatin.html [Accessed 10/04/2019].
[293] *Simplified 10% Ordnance Gelatin.* [Online] Available from: www.firearmstactical.com/tacticalbriefs/volume4/number1/article412.htm [Accessed 2010].
[294] *Dale Towert 10% Ballistic Gelatin.* [Online] Available from: www.logicsouth.com/~lcoble/dir5/gelprep.htm [Accessed 2010].
[295] Clear Ballistics LLC *Ballistic gelatin calibration for FBI and NATO standards.* 2017. [Online] Available from: https://www.clearballistics.com/shop/20-ballistic-gelatin-nato-block-16x6x6/ [Accessed 28/02/2018].
[296] Edwards, J. *Re: gelatin calibration*. [Personal Communication to James, G.] Clear Ballistics. Thu 29/03/2018 04:33.
[297] Hodgetts, T., Kirkman, E., Mahoney, P., Russell, R., Thomas, R., and Midwinter, M. UK Defence Medical Services guidance for the use of recombinant factor VIIA (RFVIIA) in the deployed military setting. *Journal of the Royal Army Medical Corps*, 2007, Vol 153(4), pp 307.
[298] Matney, M. How to Calculate the Average Cross Sectional Area. *Orbital Debris Quarterly News*, 2004, Vol 8(2), pp 7.
[299] dotPDN LLC, R.B., and contributors,. Paint.NET v3.5.10. 2011.

APPENDIX A Benefits and drawbacks of different penetration and perforation calculation methods

There are issues with some of the skin penetration/perforation data reported in the literature due to the misinterpretation of the different calculation methods and the amalgamation of data from different calculation methods when not appropriate. The skin penetration/perforation calculation method issues were noted during the literature review (Sections 3.3 and 3.4) have also been identified in (at least some of the data from) previous literature reviews (Section 3.6) within References [58; 61; 65; 68-70; 83; 84; 100-103; 286].

A very common (but least useful) method used in the literature to describe skin penetration and perforation is the use of the threshold velocity, V_{th}. This threshold velocity is entirely dependent on the velocities achieved in the experiment, with the hope that a non-perforation and perforation are achieved with close velocities to get a good estimate of where this threshold lies. However, due to obvious constraints on the number of shots possible against a particular target, this is not always possible and does not account for the rest of the shots. It is conceivable that if additional shots below the V_{th} are performed, some of these may perforate. Even if an experiment was replicated against an identical idealised material, this would likely result in a different V_{th}.

A better method for calculating skin perforation is by using a V_{50} assessment. This has the ability to account for multiple impacts in the experiment. There are a number of methods of calculation of the V_{50} velocity and it is vital to state which method has been used in addition the actual value.

The average method (e.g. Reference [210; 287]) requires an equal number of perforations and non-perforations (at least 3 of each). Based on the method for testing body armour performance [210; 287] and referred to as the STANAG or AEP 2920 method, the slowest non-perforation and fastest perforation velocity used in the calculation should be within 40 m s^{-1}. (Re)calculations based on existing data sets used the maximum (even) number of shots within the 40 m s^{-1} window. This is a simple calculation that can be performed on most of the data sets considered and does not have requirements for a ZMR. In this work, where

explicit data for each shot was not given in the literature, but the limits of the ZMR where specified, then the midpoint of the ZMR was given as an estimate of the 'average' V_{50} (and indicated as such).

The V_{50} based on the ZMR data only considers a limited number of shots. However, it is able to account for the skew of the data within the ZMR. It does not require an equal number of non-perforations and perforations and by design is suitable for instances where the ZMR is large. The obvious limitation is that it can only be used for data where a ZMR exists.

For the V_{50} based on the probit method, the statistical program R [52] was the preferred method used in this work. A probit curve was fitted to the data and enabled the V_{50} to be calculated, along with 95% confidence intervals on the measurement. This was the preferred method as it can account for every shot, including those that may be significantly above or below the V_{50}. The probit method used in this work did not require a ZMR[207]. It has the added benefits of being able to calculate the velocity required for any other probability value and the corresponding confidence interval. For example the V_{01}, which is the velocity for which the probability of perforation is 1%, is accepted as the highest velocity that never leads to a perforation [287] (V_{00} cannot be calculated as the tail of a probit curve has a horizontal asymptote). The drawback is that it is a relatively complex method and requires statistical software in order to calculate the V_{50} and confidence intervals.

The extrapolation from DoP data method is the only method that does not explicitly require non-perforation data. However, non-perforation data is likely to increase the reliability and accuracy of the prediction. This method requires multiple perforating shots with a spread in velocities where their associated penetration depths into a backing, such as tissue or a tissue simulant have been recorded. A best fit curve is then applied to the data and the point which corresponds to a DoP of 0 gives the V_{50}. There are a number of different best fit

[207] Probit calculations performed in R [52] using bias reduction in the binomial-response generalized linear model [53].

curves that can be applied. Linear, polynomial and log models can significantly under or overestimate the V_{50}, especially if there are limited data close to the V_{50}. Additionally, each will give different answers, some of which might not be rational (e.g. a negative V_{50}). In order to apply a standard approach, a direct non-linear, least squares regression model was used, as described in Reference [54]. This model assumes that the projectile does not lose mass or (significantly) plastically deform during penetration. This model fits the expected form of the data, with sufficient flexibility in the model parameters to be applied to the majority of data sets.

For isolated skin, the original equation described in Reference [54] can be applied where the residual velocity was recorded. The model is relatively complex in terms of its implementation, and does not work for all data sets. In these cases, a log model was implemented if deemed appropriate and this was indicated for data calculated in this manner.

APPENDIX B Ballistic testing experimental setups

B.1 Honed Tube Pressure Housing (HTPH)

The HTPH shown in Figure 145 is used to fire low velocity fragments from 3 mm to 20 mm diameter.

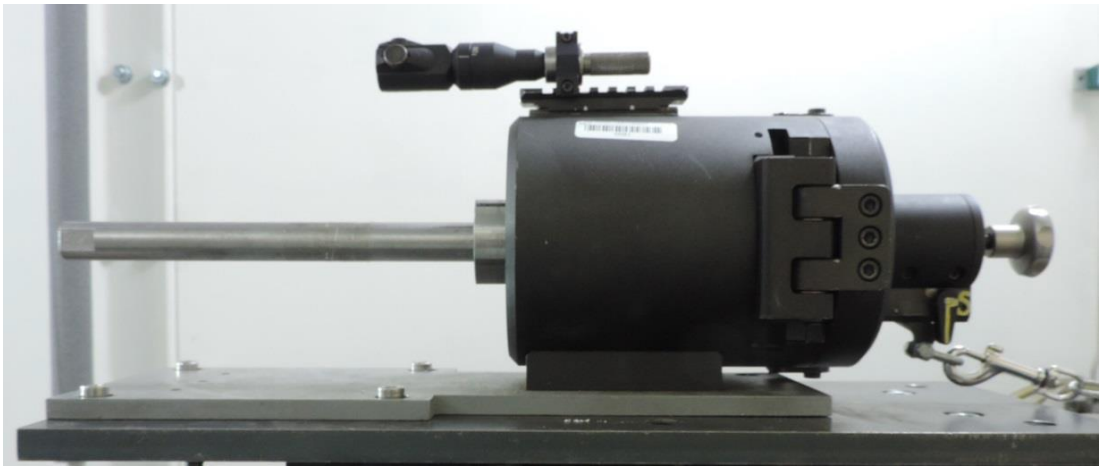

Figure 145: Photograph of the HTPH weapon system

The HTPH can accept a variety of smooth bore barrels with a typical barrel length of 300 mm. Maximum velocities of this weapon system are approximately 300 m s^{-1} for a 6 mm steel sphere. The HTPH uses rechargeable compressed air Airmunition cartridges [277] up to 20 MPa. The Airmunition cartridges are shown in Figure 146.

Figure 146: Photograph of the 37 mm Airmunition cartridge

B.2 Mann Pressure Housing (MPH)

The MPH shown in Figure 147 is used for firing projectiles from low to high velocities.

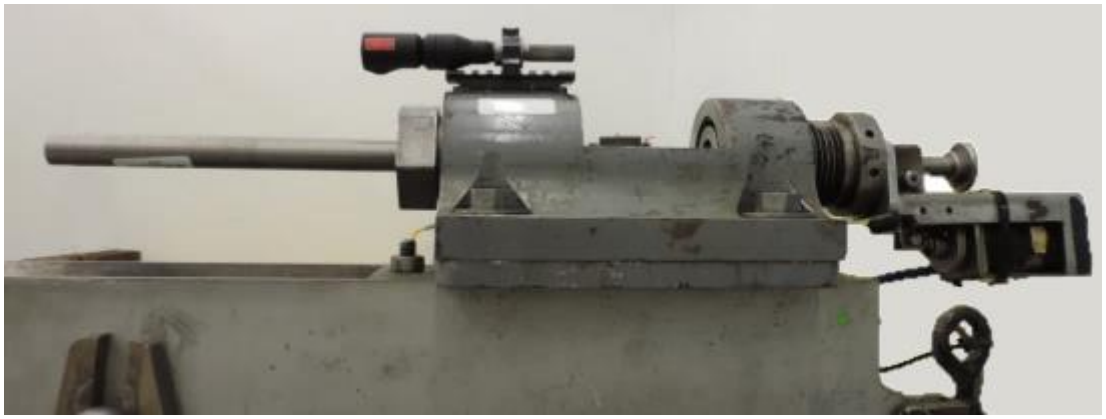

Figure 147: Photograph of the MPH weapon system

The MPH can accept the compressed air Airmunition cartridges [277] or pistol and rifle blank charges. Blank charges used include (in order of increasing velocities achievable with them); 7.65x17 mmSR (0.32” ACP) and 9x29 mmR (0.38” special) pistol blanks, 5.56x45 mm, 7.62x51 mm and 12.7x99 mm rifle blanks. These blank charges can be filled with different amounts of propellant to give the required projectile velocity. Photographs of the different blanks are shown in Figure 148 and Figure 149.

Figure 148: Photograph of 7.65x17 mmSR (0.32” ACP) blank pyrotechnic charges (unfired).

Figure 149: Photograph of a selection of blank pyrotechnic charges (all have been fired). Left to right; 12.7x99 mm, 7.62x51 mm, 5.56x45 mm and 9x29 mmR (0.38" special).

The MPH can accept the smooth bore barrels up to 20 mm calibre used for the HTPH, as well as its own dedicated rifled barrels. The MPH is also used to fire complete pistol or rifle bullets through appropriate rifled barrels.

Typical barrel lengths are 300 mm to 800 mm and velocities from approximately 25 m s^{-1} up to 1600 m s^{-1} can be achieved for <1 g projectiles.

B.3 Sabre Gas Gun

The Sabre Ballistics (part of Sydor Technologies) A1G+ gas gun [288] shown in Figure 150 is used for very low (~10 m s^{-1}) to medium velocities (~700 m s^{-1}) with fragments up to 20 mm diameter. It uses compressed air or compressed helium up to pressures of 30 MPa.

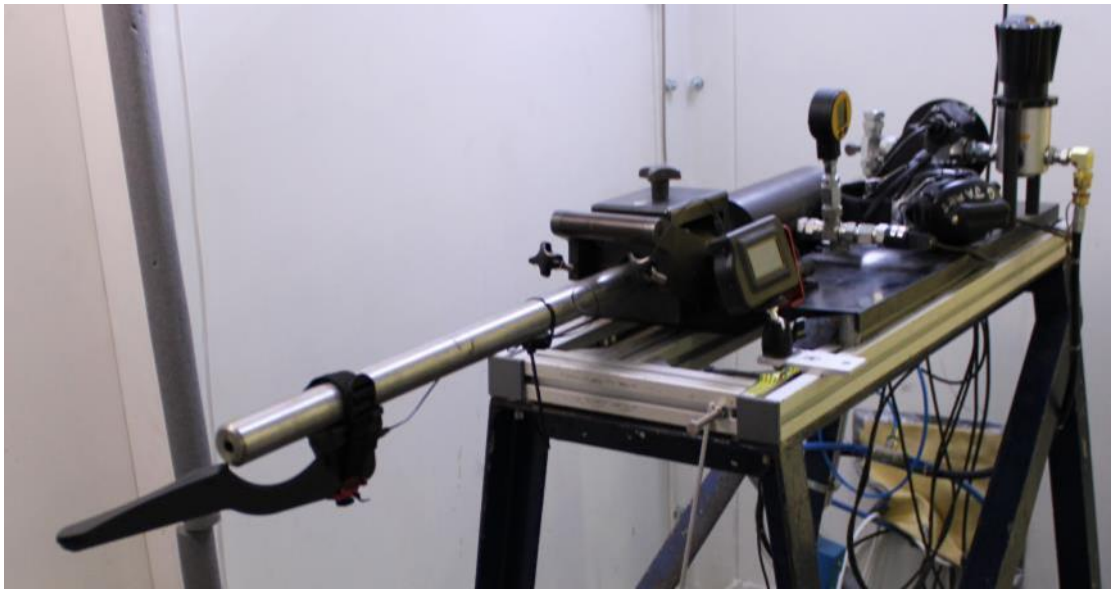

Figure 150: Photograph of the Sabre Ballistics gas gun

The Sabre Gas Gun can accept a variety of smooth bore or rifled barrels with a typical barrel length of 300 mm to 800 mm. The use of helium and longer barrels enables the higher velocities to be achieved.

APPENDIX C Expanded empirical skin penetration and perforation equation initial validation

This section provides initial validation of Equation 8: The final version of the expanded empirical skin perforation equation, for specific cases, showing the predictions against actual data. Although this validation is using data on which the model is built, it shows the model accuracy for specific cases instead of all data grouped together as in Figure 26.

The experimental data is shown against the model predictions (Equation 8) in Figure 151 to Figure 159 for the prediction type for which there is the most data. For each figure the following information are detailed: the model inputs, the source of the comparison data (all of which is given in Table 1), the number of comparison data points and the R^2 value of the prediction (where the number of comparison data points is greater than 2).

As detailed in Section 6.1.4, some of the descriptions of storage conditions given in the original references were combined. For example for fresh PMHS skin, the mixed conditions detailed as “fresh and refrigerated” [56] and “fresh and frozen-thawed” [71] were treated as “fresh” for calculations within Equation 8.

The figures are not discussed, they are shown only to provide confidence in the model predictions and provide additional evidence (albeit for a limited portion of the available data) of the relative influence of the different factors that influence the penetration or perforation response.

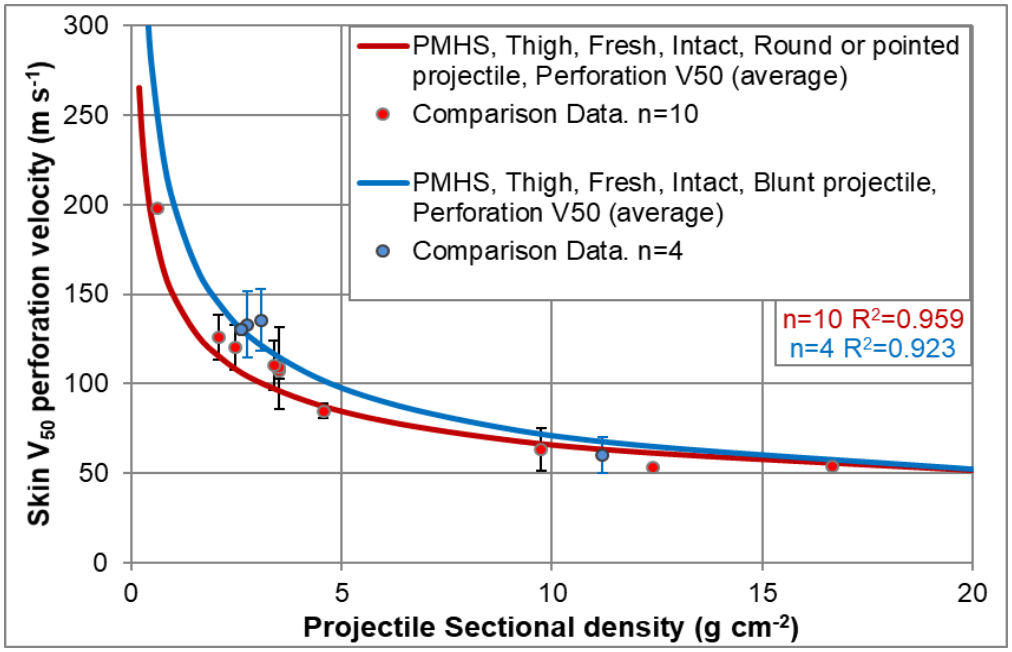

Figure 151: Equation 8 prediction for PMHS, thigh, fresh, intact, perforation V_{50} by the average method for blunt projectiles in blue and round or pointed projectiles in red. Comparison data is from References [56; 59; 62; 71]. Error bars are those stated in the original reference(s).

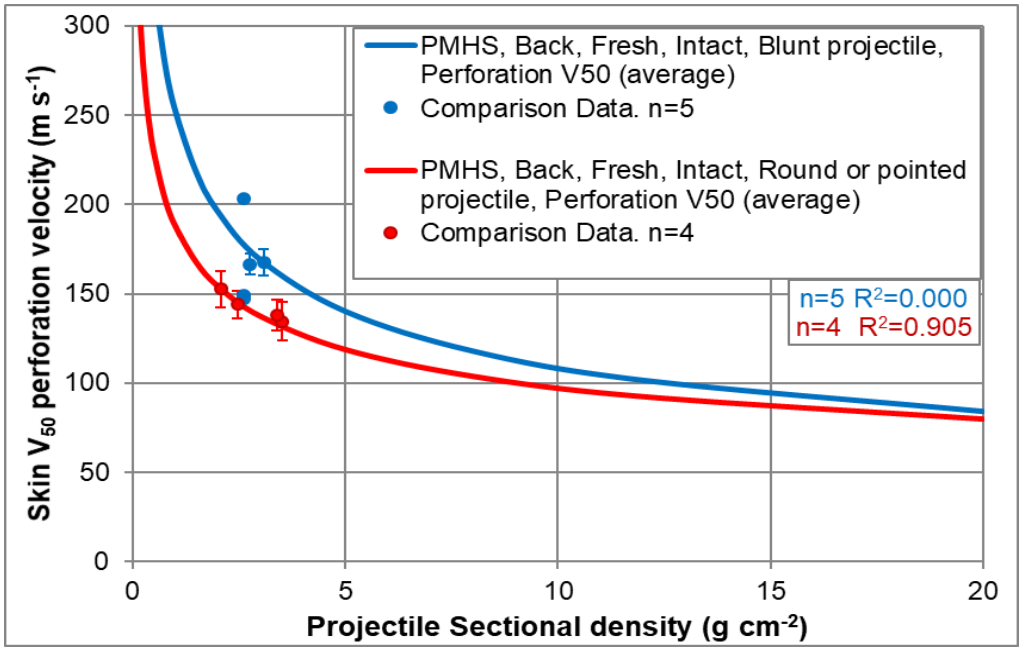

Figure 152: Equation 8 prediction for PMHS, back, fresh, intact, perforation V_{50} by the average method for blunt projectiles in blue and round or pointed projectiles in red. Comparison data is from References [56; 59; 62; 71]. Error bars are those stated in the original reference(s).

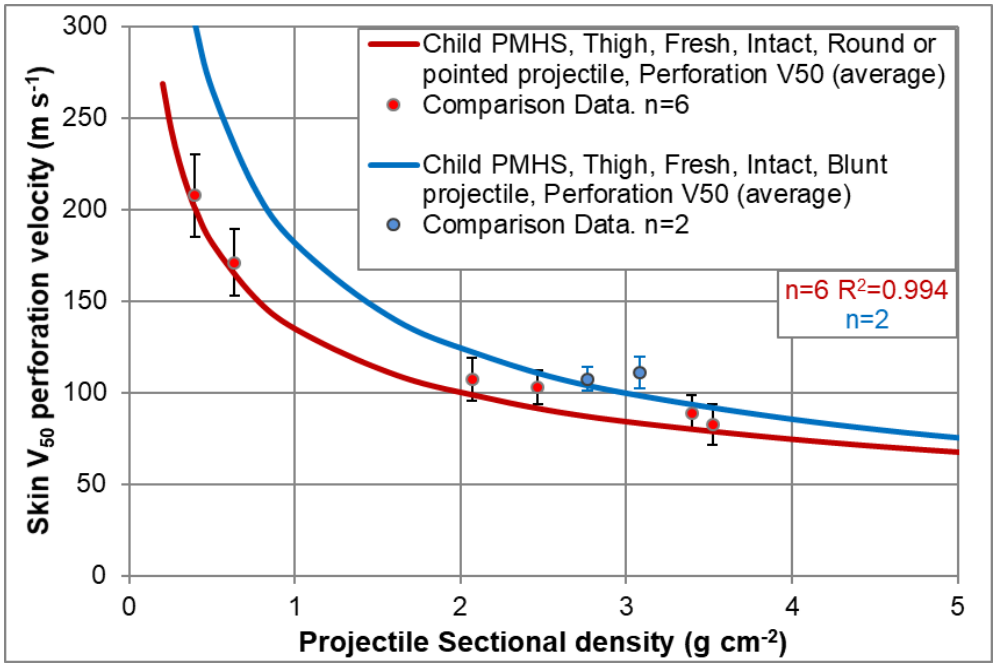

Figure 153: Equation 8 prediction for Child PMHS, thigh, fresh, intact, perforation V_{50} by the average method for blunt projectiles in blue and round or pointed projectiles in red. Comparison data is from Reference [59]. Error bars are those stated in the original reference.

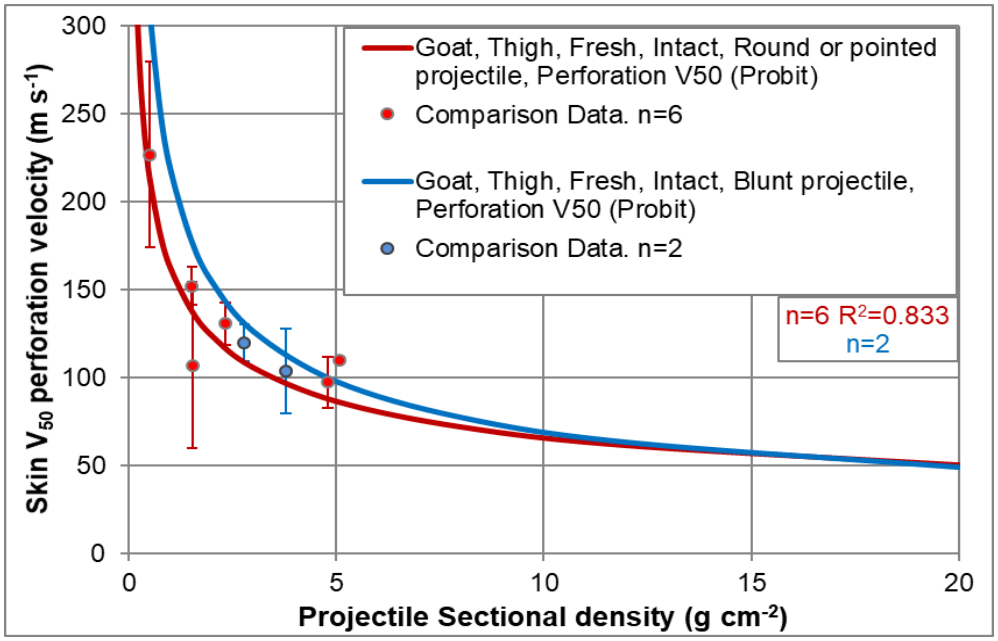

Figure 154: Equation 8 prediction for goat, thigh, fresh, intact, perforation V_{50} by the probit method for blunt projectiles in blue and round or pointed projectiles in red. Comparison data is from Reference [59; 79] and Section 5. Error bars are 95% CI.

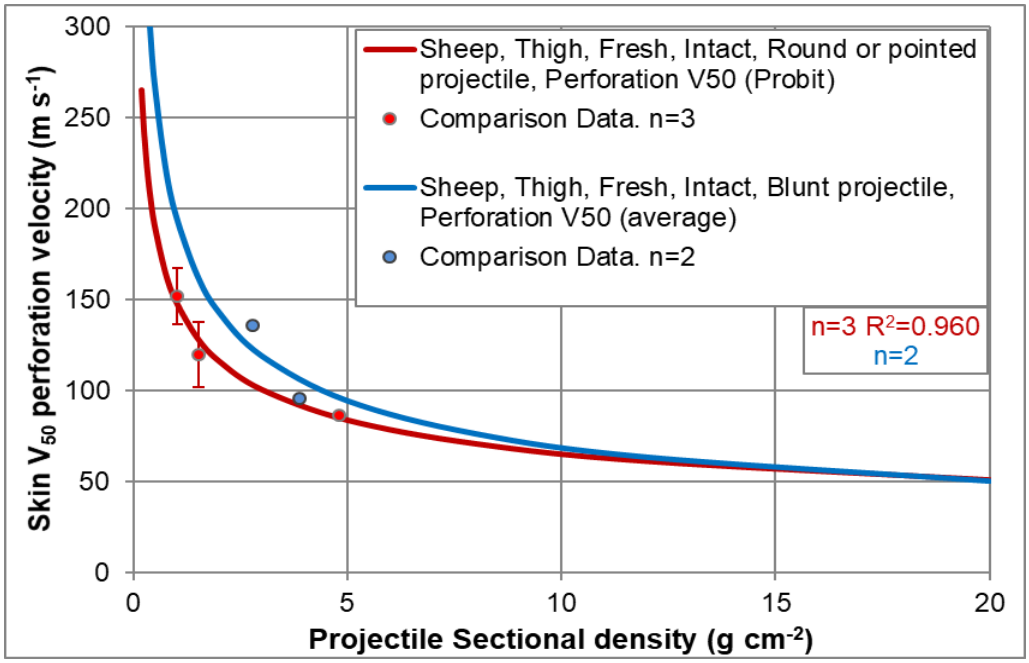

Figure 155: Equation 8 prediction for sheep, thigh, fresh, intact, perforation V_{50} by the probit method for blunt projectiles in blue and round or pointed projectiles in red. Comparison data is from Section 5. Error bars are 95% CI.

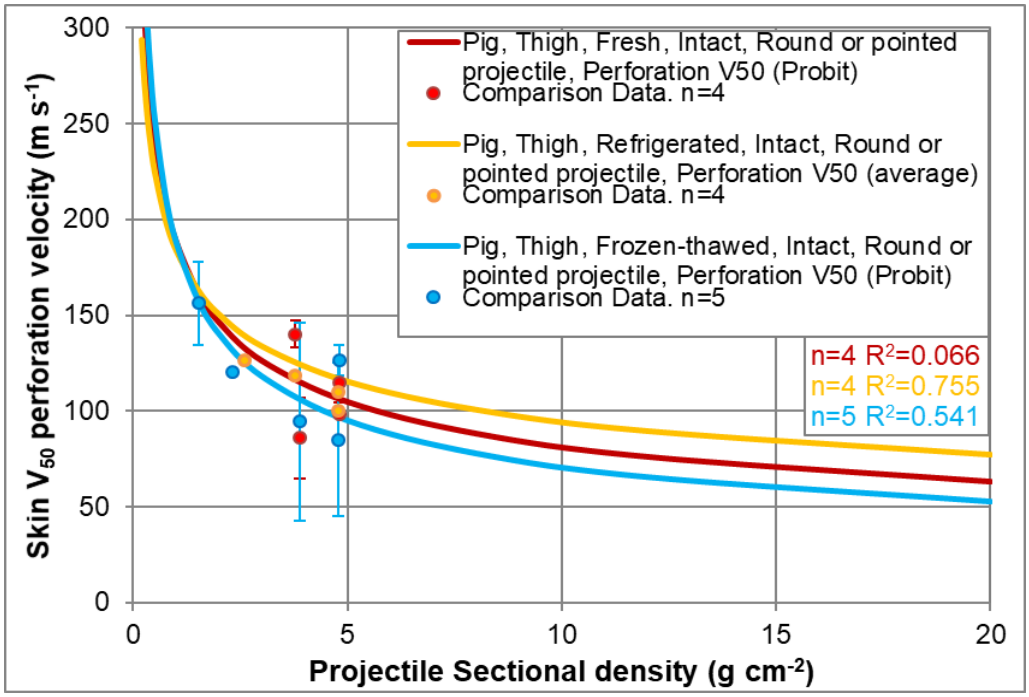

Figure 156: Equation 8 prediction for pig, thigh, intact, perforation V_{50} by the probit or average method for round or pointed projectiles for each of fresh, frozen-thawed and refrigerated storage conditions. Comparison data is from Reference [58] and Section 5. Error bars are 95% CI.

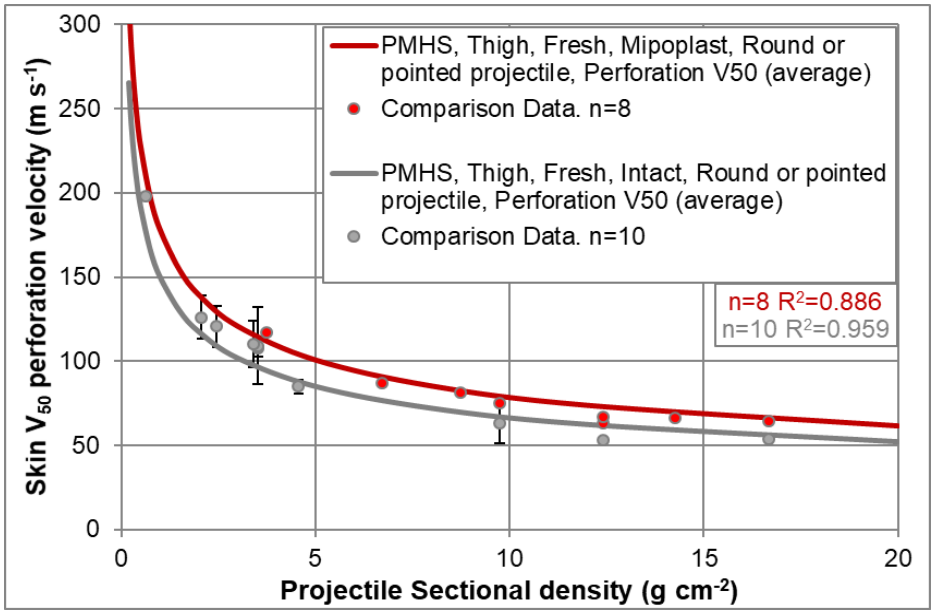

Figure 157: Equation 8 prediction for PMHS, thigh, fresh, isolated and backed by Mipoplast, perforation V_{50} by the average method for round or pointed projectiles (red). Also shown is the equivalent prediction for intact PMHS skin (grey). Comparison data is from References [56; 59; 71]. Error bars are those stated in the original reference(s).

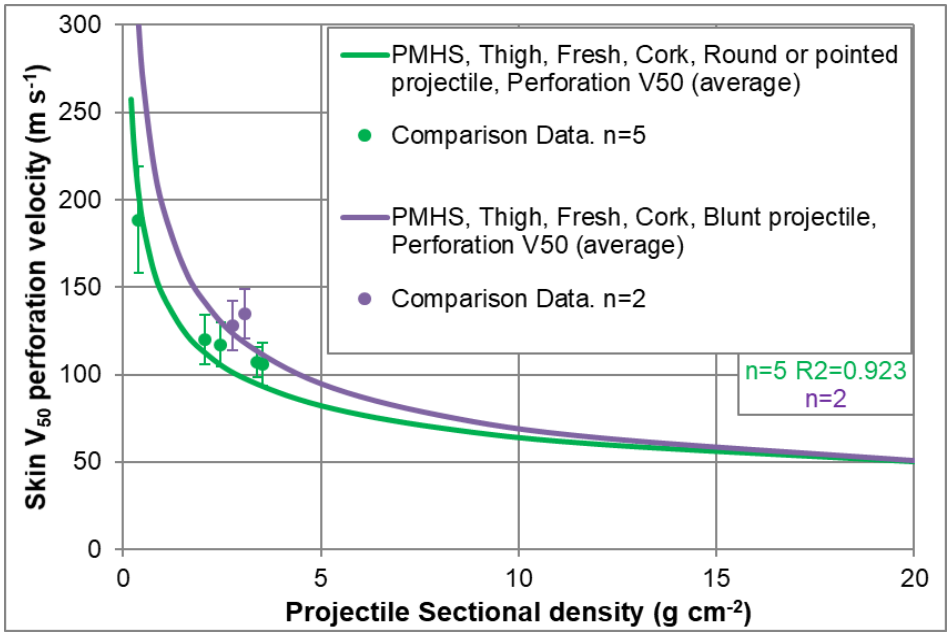

Figure 158: Equation 8 prediction for PMHS, thigh, fresh, isolated and backed by cork, perforation V_{50} by the average method for blunt projectiles in purple and round or pointed projectiles in green. Comparison data is from Reference [59]. Error bars are those stated in the original reference.

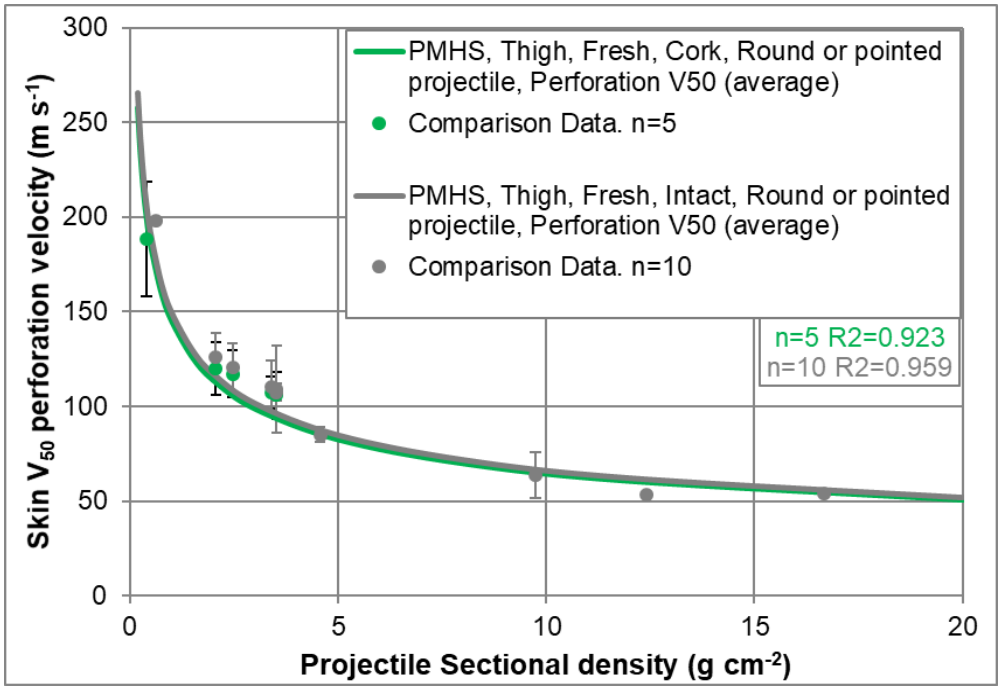

Figure 159: Equation 8 prediction for PMHS, thigh, fresh, isolated and backed by cork, perforation V_{50} by the average method for round or pointed projectiles (green). Also shown is the equivalent prediction for intact PMHS skin (grey). Comparison data is from References [56; 59; 71]. Error bars are those stated in the original reference(s).

APPENDIX D Gelatin mix methods

D.1 Dstl 20% gelatin method

The method for Dstl 20% gelatin is based on References [289; 290].

Gelatin of type A, 250 Bloom (or greater) is required.

- Heat water to 70±5°C.
- Decant the water into a suitable mixing container.
- Thymol (0.01%) or cinnamic acid (1 drop per litre) may be added into the water as a preservative against fungal growth.
- Utilising a drill with a mixing paddle, mix the water to the point of forming a whirlpool, but without introducing too much air into the mixture, slowly adding the required gelatin powder. When all gelatin is added, stir for an additional 5 minutes. Cover and allow to stand for 5 minutes. Stir once more for 5 minutes allowing it to stand for at least an hour afterwards.
- Scrape off any excess foam that may have formed on the surface of the gelatin. If the gelatin still appears opaque prior to pouring, allow to stand until clear.
- Decant the liquid gelatin into the molds.
- Place the entire mold in the conditioning cabinet at a temperature of 10±2°C, 65% Relative Humidity (RH) until set.
- Store the blocks in a conditioning cabinet at a temperature of 10±2°C, 65% relative humidity (RH) for a minimum of 16 hours.
- Blocks may be stored for up to 2 days at 10±2°C, 65% RH uncovered. Alternatively, blocks may be stored individually sealed in a plastic bag with no humidity specification up to 5 days.
- The calibration test for 20% gelatin at 10°C should be conducted on at least 1 block per batch per day. For example each batch needs to be recalibrated on each firing day, regardless of if it passed (or failed)

previously. For extended storage durations it is suggested to calibrate each block or multiple blocks from each batch where possible.

D.2 NATO 20% gelatin method

Reproduced from Reference [130]

- "*Size: A stationary gelatine block 30 cm (along line of fire) x 15 cm x 15 cm.*
- *1:4 ratio of gelatin to water by weight. For example 6 kg of dry gelatin powder is mixed with 24 kg of water at 25°C. 0.01% Thymol will be added as a preservative against mold.*
- *Let the mixture soak for 45 minutes without stirring. After swelling, the mixture is gelatinous and opaque. Then, without stirring, the mixture is heated to a temperature of 50°C in a water bath to get a clear, easy-flowing liquid. Then skim off carefully foam and bubbles from the surface.*
- *Pour the liquid into stainless steel molds of a 15 x 20 x 30cm size*[208]*. (The final height of the block has to be 14 to 16 cm). Again, skim off the foam.*
- *Cool the mixture in its mold until set at a temperature of 20°C.*
- *Gelatin block may be removed from the mold by dipping into hot water and turning it over on a flat surface. Surface ridges that are optically objectionable may be smoothed out by placing a flat pane of glass on the surface, pouring hot water over the glass and honing the glass against the surface until satisfactory. Store at 10±2ºC either with 65% RH (or sealed in a plastic bag with no humidity specification) up to 4 days. During the firing the gelatin block will have a temperature of 10±2ºC.*" [130]

D.3 Fackler 10% gelatin method

Reproduced from Reference [129]. This is also commonly called FBI 10% gelatin.

[208] 15 cm width, 20 cm height, 30 cm length.

- “*Always start with cold water (7-10°C).*
- *Always add the powdered gelatin to the water. Never pour water into gelatin. 1000 g gelatin, 9000 ml water (this gives a 10% solution)*
- *Agitate (by stirring) a bare minimum just to wet all particles (avoid violent agitation to prevent entrainment of large quantities of air).*
- *Let stand in refrigerator for 2 hours to hydrate all gelatin particles.*
- *Heat the container in a hot water bath or double cooker, and again stir gently until all gelatin is in solution and evenly dispersed throughout the container. Do not overheat (40°C). Do not stir rapidly, to prevent entrainment of air.*
- *Pour into molds, set in refrigerator or cold water bath (7-10°C) until firmly set. (Overnight for best results)*
- *After removal from molds, store in refrigerator at 4°C in airtight plastic bags. Do not use blocks until at least 36 hours have elapsed from the time gelatin was poured into molds. ”* [129]

D.4 Other gelatin mix methods

Cranfield 10% and 20% gelatin mix methods are detailed in Reference [38] (their Appendix C and D respectively) and again for 10% in References [163; 166].

The methods used to produce the 20% gelatin from References [91] and [161] were not stated. However, it is likely that the Cranfield 20% method [38] was used to produce the gelatin from Reference [91] (as it was at the same institution and by one of the same researchers as Reference [38].

There are also a number of other gelatin mix methods used by different institutions, examples include those in References [158; 215; 291-294].

D.5 DoP Calibration

D.5.1 Projectile details

A 4.4 mm (0.177 calibre) (brass coated) steel ball bearing weighing 0.35 g should be used with a 0.177" air rifle or alternative firing method for calibration.

For the purposes of calibration, **all penetration depths are measured to the shallowest part of the projectile unless stated** (i.e. do not include the projectile diameter).

It is recommended to report any calibration results (impact velocity and resulting DoP) with the studies in which it was generated to provide assurance on the gelatin verification.

D.5.2 Calibration for 10% gelatin

For gelatin of 10% concentration, it must be calibrated at 4°C (±1°C) regardless of usage temperature. There are 2 accepted methods:

- **Method 1 (fixed velocity):** With an impact velocity of 180±5 m s^{-1}, the ball bearing must achieve a penetration depth of 85±10 mm [94][209]

Or;

- **Method 2 (wider velocity range):** 2 shots at different velocities must produce DoP within the limits of the equation (which accounts for the diameter of the projectile):

$$DoP = 0.594v - 21.92 \pm 5$$

Equation 43: Calibration standard for 10% gelatin [128; 286]

Where:

[209] Reference [94] is considered to be the origin of the calibration standard for 10% gelatin at 4°C. However, the calibration standard it is not explicitly given within that paper, rather the results obtained from performing the test are reported.

DoP is in mm (measured to the shallowest part of the projectile)

v is the impact velocity in m s^{-1}, within the velocity limits $120 \leq v \leq 190$ m s^{-1}.

In all cases, the velocity and penetration depth obtained should be recorded. It is important to note the 2 calibration standards for 10% gelatin are not always mutually inclusive due to the different limits on the penetration depth for the 2 methods (± 10 mm for method 1 and ± 5 mm for method 2).

D.5.3 Calibration for 20% gelatin at 10°C

A calibration standard for 20% gelatin at 10°C is not readily available from the literature. The initial standard used is detailed below, but was revised following conclusion of the tissue simulant testing (Section 7.2.6).

Calibration should be conducted on at least one block per batch, with the block at 10±2°C.

Method 1 (fixed velocity): With an impact velocity of 180±5 m s^{-1}, the ball bearing must achieve a penetration depth of 38±6 mm [216][210].

Method 2 (wider velocity range): Following the selection and testing of Dstl 20% gelatin at 10°C, a new calibration standard for 20% gelatin was developed allowing a wider range of impact velocities. This new calibration is given by Equation 14 in Section 7.2.6, but is repeated here for completeness:

$$DoP = 0.378v - 32.6 \pm 6$$

Equation 14: New calibration standard developed for Dstl 20% gelatin at 10°C.

Where:

DoP is in mm (measured to the shallowest part of the projectile)

[210] This calibration for 20% gelatin at 10°C is also given in Reference [295]. The origin of this standard was stated as "*Come to find out NATO has not publish any official document on NATO testing standards. Our company has made its own testing standard for our version of our 20% gel. The way they came up with this standard was by making a batch of 20% natural gel and performed the BB test.*"[296]

v is the impact velocity in m s^{-1}, within the velocity limits $120 \leq v \leq 200$ m s^{-1}.

To reduce the risk of rejecting a good batch, one result that is in calibration is required per batch (or per block if calibrating each block individually). If the first shot is a valid velocity, but the resulting DoP is not, conduct an additional shot at a valid velocity. One of these 2 shots must pass the calibration. If both fail, the batch should be rejected.

D.5.4 Other sources of calibration data for gelatin

The raw Dstl 20% gelatin at 10°C calibration data and calibration standard based on Equation 14 appears to fit well and may be suitable to be applied to the Guey/Kieser 20% gelatin at 10°C from Reference [158; 160]. This is shown in Figure 160.

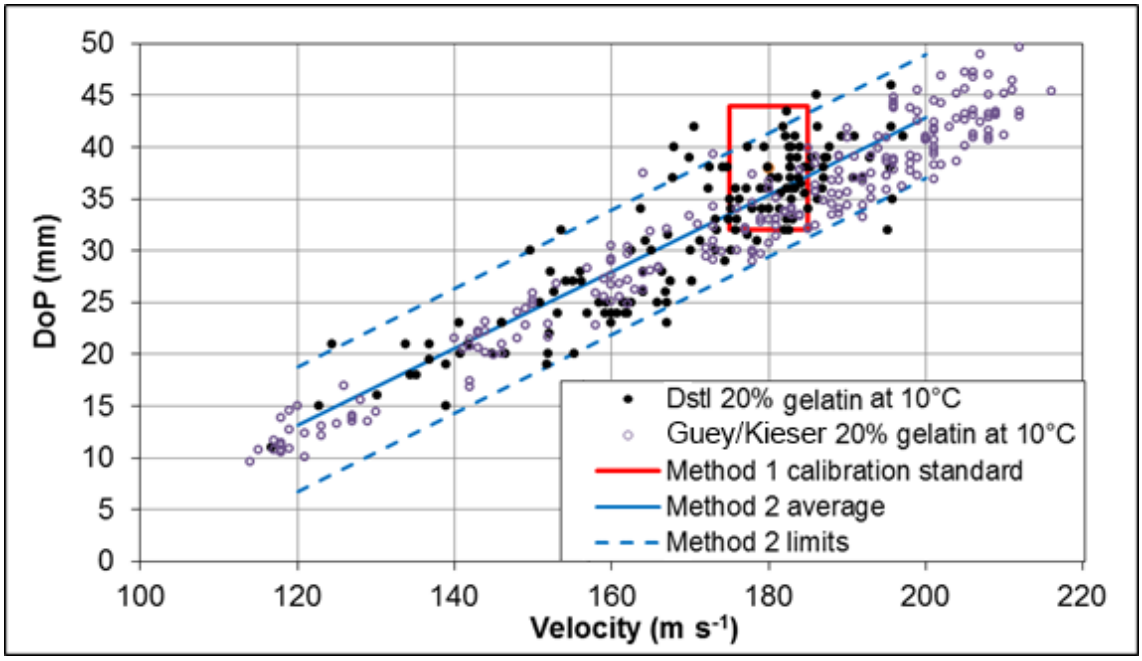

Figure 160: Calibration standards and data for Dstl 20% gelatin at 10°C (data from Section 7) and the Guey/Kieser 20% gelatin at 10°C [158; 160].

Figure 160 shows that whilst the calibration standard based on Equation 14 was produced for Dstl 20% gelatin at 10°C, it could be applied to gelatin from other manufacture methods.

However, this is not universally the case. The data for 20% gelatin at 10°C from Reference [137] does not meet either the method 1 or 2 calibration standards for 20% gelatin at 10°C. Nor does the Haag 10% gelatin at 4°C meet the method 1 or 2 calibration standards for 10% gelatin, despite the mix method based on that by Fackler [129]. Care should therefore be taken if Reference [137] is used as a source of calibration information.

References [38; 122; 166] give DoP data for calibration of Cranfield gelatin with a 5.5 mm steel sphere. However, no acceptance bounds are provided for this ‘calibration’ procedure, rather it is just to enable comparison to previous data.

APPENDIX E Additional muscle tissue and simulant penetration data and comparisons

E.1 Muscle tissue penetration comparisons

Additional comparisons between targets (various muscle tissue or muscle tissue simulants) are provided in this Appendix, in support of the data shown in Section 7.2.5.

Comparison of the penetration into animal tissue and PMHS tissue can be made and is shown in Figure 161.

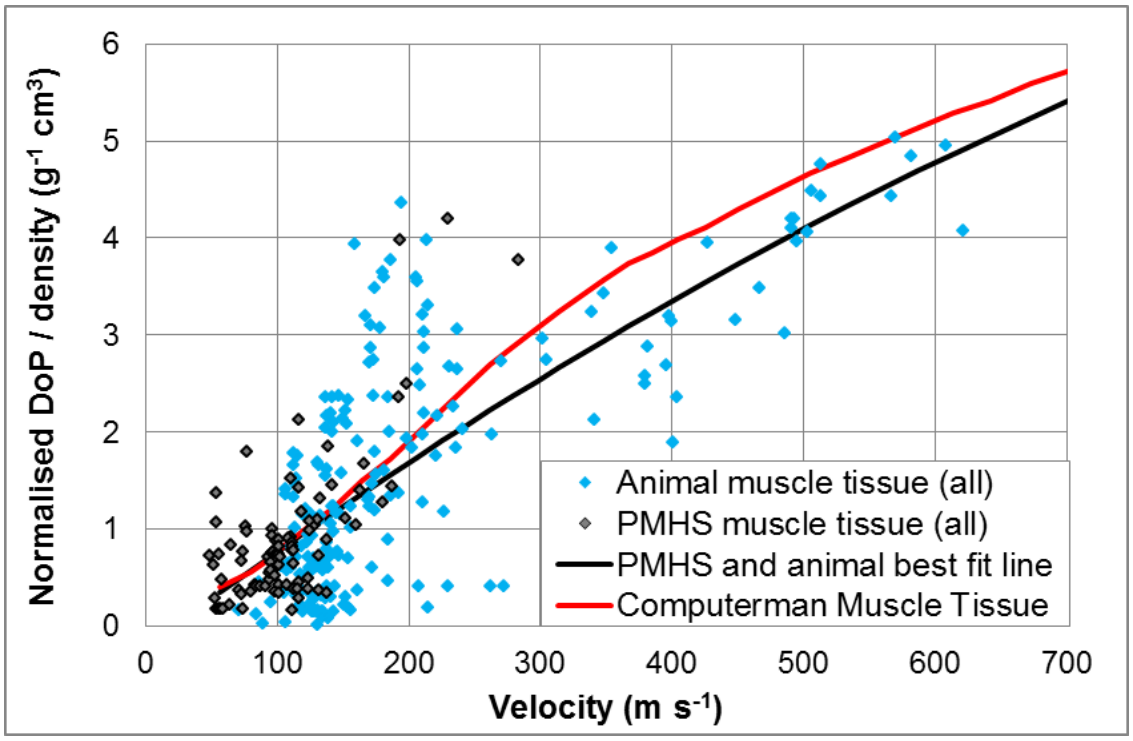

Figure 161: Comparison on depth of penetration in PMHS and animal muscle tissue (full velocity range of animal data not shown). Data summarised in Table 4.

Figure 161 shows the animal data is shifted to the right (higher velocity required for equivalent penetration) in Figure 161 compared to the PMHS data. This is likely because the majority of the animal data is for pigs (80%) which are expected to have a higher skin perforation velocity compared to PMHS (see Sections 5.5 and 6.1.5). The comparison is also hindered by the fact that only comparatively small penetrations depths have been made into PMHS muscle tissue, limited by

the size of individual muscles available in PMHS targets compared to pigs, sheep and goats.

Figure 161 shows the animal muscle tissue DoP data appears to follow a bimodal response at around 200 m s^{-1}, with one branch showing (clustering of data or) much larger normalised DoP over density values than expected based on the trends of the entire data. To investigate this further, the animal tissue data was replotted by its storage condition prior to ballistic testing which was thought to be one possible explanation for this different response. The data was separated into "fresh" and "refrigerated or frozen/thawed" animal muscle tissue (mix of pig, sheep and goat targets) and is shown in Figure 162.

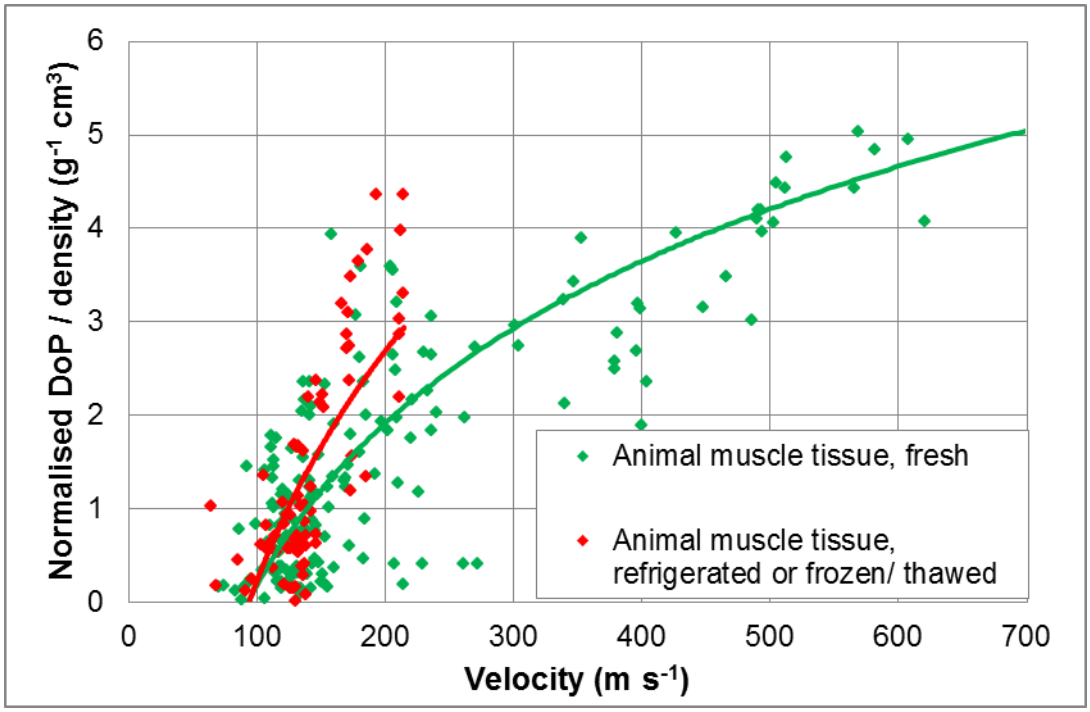

Figure 162: Comparison on depth of penetration in fresh and refrigerated or frozen/thawed animal muscle tissue. The full velocity range of fresh animal muscle tissue data not shown. Data summarised in Table 4.

Figure 162 shows that the fresh muscle tissue generally exhibited a lower normalised DoP over density value at corresponding velocities above approximately 150 m s^{-1} compared to the refrigerated or frozen/thawed animal muscle tissue. The bimodal response is not dependent on the different tissue storage types. As with the empirical skin perforation performance (Equation 8)

and testing from Section 5.4, it is likely that storing the tissue (refrigerated or frozen) prior to testing adds additionally variability into its response.

Due to limitations in the impact velocity range for the refrigerated or frozen/thawed animal muscle tissue (maximum velocities of 215 m s^{-1}), it is difficult to determine if the differences observed may be due to a difference in skin perforation response (as impacts were close to the skin V_{50}), the muscle tissue response, or a combination of these.

The penetration into different target types was additionally split into fresh pig, sheep and goat data and compared to all the PMHS muscle tissue for all storage conditions and is shown in Figure 163 with the average animal and ComputerMan muscle tissue responses.

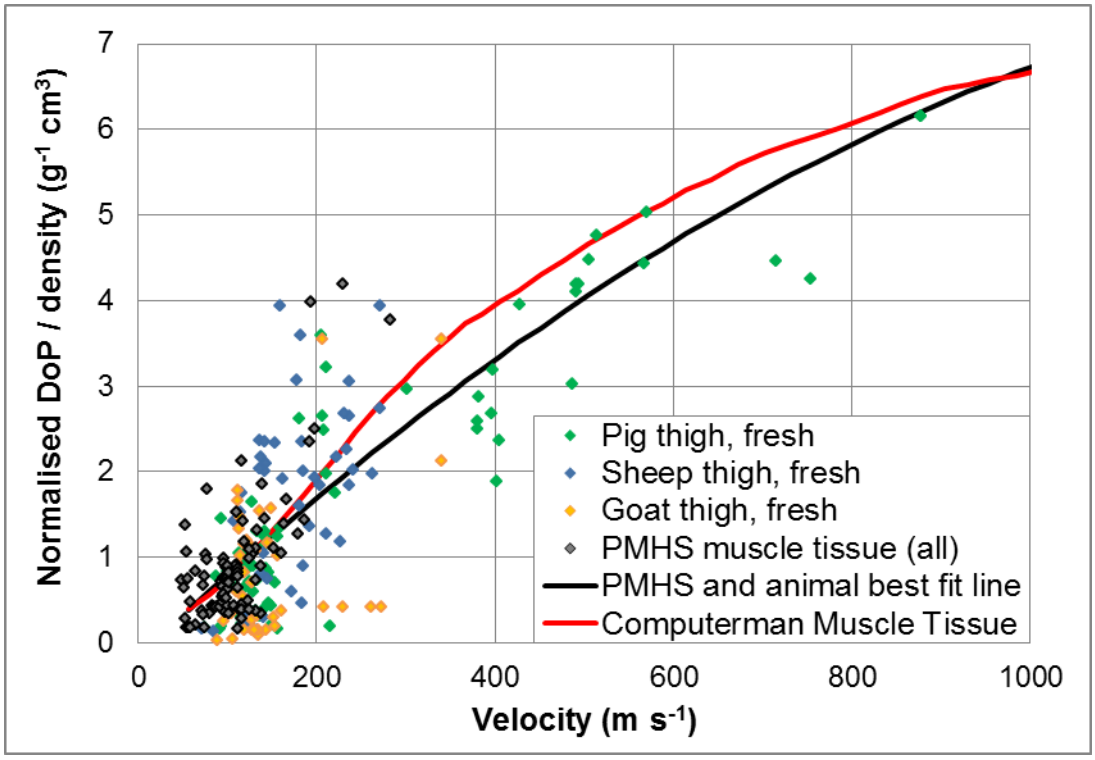

Figure 163: Comparison on depth of penetration in PMHS and different fresh animal muscle tissue, with ComputerMan muscle tissue response. Data summarised in Table 4.

Figure 163 shows that with the data available, there are no observable differences between the penetration responses in the different fresh targets. As

with Figure 162, the limited velocity range for most of the data and large inherent variability prevent further conclusions from being drawn. This comparison is limited by the fact that the PMHS targets are a mix of storage conditions and the data is for a mix of geometry projectiles (spheres, cylinders and CN cylinders).

41 data points for fresh pig abdomen and thorax from Reference [88] were also available and used to compare to the animal muscle tissue.

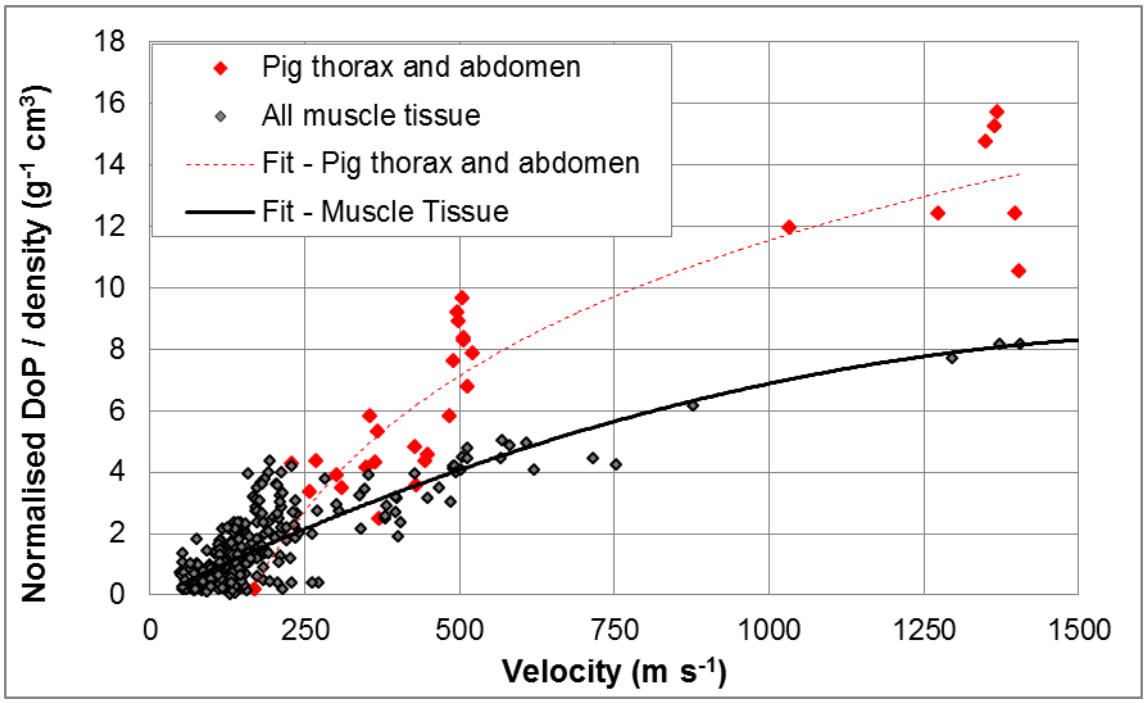

Figure 164: Penetration into animal tissue: muscle tissue compared to non-muscle tissues (thorax and abdomen). Data from Reference [88] and summarised in Table 4.

Figure 164 shows penetration into the thorax and abdomen appears to give deeper penetration depths and is more variable than the muscle tissue data (due to the number of different tissue types that the projectile would have to pass through in those body regions).

This highlights the importance of the ability to account for the different penetration or retardation response of different tissue types when considering shots through hybrid tissues (see Section 9.9).

No account was taken of which tissues were penetrated or perforated in the thorax and abdomen shots. The data points shown in Figure 164 for the thorax and abdomen that fall in line with the expected penetration in to muscle tissue may have perforated bone.

The outcomes of muscle tissue penetrations and those to the abdomen and thorax is supported by the comparisons made in Reference [88] over a smaller velocity range.

E.2 Recombinant Factor VIIa (rFVIIa) ballistic testing

E.2.1 Background to rFVIIa ballistic testing

The recombinant Factor VIIa ballistic testing described in this section supports the muscle tissue simulant energy loss comparison in Section 7.3.2.

Previous work completed for the Combat Casualty Care programme in Dstl (and its predecessor organisations) investigated the efficacy of rFVIIa for improving the survival rate in live, terminally anesthetised large white pigs that had been subjected to a ballistic penetrating injury on the muscle mass of the thigh to produce a repeatable ballistic injury.

This work was conducted under licence from the Home Office and in accordance with the Animals (Scientific Procedures) Act 1986 and contributed to clinical guidance on the use of rFVIIa [297].

The setup details and raw ballistic data were made available [96], such that the ballistic impacts conducted could be recreated with muscle tissue simulants and compared to the pig data. This is the first time that that this pig data has been reported.

E.2.2 rFVIIa testing methods

Impacts were conducted on the terminally anesthetised large white pigs with a 9.525 mm (3/8”) steel sphere (nominal mass 3.55 g) at a nominal impact velocity of 775 m s^{-1}. The exit velocity of the projectile was measured following the perforation, as was the total thickness of tissue (including skin) penetrated by the projectile.

Velocities were measured with a combination of shock pressure sensors, ballistic chronographs, sky screens and MSI infra-red light gates. In most cases, multiple velocity readings were taken prior to impact and on exit.

E.2.3 rFVIIa testing results

In total 21 impacts were conducted. Of these, two did not have associated tissue thickness measurements and a further two impacts were considered outliers, at 320 and 1026 m s^{-1}. The individual shot data for the valid impacts are provided in Table 44.

Impact velocity (m s^{-1})	Exit velocity (m s^{-1})	Tissue thickness (mm)
739.5	506.0	89
743.7	496.0	92
748.9	526.5	90
750.8	491.2	109
756.6	504.2	103
760.4	481.0	111
766.2	507.0	93
769.8	478.1	98
770.2	491.9	105
777.5	498.0	110
788.0	497.3	110
792.3	508.1	115
795.6	511.7	101
797.4	521.6	116
807.2	535.7	102
811.1	518.4	111
813.6	531.0	96

Table 44: Individual data for the rFVIIa ballistic testing.

Table 45 provides a summary of the averaged rFVIIa ballistic testing data for the valid impacts.

Number of valid impacts	17
Average impact velocity (m s^{-1})	775.8
+/- 95% on velocity (m s^{-1})	12.5
Average exit velocity (m s^{-1})	506.1
+/- 95% on velocity (m s^{-1})	8.5
Average tissue thickness (mm)	103.0
+/- 95% on tissue thickness (mm)	4.5
Average velocity loss / 100 mm (s^{-1})	262.6
+/- 95% on velocity loss (s^{-1})	9.2

Table 45: rFVIIa averaged ballistic test data

E.3 Additional energy loss comparisons

In order to differentiate the variability in the target response, to that introduced by using a mix of projectiles in Section 7.3, Figure 165 and Figure 166 show the data for energy loss in 100 mm targets for individual or very similar projectiles.

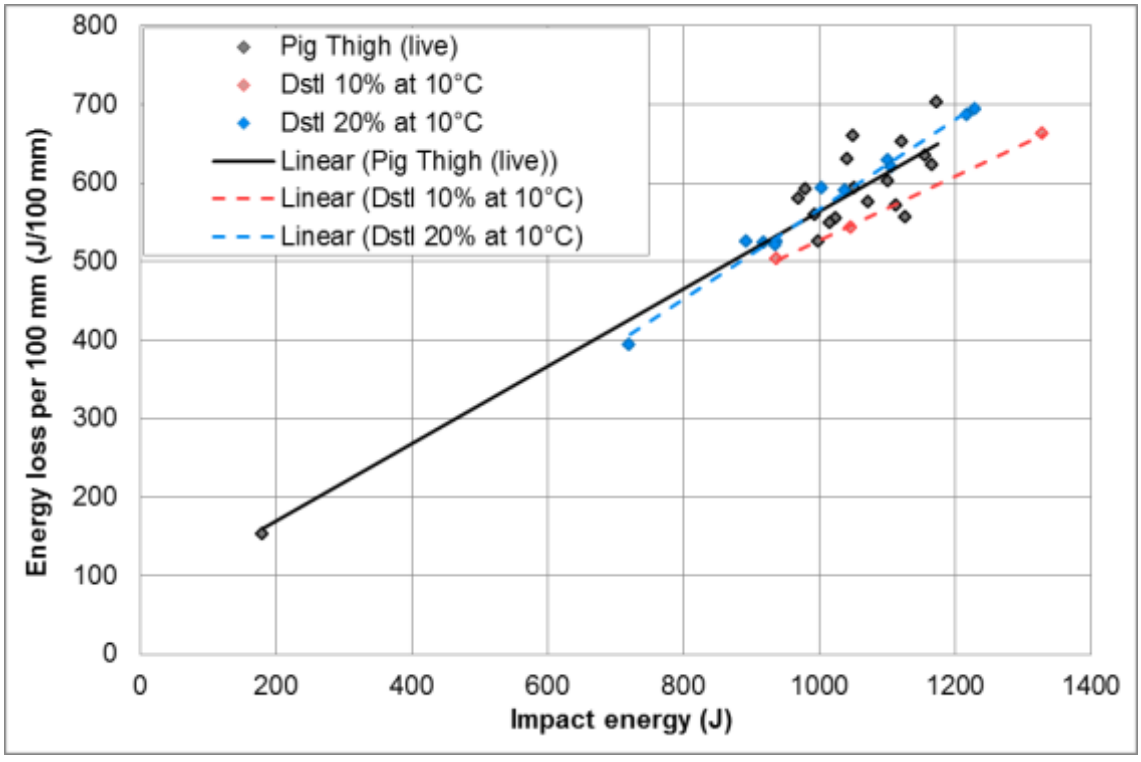

Figure 165: Energy loss per 100 mm in live pig thighs and Dstl 20% gelatin at 10°C for 9.525 mm steel spheres. Pig data from Reference [96]. Tissue simulant data is from original testing.

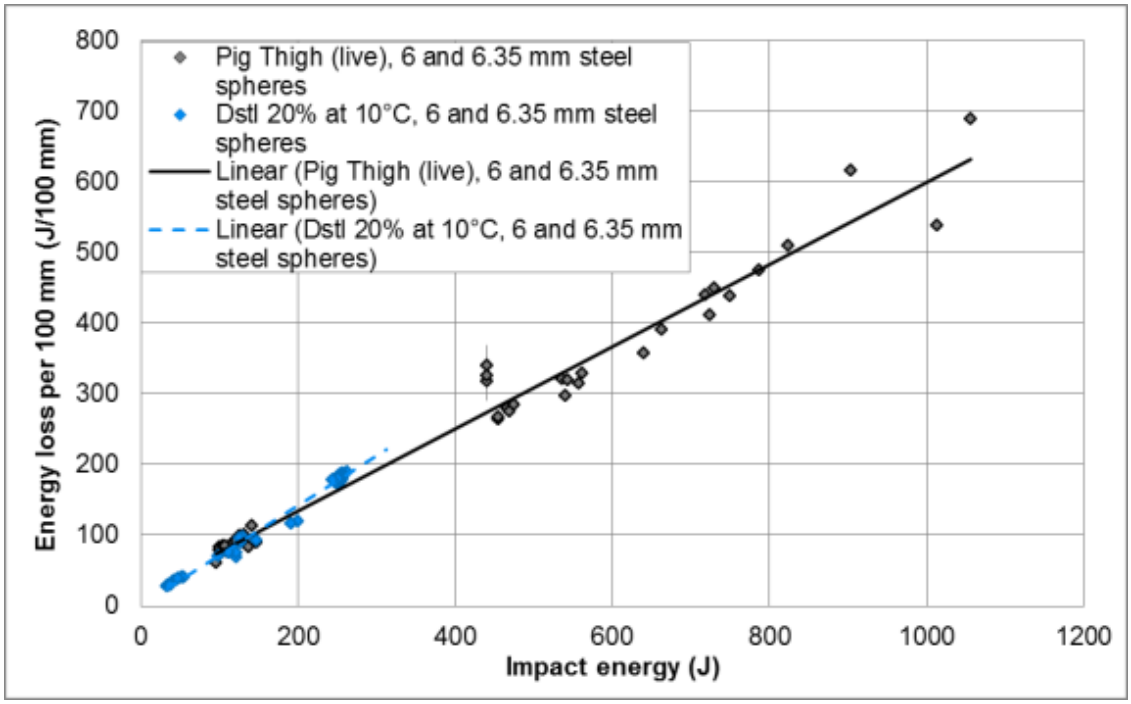

Figure 166: Energy loss per 100 mm in live pig thighs and Dstl 20% gelatin at 10°C for 6 mm and 6.35 mm steel spheres. Pig data from References [95; 113]. Tissue simulant data is from original testing.

Both Figure 165 and Figure 166 show that Dstl 20% gelatin at 10°C provides a much more repeatable target than live pig thighs, in terms of the energy loss in 100 mm thick targets, as well as supporting the suitability of Dstl 20% gelatin at 10°C as a muscle tissue simulant for these more specific data.

APPENDIX F Tabulated skin simulant V_{50} performance results

Skin simulant material	Thickness (mm)	Projectile	Probit V_{50} (m s^{-1})	+/- 95% CI (m s^{-1})
Neoprene	1.5	9 mm steel	112.4	10.5
		9 mm glass	166.2	9.5
		6 mm glass	185.4	6.3
		6 mm steel	124.1	5.8
Natural rubber	1.0	9 mm steel	101.5	7.0
		9 mm glass	149.7	7.5
		6 mm glass	167.6	12.8
Polyurethane	3.0	9 mm steel	143.5	3.0
		9 mm glass	196.0	3.5
		6 mm glass	208.6	6.8
Silicone, 50A	2.0	9 mm steel	119.4	10.7
		9 mm glass	159.0	2.1
		6 mm glass	182.3	2.1
Silicone, 80A	2.0	9 mm steel	104.7	3.8
		9 mm glass	153.0	7.0
		6 mm glass	170.4	7.3
Car inner tube	1.2	9 mm steel	89.8	3.4
		9 mm glass	147.4	6.5
		6 mm glass	170.2	2.7
		6 mm steel	105.6	9.9
		20 mm steel	71.2	2.9
Aircraft inner tube	1.5	9 mm steel	99.8	3.2
Synthetic chamois (dry), 2 layers	2.5	9 mm steel	68.5	4.5
		9 mm glass	115.0	9.0
		6 mm glass	145.1	8.3
		6 mm steel	81.0	3.2
		4.4 mm steel	96.9	n/a
		3 mm glass	263.0	12.1
		9 mm ceramic	87.6	2.1

Skin simulant material	Thickness (mm)	Projectile	Probit V_{50} (m s^{-1})	+/- 95% CI (m s^{-1})
		20 mm steel	52.3	5.1
Synthetic chamois (wet), 2 layers	2.5	9 mm steel	51.9	4.6
Real chamois in gelatin, 3 layers	1.5	9 mm steel	57.0	5.2
		9 mm glass	101.1	7.4
		6 mm glass	124.0	8.6
		6 mm steel	76.6	1.9
Real chamois dry, 3 layers	1.5	9 mm steel	110.6	18.8
RTV 428 rubber	2.0	9 mm steel	89.6	2.6
		9 mm glass	116.6	3.2
		6 mm glass	127.6	6.5
		20 mm steel	68.4	2.5

Table 46: Tabulated skin simulant V_{50} performance results.

APPENDIX G Cavity analysis method from HSV

G.1 Maximum temporary cavity size using a single HSV frame

MathShop EKE (V4.0.13) [214] software was used to manually track the cavity outline in gelatin for a given frame of HSV. This process is described below.

Initially the HSV is imported into the software and projectile impact conditions entered (camera frame rate, focal length of lens, distance from shot line, projectile mass, diameter and impact velocity if it could not be calculated from the HSV prior to impact with the block).

Scaling factors are then applied to the video to convert pixel co-ordinates into real world units. This was done from a separate calibration image taken with the same HSV settings at the beginning of each firing day, or whenever the HSV setup was changed. The calibration image consisted of a long rule positioned along the projectile shot line, such that measurements on the rule could be read, or markers at known separation distances on the rule used. The distance along the rule was divided by the pixel difference (in both x and y planes) to obtain the calibration factor (mm pixel^{-1}). The maximum identifiable separation along the rule was used in order to reduce measurement errors. An example of a typical HSV calibration image is given in Figure 167.

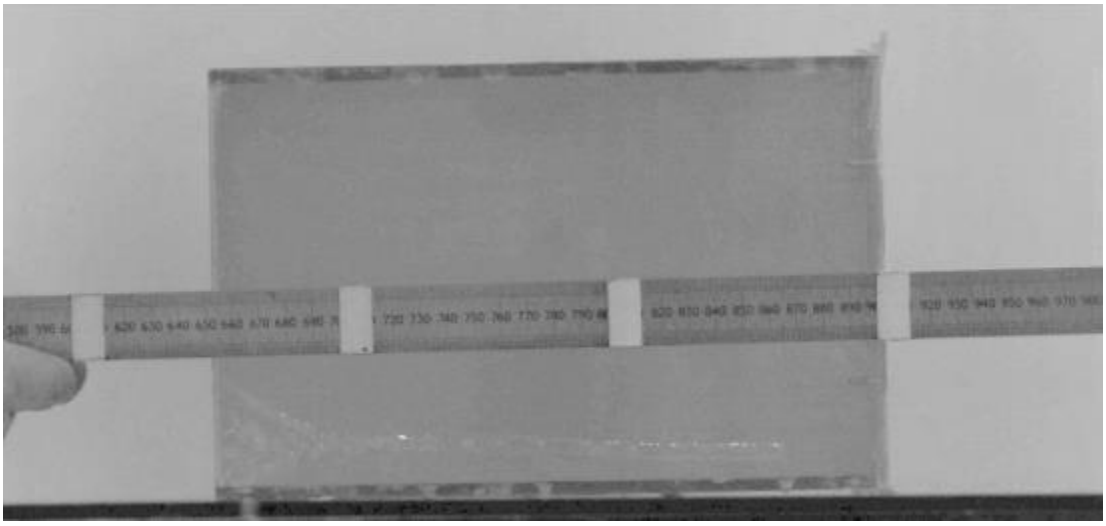

Figure 167: Example calibration image from the HSV of rule held along projectile shot line. Resolution was 1024x488 pixels. The gelatin block in the background has been moved back out of the way of the shot line for the calibration image.

After calibration, the distance of the front of the gelatin block from the reference plane and distance of the shot line from the reference plane were input. For all testing described in this thesis, the shot line was the same as the reference plane and the block was positioned such that the desired impact point was aligned with the centre of the block (distance of the front of the gelatin block from the reference plane was half the block width).

The impact face of the gelatin block was identified by selecting 2 pixels on the front face of the block. This line between those two points was used as the reference plane for penetration depth.

The position of the projectile in each frame (prior to impact and within the gelatin) was then manually tracked. This allowed the subsequent cavity radii to be calculated in relation to the projectile shot line (which is important for a later step).

The cavity outline was then manually traced by clicking points along the cavity outline in each frame of interest. The software joined the points by straight lines, to show the outline of the cavity selected. The user was responsible for choosing appropriate steps in penetration depth at which to place markers along the cavity outline. These could be at non-uniform step sizes such that particular regions of interest or sudden change could be more accurately measured. The cavity measurement was restricted to positive penetration depths (i.e. bounded by the impact reference plane). An example of the cavity outline tracing is shown in Figure 168.

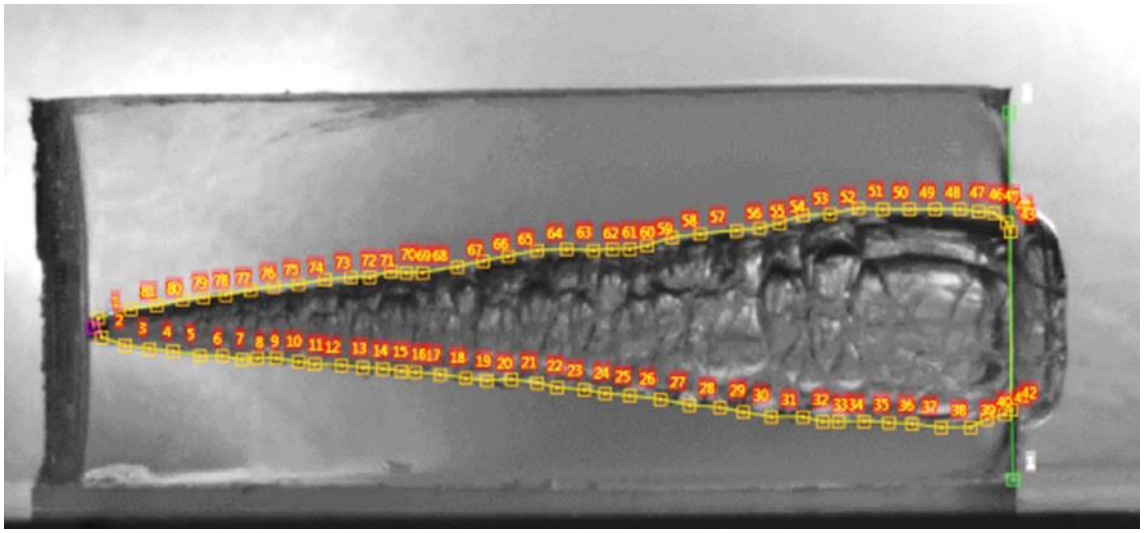

Figure 168: Example of cavity outline tracing from HSV in MathShop EKE software. Cavity outline points are yellow squares, connected by yellow lines. The green squares and connecting line show the reference impact plane. Firing direction is right to left.

The cavity outline tracing process could then be repeated on additional frames, as desired.

Once all cavity tracing was completed, the cavity was interpolated by the software by fitting ~2 mm wide trapezoids[211] to the cavity outline and could either be exported into Microsoft® Excel® or the volume could be calculated by rotating the trapezoids about the shot line. This enabled cavity volume calculations to account for instances where the shot line was not parallel to the x-axis or the shot line was divergent, whilst maintaining the correct cavity position relative to the block edges.

G.2 Maximum temporary cavity size using the entire HSV

Taking the maximum temporary cavity from a single frame of the HSV may not represent the full extent of the maximum temporary cavity of the projectile. It is less of an issue for non-deforming spheres, but is important for unstable

[211] Actual width depended on HSV resolution, calibration factor and zoom applied within the software.

(tumbling) projectiles or deforming projectiles. What is needed is the maximum temporary cavity over all time.

The software that was used to manually track the cavity outline [214] is man-power intensive as each frame requires analysis with additional post-processing to combine the output from multiple frames to generate the true maximum over all time.

Examples of instantanious temporary cavity outlines are shown for a sphere and typical military rifle bullet in Figure 169 and Figure 170 respectively.

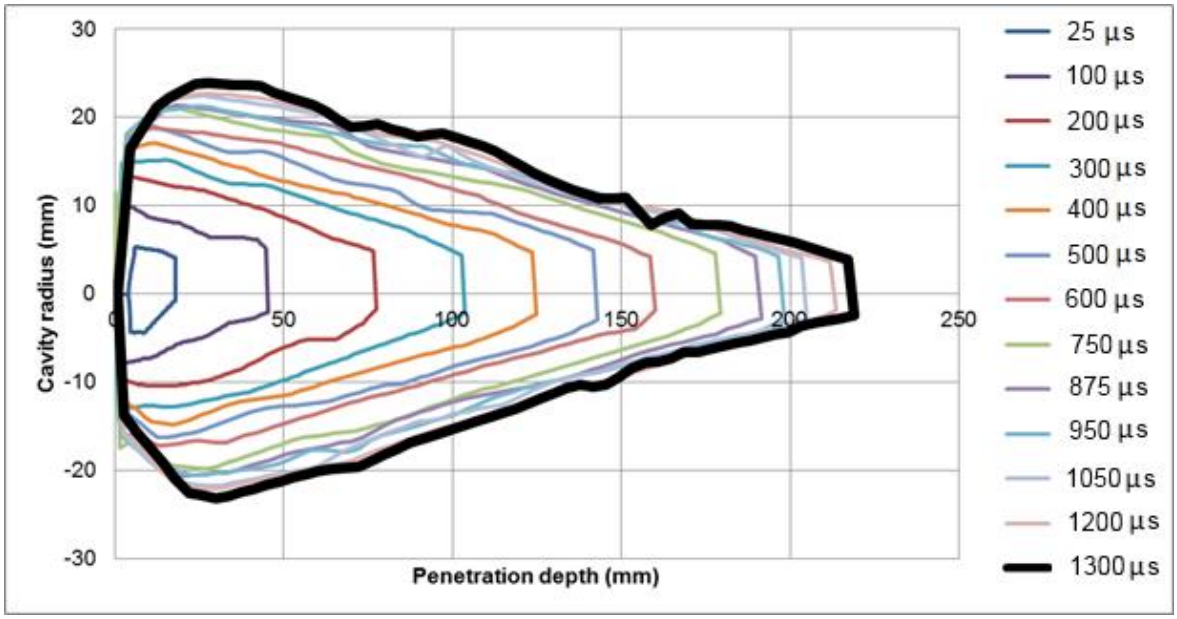

Figure 169: Example of the temporary cavity outline at various time intervals after impact up to the maximum (black outline) for a 6 mm steel sphere at 500 m s^{-1}. Firing direction is left to right.

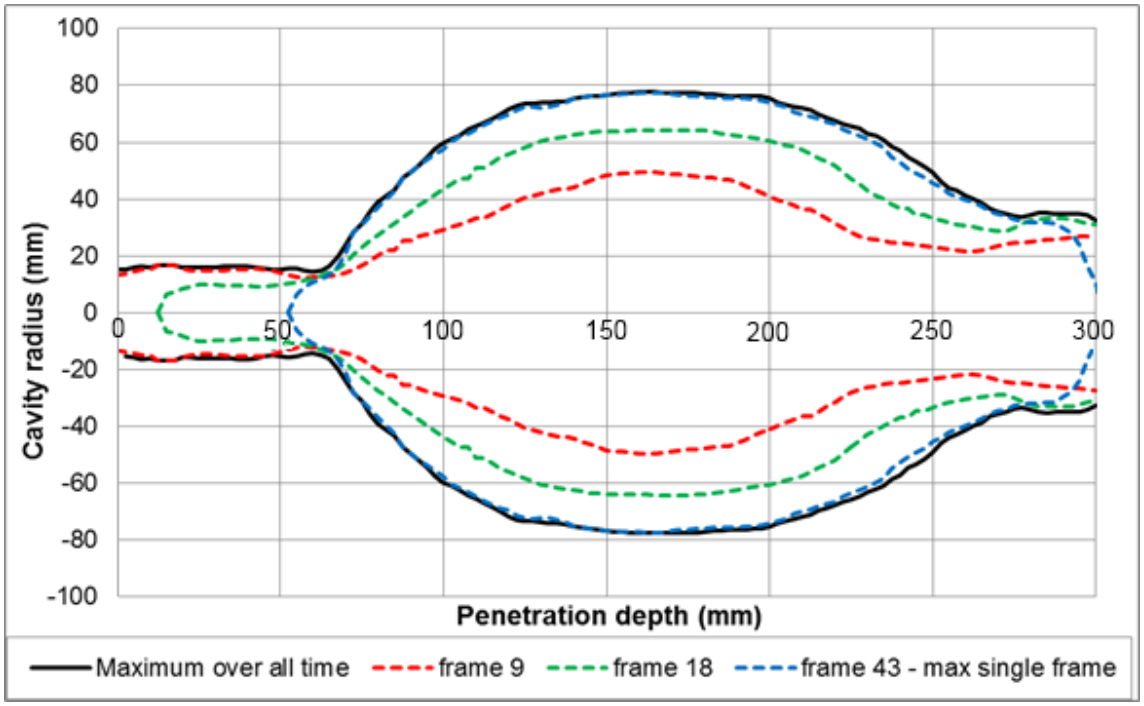

Figure 170: Example of the temporary cavity outline at 3 points in time and the maximum over all time for a typical military bullet[212]. Firing direction is left to right.

In order to analyse the maximum temporary cavity over all time, ImageJ [263] can be used to create a composite image from an (uncompressed) .avi file, or image series. This composite image can display the darkest pixel from the entire duration of the video for each pixel co-ordinate, outputting the maximum temporary cavity from all frames as the volume occupied by the cavity is darker[213,214]. This single image can then be used (with the existing cavity analysis software [214]) to extract the co-ordinates of the temporary cavity. Due to the way the software works, the 2D cavity outline is rotated around the shot line to calculate the size of the 3D cavity. In order for the software to know the location of the shot line, additional points are required to be selected over multiple frames to calculate a shot line. The extra composite cavity image can either be added as an extra frame at the beginning or end of the video file, and projectile tracking

[212] All frames were analysed and used to calculate the maximum cavity over all time. The 3 instantaneous cavities shown can be used to approximate the maximum cavity in this example.
[213] This used the image / stacks / z projection / min intensity function in ImageJ [263].
[214] The contrast of the composite image will be dependent on the original HSV, which can be adjusted prior to processing.

performed as normal on the standard frames; or, multiple copies of the composite cavity image can be saved into one .avi file and selected projectile positions chosen in subsequent copies to replicate the shot line (time and velocity information will be lost).

Examples of the composite cavity images for a sphere and typical military rifle bullet are given in Figure 171 and Figure 172.

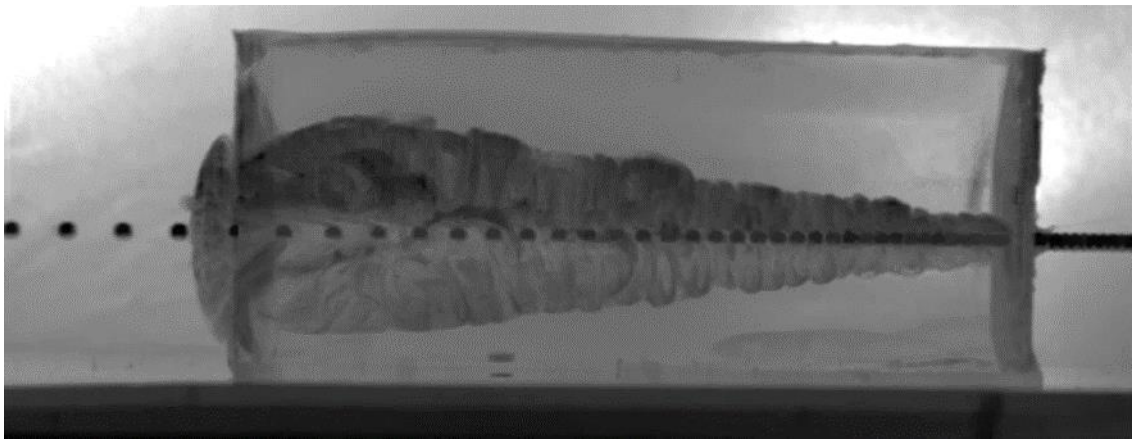

Figure 171: Composite cavity image for 6 mm steel sphere penetration into gelatin. Firing direction is left to right.

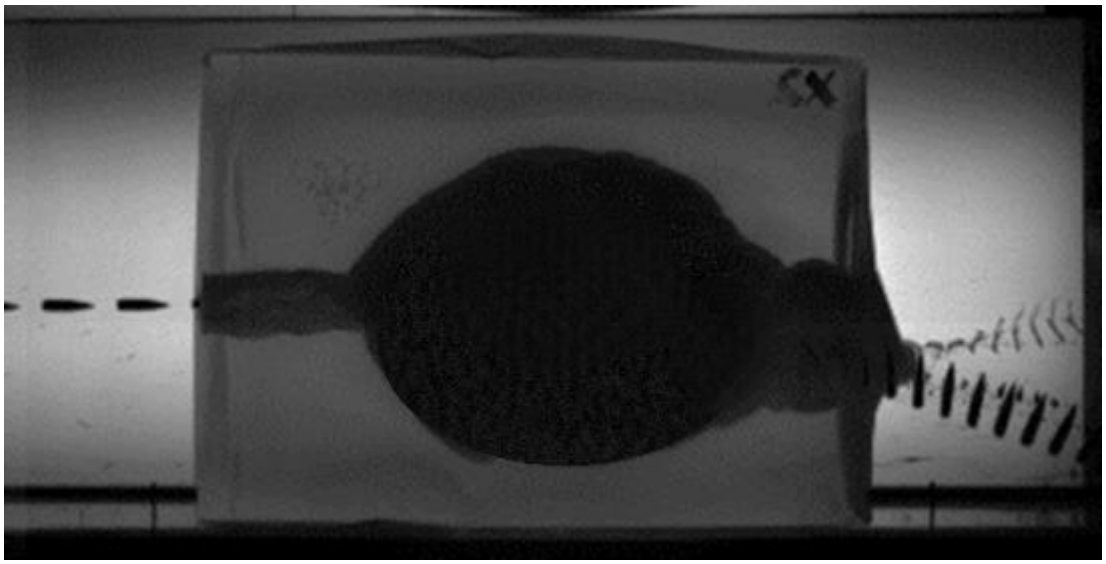

Figure 172: Composite cavity images for a typical military bullet penetrating gelatin. Firing direction is left to right.

All the temporary volume calculations performed within this thesis were using the MTC over all time method, even though it may not produce a significant difference for sphere impacts. It ensures consistency and that the methods used are applicable to other projectiles without prior assumptions on their performance.

APPENDIX H DoP equations – predictions compared to experimental data

H.1 Permanent DoP predictions

Each equation from Table 31 that was implemented was compared to the Dstl 20% gelatin at 10°C permanent DoP experimental data to determine how well the model fit. Individual graphs showing the predicted against experimental measured DoP for each equation are given in this Appendix.

Only experimental data from the 'valid' application range for each equation is shown (all data in this section is for permanent DoP and DoP>0), therefore different equations are compared against different parts of the same dataset. All equations account for different projectile diameters. The ability of each equation to predict DoP for different geometry or density projectiles is detailed in Table 31 and given in the caption for each figure below.

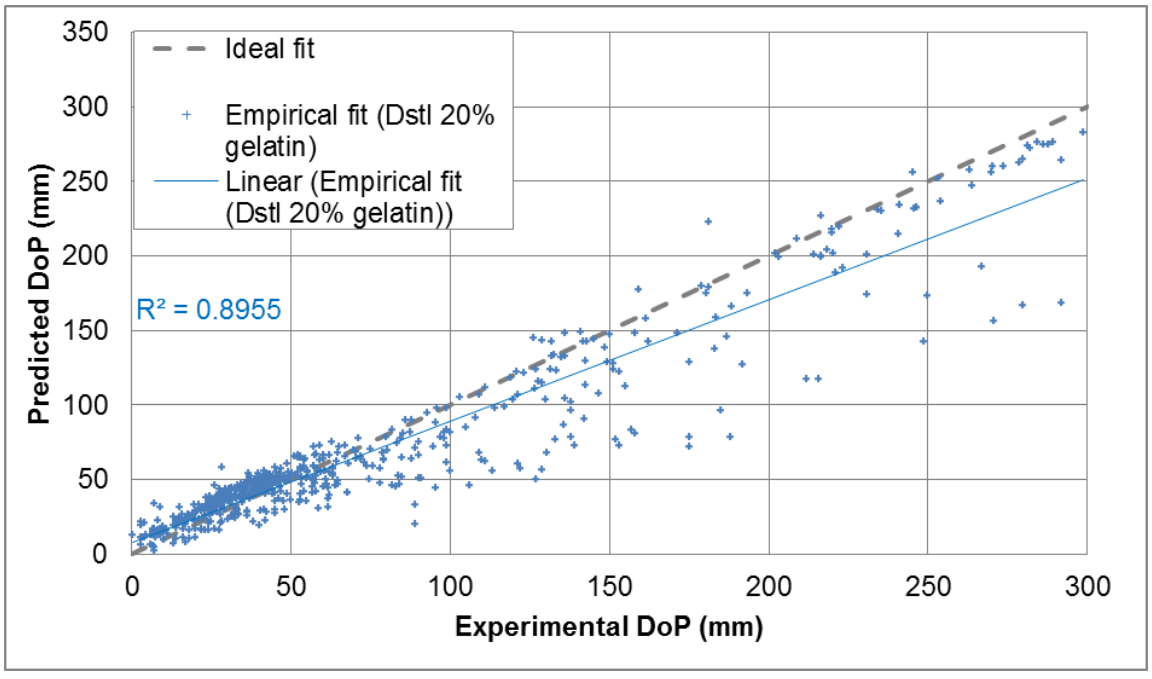

Figure 173: Predicted versus experimental measured permanent DoP in Dstl 20% gelatin at 10°C for the Dstl 20% at 10°C empirical fit equation, Equation 16. n=640 data points for different geometry and density projectiles.

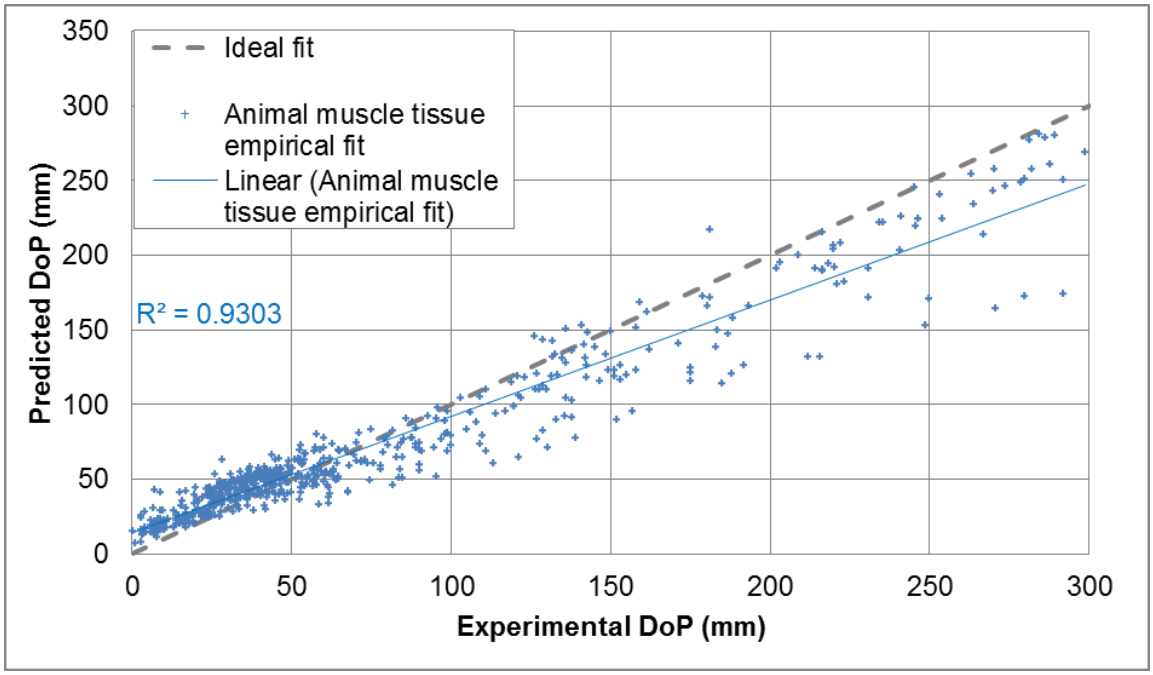

Figure 174: Predicted versus experimental measured permanent DoP in Dstl 20% gelatin at 10°C for the Animal muscle tissue empirical fit equation (Equation 12). n=640 data points for different geometry and density projectiles.

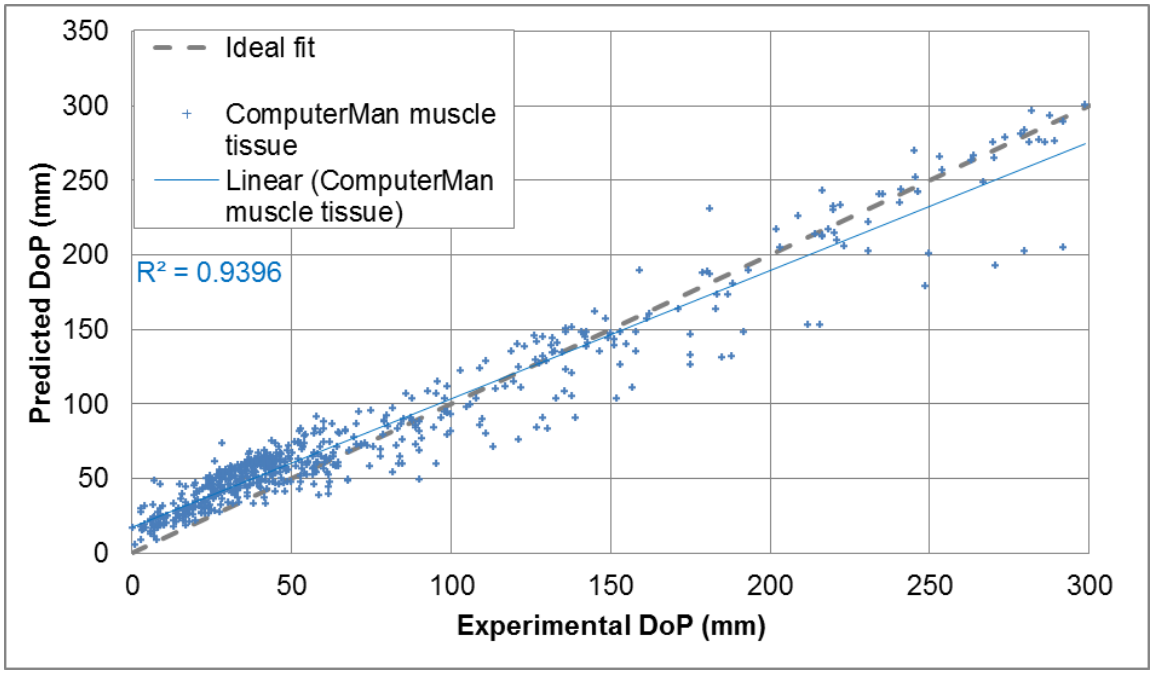

Figure 175: Predicted versus experimental measured permanent DoP in Dstl 20% gelatin at 10°C for the ComputerMan muscle tissue empirical fit equation (Equation 13) [42]. n=640 data points for different geometry and density projectiles.

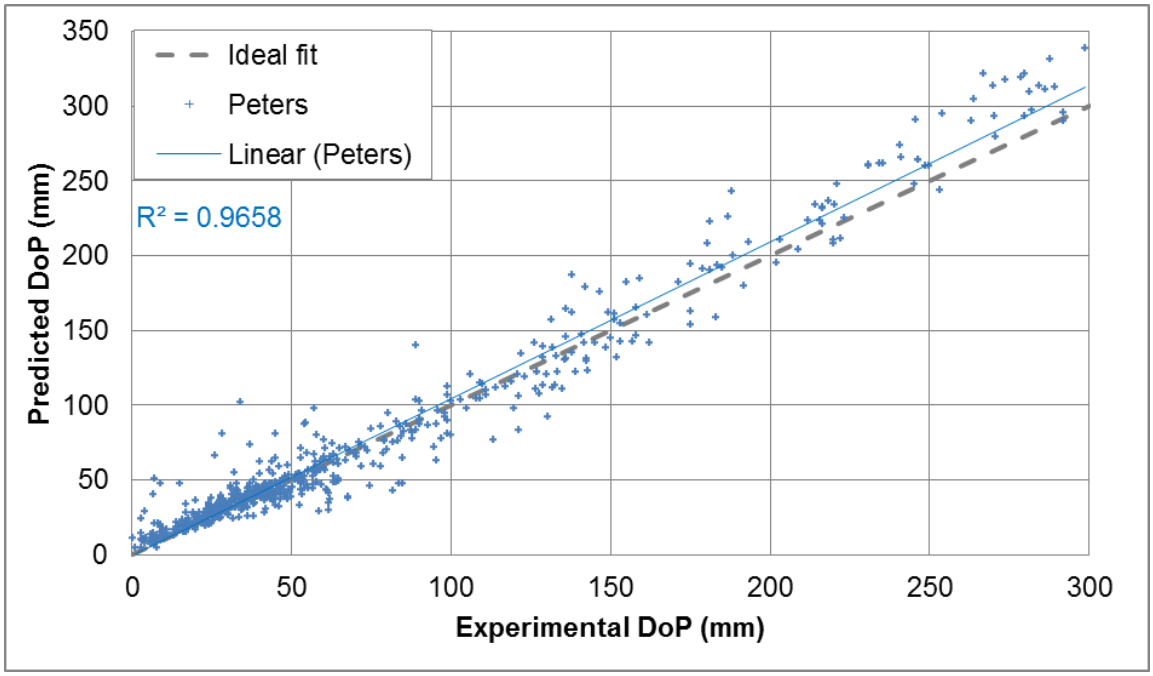

Figure 176: Predicted versus experimental measured permanent DoP in Dstl 20% gelatin at 10°C for the Peters equation [252]. n=640 data points for different geometry and density projectiles.

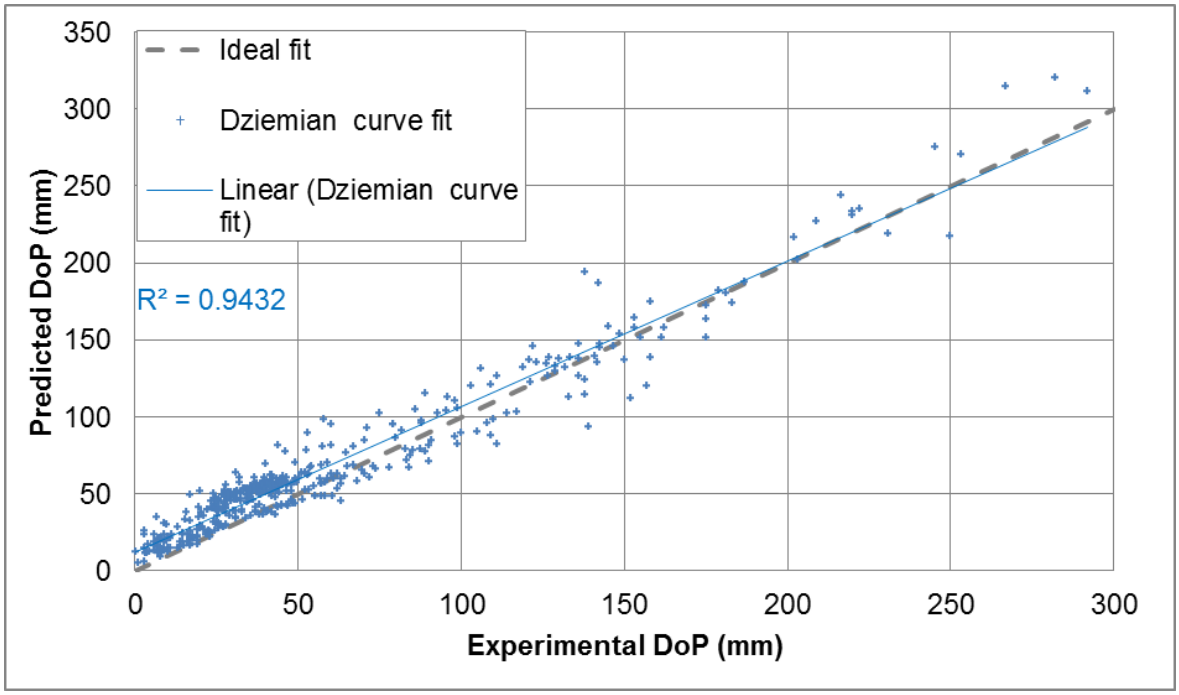

Figure 177: Predicted versus experimental measured permanent DoP in Dstl 20% gelatin at 10°C for the curve fit to Dziemian equation [161]. n=471 data points for different density spheres.

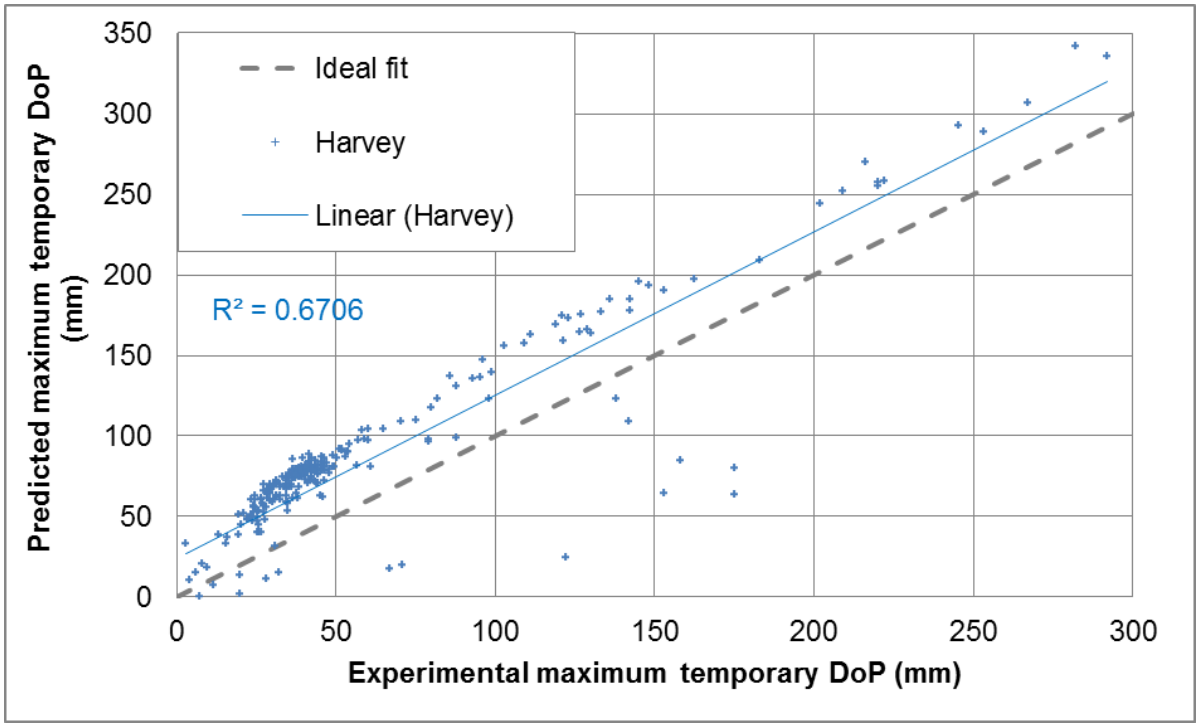

Figure 178: Predicted versus experimental measured permanent DoP in Dstl 20% gelatin at 10°C for the Harvey equation [116]. n=279 data points for steel spheres.

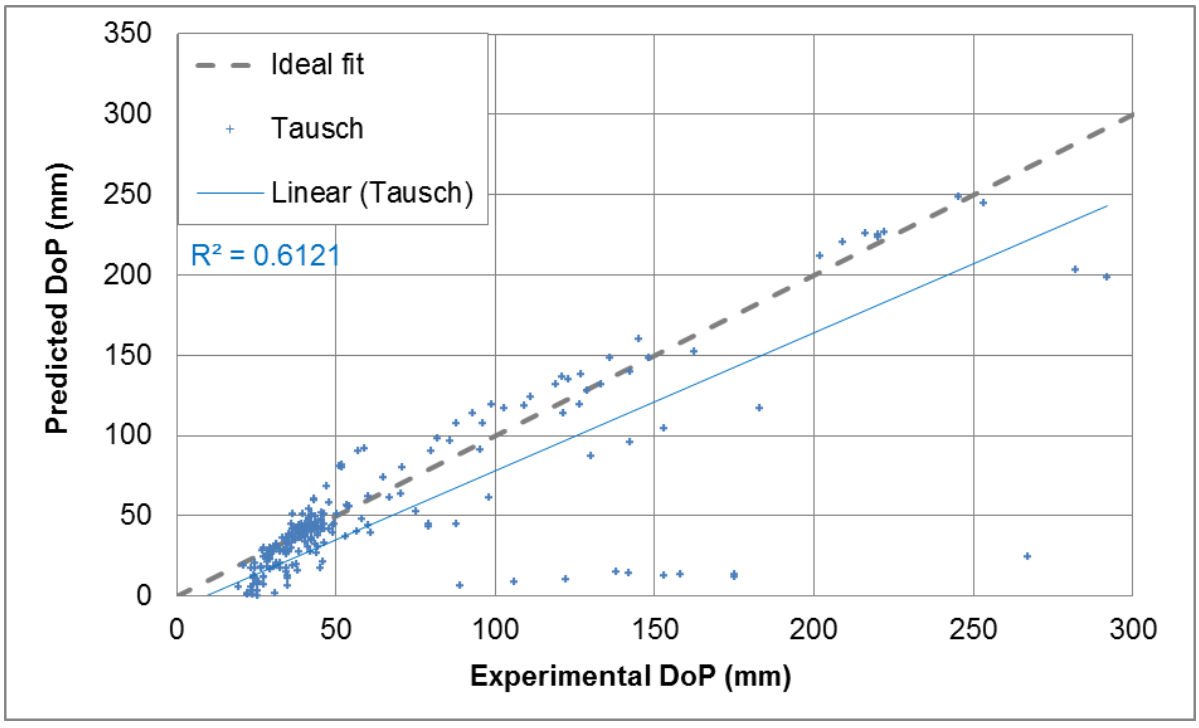

Figure 179: Predicted versus experimental measured permanent DoP in Dstl 20% gelatin at 10°C for the Tausch equation [71]. n=279 data points for steel spheres.

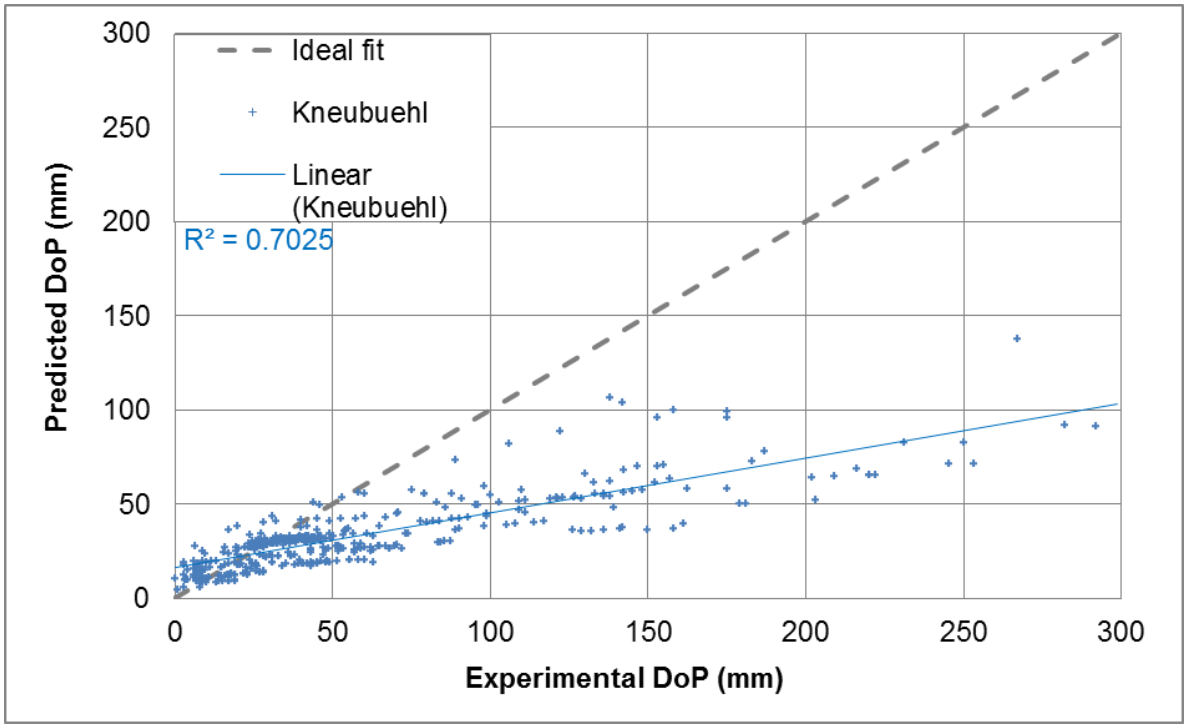

Figure 180: Predicted versus experimental measured permanent DoP in Dstl 20% gelatin at 10°C for the Kneubuehl equation [69]. n=471 data points for different density spheres.

Note that the Kneubuehl equation [69] could not be properly verified and therefore this representation of the equation should be treated with caution.

H.2 Maximum temporary DoP predictions

Some of the equations in Table 31 provide predictions of the maximum temporary DoP, rather than the permanent DoP as shown in APPENDIX H, Section H.1. The equations that are stated to predict the maximum temporary DoP are shown below (for the valid projectile range) to compare the Dstl 20% gelatin at 10°C experimental data to determine how well the model fit. Where the maximum temporary DoP was not measured experimentally, it was estimated using Equation 19.

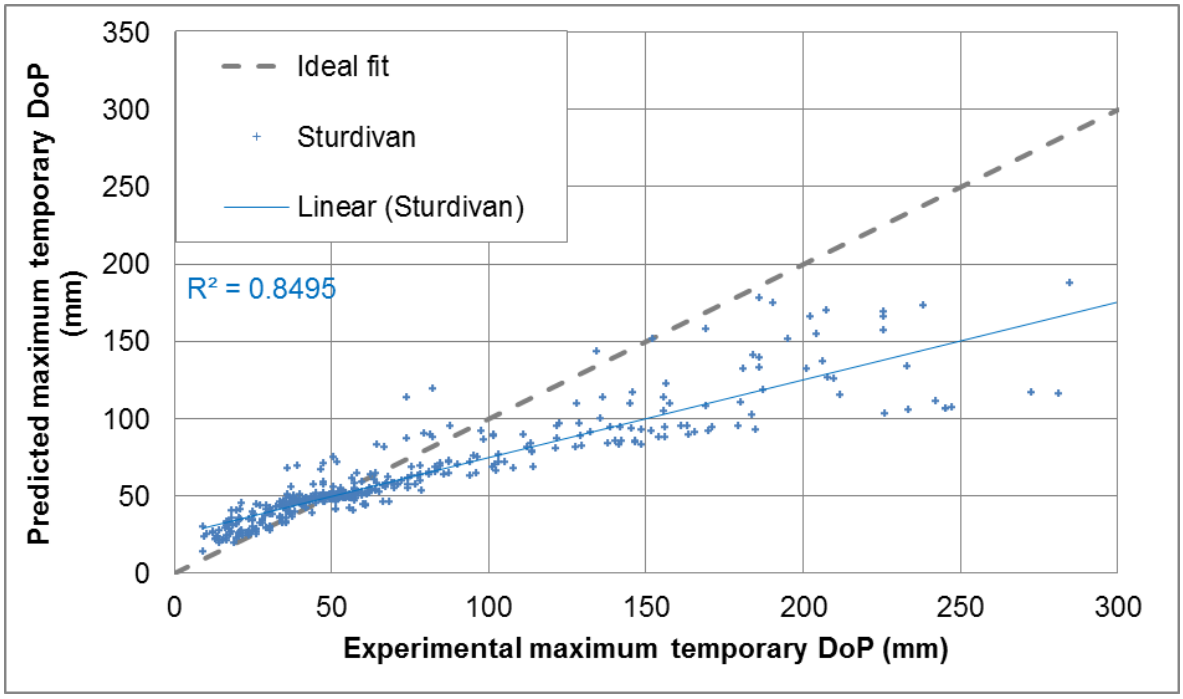

Figure 181: Predicted versus experimental maximum temporary DoP in Dstl 20% gelatin at 10°C for the Sturdivan equation [255]. n=640 data points for different geometry and density projectiles.

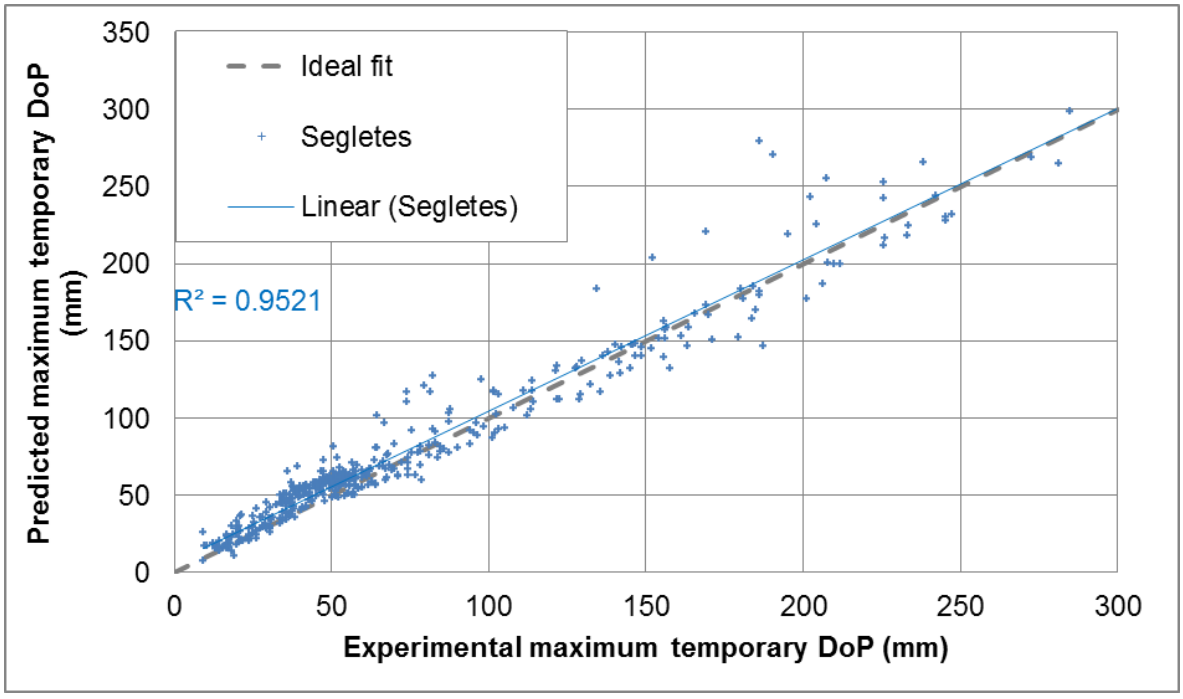

Figure 182: Predicted versus experimental maximum temporary DoP in Dstl 20% gelatin at 10°C for the Segletes equation [200] (corrected). n=471 data points for different density spheres.

APPENDIX I Retardation equations, additional validation

I.1 Block size/edge effects and projectile retardation

The NATO gelatin standard [130] specifies a particular size block to use for testing. Other mix methodologies allow the user to decide on the block size.

Reference [220] conducted testing to investigate the effect gelatin confinement on the retardation of the projectile. "*Gelatin in cylinders and unconfined cylinders was shot with APM2 bullets* [at ~2800 ft/sec] *and 1/4-inch steel spheres between 2400 and 2500 ft/sec.…there is no significant difference, by t test (p > 0. 05), between the confined cylinders and the controls with respect to the amount of energy absorbed.*" [220]

Original testing (described in Section 7.5) was conducted using 6 mm steel spheres at a nominal 750 m s^{-1} impact velocity into Dstl 20% gelatin at 10°C using different lateral sized gelatin blocks. The blocks were all 250 mm in length, but had different lateral dimensions, ranging from 50 mm by 50 mm to 150 mm by 150 mm. Some of the blocks were additionally confined within 4 mm polycarbonate square section tubes. The polycarbonate tubes constraining the gelatin broke during firing, so it was not a rigid edge constraint.

The retardation of the projectile was measured using Tracker software [213] with HSV at 25 µs intervals. The measured remaining velocity (in two orthogonal planes for each shot) for the 8 target configurations, 32 total shots, is shown in Figure 183.

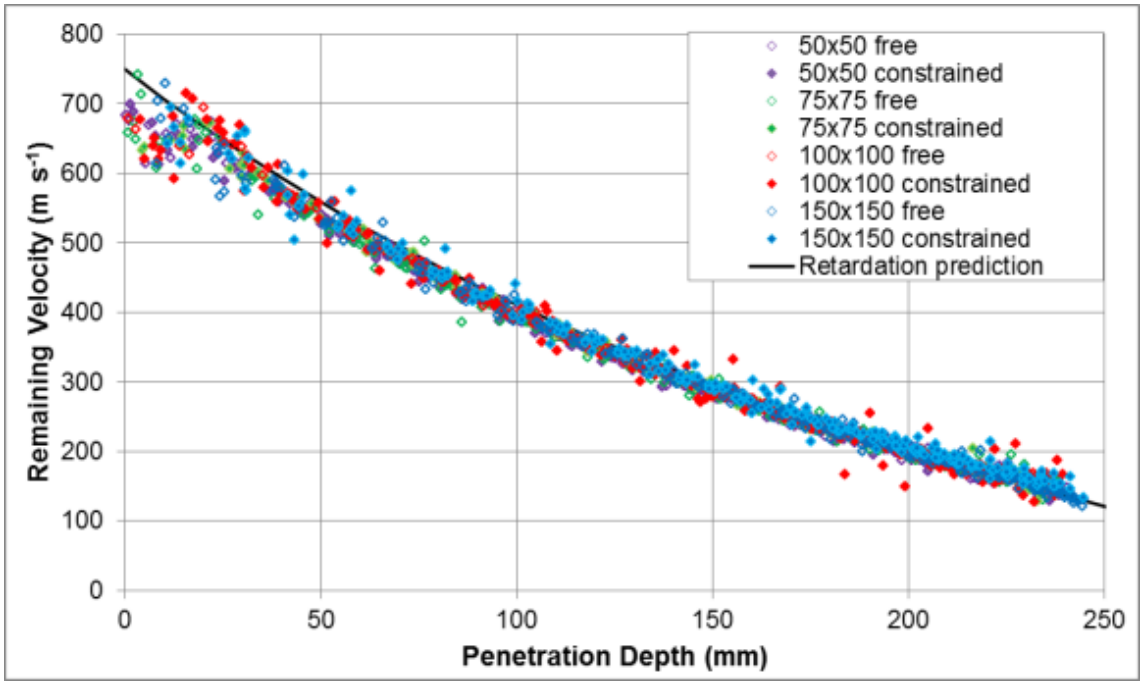

Figure 183: Retardation of 6 mm steel sphere at nominal 750 m s^{-1} impact velocity in Dstl 20% gelatin at 10°C for different lateral block dimensions and constraint (8 target configurations, 32 shots, 1911 data points), compared to the prediction (Equation 20).

Figure 183 shows that there is no difference in the measured remaining velocity when the lateral dimension or constraint of the gelatin block size is altered, even as low as 50 mm by 50 mm for a high velocity 6 mm steel sphere.

Scatter in the experimental data is due to errors in tracking of the projectile in each frame of the HSV. This included at small penetration depths due to difficulties tracking the projectile as it first penetrates into the gelatin on the HSV and one shot to the 100x100 mm target where the view of the projectile was partially obscured at larger penetration depths by the constraining mold. Automated tracking was employed to minimise user error in this respect (and gave demonstrably more consistent outcomes).

Figure 183 also shows that (with an average impact velocity of 748.5 m s^{-1}) Equation 20 provides a very good prediction of the projectile retardation. The average difference between the experimental data and prediction (ignoring the first 10 mm penetration depth due to difficulty accurately locating projectile

position in the HSV) was -1.4% of the experimental remaining velocity. Equation 20 predicted a higher velocity by an average of 1.4% (6.4 m s^{-1}) compared to the experimental data at equivalent depths. 95% of the predicted velocities were within an offset of -3.9% to +1.1% to the experimental data across the entire velocity range.

I.2 1 mm sphere impacts

Analysis of 1 mm steel sphere impacts were based on the setup as described in Section 7.3.2, using the top camera view (at 80,000 frames per second).

Projectile tracking was done by manually selecting the projectile location in each frame of the HSV (Tracker [213]). The x-y pixel locations were then converted into their position relative to the impact face of the gelatin block. The penetration depth was calculated to account for travel in the x and y plane (but not z plane, towards or away from the camera). Due to the scatter in the raw experimental data, these were converted into a 2 period moving average.

A large degree of scatter was seen in the tracked data within the gelatin. This is due to the small size of the spheres and difficulties visualising them accurately on the HSV through approximately 75 mm of gelatin, coupled with the relatively large pixel size in comparison to the projectile diameter (1 pixel = 0.68 mm for this activity due to using the existing camera setup as detailed in Section 7.3.2).

In order to compare all the 1 mm sphere penetrations against the FREM prediction (Equation 20), the data for each impact was normalised: the residual velocity was divided by the strike velocity and the transient DoP divided by the maximum temporary DoP. This was done for all 24 impacts and results are shown in Figure 184.

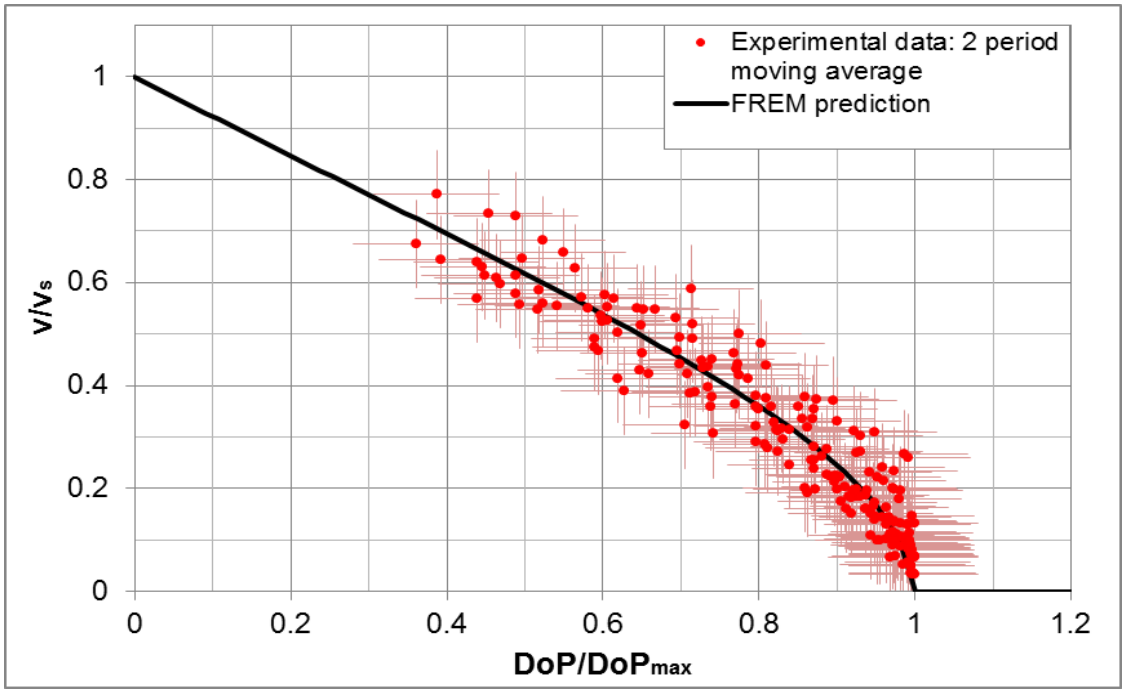

Figure 184: Retardation of 1 mm steel spheres in Dstl 20% gelatin at 10°C showing measured data (2 point moving average) compared to the prediction Equation 20.

Although the experimental data in Figure 184.shows a large degree of scatter, the FREM gives a reliable prediction of the remaining projectile velocity at a given penetration depth. Figure 184 shows that Equation 20 describes the average projectile response and there was no trend in the residual data (difference between the experimental measured and predicted normalised velocities). It should be noted that all these impacts were over a relatively narrow impact velocity range (325 ± 25 m s^{-1}).

I.3 Cylinder impacts

Four impacts with a 4.06 mm steel cylinder (0.49 g) [210] with velocities ranging between 181 m s^{-1} and 416 m s^{-1} into Dstl 20% gelatin at 10°C are shown in Figure 185 in comparison to the retardation prediction using the FREM given by Equation 20 (experimental data was measured using manual tracking of the projectile in the HSV at 10,000 frames per second).

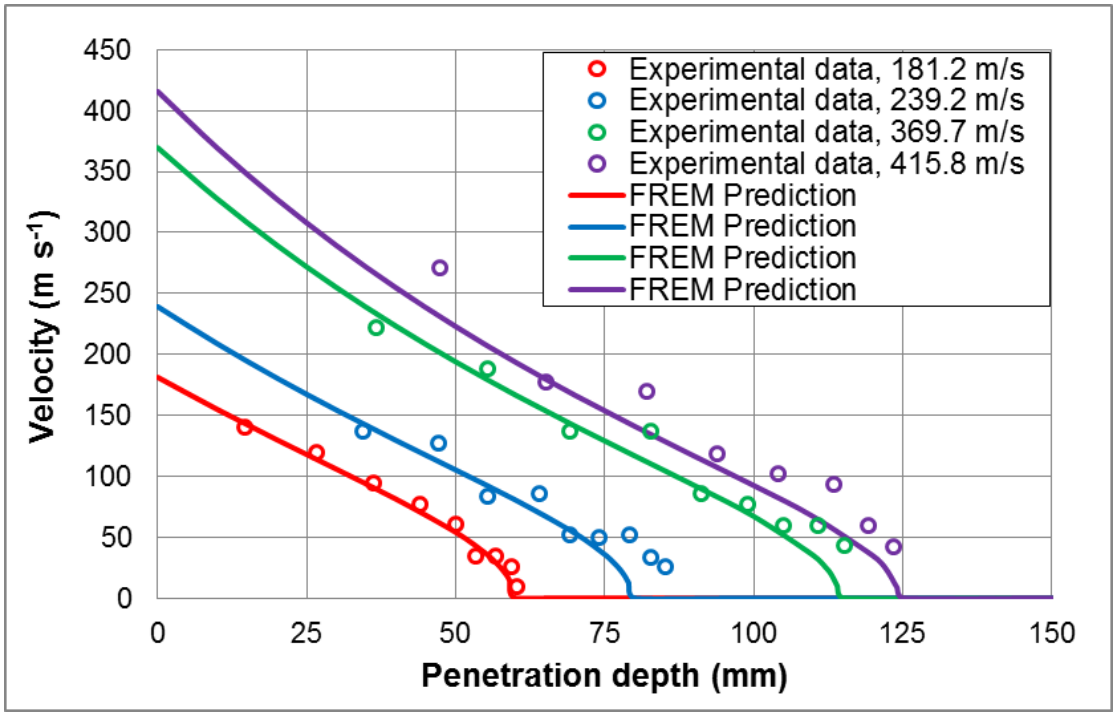

Figure 185: Retardation of 4 mm (0.49 g) steel cylinders in Dstl 20% gelatin at 10°C showing measured data compared to the prediction at 4 impact velocities.

Figure 185 shows a reasonable fit of the FREM prediction to the experimental data. In general, the FREM can be seen to slightly under-predict the remaining velocity, particularly when the projectile nears the end of the penetration process.

Firings conducted with CN cylinders (Table 23) did not have calibrated HSV and/or HSV of sufficient quality to allow projectile tracking to be related back to real world measurements.

I.4 Cube impacts

Two impacts with 5 mm steel cubes were conducted at 527.5 m s^{-1} and 719.9 m s^{-1}, with the setup as described in Section 7.3.2.

For analysis of the cube retardation and comparison to the retardation model, the following inputs were used:

- The cross sectional area of the projectile, A, was taken as the area of one cube face (0.25 cm^2).
- A single C_D value was used, C_D=0.74, the average for a randomly oriented cube in 20% gelatin at 10°C (Table 32).

Projectile tracking was performed as described for the 1 mm spheres, apart from the software was allowed to automatically track the projectile position within each frame.

From analysis the HSV, each of the cubes impacted face-on, then rotated to approximately corner-on orientation near the end of the penetration.

Figure 186 shows the projectiles' remaining velocity against penetration depth for the two experimental impacts and the corresponding model predictions (Equation 20). Whilst the model can be seen to slightly over-estimate the remaining velocity (which is more pronounced for the higher impact velocity in red), the prediction is within a factor of ±0.05 times the strike velocity, V_s (i.e. ± 5%V_s).

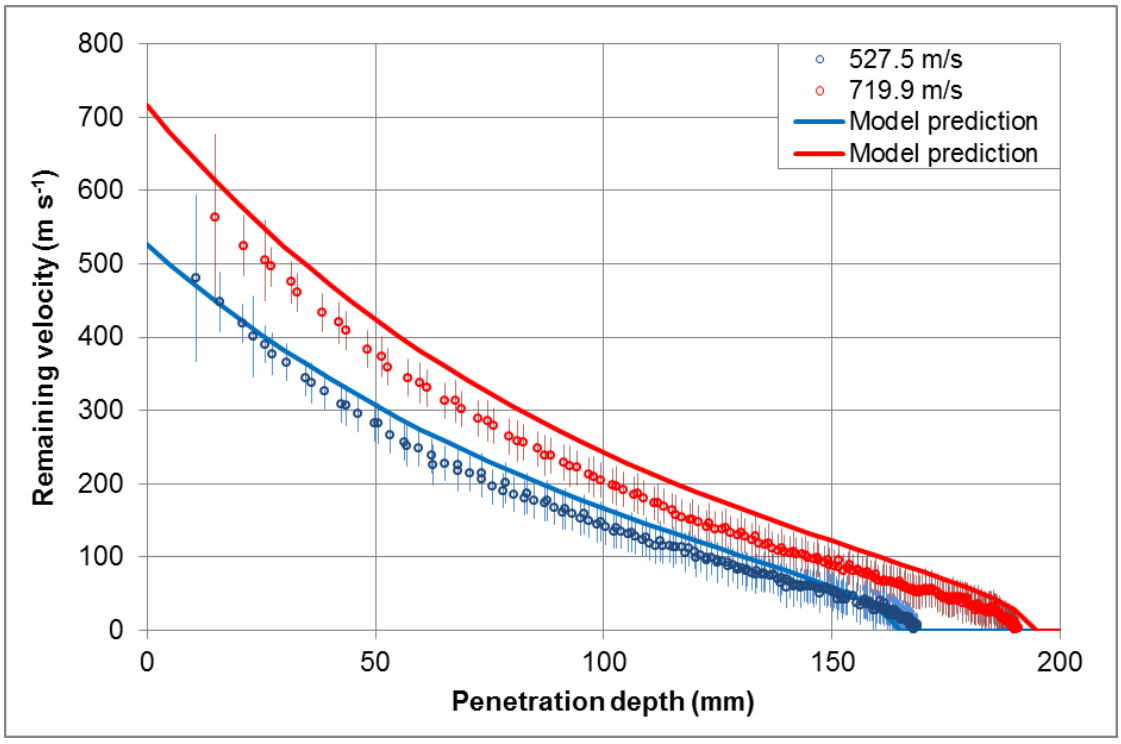

Figure 186: Retardation of 5 mm steel cubes in Dstl 20% gelatin at 10°C showing measured data compared to the prediction.

Reference [298] states that "*For any shape composed of non-concave surfaces (where every surface element can 'see' a full 2π sterradians of space, then the average projected area of the shape is a quarter of the total surface area*".

$$A_{av} = \frac{A_S}{4}$$

Equation 44: Average projected area of a shape composed of non-concave surfaces [298]

Where:

A_{av} is the average projected area

A_S is the total surface area

Using the value of A_{av} in place of the area of one cube face (denoted by A), the model predictions are less accurate, as shown in Figure 187.

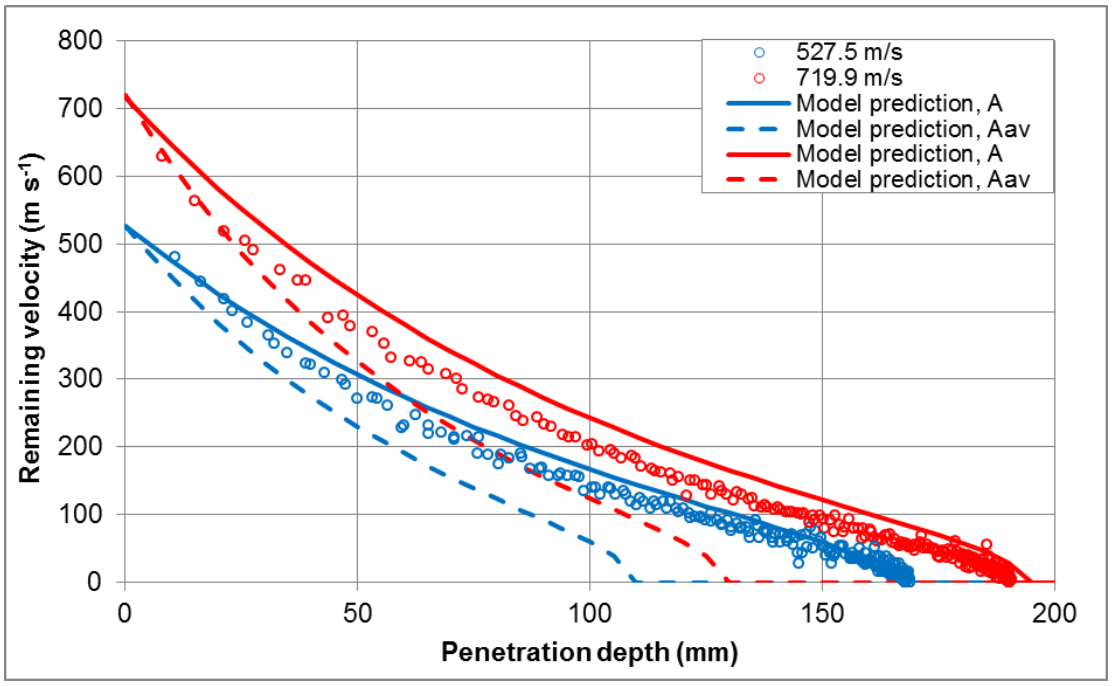

Figure 187: Remaining velocity for 5 mm steel cubes with penetration depth in 20% gelatin at 10°C. Predictions using Equation 20 are shown as solid and dashed lines using two different values for the cross sectional area.

Whilst only 2 experimental cases have been used to validate the FREM for cubes, both with flat face impacts, it gives an indication of its accuracy to cube geometry projectiles using a single average value for C_D and A as the area of one cube face. The fit of the model to the experimental cube data may be improved by refinement of the drag coefficient value. Additionally, but of less practical value,

a more detailed analysis of the HSV to determine cube orientation with depth could be used to fit a variable C_D and A function.

APPENDIX J Neoprene foam material properties

Property	Test standard	Value
Colour		Black
Cellular Structure		Closed
Density		150 – 170 kg m^{-3}
Shore hardness		38-55 sh 00
Compression Deflection according to	ASTM D1056	35-63 kPa
	NFR 99211	80-160 kPa
Water Absorption	ASTM D 1056	≤ 5%
Linear Shrinkage after 7 days at 70°C		< 7 %
Ultimate Elongation	DIN 53571	> 100 %
Tensile Strength	DIN 53571	> 500 kPa
Tear Resistance	NFR 99211-80	> 0.5 kN m^{-1}
Ozone Resistance		No cracking
Corrosive effect on copper / silver		Non corrosive
Paint staining		Staining

Table 47: Neoprene foam material properties for MDFPIM.

APPENDIX K MDFPIM analysis and example injury prediction process

K.1 MDFPIM analysis process

K.1.1 Introduction to MDFPIM analysis process

When the MDFPIM V2.0 (or V2.1, V2.2) are used to assess a threat in a ballistic or blast scenario, several different outputs are possible. This Section describes how to analyse data from each MDFPIM V2.0 deployed in a trial.

K.1.2 Recommended MDFPIM analysis

The recommended analysis route is by physical recovery of fragments:

- For assessment of corneal abrasion risk, identification of any debris adhering to the sticky polyester film indicates the potential for a corneal abrasion injury.
- For assessment of eye penetration risk, count the number of perforations to layer 1 (a or b) of the MDFPIM V2.0. The way the MDFPIM V2.0 has been developed means perforation to layer 1 indicates a (50%) risk of eye penetration, independent of projectile mass, density, diameter and geometry.
    - The number of perforations per unit area to layer 1 can be scaled from the pack area to the presented area of the eye to estimate the risk of an injurious projectile hitting the eye. This is only valid at the location where the MDFPIM V2.0 was deployed during the test.
- For assessment of skin perforation risk, count the number of perforations to layer 2 of the MDFPIM V2.0. The way the MDFPIM V2.0 has been developed means perforation to layer 2 indicates a (50%) risk of skin perforation, independent of projectile mass, density, diameter and geometry.
    - The number of perforations per unit area to layer 2 can be scaled from the pack area to the presented area of a person to estimate the worst case risk (assuming no clothing) of an injurious projectile hitting the body. This is only valid at the location where the MDFPIM V2.0 was deployed during the test.

- For projectile impact velocity estimates: Dismantle the pack, starting from the front layer. For every hole in the polythene sheeting, locate the corresponding hole or fragment in the underlying foam layer.
    - Once a fragment is located, recover it, weigh it and recorded the maximum layer it perforated.
    - Track through holes into deeper layers of the pack, progressing one layer at a time until all fragments have been accounted for. It may be beneficial to record fragment co-ordinates in terms of their impact location on the pack. The need for this will be dependent on the type of output required from the model (see Section K.2 for context on fragment impact co-ordinate recording).
    - For each fragment, the impact velocity can be predicted (Equation 39 or Equation 41).
    - Each impact velocity that is predicted can be bounded by the predicted impact velocity for the layer before and after ($L_{n\pm1}$).

Equation 41 discounts the need to consider fragment shape. However, estimates using Equation 41 may under-predict the impact velocity if the fragments have high length: diameter ratios and impact end on, or over-predict the impact velocity if the fragments are irregular or have high length: diameter ratios and impact flat face on.

K.1.3 Alternative MDFPIM analysis

An alternative analysis method if there are very large numbers of fragment impacts and/or the mass of the impacting fragments is known without having to physically recover each individually; image analysis can be used to identify and characterise the holes in the polythene witness sheet for each layer. The image analysis process is described in detail in APPENDIX L.

To summarise the image analysis method:

- A scaled photograph of the polythene sheet is taken where any perforations can be easily differentiated in terms of the pixel intensity.
- This is repeated for each layer of the MDFPIM perforated.

- Image processing software can then be used to count the number of perforations, as well as measure the average diameter and x-y impact co-ordinates.
- The data for perforations in the shallower layers need to be discounted so that only the data for the maximum perforation for each fragment remain. The x-y impact co-ordinates (in addition to the measured diameter) can be used to locate the corresponding hole in a different layer.
- The density of the fragment related to each hole needs to be estimated from knowledge of the threat and scenario. This along with the measured average diameter from the image analysis and the corresponding maximum layer perorated can be used as inputs to Equation 41.
- As for the physical fragment recovery method, each impact velocity that is predicted using Equation 41 can be bounded by the predicted impact velocity for the layer before and after ($L_{n\pm1}$).

K.1.4 Example of MDFPIM V2.0 analysis

A hypothetical example to show the analysis process for physical fragment recovery from the MDFPIM V2.0 is given below:

Assume that following testing, the MDFPIM V2.0 is deconstructed and the fragments listed in Table 48 are found:

Fragment mass (g)	Maximum layer perforated	Fragment material	Assumed density (g cm^{-3})
0.15	2	Steel	7.85
0.23	4	Plastic	0.95
0.28	4	Steel	7.85
0.05	8	Steel	7.85

Table 48: Hypothetical example fragments recovered from MDFPIM V2.0

Both layer 1 and 2 of the MDFPIM have 4 perforations, indicating there is a risk of eye penetration and skin perforation at the model location.

Substituting the values for each fragment into Equation 41 and calculating the velocity bounds using $L_{n\pm1}$ gives the values in Table 49.

Fragment mass (g)	Maximum layer perforated	Estimated impact velocity (m s^{-1})	± bounding velocity (m s^{-1})
0.15	2	96.4	21.9
0.23	4	307.9	77.8
0.28	4	131.6	19.0
0.25	8	296.1	31.7

Table 49: Hypothetical example fragments recovered from MDFPIM V2.0 and predicted velocities

The details in Table 48 and Table 49 can be used as verification data for Equation 41 if required.

K.1.5 MDFPIM V2.0 additional analysis comments

MDFPIM V2.1 or V2.2 can be used to provide assessment of eye penetration risk and skin perforation risk in the same manner as V2.0 (either by physical inspection and hole counting or by image analysis).

MDFPIM V2.2 is optimised for corneal abrasion assessment, in addition to assessment of eye penetration risk and skin perforation risk, with the transparent polythene for layer 1a.

The details in Table 48 and Table 49 can be used as verification data for Equation 41 if required. Equation 41 will give slightly different predictions to Equation 33 due to rounding errors (<0.02 m s^{-1}).

It is recommended that when the MDFPIM is used, the model version and process used to generate impact velocity predictions are detailed (physical fragment recovery or image analysis) along with the results.

The details for fragment mass and estimated impact velocity calculated from analysis of the MDFPIM can be used as inputs to other models to predict various outputs. Section K.2 describes possible routes of using the MDFPIM V2.0 outputs to provide injury estimates.

K.2 Injury prediction from the MDFPIM V2.0

The injury prediction to use for the MDFPIM depends on the requirements of the testing being performed. The most appropriate method to take the MDFPIM V2.0 outputs and convert to an injury output should be determined on a case by case basis.

As one example of how the data could be used, the steps required to apply the Sperrazza and Kokinakis (S&K) incapacitation criteria [43] to model outputs are given below:

1. Depending on desired output of model (prior to testing), map out the trials arena to locate position of each model (e.g. x, y and z co-ordinates relative to the threat).
2. Ensure each model is uniquely labelled so it can be identified after the test
3. After testing, analyse physical models to get the following information for each retained fragment:
    - Mass
    - Maximum layer perforated
    - X-y co-ordinates relative to a given corner of the model[215].
4. Use the details from mapping the trials arena to convert x-y co-ordinates of each fragment location on the pack to x, y and z co-ordinates relative to the threat [217]
5. Use MDFPIM V2.0 calibration equation (Equation 41) to estimate the impact velocity for each fragment
6. Calculate the incapacitation (P_{hk}) for each fragment using Equation 45.
    - Incapacitation calculations can be based on the co-ordinates of recovered fragments related to specific body locations[217]; or
    - Generalised over the entire body.

[215] If required depending on desired output of model.

$$P_{hk} = 1 - e^{-a\left(mv^{3}/_{2} - b\right)^{n}}$$

Equation 45: P_{hk}, the probability (given a hit) that single, random hits with steel fragments will incapacitate. Reproduced from Reference [43].

Where:

m is the fragment mass in grains

v is the fragment velocity in feet per second

a, *b* and *n* are parameters that depend on the body region, and tactical situation and time at which the incapacitation is to ensue.

7. (Create imaginary boxes to represent presented area of a person) [217]
8. Use binomial summing to calculate the total probability of incapacitation for all fragments within each model (or imaginary box) using Equation 46:

$$P_k = \prod_{i=1}^{n} \left(1 - P_{hk\,i}\right)$$

Equation 46: Total probability that n hits will incapacitate [43].

Where:

P_k is the total probability that *n* hits will incapacitate (neglecting synergistic effect of multiple wounds and assuming that P_{hk} is relatively small for each hit).

P_{hki} is the probability of incapacitation from the i^{th} fragment, calculated from Equation 45.

n is the total number of fragment impacts.

9. Present results as required.
    - One suggested way of presenting the output is to plot the outcome (P_k) for each model/box as a coloured overlay onto the trial setup or scenario.

Following the process described above, data from an explosive trial was processed, highlighting some of the key stages[216]. The models were employed in a tiled wall (Figure 188) to look at behind barrier effects from an explosive device.

Figure 188: Tiled wall of MDFPIM V2.0 in an outdoor fragmenting blast trial.

Following steps 1 and 2, the location of each pack relative to the threat was measured and packs labelled. The wall was broken down into 10 boxes (to represent the size of a standing person). Figure 189 shows a simplified plan view of the trial layout with the 10 regions on the MDFPIM wall shown.

[216] Fictitious data was used as the real data from this testing was classified.

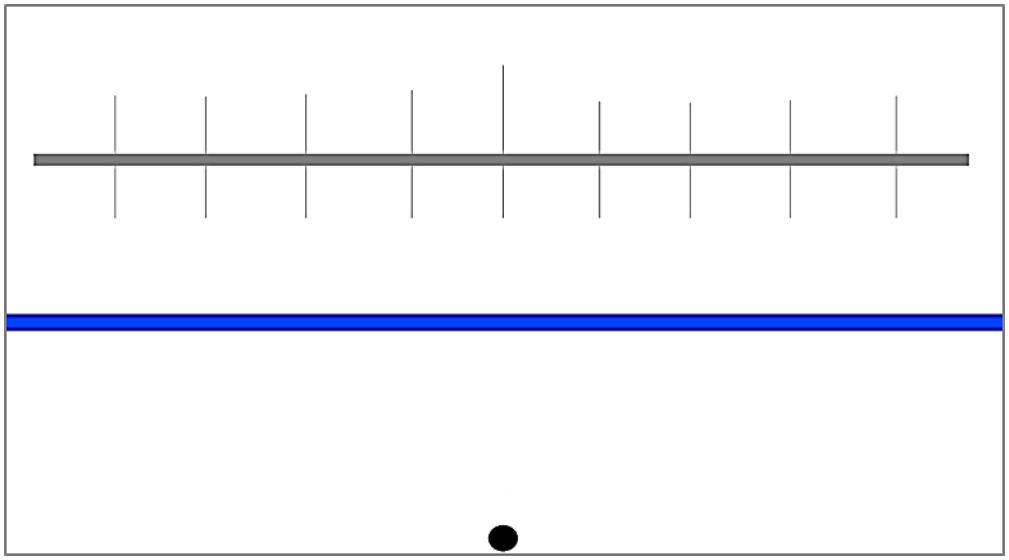

Figure 189: Diagram of plan view of the trial layout. Black circle represents the threat. Blue line is the barrier and grey line is the wall of MDFPIM. Gridlines on the MDFPIM wall indicate the 10 boxes used for analysis of the injury outcomes.

Following the testing, the mass and deepest layer perforated by each fragment was recorded and its co-ordinates measured. These co-ordinates were then translated into the relative position on the wall, rather than each pack.

The fragment mass and maximum layers perforated were used to calculate the impact velocity and then the P_{hk} value for each fragment.

The total probability of incapacitation for each box was calculated, using Equation 46 and the entire body conditions (ignoring the height from the floor component of the fragment impact locations). This process was repeated with each box shifted incrementally along the horizontal direction of the wall (discounting any boxes that overlapped the edge of the wall).The outcome for each box was then plotted in Excel® against horizontal distance along the wall of MDFPIM. A moving average was used to smooth the incapacitation predictions between each discrete box. The averaged outcomes were then assigned a colour to indicate the degree of incapacitation. Paint.Net [299] was used to manipulate the Excel® generated colour banding into an arc and overlaid back onto the trial layout as shown in Figure 190.

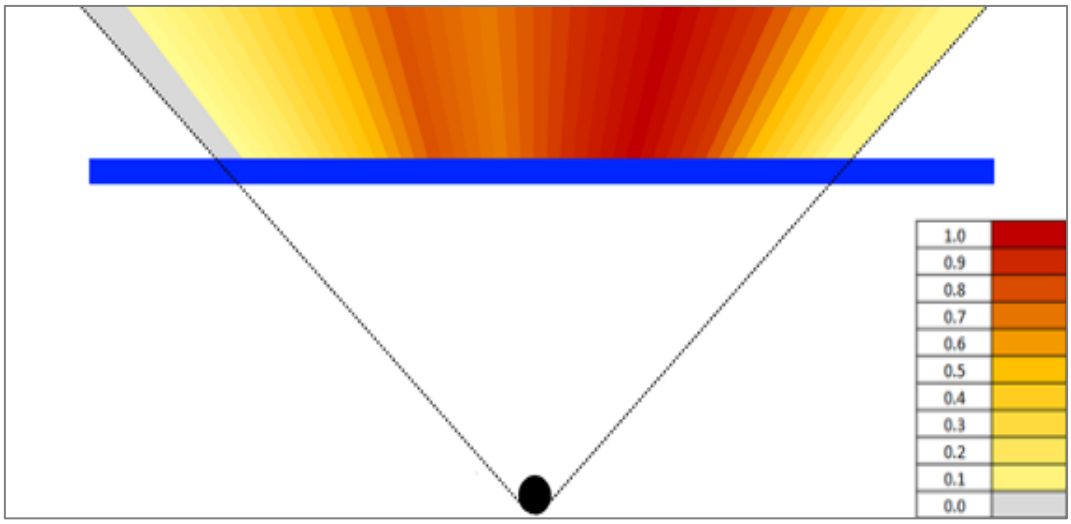

Figure 190: Example output using the incapacitation criteria, broken down into boxes and overlaid onto trial setup. The probability outcome colour key is given in the bottom right of the figure.

Figure 190 shows how the total probability of incapacitation varies along the MDFPIM wall in a simple to visualise manner. Red indicates very high risk of incapacitation, grey or light yellow indicate low risk.

This method of visualisation has been particularly useful for overlaying trial outcomes onto platforms for comparison between different scenarios with similar setups, as differences can be easily visualised.

Although not presented as part of Figure 190, regions where eye penetration and skin perforation are predicted could additionally be displayed. A zero probability of incapacitation (coloured grey in Figure 190) does not indicate a zero probability of eye penetration or skin perforation.

This analysis method highlights that the size of the impact face of the MDFPIM is not a limitation of how the results are interpreted. The MDFPIM dimensions should be chosen to simplify trial setup and analysis as far as possible.

Some brief limitations of the S&K incapacitation injury algorithm are that:

- Incapacitation is an injury output that is not always applicable or useful (it depends on the requirement as to how the outputs should be given).

- The algorithm is only valid for steel fragments (and tumbling flechettes).
- Due to the way the incapacitation is calculated in Equation 45, with a lower $mv^{3/2}$ cut-off, low mass fragments can generate a zero probability of incapacitation. Due to the design of the MDFPIM, many of the fragments that it could capture may well be below this limit (but may still cause skin perforation as determined by the model).

Synergistic effects from multiple fragments are not considered.

APPENDIX L Image analysis process for MDFPIM

L.1 Overview of MDFPIM analysis process

The ideal analysis of the MDFPIM requires the model to be completely intact post-test, so that each layer can be dissected and fragments recovered and weighed. In previous blast testing, due to the proximity the MDFPIM was placed to the device, it could be torn open or apart. When this happened (even slightly) any fragments initially captured by the pack could escape or others get in. Therefore, in these cases the mass of the penetrating fragments were estimated based on measurements of the hole in the polythene witness sheet.

Even instances where all the neoprene foam was ejected from the pack the polythene often remained in one continuous length and allowed the analysis to be conducted in this manner.

The number and dimensions of all the holes in every layer of the polythene sheets for each MDFPIM were measured using image analysis software as described in the following section.

L.2 Image analysis process using Image Pro Plus

A good quality image of the polythene sheet was taken on the light box. It was ensured that a photographic scale was included in the image, as well as an indication of which was the top of the sheet and that the image was not over or under exposed. This generated an image such as the one below, emphasising the holes in the polythene sheet.

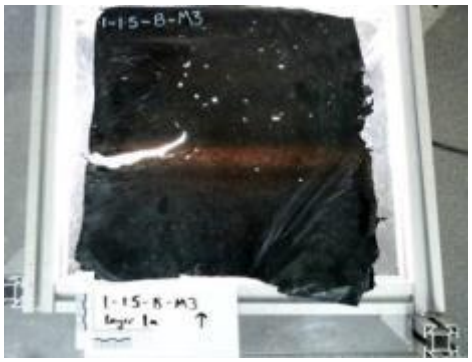

Figure 191: Photograph of polythene sheet on a light box.

The image was then imported into Image Pro Plus. The first stage was to calibrate the image to generate the numebr of pixals per millimetre. This was done by built in calibration wizard in the software, allowing the user to place a measurement curser over the scale and select the approptriate length.

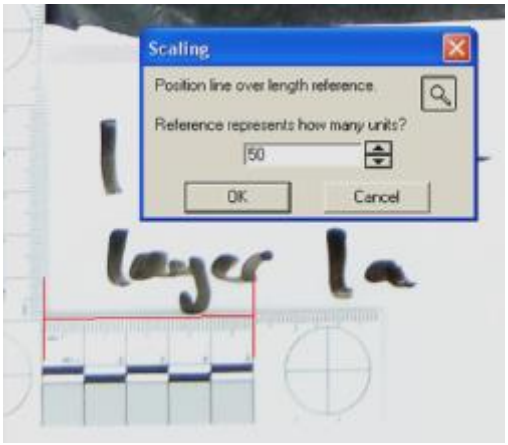

Figure 192: Screenshot of scaling process within Image Pro Plus.

The origin of the image was then altered to be the top left corner of the polythene, rather than the top left corner of the image. This later allowed the x-y co-ordinates to be calculated from a known position.

The next stage was to select the area of the image for the software to count the holes. This could be done by tracing the outline or using a tool to select areas of similar intensity. The area included in the green outline shows where the holes were counted in this image.

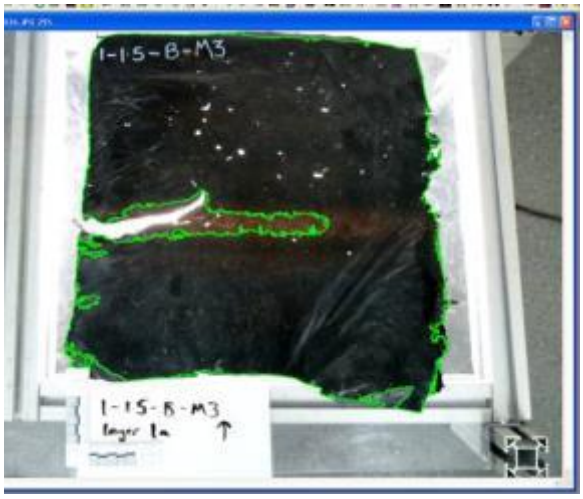

Figure 193: Area of interest in green outline selected for hole counting.

The software can then count the bright objects automatically, or be told the intensity range of objects to count. The count then outlined and numbered each object on the screen.

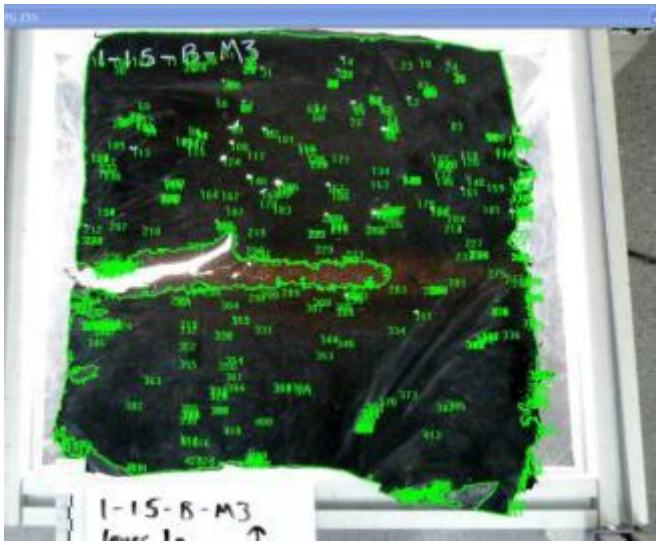

Figure 194: Holes identified after automatic counting of bright objects within the selected area of interest

The intensity range was altered by the user to screen out any light areas that weren't holes, but include all objects that were. Areas of the image could also be excluded, even if within the green outline (such as the white numbering in this image). This resulted in only the 'true' holes being outlined, as shown below.

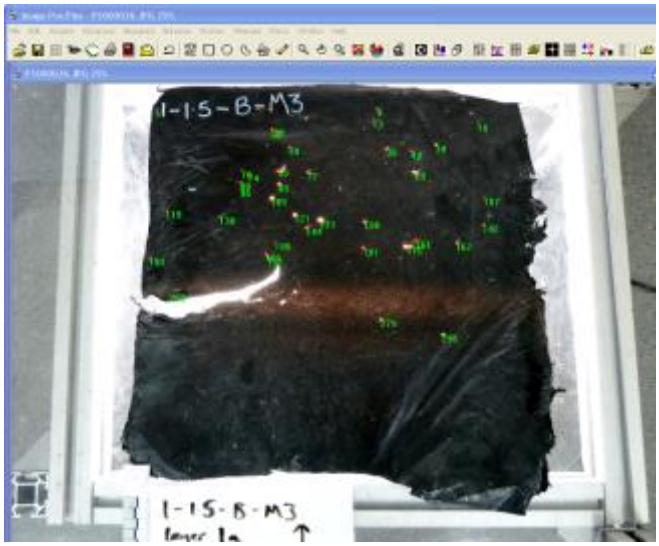

Figure 195: Holes identified after manual selection of intensity values for the count.

Multiple different measurements can be selected to measure different aspects of each object. The essential measurements for each individual hole are:

- Centre-X
- Centre-Y
- Diameter (mean)

Limits on the measurements can also be set, so that objects outside this range are automatically ignored. For example if the aspect ratio is additionally measured, objects with aspect ratios (for example above 3) can be discounted as these are likely to be rips or tears rather than perforations.

The details and measurements could then be exported to Microsoft® Excel® for further analysis. An example of the output is shown in the screenshot below.

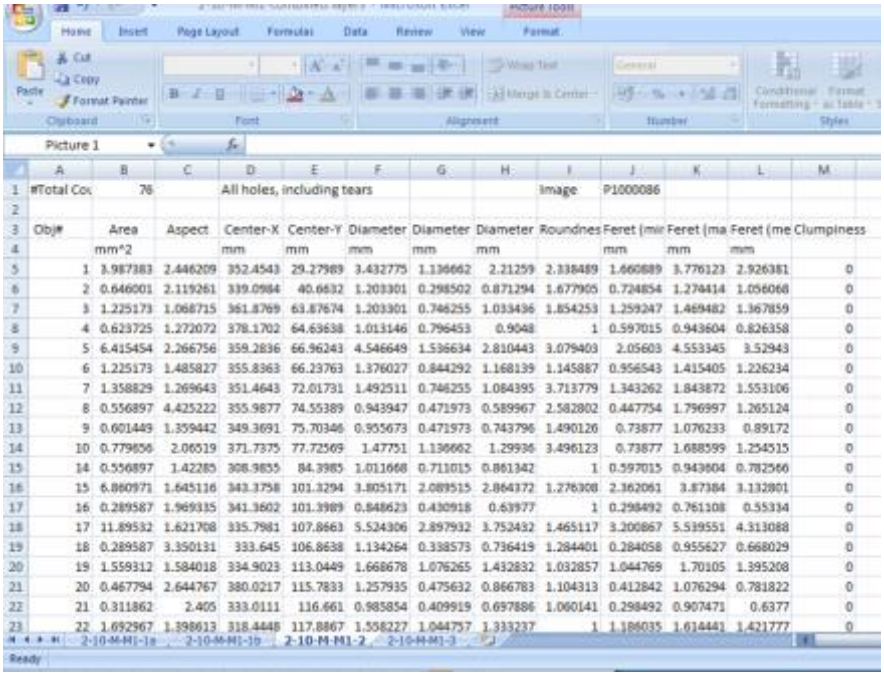

	A	B	C	D	E	F	G	H	I	J	K	L	M
1	#Total Co	76		All holes, including tears					Image	P1000086			
2													
3	Obj#	Area	Aspect	Center-X	Center-Y	Diameter	Diameter	Diameter	Roundnes	Feret (mi	Feret (ma	Feret (me	Clumpiness
4		mm^2		mm	mm	mm	mm	mm		mm	mm	mm	
5	1	3.987383	2.446209	352.4543	29.27989	3.432775	1.136662	2.21259	2.338489	1.660689	3.776123	2.926381	0
6	2	0.646001	2.119261	339.0984	40.6632	1.203301	0.298502	0.871294	1.677905	0.724854	1.274414	1.056068	0
7	3	1.225173	1.068715	361.8769	63.87674	1.203301	0.746255	1.033436	1.854253	1.259247	1.469482	1.367859	0
8	4	0.623725	1.272072	378.1702	64.63638	1.013146	0.796453	0.9048	1	0.597015	0.943604	0.826358	0
9	5	6.415454	2.266756	359.2836	66.96243	4.546649	1.536634	2.810443	3.079403	2.05603	4.553345	3.52943	0
10	6	1.225173	1.485827	355.8363	66.23763	1.376027	0.844292	1.168139	1.145887	0.956543	1.415405	1.226234	0
11	7	1.358829	1.269643	351.4643	72.01731	1.492511	0.746255	1.084395	3.713779	1.343262	1.843872	1.553106	0
12	8	0.556897	4.425222	355.9877	74.55389	0.943947	0.471973	0.589967	2.582802	0.447754	1.796997	1.265124	0
13	9	0.601449	1.359442	349.3691	75.70346	0.955673	0.471973	0.743796	1.490126	0.73877	1.076233	0.89172	0
14	10	0.779856	2.06519	371.7375	77.72569	1.47751	1.136662	1.29936	3.496123	0.73877	1.688599	1.254515	0
15	14	0.556897	1.42285	308.9855	84.3985	1.011668	0.711015	0.861342	1	0.597015	0.943604	0.782566	0
16	15	6.860971	1.645116	343.3758	101.3294	3.805171	2.089515	2.864372	1.276308	2.362061	3.87384	3.132801	0
17	16	0.289587	1.969335	341.3602	101.3989	0.848623	0.430918	0.63977	1	0.298492	0.761108	0.55334	0
18	17	11.89532	1.621708	335.7981	107.8663	5.524306	2.897932	3.752432	1.465117	3.200867	5.539551	4.313088	0
19	18	0.289587	3.350131	333.645	106.8638	1.134264	0.338573	0.736419	1.284401	0.284058	0.955627	0.668029	0
20	19	1.559312	1.584018	334.9023	113.0449	1.668678	1.076265	1.432832	1.032857	1.044769	1.70105	1.395208	0
21	20	0.467794	2.644767	380.0217	115.7833	1.257935	0.475632	0.866783	1.104313	0.412842	1.076294	0.781822	0
22	21	0.311862	2.405	333.0111	116.661	0.985854	0.409919	0.697886	1.060141	0.298492	0.907471	0.6377	0
23	22	1.692967	1.398613	318.4448	117.8867	1.558227	1.044757	1.333237	1	1.186035	1.614441	1.421777	0

Figure 196: Screenshot of Excel® spreadsheet output from hole counting and measurement in Image Pro Plus.

The output for each layer of a pack were then combined into one Excel® spreadsheet, with a different layer on each tab. The mean diameter (and roundness measurement) were then used to estimate the volume of the fragment that caused each hole. This was then used to estimate the mass of each fragemnt, based on the measured density of a number of recovered fragments, pre and post firing and validated against image analysis of recovered wieghed fragments.

These estimated masses compared well to the actual masses of the recovered fragments when direct comparisons could be made (data not shown).

The co-ordinate location as well as the estimated mass was used to plot a bubble graph for each layer of the pack. An example of some of these graphs are shown below.

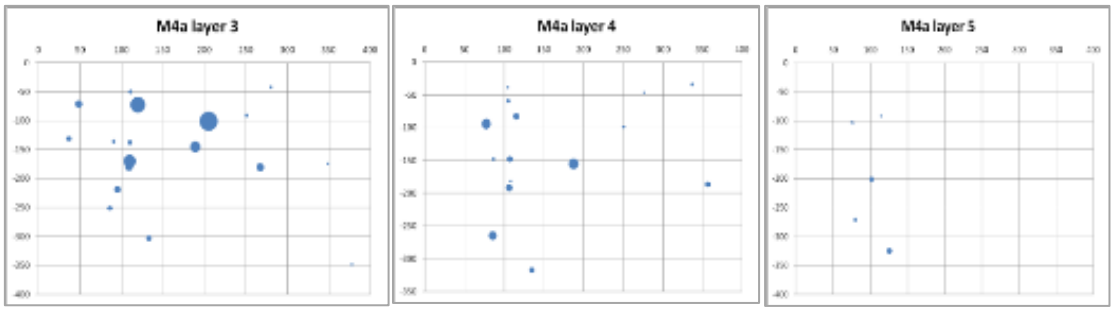

Figure 197: Bubble plots to show co-ordinates and estimated fragment mass from each hole in different polythene layers.

These graphs were used to manually determine what fragemnts had passed through multiple layers, so that they were only accounted for once, in the deepest layer that they penetrated. This therfore discounted any ‘injury’ contribution for a fragment that broke up during penetration, only considering its final mass.

The (estimated) mass of each fragment, along with the deepest layer in the MDFPIM it perforated were then fed into Equation 41.

APPENDIX M Exploitation (use) examples of MDFPIM

Figure 198 to Figure 201 show some examples of trials in which MDFPIM has been used.

Figure 198 and Figure 199 show MDFPIM V1.1 in steel frames surrounding a buried IED trial. Some packs are angled at 60° and some are covered with different PPE materials.

Figure 198: MDFPIM V1.1 in individual frames surrounding a buried IED at 1.5 m radial distance. Some models are additionally covered by ballistic materials.

Figure 199: Close up of one column of MDFPIM V1.1 in steel frames from a buried IED trial. Models are covered by ballistic materials.

Figure 200 shows impact marks on a steel plate from a small arms round with the resulting ricochet directed towards a tiled wall of MDFPIM V2.2 positioned 5 m from the plate.

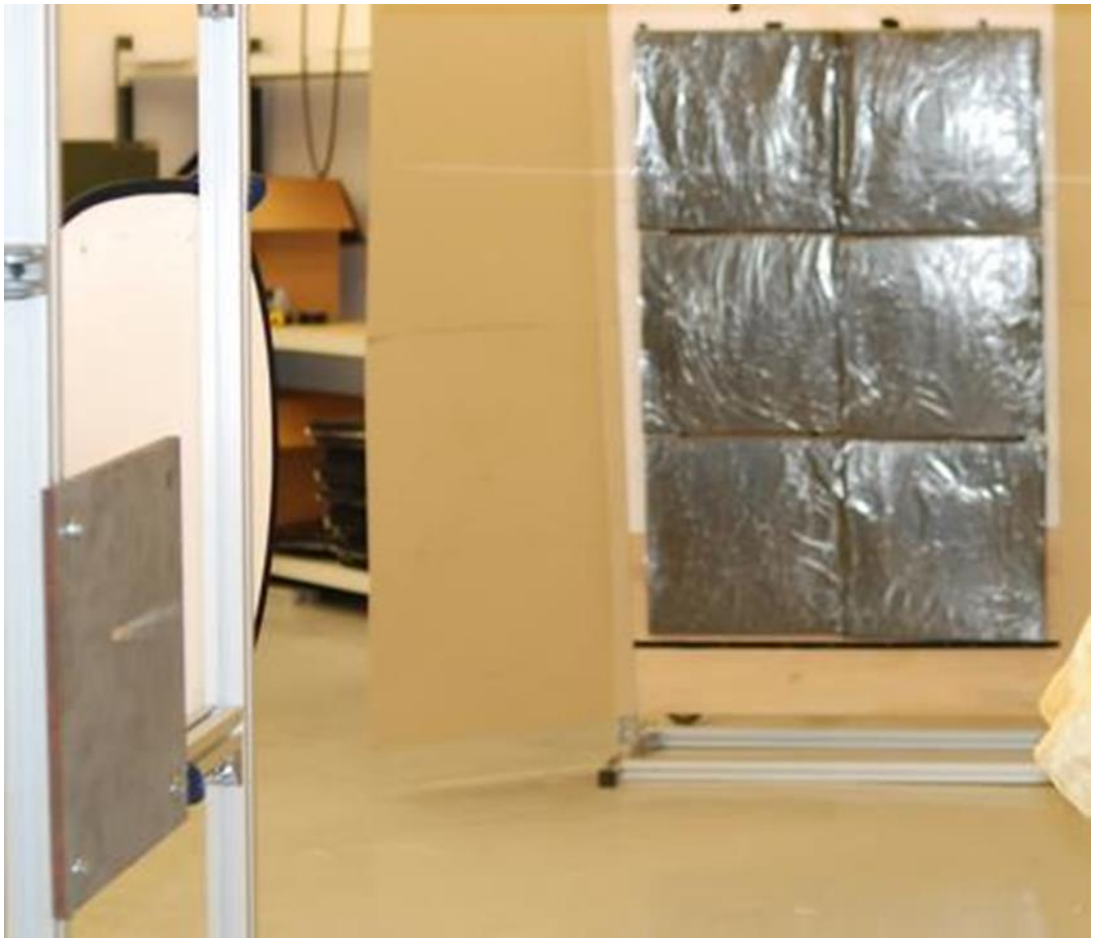

Figure 200: Tiled wall of MDFPIM V2.2, each pack 600 mm square creating a 1.8 m tall by 1.2 m wide wall used for a safety assessment trial of ricochet bullets.

Figure 201 shows a 2 m by 3.5 m tiled wall of MDFPIM V2.0 in an outdoor fragmenting blast trial.

Figure 201: Tiled wall of MDFPIM V2.0, creating a 2 m tall by 3.5 m wide wall in an outdoor fragmenting blast trial.

The trial shown in Figure 201 resulted in the a CSA (Chief Scientific Advisor) Commendation on 4th April 2019 at MOD Main Building, winning the Excellent Science or Engineering category (High quality, novel, significant and impactful science or engineering which delivers an exceptional contribution to UK Defence and Security). Additionally this work was recognised by the Dstl Annual Awards Celebration 2019 (26th September 2019 held at Tidworth Garrison).

The author as well as the MDFPIM V2.0 was integral to enable the assessment to be conducted.

A patent has been applied for covering the MDFPIM [284].

ANNEX A Presentation given to the Group Of Experts in Mitigation Systems (GEMS)

Presentation given to GEMS 18th Annual meeting, 24th-26th January 2017, Defence Academy of the United Kingdom at Shrivenham [283].

Overview

- Problem space
- Requirement for a new witness pack
- Development
- Pack design
- Calibration and validation
- Example of witness pack use
- Outcome

The problem

- Physical weapon tests - How do you assess the injury potential of the fragments generated?
- For 'conventional' metal fragments:
  - Layered metal spaced witness packs
  - Strawboard packs
  - Tissue simulant such as gelatin
  - **Impractical or potential to miss injurious fragments**
- For non-metallic fragments
  - No common or suitable method

Requirement

- A witness pack to aid injury assessment of fragments generated by buried Improvised Explosive Devices (IEDs) in Afghanistan
- Only interested in injury via penetration
- Desired attributes of witness pack:
  - Allow assessment of a range of different fragment types
  - Assess multiple impacts from a single event
  - Synthetic materials
  - Quantitative analysis

Material selection for witness pack

- Initial material selection for witness pack
  - 9 different materials assessed with range of properties
- Penetration depth in witness pack linked to animal tissue damage
- Range of fragments (different densities, masses, diameters)

Witness pack design

- Layered pack
- 2 versions – thick and thin depending on application

- Depth of penetration in witness pack linked to injury type
  - Eye penetration
  - Skin Perforation
  - Back calculate impact velocity to feed other injury predictions

Ballistic performance criteria

Eye penetration

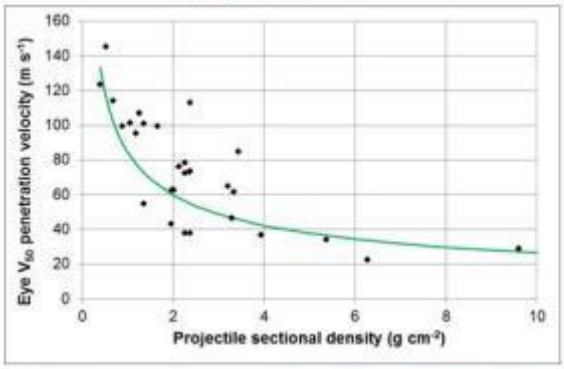

Duma, S.M et al. Determination of significant parameters for eye injury risk from projectiles. *Journal of Trauma and Acute Care Surgery, 2005, Vol 59(4), pp 960-964.*

Skin perforation

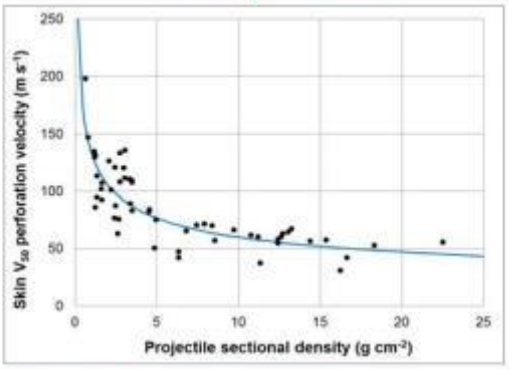

Google Patents. Skin and tissue simulant (WO2013171444 A1). Inventor: James, G. *Application: PCT/GB2013/000221. United Kingdom.*

Witness pack penetration response

- 440 shots with 9 different projectiles for the calibration of penetration response (at room temperature)
- Initial data for temperature dependence of witness pack on penetration response (from -10°C to + 40°C)

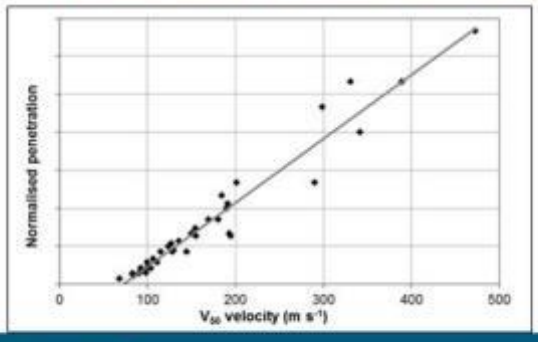

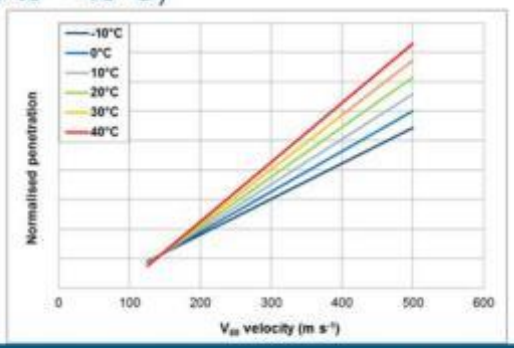

Buried IED testing with witness pack

With body armour covering

Buried explosive

Witness pack analysis

- Model deconstructed and image analysis used to determine perforations to each layer (number, size, location, etc.)

- Eye and skin injury risk
- Mass measured from recovered fragment or estimated from hole size
- Calibration data used to calculate impact velocity for each fragment
  - Degree of overmatch of mitigation

Types of assessment using the new witness pack

- Potential uses
  - Safety cases & collateral damage assessment
  - Survivability / vulnerability assessments
  - Effects of mitigation / personal protective equipment
  - Inform computer based models for injury prediction
- Threats - not just buried explosives
  - Behind barrier effects (glazing, masonry, etc.)
  - Devices producing non-metallic or low energy metal fragments

Outcome

- New witness pack supports suite of physical models for MOD and wider government injury assessments

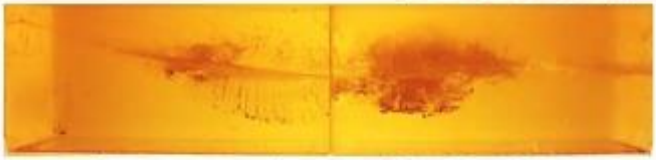

- Interest for use as a witness pack outside Dstl?

Questions?

Gregory James
grjames@dstl.gov.uk

 Dstl/PUB099788

[dstl] 24 January 2017 © Crown copyright 2017 Dstl UK OFFICIAL Ministry of Defence